Using Earth Observation and ground-based data to improve modelled CO_2 and CH_4 fluxes from peatlands

Natasha Louise MacBean

Department of Geography,

University College London

Thesis submitted for the fulfillment of a

degree of Doctorate of Philosophy

August 2011

Declaration

I, NATASHA MACBEAN, confirm that the work presented in this thesis is my own. Where information has been derived from other sources, I confirm that this has been indicated in the thesis.

Signed:

Date:

Abstract

Peatlands are an important store of carbon; they contain ~15-30% of the world's soil C while covering only ~3% of the land area. They are also the largest natural source of methane (CH_4), but the global estimate is highly uncertain. Here, this issue is addressed by developing a combined data - modelling framework to provide optimal estimates of CO_2 and CH_4 fluxes from an upland UK peat site. An Observing Systems Simulation Experiment (OSSE), using a Bayesian inversion method, is implemented to investigate the CH_4, NEP and soil moisture observation temporal frequency and uncertainty required to accurately constrain model parameters and to estimate model predictive uncertainty. The OSSE is used to examine the impact of parameter correlations, bias in low-resolution observations, and unknown model error. The highly model-sensitive parameters are constrained by almost all observations, with a corresponding improvement in model predictive uncertainty. However there is high degree of model equifinality. Biased observations and unaccounted-for model error can result in false confidence in inaccurate model predictions. The OSSE results demonstrate the importance of performing a synthetic experiment prior to using actual data. Finally, real data are used to calibrate the model, which is then used to determine the net CO_2 and CH_4 flux for the site. The results highlight a possible source of error in the model. It is suggested this is because of an inaccurate representation of the coupling between CO_2 and CH_4, due to an unaccounted for lag in the methanotrophic activity. This has significant implications for CH_4 flux modelling, as many models use a similar formulation for CH_4 dynamics. Results are compared with satellite and ground-based measurement characteristics and recommendations are made for the observation and modelling of ecosystems at small spatial scales. This information is useful for modellers, space agencies and field biologists.

Acknowledgements

I would like to dedicate this thesis to my father and maternal grandmother, who unfortunately are no longer with us. Their strength of character and presence of mind have undoubtedly served as a shining example to me throughout my life.

I'd like to start by thanking my principal supervisor Mat Disney for his straight-talking guidance and support throughout the last four years. He has been very encouraging and has always made the time to talk things through with me, for which I am very grateful. I'd also like to thank my second supervisors Philip Lewis and Phil Ineson for their advice and support. Particular thanks goes to Jose Gomez-Dans for his patience in answering my many questions. I am immensely appreciative of all the time he has taken to discuss the various aspects of my research with me. I would also like to thank Tristan Quaife for useful discussions in the earlier stages of my PhD. I'd like to express my sincere thanks to my friends and former PhD student 'buddies' Martin De Kauwe and Steve Hancock, who have been very supportive and encouraging over the past four years.

I am sincerely grateful to Andreas Heinemeyer, James Stockdale and Matthew Carroll for providing data that was used in these thesis, and for taking the time to discuss the data with me. I have found their input very helpful and their contribution has made all the difference to my PhD work. My wholehearted thanks also goes to the many members of the UKPopNet team who helped set up the weather stations at the Lake Vyrnwy site and who collected the C flux data, including Robert Holden, Catherine Moody, Anna Bing, Debbie Coldwell, Matt Walker, Sylvia Toet, James Stafford and Graham Hambley. I would like to thank the RSPB and the Countryside Council for Wales for providing access to the Lake Vyrnwy Reserve and the RSPB staff at Lake Vyrnwy who were also very helpful in solving practical problems in the field. Thanks also goes to CCW for providing access to aerial photography for the site, and to Liz Jones and Dietmar Backes in the Geomatics Department at UCL for loaning me the GPS.

I owe a debt of gratitude to my friends and fellow UCL PhD students Kate Littler and Rakia Meister for many lunch-time chats over the last few years on just about everything, including the ups and downs of our PhD work. Life at UCL would not have been quite the same without them, and I thank them for their encouragement and support, especially

in the last few months.

I am especially grateful to my boyfriend Rob for his care, love and support over the past two years. He has been incredibly patient with me at times when I've felt stressed. I hope I can do the same for him as he continues his PhD. I'd also like to express my heartfelt thanks to my dear friend and house-mate over the last three years, Lillie Dunn. She always provides very balanced and thoughtful advice which keeps me grounded. She has been immensely supportive of me and for that, and her friendship, I am extremely grateful. My thanks also goes to my other two friends and house-mates over the last year, Alice and Olivia Dunn, who have also been very encouraging and supportive whilst I've been writing up my PhD, and to Jo Caroussis, my friend and former house-mate, for her support and encouragement. I would like to extend my thanks to all my wonderful friends who have all been there for me at various points in the last few years.

Lastly I'd like to thank my family who have provided me with a strong and stable support network throughout my life. In particular I'd like to thank my step-dad Martin, for his encouragement and support, especially "behind-the-scenes". I cannot express enough thanks to my mother who has always showered me with love, who has always believed in me, and who always let me know that she was proud of me. She has always encouraged me to just to do the best I can and supported me in all my endeavors. For that, and for everything she has done for me in my life, I am eternally grateful.

Contents

List of Figures

List of Tables

List of Acronyms

AATSR: Advanced Along-Track Scanning Radiometer
AIRS: Atmosperic InfraRed Sounder
ALOS: Advanced Land Observing Satellite
ASCAT: Advanced SCATterometer
AVHRR: Advanced Very High Resolution Radiometer
BATEA: BAyesian Total Error Analysis
BEPS: Boreal Ecosystem Productivity Simulator
BETHY: Biosphere-Energy-Transfer-HYdrology
CASA: Carnegie-Ames-Stanford-Approach
COLM: COmmon Land Model
CCW: Countryside Council for Wales
DA: Data Assimilation
DEMC: Differential Evolution Markov Chain
DOAS: Differential Optical Absorption Spectroscopy
DVM: Dynamic Vegetation Model
ECMWF: European Centre for Medium Range Weather Forecasting
EET: Estimated EvapoTranspiration
EO: Earth Observation
ERS: European Remote Sensing
FAO: Food and Agriculture Organisation
fAPAR: fraction of Absorbed Photosynthetically Active Radiation
FPAR: Fraction of PAR
GCM: Global Climate Model
GHG: GreenHouse Gas
GOSAT - Global greenhouse gas Observation by SATellite
GPP: Gross Primary Production
IASI: InfraRed Atmospheric Sounding Interferometer
IEM: Integral Equation Model
IMAP-DOAS: Iterative Maximum A Posteriori - DOAS
IPAR: Intercepted Photosynthetically Active Radiation
IRGA: InfraRed Gas Analyser
JAXA: Japanese Aerospace Exploration Agency
JULES: Joint UK Land Environment Simulator
LAI: Leaf Area Index
LPJ: Lund Potsdam Jena
LPJ-WHyMe: LPJ Wetland Hydrology and Methane emission
LPRM: Land Parameter Retrieval Model
LST: Land Surface Temperature
LUE: Light Use Efficiency
LUT: Look Up Table

LST: Land Surface Temperature
MAP: Maximum A Posteriori
MERIS: MEdium Resolution Imaging Spectrometer
MCMC: Markov Chain Monte Carlo
MDF: Model Data Fusion
MH-MCMC: Metropolis Hastings MCMC
MODIS: MODerate resolution Imaging Spectrometer
NDVI: Normalised Difference Vegetation Index
NEP: Net Ecosystem Product
NIR: Near-InfraRed
NPP: Net Primary Production
NPPann: annual NPP
OAT: "One-At-a-Time"
OCO: Orbiting Carbon Observatiory
OSSE: Observation System Simulation Experiment
PALSAR: Phased Array type L-band Synthetic Aperture Radar
PAR: Photosynthetically Active Radiation
PCARS: Peatland CARbon Simulator
PDM: Peat Decomposition Model
PEM: Production Efficiency Model
PET: Potential EvapoTranspiration
PFT: Plant Functional Type
PDF: Probability Distribution Function
PPDF: Posterior PDF
RDR: Relative Drying Rate
RMSD: Root Mean Squared Difference
SA: Sensitivity Analysis
SAC: Special Area of Conservation
SAR: Synthetic Aperture Radar
SCIAMACHY: SCanning Imaging Absorption spectroMeter for Atmospheric CHartographY
SEM: Standard Error of the Mean
SMAP: Soil Moisture Active Passive
SMEX: Soil Moisture EXperiments
SMOS: Soil Moisture and Ocean Salinity
SOM: Soil Organic Matter
SWI: Soil Wetness Index
SVAT: Soil-Vegetation-Atmosphere-Transfer
TEM: Terrestrial Ecosystem Model
TOPLATS: TOPmodel - based Land Atmosphere Transfer Scheme
TOVS: Tiros Operational Vertical Sounder
UNFCC: United Nations Framework on Climate Change
USDA: United States Department of Agriculture

VCD: Vertical Column Density
WFM-DOAS: Weighting Function Modified - DOAS
WMEM: Wetland MEthane Model
WTD: Water Table Depth

Chapter 1

Introduction

The concentration of greenhouse gases (GHGs), most notably CO_2, have been increasing in the atmosphere for the last 250 years as a result of human activity, causing a change in the radiative forcing of the atmosphere (*Denman et al.*, 2007). Much evidence points to this causing a rise in the global average temperature. How high the temperature will rise, however, is still the subject of much debate. Many groups from around the world are contributing to efforts to model the climate and its feedbacks with the land and ocean. Around 55% of the total carbon dioxide (CO_2) emissions over the last four decades were taken up by the land and ocean sinks (i.e. stores of C), but it is widely thought the efficiency of these sinks will decrease in the future (*Le Quéré*, 2010). This decrease is not fully understood, however, and the uncertainties on the estimates are large. The largest uncertainty is associated with the land surface, both through the natural carbon (C) cycle of uptake and release via photosynthesis and respiration (amongst other processes), and through land use change (Figure 1.1). Thus there is an urgent need to improve our knowledge of the C cycle through observations and modelling, which provides a tool for combining our understanding of the relevant processes.

The 4th Assessment Report from the Intergovernmental Panel on Climate Change highlighted the fact that climate change might significantly impact northern peatlands (*Denman et al.*, 2007). Peatlands are wetlands with an organic soil layer of >30cm (*Limpens et al.*, 2008) that occurs beneath a living plant layer as a result of the water-logged nature of the soil restricting complete decay of the biomass (*Charman*, 2002). Peatlands are important ecosystems; Boreal and subarctic peatlands are estimated to contain 455Pg of carbon (*Gorham*, 1991), about 15-30% of the world's soil carbon (*Limpens et al.*, 2008), and yet constitute less than 3% of the world's total land area (*Lai*, 2009) (Figure 1.2). More recent estimates which include deeper peats and permafrost soils, show even higher values of ~1600 Pg (*Tarnocai et al.*, 2009).

Peatlands not only sequester CO_2 through photosynthesis but also release C during microbial decomposition of soil organic matter (SOM), either as CO_2 under aerobic conditions or as methane (CH_4) under anaerobic, water-logged conditions. However, not all CH_4 is emitted to the atmosphere as microbial consumption of CH_4 occurs in the unsaturated soil layers, resulting in CO_2 instead of CH_4 being emitted to the atmosphere. Water table depth (i.e. the depth of the top of the saturated zone in the soil) is therefore a key environmental variable controlling the net C flux in peatlands. As climate changes this might also cause significant changes in peat accumulation

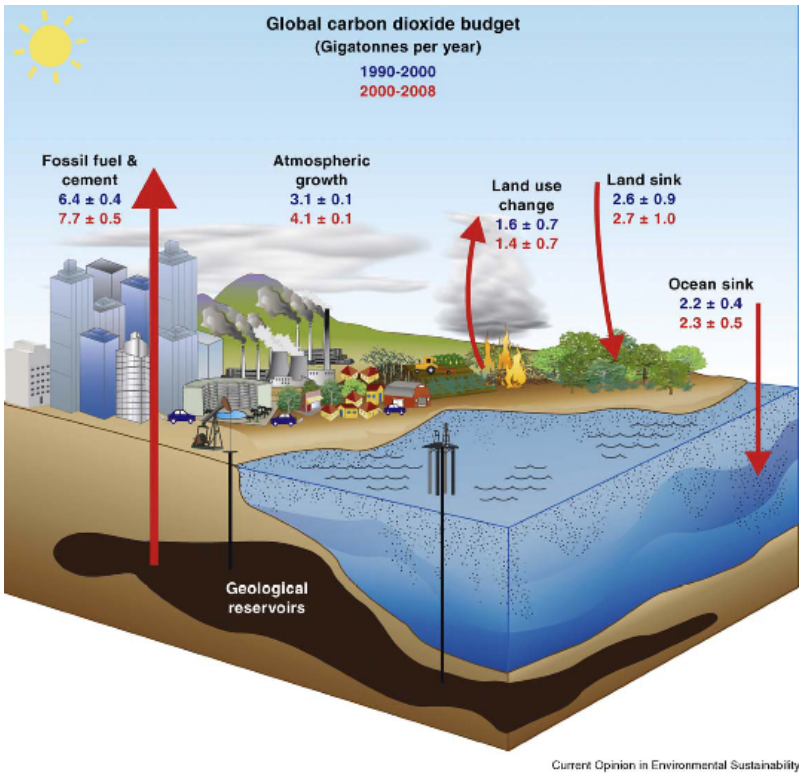

Figure 1.1: The Global CO_2 budget for both the 1990-2000 (blue) and 2000-2008 (red) periods. Taken from *Le Quéré* (2010).

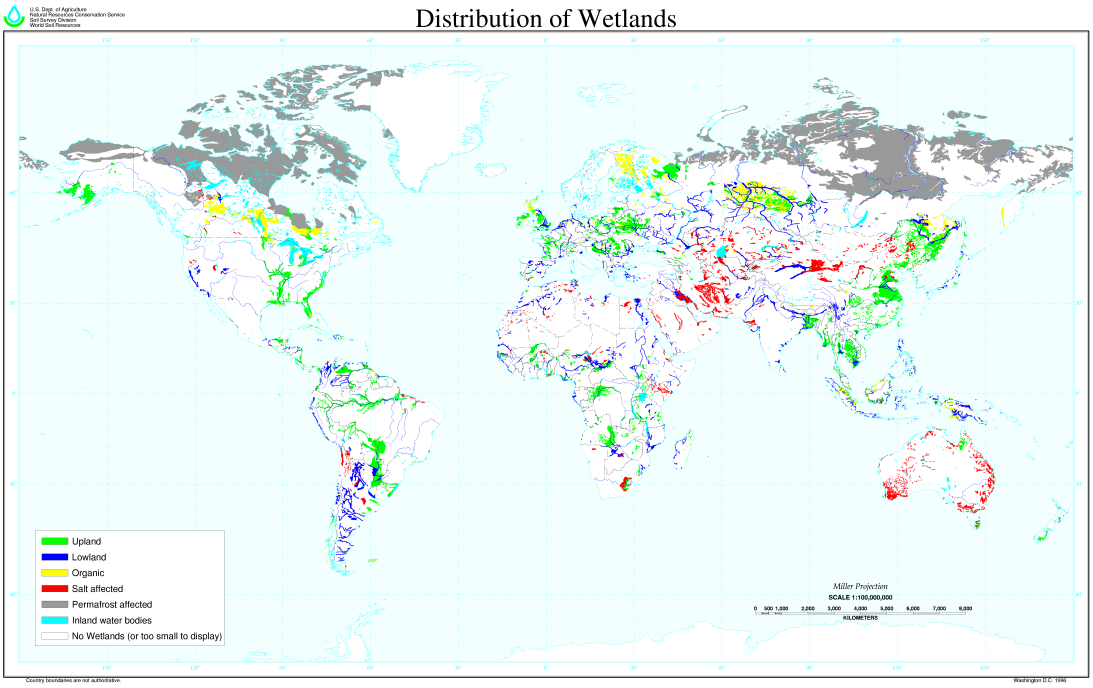

Figure 1.2: US Department of Agriculture Map of the Global Distribution of Wetlands. Organic wetlands (i.e. peatlands) are highlighted in yellow.

versus decomposition and its C emissions (*Heinemeyer et al.*, 2010).

Natural sources are responsible for about 30% of annual global CH_4 emissions, with wetlands being the main contributor (*Le Mer and Roger*, 2001; *Denman et al.*, 2007). *Denman et al.* (2007) reported CH_4 budgets of between 100 - 230Tg(CH_4)yr^{-1}. Uncertainties on estimates of the global CH_4 budget are high (e.g. Figure 1.3). *Bubier and Moore* (1994) (and references therein) estimated the contribution of northern wetlands is 35Tg(CH_4)yr^{-1}. Measurements span a range of three orders of magnitude however, from 1 mg$CH_4m^{-2}y^{-1}$ to 2200 mg$CH_4m^{-2}y^{-1}$. CH_4 has a short residence time in the atmosphere (10 years) but it is 20 to 30 times more efficient at absorbing infrared radiation than CO_2 (*Le Mer and Roger*, 2001).

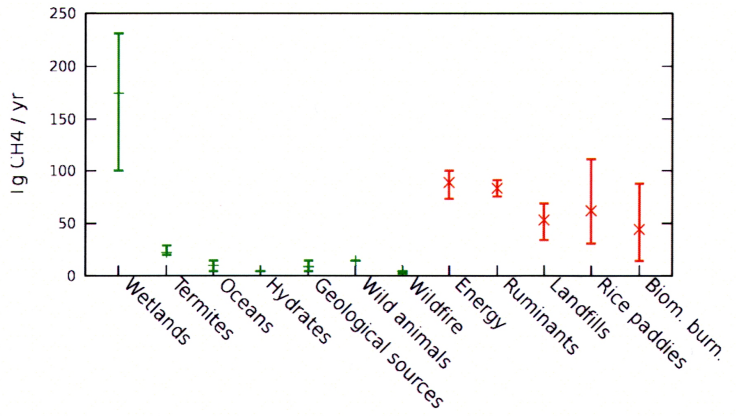

Figure 1.3: Estimates of methane emission from various sources. Taken from *Wania* (2007).

Peat-covered landscapes are highly sensitive to changes in land management, climate and pollution (*Bragg and Tallis*, 2001). Many have suffered degradation due to afforestation, encroachment by alien species, over-grazing, artificial drainage, and either deliberate or accidental burning, resulting in erosion, flooding, poor water quality and loss of ecological biodiversity (*Holden et al.*, 2004). Such damage is thought to be causing peatlands to be converted from net sinks to net sources of carbon (*Holden*, 2005).

It is widely hypothesised that with higher temperatures, and a potentially more vigorous hydrological cycle resulting from climate change, decomposition rates in peatlands could increase, thus releasing all the locked up C and turning the soil into a net source as opposed to a sink (*Parry et al.*, 2007). This is especially true in the Arctic where the C is unreactive in permafrost regions as the soil is frozen. With increasing temperatures it is thought that the soil will thaw, opening up a new source of C which could be released back to the atmosphere (*Denman et al.*, 2007).

Understanding the impact of changing management, land use and climate on peatlands is of great importance, as peatlands are such sensitive ecosystems. The balance between CO_2 uptake and CO_2 and CH_4 emission is complex and poorly quantified, it is clear that reducing the uncertainty on estimates of CO_2 and CH_4 emissions is imperative to improving our understanding of how important a role peatlands play in the land carbon cycle and climate change.

To address these issues several options are available. Ground-based observations can be used to provide detailed process information but only at a small scale and over a limited region. In addition ground-based measurements are often only taken over a short period of time. Earth

Observation (EO) data are available, both of biophysical variables which affect the carbon flux, such as soil moisture, or of trace gas fluxes calculated from columnar concentration measurements. EO data have the advantage of covering a wide area and are taken at regular time intervals over a relatively long time period. Such observations are not direct measurements of the variables in question and therefore a retrieval algorithm is required in order to derive the observations from raw radiance data. As such these observations are often highly uncertain.

Models are available which link together the processes involved in the carbon cycle based on current understanding. These are useful as a diagnostic and prognostic tool to test the current level of process knowledge and future scenarios relating to changes from management or climate change. However the models are imperfect or incomplete representations of the system, either because of lack of knowledge or because the scale or purpose of the model doesn't require more detail.

In recognising the drawbacks in solely using observations or models to understand the system, combined modelling-observation approaches for estimating variables relating to the land surface (energy, hydrology, C flux) have been investigated over the last decade or so. This field is called data assimilation (DA) or model-data fusion (MDF), and is the process of statistically combining observations and models in order to provide the best estimate of the variables being studied, and to improve our knowledge of the system. Many studies have been successful in doing this with land-based C flux observations and models (*Rayner*, 2010). These are reviewed further in Chapter 2. Many problems still persist however. Whilst land surface models are evolving at an increasing rate there is notably a lack of availability of observations to test, constrain and improve them. Satellite observations of C fluxes, and the variables which control C flux (e.g. measurements of vegetation dynamics including biomass and leaf area index (LAI), land surface temperature (LST) and soil moisture), are increasingly available, and as discussed offer a clear advantage over ground-based datasets. In order to combine the observations and the models it is imperative that an honest assessment of the uncertainty of the data is available, as discussed by *Raupach et al.* (2005). This is a challenging requirement and is an area which is severely lacking for many different types of observation. There is a growing realisation that observational errors need to be well-characterised in order for meaningful conclusions and estimates to be derived from looking at or using the data (*Hollinger and Richardson*, 2005; *Richardson et al.*, 2010; *Dorigo et al.*, 2010). This is reviewed further in the sections on the various observations in Chapter 2.

As the process of combining observations and models, with associated uncertainty, is quite involved it is important to understand which type of observations and their error and temporal sampling interval characteristics are needed to result in improved model estimates. Observation System Simulation Experiments (OSSEs) are useful in that regard as they implement the DA algorithms with synthetic "observations" with known characteristics, leading to an assessment as to whether the necessary data are available to achieve better estimates of the C flux and its uncertainty.

1.1 Objectives of this thesis

The aim of this thesis is to test the ability of a combined observation - modelling approach to improve peatland C flux estimates. A Bayesian inversion technique is used to calibrate the parameters of a simple C flux model that contains a representation of CH_4 flux dynamics, with the intention of constraining the model predictions of CO_2 and CH_4 flux.

The objectives of this thesis are as follows:

1. To choose a suitable model that can be used to estimate CO_2 and CH_4 estimates of peatland ecosystems.

2. To perform a model evaluation and sensitivity analysis so as to determine the parameters to which the C fluxes are most sensitive, and therefore which require calibration, and the observations that can be used to do so.

3. To develop and implement a synthetic experiment framework (OSSE) to determine which type of observation, and the required characteristics (i.e. temporal sampling interval and uncertainty), that should be used to calibrate the model using the Bayesian inversion technique.

4. To apply the inversion approach, drawing on conclusions from the OSSE studies, to a test site in North Wales, in order to obtain estimates of the magnitude and uncertainty of the net C fluxes.

This thesis provides an example of a generic framework that could be used to test and improve models, whether of the land surface C cycle or not. It also shows that, as well as understanding the requirements of the observations in performing a model calibration, an OSSE is a powerful tool that can be used to gain a better understanding of the results of the Bayesian inversion.

1.2 Outline of this thesis

This thesis is organised as follows:

1. Chapter 2 summarises the relevant literature on the peatland C cycle, C cycle models, especially those which include peatlands and CH_4 dynamics, DA methods, examples of studies using DA to improve C flux estimates, the available, relevant ground-based and satellite observations, and finally a brief review of OSSE studies.

2. Chapter 3 outlines the methods used in the thesis, including a description of the study site, the C flux model and driving data, the DA algorithm, and the OSSE method. Finally the real observations used in the final chapter are described.

3. Chapter 4 briefly reviews the model and the modifications made to it, before detailing the results of a global model sensitivity analysis.

4. Chapters 5 to 7 discuss the results of the OSSE studies using CH_4 flux, NEP and soil moisture observations.

5. Chapters 7 and 8 use the same OSSE framework to examine issues relating to biased observations and unknown model error that may arise when performing the calibration.

6. In Chapter 9 the available ground-based C flux and satellite soil moisture observations are used to constrain the model and provide a prediction of the daily C fluxes and the annual net C balance with uncertainty estimates for the test site in North Wales.

7. Chapter 10 summarises the main findings of the work in this thesis, the contributions to science, and makes suggestions for future work.

Chapter 2

Literature Review

This chapter will review the literature which is relevant to the work in this thesis. Firstly peatland C dynamics are summarised. The importance of understanding and improving estimates of peatland C dynamics was discussed in Chapter 1. Then a brief review of C flux models, and in particular those which contain a representation of peatland C dynamics, is provided. Following this ground-based and satellite approaches to measuring C fluxes and soil moisture are outlined. The theory behind data assimilation and the different data assimilation techniques are then described, together with examples of C cycle model parameter calibration studies. Issues relating to the difficulties of using observations to calibrate a model are briefly discussed at the end of this chapter.

2.1 Carbon flux dynamics

2.1.1 Processes controlling CO_2 assimilation and emission

Photosynthesis and Net Primary Production

CO_2 is assimilated into vegetation via photosynthesis. This is a process where light energy in the visible part of the electromagnetic spectrum (photosynthetically active radiation (PAR)) is used to convert CO_2 into organic carbon compounds in the chloroplasts of green leaves (*Chapin et al.*, 2002). This process is carried out by autotrophic organisms (*Killham*, 1994), via the reaction:

$$CO_2 + H_2O \rightleftharpoons CH_2O + O_2 \tag{2.1}$$

The total amount of CO_2 fixed by the plant in photosynthesis is termed Gross Primary Production (GPP). There are several controls over photosynthesis, namely the availability of the reactants: light energy, water and CO_2 over timescales of seconds to minutes and nitrogen, which is required to produce photosynthetic enzymes such as rubisco, over timescales of days to weeks (*Chapin et al.*, 2002).

The diurnal and seasonal change in light availability, due to the earth's orbital parameters, explain most of the temporal change in C assimilated into the ecosystem (*Chapin et al.*, 2002). The leaf area and leaf angle distribution are major factors controlling the amount of visible light a plant can absorb. Plants have a relatively constant relationship between the amount of absorbed PAR and the net amount of photosynthesis; a relationship is referred to as a plant's light-use efficiency

(LUE). If one of the reactants in the photosynthesis reaction is limited plants will acclimate over long timescales to reduce photosynthetic pigments and enzymes or the amount of light absorbed so the photosynthetic capacity matches the stomatal conductance and the soil resources that can support growth; the "co-limiting principle" (*Chapin et al.*, 2002). For example, plants in dry environments often have lower leaf area to try to reduce the amount of water lost, or they try to minimise the amount of radiation absorbed (to match the reduction in CO_2 availability) by inclining their leaves (*Chapin et al.*, 2002).

Plants uptake CO_2 and transpire water through their stomata. The flux of water and CO_2 is regulated by the opening and closing of the stomata. This flux is called stomatal conductance. If a plant is experiencing water stress it will close its stomata and there will be a resultant decrease in stomatal conductance. This reduces the supply of CO_2 to the plant and therefore its photosynthetic rate. However, the indirect effect of increased soil moisture with decreased stomatal conductance may result in an increase in plant growth (*Chapin et al.*, 2002). CO_2 limitation is more likely to be a result of a change in stomatal conductance than variation in atmospheric CO_2 concentration as the atmosphere is fairly well mixed.

Also important is temperature, which limits the rates of reaction and have an effect on photosynthesis (*Chapin et al.*, 2002). At high temperatures photosynthesis declines due to enzyme inactivation, destruction of photosynthetic pigments and an increase in photorespiration. At lower temperatures enzyme activity is also reduced. Leaf temperature is often different from air temperature due to the cooling effect transpiration has on the plant. The photosynthetic rate is often highest near the temperatures experienced on sunny days, as the plants have adapted to that temperature.

Other environmental factors which affect stomatal conductance and therefore the amount of CO_2 uptake are wind speed and relative humidity. Wind speed influences the temperature gradient and CO_2 and water concentration gradients across the leaf-atmosphere boundary (*Chapin et al.*, 2002). Steeper gradients result in more rapid diffusion across this surface. The concentration gradient of water is similarly affected by relative humidity.

Temperature and water availability effects can also be felt indirectly through the nutrient supply by affecting decomposition rates. The nutrient supply will in turn influence the growth rate of the plant which affects the photosynthetic rate (*Chapin et al.*, 2002). Environmental controls on decomposition will be discussed in the following section.

Respiration

The net accumulation of carbon into the ecosystem is the balance between Gross Primary Production and ecosystem respiration. CO_2 is returned to the atmosphere through plant and soil respiration. Plant respiration involves mitochondrial oxidation of carbohydrates produced during photosynthesis which produce energy for the plant (*Chapin et al.*, 2002). CO_2 is produced in the process and released back into the atmosphere. It is essentially the inverse reaction of photosynthesis. Energy from plant respiration is used for growth, maintenance and ion transport across membranes.

The carbon which has been assimilated by plants and not respired is transferred to the soil organic matter (SOM) pool via several pathways. These are i) via litterfall, the shedding of dead leaves, branches and root detritus during senescence, or plant death, ii) via soluble organic compounds

that are secreted by the roots, and iii) via carbon transfer to microbes which are symbiotically associated with the roots, such as mycorrhyzae, and iv) via the waste products of animals (*Chapin et al.*, 2002; *Killham*, 1994). Plants allocate carbon between the leaves and roots depending on where the limiting resources are (*Chapin et al.*, 2002).
Soil organic matter is aerobically decomposed by heterotrophic organisms in the microbial soil pool. This occurs via the same reaction as that of plant respiration and the CO_2 produced is released back to the atmosphere. Decomposition results in carbon either being released as CO_2, incorporated into the cell walls of the decomposing microbes or entering a stable soil carbon pool where decomposition rates are very low. The stable pool contains carbon that is protected physically (relating the structural characteristics of the soil) or chemically (soil humus) from decomposition(*Killham*, 1994). Over long timescales autotrophic fixation of carbon is balanced by heterotrophic respiration (*Killham*, 1994). Decomposition also results in nutrients being released that can be used for plant growth (*Chapin et al.*, 2002).
Several factors such as temperature, moisture content, pH, Eh (reduction potential) and soil texture influence heterotrophic activity and therefore organic matter decomposition in the soil (*Killham*, 1994). The quality of the litter is also important which is species specific. An increase in temperature results in higher rates of microbial production and therefore influences decomposition directly (*Chapin et al.*, 2002). Colder temperatures may kill the microbes which would result in an increase in available organic matter which might conversely promote decomposition. Temperature also affects the amount of evapotranspiration and therefore the soil moisture content which in turn influences decomposition.

In addition to emission of CO_2 from respiration, CH_4 produced in the saturated zone can be oxidised to CO_2 during diffusion through the unsaturated soil layers. This adds to the net CO_2 flux. This is discussed in more detail in the following sections.

2.1.2 Processes controlling net CH_4 emission

CH_4 production and consumption

CH_4 production and consumption in the soil column are the result of microbial activity. Different populations of bacteria control these two processes. CH_4 production takes place through the activity of methanogenic bacteria which require water-logged, anoxic conditions, whereas CH_4 consumption is the result of CH_4 oxidation by aerobic methanotrophs in the unsaturated (oxic) zone (*Bubier and Moore*, 1994; *Le Mer and Roger*, 2001; *Lai*, 2009). Most methanotrophic activity occurs near the boundary between the anoxic and oxic zones where the ratio of CH_4 to oxygen is highest (*Lai*, 2009).

The water table position determines the anoxic and oxic zones in the soil profile (*Lai*, 2009), and therefore is the main factor controlling the amount of CH_4 production versus consumption. In many studies a negative correlation (or negative logarithmic correlation) has been found between CH_4 flux and water table depth, and with methanotrophic activity and soil water content (*Le Mer and Roger*, 2001). An increase in water table depth can cause a substantial decrease in the CH_4 flux as the zone of CH_4 production is reduced and the zone of oxidation increased (*Lai*, 2009). The water balance in the soil is the product of several variables including precipitation, evapotran-

spiration, run-on and run-off. Environmental variables such as air temperature, solar radiation and precipitation therefore indirectly affect the amount of CH_4 production versus consumption as they control the temperature and moisture profiles within the soil. Temperature and soil moisture in turn are interrelated; soil moisture controls thermal diffusivity in soil (*Bubier and Moore*, 1994), and temperature will affect the amount of evapotranspiration.

Under saturated conditions organic substrate is considered a major limiting factor for CH_4 production (*Segers*, 1998; *Lai*, 2009) as plant root exudates provide substrates for methanogenesis (*Bellisario et al.*, 1999). Litter supply, quality and decomposability are all important (*Valentine et al.*, 1994). Previous work has indicated that methanogenesis is highly correlated with Net Primary Production (NPP) and Net Ecosystem Production (NEP), amount of biomass and plant density (*Valentine et al.* (1994), and references therein; *Bellisario et al.* (1999)), with ^{14}C studies suggesting that most CH_4 is produced from recent organic matter (*Chanton et al.*, 1995). Plant species composition affects the quality and decomposability of the substrate and also influences the physical properties of the peat (*Limpens et al.*, 2008), as different plants produce peat with different structures and hydraulic conductivity.

Soil temperature is an important factor in controlling the rate of microbial activity of the CH_4 producers and consumers (*Bubier and Moore*, 1994; *Bellisario et al.*, 1999). This is particularly the case when organic substrate quality is high (*Valentine et al.*, 1994), although methanotrophs appear to be less sensitive to temperature than methanogens (*Le Mer and Roger*, 2001). Soil temperature will also have an impact on the growth cycle of vascular plants (*MacDonald et al.*, 1998), which in turn affects the amount of available substrate.

CH_4 emission

Transport of CH_4 produced in the anaerobic zone beneath the water table takes place (1) via diffusion through the possibly unsaturated top layer of soil (where it may be oxidised by methanotrophs), (2) through the episodic, rapid release of CH_4 bubbles in solution below the water table (ebullition), and (3) via plant-mediated transport of CH_4 through the aerenchyma (internal gas-space ventilation systems) of vascular plants (*Joabsson et al.*, 1999; *Lai*, 2009). Vascular plants are those which have complex tissue for conducting resources through the plant.

Diffusion is driven by the CH_4 concentration gradient from the anaerobic peat layers to the atmosphere (*Lai*, 2009). Ebullition occurs when the partial pressure of the dissolved gases in solution is greater than the hydrostatic pressure in the peat (*Lai*, 2009). Plant-mediated transport can occur through molecular diffusion and bulk flow (*Joabsson et al.*, 1999) and has been shown to account for a high percentage of the CH_4 flux from vascular plants. *Bellisario et al.* (1999) for example observed higher fluxes at sites where *Carex* spp. (sedges) had not been clipped compared to sites where it had. The method of transport controls how much CH_4 bypasses the zone of oxidation and also the rate at which CH_4 reaches the atmosphere (*Bubier and Moore*, 1994).

In addition to being an important variable in controlling CH_4 production and consumption soil temperature also influences the amount of CH_4 released through ebullition and plant-mediated transport. This is because an increase in temperature would result in increased bubble volume and increased bulk flow due to higher pressure in the soil (*Lai*, 2009).

Soil characteristics also play a role in regulating CH_4 emissions. Soil texture impacts the

transfer of CH_4 gas in the soil column (*Le Mer and Roger*, 2001). The pH of the soil can affect the microbial population; most methanogenic bacteria have their optimum pH at 7 (*Segers*, 1998), though more acidophilic methanogens have been found.

It is not thought that the size of the methanogenic or methanotrophic populations is a major factor regulating CH_4 flux as studies show that they maintain their populations under unfavourable conditions of either drainage/drying-up or flooding respectively (*Le Mer and Roger*, 2001).

In summary, net CH_4 emission from peatlands is a function of the competing processes of production, consumption and the various transport mechanisms (*Limpens et al.*, 2008). Variations in CH_4 emissions are related to temporal and spatial changes in climate and the resultant phenology of the vegetation (*Le Mer and Roger*, 2001), plant species distributions and soil characteristics.

2.2 Carbon flux modelling in peatlands

2.2.1 General overview of Carbon flux and land surface models

As discussed in Chapter 1, models are useful in combining the current theoretical understanding of the physical, chemical and biological processes of a system together, in order to better understand how they interact, and for obtaining estimates of model state variables over wide regions. C flux models range in complexity, mostly in the way the C is assimilated into the system. *Cramer et al.* (1999) published a review of the global NPP models. They split the models up into three categories. The first include those that simulate the phenology of the system using a satellite-derived normalised difference vegetation index (NDVI). The models calculate the amount of C assimilated into the system based on empirical relationships between the NDVI and the fraction of absorbed photosynthetically active radiation (fAPAR). The fAPAR is transformed into the GPP or NPP based on a light use efficiency parameter. This type of model is known as a Production Efficiency Model (PEM). *McCallum et al.* (2010) provide a comprehensive review of the different formulations based on this concept.

The second group of models identified by *Cramer et al.* (1999) use a vegetation map to initialise structural (i.e. leaf area index (LAI)) and functional parameters. The assimilation of C into the canopy is driven by climate, soil variables and phenology-related parameters. This provides a measure of the amount of C into the system, which is used to "grow" leaf biomass, but a structurally explicit canopy is not modelled. Processes working on a leaf-scale are scaled up to the canopy using a measure of LAI. These models are referred to as biogeochemical models.

The third group specified in *Cramer et al.* (1999) are the dynamic vegetation models (DVMs) which use rules of process optimisation and competition to model the growth of specific vegetation types. Hence no predefined vegetation maps are needed. Instead plant functional type (PFT) parameters are required to establish the vegetation types. This modelling approach results in an explicitly modelled vegetation structure, as well as function (i.e. C flux). Such models include the Lund Potsdam Jena (LPJ) model (*Sitch et al.*, 2003), ORCHIDEE (*Krinner et al.*, 2005), Sheffield DVM (*Woodward et al.*, 1995) and TRIFFID (*Cox*, 2001). These models are generally the ones coupled to the larger global climate models (GCMs) as they have the functionality to re-distribute the vegetation under changing atmospheric CO_2 concentrations and climate.

The models are also linked to soil C models, which calculate the transfer of C between the

different litter and soil pools, based on differing rates of decomposition and microbial efficiency. The soil C model most used in larger models of the C cycle or land surface is based on the the CENTURY model (*Parton et al.*, 1987).

These models are also coupled to energy balance and hydrology models and together they form "land surface models". All three cycles (energy, water and C) are linked via canopy conductance, which is coupled to photosynthesis through the opening of the stomata, and via the available plant and soil moisture which in part controls photosynthesis. It therefore makes sense to combine them in order to achieve a proper representation of the land surface fluxes (*Sellers et al.*, 1997). A review of the evolution of energy balance and hydrology model formulation through to land surface models is provided in *Pitman* (2003).

Using EO data to drive the model limits it's predictive capability. However models which predict the amount of vegetation often suffer from being complex and requiring many parameters. Such models require several assumptions or are limited by the vegetation types they include in the model. Therefore in terms of understanding other model processes, such as the effect of the hydrology on carbon fluxes, it is useful to have a relatively simple measure of vegetation amount that gives a realistic measure of carbon input to the system.

2.2.2 Peatland C flux models

Several different ecosystem models have been developed or adapted to model CH_4 dynamics from peatlands and wetlands. *Cao et al.* (1996) developed the Wetland Methane Emission Model (WMEM) which models the amount of CH_4 production simply as a function of scalars on the C decomposition, which are dependent upon water table and temperature. Methane oxidation is a fraction of the production, based on a measure of physiological activity. The Terrestrial Ecosystem Model (TEM) (*Raich et al.*, 1991) was used to calculate C inputs to the system (NPP, litter C deposition and organic C deposition), with the vegetation type specified. The water table is calculated using a simple 1D bucket model. A fraction of precipitation is intercepted and evaporated before entering the soil. The model requires monthly air temperature, precipitation radiation and PAR.

Potter (1997) modified the existing Carnegie-Ames-Stanford-Approach (CASA) model (*Potter et al.*, 1993) to account for CH_4 dynamics (hereafter referred to as the CASA-CH_4 model). The CASA model is essentially a PEM coupled to a simplified version of the CENTURY model for soil C and N dynamics. *Potter* (1997) increased the complexity of the soil hydrology and temperature submodules by adding extra layers, in order to calculate more localised values of soil moisture within the profile, and by modelling the diffusion of heat in the soil to better account for changes in temperature down the profile. These factors were then used to modify the decomposition of C in the soil. The C produced during decomposition was partitioned into CO_2 and CH_4 flux through an empirical relationship which gave the ratio of CH_4:CO_2 as a function of the water table depth. The CH_4 produced exits the soil via the three main pathways known to affect CH_4 emissions: diffusion through the soil, and possible oxidation to CO_2, plant-mediated transport (i.e. the rapid release of CH_4 via aerenchymous tissues in vascular plants), and ebullition. The model requires daily climate drivers (air temperature, solar radiation and precipitation), daily satellite-derived NDVI timeseries, and a vegetation map. The CASA-CH_4 model is the one used in this thesis. The reason for this choice and a more detailed descriptions of the workings in the model

are described in Chapter 3.

The model developed by *Walter and Heimann* (2000) was again designed to simply model the amount of CH_4 production below the water table as a function of NPP, which was used as a measure of substrate availability, and soil temperature. The water table depth, soil temperature and NPP were inputs to the model, with NPP being modelled by the larger ecosystem model BETHY (Biosphere-Energy-Transfer-Hydrology) (*Knorr*, 2000). The water table and soil temperature were not taken from BETHY however, but were either driven with site-based data or using data from the European Centre for Medium Range Weather Forecasting (ECMWF). The three CH_4 emission pathways were represented, with more physically based descriptions of the physics than in *Potter* (1997) who tended to use semi-empirical functions. The PEATLAND model (*van Huissteden et al.*, 2006), later PEATLAND-VU model (*Petrescu et al.*, 2008) also used a version of the Walter-Heimann model.

Segers and Leffelaar (2001) published results of a more complex model formulation which models the species (i.e. CO_2, CH_4, electron acceptors, oxygen, nitrogen) as a function of physically based transport processes and kinetics with depth. They modelled the gas concentrations in the profile as a function of the diffusion and aqueous convection of gases in the saturated and unsaturated zone, and the gas exchange at roots and by diffusion in gaseous pores. The diffusion of water and temperature were also physically modelled using the 1D Richards' equation and a simple diffusion equation respectively. Model inputs included climate and biomass data.

The Peatland Carbon Simulator (PCARS) model (*Frolking et al.*, 2002) is a different class of model. It used the Peat Decomposition Model (PDM) (*Frolking et al.*, 2001), which builds the peat up as a series of layers ("cohorts") of partially decomposed litter. Thus the peat "accumulates" over many thousands of years of model spin-up.. The amount of C assimilated into the system was based on a simple light use efficiency model with the Beer-Lambert law used to attenuate PAR through a vertically stratified canopy. Respiration, phenology and C allocation were modelled in a very similar way to other biogeochemical models. CO_2 and CH_4 were produced in equal amounts under anoxic conditions and all the CH_4 goes into a single dissolved pool equal to the volume of water in the pore spaces. This can be released via ebullition, plant-mediated transport or diffusion and possible oxidation. Methane oxidation was modelled as a simple function of water table depth and a simple population distribution of methane oxidisers. The PCARS model required air and soil temperature, radiation, water table depth and runoff as drivers. Many other site-specific parameters were also required to initialise the PDM model. The recently published McGill Wetland Model (MWM) (*St-Hilaire et al.*, 2010) used PCARS as its methane module but the multi-layered PDM model was replaced by a two layer model divided by the depth of water table.

Heinemeyer et al. (2010) have also recently published a peat cohort model called MILLENNIA. They argued that such a model is needed for peatlands as the CENTURY-type models were based on concepts relating to mineral soils, where microbial processes thoroughly mix the layers. This results in a higher soil bulk density compared to peat. The bulk density in turn affects the hydrology through its impact on the soil water retention. They noted that DVMs have not been able to produce the C stocks or peat depths measured in various peat regions and they suggested that as a result predictions of CO_2 and CH_4 will be inaccurate. It remains to be seen whether such specific peatland processes will be incorporated into larger land surface models, but given this

would require two different soil modules this is unlikely

Kettunen (2003) produced a similarly complex model to *Segers and Leffelaar* (2001) based on modelling the populations of the methanotrophic and methanogenic bacteria as state variables together with the CH_4, substrate and O_2. The model was a 1D partial-differential model which modelled the state variables with depth. The methane production by bacteria is dependent upon the available substrates from vascular plants, which is in turn dependent upon the GPP (modelled as a function of PAR and temp) and the oxygen concentration. Plant mediated transport of the CH_4 produced was considered. The model used daily PAR, the soil temperature profile and water table depth as drivers.

The methane dynamics model as summarised in *Zhuang et al.* (2004) is similar to the others in that it had CH_4 production occurring below the water table and CH_4 oxidation occurring above it. CH_4 production is a function of the ecosystem-specific maximum production rate, which was scaled by the availability of the substrate (as a function of NPP), temperature, pH and electron acceptor availability. CH_4 oxidation is also decreased from its maximum potential values by temperature, moisture and redox potential. Transport of CH_4 to the atmosphere can occur via the three pathways discussed above. The model is coupled to the Terrestrial Ecosystem Model, which provides C, vegetation and soil temperature inputs, whilst a separate hydrology module provides the hydrological inputs of soil moisture and water table depth. These two models require normal climate and vegetation drivers.

More recently peatland CH_4 dynamics have been incorporated into the larger DVMs. The first to do this were *Wania et al.* (2009a,b) with the LPJ model. They added two extra PFTs which were specifically able to deal with water-logged conditions, and added a methane emission model to produce the LPJ Wetland Hydrology and Methane Emission model (LPJ-WhyMe). CH_4 production is dependent upon the available substrates and upon the level of soil saturation, rather than the water table depth, as they recognise that some CH_4 can also be produced in the near-saturated soil above the water table. The peatland hydrology and methane emission is only "switched on" with organic soil types.

Most of these studies model CH_4 production in a similar way, but there is a varying amount of complexity as a result of the number of parameters and whether the model formulations are semi-empirically or physically based. Many need water table depth as a driver, which can be provided from site-based meteorological data or from a larger land surface model. Either way this adds a logistical problem when modelling a small site where ground-based monitoring stations have not already been set-up, calibrated and validated for a certain time period.

2.3 C flux observations

2.3.1 Ground-based C flux measurements

Two different systems are used to make C flux (and other trace gas) measurements on the ground: i) chamber measurements, ii) flux towers, which use the 'eddy covariance' technique. The first are limited to the plot scale (tens of centimetres), and the second measures the fluxes over an ecosystem scale (area - km^2 to tens of km^2).

Chamber methods

Closed-chamber measurements are often used to measure the net flux of trace gases between the atmosphere and soil/vegetation of bogs, peatland and wetland (and other) ecosystems (e.g. *MacDonald et al.* (1998); *McNamara et al.* (2008); *Schrier-Uijl et al.* (2008); *Dinsmore et al.* (2009); *Moore et al.* (2011)). A chamber, of known dimensions, is sealed over the surface of the soil and vegetation for a certain period of time, ranging from a few minutes to around an hour and a half (depending on the background concentration of the gas being measured), during which the concentration of the gas is recorded. Opaque chambers measure soil and root respiration as well as other gas fluxes (like CH_4), and transparent chambers measure the NEE or net CO_2 exchange, including the uptake of CO_2 via photosynthesis.

Two different systems are used to measure gases concentrations in the chamber; 'dynamic' and 'static' chambers. In the dynamic system an instrument, usually an infrared gas analyser (IRGA), is used to continuously measure the change in gas concentration in the chamber. It is connected to the chamber by a pipe and a flow of air circulates the air from the chamber to the IRGA. In a static system samples of gas are taken from the chamber at regular intervals whilst the chamber is sealed over the surface. These are typically taken using syringes inserted into a small plastic tube connected to the chamber which is also sealed. The samples are then stored in pre-evacuated exetainers and later analysed, often using a gas chromatograph, for the concentration of gases. In both systems a change in concentration of the gas in the chamber headspace with time is then converted into a flux, often using a simple linear regression (though some studies, discussed later, have shown this can lead to inaccurate results). Most studies only accept the calculated flux value if the R^2 value for the linear regression is greater than a certain value (usually 0.9).

More sophisticated designs have climate-control systems that circulate air through cooling systems to keep the temperature to within 1^oC of the outside temperature and on very hot days ice water is circulated through a heat exchanger attached to the chamber walls (e.g. *Burrows et al.* (2005)). The relative humidity is also kept constant level to prevent condensation. Many systems have a fan inside to keep the air well-mixed. Several known sources of error are discussed in a variety of studies (e.g. *Norman et al.* (1997); *Davidson et al.* (2002); *Myklebust et al.* (2008); *Forbich et al.* (2010)). These include i) leaks of the gas due to incomplete sealing of the chamber, ii) pressure differences between the inside of the chamber and the outside caused by in air flow restrictions in dynamic chambers, iii) changes in concentration gradient of the gas in the chamber headspace as a result of the chambers being sealed over the surface for a long time, resulting in an underestimate of the flux, iv) changes in flux during the initial deployment of the chamber, causing changes in pressure, concentration gradient and turbulent flow, v) changes in CO_2 flux from roots cut when collars, used to connect the chamber to the soil, are inserted too far into the soil.

Whilst possible sources of systematic error in chamber measurements are known, these are rarely cited in studies reporting C flux budgets from a variety of ecosystems, including peatlands. *Savage et al.* (2008) suggest that whilst a few studies have compared chamber designs and anaylsed the possible resultant biases, a protocol for evaluating the data uncertainties has not been developed for chamber measurements, partly because datasets generally contain relatively few data. They argue this is needed, especially with the introduction of automated chamber measurements which gather large quantities of data, and with the increasing use of C flux measurements in model-data

fusion studies.

Savage et al. (2008) propose that sampling uncertainty is a source of systematic error, i.e. the error resulting from sampling limited locations in a heterogeneous landscape results might result in biased flux values. As for many other studies they estimate the sampling uncertainty as the standard error of the mean of replicates of chamber measurements taken at different locations. They suggest the random error of the measurement comes from instrument glitches and other stochastic events and following *Hollinger and Richardson* (2005) use a paired flux measurements taken at the same location but 24 hours apart (except for when there's been precipitation in between) to assess the magnitude of the error. They found the errors do not have a constant variance but increase with the magnitude of flux, as did the sampling uncertainties. The resultant PDF of the errors approximated a Laplacian function (also called a double-exponential, i.e. two exponential functions back-to-back), rather than a Gaussian. They find the magnitude of the random error is similar to that of the sampling uncertainty for individual flux measurements (*Hollinger and Richardson*, 2005).

The proposed scheme for assessing the random error in the measurement is potentially flawed as the fluxes are known to vary from day to day dependent upon the environmental conditions, especially in a location with rapidly changing weather, although *Hollinger and Richardson* (2005) specify limits of changing environmental conditions above which the method cannot be used. Even if it does provide a good estimate of the random measurement error it has not been used to provide error estimates in most chamber flux studies, with authors suggesting the standard error of replicate measurements provides a good estimate of both the measurement and sampling uncertainty.

Whilst the study by *Hollinger and Richardson* (2005) goes further than any previous studies in formulating a scheme for characterising the error in chamber C flux measurements it does not consider the systematic errors in the actual measurement of the flux, as discussed above, and in the assumptions used in the analysis of the data. The systematic error is solely attributed to sampling uncertainties, rather than, for example, having a chamber sealed over the surface for too long, which has been reported to result in changes in concentration gradient that might result in a biased (underestimated) flux estimate, or incorrect assumptions made in the data analysis. Most studies try to account for potential biases in the observations by modifying the chamber design or the method of analysis used. *Davidson et al.* (2002) suggest that CO_2 fluxes are underestimated by <15% and can be corrected for with curve-fitting and/or having a sealed chamber for a short period of time. *Kutzbach et al.* (2007) suggest using an exponential regression model instead of a linear regression between the concentration of the gas and the time of measurement, to account for the changes in concentration gradient discussed above. They found the underestimate of the flux using a linear regression model could be as high as 40%, depending on the vegetation type, soil conditions and the CO_2 flux strength. *Forbich et al.* (2010) also tested linear and exponential regression functions on CH_4 data. They found most measurements showed linear increases in CH_4 with time and thought non-linear changes occurred during periods of changing water table (ebullition flux perhaps). They argue that without further knowledge of CH_4 concentration profiles in the soil they could not determine if the non-linear changes in concentration were natural or an artifact of the measurement. They state that flux estimates from the exponential function at the beginning of the measurement time period can be significantly higher than the linear regression

function for those data that might contain non-linear changes in concentration, but as the source of the non-linearity is unclear they suggest using both the initial and final slope of the exponential function as the measure of uncertainty in the flux estimate.

Clearly no scheme of data analysis has yet been universally adopted as studies are reporting different findings on the nature of the increase in gas concentration in the chamber headspace. The ability to detect an exponential increase in concentration will also depend on the sampling interval of the concentration measurements (*Forbich et al.*, 2010). Few studies include a measure of the random measurement error and systematic biases. Repeat measurements in space and time with the same instrument/experiment design cannot assess systematic biases in the actual measurement, only independent methods of measuring fluxes can do that. Some studies, discussed later, have compared chamber measurements with eddy covariance (flux tower) measurements and even with aircraft data. These have the potential of assessing biases in the measurement techniques.

No study so far has also included the effects of gap-filling and scaling of errors temporally or spatially. More work is to be done if all sources of measurement error, sampling uncertainty and uncertainty relating to data analysis are to be compounded into one estimate of uncertainty of a flux, which is crucial for model-data fusion studies. Error characterisation is an issue for most observations, but more and more studies that are attempting to address these issues are now appearing in the literature (e.g. *Hollinger and Richardson* (2005); *Savage et al.* (2008).

Eddy covariance techniques

Eddy covariance is a technique that is used to measure the net flux of trace gases across the atmosphere - soil/vegetation surface. It is based on the principle of conservation of mass, that states that the rate of change of the mixing ratio (concentration - i.e. $\rho_{tracegas}$ / ρ_{air}) of a trace gas is balanced by the mean horizontal and vertical advection, by the flux divergence/convergence in three dimensions and by the strength of the source/sink across the atmosphere - soil/vegetation surface (*Baldocchi et al.*, 1988; *Baldocchi*, 2003). It is assumed that the rate of change of the mixing ratio is zero and that the underlying surface is homogenous and on flat terrain, therefore the advection term is zero as are the horizontal components of the flux divergence (*Baldocchi*, 2003). Hence the equation reduces to the balance between the vertical flux divergence and the source/sink strength. The instantaneous mass flux density is a product of the wind speed and the density of the trace gas. The eddy covariance technique aims to estimate the mean vertical flux density by a statistical analysis of the covariance between the wind speed and the change in the mixing ratio of the trace gas over a certain time span. (*Baldocchi*, 2003). It therefore samples the turbulent movement of upward and downward flowing air parcels (eddies) that contain the trace gases. Sonic anenometers are often used to measure the vertical wind speed and direction and infrared gas analysers are used to measure the trace gas flux concentration.

Random errors in eddy covariance systems result from the different instruments used to measure the flux (infrared gas analyser, sonic anenometer etc), errors associated with the turbulent transport and errors relating to the heterogeneity of the flux tower footprint (*Hollinger and Richardson*, 2005; *Richardson et al.*, 2006). Several recent studies have tried to characterise the random measurement error of eddy flux measurements through statistical analyses; systematic errors need to be identified via a different method (*Hollinger and Richardson*, 2005). The studies use

the standard deviation of pairs of independent flux measurements made repeatedly under identical conditions to calculate random error. This can be achieved by analysing data from two flux towers located close together (*Hollinger and Richardson*, 2005), or by analysing measurements taken 24 hours apart at the same flux tower (*Hollinger and Richardson*, 2005; *Richardson et al.*, 2006). However one tower approach is unlikely to represent full spatial uncertainty in an ecosystem, resulting in an underestimate of the uncertainty. In addition if the environmental conditions between the days are not perfect this could result in an overestimation of the uncertainty (*Richardson et al.*, 2008).

All the studies find that the flux errors are represented Laplacian (double-exponential) PDFs, rather than Gaussian distributions. The data are heteroscedastic (i.e. have differing variance) with the variance increasing with the magnitude of flux (*Richardson et al.*, 2006). Random errors are roughly three times higher for peak fluxes in the summer growing season. This is compounded by the fact that low flux magnitudes are more common than high flux. The other factor contributing to the shape of the PDF is the fact that eddy flux data often contain extreme outliers due to problems with the measurement systems including power fluctuations and insects in the sonic anenometers (*Hollinger and Richardson*, 2005). *Richardson et al.* (2006) report that the random error decreases with increasing wind speed and when a closed-path , rather than an open-path, gas analyser is used. The one tower approach is even less likely than the two-tower approach to represent full spatial uncertainty in an ecosystem, which would result in an underestimate of the uncertainty. If the environmental conditions between the measurement periods are not perfect however this could result in an overestimation of the uncertainty (*Richardson et al.*, 2008). If the assumptions of horizontal and homogenous terrain are not met inaccuracies can be introduced into the flux measurements as a result of the other terms in the conservation of mass equation being ignored. *Baldocchi* (2003) discuss these sources of error in more detail and the methods that have been derived to solve the problems. Changing footprints, as discussed, are also a cause of uncertainty due to changing wind direction (*Oren et al.*, 2006; *Papale et al.*, 2006). *Oren et al.* (2006) compared the difference in the standard deviations from six flux tower eddy covariance measurements arising from gap-filling methods, instrument errors and spatial variability. They found gap-filling tends to contribute the most to the overall uncertainty (range from 47 to 93% for 7 years), followed by the spatial variability (6 to 49%) and then the instrument error (1 to 6%). The spatial variability can clearly be quite high even over a uniform vegetation type (*Oren et al.*, 2006). *Oren et al.* (2006) also found that increasing averaging time resulted in lower errors from spatial variability; at an averaging time of 30 minutes, half the observed variability was due to spatial variability. This is obviously affected by the distance between flux towers compared to the spatial heterogeneity of the scene and needs to be considered if using eddy covariance data that is an average of several towers.

Systematic errors are more difficult to quantify and tend to affect the flux on varying timescales (*Richardson et al.*, 2008). If the assumptions of horizontal and homogenous terrain are not met inaccuracies can be introduced into the flux measurements as a result of the other terms in the conservation of mass equation being ignored. *Baldocchi* (2003) discuss these sources of error in more detail and the methods that have been derived to solve the problems. There are time periods when the turbulent flux crossing the location of the sensors is not high enough to be able to use to calculate the source/sink strength. This can occur during the night when thermal

stratification of the atmosphere prevents vertical flow of the air, resulting in an underestimate of the nighttime trace gas flux (*Baldocchi*, 2003). As the sun heats the air in the morning a more vigorous mixing of the previously stratified layers results in an overestimate of the trace gas flux due to the sudden release of high concentrations of trace gas stored in the canopy air below the instruments (*Baldocchi*, 2003; *Papale et al.*, 2006). Techniques have been adopted to correct for these conditions. A correction can be made for canopy trace gas storage, but this requires trace gas concentration profiles through the canopy, which are not always available (*Papale et al.*, 2006). The "u^*" (friction velocity) correction is used to discriminate between periods of poorly mixed and well mixed air. When the air is not well mixed the data is replaced by the expected flux given the climate and time of day from well-mixed periods. This is based on an assumption of equivalent fluxes which is not proven (*Papale et al.*, 2006). These corrections do add uncertainty to the data, but eliminate outliers and biases.

The errors in eddy covariance C flux measurements are dependent upon the meteorological conditions, the land surface type, whether good corrections have been made. The characterisation of those errors relies upon independent measurements. *Richardson et al.* (2006) argue fairly that quantification of the random error in the flux measurements is a prerequisite to model-data synthesis but systematic measurement errors need to be accounted for. Whilst several studies, some of which are summarised here, have examined the systematic errors, to date no formalised method for accounting for all these errors has been put forward. Indeed *Richardson et al.* (2008) conclude that a logical further step would be to reconcile random and systematic errors under a common framework so an estimate of the total uncertainty is achievable. They also suggest that differing time scales of error should be investigated and distinguished as well as the differences between random and systematic errors.

Comparison of ground-based techniques

The eddy covariance technique provide observations at an ecosystem scale which is intermediate between very small scale chamber measurements and observations provided by aircrafts or even satellites (*Myklebust et al.*, 2008). They are near-continuous and therefore can be scaled up to any time period of interest for comparison with C flux models. *Savage et al.* (2008) report that eddy covariance errors are larger on the whole than chamber measurements, both in relative and absolute terms. Flux towers are also expensive and difficult to set-up and maintain. Chambers on the other hand are low-cost and portable, therefore they can be set up anywhere in the landscape. This enables a better exploration of the effect of spatial heterogeneity on the C fluxes. Clearly much work to be done in characterising the uncertainties associated with both sets of observations, and in developing a framework which can provide full uncertainty estimates with the observations. They don't provide an estimate of the fluxes over a wide area however, which therefore results in a large discrepancy in the spatial scale between the observations and the models.

2.3.2 Satellite C flux measurements

The "top-down" approach to calculating surface C flux involves measurement of the spatial and temporal concentration of the trace gases in the atmosphere, either from a ground-based station or

a satellite. Following this an atmospheric chemistry - transport inversion model is used to calculate the magnitude and spatial distribution of the net surface flux (*Hungershoefer et al.*, 2010). The measurement of trace gas concentration is based upon the absorption of different wavelengths of the electromagnetic spectrum by different trace gases. Two different wavelengths are used, <3μm (solar spectroscopy), and the thermal infrared region (>4μm) (thermal infrared sounding) (*Breon and Ciais*, 2010). The atmospheric transmission of light is also dependent upon temperature and pressure. The TIROS Operational Vertical Sounder (TOVS) instrument onboard the NOAA meteorological satellites, the Atmospheric Infrared Sounder (AIRS) onboard NASA's Aqua satellite and Infrared Atmospheric Sounding Interferometer (IASI) onboard ESA's MetOp satellite were originally designed to estimate the atmospheric temperature profile, assuming a known concentration of trace gases. More recently they have been used to estimate CO_2 concentrations by assuming a known temperature profile. *Breon and Ciais* (2010) give a detailed review of these studies but in general the results are not promising. This is partly because the sensitivity to CO_2 concentration is smaller than to temperature. In addition the measurements are sensitive to the upper troposphere whereas a sensitivity to the lower troposphere is needed for deriving surface flux measurements.

Solar spectroscopy provides another option for measuring trace gas concentrations as it is sensitive to gas concentrations in the lower troposphere. The radiance received at the satellite is from reflected sunlight, either from the surface or atmospheric constituents. Again there are narrow wavelength bands in which certain trace gases absorb the reflected radiation. The width of the absorbing band is proportional to the amount of trace gas present (*Breon and Ciais*, 2010). The method requires a high sun angle to limit scattering in the atmosphere, and as with all optical reflectance measurements, no clouds. This results in fewer observations in cloud free areas and also limits the time that the measurements can be taken (*Breon and Ciais*, 2010).

At present there are two satellites with spectrometers that use this technique to measure trace gas concentrations in the atmosphere: the Scanning Imaging Absorption Spectrometer for Atmospheric Chartography (SCIAMACHY) onboard the European ENVISAT satellite (launched in 2002) and a spectrometer on board JAXA's Global Greenhouse Gas Observation by Satellite (GOSAT - launched in 2009).

Most studies use algorithms based on Differential Optical Absorption Spectroscopy (DOAS), which compares the measured absorption lines with reference spectra which have passed through little/none of the trace gas(es) in question, to calculate vertical column densities. The Weighting Function Modified-DOAS (WFM-DOAS) algorithm fits reference spectra, based on different climatological regimes, to the observations using a least squares regression (e.g. *Buchwitz et al.* (2000). The fit parameters are weighting functions for each vertical profile of trace gas and temperature. They represent the change in radiance as a function of change in the concentrations of the respective variable (*Barkley et al.*, 2006b). Error estimates are provided from the covariance matrix. In the original version a look up table (LUT) of reference spectra was used. In a later paper *Barkley et al.* (2006a), the algorithm was improved by using a reference spectrum that is calculated for each observation based on known properties of the surface and atmosphere at the time of the measurement. This is termed the Full Spectral Initiation WFM-DOAS. A radiative transfer algorithm is used to create the reference spectra, and is dependent upon inputs such as surface albedo, temperature, pressure and water vapour profiles, aerosol concentration and a prior

trace gas vertical profiles. *Frankenberg et al.* (2006) use a different algorithm called the Iterative Maximum A Posteriori - DOAS (IMAP-DOAS) which iterates over the possible vertical column densities (VCDs) from a model representation until the modelled total optical density fits the measurement. The VCD is then normalised to produce vertical mixing ratio. To do this the total atmospheric column which has been measured, which depends on the atmospheric pressure and light path (*Frankenberg et al.*, 2006).

As well as instrument noise the sensitivity of the retrieved total column mixing ratios depends upon the possible systematic and random errors in the retrieval algorithm which include errors in the temperature, pressure and water vapour profiles (*Buchwitz et al.*, 2005; *Frankenberg et al.*, 2005), interferences between different absorbers (*Frankenberg et al.*, 2005), aerosols, surface albedo and inaccuracies in the cloud detection algorithms (*Buchwitz et al.*, 2005). The errors in the retrieval algorithms have been characterised using simulated reference spectra.

The trace gas VCDs or mixing ratios are often validated using aircraft or balloon data (*Bergamaschi et al.*, 2009), ground-based spectrometer measurements or a global chemistry-transport model (*Barkley et al.*, 2006b; *Frankenberg et al.*, 2011). *Barkley et al.* (2006b) report accuracies of ~1% and a bias of <4% for CO_2 concentrations from SCIAMACHY. *Frankenberg et al.* (2011) show that accuracies can be as high as 0.3% when comparing SCIAMACHY CH_4 concentrations to ground-based data over the Sahara where "ideal comparison conditions are met". Elsewhere they report accuracies mostly <1% but in the tropics they find negative anomalies which may be due to pixel degradation and in SE Asia they find positive anomaly between August and November which does correspond to chemistry-transport models but the origin is as yet unknown. This could be due to inaccuracies in the retrieval algorithm, though this is unlikely as it corresponds well to atmospheric chemistry-transport models, or it could be due to incomplete knowledge of the CH_4 cycle. A pronounced period of an increase in CH_4 is seen in the model and observations from the beginning of 2007 for each of the areas focused on in *Frankenberg et al.* (2011): Australia, Africa, South America and SE Asia. Two problems with using SCIAMACHY data are the low spatial resolution (typically 30 x 60km), which means that completely cloud-free pixels are unlikely to be achievable, and the spectral resolution, which is not fine enough to resolve individual absorption lines (*Breon and Ciais*, 2010). Several groups are currently working on CO_2 and CH_4 concentrations from GOSAT, though no validated results from the post-calibration period have yet been published.

As stated above, surface C flux estimates are derived from the satellite total column C concentrations using a Bayesian inversion approach. This essentially "updates" the prior knowledge of the surface fluxes, which can be from inventory data or model estimates or both, with the use of an atmospheric chemistry-transport model. *Meirink et al.* (2008) find that CH_4 observations from SCIAMACHY result in error reductions in the annual CH_4 emissions estimates of up to 60-80% compared to the prior uncertainty estimates. *Bergamaschi et al.* (2009) report that CH_4 emission patterns at small scales are greatly constrained by the concentration measurements but that the fluxes are show a high sensitivity to the a prior emission inventories. They found significantly different spatial patterns compared to bottom-up inventories, which they suggest is due either to inaccuracies in the bottom-up inventories, such as the magnitude of the wetland emissions, or unidentified sources. They note that independent validation of C fluxes over large regions is dif-

ficult but that further validation needs to take place. *Bergamaschi et al.* (2010) go on to compare CH_4 emissions over NW Europe ground-based stations which measure the concentration of trace gases in air (flask) samples taken at regular intervals over the day. They also find that the observations constrain the prior flux estimates and region emission patterns that correspond to those of the bottom-up inventory and United Nations Framework on Climate Change (UNFCCC) values. The inversion results overestimate both of the other datasets by 21 and 40% respectively. As they report the uncertainties on the observations are not well-characterised due to the difficulties in doing so, but given their assumption of 30% uncertainty, the three datasets are consistent with each other.

Several synthetic studies have been carried out to investigate the relative magnitude of possible error sources on the C flux inversions from SCIAMACHY (*Meirink et al.*, 2006; *Hungershoefer et al.*, 2010), GOSAT (*Chevallier et al.*, 2009; *Hungershoefer et al.*, 2010) and NASA's Orbiting Carbon Observatory (OCO), which was destroyed during launch in 2009 (*Chevallier et al.*, 2007; *Feng et al.*, 2009; *Baker et al.*, 2010; *Hungershoefer et al.*, 2010). *Meirink et al.* (2006) suggest that if the accuracy of CH_4 concentrations is less than the estimate precision of 1.5 - 2% will contribute greatly to the reduction in error of CH_4 flux estimates. If systematic biases are lower than % good retrieval will also be necessary, but identification and elimination of systematic biases must be a priority. They suggest that pixels partially covered by clouds must be taken into account in order to get enough data for the inversions, but that ultimately the presence of clouds might result in higher uncertainties than measurement error. *Chevallier et al.* (2009) report error reductions in the yearly CO_2 flux estimates of 50-80% for sub-continental regions using GOSAT data and *Chevallier et al.* (2007) suggest error reductions of up to ~40-50% over vegetated areas for the 8-day and monthly means with a model grid cell resolution of 3.75^o x 2.5^o for OCO data.

Hungershoefer et al. (2010) performed an extensive synthetic study to test the reduction in uncertainty between prior and posterior CO_2 flux estimates from existing and hypothetical surface networks, all three satellites mentioned above, from a potential active lidar system, which also would measure the absorption spectra and from various combinations of the above observing systems. They use observation uncertainty estimates from theoretical studies done by the retrieval algorithm teams of the respective satellites. They provide therefore a useful summary of the contribution of different variables to the different instruments' retrieval algorithms. For example for OCO simple radiative transfer simulations show that viewing geometry, aerosol amount and characterisation of the surface reflectance cause variation in the magnitude of error. The same issues apply to SCIAMACHY but the observations have a larger random error due to the lower signal-to-noise ratio and the lower spectral resolution (*Hungershoefer et al.*, 2010). Of course ground-based concentration measurements are more precise but may not be as representative of the model grid cell. *Hungershoefer et al.* (2010) provide results of weekly averaged and annual posterior uncertainties as well as the % reduction in uncertainty. All systems provide useful information on constraining the surface CO_2 fluxes. Weekly flux posterior uncertainties range from 0.51 to $2.12 gCm^{-2}d^{-1}$ for one single region (France) using each individual satellite data. The active lidar system achieves the best results and the AIRS instrument the worst. This amounts to reduction in uncertainty of ~20 to 80%. The posterior uncertainty is improved if the existing networks are included in the retrieval, and if the estimates are produced for a larger area. For example over

Europe the range in posterior uncertainty decreases to 0.06 to 0.28gCm^{-2}d^{-1} using the individual satellites.

This is an extremely comprehensive OSSE. However the errors in the transport model are not included. *Meirink et al.* (2006) argue that transport errors are not as important as they will not affect the total column concentrations measured by the satellite and are lower resolution than the satellite data themselves. A simulation study by *Houweling et al.* (2010) suggests that inaccuracies in the transport models will lead to limitations on the possible error reduction in the flux measurements.

Whilst useful, the OSSE studies do not provide a full error characterisation as would independent validation. As is the case with other EO data, validation exercises, the results tend to show that observation uncertainties are larger than the theoretical estimates from retrieval algorithm simulations due to unaccounted for processes or effects. *Houweling et al.* (2010) point out that while useful, it is difficult to account for correlated uncertainties and biases in OSSE studies. Clearly further validation is required before the nature of the random and systematic uncertainties is fully understood. Validation of bottom-up inventories are also needed (*Bergamaschi et al.*, 2010).

Several websites routinely provide C flux inversions using satellite concentration observations. For Europe these include the CarbonTracker Europe project (http://www.carbontracker.eu/index.html) which would provide 1 x 1 degree fluxes at a three-hourly resolution, and CarboScope (http://www.carboscope.eu/), which provides the results of different inversion algorithms from different research groups (and different version) for CO_2 and CH_4 flux monthly and yearly timeseries at the scale of continents, hemispheres or the entire globe.

Meirink et al. (2006) recommend that C flux observations could be improved with finer spectral resolution, a smaller pixel size, in order to retrieve more cloud-free pixels, and better characterisation of aerosols and clouds. The OCO satellite had the possibility of aiming at specific targets. If another OCO satellite is launched this will mean that the instrument could regularly point at specific location for calibration purposes and more extensive validation exercises could be carried out (*Breon and Ciais*, 2010). It does not appear to be the case, from this literature review, that satellite C flux data are compared to eddy covariance tower measurements of C fluxes. It is possible these data would be useful in validation studies, even though their footprint would not be as large as the size of the satellite pixel. Full uncertainty analysis, including all possible sources of random and systematic errors, and validation studies, are needed before these data can be reliably used in data-model fusion studies. Having said that the flux retrieval algorithm effectively does just that, it updates the model flux estimates. The concentration data could therefore be used in a similar data assimilation inversion approach to update the state variables, and the parameters, of any C flux model, as long as anthropogenic emissions were also taken into account.

2.4 Soil moisture observations

2.4.1 Ground-based soil moisture observations

Ground based soil moisture measurements are usually measured with a theta probe, which measure the electrical impedance of the soil (related to the dielectric constant) or a neutron probe. In the latter method “fast” neutrons produced by the decay products of americium are released into

the soil. When they collide with hydrogen atoms (in a water molecule for instance) they lose much of the energy. The probe detects the "slow" neutrons, allowing an estimate of the soil moisture. Several ground-based soil moisture networks and campaigns have been run over the past ten to 15 years. The Soil Moisture Experiments (SMEX) in 2002-2005 inclusive, run by the Hydrology and Remote Sensing Laboratory of the United States Department of Agriculture Agricultural Research Service (http://hydrolab.arsusda.gov/smex05/) were undertaken to facilitate the validation of satellite soil moisture data, and have been extremely useful in this regard. The SMOSREX (Surface Monitoring Of the Soil Reservoir EXperiment) campaign (*de Rosnay et al.*, 2006) has also been used for satellite soil moisture validation, as have in-situ networks including the REMEDHUS (Soil Moisture Measurement Stations Network) network in Spain and the SMOSMANIA network in southern France (*Calvet et al.*, 2007), which was designed for the validation of soil moisture observations from ESA's Soil Moisture and Ocean Salinity (SMOS) radiometer.

Until recently the Global Soil Moisture Data Bank was held at Rutgers University (*Robock et al.*, 2000). It consisted of soil moisture observations from around the globe, most taken in-situ using gravimetric methods, and was used not only for validating soil moisture retrievals from satellites but for validation of atmospheric and land surface models, to examine trends in soil moisture, and for the design of soil moisture networks. The gravimetric method uses the difference in weight of a sample of soil before and after it has been oven-dried to calculate the soil moisture percentage.

Recently *Dorigo et al.* (2011) have announced the start-up of the International Soil Moisture Network (ISMN - http://www.ipf.tuwien.ac.at/insitu) whose aim is to collate ground-based soil moisture measurements from around the globe in order to provide more data for the validation of satellite soil moisture observations and land surface model predictions. The data from the Global Soil Moisture Data Bank has now been moved to the ISMN, along with other datasets. *Dorigo et al.* (2011) suggest this is the first step towards a global soil moisture observing system.

2.4.2 Satellite-based microwave remote sensing of soil moisture

Why use microwave wavelengths?

The theoretical basis for using the microwave part of the spectrum to measure soil moisture is due to the fact the microwave signal is partly dependent upon the dielectric properties of the soil, which are very different in wet and dry soils. For example at L-band microwave frequency the dielectric constant of water is ~80, whereas the dry soil has a dielectric constant of ~3-5 (*Engman and Chauhan*, 1995). In addition the relatively long microwave wavelengths are unaffected by clouds and other atmospheric constituents and can penetrate deeper into the soil when compared to optical and thermal domains (*Moran et al.*, 2004). Optical and thermal wavelengths have been used to look at soil moisture indirectly, through it's affect on surface temperature, evapotranspiration or the direct reflectance of bare soil, but all of these measures have shown a relatively weak relationship to soil moisture, unless an empirical calibration is carried out for a particular site,and no conclusive methods have been developed (*Moran et al.*, 2004).

Measurement principles

Three different measurement principles are used in satellite remote sensing of soil moisture; radiometry, scatterometry and Synthetic Aperture Radar (SAR). Radiometry is a passive technique which measures the intensity of microwave emission from the surface and near-surface (*Engman and Chauhan*, 1995). This is referred to as the brightness temperature (T_B) (*Wagner et al.*, 2007a). T_B is proportional to the product of the surface emissivity and surface temperature (*Engman and Chauhan*, 1995). Scatterometry and SAR are active techniques, which transmit a pulse of microwave energy and measure the backscattered radiation (given as the backscatter coefficient - σ^o) from the interaction of the radar wave with the surface and vegetation. The difference between the two is that scatterometers use a real-aperture radar, whereas the synthetic aperture radar systems synthesise a longer antenna length electronically by processing the phases of many transmitted pulses of energy as the satellite moves past the target using Dopler principles (*Ulaby et al.*, 1982). The purpose is to achieve a higher azimuthal (along-track) resolution. Azmiuthal resolution is inversely proportional to wavelength, therefore very long antennas (hundreds of metres) would need to be constructed to achieve a resolution of hundreds of metres to kilometres at microwave wavelengths. SAR instruments are thus able to produce higher resolution datasets (tens of metres) than scatterometers (tens of kilometres).

Different microwave instruments use different wavelengths, with the most common being wavelengths in the 2.4 - 3.8cm (X-band), 3.9 - 7.5cm (C-band) and more recently 15 - 30cm (L-band) ranges. The longer the wavelength the greater the penetration depth through the canopy and into the subsurface (*Jensen*, 2000). Longer wavelength microwaves interact with smaller scale scattering objects in the vegetation canopy such as leaves and small branches, whereas L-band wavelengths will penetrate through even thick vegetation canopies and into the top surface of the soil. The penetration depth is commonly calculated as $\frac{1}{4}$ to $\frac{1}{2}$ the wavelength of the transmitted pulse, therefore longer wavelengths are preferred for remote sensing of soil moisture.

Retrieval algorithms

Several variables, other than soil moisture, affect the emitted or backscattered microwave signal and therefore the measurement of soil moisture; surface roughness, vegetation and to a lesser extent, soil texture, which impacts the soil dielectric constant (*Engman and Chauhan*, 1995). In radiometry the brightness temperature is proportional to the product of the surface emissivity and surface temperature, if the negligible contributon of the atmosphere is ignored (*Engman and Chauhan*, 1995). The emissivity (1 - reflectivity) is related to the reflection coefficient, which can be calculated from the Fresnel equations, and is dependent upon polarisation and the soil dielectric permittivity and view angle. The soil dielectric permittivity is mainly dependent upon soil moisture and texture. Several models exist which relate these two variables (e.g. *Dobson et al.* (1985). The reflectivity is also affected by surface roughness, which is relative to the wavelength of the microwave wavelength. The surface roughness enhances emission of the microwave signal and decreases the reflectivity. Surface roughness effects are commonly accounted for using two parameters, 'Q' and 'h', which modify the soil specular (smooth surface) reflectivity and which depend on the root mean squared height of the surface variations, wavelength (*Wang and Choud-*

hury, 1981; *Engman and Chauhan*, 1995; *Wigneron et al.*, 2003).

If vegetation is present it acts to attenuate the emission from the soil and to add to the microwave emission, depending upon the amount of vegetation and the wavelength of the microwave signal (*Engman and Chauhan*, 1995). A simple radiative transfer model, known as the tau-omega ('τ - ω') model, is often used to account for vegetation attenuation and scattering effects in radiometry at low microwave frequencies (*Wigneron et al.*, 2003). τ is the optical depth and ω is the single scattering albedo, both of which are used to modify the soil reflectivity. τ has been shown, (e.g. by *Jackson and Schmugge* (1991)), to be linearly related to the vegetation water content via the 'b' parameter which is dependent upon vegetation type, polarisation and frequency, and which has to be calibrated.

To estimate soil moisture the surface roughness and vegetation effects need to be accounted for, either by empirical calibration for the site or vegetation type, or explicitly in the retrieval algorithm. Most passive algorithms use a version of the τ-ω model but parameterise the model in different ways. For example *Yang et al.* (2007c) use a different method of calculating the optical depth to *Kerr and Njoku* (1990). *Wang and Schmugge* (1980) use a relationship between the soil dielectric constant and specular emissivity whereas *Dobson et al.* (1985) developed an equation between the soil dielectric constant and reflectivity. In some models the vegetation water content is a function of LAI (*Koike et al.*, 2004), which can be prescribed from ancillary EO information. Soil textural prorperties and soil porosity also need to known or estimated a priori from independent sources. This can be difficult on a global scale. As the variables are mostly either polarisation or frequency dependent, and vary with viewing angle, multi-polarisation, multi-frequency and multi-angular measurements can be used to distinguish the variables. For example at increasingly lower frequencies the soil emission increasingly becomes the dominant contribution to the microwave signal and at higher viewing angles the signal has a longer pathway through the vegetation, therefore the microwave signal is increasingly attenuated (*Wigneron et al.*, 2003).

Wigneron et al. (2003) give an excellent review of the retrieval algorithms that are used in passive microwave remote sensing and how they each account for the various variables that contribute to the microwave signal. They separate the algorithms into four groups; i) those that use ancillary information based on land cover type to give information on vegetation and soil properties, ii) ancillary information from remote sensing indices to account for the vegetation effects and/or surface temperature, iii) and iv) two and three parameter retrievals, which make use of the multi-configuration characteristics of the of the sensor. Some non-parameteric models (i.e. linear empirical functions that fit soil moisture to T_B) have been successful in obtaining good estimates of soil moisture, especially with microwave indices, such as polarisation ratios, but these tend to be site-specific and unable to retrieve good results elsewhere (*Wigneron et al.*, 2003). Even the third and fourth algorithm types cannot solve for all parameters in the model and therefore a good representation of the vegetation attenuation properties needs to be obtained from ancillary information, however these algorithms have been more successful in general (*Wigneron et al.*, 2003).

Examples of multi-configuration retrieval algorithms include *Owe et al.* (2001) who assumed that τ and ω were polarisation independent in all vegetation types except those with extreme preferential orientation such as vertical stalks in crops. They therefore used the T_B equations at V and H polarisation (multi-polarisation difference index) to solve for the soil moisture and τ

simultaneously. It assumes constant values for ω and surface roughness. The surface temperature is derived from the 37GHz frequency channel based on the fact that 37GHz T_B is highly correlated with land surface temeperature (*Owe et al.*, 2001). This model is later referred to as the Land Parameter Retrieval Model (LPRM). Some studies use a ratio of vertically polarised 18.7GHz to 6.9GHz T_Bs to account for surface temperature by assuming a constant temperature at low microwave frequencies, (e.g. *Yang et al.* (2007c); *Qin et al.* (2009)).

One issue of using a simple radiative transfer algorithm such as the τ-ω model in radiometry is the relatively low resolution (~50km), which results in pixels which cover heterogeneous landscapes where the vegetation and surface roughness are dramatically different from one vegetation type to another. Setting pixel average values for vegetation properties can lead to errors in the satellite measurements.

Although surface roughness does need to be taken into account in passive microwave retrieval algorithms, it is not as serious a limitation as for active techniques, as there is more interaction between the microwave energy and the surface (*Engman and Chauhan*, 1995). A rough surface (relative to the wavelength of the microwave radiation) increases the amount of backscattered energy, however the backscatter is increasingly insensitive to soil moisture due to the sharp decrease in reflectivity with increasing roughness. Therefore for active systems the effect of roughness on backscatter can be greater than the effect of soil moisture, and for this reason it is imperative to accurately account for the vegetation and surface roughness effects in active microwave soil moisture retrieval algorithms (*Engman and Chauhan*, 1995).

Moran et al. (2004) and *Wagner et al.* (2007a) both provide a good overview of the current status of active microwave retrieval algorithms. They conclude that whilst a vast body of work has been carried out in this area there is still no widely used, operational retrieval algorithm. This is due to the complexity of the interaction of the microwave pulse with the surface, and the fact that most instruments don't have multi-configuration capabilities. In addition SAR systems, though capable of high resolution, consequently have a long revisit time and are therefore not useful for change detection algorithms (discussed below).

σ^0 is comprised of more components than T_B, which is just the result of direct emission from the soil attenuated by the canopy, direct vegetation emission and emission from the vegetation which is reflected by the soil and then attenuated by the canopy. σ^0 is a function backscatter from the soil surface, the two-way attenuation of the vegetation, direct backscatter from the vegetation and multiple scattering between the vegetation and soil elements (*Moran et al.*, 2004)

Empirical approaches require parameter calibration and are therefore site-specific or only valid for a given sensor, land cover, climate and possibly season (*Moran et al.*, 2004), therefore *Wagner et al.* (2007a) suggests that the more physically based radiative transfer models that account for multiple-scattering effects are the most useful. Some semi-empirical approaches try, as in passive retrieval algorithms, to account for the vegetation-related backscatter using a simple radiative transfer algorithm, before forming an empirical relationship between the *surface* backscatter component and the soil moisture. One often used semi-emipirical model which accounts for the effects of vegetation scattering is the 'water cloud model'. This represents the canopy as a uniform cloud of spherical droplets where the canopy is defined by LAI or vegetation water content (*Moran et al.*, 2004). More complex approaches expand on this idea by using explicit descriptions of the differ-

ent elements of the canopy (*Wagner et al.*, 2007a). Purely theoretical radiative transfer approaches usually require surface roughness parameters to be defined a priori, but choosing such a parameter which adequately describes this variable is difficult (*Wagner et al.*, 2007a). As with passive approaches this is usually described using the root mean squared height of the surface vegetation and correlation length (i.e. an autocorrelation function). Probably the most widely used microwave backscatter radiative transfer model is the 'Integral Equation Model' (IEM) (*Fung et al.*, 1992; *Wagner et al.*, 2007a) which is a bare soil model. Many additions and refinements have been made to the IEM to account for vegetation effects. However *Moran et al.* (2004) report that numerous studies have shown the IEM doesn't always work well, even with a very good, ground-based, characterisation of surface roughness. In general *Wagner et al.* (2007a) conclude that models have failed to accurately account for the surface roughness, partly due to the complex geometry of the surface, and partly due to the fact that microwaves can be longer, comparable to or shorter than the scales of variations in the vegetation elements (leaves, branches etc). As most SAR systems are not multi-angular and do not operate at more than one frequency it will be difficult to account for surface roughness and vegetation effects and therefore accurate determination of soil moisture is limited (*Moran et al.*, 2004).

In order to take into account the surface roughness and vegetation effects *Wagner et al.* (1999b) and *Wagner et al.* (1999a) at TU-Wien University proposed a change detection method for scatterometer data from the instrument on board the European Remote Sensing (ERS) satellite (Table 2.1) which exploited the multi-angular nature of the data to account for the changes in backscatter due to the vegetation phenology (the contribution of surface roughness is assumed constant). The data are normalised to a reference angle of 40^o and are then related to reference backscatter timeseries for completely dry and wet soil conditions, calculated from many years of data, that take into account the vegetation phenology. The dry reference backscatter value at time t is subtracted from the measured value and this is then normalised to range in the dry and wet reference backscatter values, in order to derive a relative measure of soil moisture (assuming a linear relationship between soil moisture and backscatter) (*Wagner et al.*, 2003; *Naeimi et al.*, 2009a). The TU-Wien model has been used in the same way to derive relative soil moisture measurements from the Advanced Scatterometer (ASCAT) onboard the MetOp satellites (*Naeimi et al.*, 2009b,a).

Current Satellites

Table 2.1 provides an overview of the current operational satellites that are capable of measuring soil moisture and one planned future mission. The instruments are grouped according to measurement technique. The satellite is detailed along with the launch data and then the instrument charactersitics. The revisit time is dependent upon the swath width, which tends to be higher for lower resolution satellites, offering a temporal trade-off with poorer spatial resolution. SAR instruments provide the highest spatial resolutions compared to radiometer and scatterometer data. As discussed above the longer the wavelength the greater the penetration of the canopy and surface soil, which is important for remote sensing of soil moisture. A summary of the observation uncertainty resulting from validation studies is provided in the next section.

Measurement Technique	Instrument	Satellite (Agency)	Launch Date	Frequency (GHz)	Polarisation	Resolution (km)	Swath Width (km)	Re-visit Period (days)
Passive - Radiometry	AMSR-E	Aqua (NASA)	2002	6.925, 10.65, 18.7 23.8, 36.5, 89	HV	56, 38, 21 24, 12, 5.4	1445	1-2
	MIRAS	SMOS (ESA)	2009	1.4 (L-band)	HV	30-50	1000	3
Active - Scatterometry	ASCAT	MetOp (ESA)	2006	5.255 (C-band)	VV	25-50	500 (x2)	1-2
	Wind Scatter.	ERS-2 (ESA)	1995	5.3	VV	50	500	2-7
Active - SAR	SAR	ERS-2 (ESA)	1995	5.3	VV	0.03	100	35
	ASAR	ENVISAT (ESA)	2002	5.3	HH/VV	0.03-1	0.005-0.4	35
	PALSAR	ALOS (JAXA)	2006	1.27	combination	0.007-0.1	70-360	46
Future - SAR	C-band SAR	Sentinel-1 (ESA)	2013	5.405	VV+VH,HH+HV	0.005-0.02x0.04	80-400	12
Future - both	SMAP	(NASA)	2014	1.26 (Radar)	VV HH HV	1-3	1000	1-2
				1.41 (Radiometer)	HV	40		

Table 2.1: The characteristics of various satellite-based microwave instruments used to retrieve soil moisture observations.

Observation uncertainty and validation

The uncertainty in satellite soil moisture observations is determined by sensor characteristics and retrieval algorithms (*Wagner et al.*, 2007b). Satellite soil moisture products have mostly been validated by comparing the data with ground-based in-situ soil-moisture observations. However validation with point measurements of soil moisture is problematic as discussed below. The resolution of the satellite data, particularly passive systems, is often large (few km^2 to several thousand km^2) and soil moisture can change over small spatial scales due to topography and soil processes (*Wagner et al.*, 2008). Variability in atmospheric forcing (i.e. precipitation, temperature, wind, humidity etc) can be large enough to have an effect on the spatial soil moisture patterns within the resolution of some satellite instruments. Heterogenous land cover and soil type within a pixel also contribute to uncertainty in the soil moisture signal, especially if the variability in surface characteristics are not accounted for in the retrieval algorithm *Jackson et al.* (2010). Differences between the ground-based observations and the satellite data may not be due to errors in the retrieval algorithms, sensor characteristics or instrument calibration but may just be the result of comparing datasets which actually represent different things. Often the mean of point measurements made across the pixel is used to compare with the spatial average recorded by the satellite sensor. The ground-based observations often have a high spatial variability due to the reasons discussed above (*Owe et al.*, 2008). In addition the satellite footprint size is not fully known for radiometers and a specific ground location might be located in a different part of the satellite footprint with every satellite pass (*Jackson et al.*, 2010). The vertical resolution of the data may not be the same either. Ground-based observations are often made at depths of >5cm, which is below the penetration depths of most microwave wavelengths, whereas only the topmost ~<=2cm of the soil contributes to the signal received at the satellite. The penetration depth also changes with the saturation of the soil (*Owe et al.*, 2008; *Jackson et al.*, 2010). Differences in the time of day, or date, that the ground-based and satellite data are acquired will also possibly result in differences between the datasets, especially if there has been precipitation in-between. This is more of a problem for regions which experience high, frequent rainfall.

Despite several large campaigns aimed at measuring ground-based soil moisture for satellite validation, as summarised in Section 2.4.1, *Owe et al.* (2008) point out there are very few observational datasets that exist at the temporal and spatial scales necessary (both horizontally and vertically) for good quality validation of the satellite data and therefore suggest it is more mean-

ingful to compare the temporal trends rather than the absolute values. Many of the validation studies that have been undertaken for currently operating satellites are summarised in Table 2.2. Whilst no validation studies have been carried out over the peatlands, the literature summarised in Table 2.2 covers validation studies of similar vegetation types to the shrubs and grasses found in UK peatlands. Some of the main issues arising from these studies are discussed below.

In the majority of validation studies the satellite soil moisture corresponds well with the low frequency, seasonal scale, temporal dynamics, but the absolute values are over- or underestimated (e.g. *Gruhier et al.* (2010)). The satellite observations often show higher variability than ground-based measurements on a shorter timescale (e.g. *Paris Anguela et al.* (2008); *Albergel et al.* (2009)). This is thought to be due to the fact that most ground-based sensors are positioned at a depth of >5cm whereas the satellites 'see' only the top few cms of the soil, which responds faster to atmospheric forcing (precipitation, humidity, temperature and wind) than lower layers (*Wagner et al.*, 2007a). Many studies report a good response of the satellite data to precipitation (e.g. *Mladenova et al.* (2010)), and in some studies rainfall has not been captured by the in-situ data (*Gao et al.*, 2006). A quicker 'dry-down' is sometimes observed in satellite data when compared with ground-based observations (*Gao et al.*, 2006). High RMSE values might result from high soil moisture variability in response to highly changeable precipitation forcing, such as in a Monsoon period (*Gruhier et al.*, 2010), where high biases might just be the result of a lag time between the satellite measured surface soil moisture and the in-situ soil moisture measured at a greater depth. If high correlations are found during these periods, however, then the the algorithms are capturing the dynamics well, which is important in areas where the land-atmosphere feedback to precipitation is strong (*Gruhier et al.*, 2010).

To understand what temporal scales are contributing to the correlation *Rudiger et al.* (2009) computed the soil moisture anomaly correlations, i.e. the difference from the mean over a time window. They found that the correlation was mainly due to seasonal effects as the anomaly correlations are lower at certain parts of the year. The satellite data and ground observations didn't correlate as well in winter, which they propose is due to soil freezing and the reduced dynamics of the soil moisture signal. On the contrary *Albergel et al.* (2009) found that the anomalies had as high a correlation as the soil moisture timeseries, and therefore suggested the correlations were not dominated by the seasonal dynamics. *Gao et al.* (2006) grouped the data into seasons before examining the correlations and found a large seasonal variability in the correlation values, with the highest correlations found in autumn and the lowest in winter.

From studies which look at several different locations it is obvious that soil moisture data can have very different error characteristics, possibly due to differences in the climate, soil properties and vegetation type and amount (*Reichle et al.*, 2004; *Ni-Meister et al.*, 2005; *Gruhier et al.*, 2010). Therefore, a validation study from one location or region cannot be relied upon to give an idea of the error characteristics of another region. A number of issues arise when transferring the results of a validation exercise at one site to another location. Error estimates might be small due to low soil moisture values or dynamic range (e.g.*Li et al.* (2010); *Gruhier et al.* (2010)). Differences can also result from inadequate parameterisations in the retrieval algorithms which give accurate parameter estimates for one region but not for another (*Reichle et al.*, 2004). It is therefore potentially not very useful to obtain an average RMSE for a range of locations (*Li et al.*,

2010), and/or dates as many studies do. *Champagne et al.* (2010) argue that long term datasets are required to truly validate soil moisture accuracy and evaluate the dynamics, not just as because of changing seasonal dynamics, but because of longer term changes in surface vegetation or climate.

The RMSE between satellite observations and ground-truth data is often affected by the spatial uncertainty in the ground-based data. Data from different stations within the pixel area are used calculate a mean value to compare with the single satellite observation. Some studies report a relatively high spatial scaling error between the stations, (e.g. $0.034 m^3 m^{-3}$, *Ceballos et al.* (2005) and $0.03 m^3 m^{-3}$, *Reichle et al.* (2004)). Point-based soil moisture measurements follow the same temporal trend as the mean so taking a linear average is valid (*Ceballos et al.*, 2005). *Ni-Meister et al.* (2005) point out the need to account for in-situ measurement error and for horizontal *and* vertical scaling errors, as the satellites will mostly likely be measuring the soil moisture of a thinner surface layer than the ground-based observations.

Gruhier et al. (2010) compared five different passive and active sensors and retrieval algorithms and found the soil moisture products varied greatly in terms of the overall range and variability. However the mean relative difference between the five products was very low, showing the mean values correspond well over longer time periods. The two AMSR-E products (Table 2.2) showed a strong temporal correlation but the absolute values varied, especially in the dry season, resulting in an RMSE of 0.058 (*Gruhier et al.*, 2010). The two ERS Scatterometer products (Table 2.2) compared well in terms of temporal variability and absolute value (*Gruhier et al.*, 2010) as did the two different sensors that used the LPRM algorithm (*Owe et al.*, 2001), with a particularly high correlation of 0.82. *Gruhier et al.* (2010) concluded that both frequency, sensor type and retrieval algorithm are important in determining an accurate estimate of soil moisture. *de Jeu et al.* (2008) suggest that if soil moisture products from different sensors and retrieval algorithms have similar error statistics for a given region then they likely do represent the actual soil moisture dynamics as it is very unlikely to see the same systematic errors in independent datasets. However this does not suggest they have the correct absolute values as a bias can still be present due to vertical and horizontal scaling errors etc.

Several studies calculated the profile average soil moisture (SWI - Soil Wetness Index) from the surface, satellite-derived soil moisture using a two-layer water balance model and found the profile average to compare better with in-situ profile averaged soil moisture, as the high temporal variability of the satellite observations is dampened with depth (*Ceballos et al.*, 2005; *Brocca et al.*, 2010). This is potentially an important finding for data assimilation studies because the SWI might contain more information on soil dynamics than the surface soil moisture. The profile average soil moisture can easily be calculated in the model and compared to the data.

When comparing with relative soil moisture measurements (i.e. % saturation) the ground based data are either transformed into relative soil moisture by scaling between the minimum and maximum of the in-situ observations (*Rudiger et al.*, 2009), or alternatively the satellite relative soil moisture data are transformed into absolute values using the known or theoretical porosity and wilting point, (*Drusch et al.*, 2004) or the dynamic range of the in-situ data (*Albergel et al.*, 2009). There is a potential issue in comparing "like-with-like" in these data in terms of what is defined as the minimum and maximum. The change detection algorithms use the minimum and maximum value of a climatology of microwave backscatter data spanning several years and assume that these

values correspond to completely dry and wet conditions (*Wagner et al.*, 2003). For some areas the minimum and maximum of the satellite data might not correspond to the actual wilting point and porosity of the soil, yet the porosity is used to transform the data into absolute values. Equally, the minimum and maximum of the in-situ data is often used to transform the data into relative soil moisture and this might not correspond to the same conditions which resulted in the minimum and maximum backscatter data that is used to calculate the satellite observations. *Wagner et al.* (2003) recognise this issue and discuss an empirical correction that is applied to very dry soils which might never reach saturation. They also discuss using the backscatter value for frozen soils at high wet latitudes where the opposite is true. However in temperate, wet climates the soil may never reach its wilting point or be frozen. Whether this is indeed a problem for near-saturated soils in these climates, and whether it is accounted for in the model needs further clarification.

Wagner et al. (2007a) argue that evaluation with ground-based data alone is insufficient due to the problems discussed above, and that pair-wise comparison with other datasets can alleviate this problem. Recently other methods of determining the error characteristics of satellite soil moisture datasets have been introduced. *Scipal et al.* (2008) introduced the "triple collocation" technique for understanding error characteristics of various soil moisture products, even in the absence of ground-truth data. The method allows systematic differences between the "truth" and satellite data to be taken into account. This is achieved by assuming a linear relationship between the measured and "true" soil moisture, including the residual random error (+ e), and solving for the "calibration constants" of the linear function for each dataset in order to calculate the residual RMSE (*Scipal et al.*, 2008). This approach assumes the errors of the individual datasets are uncorrelated. It also requires enough coincident data points; *Dorigo et al.* (2010) suggest over 100. *Scipal et al.* (2008) only included data points which had a correlation of higher than 0.2 between the measured and true values in order to make sure the datasets were measuring the physical soil moisture. One problem with the method is that the user needs to define a "truth" or reference dataset and therefore the resultant RMSE values are relative to the reference dataset and will change depending on the dynamic range of that dataset (*Dorigo et al.*, 2010). To determine the relative magnitude of the errors, independent of the reference dataset, *Scipal et al.* (2008) normalise the values by scaling between the maximum and minimum of the reference dataset soil moisture. They compared the ERS-2 Scatterometer and the TRMM TMI instrument with the ERA-Interim climatology as the reference dataset. The resultant RMSE (and relative error) values were $0.028 m^3 m^{-3}$ (9.4%), $0.046 m^3 m^{-3}$ (15.6%) and $0.02 m^3 m^{-3}$ (6.9%).

Dorigo et al. (2010) used the triple collocation method but defined the problem slightly differently. They looked at the trends in the uncertainty due to the different observation principles of active and passive systems and for different frequencies. Instead of examining the absolute soil moisture values they investigated the temporal anomalies so as to investigate the ability of the data to capture the temporal dynamics (*Dorigo et al.*, 2010). They found global average RMSE values of $0.017 m^3 m-3$ for the ASCAT anomalies and $0.019 m^3 m^{-3}$ for AMSR-E compared to the ERA-Interim reference dataset with RMSE of $0.018 m^3 m^{-3}$. They find AMSR-E performs better than ASCAT in dry areas, probably due to the volumetric scattering confounding effects in the active ASCAT data. However AMSR-E has a higher RMSE value in dense vegetation, which they ascribe to problems in the simple linear radiative transfer retrieval algorithm of the AMSR-E data

(*Owe et al.*, 2001), which doesn't fully account for higher order scattering effects in the vegetation canopy, compared to the change detection algorithm *Wagner et al.* (2003), which by its design deals with the problem of characterising the vegetation effects on microwave scattering. No RMSE value greater than $0.05 m^3 m^{-3}$ is reported in *Dorigo et al.* (2010).

Although this method effectively takes the systematic errors into account in order to determine the random error in the observations, it is still necessary to determine and specify the absolute biases between the satellite data and the in-situ truth for data assimilation studies using the satellite soil moisture data. But this method allows a more in depth exploration of the different possible sources of error in datasets.

Rudiger et al. (2009) point out that for atmospheric studies it is more important to capture the right temporal dynamics than to obtain the correct absolute value, however *Ni-Meister et al.* (2005) stressed the need for accurate soil moisture initialisation in data assimilation systems, therefore ascertaining the differences between the satellite data and observations is crucial. *Reichle et al.* (2004) argue therefore that the bias needs to be accounted or corrected for, or the values re-scaled, before incorporating the data into the data assimilation system. For parameter calibration exercises an accurate value of the soil moisture is necessary, as it is not the temporal trend of the model which is being "updated/adjusted" by the observations.

It is clear that a wide range of RMSE and bias values are possible and that validation studies from one site cannot be transferred even to a nearby location. Thus until a wider databank of validation studies has been carried out, it is imperative to validate any soil moisture data with ground-based data from individual study sites, or at least similar ecosystems, before using it in model calibration or data assimilation studies. *Wagner et al.* (2007b) discussed the need for introducing a standardised validation method (as has been done for other EO datasets such as LAI, e.g. *De Kauwe et al.* (2010)), and collective datasets that can be used for validation, in order to directly compare the accuracy obtained from the evaluation of different satellite products. This would go a long way in improving understanding of the error characteristics of satellite soil moisture. The need for robust error characterisation is increasingly being realised with many observation datasets, including for EO data. Studies such as those by *Dorigo et al.* (2010) are also an important step towards understanding the observation uncertainty. Hopefully in the near future good quality error fields will be provided with each dataset. This will in turn encourage more people to use the data, as an independent validation is not always possible, and if a global modelling study is being undertaken, it is simply impossible.

Unfortunately the only operational soil moisture products currently available are based on radiometer or scatterometer data, both of which have a low resolution. The benefit of this is that high temporal revisit period is possible, but significant biases can occur in the pixel values if the pixel covers a heterogeneous landscape and only one part of the pixel is being studied. SAR enables a much finer resolution to be achieved and therefore more detailed spatial patterns of soil moisture fields. Results from *Pathe et al.* (2009) show a very high correlation (0.9) between ERS scatterometer soil moisture data and co-registered 50km linearly-averaged ASAR data with a low RMSE and bias of $0.04 m^3 m^{-3}$ and ~0.008 respectively. It is possible that high resolution coincident SAR soil moisture data can bridge the gap in scale between the point-based in-situ data and the coarser resolution radiometer and scatterometer data for validation purposes or for

downscaling low resolution data *Wagner et al.* (2008). Although as SAR validation studies show (Table 2.2), there is a need for improvement in the SAR retrieval algorithms before this will be possible. Other optical and thermal datasets have also been used for to disaggregate low resolution soil moisture data (e.g. *Merlin et al.* (2009, 2010), resulting in reasonably low RMS errors (~0.01 - 0.06m^3m^{-3}) and biases -0.045m^3m^{-3} and high correlation coefficients (>0.9). Standardised algorithms may soon become available to create higher resolution datasets from low resolution radiometer and scatterometer data. NASA's Soil Moisture Active Passive (SMAP) satellite, currently planned for launch in 2014, will contain, for the first time onboard a satellite, an L-band radar and an L-band radiometer. Algorithms have been developed to merge the two datasets to provide high resolution (9km) soil moisture datasets that will meet or better the 0.04m^3m^{-3} mission accuracy requirement (*Das et al.*, 2011) and daily composite products will be provided (http://smap.jpl.nasa.gov/science/dataproducts/). This might be the best option for retrieving high resolution data as the instruments are onboard the same satellite.

No validation studies have yet been undertaken to compare low resolution satellite soil moisture with ecosystems which have near-saturated soil for most of the year, as is the case for peatlands and areas of wetlands which are not inundated. It is unclear whether any biases will be present in the data as a result of systematic errors in the retrieval algorithms, or whether the random error increases or decreases for higher values of soil moisture. As is the case for many ecosystems further validation and error characterisation is needed before the data can be used with confidence without site-specific validation.

Sensor	Retrieval Algorithm	Location	Vegetation Type	RMSE ($^3m^{-3}$)	Bias (m^3m^{-3})	correlation Coefficient	No. of obs.	Reference
AMSR-E	LSMEM[a]	IA, USA (SMEX02)	crops	0.041	-	0.75	8	*McCabe et al.* (2005)
AMSR-E	LPRM (VUA)[b]	Australia	grassland	0.05 to 0.20	-0.01 to 0.19	0.45 to 0.92	200-282	*Draper et al.* (2009)
AMSR-E	NASA [c]	Spain (REMEDHUS)	crop	0.089	-	0.0	-	*Wagner et al.* (2007b)
	LPRM (VUA)[b]			0.044	-	0.83	-	
AMSR-E	NASA [c]	SW France (SMOSREX)	mostly fallow	0.107	0.04	0.132	698	*Rudiger et al.* (2009)
	LPRM (VUA)[b]			0.0582	0.0216	0.775	606	
AMSR-E	NASA [c]	Mali (Sahel)	herbaceous savanna,	0.0591	0.053	0.59	334	*Gruhier et al.* (2010)
	LPRM (VUA)[b]		rocky plain, forest	0.033	0.013	0.82	335	
AMSR-E	NASA [d]	OK,GA,AZ,ID (USA)	shrubs, crops, grass	0.045 to 0.076	0.016-0.072	0.31-0.57	555-1894	*Jackson et al.* (2010)
	LPRM (VUA)[b]			0.088 to 0.220	0.061-0.072	0.36-0.72	534-1881	
	JAXA [e]			0.037 to 0.105	0.02-0.08	-0.03-0.72	552-1695	
	SCA (USDA)[f]			0.021 to 0.053	0.017-0.034	0.41-0.67	554-1757	
ERS Scat	change detection (TU Wien)[g]	SW France (SMOSREX)	mostly fallow	0.0732	-0.0255	0.618	133	*Rudiger et al.* (2009)
ERS Scat	change detection (TU Wien)[g]	OK, USA	grass	0.057	0.018	0.66	-	*Drusch et al.* (2004)
ERS Scat	change detection (TU Wien)[g]	Spain (REMEDHUS)	agricultural	0.07	-	0.64	-	*Wagner et al.* (2007b)
ERS Scat	change detection (TU Wien)[g]	Spain (REMEDHUS)	agricultural	0.038 to 0.073	0.068	0.62 to 0.84	-	*Ceballos et al.* (2005)
ERS Scat	change detection (TU Wien)[g]	SE Paris, France	agriculture, forest	0.05	0.004	0.73	-	*Paris Anguela et al.* (2008)
ERS Scat	change detection (TU Wien)[g]	Mali (Sahel)	herbaceous savanna	0.0541	0.042	0.52	151	*Gruhier et al.* (2010)
	CETP[h]		rocky plain, forest	0.0523	0.041	0.63	83	
ASCAT	change detection (TU Wien)[g]	SW France (SMOSREX and SMOSMANIA)	grass, trees	0.044 to 0.09	-	0.09 to 0.73	36-61	*Albergel et al.* (2009)
ASCAT	change detection (TU Wien)[i]	central Italy	-	~0.08	-	0.672	342	*Brocca et al.* (2010)
ERS SAR	*Quesney et al.* (2000)	France	forest, crop, grass	0.0174 to 0.035	-	0.79 to 0.92	13	*Le Hegarat-Mascle et al.* (2002)
ASAR	change detection (TU Wien)[g]	OK, USA (MESONET)	grass, crops	0.056 to 0.136	-0.152 to 0.0016	0.17 to 0.78	-	*Pathe et al.* (2009)
ASAR	change detection (TU Wien)[g]	SE Australia	crops and grass	0.088	-	0.75	29	*Mladenova et al.* (2010)
ASAR	2-step AIEM[j]	NW China	farmland with crops	0.04 and 0.06	-0.02 and -0.03	0.7 and 0.35	-	*Wang et al.* (2011)
PALSAR	based on IEM *Verhoest et al.* (2008)	Belgium and Luxembourg	bare soil	0.0536	-	-		*Verhoest et al.* (2008)
PALSAR	NMBI[k]	Hokkaido, Japan	bare soil	0.044	-	-		*Sonobe et al.* (2008)
PALSAR	constrained min IEM	S Italy	crops	0.05	-	-		*Mattia et al.*

Table 2.2: Summary of the root mean squared error (RMSE), bias and correlation coefficient of the validation studies for various types of measurement technique (radiometry, scatterometry and SAR), instrument and retrieval algorithms. A **-** denotes where the information was not provided in the literature. (References for the retrieval algorithms: [a]Land Surface Microwave Emission Model *Drusch et al.* (2004), [b]Land Parameter Retrieval Model (Vrije Universiteit Amsterdam) *Owe et al.* (2001), [c]*Njoku et al.* (2003); [d]*Njoku and Chan* (2006); [e]*Koike et al.* (2004); [f] *Jackson* (1993); [g]*Wagner et al.* (1999b,a); [h]Centre d'Etudes Terrestres et Planetaires *Zribi et al.* (2009); [i]*Naeimi et al.* (2009b); [j]*Wang et al.* (2011); [k]*Shoshany et al.* (2000); and for the global soil moisture network: [l]*Robock et al.* (2000)).

2.5 Data assimilation - optimal combination of observations and models

Data assimilation (DA) comprises of a set of statistical techniques aimed at integrating models (prior knowledge of a system) and observations (new information) to improve model predictions and to obtain an estimate of the distribution of the model prediction (i.e. the uncertainty) (*Wikle and Berliner*, 2007). This follows Bayes' Theorem which is described. Following this a brief summary of the different DA techniques is presented along with their comparative advantages and disadvantages. Examples of carbon cycle DA studies are then provided and finally the benefits and potential issues that may arise when using this method are discussed.

2.5.1 Bayes' Theorem and Bayesian Inference

Bayes' Theorem is a theory of probability which relates a conditional probability of one event upon another, to its inverse probability and a prior knowledge of the independent probability of each event occurring. It can be derived from the multiplication rule in probability theory and the definition of conditional probability.

$$P(A \cap B) = P(A)P(B|A) \tag{2.2}$$

This is the probability of both event A and event B occurring together if event B is conditional on event A having already happened (P(B|A)). The probabilities are expressed as probability distributions, which are summarised in the form of a mean vector and a covariance matrix. Similarly:

$$P(A \cap B) = P(B)P(A|B) \tag{2.3}$$

From this we can derive Bayes' Theorem which states the probability of event A occurring given event B has already occurred is dependent on the probability of event B occurring given event A, multiplied by the unconditional probability of event A occurring, and divided by the probability of event B occurring:

$$P(A \cap B) = P(B|A)P(A) = P(A|B)P(B) \tag{2.4}$$

$$P(A|B) = \frac{P(B|A)P(A)}{P(B)} \tag{2.5}$$

P(A|B) and P(B|A) are conditional probabilities. P(A|B) is referred to as the posterior distribution and P(B|A) is called the "likelihood function". P(A) as the prior distribution and P(B) is a normalising constant.

Bayes' theorem is appropriate in addressing scientific questions, as it provides a simple way of updating the prior probability of a hypothesis given new observations or evidence (*Sivia*, 2006). Say event A is the hypothesis and event B is the data. So the equation can now be expressed as:

$$P(\textit{hypothesis given the data}) \propto P(\textit{hypothesis}) \text{ x } P(\textit{data given the hypothesis}) \tag{2.6}$$

P(hypothesis) describes the prior knowledge of the hypothesis. This provides a method of improving our knowledge of a quantity of interest, using not only the new data but also the knowledge of the hypothesis we already have. This approach is often referred to as Bayesian Inference (*Wikle and Berliner*, 2007). It is useful also in that it applies a *probability* to a hypothesis, rather than just accepting or rejecting it. Bayes' Theorem therefore allows conclusions to be drawn even with uncertain information.

This is the basis of DA; the process of combining data with prior knowledge of the variables of a physical system to obtain an improved estimate of the variables. The framework can be used to analyse a model when combined with observed data. The model is the hypothesis in the above example, i.e.:

$$P(\textit{model, given the data}) \propto P(\textit{model}) \text{ x } P(\textit{observations given the model}) \tag{2.7}$$

The observations are used to update a model parameters, the initial state vector or both. Taking the example of updating the model parameters, using Bayes' Theorem the probability distribution of the parameters, θ, of the model, given the data, is a function of the prior probability of the model parameters and the probability distribution of the data given the model parameters:

$$P(\theta|D) \propto P(\Theta)\, P(D|f(\Theta)) \tag{2.8}$$

where f(θ) is the model with specified parameters.

Even if little information about the prior probability distribution of the parameters is available this prior knowledge is still utilised. For example if only the physically limiting intervals of a parameter are known a simple uniform distribution can be used.

The likelihood function, which is the probability distribution of the differences between the observations and the model, can be determined by running the model using a certain set of parameters and comparing the resultant modelled state variables with observed values. Data can be used in a very simple way to improve the probability distribution of the parameters and is therefore useful as a calibration tool. As new data becomes available the probability distribution of the parameters can be further constrained. This process is often called optimisation and/or inversion.

In summary a Bayesian inference approach can be used to provide improved estimates of the parameters of a model with associated uncertainty, uncertainty in model outputs and information on the correlations between parameters. To use this approach you need an estimate of the prior distribution and estimates of the uncertainties in your observations. Bayesian inference is a powerful tool. *Wikle and Berliner* (2007) argue that it is an ideal probabilistic framework for combining all the relevant information including any prior knowledge of the system, the available observations and the model, including the associated uncertainties.

2.5.2 Methods of Data Assimilation

Wikle and Berliner (2007) provide an excellent overview of the different methods of DA in a Bayesian context. Many authors distinguish two types of DA techniques: sequential and batch. Sequential methods (sometimes referred to as 'filters') update the model parameters or the state variables at the point that a new observation becomes available. Batch methods (sometimes re-

ferred to as 'smoothers') change the initial parameterisation to produce a model run which best fits the observations over a certain time window, thereby incorporating more information.

One example of a sequential method is the Kalman Filter. This essentially calculates a weighted average of the uncertainty in both the observations and the model, with the highest weight given to whichever has the lowest uncertainty (*Maybeck*, 1979). Hence the model state and/or parameters are updated by the observations if they provide useful information. The Kalman Filter assumes that the model and observation operator are linear and that the model parameters have a Gaussian distribution. The Ensemble Kalman Filter (*Evensen*, 2003) works around the assumption of a linear model by creating ensembles of model runs which provide the error statistics for the model. However Gaussian distributions are still assumed for the observation operator and observations.

Variational DA techniques attempt to minimise a cost function which represents the difference between the models and the observations. The errors in the forward model, priors, observations and observation operator need to be included as terms in the cost function. The model can therefore act as a constraint in how well the observations improve the prior information.

Variational methods look for the maximum value of the posterior distribution (i.e. the most likely value of the parameters or state variable being estimated) by solving for the minimum of the cost function. This can be found using gradient descent methods such as the Newton Raphson method. The second derivative (Hessian) of the cost function provides an estimate of the covariance. To obtain the minimum of the cost function, the derivative of the cost function has to be derived and for that the partial derivatives of the model, with respect to the parameters or initial variables are required. This is called the adjoint (Jacobian) and describes the linear sensitivity of the model to all the other model variables and parameters. The adjoint is the transpose of the tangent linear model which gives the derivatives of the state vector. The tangent linear model can be used without the adjoint but this takes longer as the model has to be run with every change in the initial state variables or parameters. This method is often referred to as "3d-var". If observations are used over a time window the method is termed "4d-var". The major disadvantage of this method is that the adjoint needs to be calculated. This can be particularly difficult if the processes in the model are formulated in a non-differentiable way, for example if there are switches between one function and another depending on certain inputs or conditions.

In cases where an analytical derivation of the posterior distribution is not possible because the observations, parameters and model are strongly non-linear, the uncertainties are non-Gaussian, or the adjoint is difficult to calculate, Markov Chain Monte Carlo (MCMC) approaches are useful (*Wikle and Berliner*, 2007). MCMC methods obtain the posterior distribution by sampling the prior parameter space. These are termed "global search" methods. The technique is more flexible as no assumptions of the distribution of the model parameters, state variables or observations, and no linearisation of the model is required. However MCMC is more computationally expensive which prohibits its use for optimising larger models.

MCMC methods can be both sequential or batch. They also differ mostly in how they sample the prior distribution and in how they accept or reject the values to produce the posterior distribution. The particle filter is an example of a sequential MCMC algorithm, and the Metropolis-Hastings algorithm is used in a variational framework. The chosen data assimilation method is described in more detail in Chapter 3.

2.6 Carbon cycle data assimilation

Rayner (2010) provides a good general overview of the carbon cycle DA studies to date and the current status of field. The field of carbon cycle DA is divided between "top-down" inversions of satellite atmospheric C concentration measurements to provide land surface flux estimates, which do not include the use of a process-based model (except perhaps for the provision of prior flux estimates), and "bottom-up" approaches which use a process-based model to infer land surface C fluxes (*Wang et al.*, 2009; *Rayner*, 2010). *Wang et al.* (2009) review the advances made in five different applications of carbon cycle data assimilation: flux estimation, parameter estimation, model error analysis, evaluation of sampling strategies and forecasting. The inversion approach is essentially the same for all studies, though different studies use different assimilation techniques to suit their purposes. A few studies have combined both approaches (*Rayner et al.*, 2005; *Scholze et al.*, 2007).

The "top-down" approach was discussed in some detail in Section 2.3.2, so it is not discussed further here. Both approaches are also used to infer oceanic C fluxes as well as terrestrial, but the following discussion focuses solely on the land surface.

Most carbon cycle data assimilation studies to date have used either satellite-derived vegetation indices, LST or evapotranspiration, satellite observations of atmospheric CO_2 and CH_4 concentrations, eddy covariance data and soil carbon measurements to constrain the parameters or state variables of a model. A brief outline of some of these studies is given below. Other observations could also be used, including intensive chamber-based measurements of C flux, hydrological observations, and historical data on land use, land use change and disturbance (*Raupach et al.*, 2005).

2.6.1 DA with ground-based C flux observations

The majority of carbon cycle Bayesian inversion studies with process-based models have used eddy covariance C flux data to constrain the parameters, and in some cases C pool sizes, of an ecosystem or land surface model (*Braswell et al.*, 2005; *Knorr and Kattge*, 2005; *Williams et al.*, 2005; *Santaren et al.*, 2007; *Chen et al.*, 2008; *Richardson et al.*, 2010; *Vuichard et al.*, 2010; *Bonan et al.*, 2011; *Ricciuto et al.*, 2011; *Verbeeck et al.*, 2011). These studies not only looked at the constraint of different types of parameters but also the reduction in uncertainty between the prior and posterior PDF and the correlations between the parameters. Some discussed the impact of different time periods of data that were included in the inversion and the ability of this approach to identify errors in the model.

Knorr and Kattge (2005) found half-hourly eddy covariance CO_2 and H_2O fluxes substantially reduces the uncertainty of 5 parameters of the BETHY model. They found that in some cases the result depended strongly on the choice of prior uncertainties, suggesting the need for a full assessment of the information that might be available to provide accurate priors.

Santaren et al. (2007) used eddy covariance CO_2 flux data, as well as latent and sensible heat fluxes and net radiation to constrain the parameters of the ORCHIDEE model. They tested the timescales of improvement and found the fit to the diurnal cycle of the flux was better than the seasonal cycle, even when using a whole year of flux data. The parameters controlling photosyn-

thesis and the energy balance were well constrained whereas the parameters controlling respiration were not. The autotrophic and heterotrophic respiration terms could not be distinguished. They also discussed the ability of "edge-hitting" parameters (i.e. where the parameter is constrained to one end of the posterior PDF (PPDF)), in identifying structural deficiencies in the model.

Richardson et al. (2010) focused on the impact of different types of data, including eddy covariance, on the posterior PDF of C stocks and fluxes in the DALEC model. They also emphasised the need for a proper characterisation of the observation uncertainty and propagation of the uncertainty through the models. Most parameters were well-constrained by the available data apart from initial values of the fine root and soil C pool. *Richardson et al.* (2010) suggested this is not due to their limited impact on the model but down to the fact correlations with other parameters are compensating for the values. This is known as model equifinality (*Beven*, 2006). They concluded that including structures in the model for which observations cannot be readily obtained is not very beneficial, and will lead to a higher degree of model equifinality. A crucial finding of this study was that multiple streams of data both improves the model predictions and reduces the associated uncertainties.

Eddy covariance data were also used to constrain the Local Terrestrial Ecosystem Carbon model (*Ricciuto et al.*, 2011). The headline result of this study was that the uncertainty in the parameters and model predictions were strongly dependent on the length of the time period of observations. The uncertainty reduction increased as up to and including 5 years worth of data were added. As expected, parameters associated with short timescale processes such as photosynthesis and hydrology were well-constrained by short data records and vice versa. Adding in observations relating to the initial C pools and annual aboveground woody increment reduced the uncertainty in NEE predictions by 50%, as the model was very sensitive to these variables. They found that the number of parameters which were correlated increased with the length of the data record, suggesting there needs to be a trade-off between length of calibration and the number of well-constrained parameters. This was one of the only studies to perform a synthetic experiment prior to using actual data, which allowed an evaluation of the ability of the method without confounding factors such as model error. When actual data were used the inability of the model to reproduce the observations signified the presence of structural deficiencies in the model, which they suggested would need addressing in future modelling studies.

The use of chamber-based C flux data in model inversion has been demonstrated by *Yeluripati et al.* (2009), *Richardson et al.* (2010) and *Hashimoto et al.* (2011). *Richardson et al.* (2010) found that, in addition to eddy covariance observations, chamber measurements of soil respiration provided a valuable constraint on the model parameters and argued that this type of observation should be included as they are routinely made by field biologists. *Yeluripati et al.* (2009) constrain the initial values of soil C pools of the DAYCENT model (the daily timestep version of the CENTURY model), which they argue is necessary as the soil C pools may not be in equilibrium due to changing management and land use. They showed the uncertainty on the initial pool sizes could be reduced by the inversion. This was based on accurate information on the total soil C at the site, which was used as prior information. Arguably if this had not been available the results would not be as good quality. This information is hard to obtain for most sites.

Site-based vegetation characteristics and data available on C stocks was often used as ancillary

information to C flux measurements (e.g. *Van Oijen et al.* (2005); *Xu et al.* (2006); *Richardson et al.* (2010); *Hashimoto et al.* (2011). *Xu et al.* (2006) used datasets of woody biomass, foliage biomass, litterfall, C content in the litter layers and C content in the mineral soil, together with measurements of soil respiration, to constrain estimates of C transfer coefficients between the soil C pools. This resulted ina good constraint of the transfer coefficients of the biomass and litter pools but not the microbial, slow and passive soil C pools. This was attributed to either the lack of experimental data or the mismatch in timescales between the available data and the parameters.

2.6.2 DA with satellite observations of variables related to C flux

Vegetation dynamics

Several satellite data relating to the vegetation phenology have been assimilated into ecosystem models in order to constrain the C flux estimates. *Demarty et al.* (2007) used two years of satellite LAI data from the MODIS instrument onboard NASA's Terra and Aqua satellites to constrain the phenology-related parameters of the ORCHIDEE model. The inversion resulted in advances in the onset and end of the growing season at high northern latitudes which reduces the global annual estimates of GPP and NPP by 5 and 3% respectively. They find that the assimilation of LAI results in a better fit to independent eddy covariance data despite the errors in the LAI retrieval, unknown model errors and the mismatch between the scale of the flux tower footprint and the model grid cell.

Knorr et al. (2010) used satellite-derived fAPAR from the Medium Resolution Imaging Spectrometer (MERIS) onboard ESA's Envisat satellite to constrain 14 phenology- and 24 photosynthetic-related parameters of a generic phenology model. They found that one parameter set can accurately reproduce the fAPAR measured at 20 flux tower sites across boreal, temperature, semiarid and humid-tropical climates, with corresponding moderate reductions in the NPP uncertainty estimates. They suggested that the data could also be used to infer PFT fractions and the maximum plant available water content parameter of the model.

Quaife et al. (2008) argued that instead of using satellite-derived LAI or fAPAR, which are "high-level" EO products, i.e. those which require the use of an observation operator to convert the raw radiances into the observations required, surface reflectance data should be used in the assimilation. Surface reflectance, corrected for angular effects resulting from the viewing and illumination geometry, is a "low-level" product, i.e. only the correction of atmospheric effects and the conversion to reflectance from radiance is required. No further retrieval algorithm, which is either semi-empirically based, therefore probably calibrated to certain sites, or physically based, therefore involving assumptions on the type of vegetation, its structure, extent etc, is required. Products of the same variable but from different satellites might make different assumptions in their retrieval algorithms, and this may not match with the assumptions that the process-model makes for that same variable. Hence *Quaife et al.* (2008) argued that the reflectance should be modelled forward using a radiative transfer algorithm and then matched to the satellite observations. The errors in the retrieval can therefore be tracked and included in the inversion. They followed this approach in constraining the parameters of the simple ecosystem model DALEC, and the parameters of the observation operator. The results were compared to eddy covariance measurements. The results

showed a reduction in the CO_2 fluxes (NEP and total respiration) but the foliar biomass (and to some extent GPP) is overestimated after calibration. This is attributed to a few possible sources including error in the retrieval algorithm, lack of observations in the winter and shortcomings in the model, including the issue of setting the initial state and rate parameters which are taken from another study and assumed constant over the study area.

Land surface temperature and soil moisture

Other related EO variables which are important in terms of carbon fluxes are Land Surface Temperature (LST) and soil moisture. LST and soil moisture are important in calculating how much carbon enters the system by controlling the optimal conditions that the plants can function at. LST is useful in determining the surface energy balance and therefore the soil temperature profile and the amount of water in the system. LST influences the amount of evapotranspiration and therefore the water available in the surface layer and soil moisture changes the thermal conductivity of the soil. Although ideally for the modelling of CH_4 fluxes, observations of water table depth would be available, soil moisture is useful in modelling water table dynamics. Soil moisture and temperature also determine the amount of decomposition and therefore CO_2 loss from the system.

Several LST products are available from satellite instruments which have thermal channels, e.g. the Moderate Resolution Imaging Spectrometer (MODIS) on board NASA's Terra and Aqua satellites and Advanced Along-Track Scanning Radiometer (AATSR) on board ESA's Envisat satellite. Daily observations (both day and night) of LST are available at 1km from MODIS. LST observations at a resolution of 1km every couple of days are available from AATSR. Both instruments will likely have gaps in the data at this location due to cloud cover.

Relatively few studies to date have assimilated soil moisture or LST into land surface models, and the number decreases if only studies using satellite observations are considered. No studies have rigorously quantified the impact on the C flux predictions and uncertainties. *Zhu et al.* (2009) constrained the parameters of the terrestrial ecosystem model BEPS (Boreal Ecosystem Productivity Simulator) using soil moisture data derived from MODIS data. Their aim was to improve the soil moisture predictions of the model, but parameters relating to canopy transpiration were also considered which would have an impact on the C fluxes, though this was not discussed.

The improvement in modelled LST and evapotranspiration from assimilating LST into the Common Land Model (COLM) was investigated by *Meng et al.* (2009). They reported that, aside from time periods with heavy rainfall, a better comparison with in-situ data was achieved when the assimilation was performed once per day. They found no noticeable improvement if the assimilation was performed twice in most cases. *Barbu et al.* (2011) assimilated the soil wetness index (as well as LAI) derived from ground-based instrumentation into the ISBA-A-gs model (Interaction between Soil Biosphere and Atmosphere - with CO_2 dynamics). They mainly looked at the improved estimates of root zone soil moisture and LAI but provided a brief discussion on the effect of data assimilation on the model CO_2 fluxes, reporting a decrease in the RMSE between observed and modelled NEE of 5%.

Ghent et al. (2011) assimilated satellite-derived LST into the land surface model JULES (Joint UK Land Environment Simulator). They examine the improvement in soil moisture model estimates after the assimilation using satellite-derived soil moisture from the ERS Scatterometer,

showing how EO data can also be useful in validating models as well as for assimilation. They show the RMSE between the model and the satellite-derived estimates of soil moisture are 27.4 and 32.2% lower for West and North Africa respectively. The assimilation results in a reduction in the mean daily evapotranspiration and NPP but the reduction in the uncertainty of these estimates is not quantified.

Other studies which present results from satellite soil moisture assimilation with a land surface model include *Pathmathevan et al.* (2003), *Yang et al.* (2007c) and *Qin et al.* (2009). Again, they only look at the soil moisture, water balance and/or the energy balance and don't go further to comment on the impact on C fluxes. This coupled effect should be considered in the near future if full use of satellite-based LST and soil moisture observations is to made.

2.6.3 Energy balance and hydrological model data assimilation

Examples of studies using satellite based estimates of LST and soil moisture to improve models of the energy balance and hydrological cycle in a data assimilation framework are briefly summarised. Those studies which have attempted to use these observations to improve model estimates of C flux in LSMs were detailed in the previous section.

Walker and Houser (2005) provide a review of hydrology-related data assimilation as does *Moradkhani* (2008). Many studies have looked at assimilating soil moisture observations into hydrological models. This includes soil-vegetation-atmosphere-transfer (SVAT) models (*Wigneron et al.*, 1999), conceptual rainfall-runoff models (*Crow et al.*, 2005; *Brocca et al.*, 2010), simple 1-d hydrological models (*Walker et al.*, 2001), and semi- to fully distributed catchment and watershed models (*Walker et al.*, 2002; *Reichle et al.*, 2007; *Yang et al.*, 2007a; *Pan et al.*, 2010; *Chen et al.*, 2011), as well as combinations of a catchment and SVAT model (e.g. the TOPMODEL - based Land Atmosphere Transfer Scheme (TOPLATS) - *Crow and E.F.Wood* (2003)). Many of these studies show the soil moisture observations help to correct for inaccurate precipitation inputs, which is a particular problem for reanalysis data. Several synthetic studies have also been carried out (e.g. (*Hoeben and Troch*, 2000; *Li et al.*, 2010).

As discussed in the previous section, whilst some soil moisture studies have been used to improve estimates of the energy balance or hydrology in existing land surface and terrestrial biosphere models, they have stopped short of assessing the impact on C flux estimates. Catchment-based hydrological models in the past decade or so are now being included in land surface models to provide a 2-dimensional modelling capability. These examples offer "proof-of-concept" studies for when soil moisture and LST are used in more complex land surface models.

2.7 Issues with data assimilation and model calibration

There has been a general move over time to produce more complex, physically-based models, with a corresponding increase in the number of parameters. This can lead to the problem of model "equifinality" (*Franks et al.*, 1997), where many combinations of the parameters of a model result in similar model outputs. In a calibration framework the model can display a degree of model equifinality if there is not enough information in the observations, or the priors (if a Bayesian method is used) to find a unique solution to the values of the parameters. The problem is therefore

"ill-posed". If the model calibration is ill-posed due to the high number of parameters, or the complex interactions between the parameters, more information has to be determined a priori (*Combal et al.*, 2002; *Wang et al.*, 2009; *Williams et al.*, 2009). Sensitivity analyses which determine the relative importance of the parameters can aide in determining a) to which parameters the model most sensitive, therefore which require calibration, and b) the interactions between the parameters (*Saltelli et al.*, 2006). This type of analysis should therefore be performed prior to a model calibration.

Chapter 3

Data and Methods

This chapter outlines the main tools used in this thesis. First the study site is described, and then the decisions made in choosing a peatland C flux model are summarised. Following this the CASA-CH_4 model formulation is outlined together with some assumptions that were made in coding up the model. The model parameters are then summarised, including the references used and decisions made in defining the default value (used as the "true" value in the OSSE experiments), and ranges of each parameter. After that the driving data are detailed and the source of the data is specified. Where the raw data required further processing a description of these steps is also provided. The model setup, including the spin-up period and the specific driving data used in the OSSE experiments is then detailed. Following this, a sensitivity analysis method is outlined and then the Bayesian inversion framework, used in the model calibration, is described. The OSSE method is then set out, including the experiments which will be performed and the metrics used to evaluate the results. Finally the real observations that are used to constrain the CASA-CH_4 model for the Lake Vyrnwy site in Chapter 9, are described.

3.1 Study Area

The study site is an upland blanket peatland site on the RSPB Lake Vyrnwy Reserve in the Berwyn Special Area of Conservation (SAC), North Wales (52.8^{o}N, 3.5^{o}W). his site was used because of the availability of C flux data. However the site is very representative of UK peatlands, which in total cover about 8% of the UK land surface (*Bragg and Tallis*, 2001). The British Isles contains 10-15% of the world's blanket peat (*Tallis*, 1997). The land is mainly used for sheep grazing and the vegetation forms a heterogeneous landscape of patches of *Calluna vulgaris* (heather), *Carex* sp. (sedge), *Molinia* sp. (grass), *Sphagnum* sp. (moss) and *Juncus* sp. (rush) patches. Recent management practices (past 5 years) include the blocking of grips and heather mowing. Figure 9.1 shows the test site with the paired catchments set up to test the impact of management on the area. This management is being carried out as part of the EU-LIFE Active Blanket Bogs in Wales Project (www.blanketbogswales.org).

Table 3.1 provides a summary of the ground-based data that were available at the Lake Vyrnwy site. These are detailed further later in this chapter in Section 3.8, together with satellite-derived soil moisture data which cover this location for the time period studied (2009).

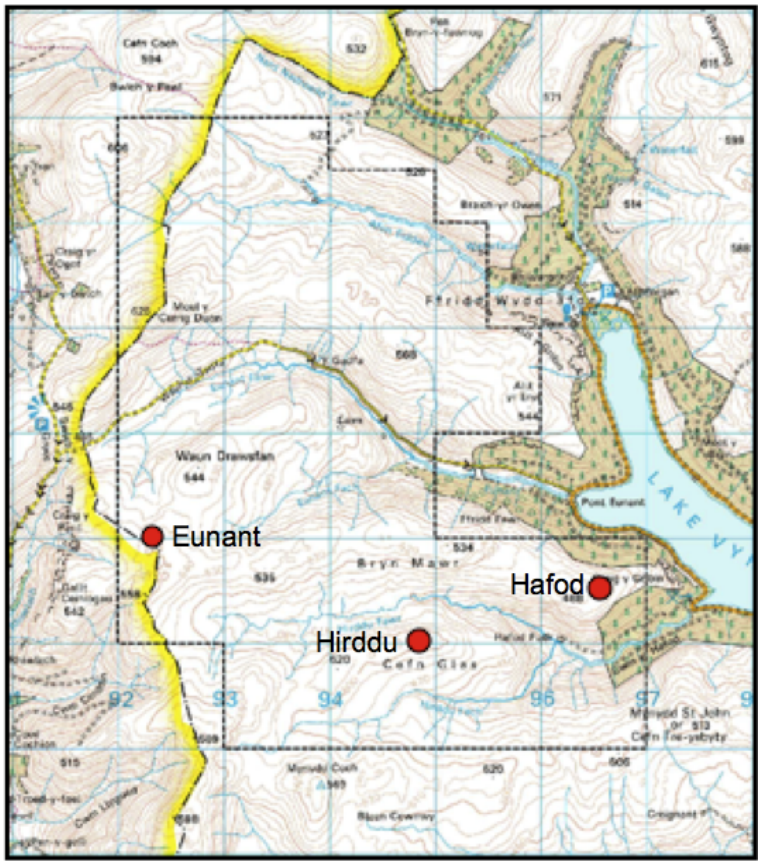

Figure 3.1: Map of the RSPB Lake Vyrnwy Reserve site and the management set-up. Red circles show the locations of the meteorological stations and ground-based CH_4 flux measurements (Section 3.3.6 and Chapter 9).

Data	Method	Date of collection
CH_4 flux	Chamber	2009 (monthly)
Total CO_2 respiration	Chamber	2009 (monthly)
NEP	eddy covariance flux tower	(only four dates processed so far)
Soil moisture	theta probe	2009, 2010 (19 dates in months of May-July)
Air temp.	weather station	2009 (hourly)
Solar radiation	weather station	2009 (hourly)
Precipitation	weather station	2009 (hourly)

Table 3.1: Table summarising the ground-based data which were available at the Lake Vyrnwy site.

3.2 Choice of model

The aim of this thesis is to test a combined observation - modelling framework and to investigate how observations can be used to improve and better understand a model. The task of using observations to constrain models is not easy. More complex models necessarily have more parameters which require calibration and this in turn makes the task of data assimilation quite difficult. Therefore the choice of model is directed by the requirement of the simplest possible model of CO_2 and CH_4 dynamics that allows the desired level of process understanding and represents the main factors which control the C fluxes. This is so the results of the combined observation - modelling experiments can be easily interpreted and understood, and not lost in the complexity of a larger model at this stage.

The CASA-CH_4 model (briefly described in Chapter 2 Section 2.2.2) was chosen to model the CO_2 and CH_4 fluxes at this site, because from the reviews of the peatland C models, it was the simplest, yet fullest description of CO_2 and CH_4 dynamics (for example it included a representation of all three CH_4 transport pathways). It also required the fewest driving data. Most of the other models, whilst using a similar approach to modelling the partitioning of C decomposition into CO_2 and CH_4 flux based on water table depth, required the water table depth as an input. Such data were not available at the timescales required at the study site. A larger land surface model could have been used, but again this would have added to the complexity. Most of the other peatland C flux models had many more site-specific parameters which would require calibration and some papers detailing the model descriptions failed to outline the derivation of all the parameters. Some models contained representations of processes that could not readily be measured and therefore were too complex, for example *Kettunen* (2003) modelled the populations of methanotrophic and methanogenic bacteria in the soil, which. Others did not include model formulations which could be easily compared to any observations (*Cao et al.*, 1996; *Segers and Leffelaar*, 2001).

The final deciding factor in choosing a model was the availability of the code. None of the model codes were available which meant the model had to be coded up. A simpler model suited that demand much better than some of the more complex models which either didn't have a complete description in the literature or were too complex (e.g. *Kettunen* (2003) model the methanogenic and methanotrophic bacteria populations) to be considered. *Potter et al.* (1993) and *Potter* (1997) provided a near full description of the model, and where detail was lacking some basic assumptions were made as detailed below.

The fact that the CASA-CH_4 model uses EO data as a driver demonstrates another use of EO data in improving model estimates. The landscape at this site is extremely heterogeneous. Some of the more complex models would require many parameters to model the C assimilation into the system. In addition, unless a DVM such as LPJ-WHyMe were used, the impact of management practices at the site could not be effectively modelled. A satellite-based dataset to prescribe the vegetation phenology gets round these complexities. This is a relatively simple approach. Further work could compare this model formulation to other more complicated biogeochemical representations of C assimilation. Model comparisons, whilst interesting, were not the focus of this thesis however, and there is not enough data on C assimilation (GPP, NPP) available from the study site to do so.

3.3 The CASA-CH_4 model

The original Carnegie-Ames-Stanford approach (CASA) biosphere model (*Potter et al.*, 1993) was developed with the purpose of simulating global terrestrial ecosystem production and soil microbial respiration using monthly satellite, climatological and soil attribute data as drivers. This was further modified by *Potter* (1997) to model daily methane production and emission from wetlands. The combined model is described below and a schematic of the model is shown in Figure 3.2.

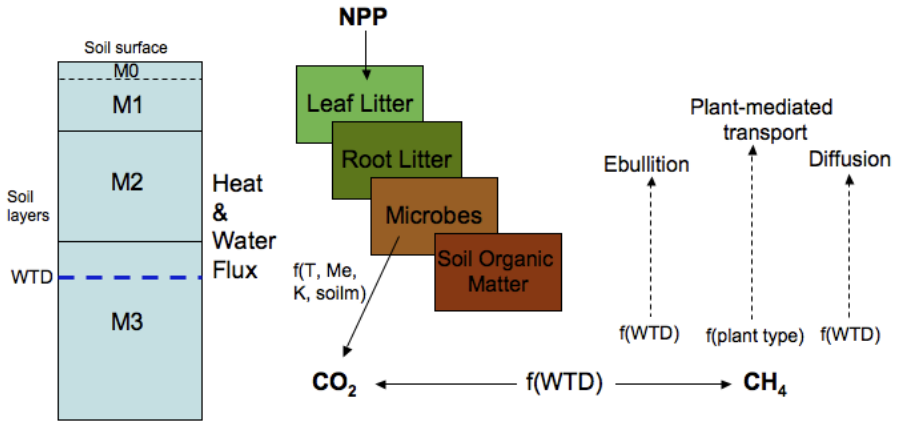

Figure 3.2: A schematic of the CASA-CH4 model (following *Potter* (1997)).

3.3.1 Net Primary Production

Net primary production (NPP) is modelled as a product of the intercepted photosynthetically active radiation (IPAR) and a light use efficiency term (LUE) that is scaled by temperature (T) and moisture (W) stress terms, (*Potter et al.*, 1993):

$$NPP(x,t) = IPAR(x,t)\, LUE\, T(x,t)\, W(x,t) \tag{3.1}$$

where x and t are the location and time respectively. IPAR is the product of the total solar radiation (SOL) incident on the grid cell and the fraction of PAR (FPAR) intercepted by green vegetation. A factor of 0.5 accounts for the fact that approximately half the radiation is in the PAR waveband (0.4μm - 0.7μm),

$$IPAR(x,t) = SOL(x,t)\, FPAR(x,t)\, 0.5 \tag{3.2}$$

FPAR is calculated as a linear function of the simple ratio (SR), originally developed for the Advanced Very High Resolution Radiometer (AVHRR) by *Sellers et al.* (1996):

$$FPAR(x,t) = min[\frac{SR(x,t)}{(SR_{max} - SR_{min})} - \frac{SR_{min}}{(SR_{max} - SR_{min})}, 0.95], \tag{3.3}$$

where SR is a function of the normalised difference vegetation index (NDVI), (equation 3.4),

$$SR(x,t) = \frac{1 + NDVI(x,t)}{1 - NDVI(x,t)} \tag{3.4}$$

NDVI identifies vegetated amount and dynamics by exploiting the large difference in the red (RED) and near-infrared (NIR) reflectances of green leaves compared with other materials.

$$NDVI = \frac{NIR - RED}{NIR + RED} \tag{3.5}$$

NDVI is calculated from the surface reflectance of the RED and NIR bands of a satellite (e.g. the Moderate Resolution Imaging Spectroradiometer, MODIS) before being input into the model. SR_{min} in equation 3.3 represents the SR for unvegetated areas and is set to 1.08 in *Potter et al.* (1993). SR_{max} is an approximation of the value at which all radiation is intercepted and is designed to correct for effects of canopy architecture and residual cloud contamination. An upper limit of 0.95 for FPAR has been included to take into consideration the finite limit of leaf area.
The temperature stress scalar (equation 3.1) is the product of two terms, $T_{\epsilon 1}$ and $T_{\epsilon 2}$. $T_{\epsilon 1}$ depresses the light use efficiency term (ϵ) at very high and low temperatures and when the temperature is above or below the optimum temperature (T_{opt}). T_{opt} is the optimum growing temperature and is defined as the mean daily temperature in the month in which the NDVI reaches a maximum for the year. This assumes that plant growth is adapted to local ambient conditions.

$$T_{\epsilon 1}(x,t) = 0.8 + 0.02T_{opt}(x) - 0.0005(T_{opt}(x))^2 \tag{3.6}$$

This scalar represents the fact that plants in very cold environments have very low growth rates and plants in very hot environments have high growth rates but are limited in their efficiency by simultaneous high rates of respiration (*Potter et al.*, 1993).
The $T_{\epsilon 2}$ term is incorporated in the temperature stress scalar to account for the reduced efficiency of the light utilisation of the plant when the temperature is not T_{opt}.

$$T_{\epsilon 2}(x,t) = 1.1814/(1 + e^{(0.2(T_{opt}(x)-10-T_{air}(x,t)))})(1 + e^{(0.3(-T_{opt}(x)-10+T_{air}(x,t)))}) \tag{3.7}$$

The water stress scalar on net primary production is a function of the estimated and potential evapotranspiration (EET and PET respectively), which are calculated in the soil moisture submodel, (3.3.4).

$$W_{\epsilon}(x,t) = \frac{1}{2}[1 + \frac{EET(x,t)}{PET(x,t)}] \tag{3.8}$$

This scalar depresses the efficiency of the plant photosynthesis in drier environments. If the temperatures are below zero, snow accumulates on the surface (see the soil moisture submodel) and therefore the W_{ϵ} from the previous timestep is used.

3.3.2 Litter allocation and soil carbon flux

The CASA model contains litter, microbial and soil organic (slow and old) carbon pools, (*Potter et al.*, 1993). The model formulation is based on the CENTURY soil C and N dynamics model (*Parton et al.*, 1987). Organic soils were assigned to the coarse/medium Food and Agriculture Organisation (FAO) texture class (*Potter et al.*, 1993). Annual NPP (NPP_{ann}) is distributed over

the year as an input to the soil carbon submodel in the form of litterfall (LT_{LAI}) which is a function of changes in leaf area index (LAI).

$$LT_{LAI}(x,t) = NPP_{ann}(x)(LT_{con}(x) + LT_{var}(x,t)), \tag{3.9}$$

where $$LT_{con}(x) = (LAI_{min}(x)/LAI_{av}(x)) \ / \ n$$

and $$LT_{var}(x,t) = [\Delta LAI(x,t)/\Sigma\Delta LAI(x,t)][1 - (LAI_{min}(x)/LAI_{av}(x))]$$

where n is the number of timesteps in one year and LAI_{min} and LAI_{av} are the minimum and average LAI values for that year respectively. The litterfall term is a product of constant and varying fractions of NPP. A fraction of NPP is distributed evenly throughout the year (LT_{con}), and a fraction unevenly (LT_{var}), depending on the phenological cycle of the plants in question. The LT_{var} term is therefore calculated as a function of the sum of all the timesteps where there is a decrease in LAI. For completely constant evergreen ecosystems the LT_{var} term is zero for all timesteps and for ecosystems which contain completely deciduous vegetation the LT_{con} term is zero (*Potter et al.*, 1993).

The litterfall fraction is allocated evenly between leaf, roots and wood plant tissue (or only between leaf and roots if the plant functional type (PFT) is non-wood). For the leaf and root pools the carbon is then partitioned between the metabolic and structural fractions dependent upon the lignin-to-nitrogen ratio (LN) according to the relationship:

$$MT_f(x,t) = 0.85 - (0.018\, LN(x,t)) \tag{3.10}$$

where MT_f is the metabolic fraction. *Potter and Klooster* (1997) fixed the lignin-to-nitrogen ratio in the CASA model depending on ecosystem type. The same approach was adopted in this study; the ratio is a fixed parameter that can be calibrated. This can be updated by adding nitrogen (N) dynamics into the model.

All the lignin residue resides in the structural pool (*Potter et al.*, 1993). The lignin has an impact on the transfers of C from the leaf and root litter structural pools to the soil C pools *Parton et al.* (1993). Firstly the fraction of lignin in the litter structural pool is determined from the vegetation lignin fraction, and then the effect on the C transfers is calculated as per:

$$structural\,lignin', fraction = ((vegegtation\,lignin\,fraction * 0.65)/0.45)/(1 - metabolic\,fraction) \tag{3.11}$$

$$lignin\,effect = exp^{-3 * structural\,lignin\,fraction} \tag{3.12}$$

The lignin fraction for each vegetation class is given in *Potter et al.* (1993). An average of the values for the perennial grasslands and broadleaf shrub with grass ecosystems was therefore used here (0.15).

The cycling of carbon in the soil is shown in Figure 3.3. Transfer of carbon from the litter to the microbial pools and microbial to the soil organic pools is governed by the equation:

$$C_{trans}(x,t)_i = C(x,t)_i\, k_i\, W_s(x,t)\, T_s(x,t)\, M_e \tag{3.13}$$

where C is the carbon content of pool i, k is the maximum decay rate constant for pool i, W_s

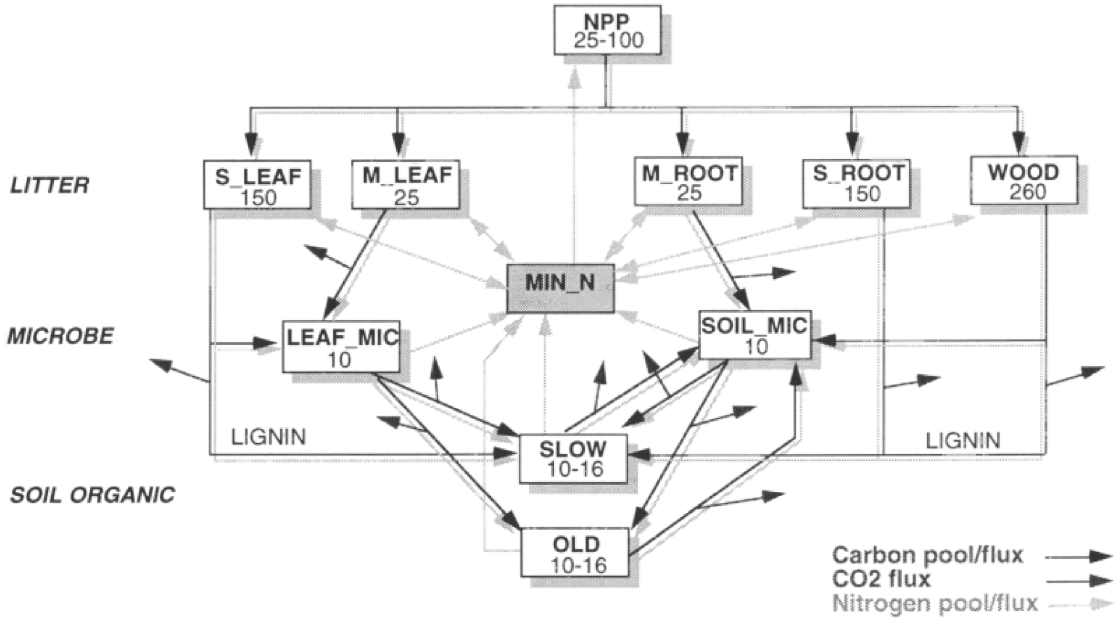

Figure 3.3: Schematic diagram of the ecosystem carbon model pools and fluxes, *Potter et al.* (1993). Dark arrows connecting boxes are the carbon transfers between pools with associated CO_2 loss as a result of decomposition (shorter dark arrows). The values in the boxes are the C:N ratios, which would be used in the full CENTURY model which includes N dynamics.

and T_s are scalars for the effect of soil moisture and temperature on decomposition in pool i respectively and M_e is carbon assimilation efficiency of the microbes. The amount of CO_2 lost due to microbial decomposition during each transfer between the carbon pools is calculated using the above equation, with (1-M_e) in place of M_e.
The temperature scalar in the decomposition equation is modelled as a Q_{10} response function (*Potter et al.*, 1993), i.e.

$$T_s(x,t) = Q_{10}^{((T_{air}(x,t)-30)/10)} \tag{3.14}$$

where T(x,t) is the air temperature and Q_{10} is the increase in soil biological activity with a 10^oC rise in soil temperature. *Potter et al.* (2001) recommend using a different value for the C transfers from litter and the soil. Therefore two different parameters Q10 litter (Q10_l) and Q10 for the soil (Q10_s) are included as parameters in the model.

The scalar for the effect of soil moisture stress on decomposition was modeled as in *Potter* (1997). This was modified from the original formulation in *Potter et al.* (1993) to account for reduced decomposition rates in poorly-drained organic soils following the algorithms of *Doran et al.* (1990). The scalar is a function of water-filled pore space or volumetric soil water content (Θ_w). The equation for medium-to-fine textured soils is used:

$$W_s(x,t) = 5.63\,\Theta_w - 4.64\,\Theta_w^2 - 0.745 \tag{3.15}$$

In this interpretation of the decay rate constant for each pool, the model values were taken from *Parton et al.* (1993) apart from the wood pool which was taken from *Potter et al.* (1993). M_e is set to 0.45 for most soil carbon pool transfers (*Potter et al.*, 1993). The two exceptions are i) the transfer of lignin from the structural and wood pools straight to the slow pool with a M_e of 0.7 (*Parton et al.* (1987); *Potter et al.* (1993)) and ii) the carbon assimilation efficiency of microbes for transfers from the soil microbial (active) pools to the slow pool. The latter is a function of silt plus clay (SC) content, which for organic soils assigned to the coarse/medium texture class. The equation for fraction of C lost as CO_2 from soil microbes during the transfer to the slow pool (i.e. 1-Me) is:

$$SLOW_f = 0.85 - 0.68\,(SC), \tag{3.16}$$

therefore the M_e for this transfer is set to 0.422. The carbon content of each pool is updated according to the amount of carbon transferred in or out of that pool for each timestep. The net amount of CO_2 lost during decomposition (soil respiration) is used to calculate the amount of methane produced, (section 3.3.3).

3.3.3 Methane submodel

Methane production

Methane production is estimated from the CO_2:CH_4 microbial production ratio which is in turn a function of water table depth (WTD). This is a hypothesised relationship based on experimental studies by *Moore and Knowles* (1989) and *Funk et al.* (1994) for water table depth intervals of 5cm and a range ±20cm, with the soil surface at 0cm and a positive value of water table depth above the surface.

Methane transport and emission

As outlined in Chapter 2 Section 2.1.2, methane emission from the soil profile occurs through 3 main pathways: diffusion though the soil column, ebullition and vascular plant-mediated transport.The methane sub-model of *Potter* (1997) implemented these processes as functions of CH_4 production, water table depth and plant-type.

If the water table depth is below the surface, gaseous diffusion of methane produced beneath the water table through the unsaturated soil column will result in oxidation of some or all of the methane. *Potter* (1997) simulated diffusion empirically based on a hypothesised relationship between potential methane oxidation and water table depth that is derived from data reported by *Sundh et al.* (1995). All the methane is oxidised if the water table depth is > -20cm and no methane oxidation occurs if the water table is at or above the surface.

Ebullition is the release of methane gas bubbles that have formed beneath the water table. It occurs when the partial pressure of the gases in solution exceeds the hydrostatic pressure of the water column (*Potter*, 1997). *Potter* (1997) used a declining water table as a proxy for a reduction in hydrostatic pressure, based on studies by *Moore et al.* (1990) and *Shurpali et al.* (1993) and summarised in *Bartlett and Harriss* (1993). Therefore an ebullition event occurs in the model when the water table drops by 1cm d^{-1} over four consecutive days. All the methane in the saturated zone beneath the water table is released during the event.

Following studies of *Chanton and Dacey* (1991), *Morrissey and Livingston* (1992) and *Schimel* (1995) plant-mediated transport through vascular plants took precedence over the other methods of methane transport in the *Potter* (1997) model, with the fraction emitted dependent upon the plant types of the *Schutz et al.* (1991) grouping scheme. For the purposes of modelling upland peat ecosystems the important groups are i) freshwater rooted with soft epiderm, including species such as *Carex, Eriophorum* and *Typha*, and ii) freshwater rooted with hard epiderm, including *Juncus, Cladium, Glyceria* and *Scirpius*. No methane is emitted via this pathway for non-vascular plants.

3.3.4 Hydrology and Temperature submodel

In the modified version of the CASA model for methane, *Potter* (1997) divided the soil profile into 3 layers: surface organic matter (M_1, 0-0.3m), topsoil (M_2, 0.3-1.0m) and subsoil to rooting depth (M_3, 1.0m). This allows the scalars for the effect of moisture and temperature on decomposition to represent the conditions at the depth of each carbon transfer. The temperature and soil moisture amount for the surface organic matter are used to calculate the scalars for decomposition of the litter pools, and decomposition of the soil carbon pools use the topsoil values. The soil moisture and temperature are uniform within each soil layer, as is the porosity.

Hydrology

The soil moisture storage was modelled in *Potter et al.* (1993) as a function of inputs of precipitation or volumetric percolation minus outputs of evapotranspiration for each layer, scaled by a relative drying rate (RDR) term if the precipitation (PPT) is less than the potential evapotranspiration (PET), equation 3.18.

$$
\begin{aligned}
SOILM(x,t) &= SOILM(x,t-1) - \\
&\quad RDR(PET(x,t) - PPT(x,t)) \\
&\quad for\ PPT(x,t) < PET(x,t) \qquad (3.17)
\end{aligned}
$$

(3.18)

$$
\begin{aligned}
SOILM(x,t) &= SOILM\,(x,t-1) + \\
&\quad PPT(x,t) - PET(x,t) \\
&\quad forPPT(x,t) \geq PET(x,t) \qquad (3.19)
\end{aligned}
$$

PPT is the average amount of precipitation for that timestep. Potential evapotranspiration (PET) is modelled using a modified version of the *Priestly and Taylor* (1972) method, described in *Bonan* (1989). The algorithm uses inputs of air temperature (^oC) and solar radiation (R_s - cal cm^{-2} d^{-1}), equation 3.20.

$$PET(x,t) = a\,(T_s + b)\,R_s \qquad (3.20)$$

where T_s is the temperature at the litter-soil surface following empirical relationships in *Yin and Arp* (1993); *Potter* (1997). The calculation of T_s is detailed in equation 3.29. The constants a and b are functions of saturation vapour pressure and elevation (*Jensen and Haise* (1963); *Jensen* (1973)).

$$a = [38 - (2E\ /\ 305) + (380\ /\ (e_2 - e_1))]^{-1} \qquad (3.21)$$

$$b = 2.5 + 0.14\,(e_2 - e_1) + E\ /\ 550 \qquad (3.22)$$

where E is elevation in metres and e_1 and e_2 are the saturation vapour pressures (mbar) during the mean maximum and mean minimum daily temperature (T_{air}) of the warmest month of the year respectively, using an approximation from *Bosen* (1960):

$$e_1 = 33.8639\,[\,(\,0.00738\,T_{air\_max} + 0.8072\,)^8 - 0.000019\,|\,1.8\,T_{air\_max} + 48\,|\,+ 0.001316\,] \qquad (3.23)$$

$$e_2 = 33.8639\,[\,(\,0.00738\,T_{air\_min} + 0.8072\,)^8 - 0.000019\,|\,1.8\,T_{air\_min} + 48\,|\,+ 0.001316\,] \qquad (3.24)$$

Potter (1997) noted that conversion of PET to units of cm d^{-1} can be achieved by dividing by the latent heat of vapourisation and that soil surface temperature could replace air temperature in equation 3.20.

The relative drying rate in equation 3.18 was designed to simulate a reduced rate of soil drying with decreasing soil moisture content. *Potter et al.* (1993) used a transformation of the relationship between soil water potential and volumetric water content (*Saxton et al.*, 1986) to derive the RDR scalar.

$$RDR(x,t) = (1 + a)\ /\ (1 + a\,\Theta^b) \qquad (3.25)$$

The constants a and b are texture-dependent empirical coefficients (*Potter et al.*, 1993) and are calculated from equations 5 and 6 of *Saxton et al.* (1986) using the coarse/medium clay and sand percentages given in *Potter et al.* (1993). Θ is the volumetric water content, which is the ratio of the volume of water to the total volume of the soil column.
The estimated evapotranspiration (EET) used in the NPP soil moisture scalar is calculated using parameters defined above and the soil moisture storage at the previous timestep. If the precipitation is greater than the potential evapotranspiration then EET is set to PET, else it is based on the amount of water available for evapotranspiration.

$$\begin{aligned} EET(x,t) &= min[\, PPT\,(x,t) + RDR(PET(x,t) - PPT(x,t))\,], \\ &\quad [\, PPT(x,t) - (SOILM(x,t-1) - WPT(x))\,] \\ &\quad for\ PPT(x,t) < PET(x,t) \end{aligned} \tag{3.26}$$

$$\begin{aligned} EET(x,t) &= PET(x,t) \\ &\quad for\ PPT(x,t) \geq PET(x,t) \end{aligned} \tag{3.27}$$

Note therefore that equations 3.18 and 3.19 can be written as:

$$SOILM(x,t) = SOILM(x,t-1) + (PPT(x,t) - EET(x,t)) \tag{3.28}$$

Potter (1997) assumes a "three-layered bucket model" in that the top layer fills up to water holding capacity (pore saturation) before excess water percolates through to next layer down in the soil profile and so on. Water accumulates in a ponded surface layer (M_0) if all the layers exceed their pore capacity. An approximate water table depth is modelled as the change in net soil water balance (*Potter*, 1997).

Temperature

As stated earlier, *Potter* (1997) recommended using empirical relationships from *Yin and Arp* (1993) to derive the temperature at the litter-soil surface. This is calculated as follows:

$$T_s = T_{air} + [(-0.11 + 0.96T_{air} - 0.00008T_{air}^3) - T_{air}]\, ln[1 + min(LAI, LAI_{max})] \,/\, ln(1 + LAI_{max}) \tag{3.29}$$

T_s was used to force the upper boundary of the soil temperature profile, as detailed below.

The soil temperature profile was calculated using Fick's Laws of Diffusion (*Potter*, 1997). The equation calculates the amount of heat conducted across a unit area (δz) per timestep (δt):

$$\frac{\delta T}{\delta t} = \frac{\delta^2 T}{\delta z^2}\left(\frac{K}{C}\right) \tag{3.30}$$

where K is the soil thermal conductivity and C the thermal diffusivity. K and C are a function of soil moisture content.

3.3.5 Model assumptions

It was assumed that the PEM approach for calculating the C assimilation into the soil (equation 3.1 calculates GPP and not NPP, following other PEM models (*McCallum et al.*, 2010). Therefore an "autotrophic respiration parameter" was added to the model to determine the fraction of GPP that was respired as CO_2. This was subtracted from the amount of C calculated in equation 3.1 in order to provide an estimate of NPP.

Potter (1997) does not detail how the plant-mediated transport process worked in the model, particularly with reference to how much plant mediated transport dominated over the other methods of methane transport and whether there was a difference in plant-mediated flux between the two vascular plant types of *Schutz et al.* (1991). Therefore the following additional information was used to implement this component of the model.
Many studies (*Sebacher et al.*, 1985; *Chanton and Dacey*, 1991; *Whiting and Chanton*, 1992; *Morrissey and Livingston*, 1992; *Schimel*, 1995; *Shannon et al.*, 1996; *MacDonald et al.*, 1998) have reported that up to 90% of methane emission in wetlands is via plant-mediated transport through the aerenchymous tissue of species in the the first plant group of *Schutz et al.* (1991). However, only *Sebacher et al.* (1985) presented a study of plant-mediated transport from the second plant group (freshwater rooted with hard epiderm) of *Schutz et al.* (1991). The methane emitted from *Juncus* in the *Sebacher et al.* (1985) study is 4.1% of the average amount of methane emitted by the first group. Taking the reported average percent of the total methane flux emitted by *Carex* and *Eriophorum* in *Schimel* (1995) of 75%, the fraction of methane emitted through plant-mediated transport by the soft epiderm plant group was therefore set to 0.75 and the value for the hard epiderm group to 0.0375.

The diffusion equation for soil temperature profile was solved using a Crank-Nicholson scheme (*Xi*, 2008) as the method for doing so was not specified in *Potter* (1997). This uses weighted contributions of the temperature in the layers above and below and at the previous and current timestep to calculate the value for that layer for the current timestep (*Stroud and Booth*, 2003). The thermal diffusivity, C, in equation 3.30 is calculated for each layer in the soil profile as a linear sum of the volumetric heat capacities of soil (C_s, 1.26 x10^6Jm^{-3}K^{-1}), water (C_w, 4.2 x10^6Jm^{-3}K^{-1}) and air (C_a, 1004 Jm^{-3}K^{-1}), weighted by volumetric soil water content (*Xi*, 2008), e.g.

$$C(\Theta_w) = \Theta_w C_w + (1 - \Theta_s) C_s + (\Theta_s - \Theta_w) C_a \tag{3.31}$$

where Θ_s is the maximum volumetric soil water content (porosity). Θ_w(x, t) is calculated in the hydrology submodel and used in the soil temperature calculation. The thermal conductivity, K, is also calculated for each layer in the soil profile and has the form:

$$K(\Theta_w) = 420\, e^{-(2.7+Pf)} \qquad Pf \leq 5.1 \tag{3.32}$$

$$K(\Theta_w) = 0.1774 \qquad Pf > 5.1 \tag{3.33}$$

following *Xi* (2008). Pf is a power function derived in *Cosby et al.* (1984) relating Ψ_s, the

saturated soil potential (suction), and Θ (*Xi*, 2008),

$$Pf = log\,(\Psi_s\,(\Theta_s\,/\,\Theta_w)^b) \tag{3.34}$$

where b is the slope log Ψ_s versus log $(\Theta_s/\Theta_w)^b$) regression. Ψ_s, Θ_s and b depend on the soil texture. *Cosby et al.* (1984) used the United States Department of Agriculture (USDA) soil texture classification which differs from the FAO classification used by *Potter et al.* (1993). Based on the sand, clay and silt percentages of the coarse/medium FAO texture class to which organic soils belong, the "sandy clay loam" USDA texture class values of Ψ_s and b in *Cosby et al.* (1984) were used in the initial model runs. In *Xi* (2008) the upper boundary was forced with air temperature. Here the model was forced at the upper boundary with T_s, as detailed above.

Potter (1997) specified that evapotranspiration outputs would be subtracted from the water inputs for each soil layer. However it was not suggested how the total amount of PET, already calculated using equation 3.20 should be divided up between the layers. To account for this, the PET was divided up so equal amounts were subtracted from the top layers (down to a depth of 1m - as the roots of some vegetation types such as sedge and juncus will extend to this depth). As the layers get thicker with depth, this means a smaller proportion of the PET will be subtracted from each layer.

3.3.6 Driving data

Inputs to the model include (daily or monthly) climate drivers for solar radiation (Wm^{-2}), air temperature (^oC) and precipitation amount (mm) from meteorological station data, the Normalised Difference Vegetation Index (NDVI), derived from satellite optical reflectance data, as a proxy for vegetation amount and dynamics, and finally fractional plant cover data sets derived from a classification of airborne imagery.

Meteorological data

Meteorological data were collected at three weather stations (WS-GP1, Delta-T Devices, Cambridge, UK) located at (OSGB coordinates) SH 292336 322015 ("Eunant" location), SH 296619 321523 ("Hafod" location) and SH 294839 321011 ("Hirddu" location) at the Lake Vyrnwy site during 2009 (Figure 9.1). Air temperature and relative humidity were measured using a combined sensor (RHT2nl-CA) which was positioned 2m above the ground. Precipitation was measured with a rain gauge (RG2+WS-CA), and solar radiation was measured in the 300 and 3000nm range (D-PYRPA-CA).

Satellite-derived NDVI data

Surface reflectance data collected by the Moderate Resolution Imaging Spectrometer (MODIS) instrument on board NASA's Terra and Aqua satellites were used to calculate the NDVI timeseries. The NDVI values were calculated from the red and NIR reflectance bands of the Nadir BRDF-Adjusted Reflectance 16-Day L3 Global 500m product (MCD43A4) with quality flags derived

from the BRDF-Albedo product (MCD43A2) (*Schaaf et al.*, 2002). MODIS data were used as the Nadir-adjusted reflectance product was available and easy to download. The two products were downloaded using the MODIS Python (http://www.python.org/) client, which is available through the MODIS web service (http://daac.ornl.gov/MODIS/MODIS-menu/modis_webservice.html). The client allows the user to download subset the MODIS tiles for certain products by date and location (pixel number or latitude and longitude).

The nadir BRDF-adjusted reflectance was used so as to eliminate any spurious data points that might result from angular effects due to changes in the illumination - viewing angle geometry. Only the "good" or "best" quality, full inversion data were used. Due to the presence of clouds relatively few data points could be retrieved over this site, therefore to derive a daily timeseries a spline was fitted to the data. Two different splines were tested for interpolation; a univariate spline a and B- spline, both using the Python Scipy (scientific tools for Python - http://www.scipy.org/) interpolation module.

A B-spline with a k value of 4 and an s value of 3 was chosen as the best fit to the data.

Vegetation classification

Fractional cover was derived from 25cm resolution aerial images collected in 2006 (Cowi Vexcel 2006, Nextmap) and were licensed for use through the Countryside Council for Wales (CCW). The fraction of each vegetation type (across the site) was calculated using a *maximum likelihood supervised classification* (*Mather*, 2004) in the ENVI image processing software (© ITT Visual Information Solutions). The outline is in conjunction with the edge of MODIS pixels that cover the site. It covers most of the peatland area to the west of Lake Vyrnwy but masks the surrounding mineral soils and forested regions. It also encompasses three separate catchments of the Lake Vyrnwy reservoir. Ground-truth data, used to "train" the maximum likelihood algorithm, were collected across the site in 2008-2010 using a Thales MobileMapper differential GPS handheld device, which had an accuracy of <2m, and the accompanying PocketGIS software. The coordinates of polygons depicting areas of homogeneous vegetation cover were taken and converted to shapefiles. The fractional cover of seven different cover types were derived in the classification: bracken, sedge, heather, grass, forest, road and juncus. Figures 3.4 and 3.6 shows the original RGB image and the classified image. A small subset (~2%) of the training pixels were used to validate the classification. The overall accuracy of the classification was 73% and 2.6% of the pixels remained unclassified. *The algorithm had the most difficulty identifying the sedge cover type. This is not surprising, as the sedge can appear very different even on the ground. It can be clumped into tufts or can have a very similar appearance in texture to grass. The landscape at the Lake Vyrnwy site is very heterogeneous. The length scales of change in vegetation type can be as small as a few metres. It was extremely difficult to find homogeneous patches of vegetation that were large enough to collect the coordinates for use as training and validation data. Ideally with more time, more ground-truth data would be collected and a higher resolution dataset would be used for the classification.* The classification was then split up into the MODIS pixel areas using the coordinates given by the MODIS Python client, and the fractional cover of each vegetation type was calculated for each pixel.

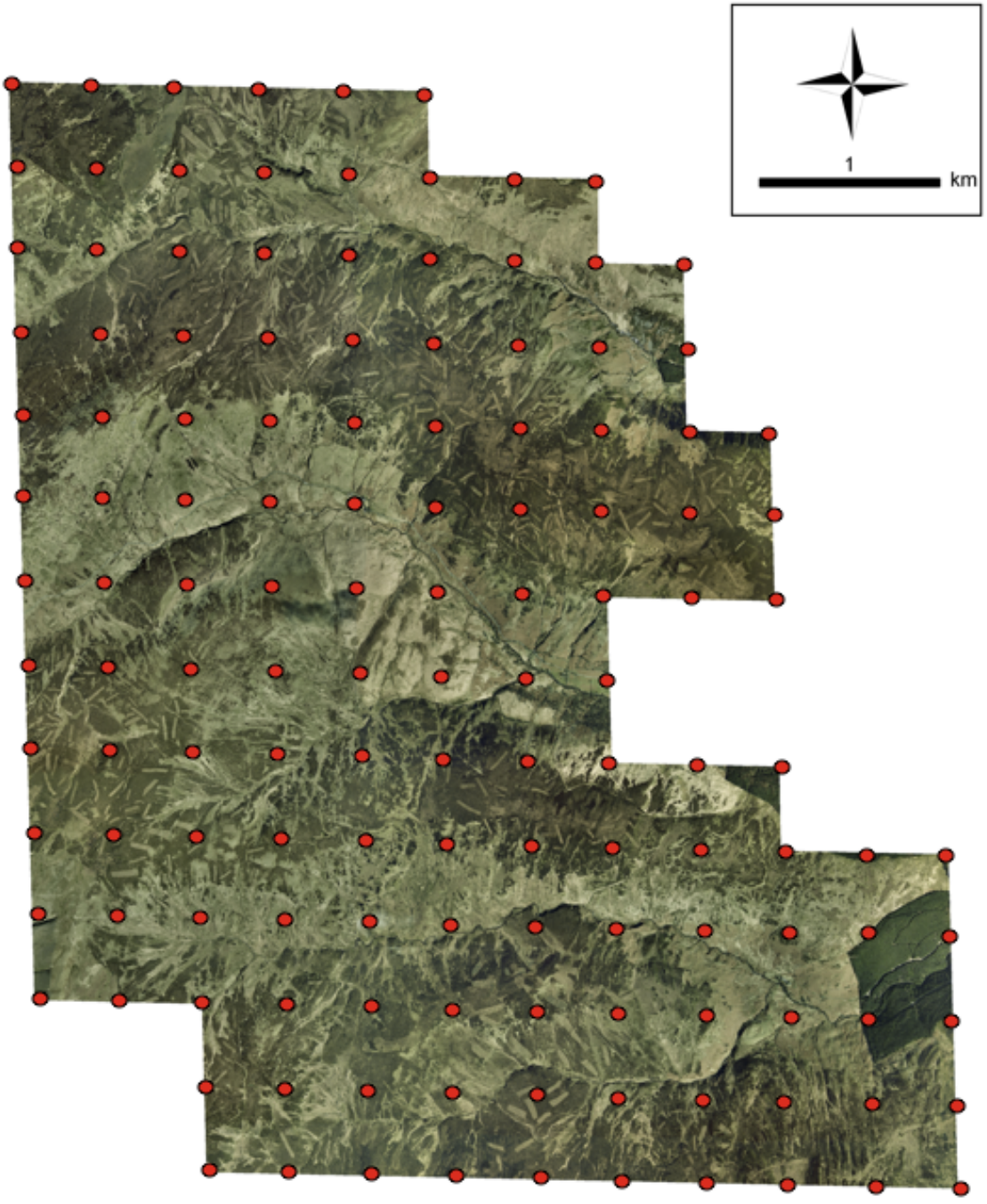

Figure 3.4: Original RGB aerial image (Red dots show the location of the MODIS pixels).

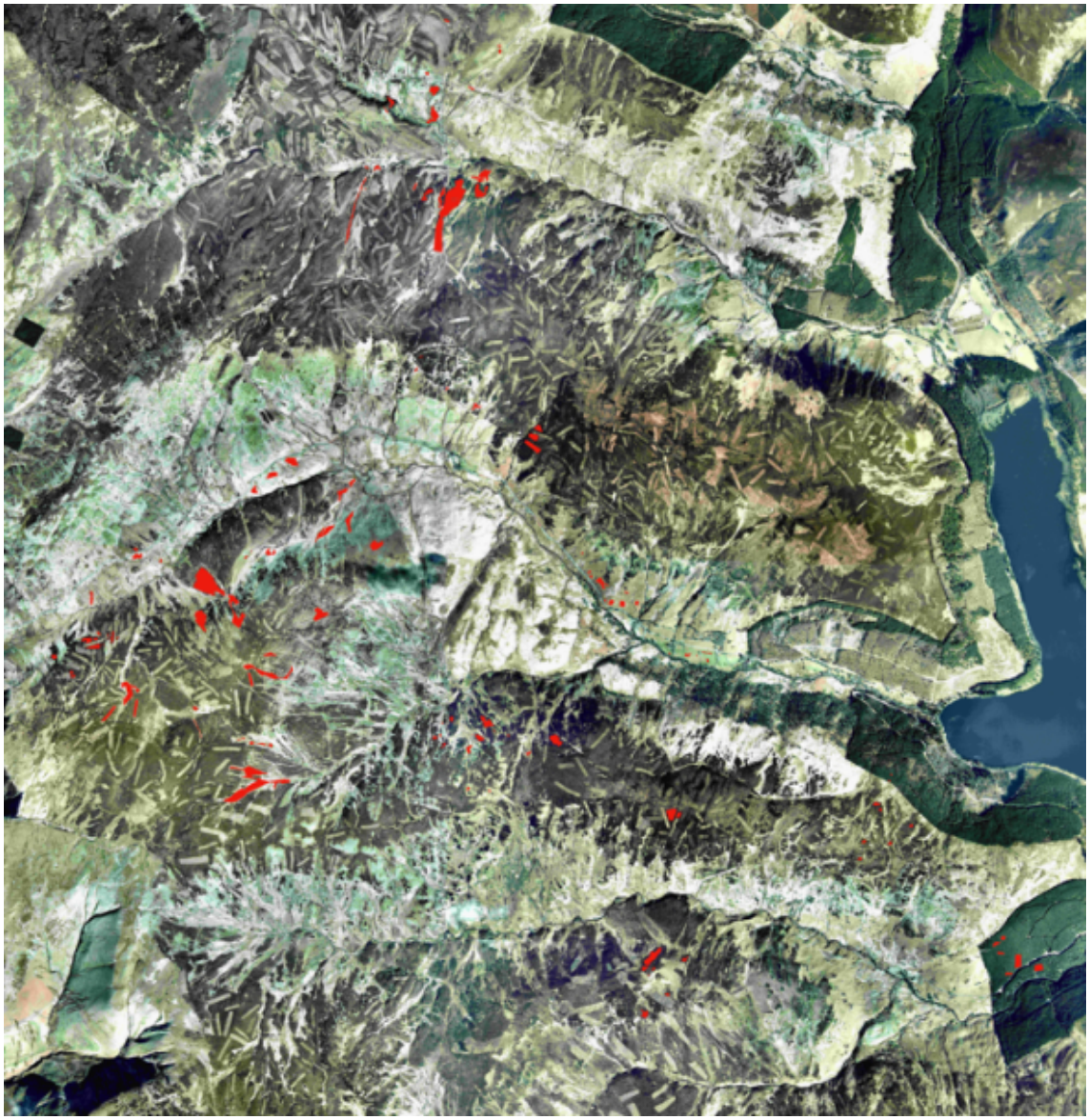

Figure 3.5: Location of the training pixels used in the classification shown in red.

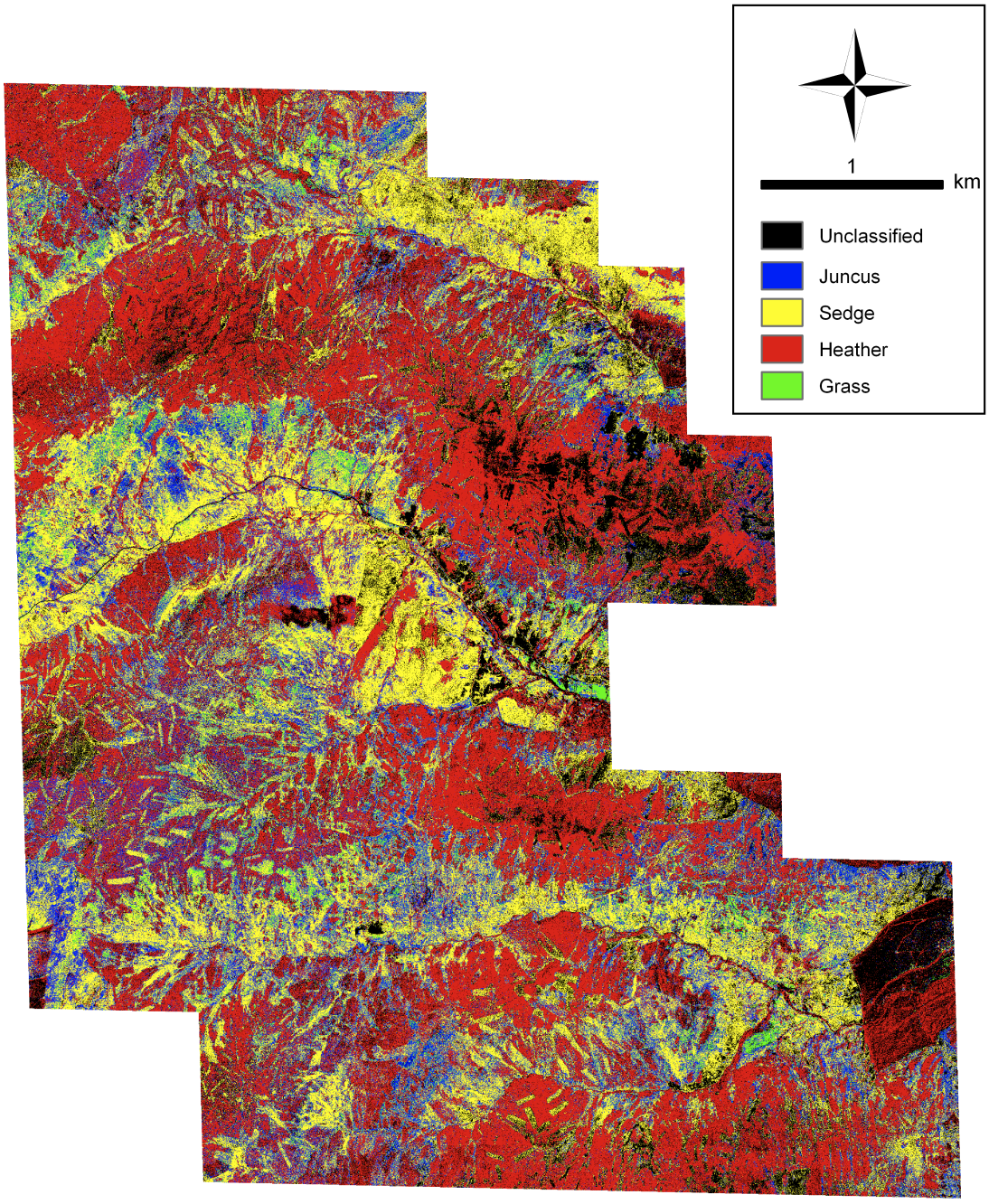

Figure 3.6: Maximum Likelihood Classification for the Vyrnwy site. (Colour codes of the classified vegetation types are listed in the key).

3.3.7 Model set-up

Each model grid-cell which contained the weather stations, with its respective driving data was spun-up for 1000 years, using the mean daily values of each model input from the previous five years (2003-2008), until the litter and soil C pools were stabilised. The weather stations were not set up at the Lake Vyrnwy site until the end of 2008, so the meteorological drivers were taken from a UK Meteorological Office MIDAS weather station located next to Lake Vyrnwy (grid reference 52.757^{o}N 3.46411^{o}W). The data were downloaded from the British Atmospheric Data Centre. The use of only five years worth of recent driving data is a limiting factor in the model calculations. However, as no data are available for the past 1000 years another source of data is required. In this study it was decided that meteorological data from a weather station close to the site would be better than reanalysis datasets as such data consistently underestimate the precipitation for this site. Using NDVI data will not reflect the vegetation phenology over the last 1000 years due to climate and land use change. Again it is difficult to quantify the uncertainty in these driving data, and it is recognised that this might introduce significant uncertainties into the C flux estimates. In addition as only three model grid-cells were spun-up due to time constraints, the spatial estimates of C fluxes of grid cells that do not cover the weather stations might be biased. However it is assumed that this source of uncertainty will be smaller than that introduced from only using 5 years worth of recent data for the spin-up period.

Another source of uncertainty in the spun-up C pool and NPP estimates is that only the default parameters were used, which may be inaccurate. It is too time consuming to run the Bayesian inversion with the 1000 year spin up period. A possible solution to this problem would be to include the C pool sizes as initial states in the model calibration. This is outside the scope of this study however.

The annual NPP from the previous year was also recorded. These litter and soil C pool sizes, and the annual NPP, were then set in the model, but the other state variables which required spinning up were set to zero (such as the soil temperature and soil moisture). Each model iteration in the Bayesian inversion was then spun-up for a further three years before the actual model run, which provided the necessary spin up time for the state variables which were not set in the model. This was particularly necessary for the soil moisture submodule during calibration, as if the values of porosity for example, changed dramatically between the spin up and calibration runs the result would be an odd pattern in the soil moisture at the beginning of the year. Of course this would also be a problem for the litter and soil C pools, but the changes in the values there are much smaller and only really affect the slow and old C pools which stabilise over a longer period of time. The effect of the amount of C in the slow and old pools on the daily C fluxes is very small, so it was assumed that the values could be set in the model. The Bayesian inversion could be used to calibrate the initial conditions, such as the C amount in the litter and soil C pools, and indeed this was the focus of the study by *Yeluripati et al.* (2009). This is beyond the scope of this thesis however.

For the initial model evaluation and OSSE experiments, the model was run using the meteorological input data from the Hirddu weather station, the NDVI data from the pixel which covers the Hirddu weather station and the corresponding fractional vegetation cover. In Chapter 9, real data (where available) are used to calibrate the model at all three weather station locations, using

the respective meteorological data and NDVI and fractional cover from the corresponding MODIS pixels. Following this, the calibrated parameters are used to derive the annual fluxes for the whole site as outlined in Figure 3.6.

3.4 Model parameters

The full set of model parameters are outlined in Table 3.2. A description of their purpose is given and the "default" value used in the initial model evaluation and OSSE experiments, as well as the range. The first reference in the last column of Table 3.2 was the one used to define the default parameter value, and the second (if given) was the one used to define the parameter range. If the parameter is a scalar between 0.0 and 1.0 a reference is not given as these bounds define the range. A second reference is also not given if the first reference was used to define both the default value and the range.

The autotrophic respiration scalar is the fraction of GPP that is partitioned into autotrophic respiration. The decision to model the autotrophic respiration as a constant fraction but which could be calibrated followed an extensive literature review but is summarised in *Gifford* (2003) who suggested that a constant fraction of GPP is a simple and practical way to model autotrophic respiration and is just as good as other more complex methods. The default value for the autotrophic respiration scalar (0.5) was derived following *McCallum et al.* (2010) who reported that autotrophic respiration is roughly half of GPP (range 48 to 60%) in their review of satellite-based terrestrial production efficiency modelling.

The SR_max parameter is described in the model description (equation 3.4). *Sellers et al.* (1996) derived the value of SR_{max} for different ecosystem groups. For the study of upland peat ecosystems a value of 5.13 has been used as this is value given to perennial grasslands and broadleaf shrub with grass ecosystems. The maximum LAI is also set for these vegetation types as per *Sellers et al.* (1996), as is the lignin fraction. *Potter et al.* (1993) give values for the light use efficiency for each vegetation class for months when the temperature is greater than zero. The light use efficiency values for the perennial grassland and broadleaf shrub ecosystems are 0.299 and 0.229 respectively, therefore an average of 0.264 is used here.

The value for porosity was given in *Potter et al.* (1993) based on the fact that organic soils were assigned to the coarse/medium texture class. The wilting point followed the same reasoning but was set to a percentage of the porosity for calibration purposes.

Several parameters were calculated on the basis of the soil textural properties (Me_a, soil suction, Kb, rdr_a and rdr_b). The references in Table 3.2 give the calculations used for the respective parameter. There is no soil texture parameter that can be used to define an organic soil in the CENTURY soil module. To account for this the percentage of sand, silt and clay are set to 98, 1 and 1% respectively following (*Raich et al.*, 2000) and (*Chimner et al.*, 2002) and the calculations are based on those percentages. For these parameters their range is based on the range of percentages of the different soil textural classes. The inundation ratio parameter is discussed more in Chapter 4 Section 4.2.

Parameter	Description	Calculation	Default Value	Range	Reference
auto. resp.	autotrophic respiration scalar	NPP	0.5	0 - 1	*McCallum et al.* (2010)
LUE	light use efficiency	NPP	0.264	0 - 2.88	*Potter et al.* (1993)
SR_max	maximum value of SR ratio	NPP	5.13	4 - 9	*Sellers et al.* (1996), *Potter et al.* (1993)
LAI max	maximum value of LAI	temp. at the litter-soil surface and LAI from FPAR	5	1e-5 - 15	*Sellers et al.* (1996), *Asner et al.* (2003)
Q10_l	Q10 value for litter	temp. scalar on litter C decomposition	1.5	1 - 30	*Raich and Potter* (1995), *Potter* (1997)
Q10_s	Q10 value for soil	temp. scalar on soil C decomposition	2	1 - 30	*Raich and Potter* (1995), *Potter* (1997)
Me_s	microbial C assimilation efficiency	standard transfer of C between soil C pools	0.45	0 - 1	*Potter et al.* (1993)
Me_l	microbial C assimilation efficiency	lignin transfers in the soil C submodule	0.7	0 - 1	*Potter et al.* (1993)
Me_a	microbial C assimilation efficiency	active to slow pool soil C transfers	0.1636	0 - 1	*Potter et al.* (1993)
sm_scalar	soil microbial scalar	scales C transfers from slow pool ($SLOW_f$ in eqn 3.16)	0.985	0 - 1	*Potter et al.* (1993)
lig. frac	vegetation lignin fraction	scales C transfers from structural litter pools	0.15	0 - 1	*Potter et al.* (1993)
LN ratio	lignin to nitrogen ratio	partition litterfall into metabolic and structural fractions	15	0 - 40	*Potter and Klooster* (1997)
inund. ratio	inundation ratio	determines max. CH_4:CO_2 ratio in saturated soil	0.2	0.001 - 1.7	*Wania* (2007)
poros.	porosity	max. soil moisture	0.55	1e-5 - 1	*Potter et al.* (1993)
rdr_a	relative drying rate parameter A	scale hydrological fluxes	7.01e-3	1.81e-24 - 1.24	*Saxton et al.* (1986)
rdr_b	relative drying rate parameter B	scale hydrological fluxes	-3.48	-60.18 - -3.41	*Saxton et al.* (1986)
wpt	wilting point	min. soil moisture	0.3 (* poros.)	0. - 1.	*Potter et al.* (1993)
soil suc.	saturated soil water potential (suction)	soil temperature	0.069	1e-5 - 12	*Cosby et al.* (1984), *Letts et al.* (2000)
Kb	constant	thermal conductivity calculation	2.7	1 - 16	*Letts et al.* (2000) and *Lawrence and Slater* (2008)
s_pmt	fraction of plant-mediated transport in sedge	CH_4 dynamics	0.75	0 - 1	(see Section 3.3.5)
j_pmt	fraction of plant-mediated transport in juncus	CH_4 dynamics	0.0375	0 - 1	(see Section 3.3.5)

Table 3.2: Description, default value and range of the CASA-CH_4 model parameters, and the references used to define these values.

3.5 Morris Sensitivity Analysis

The motivation for performing a sensitivity analysis (SA) was discussed in Chapter 2 Section 2.7. It is imperative in a modelling framework to define the uncertainty in a model prediction. A sensitivity analysis identifies what the uncertainty in the model outputs is attributable to in the model inputs (parameters in this case). This is achieved by running the model for many different random samples of the parameter space to determine their impact on the model outputs. It provides information on how much of the output variance is controlled by each parameter. The more complex, variance based SA methods (e.g. Sobol', FAST ETC) give a quantitative estimate of the percentage of the variance that each parameter is responsible for. Less complex "screening" methods provide qualitative information by ranking each parameter in terms of how great an impact they have on the model outputs. These methods are less computationally expensive. The Morris method is an example of a screening method which can efficiently determine the importance of the parameters (*Yang*, 2010), and produces results comparable to the more complex methods (*Confalonieri et al.*, 2010).

The Morris method is based on determining incremental ratios, or "elementary effects",from which basic statistics are used to define the model sensitivity (*Morris*, 1991; *Campolongo et al.*, 2007). The elementary effects are based on changing the value of one parameter at a time in sequence for many (r) trajectories which populate the parameter space. The difference in the model outputs is recorded and the mean and standard deviation of the difference from all trajectories for each parameter is calculated once the sampling has finished. Therefore the parameter values are changed as per a "one-at-a-time" (OAT) sensitivity analysis, but the value of the other parameters are different each time the parameter in question is changed. This is therefore a global search method. It aims to determine which parameters have a negligible impact on the model, those which have a linear and additive effect, and those which are non-linear and are involved with interactions with other factors (*Campolongo et al.*, 2007).

The individual randomised OAT experiments are set up over the whole joint parameter space with θ_i, i=1,...k (where k equals the number of parameters) varying over p set levels (*Campolongo et al.*, 2007). At each point in the trajectory the model is run with a step change (Δ) in only one of the parameters. Therefore the entire parameter space is explored using a k-dimensional, p-level grid. Under the assumption that the parameters are uniformly distributed in [0,1] (if not they should be transformed or re-scaled) the elementary effect of the i^{th} parameter is:

$$EE_i = \frac{M(\theta_1, ...\theta_i + \Delta, ...\theta_k) - M(\theta)}{\Delta} \tag{3.35}$$

where Δ is the step in the p by k grid and is equal to p/[2(p-1)] (*Campolongo et al.*, 2007). The r trajectories of parameters (θ) are sampled from the p by k grid. The starting point in the p by k grid is randomly chosen for each trajectory. In this thesis the number of levels in the grid (p) was set to 30 and 400 trajectories were used to sample the parameter space. The values for the number of levels and trajectories were increased until the rankings of the parameters from the sensitivity analysis did not change.

The model outputs daily values. For this sensitivity method one value for the model output is required. The annual C flux could be used, but as the observations are also provided as daily

estimates it is important to determine the influence of the parameters on the daily model outputs. In this study therefore the mean of the difference in the daily model outputs with each iteration was used to calculate the elementary effects.

Once the model has been run for each of the k parameters in each trajectory, the mean μ, and standard deviation σ, of the elementary effects for each parameter are calculated. *Campolongo et al.* (2007) suggest also looking at the mean of the absolute values μ^*, which solves the problem that changes in the parameter value might result in model outputs with changing sign. The value of μ^* can be used to rank the importance of the parameters in terms of their relative influence on the model (higher values equal higher sensitivity of the model to that parameter) but the information on the sign of the effects is also interesting. The μ or μ^* of the elementary effects determines the overall sensitivity of the model to the parameter, and σ provides information on the higher-order effects, i.e. if the model exhibits non-linear behaviour with changing parameter value or if the parameters are correlated. The values of μ^* and σ are plotted on the same graph to compare the behaviour of the parameters, and μ^* of each parameter is used to rank them. The rankings of the parameters and the values of μ^* are used to determine which parameters should be included in the model calibration, i.e. which are the most important parameters that contribute most to the variance in the output.

3.6 Bayesian model inversion

The method used to constrain the parameters of the model was based on a Markov Chain Monte Carlo (MCMC) method, which was briefly described in Chapter 2. This technique was chosen over other methods as no assumptions are made as to the distributions of the prior parameters and a linear model is not a requirement. As the CASA-CH_4 is a non-linear dynamic model, and there is little information on the prior distributions of the parameters, this method is appropriate to use. It also does not require an assumption of a Gaussian distribution of the observation uncertainty and therefore provides a framework for testing the error structures in the observations. It is a very versatile method as all the different sources of error with potentially differing distributions can be taken into account. In addition it allows an exploration of the correlations between the parameters.

Two studies have compared optimisation algorithms and found the different algorithms were able to find similar parameters estimates (*Fox et al.*, 2009) and that choice of algorithm did not have as much of an influence as the choice of the cost function (used to describe the differences between the model and the observations) (*Trudinger et al.*, 2007). Many studies have adopted an MCMC approach in the inversion of C flux models, as reviewed in Chapter 2, e.g. *Knorr and Kattge* (2005); *Xu et al.* (2006); *Ricciuto et al.* (2011).

MCMC is rooted in Bayesian inference (Chapter 2 Section 2.5.1). It provides a method of finding the posterior distribution of parameters, given the data, by sampling from the prior distribution of the parameters and accepting or rejecting the parameter value with a given probability (Chapter 2 Section 2.5.2). The algorithm used is based on the Metropolis Hastings MCMC algorithm (MH-MCMC), which provides a method for the acceptance or rejection of a parameter based on the acceptance probability. An adaptation to this which uses a more sophisticated sampling algorithm, the Differential Evolution Markov Chain with snooker updater and fewer chains

(DE-MC$_{ZS}$) (*ter Braak and Vrugt*, 2008), was used to sample from the joint prior parameter probability distribution. Firstly the general Metropolis Hastings MCMC algorithm is described, and following this the DE-MC$_{ZS}$ sampler in Section 3.6.2.

3.6.1 MCMC and the Metropolis-Hastings algorithm

In MCMC, a parameter value is accepted or rejected in a model calibration or data assimilation sense by comparing how well a model output, using a given parameter value(s), is able to produce (match) the observed data. This information is contained in the likelihood function as we'll see below. The acceptance of only certain parameter values leads to convergence on the posterior distribution of the parameters. Figure 3.7 shows a schematic diagram of the Bayesian inversion.

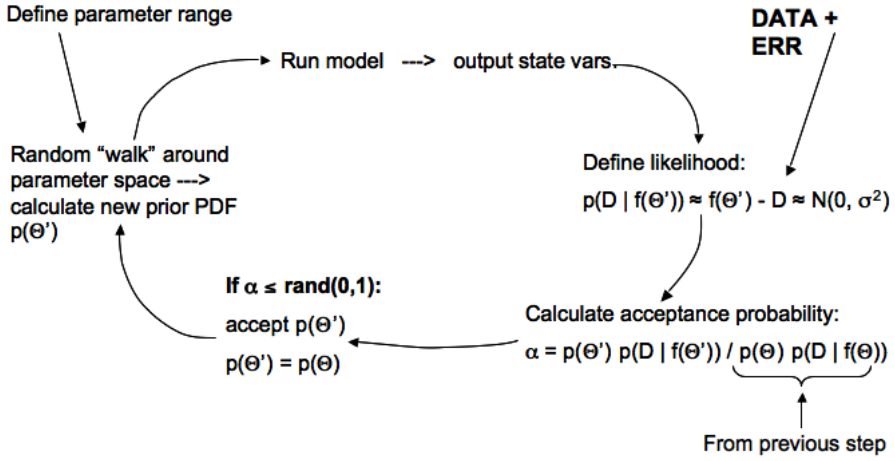

Figure 3.7: A schematic of the Bayesian inversion.

Markov Chain Monte Carlo simulation offers a way to systematically sample the parameter space of the **prior distribution**. The prior distribution of the parameters, (P(θ)), describes the knowledge of the distribution of the parameters values prior to the calibration. In this thesis, the prior of each parameter is taken from the literature of all possible values for that parameter, or is set to the physical limits of the parameter. The prior predictive uncertainty of the model outputs can be determined by random sampling of the parameters from the prior distribution. The **posterior distribution** of the parameters P(f(θ)|D) is the joint probability distribution of the parameters of the model after calibration. The posterior probability distribution function will be referred to as PPDF from here on.

At each iteration of the Markov Chain a new parameter value is proposed. This "candidate" value or values can be generated by taking a small step from the existing value. The small step can be chosen from a proposal distribution which depends on the current value and the covariance matrix, (*Gelman et al.*, 2004) or the proposed candidate can be drawn independently of the current step from the proposal distribution. A chain is set up to take a random walk through the defined parameter space. The step size and chain length should be sufficient to sample all of the parameter space. MCMC therefore allows for a complete sampling and characterisation of the PPDF, whatever form that takes.

At each step in the chain a new parameter set is defined and the new distribution of the parameters p(Θ') calculated. The model is then run using the new parameter set. The **likelihood function** is then calculated. The likelihood is the probability distribution function of the data, given the parameters (P(D|f(θ)):

$$P(D|f(\Theta)) = f(\Theta) - D = N(0, \sigma^2) \tag{3.36}$$

This is essentially the probability that the data and corresponding modelled state variable are equivalent. In practice several sources of uncertainty will result in a disagreement between the values: error in data collection, model formulation and driver inputs and issues relating to autocorrelation. These sources of error are described by the likelihood function by fitting a probability distribution to the differences between the model outputs and the data.

In this thesis it is assumed that the differences between the model and the observations are a result of uncertainty in the observations only (σ^2) and that they have a Gaussian distribution about a mean of zero. It is assumed that the model has no uncertainty associated with it. The impact of this assumption being incorrect on the results of the calibration is explored in Chapter 8. It is also assumed that the observations are independent, i.e. they are not temporally or spatially correlated. Different error models could be used and the likelihood function could be adapted to account for correlations in the observations. This is discussed in more detail in later chapters. *Trudinger et al.* (2007) emphasised the need to choose the error model carefully.

The Metropolis Hastings algorithm assigns an acceptance probability (α)to the new parameter set. This is calculated by taking the ratio of the prior distribution of the proposed parameter set (Θ') multiplied by the likelihood of the proposed parameter set to the prior distribution of the current parameters P(θ) multiplied by the likelihood of the current parameter set in the Markov chain.

$$\alpha = \frac{P(\Theta')\,P(D|f(\Theta'))}{P(\Theta)\,P(D|f(\Theta))} \tag{3.37}$$

If the model run using the new parameters produces a value of a state variable which more closely matches the observed data the acceptance probability will be higher than 1.0 and that parameter set will be accepted. If not, the parameter set is accepted only if the acceptance probability is greater than a randomly generated number between 0 and 1. This ensures the parameter space is properly sampled as the chain will not get 'stuck' at the margins of the parameter set on values which do not have a high likelihood. As stated above a sophisticated method of sampling the parameter space was used in this thesis. This is described in the following section (Section 3.6.2. If the acceptance ratio is lower than the generated random number the parameter set is rejected and the previous one retained for the next iteration of the chain (*Gelman et al.*, 2004).

Convergence of the chain will occur when each step in the chain produces a parameter set which gives a similar likelihood ratio to the one before and therefore the acceptance ratio will near unity. Once convergence has occurred the PPDF of the parameters has been found. Several methods can be employed to ascertain whether convergence has been reached. This simplest of these is a visual inspection of the trace plots of the parameter values for each iteration. These will show that the parameter space has been adequately sampled. Other more sophisticated methods

can also be used (*Gelman et al.*, 2004) such as running parallel chains to confirm that both reach the same distribution. A commonly used diagnostic is the "rhat" ($\hat{R}$) statistic (*Gelman and Rubin*, 1992). This is based on assessing the total variance of the target (posterior) distribution which is a weighted average of the "within chain" and "between chain" variance. Only when the the total variance is comparable to the "within chain" variance has convergence been reached. Typically an $\hat{R}$ value of 1.2 is used to confirm the chains have converged on the posterior distribution. Once convergence is reached the PPDF of the parameters has been found.

Once the algorithm has converged on the joint PPDF of all the parameters the marginal distribution of each parameter is examined to see if the observations have been able to improve on the information provided in the prior distribution of the parameter. The reduction in 95% confidence interval between the prior and the posterior of the parameter is also examined to see how "well-constrained" the parameters are as a result of the calibration. If the parameter has been well-constrained by the observations the shape of the marginal PPDF is used to ascertain which probability distribution the parameter most corresponds to. The correlations between the parameters is also investigated using their marginal distributions. To determine the impact on the model predictions and uncertainty in those predictions as a result of the parameter constraint, the model is run 500 times ("forward runs") using random samples from the joint PPDF of the parameters. 500 forward runs were used to ensure adequate sampling of the joint PPDF. This was typically required for the less well-constrained PPDFs. The mode and the 95% confidence interval of the forward runs for each model output is then calculated. This is referred to as the posterior distribution of the model state variable in question. The prior distribution of the model state variable is also determined using random runs from the prior joint distribution of the parameters and the 95% confidence interval determined. Therefore the reduction in model predictive uncertainty is calculated between the prior and posterior 95% confidence intervals of the model runs.

3.6.2 The DE-MC$_{ZS}$ sampler

DE-MC$_{ZS}$ stands for Differential Evolution Markov Chain (DE-MC) with snooker updater and fewer chains (*ter Braak and Vrugt*, 2008). It is a more robust algorithm for sampling the whole parameter space. DE-MC is based on the MCMC algorithm but has multiple chains running in parallel in order to sample the parameter space more fully. It helps in exploring multi-modal distributions and was shown to be more efficient than the normal random walk Metropolis sampler. It solves the difficult problem of choosing the scale and orientation of jump between the current and proposed parameters (*Braak*, 2006). The Metropolis ratio, outlined in the previous section, is still used to accept or reject the proposed parameter.

In DE-MC N chains are run in parallel and the jump is generated from the other N-1 chains. In brief the jump is created by randomly choosing two vectors, taking the difference, scaling it by a factor γ, and adding this to another random vector. The idea is that the difference between the two randomly chosen chains contains the information on the scale and orientation of the jumping distribution (*ter Braak and Vrugt*, 2008). A problem with DE-MC is that for it to work well the number of chains must be larger than the number of parameters d. *Braak* (2006) showed that for distributions that are more complicated than a unimodal distribution, $N = 10d$ to $20d$ should be used. However this results in the convergence time increasing by a factor of N than for a

single chain presenting a real problem for slowly converging chains (*ter Braak and Vrugt*, 2008). Fewer chains would therefore be desirable. This also reduces the possibility of an "outlier" chain taking a much longer time to find the mode than the other chains. It also makes the problem less computationally expensive.

ter Braak and Vrugt (2008) presented an update to the DE-MC algorithm to account for the high number of chains required when the posterior is complex and/or the number of parameters is high (high-dimensional problem). They sample the difference vectors (difference between two other randomly chosen chains) from past states of the chains. This makes the algorithm an adaptive Metropolis sampler (*ter Braak and Vrugt*, 2008). The chains' history will initially represent the entire parameter space. The past states only include those parameters that have been accepted by the algorithm so as the chains converge on the mode of the posterior the past states will contain an increasingly higher number of parameters that are close to the mode. In addition to this they add a "snooker-update". This effectively randomly pushes a chain in a different direction, which aims to solve the problem of a chain getting stuck in a local minimum.

The exact steps of the algorithm are detailed in *ter Braak and Vrugt* (2008). They show that DE-MC can work for d of up to 50-100 with far fewer chains N=3. The initial matrix of past states for all chains can be found by randomly sampling from the prior distributions of the parameters. *ter Braak and Vrugt* (2008) found that a reasonable size (M_o) for this sample was $10d$. Different values for M_o (80-500) and N (3-10) were tested in several trial-runs of the DE-MC$_{ZS}$ algorithm with the maximum number of parameters that would be calibrated. The iterations were compared based on the speed of convergence and the ability to retrieve the correct parameter values. Following this the values of N=6 and M_o=100 were chosen for all the DE-MCZS runs. The scaling factor, γ was chosen as suggested by *Braak* (2006) to be equal to $2.38/\sqrt{2d}$.

3.6.3 Experimental set-up

Priors

The prior distributions of the parameters in this study are based on the range of values reported in the literature, as detailed in Table 3.2. As no further information is available on the distributions, uniform prior distributions are used, with the minimum and maximum value corresponding to the lower and upper limit of the range respectively. The prior distributions of the parameters used in each model calibration exercise are summarised in the experimental set-up sections in each chapter.

Observations

The uncertainty in the observations is used as the standard deviation of the normal distribution of the differences between the model and the observations in the likelihood function. This is assuming that the differences are solely due to uncertainty in the observations and not the model. In the synthetic experiments, detailed in Section 3.7, random Gaussian noise is added to the observations. The standard deviation used to generate the random noise is therefore defined as the standard deviation of the observations. It is this value that is used to calculate the normal distribution in the likelihood.

The real data, and associated uncertainties, used in the Bayesian calibration in Chapter 9, are described at the end of this Chapter (Section 3.8). Again the uncertainty associated with each dataset is used to define the standard deviation of the normal distribution of the differences between the model and the observations in the likelihood, assuming no model error.

Outputs of the Bayesian inversion

Once the algorithm has converged on the joint PPDF of all the parameters the marginal distribution of each parameter is examined to see if the observations have been able to improve on the information provided in the prior distribution of the parameter. The reduction in 95% confidence interval between the prior and the posterior of the parameter is also examined to see how "well-constrained" the parameters are as a result of the calibration. The correlations between the parameters is also investigated using their marginal distributions.

To determine the impact on the model predictions and uncertainty in those predictions as a result of the parameter constraint, the model is run 500 times ("forward runs") using random samples from the joint PPDF of the parameters. The mode and the 95% confidence interval of the forward runs for each model output is then calculated. This is referred to as the posterior distribution of the model state variable in question. The prior distribution of the model state variable is also determined using random runs from the prior joint distribution of the parameters and the 95% confidence interval determined. Therefore the reduction in model predictive uncertainty is calculated between the prior and posterior 95% confidence intervals of the model runs.

3.7 Observation Systems Simulation Experiment

As previously discussed data assimilation is used as a tool for integrating models and observations in order to provide optimal estimates of state variables. EO data is useful in allowing this approach to be applied over wide spatial scales. As well as obtaining an improved characterisation of the uncertainty on model outputs, the observations are useful in testing our model understanding. Using the MH-MCMC approach, the advantages of which were discussed in Chapter 2 Section 2.5.2, if no set of parameters is able to bring the model closer to the observations then we can infer that the underlying model formulation needs improvement. This is based on the assumption that we trust our observations more than the model. In practice both the observations and the model have uncertainty associated with them, and therefore combining the two is the optimal use of the information in providing an estimate, given the current state of our knowledge and available data. The observations are used to update the prior knowledge, which is represented by the model. Firstly though it is important to determine the characteristics of a set of observations that would be required to test the model and improve estimates of uncertainty. The model formulation might be such that it needs updating with frequent observations that have low uncertainty. Real data that match these requirements may not currently be available. It is useful therefore to perform an experiment with synthetic observations before calibrating the model with real observations.

The aim of Chapters 5 to 8 is to use an Observation Systems Simulation Experiment (OSSE) to identify which observational characteristics (temporal sampling interval and observation error) result in accurate and well-constrained CASA-CH_4 model parameters and a reduction in the model

predictive uncertainty. The temporal sampling interval is examined as well as differing amount of observation uncertainty. In addition the impact on the model of different types of observations can be investigated. The OSSE is a powerful tool, as it allows an exploration of how the algorithm would work under different scenarios, for example with unidentified model error or inaccurate observations. It tests the ability of the observations to improve quantities of interest and tries to elucidate whether the observations have enough information to constrain a model inversion. A set of experiments in this regard have been performed in this thesis to demonstrate the usefulness of this tool. These experiments are only performed under one set of driving conditions (i.e. specific climate and ecosystem type). A more extensive study would explore many different climatic regimes and ecosystem types. The OSSE also enables an exploration of the workings of the model, what is possible to achieve with the model and what is not. Therefore an assessment can be made as to the validity of the model in answering the scientific questions posed. Even with a relatively simple model with relatively few parameters, such as the CASA-CH_4 model, it is impossible to track the subtle workings of the model behaviour simply by understanding the calculations involved, as the relationships between the model physics and parameters are quite complex. In a calibration exercise the observation characteristics only add to this complexity. A synthetic experiment is the only way to gain even a simple understanding of the model, and the assimilation of the observations with the particular model, as the "true" parameter values and model outputs are known.

The following questions shall be addressed in the OSSE experimental results chapters:

1. Which observational characteristics, for each type of observation, result in accurate and well-constrained model parameters and a reduction in the predictive uncertainty of the daily and annual modelled C flux?

2. Which type of observations are most useful in constraining the model parameters and state variables?

3. What is the impact of unknown model error on the Bayesian inversion results, and can the results identify this error and/or account for it?

4. What is the impact of unknown bias in the observations on our ability to constrain the model parameters, and what is the best way to account for it?

3.7.1 Method

The OSSE involves synthetic "twin" experiments, i.e. synthetic observations are generated from a default model output with a known (true) set of parameters. These "observations" are degraded by adding random Gaussian noise and thinned to create differing temporal frequencies. The observations are then used in the Bayesian inversion to test the calibration of the model parameters. A schematic of the OSSE is presented in Figure 3.8.

The synthetic "observations" are taken from the state variable outputs of the default run of the model with the parameter values specified in Table 3.2. Subsequently the uncertainty of the observations is increased by adding random Gaussian noise with increased standard deviation to the observations. Following this, the temporal sampling interval of observations is reduced by

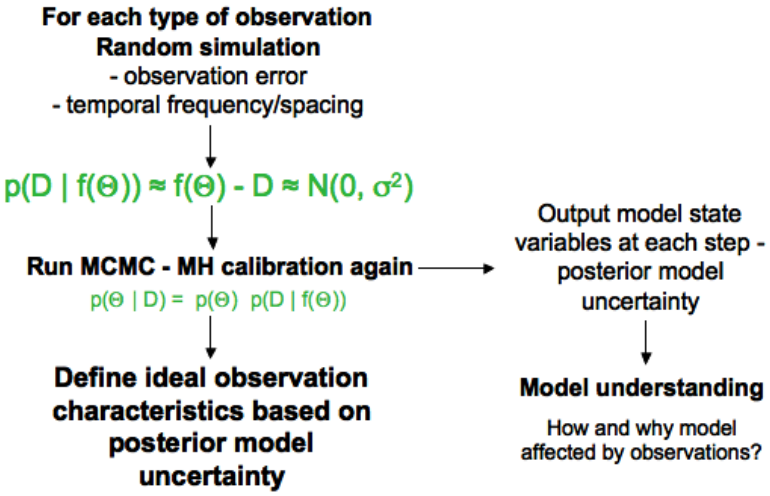

Figure 3.8: A schematic of the sythentic experiment used to determine the 'ideal' characteristics of observations require to improve model estimates.

taking an observation every t^{th} day, where t is the temporal sampling interval. The seasonality of observations is also tested by concentrating observations in different seasons of the year. The prior parameter distributions used in the algorithms are also outlined in Chapter 4. The set of observations created by this process is then combined with the model by specifying the difference between the observations and the model, and the standard deviation of the difference, in the likelihood of the MH-MCMC algorithm. The prior is combined with the likelihood function resulting from the synthetic observations, to find the posterior distribution of the model parameters. This is repeated for each set of observational characteristics with increasing error and decreasing temporal sampling interval.

Choice of observation error and temporal sampling interval

The typical magnitude of errors that are associated with ground-based and satellite measurements of soil moisture and C fluxes were taken from the literature (Chapter 2 Sections 2.4 and 2.3). The range of errors associated with the satellite soil moisture measurements were from studies across many different types of ecosystem, but mostly temperate grass and croplands (Table 2.2), as there were no specific studies that had looked at temperate or boreal peatland ecosystems. The range of errors associated with the C flux measurements are from specific peatland C flux studies (for ground-based measurements) and from the limited existing literature on satellite C flux data, including the results of OSSE experiments that look at the theoretical uncertainty associated with the retrieval of C flux data from current and future satellites that can be used, or have been designed, for this purpose (e.g. *Hungershoefer et al.* (2010)). The range of observation errors for each observational type is listed in Table 3.3. The spacing of the errors was non-linear, as there tended to be a higher number of smaller errors for all observation types, therefore a smaller spacing between different magnitudes of error is needed.

The parameters which were shown to have a greater sensitivity in mean daily flux than the smallest error were therefore chosen for each model output/observation type. In practice this in-

volved choosing parameters which had an absolute mean elementary effects value that was double that of the smallest error, due to the way in which the elementary effects are calculated in the Morris algorithm (see Section 3.5). The chosen parameters for each observational type are listed in Table 3.4. The same temporal sampling interval was chosen for all observational types and reflected typical sampling frequencies available for measurements both in the field and from satellite data, in particular the higher sampling intervals were chosen to reflect typical satellite revisit periods (see Chapter 2 Sections 2.4 and 2.3). It also included the possibility that only a few observations are available over an extended period of time, which is the case for some agencies or companies which only provide satellite data for targeted aquisitions. The choice of observational temporal sampling interval is also listed in Table 3.3.

Temporal Sampling Interval	**Vol. soil moist. error (m^3m^{-3})**	**Relative soil moist. error (%)**	**CH_4 flux error ($gCm^{-2}d^{-1}$)**	**NEP flux error ($gCm^{-2}d^{-1}$)**
1	0.02	2	0.002	0.05
5	0.04	5	0.005	0.1
10	0.06	10	0.01	0.2
15	0.08	15	0.02	0.5
30	0.1	20	0.05	1.0
60	0.15	30	0.1	2.0
180	0.2	50	0.2	5.0

Table 3.3: The temporal sampling interval used to 'thin' the synthetic observations and random Gaussian error added to the synthetic observations in each OSSE experiment.

Soil moisture	**CH_4 flux**	**NEP flux**
porosity	Q10_l	Q10_l
rdr_a	Q10_s	LUE
rdr_b	LUE	SR_max
wilting point	porosity	porosity
	Me_s	auto. resp.
	Me_l	
	LN ratio	
	lignin frac.	
	SR_max	
	innund. ratio	
	auto. resp.	

Table 3.4: The parameters chosen to be included in the Bayesian inversion for each observation type, based on the sensitivity of the model outputs relating to each observation type to the model parameters. (See Chapter 4 Section 4.4).

Experiment outputs

The outputs of the experiments and metrics used to evaluate the efficacy of the algorithm and different observation characteristics are listed below:

- Histograms of each parameter posterior PDF (PPDF) for all observational characteristics.
- Table of the bias between the Maximum A Posteriori (MAP), or mode, of the PPDF and the "true" (default) parameter value for all observation characteristics. A negative bias suggests the mode is lower than the true value and vice versa.
- Table of the reduction in 95% confidence interval between the prior and posterior parameter distributions.
- Plots of the forward model outputs of NEP and CH_4 flux (and where appropriate, other model outputs) for each observational characteristic showing an ensemble of 500 model runs sampled from the posterior parameter distribution (with all non-calibrated parameters remaining at the default values), with the prior and posterior forward model ensemble 95% confidence intervals and the "true" model output derived from the default model parameters.
- Histograms of the annual flux PPDF for both the NEP and CH_4 flux for all observational characteristics.
- Table of the bias between the Maximum A Posteriori (MAP), i.e. mode, of the posterior annual C flux PDF and the "true" (default) annual C flux value for all observation characteristics. A negative bias suggests the mode is lower than the true value and vice versa.
- Table of the reduction in 95% confidence interval between the prior and posterior annual C flux distributions.
- Plots of the root mean squared difference (RMSD) between the daily forward model mode and the true value for all observational characteristics.
- Correlations between each parameter pair for each observation characteristic.

The aims of the metrics are to quantitatively assess both how well the algorithm constrains the parameter and flux estimates (through the reduction in 95% confidence interval) and whether the true values are accurately retrieved (through the mode - truth bias). The correlation coefficients between the parameters describe the level of interaction between each parameter pair, and the resultant influence on the model outputs.

This is real advantage of a synthetic twin experiment. If such a synthetic experiment is not performed there is no confidence that the data assimilation exercise will produce a true estimate (± uncertainty) of the model output.

The discussion following the OSSE results in each chapter will address the questions posed for this chapter and will also comment on the suitability of the model and the Bayesian inversion for deriving accurate flux estimates. The results of each experiment are compared to determine which circumstances result in improved model estimates, and the required "ideal" sets of observations are compared with the available datasets that can or will be obtained from current and future satellite missions and ground-based datasets.

Notation

There are many instances in the OSSE chapters where the characteristics of the synthetic observations need to be referred to. However it is a bit long-winded to keep describing the observational characteristics with a phrase such as "observations with a temporal sampling interval of t days and an uncertainty of ε (units of measurement)". Instead, the following notation is adopted throughout this thesis in order to refer more easily to the observational characteristics. The temporal sampling interval and uncertainty of a set of synthetic observations is specified by two numbers, enclosed in curly brackets, and separated by a forward slash. For example a set of observational characteristics is referred to as "the $\{t/\varepsilon\}$ observations", where the temporal sampling interval is denoted by t (in days) before the forward slash and the observation uncertainty is indicated by ε after the forward slash. The units of the uncertainty are the same as the units of the observations, i.e. m^3m^{-3} for volumetric soil moisture observations, % for relative soil moisture observations and $gCm^{-2}d^{-1}$ for both the CH_4 and NEP flux observations.

Figure and table captions

In the OSSE chapters in order to avoid long figure captions which essentially repeat the same information, the details of what the tables, histogram and forward model figures show are given here. This will be repeated for the first figure (for both the histograms and the forward model plots) and table of each OSSE results chapter.

The histogram plots, which compare the prior and posterior parameter distributions of the parameters and annual C fluxes, are arranged with increasing observation uncertainty along the columns and increasing temporal sampling interval down the rows. The magnitude of the observation uncertainty is given in the top row, and the temporal sampling interval is given in the right-hand column.

The axes are the same for all histograms, and are shown at the bottom and left hand side of the figure. The red line shows the prior distribution and the blue, the posterior. The vertical black dashed line shows the true value.

Tables of both the reduction in the 95% confidence interval between the prior and posteriors, and the bias between the MAP estimate of the posterior distribution and the true value, for both the parameters and annual C fluxes, are also arranged with increasing observation uncertainty along the columns and increasing temporal sampling interval down the rows. The magnitude of the observation uncertainty is listed in the top headings of the table, and the temporal sampling interval is listed in the headings in the left-hand column. Both are shown in bold.

The units of the temporal sampling interval are days. For OSSE studies using CH_4 flux and NEP observations (Chapters 5 and 6 respectively), the units of the observation uncertainty are $gCm^{-2}d^{-1}$. For the OSSE studies using volumetric soil moisture observations (Chapter 7 Section 7.3), the units of the observation uncertainty are m^3m^{-3}. For the OSSE studies using relative soil moisture observations (Chapter 7 Section 7.6), the units of the observation uncertainty are %.

In the forward model plots the green area shows the prior 95% confidence interval of the respective model state variable, using 3000 random samples from the joint prior distribution of the parameters that are being calibrated in that OSSE experiment. The pink area is the posterior

95% confidence interval and the red line is the forward model mode for an ensemble of 500 model runs sampling randomly from the posterior parameter PDFs. These results are compared to the model run with the true set of parameters, which is denoted by the blue dashed line. For OSSE experiments which examine model error in Chapter 8, the blue line represents the altered (now "true") model timeseries and the black line represents the original (now "inaccurate") model timeseries.

This information will be provided in the first figure and table of each of the OSSE chapters, but thereafter only the relevant new information on each figure and table will be provided in the caption.

3.7.2 Outline of the OSSE experimental chapters

The results of the OSSE experiments are outlined in Chapters 5 to 8. Chapter 5 describes the OSSE experiment using synthetic CH_4 flux observations to constrain the CH_4 flux sensitive parameters. Chapter 6 does the same for NEP flux observations, which are used to constrain the NEP flux - sensitive parameters. Chapter 7 presents the results of OSSE experiments using both absolute volumetric soil moisture observations and relative (%) soil moisture observations. It also examines the impact on the OSSE results of a) poorly defined prior parameter distributions and b) biased observations, as this is likely to occur with the available satellite soil moisture observations for this area. Finally Chapter 8 investigates the effect of an unknown, and therefore unaccounted for, model structural error on the ability of the Bayesian inversion to constrain the parameter and model predictive uncertainty.

3.8 Real data sources

The observations which are used to constrain the CASA-CH_4 model at the Lake Vyrnwy site are presented in this section. The temporal trend, magnitude and variability are discussed and compared to both ground-based observations, in the case of satellite data, and to the model run with the default (un-calibrated) parameter values.

3.8.1 Ground-based CH_4 observations at Lake Vyrnwy

Monthly ground-based CH_4 flux chamber measurements were available for the Lake Vyrnwy for the whole of 2009. The data were collected and provided by J. Stockdale (Department of Biology, University of York. pers. comm.). The data were collected at three different locations across the Lake Vyrnwy site, named "Eunant", "Hafod" and "Hirddu", corresponding to the names of the catchments in which the measurements were taken. Meteorological stations at each location measured the air temperature, precipitation and the irradiance, which were used to drive the model.

The CH_4 measurements were taken using the static chamber technique (see Chapter 2 Section 2.3.1), with samples taken every 20 to 30 minutes over a total sampling time of around 100 minutes. The inert gas SF_6 was injected into the chamber headspace in order to detect and correct for leakages from the sealed chamber. The samples were stored in exetainers and analysed in the lab using a Perkin Elmer AutoSystem XL gas chromatograph (GC; PerkinElmer Instruments,

Shelton, CT, USA) for CO_2, CH_4 and SF_6. The fluxes (in $mgCH_4m^{-2}hr^{-1}$) were subsequently calculated using a linear regression relating the concentrations of each gas to time (J. Stockdale, pers. comm.).

The data were then converted to $gCm^{-2}d^{-1}$ by multiplying the hourly measurements by 24, following *Moore et al.* (2011). Some studies have observed a diurnal cycle in CH_4 observations (e.g. (*Hendriks et al.*, 2010)) but the cycles are not as clear or as pronounced as the diurnal cycle of CO_2. Given the observations were mostly taken in the middle of the morning or afternoon, and given the lack of information on the CH_4 diurnal cycle, the assumption of scaling by 24 hours is justified, but may result in a slight overestimate of the flux.

The CH_4 flux was measured at five different plots for each of the four different vegetation types, grass, sedges, juncus and heather, at each location. The mean and standard error of the mean (SEM) were calculated for the five replicates for each vegetation type at each location. Figure 3.9, Figure 3.10 and Figure 3.11 show the mean and SEM of the ground-based CH_4 flux observations for each vegetation type at the Eunant, Hafod and Hirddu locations, compared to the site-averaged value and the vegetation-weighted value. The ground-based observations are also compared to the CASA-CH_4 model run using the default (un-calibrated) parameters, for reference. It appears that the model is overestimating the flux observations in the winter and autumn months. However until the calibration has been performed an analysis of the possible causes discrenpancy between the two cannot be carried out. It is possible that the simple partitioning of decomposed C into CO_2 and CH_4 fluxes is too simplistic, or that the hydrology submodule is inaccurate. This is discussed further in Chapter 9 which details the results of the model calibration using these data. In order to compare to the model, and because there is a clear difference in the magnitude of CH_4 flux from the different vegetation types, the fractional cover of each vegetation type was used to scale up the mean and SEM of the fluxes for each vegetation type to the area of the MODIS NDVI pixel used to drive the model, using the classification produced for the site (Chapter 3). In many cases the vegetation-weighted mean was not much different to the un-weighted mean for each site, as seen in the figures below.

The mean flux is close to zero, or negative, in the first ~5 months of 2009 for all locations and vegetation types. The increase in flux in the summer months occurs later than in the modelled values (end of June), suggesting the temporal trends might be out of phase, although the model has not been calibrated. The flux magnitude is greater at the Hafod location for the summer and autumn months when the flux is higher, and the increase in flux starts earlier in the year, around the end of May. There is a gradual increase in CH_4, apart from the end of July where the flux is lower, until the peak flux in the middle of August. By comparison the peaks in CH_4 in the model occur in June. For the Eunant and Hirddu sites the magnitude of peak flux is lower and broader. The fluxes do not start increasing until the end of June for these sites and the maximum flux is seen at the end of July. The CH_4 flux declines almost to zero again in November and December for the Eunant and Hirddu location, whilst the flux at the Hafod location remains high.

In general the lowest fluxes throughout the year, and particularly in the summer and autumn months, are from measurements taken over grass and heather. This is expected as these vegetation types do not have aerenchymous tissues which result in rapid transport of CH_4 from beneath the water table to the atmosphere. The highest fluxes are seen for the sedge and juncus, which do

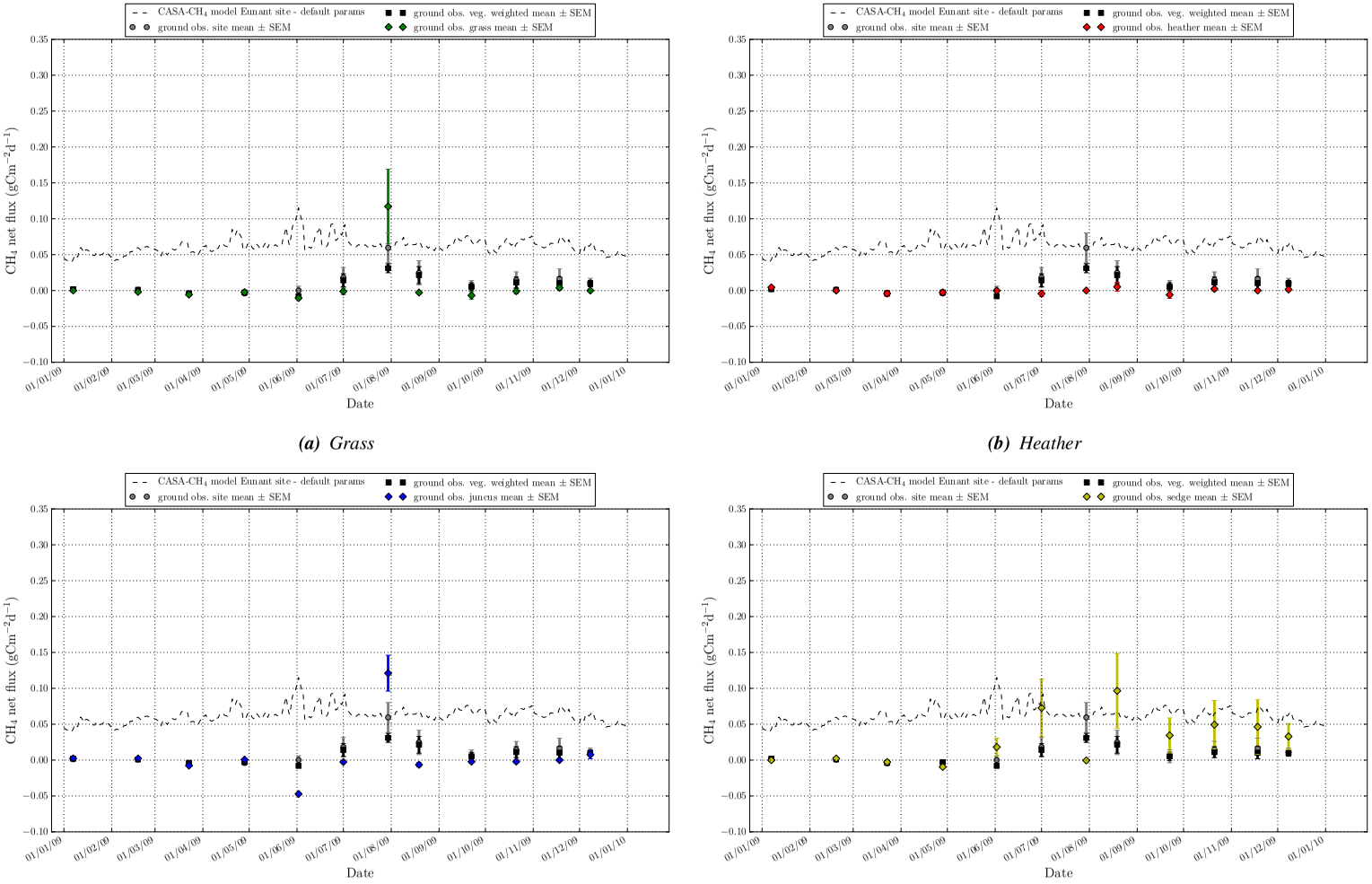

Figure 3.9: Plots showing the mean and SEM of the ground-based CH_4 observations for the Eunant location for each vegetation type, compared to the Eunant location-mean CH_4 flux, the up-scaled percentage vegetation cover-weighed mean and SEM. All ground-based observations are compared to the CASA-CH_4 modelled CH_4 output using the default parameters, prior to calibration.

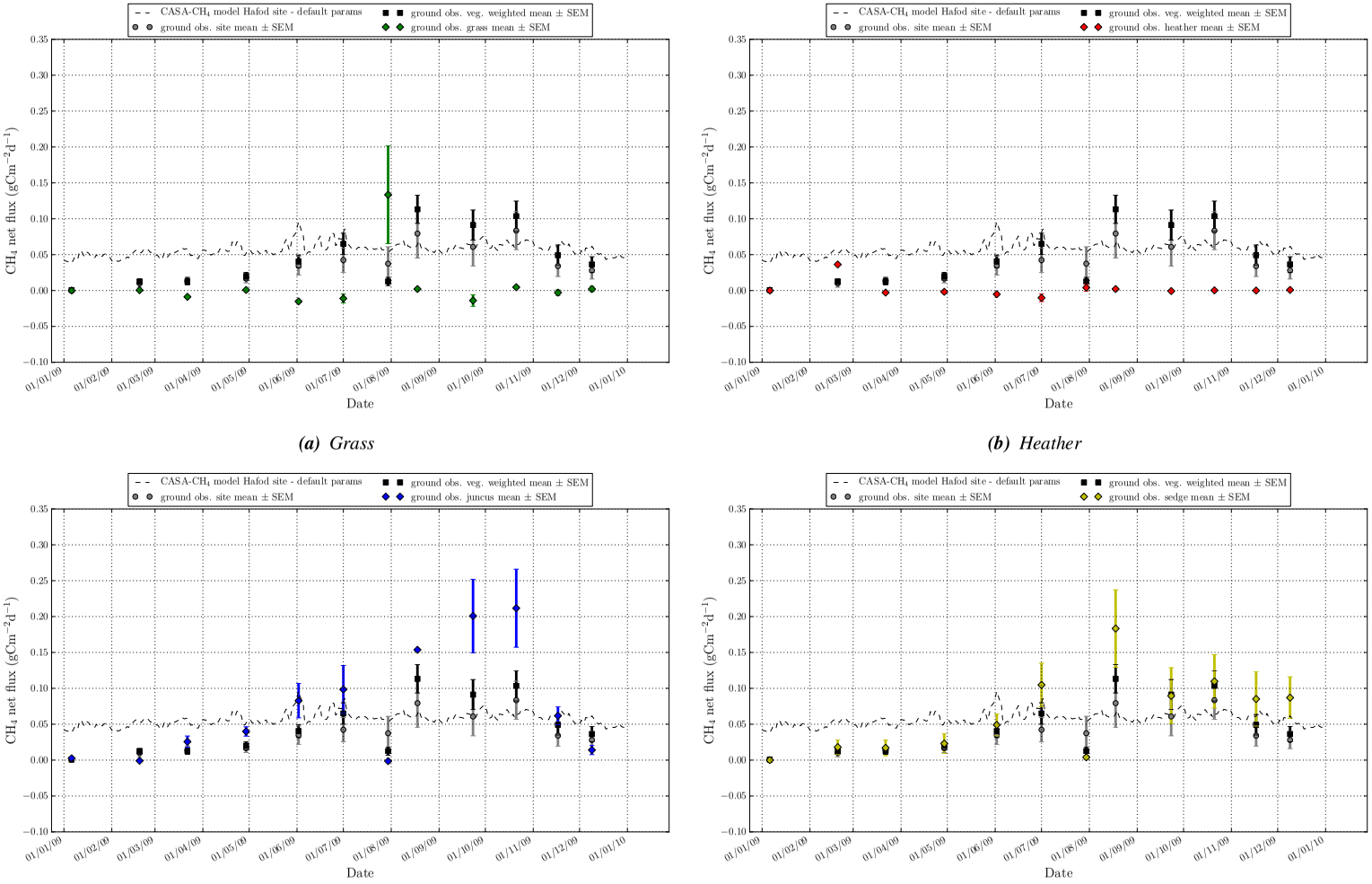

(a) *Grass*

(b) *Heather*

(c) *Juncus*

(d) *Sedge*

Figure 3.10: Plots showing the mean and SEM of the ground-based CH_4 observations for the Hafod location for each vegetation type, compared to the Hafod location-mean CH_4 flux, the up-scaled percentage vegetation cover-weighted mean and SEM. All ground-based observations are compared to the CASA-CH_4 modelled CH_4 output using the default parameters, prior to calibration.

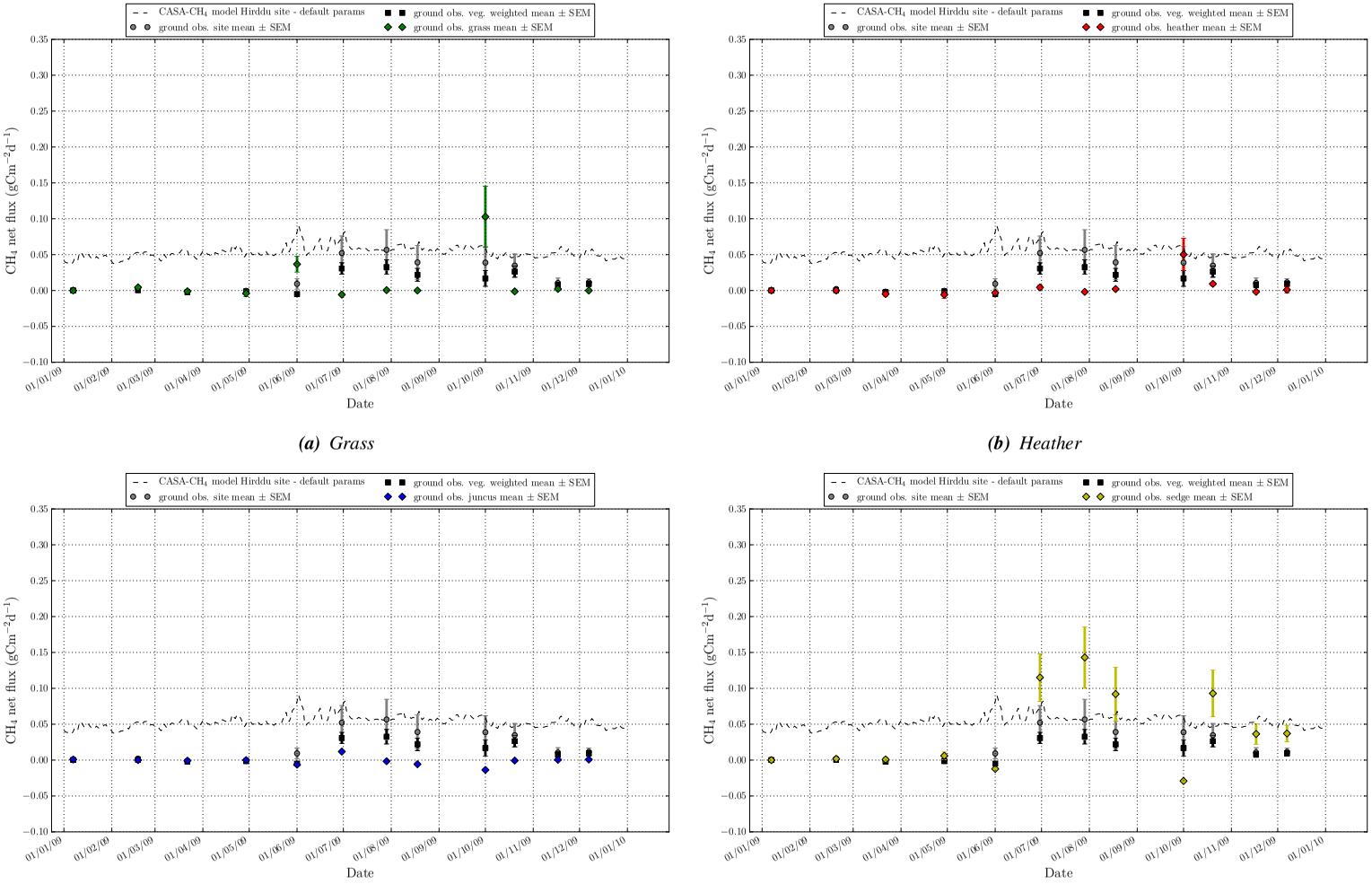

(a) *Grass*

(b) *Heather*

(c) *Juncus*

(d) *Sedge*

Figure 3.11: Plots showing the mean and SEM of the ground-based CH_4 observations for the Hirddu location for each vegetation type, compared to the Hirddu location-mean CH_4 flux, the up-scaled percentage vegetation cover-weighted mean and SEM. All ground-based observations are compared to the CASA-CH_4 modelled CH_4 output using the default parameters, prior to calibration.

have aerenchymous tissue, in the summer and autumn months. Exceptions to this are seen for grass and sedge at the Eunant and Hafod locations at the end of July, where the grass flux is much higher than the sedge. It is not clear why this is the case. The fluxes measured for the juncus at the Hirddu location are uncharacteristically low given they have roots which extend deep into the soil and aerenchymous tissue that can rapidly transport the CH_4 produced below the water table to the surface. This may be due to the fact that the measurements (at all sites) were taken from sites at the hill top, where the water table might be lower than it otherwise would be elsewhere. However high fluxes are still seen for other vegetation types and at other locations so it is probably a more localised effect.

These observations show that the variability, even for one vegetation type measured on one day and at one location, is quite high. The variability increases with the magnitude of flux, and the change in magnitude of the flux between months can be considerable, even during the months where the fluxes are the highest. There is an underlying factor that results in higher fluxes from the Hafod location compared to the other two sites. The high variability suggests that the factors which control the CH_4 flux are quite complex and clearly operate on a number of scales. The SEM associated with these measurements in part include the measurement error, but they also include a measure of the spatial uncertainty in the observation as a result of measuring the flux at one location over another. It is therefore probably an overestimate of the real error in the observation. This is remedied in part by taking the standard error of the mean, but the associated errors are still significant, especially for the months where the CH_4 flux is highest.

3.8.2 Ground-based NEP observations

Two flux towers taking eddy covariance measurements of CO_2 net flux (NEP) were located approximately 100m apart at the Lake Vyrnwy site for part of 2009 (grid reference: OSGB 2934 3232). Only data collected on the same four dates as ground-based NEP chamber measurements have so far been processed, but these data have been provided by A. Heinemeyer (Stockholm Environment Institute, University of York. pers. comm.). All four dates contain gaps in the data, but two were considered to have too many gaps to be useful. The remaining two dates (17th and 18th August) contained only small gaps in the dataset (less than a few hours). Without any ancillary data at the time of the gaps which could be used for gap-filling, the missing points were replaced with an average of the data points either side of the gap. The SEM of the two flux towers was taken as a representation of the random error associated with the observations, which were recorded every half an hour. The data were summed, and the SEM combined to calculate a daily flux in $gCm^{-2}d^{-1}$. The data are shown, together with the standard error of the mean in Figure 3.12, and are compared to the default model run for the Eunant location, as this is the nearest weather station to the flux tower. The observations are ~1-1.5$gCm^{-2}d^{-1}$ higher than the default model using the uncalibrated parameter set, but given the prior range in the NEP flux model for the NEP-flux sensitive parameters, it is very possible that parameter calibration with adequate observations would result in the model correctly capturing the magnitude of the observations. The prior model distribution (for example see Figure 6.6 in Chapter 6) encompasses the observations, therefore an analysis of any possible discrepancy between the model and the NEP observations should be carried out after the calibration, as was the case for the CH_4 flux observations. This is discussed

further in Chapter 9.

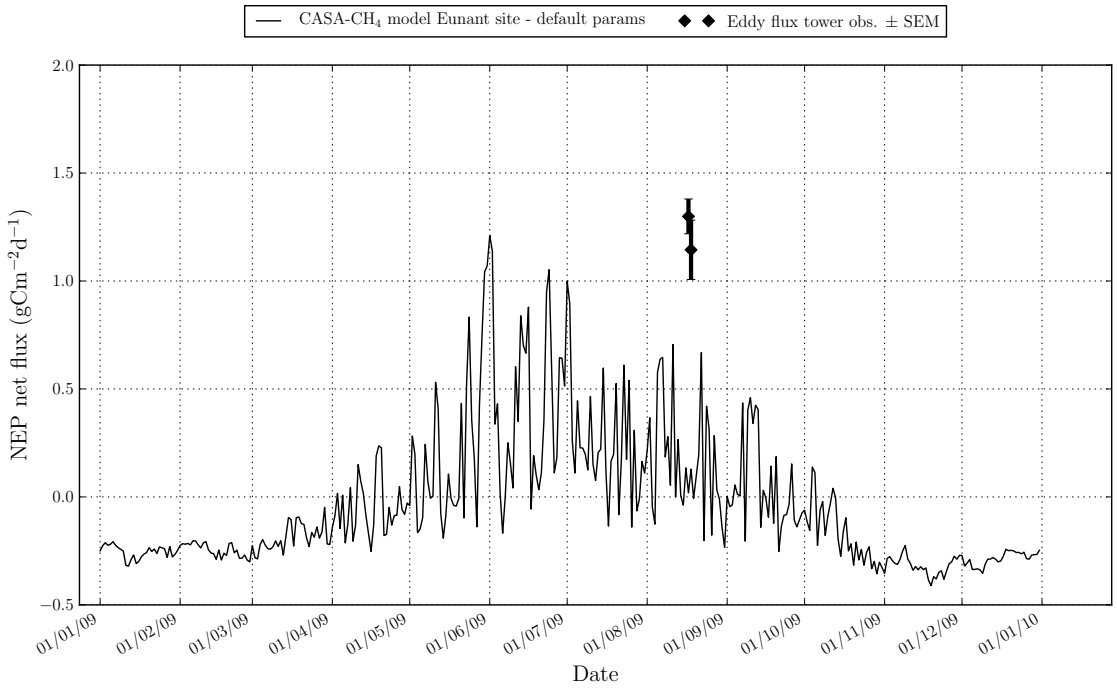

Figure 3.12: Graph showing the NEE observations from the eddy covariance measurements compared to the default model run for the Eunant location.

3.8.3 Satellite soil moisture data

Satellite soil moisture data from the AMSR-E radiometer onboard NASA's Aqua satellite are available for the Lake Vyrnwy site for 2009. The algorithm used to derive the soil moisture data is referenced below and the data are compared, where possible, to the available ground-based soil moisture data (M. Carroll, unpub.). Ground-truth data were kindly provided by M. Carroll (Department of Biology, University of York. pers. comm.). The soil moisture was measured at randomly sampled locations across the Lake Vyrnwy site using a theta probe. These values were averaged to give a site-mean value for each day of data collection, in order to compare with the low resolution satellite data.

AMSR-E data

The AMSR-E volumetric soil moisture data were derived using the LPRM (VUA) algorithm (*Owe et al.*, 2001) and described in Chapter 2 Section 2.4.2. The data can be downloaded, along with dataset product description pages and related documents, from the VUA website

(http://geoservices.falw.vu.nl/). The data were then processed to obtain only the pixels that were flagged as "good quality" as specified on the dataset product pages. The spatial resolution of the data is ~50km. The resultant timeseries is compared to the available ground-based data in 2009 and 2010, though only 2009 data will be used in the model calibration. No estimate of error is provided with these observations but (*de Jeu et al.*, 2008) estimated the accuracy of the observa-

tions is 0.06m^3m^{-3}. *Scipal et al.* (2008) and *Dorigo et al.* (2010) examined the random error in the AMSR-E observations as opposed to the systematic error from biases in the observations. Their results suggest that the 0.06m^3m^{-3} estimate appears to be fair representation of the magnitude of the error in the observations, though these studies were not for sites with near-saturated soils.

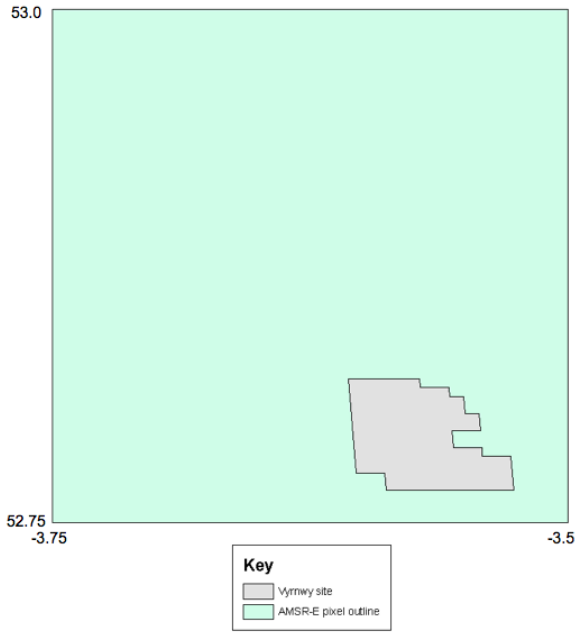

Figure 3.13: Plot to show a comparison of the coverage of the AMSR-E pixel with the Lake Vyrnwy site.

As the AMSR-E pixel resolution is larger than the Lake Vyrnwy site (see Figure 3.13), it was expected that the AMSR-E data would underestimate the ground-based soil moisture observations, as the surrounding mineral soils will have lower soil moisture values. As Figure 3.14(a) shows this is indeed the case. Although the satellite soil moisture observations are negatively biased, the timeseries shows the temporal variability is well-approximated by the AMSR-E observations. The correlation between the satellite and ground-based soil moisture (0.44) is shown in Figure 3.14(b). This increases to 0.79 if the data point on the 29th June is excluded, where the ground-truth data are close to 1.0m^3m^{-3}. These values are only based on a limited dataset for the summer months, but the results are encouraging. In particular the high variability of the soil moisture, expected of the thin upper layer of the soil is seen in both the satellite data and ground-truth data, also suggesting the two datasets are capturing the dynamics of the system well.

Figure 3.14(d) shows a comparison of both the AMSR-E and ground-truth observations with the default model run. The dips in the model appear to correspond well to both sets of observations, though the AMSR-E observations in particular are more highly variable than the model and do not appear to reach a maximum value. This may be due to the bias in the satellite observations. It might also be due to the fact the AMSR-E observations are probably "seeing" a thinner, more variable, surface layer of the soil than the 5cm surface layer of the model. It is very difficult to know the exact penetration depth of the microwave signal, but it might help if the model had five 1cm-thick layers at the surface with which to compare to the satellite observations, instead of one, 5cm thick layer. The default model run is based on a porosity of 0.55. This incidentally

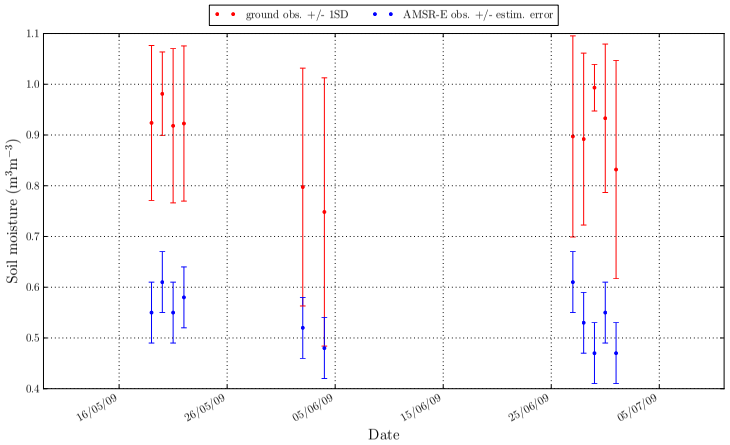

(a) *Comparison of the AMSR-E and ground-based volumetric soil moisture data for the available ground-truth dates*

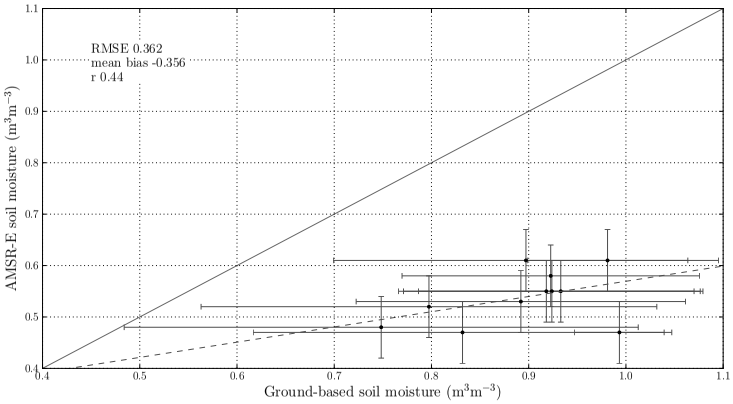

(b) *Correlation between the ground-truth and AMSR-E volumetric soil moisture data.*

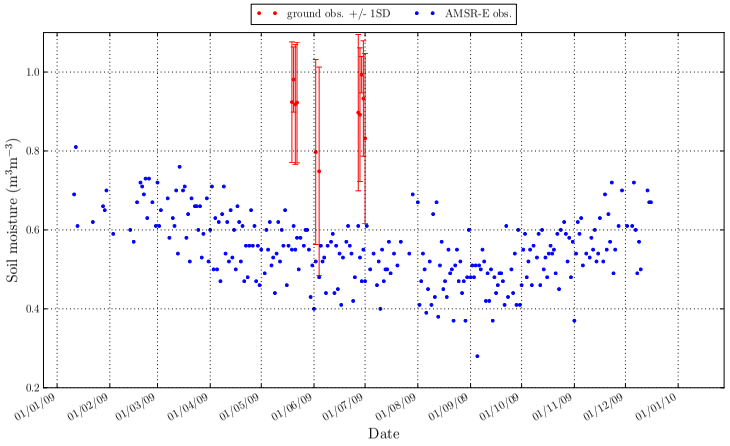

(c) *Comparison of the complete 2009 AMSR-E timeseries with the available ground-truth data.*

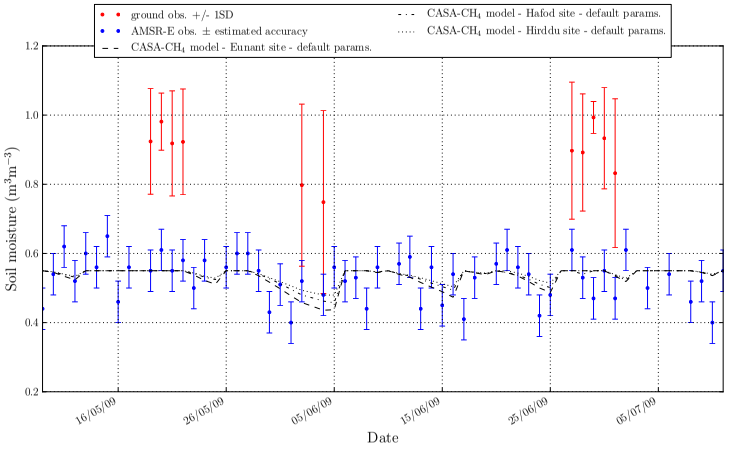

(d) *Comparison of the AMSR-E and ground-truth data with the model run using the default parameters for all three locations at the Lake Vyrnwy site.*

Figure 3.14: Plots to show the validation of the AMSR-E volumetric soil moisture data with ground-truth data and a comparison to the default model run.

corresponds well to the AMSR-E observations. However as already discussed the satellite data contain a bias will needs to be taken into account when performing the model calibration. This is discussed further in Chapter 9 Section 9.3.

Chapter 4

Model evaluation and sensitivity analysis

4.1 Introduction

The aim of this chapter is to perform an initial model evaluation, detail the modifications made to the original model formulation as set out in *Potter et al.* (1993) and *Potter* (1997) and to conduct a sensitivity analysis on the model.

The model evaluation is intended to provide a brief overview of the model. In particular it is used to investigate which inputs and/or subsidiary state variables, such as soil moisture and temperature, control the magnitude, variability and trend of the different C fluxes.

The objective of the sensitivity analysis is to determine which parameters the model state variables, in particular the C fluxes, are most sensitive to. This is key for determining which parameters should be included in the Bayesian model calibration.

Both the initial model evaluation and the sensitivity analysis are used to determine which observation datasets would be most useful for constraining the model parameters and model predictive uncertainty, with particular reference to EO datasets.

The model modifications are described at the beginning of the chapter so that the model runs with the default parameters are consistent for the remainder of the thesis. Following this a brief summary of the model state variables is provided. Finally the results of the sensitivity analysis are detailed and discussed. The main findings of this chapter are discussed and summarised at the end of the chapter.

4.2 Modifications to the model

Two main modifications were made to the model in addition to those mentioned in Chapter 3 Section 3.3.5. Firstly the formulation for calculating the ratio between the CO_2 and CH_4 flux, as described in *Potter* (1997) resulted in CH_4 fluxes that were too low, based on the ground-based flux results that were available from the Lake Vyrnwy site. The water table is mostly below the surface by up to 40cm at the Lake Vyrnwy site. *Potter* (1997) gives ratios of CH_4:CO_2 of <=0.01 for water tables at or below the surface (0.01 for a water table of 0.0m, decreasing logarithmically

to 0.0001 for water tables of -0.2m). Figures 4.1(a) and 4.1(b) show examples of the CH_4:CO_2 ratios for the two locations where C flux observations were taken throughout 2009; the first for a grass patch, and the second for a sedge patch. It was hypothesised that the grass would not emit much CH_4, especially compared to the sedge, which has aerenchymous tissues. Yet both show the maximum ratio exceeds 0.01, even when the water table is >0.2m below the surface. The CH_4:CO_2 ratio reaches values of ~0.21 for the sedge.

The magnitude of the ground-based flux measurements could not have been achieved with the ratios of CH_4:CO_2 that were given in *Potter* (1997). *Wania* (2007) concludes that the ratio of CH_4:CO_2 is difficult to predict, given the high range of values in the literature (0.001 to 1.7) Figures 4.1(a) and 4.1(b) support this finding, as clearly the ratio can be very different even for measurements taken on the same day and at a similar time, in the same location and for the same vegetation type. They therefore chose to have the ratio at soil saturation as a parameter that can be calibrated, and to decrease the ratio based on the degree of soil saturation. This formulation was adopted for the CASA-CH_4 model. Figure 4.1(c) shows a comparison of the original and the LPJ-WHyMe model formulation. The original formulation never produced a flux that increased much above ~0.0g$Cm^{-2}d^{-1}$, whereas the LPJ-WHyMe formulation can capture the magnitude of the higher summer fluxes. The "inundation ratio" parameter, i.e. the ratio of CH_4:CO_2 when the soil is saturated, can be calibrated to account for the changing magnitude of the fluxes throughout the year. Based on *Wania et al.* (2009a,b) a range of 0.001 to 1.7 was chosen for the inundation ratio parameter. The other benefit of using the LPJ-WHyMe formulation is that it depends on the saturation of the soil, and therefore the volumetric soil moisture, rather than the model water table depth, which appeared to be much higher than the low water table depths seen in the initial measurements. Volumetric soil moisture is much easier to measure that water table depth in the field and satellite-derived soil moisture estimates of the thin layer near the surface are also available.

The CH_4 flux dynamics of the observations do not seem to be represented well by either of the model formulations however. A full assessment of this discrepancy is not possible until the model has been calibrated. However it might be the case that the ratio used to partition the C into CO_2 and CH_4 flux may not be accurate, and the model formulation may need to be changed.

The ground-based observations occasionally were negative as a result of the uptake of CH_4 into the soil. The CASA-CH_4 model does not take into account CH_4 uptake and therefore no negative fluxes can be predicted. As the magnitude of the CH_4 uptake is very small, a decision was taken not to add further complexity to the model by adding a submodule that could account for the uptake of CH_4 into the soil.

The second modification made to the model was to add a thin surface layer (5cm thick) to the soil temperature and moisture submodules. This is because satellite soil moisture estimates are derived from the top few cm (wavelength dependent) of the soil, due to the fact the microwave wavelengths cannot penetrate to greater depths. In order to use satellite soil moisture measurements to calibrate the model it is necessary to compare them to the model output from an equivalent depth in the soil, otherwise the disparity might simply be due to the different vertical resolution of the measurement. The depths of the other boundaries in the soil remained the same at 30cm, 1m and 2m. This modification resulted in a greater magnitude of variability in soil moisture in the uppermost layer, as it is only 5cm thick instead of 30cm, and a subsequent slight reduction

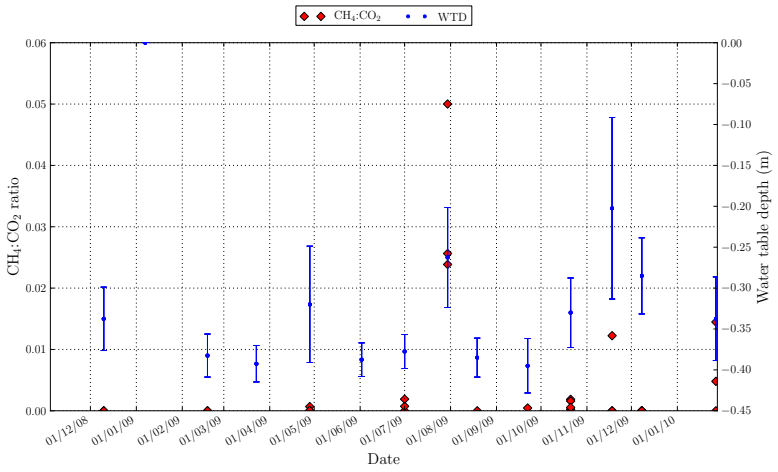

(a) *Comparison of the ground-based CH_4:CO_2 ratios with the water table depths for a grass location at the Lake Vyrnwy site.*

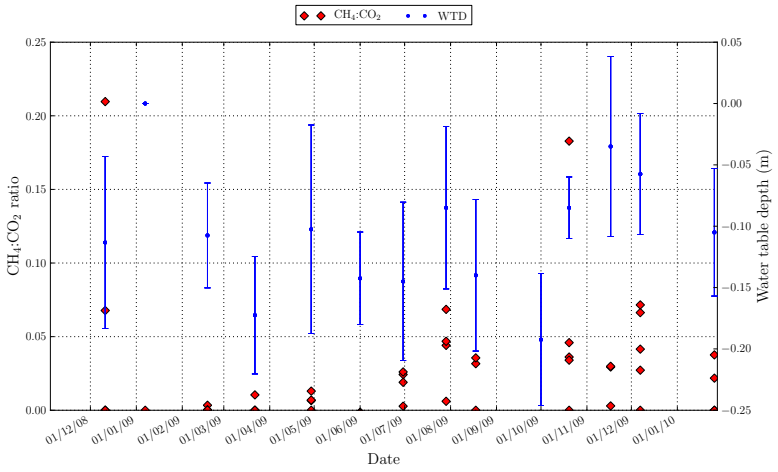

(b) *Comparison of the ground-based CH_4:CO_2 ratios with the water table depths for a sedge location at the Lake Vyrnwy site.*

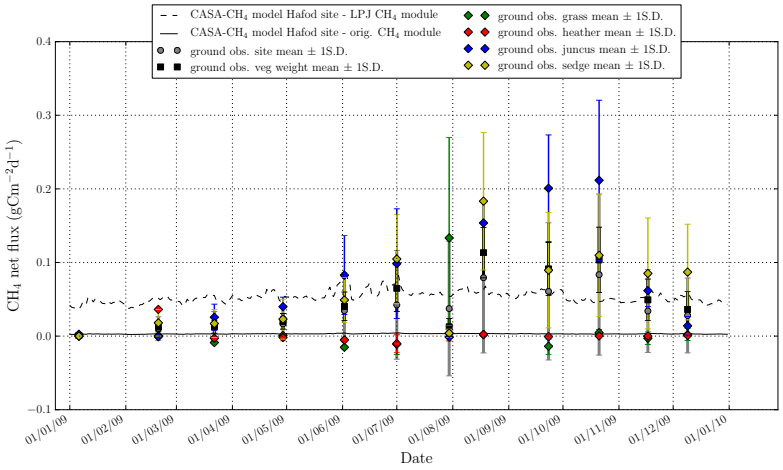

(c) *Model CH_4 timeseries with the original and LPJ-WHyMe model formulations, compared to ground-based observations.*

Figure 4.1: Plots to show the of the original CH_4:CO_2 ratios put forward in *Potter* (1997)

in the lower layers, as seen in Figure 4.2. However the total variability of soil moisture hardly changes. Only a very, slight increase in the reduction in soil moisture is seen for the largest dip in soil moisture in the summer months (data not shown). Therefore the overall magnitude of the C flux is only fractionally larger. This is due to the fact that there is an overall increase in the moisture variability of the upper two layers that are used to calculate the scalars that control the decomposition of the litter, which produces a higher fraction of the total daily soil C flux than the microbial and soil layers.

4.3 Model Evaluation

The initial model evaluation is based on model runs using the default parameters as detailed in the Chapter 3 Table 3.2. Most of the behaviour of the model can be predicted from the model physics. NPP is dependent mainly upon the temporal evolution of air temperature, solar radiation and NDVI. It is also affected to a lesser extent, by the soil moisture, as the EET, used to calculate the moisture scalar for the NPP calculation, is influenced by the saturation of the soil. The soil C fluxes (CO_2 and CH_4) correspond closely to each other, as expected (Figure 4.3(a)). As already discussed the temporal trend of the CH_4 flux, i.e. the "long autumn shoulder" seen in the observations, may be different to the temporal trend of the soil respiration. As such the model representation of CH_4 flux dynamics may be incorrect. The temporal variability of the NEP flux is dominated by that of the NPP, and not the soil respiration as its magnitude is much smaller (Figure 4.3(b)).

The magnitude of the soil C fluxes depends on the amount of C entering the system, the cycling of C between the various C pools and the soil temperature and moisture. Soil temperature and moisture are used to calculate the scalars which, in part, control the amount of C decomposition in the soil and the transfers between the C pools at various depths. An increase in soil temperature and a decrease in soil moisture result in an increase in C flux.

Whilst the magnitude of the C flux is controlled by the amount of C assimilation and the soil temperature and moisture, the daily variability in C flux is modulated by that of the soil temperature and moisture. This can be seen if the soil temperature submodule is driven with a sinusoidal variation of temperature about the annual mean temperature, rather than the actual air temperature, as was initially put forward in *Potter* (1997). Figure 4.4(a) shows a comparison of the soil respiration that results with the soil temperature being forced at the upper boundary with air temperature and with the sinusoidal oscillation. The trend in soil temperature and moisture is also shown. The smooth oscillation used to force the soil temperature submodule results in a smooth C flux temporal trend, except for the time periods where there is a dip in the soil moisture (Figures 9.10(i) and 9.10(i)). Decomposition is severely inhibited when the soil is saturated and therefore the temporal variability is dominated by the soil temperature. When the soil is saturated sharp peaks in the C flux are seen. This is clearly evident even when the soil temperature is driven with the variable air temperature timeseries, suggesting a reduction in soil moisture has a more dramatic impact on the C flux than the soil temperature.

This behaviour is demonstrated for the soil respiration, but the same behaviour is seen for the CH_4 flux, which as already discussed, is closely linked to the soil CO_2 flux. As discussed the magnitude of the soil respiration and CH_4 flux is also controlled by the assimilation of C into

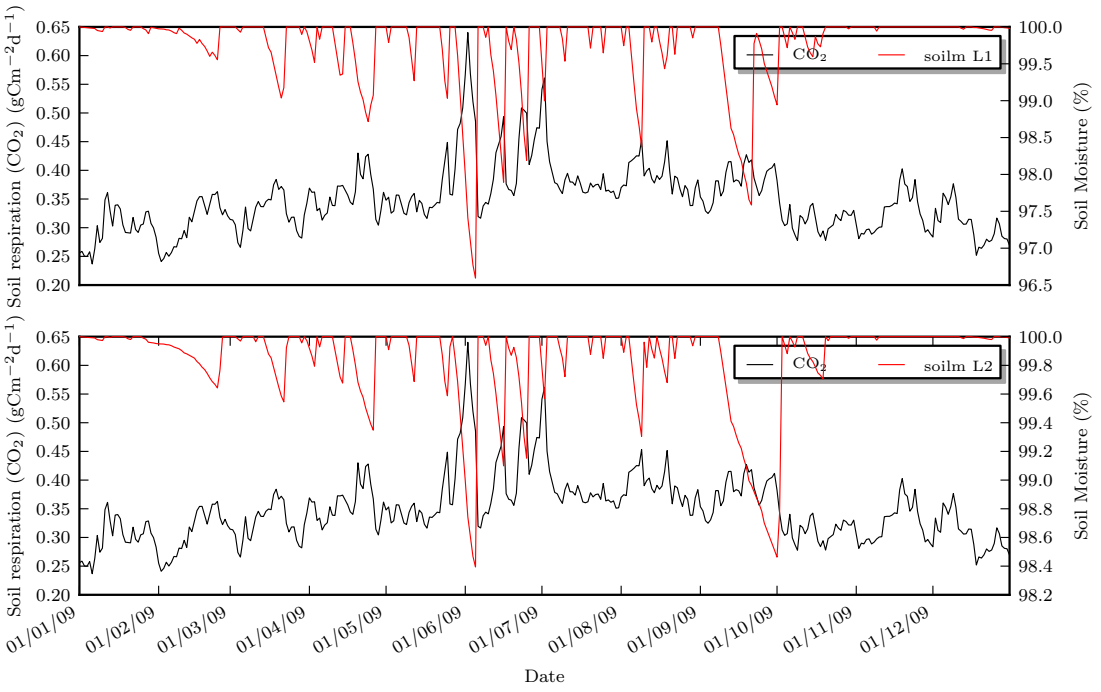

(a) *Three-layered model.*

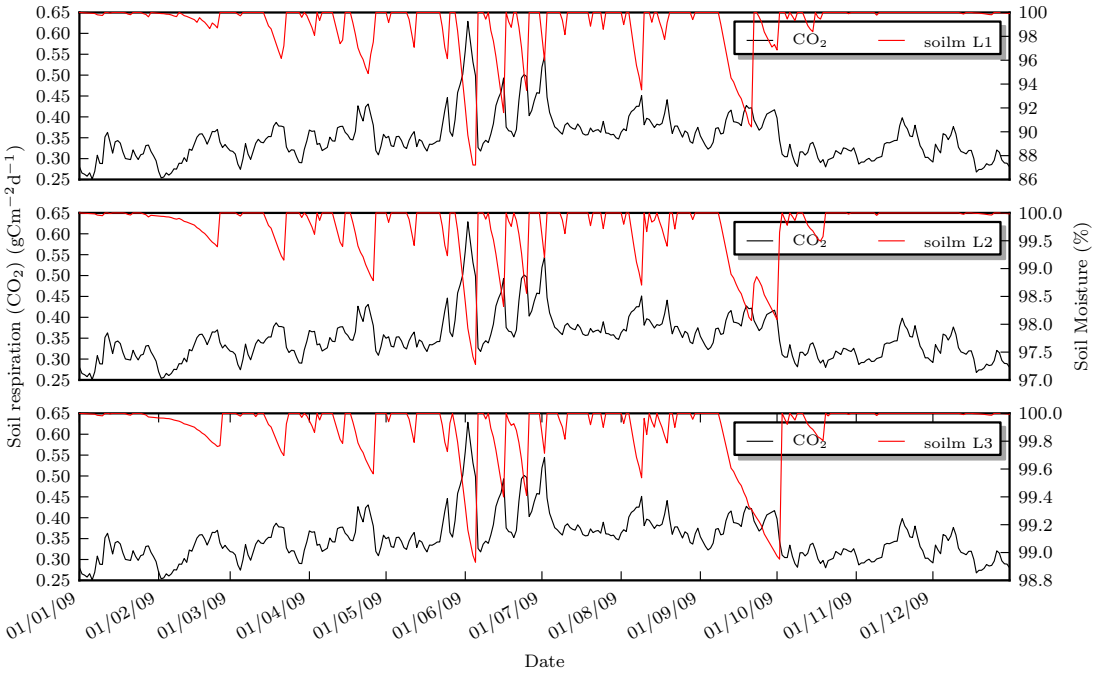

(b) *Four-layered model.*

Figure 4.2: Plots to show the change in soil moisture of the layers in the upper 1m of the soil and the subsequent soil respiration (CO_2) flux for the three- and four-layered model (resulting in two and three layers respectively in the uppermost 1m of the soil).

(a) *Soil respiration (CO_2) compared to CH_4 flux.*

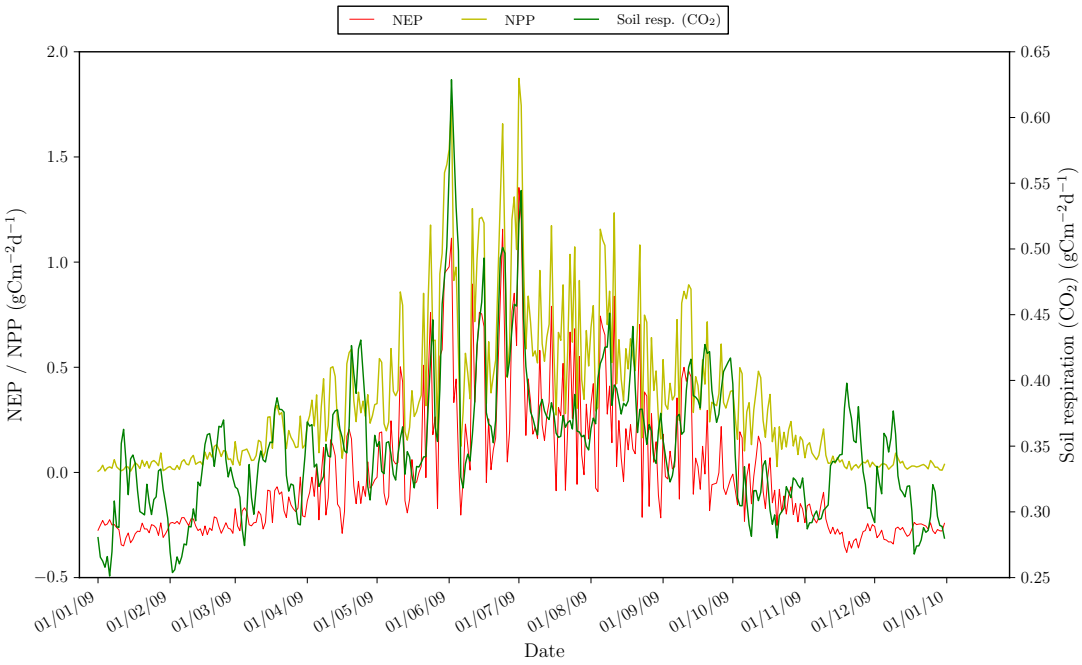

(b) *NEP compared to NPP and soil respiration (CO_2) fluxes.*

Figure 4.3: Plots to show the relationships between the various C fluxes of the CASA-CH_4 model.

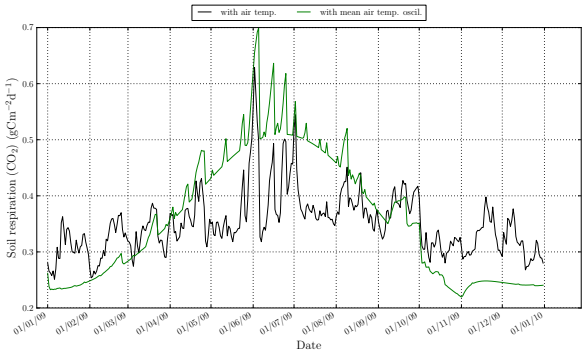

(a) *Comparison of the soil respiration flux when the soil temperature submodule is forced at its upper boundary with air temperature and with a sinusoidal oscillation about the annual mean air temperature.*

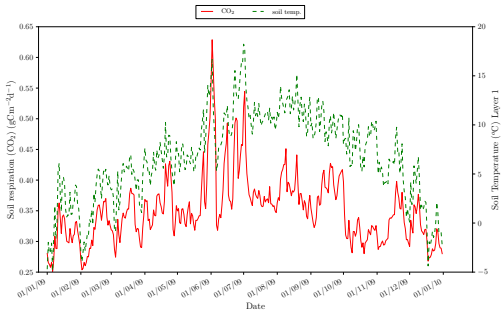

(b) *Soil respiration compared to the soil temperature timeseries of the uppermost layer when forced with air temperature.*

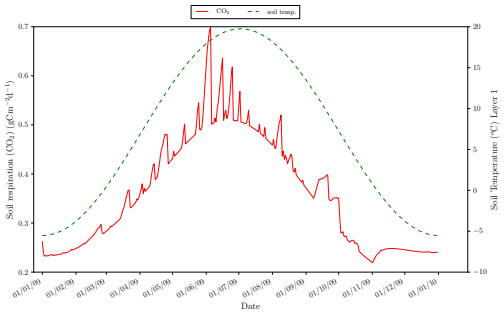

(c) *Soil respiration compared to the soil temperature timeseries of the uppermost layer when forced with a sinusoidal oscillation about the annual mean air temperature.*

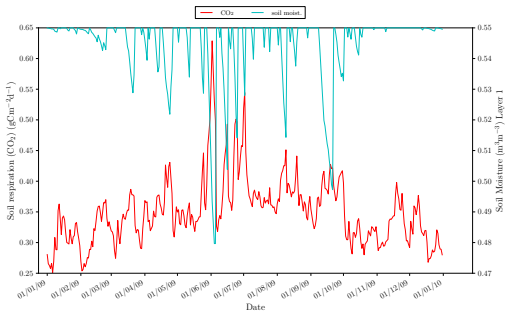

(d) *Soil respiration compared to the soil moisture timeseries of the uppermost layer when the soil temperature submodule is forced with air temperature.*

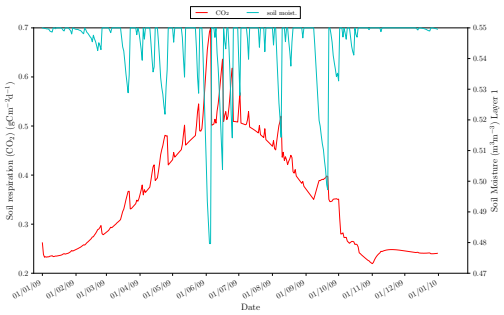

(e) *Soil respiration compared to the soil moisture timeseries of the uppermost layer when the soil temperature submodule is forced with a sinusoidal oscillation about the annual mean air temperature.*

Figure 4.4: Plots to show the effect of soil temperature and moisture on the daily variability in soil C fluxes.

the soil. This is dependent upon many parameters and the model physics, but is crucially driven by the NDVI and meteorological data. The NDVI timeseries is doubly important as it is used to calculate the LAI, from which the timing of litterfall is approximated. A visual assessment of the importance of the magnitude and trend of NDVI data on the NPP is also provided. Figure 4.5 shows the original NPP compared to the interpolated NDVI timeseries, followed by the change in NPP that would be expected a) for a shift in the magnitude of NDVI of ±0.1 (Figure 4.5(b)), and b) a shift in the phase of the NDVI timeseries of ±1 month (Figure 4.5(c)). The annual flux is also given in the top right hand corner. The plots suggest an error in the magnitude of the NDVI would have a greater impact on the daily variability, and the annual flux, than an error in the temporal trend. This is most likely due to the fact slightly different temporal trends of the air temperature and solar radiation have a more direct control on the annual cycle of the NPP. It is important to use good quality satellite NDVI data that has been corrected for atmospheric, cloud and angular effects associated with the viewing and illumination geometry. Additionally a robust interpolation of the satellite NDVI data is also required.

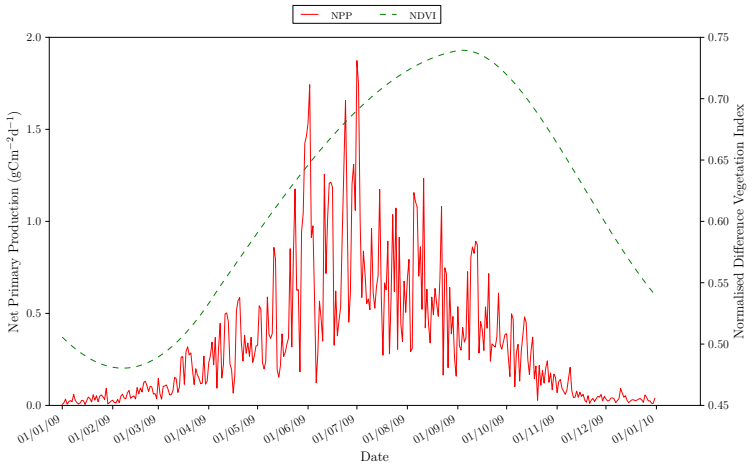

(a) *Comparison of the default NPP with the NDVI timeseries.*

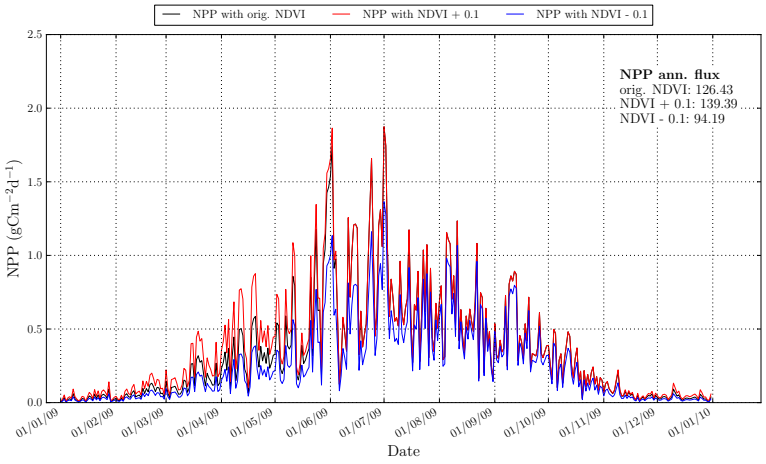

(b) *Comparison of the default NPP with the NPP calculated using the NDVI with a change in magnitude of ±0.1.*

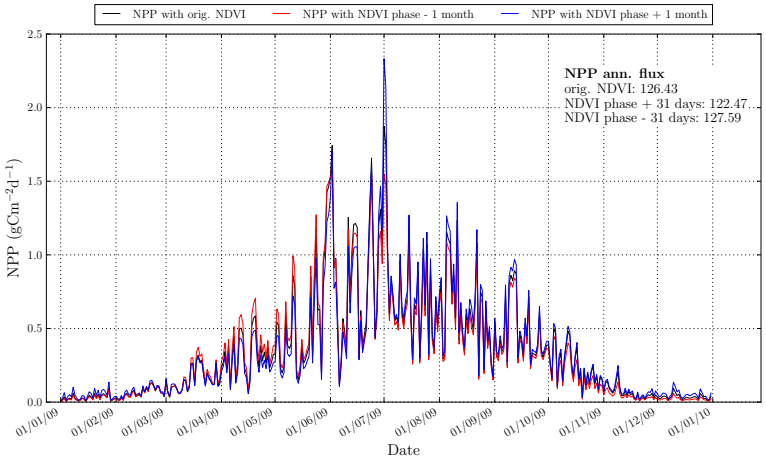

(c) *Comparison of the default NPP with the NPP calculated using the NDVI with a shift in the phase of ± 1 month.*

Figure 4.5: Plots to show the influence of the NDVI magnitude and temporal trend on the NPP.

4.4 Results of the Morris sensitivity analysis

The Morris sensitivity analysis method was detailed in Chapter 3 Section 3.5. The sensitivity analysis was performed for the model NPP, soil respiration (CO_2), NEP and CH_4 flux. The results are presented below.

The Morris sensitivity analysis of the mean daily differences in model outputs as a result of changing parameter values produced the parameter rankings for each model output shown in Table 4.1. The rankings are based on the mean of the absolute value of the elementary effects. The highest ranking parameters for all of the C flux model outputs are those directly involved in the calculation of C flux, either through the NPP calculation, the soil CO_2 respiration, or the CH_4 flux calculation, where relevant. The next most important parameters are those involved in the soil moisture calculations, and in particular for the NEP and CH_4 flux, the porosity. None of the soil temperature related parameters have a significant impact on any of the model outputs, and are always the lowest ranked parameters.

Ranking	**NPP**	**Soil respiration (CO_2)**	**NEP**	**CH_4 flux**
1	LUE	Q10_l	auto. resp.	Q10_l
2	auto. resp.	Me_s	LUE	Me_s
3	SR_max	auto. resp.	SR_max	auto. resp.
4	poros.	LUE	Q10_l	inund. ratio
5	rdr_b	inund. ratio	poros.	LUE
6	rdr_a	LN ratio	Me_s	LN ratio
7	wpt	Q10_s	rdr_b	Q10_s
8	LAI_max	SR_max	wpt	lig. frac.
9		lig. frac	inund. ratio	SR_max
10		Me_l	rdr_a	Me_l
11		poros.	Q10_s	poros.
12		Me_a	LN ratio	LAI_max
13		wpt	lig. frac.	wpt
14		sm_scalar	Me_l	Me_a
15		LAI_max	Me_a	sm_scalar
16		rdr_b	LAI_max	rdr_b
17		s_pmt	sm_scalar	s_pmt
18		rdr_a	s_pmt	j_pmt
19		j_pmt	soil suc.	rdr_*a*
20		soil suc.	j_pmt	soil suc.
21		Kb	Kb	Kb

Table 4.1: The Morris rankings for each parameter for each C flux in the CASA-CH_4 model. See Chapter 3 Table 3.2 for a description of the parameters.

NPP is related to parameters that control assimilation of C into the soil in equations 3.1 and 3.3 (LUE, autotrophic respiration scalar and SR_max), as well as parameters controlling moisture limitation (equation 3.8), either directly by controlling the soil moisture (porosity and rdr parameters) or indirectly through its impact on the PET (LAI_max).

For the soil CO_2 respiration flux the two most important parameters are directly related to the cycling of the C through the litter and soil C pools (Figure 4.7). The next most parameters important

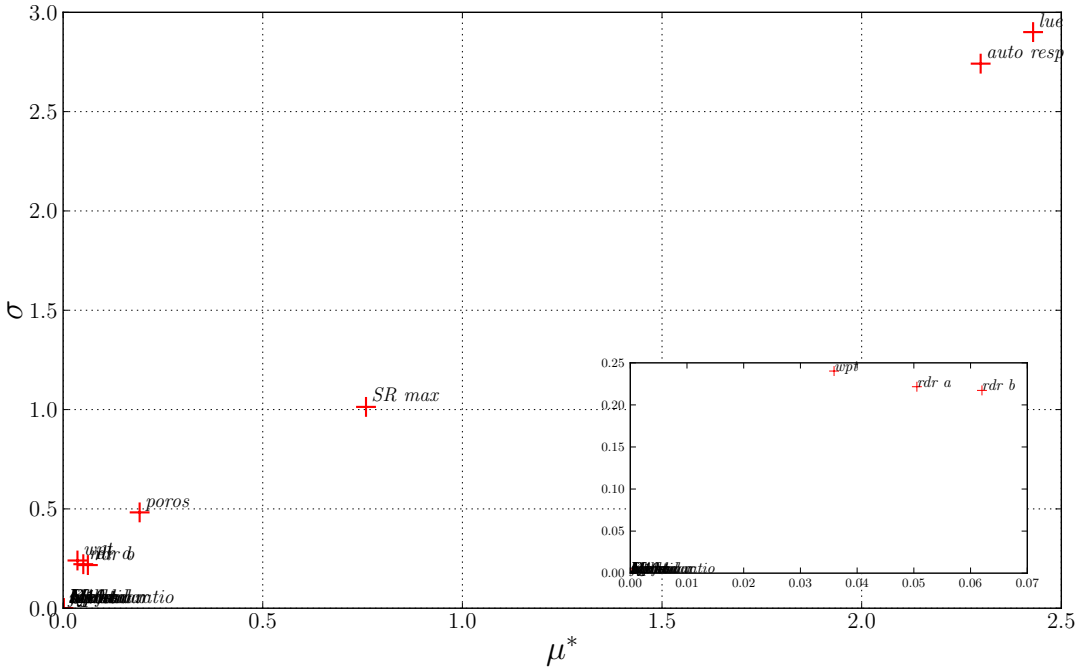

Figure 4.6: Morris sensitivity analysis of the NPP flux. μ^* is the mean of the absolute values of the elementary effects σ is the standard deviation. The parameters that do not affect the the NPP as much are shown in the inset.

are those involved in the calculation of NPP, which controls the amount of C assimilated into the litter and soil on a daily basis. Following these parameters the next most important parameter is the inundation ratio, which controls the partitioning of decomposed C into CO_2 and CH_4 flux and is dependent on saturation of the soil. The remaining parameters which have a significant impact on the soil CO_2 are again related to the assimilation of C into, or the cycling of C within, the litter and soil C pools.

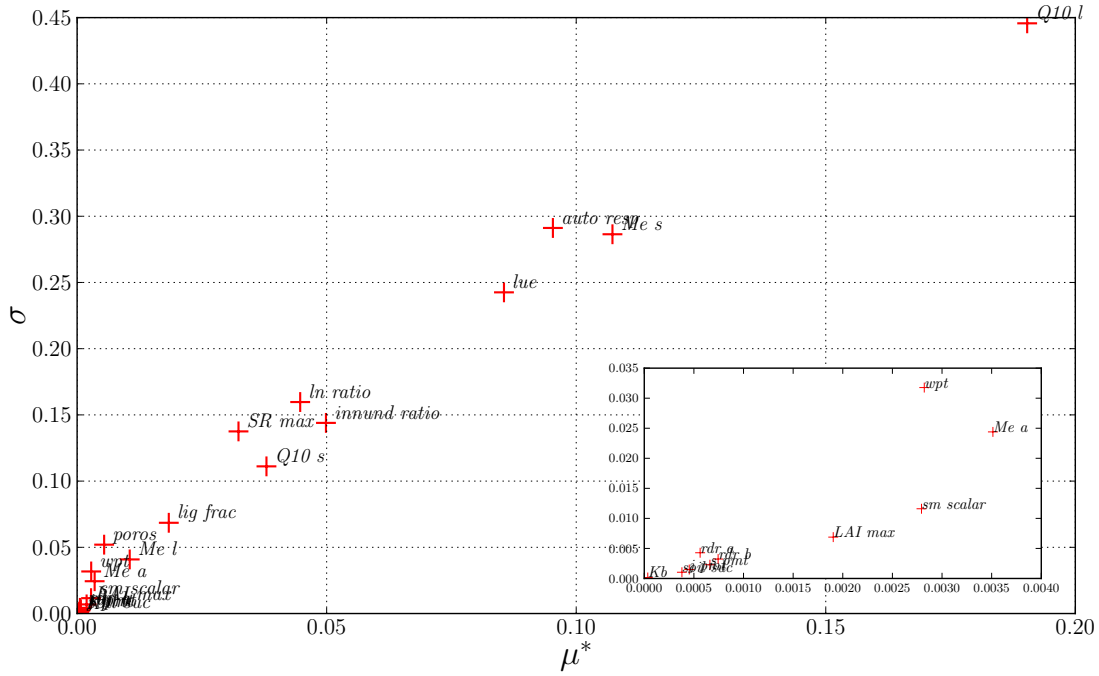

Figure 4.7: Morris sensitivity analysis of the soil CO_2 flux. μ^* is the mean of the absolute values of the elementary effects σ is the standard deviation. The parameters that do not affect the the CO_2 flux as much are shown in the inset.

The NEP flux is clearly most sensitive to the three parameters involved in the NPP calculations, the autotrophic respiration scalar, LUE and SR_max (Figure 4.8). This is not surprising given the obvious dominance of NPP in the temporal trend of the NEP flux (Figure 4.3(b)). Interestingly the NEP flux is more sensitive to the porosity parameter than to any of the parameters involved in the calculation of soil respiration CO_2 flux because it is used in both the NPP and soil respiration CO_2 flux calculations, through the soil moisture scalars on C transfer in the soil (assimilation or decomposition). Following this the NEP flux is sensitive to parameters related to the cycling of soil C, with Q10_l being the highest ranking, and to the rdr parameters (see inset of Figure 4.9).
As was the case for the soil CO_2 flux, the CH_4 flux is unsurprisingly most sensitive to the parameters involved in the cycling of C in the litter and soil (Figure 4.9), as the C produced during decomposition is divided between the CO_2 and CH_4 flux through the inundation ratio parameter, as already discussed. The order of the rankings of parameters the CH_4 flux is sensitive to is very similar to the CO_2 flux, however it appears the CH_4 flux is more sensitive to the inundation ratio, which has a higher ranking, as does the Me_s parameter, especially in relation to the LUE and autotrophic respiration scalar parameters. This is to be expected as the CH_4 flux is a) further down

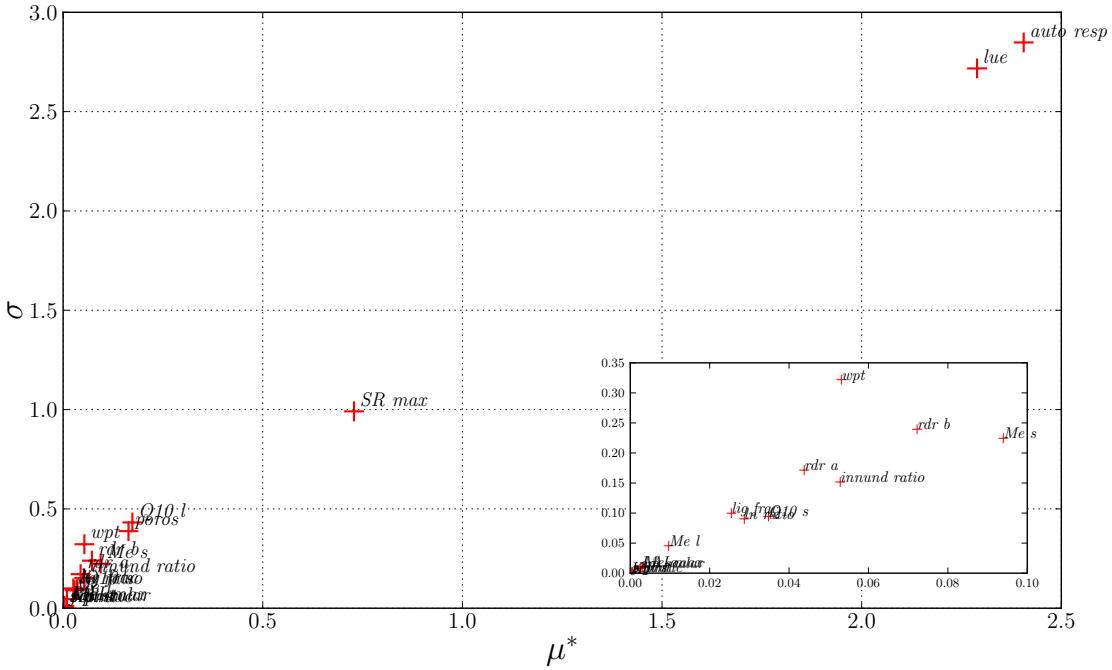

Figure 4.8: Morris sensitivity analysis of the soil NEP flux. μ^* is the mean of the absolute values of the elementary effects σ is the standard deviation. The parameters that do not affect the the NEP as much are shown in the inset.

the chain of calculations involving C flux, thereby less responsive relatively to the NPP calculations, and b) the CH_4 flux is much smaller in magnitude than the soil CO_2 flux, and therefore a change in the inundation ratio produces a higher relative magnitude of change for the CH_4 flux. There is a limited body of literature on the Q10 parameters which are often used in C flux models (e.g. *CHEN and TIAN* (2005)). If the C fluxes are very sensitive to this parameter then more experimental work needs to be done to better quantify the value of Q10 for different soil processes in different ecosystems.

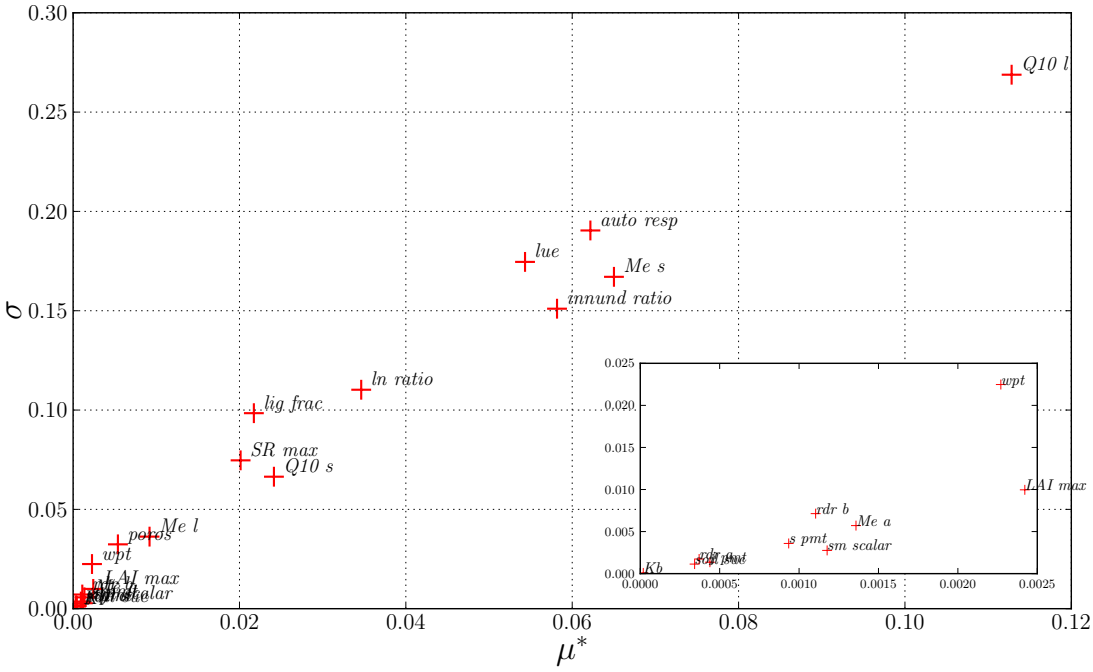

Figure 4.9: Morris sensitivity analysis of the soil CH_4 flux. μ^* is the mean of the absolute values of the elementary effects σ is the standard deviation. The parameters that do not affect the the CH_4 flux as much are shown in the inset.

4.5 "One-at-a-time" (OAT) sensitivity analyses

OAT sensitivity analyses are performed by changing only one parameter at a time. The other parameters remain fixed at their default value (see Chapter 3 Table 3.2). The following plots show the response of a change in each parameter on the soil moisture, NEP and CH_4 flux observations, as corresponding observations will be used in the Bayesian inversions later in the thesis. The parameter space was divided into five equal segments and the model run for each value of each parameter. The outputs are compared to the default value of the parameter.

Whilst local OAT sensitivity analyses are not useful for understanding the impact of the whole model parameter space on the model outputs, it is informative to look at plots of OAT analyses of parameter behaviour on the model output in question, keeping all other parameters than the one in question set to their default values, as it gives an idea of the kind of response that might be expected in the model output with changing parameter value. However it is imperative to keep in mind that for different values of the other parameters, the behaviour, and in particular the magnitude, of

changes in the model outputs might be very different. Rather than show numerous plots of the response of each model output to all the parameters, plots of the OAT analyses of parameters that most affect the model outputs to be constrained by the MH-MCMC algorithm in later chapters are shown. The effect of all parameters on the various model outputs is briefly summarised however.
The volumetric soil moisture is affected by the porosity, which mainly controls the maximum value (Figure 4.10(a)) and the relative drying rate (rdr) parameters, which control the amount the volumetric soil moisture decreases from the maximum value, which happens when the outputs of the hydrology module (i.e. evapotranspiration) are greater than the inputs (i.e. rainfall). An increase in the rdr_a parameter reduces the drop in soil moisture during times when the soil moisture dips below its maximum value (Figure 4.10(b)). An increase in the rdr_b parameter results in the opposite effect, and Figure 4.10(c) shows that the volumetric soil moisture is potentially not sensitive to the whole range of parameter values (although this cannot be assumed for different values of other parameters).

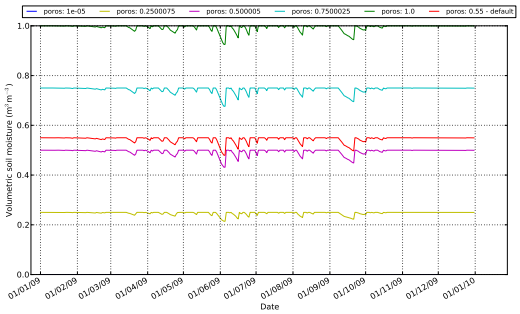

(a) porosity

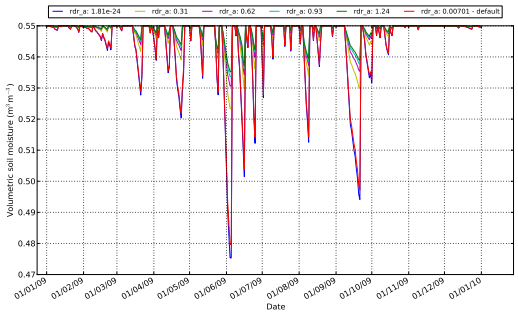

(b) rdr_a scalar

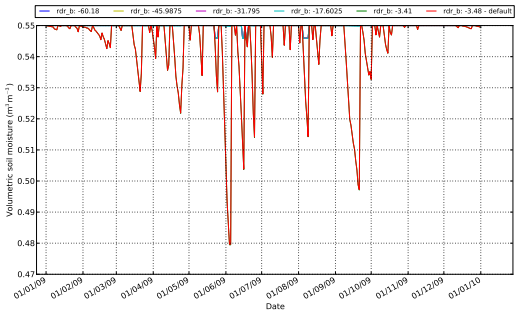

(c) rdr_b scalar

Figure 4.10: OAT sensitivity analyses of the effect of different related parameters on the volumetric soil moisture.

It is clear from the sensitivity analysis of the soil moisture that whilst the wilting point parameter is used in the calculations relating to the soil moisture, in this type of climate with high precipitation that the wilting point parameter is not important as the soil moisture never reaches the wilting point. Therefore it is a redundant parameter and should not be included in the calibration.
The response of the relative soil moisture to porosity is different from the volumetric soil moisture as it is a relative measure (Figure 4.11(a)). At very low values of porosity the relative soil moisture drops dramatically at times when there is a big drop in soil moisture due to limited rainfall or increased evapotranspiration. The response of the relative soil moisture to the rdr parameters

(Figures 4.11(b) and 4.11(c)), is much the same as for the volumetric soil moisture.

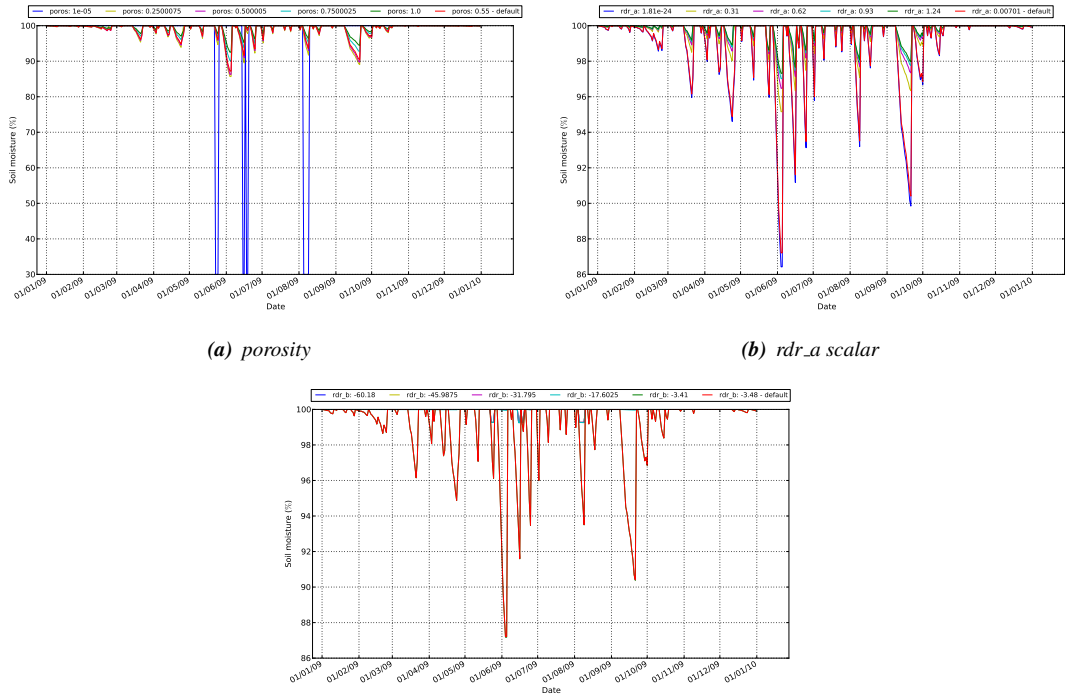

(a) *porosity*

(b) *rdr_a scalar*

(c) *rdr_b scalar*

Figure 4.11: OAT sensitivity analyses of the effect of different related parameters on the relative (%) soil moisture.

The effect of the parameters on the NEP flux is discussed in order of their importance. An increase in the autotrophic respiration scalar results in a decrease in the NEP flux if above ~-0.15gCm^{-2}d^{-1}, and an increase if below, and therefore a decrease in the amplitude of the annual cycle (Figure 4.12(a)). At values close to 1.0 it appears the daily variability is greatly reduced and shows the opposite sign to the NEP flux for other values of the autotrophic respiration scalar. The magnitude of variability is greater for higher values of NEP flux. The same pattern emerges for the LUE parameter but with a decrease in the flux above zero and an increase below (Figure 4.12(b)). LUE appears to result in the largest variability in NEP but this is contingent on the choice of the other default parameters.

The SR_max parameter shows different behaviour at different times of the year. Mostly an increase in the value of the parameter results in a decrease in flux when the NEP values are greater than ~-0.2gCm^{-2}d^{-1} and an increase if below. However the amount the flux decreases when the values are greater than zero is different throughout the year, resulting in slightly non-linear behaviour (Figure 4.12(c)). Generally an increase in porosity results in an increase in NEP flux for values above ~-0.2gCm^{-2}d^{-1} and a decrease below (Figure 4.12(d)). The magnitude of the variability is much greater for higher values of NEP flux. The final parameter which the NEP flux is significantly sensitive to is the Q10_1 parameter. An increase in the Q10_1 parameter results in an increase in the NEP flux, however the behaviour is non-linear. Above a value of ~8gCm^{-2}d^{-1} the NEP flux doesn't change. In addition at lower values of NEP flux the sensitivity of the flux to changing parameter value is higher.

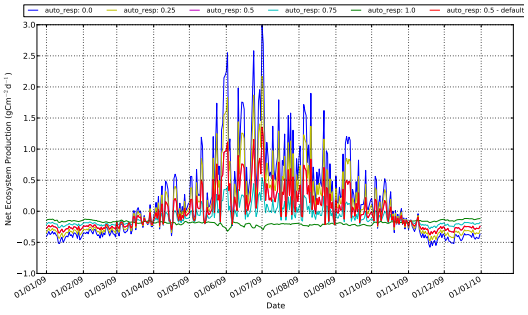

(a) *Autotrophic respiration scalar*

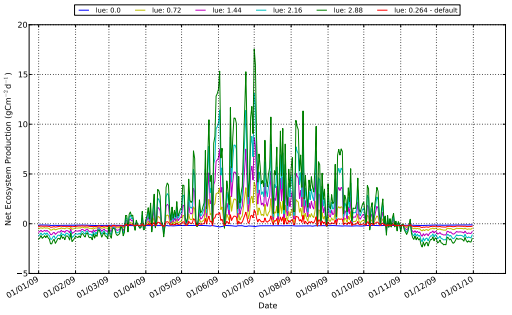

(b) *LUE*

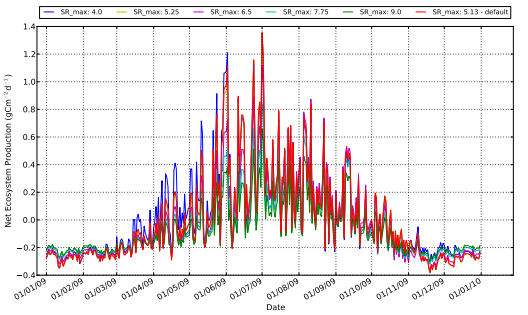

(c) *SR_max*

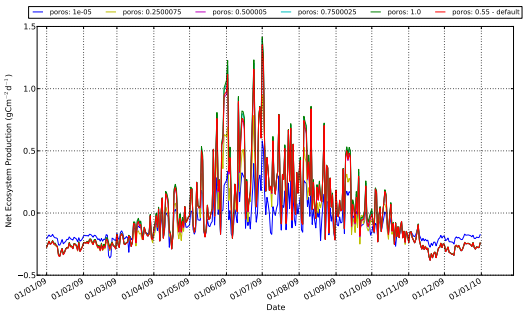

(d) *Porosity*

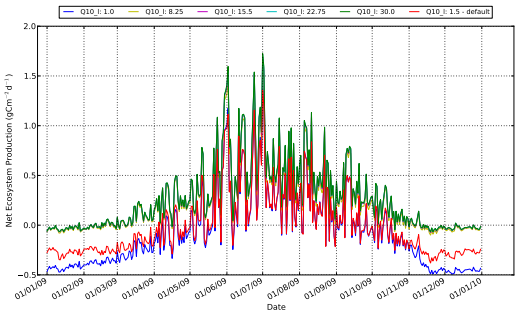

(e) *Q10_I*

Figure 4.12: OAT sensitivity analyses of the effect of different related parameters on the NEP flux.

The NEP flux is less sensitive to the remaining parameters, but a change in their value does result in a small change in the flux. An increase in the wilting point parameter results in a decrease in the NEP flux above a value of ~-0.2gCm^{-2}d^{-1} and an increase below it, though the behaviour appears to be sensitive only to a small region of the parameter space between the values of 0.3 and 0.5. An increase in the rdr_a parameter results in a small decrease in NEP flux but only at higher values, whereas an increase in the lignin-to-nitrogen ratio results in a very small increase in NEP flux in the winter months (November to February) when the NEP flux is negative. Higher values of the inundation ratio, lignin fraction, Me_s, Me_l and Me_a parameters all result in a linearly spaced but small increase in the NEP flux at all times of the year. The Q10_s parameter shows the same behaviour as its litter counterpart, with limited change to the NEP flux above a value of ~8gCm^{-2}d^{-1}, and increasing variability with changing parameter value at lower fluxes. An increase in the soil microbial scalar results in a non-linearly spaced and very small decrease in the NEP flux. The NEP flux hardly changes with changing value of the maximum LAI or the soil suction and Kb parameters, which are involved in the soil temperature calculations. Finally, the NEP flux is insensitive to the sedge and juncus plant mediated transport parameters as these are only involved in the CH_4 flux calculations.

The CH_4 flux is most sensitive, according to the Morris sensitivity analysis (Table 4.1), to the Q10_l parameter, as this is the biggest control on the soil C decomposition. With increasing Q10_l, the CH_4 flux decreases in a non-linear way (Figure 4.13(a)). Much the same as the NEP flux, above a certain value of Q10_l the CH_4 is relatively insensitive to changing parameter value. Notably, towards a value of 1.0, the CH_4 flux annual temporal trend is inverted.

With increasing Me_s there is an increasing decrease in the CH_4 flux (Figure 4.13(b)). The response to the autotrophic respiration scalar however shows a linear decrease in CH_4 flux with increasing parameter value (Figure 4.13(c)).

The CH_4 flux increases with increasing values of the LUE parameter (Figure 4.13(d)). An increase in the inundation ratio results in a gradually smaller increase in CH_4 flux (Figure 4.13(e)). Changes in the Q10_s parameter result in the same behaviour in the CH_4 flux as for the Q10_l parameter except for the fact the annual temporal trend does not change at values close to 1.0 (Figure 4.13(f)).

In general an increase in the lignin-to-nitrogen ratio results in a decrease in the CH_4 flux, but the magnitude of change in the flux is not the same throughout the year (Figure 4.14(a)). In the months of October and November it appears that the lowest values of the ratio result in a decrease in flux, clearly demonstrating the non-linear behaviour of this parameter. The is also true for the SR_max parameter, which generally shows a linear increase in CH_4 flux with decreasing parameter value, but for the months of mid-October to mid-December, where the lowest value of SR_max does not result in the highest flux (Figure 4.14(b)).

The CH_4 flux decreases linearly with increasing lignin fraction up to a value of 0.5, above which the CH_4 flux does not appear to change (Figure 4.14(c)). An increase in the value of Me_l results in a linear decrease in the CH_4 flux (Figure 4.14(d)). The CH_4 flux is mostly sensitive to changes in low values of the porosity parameter, although at times of peak flux, when the soil moisture decreases from the maximum value, it is clear that an increase in the porosity results in a decrease in the CH_4 flux (Figure 4.14(e)).

The results of the Morris sensitivity analysis show the CH_4 flux is relatively insensitive to the

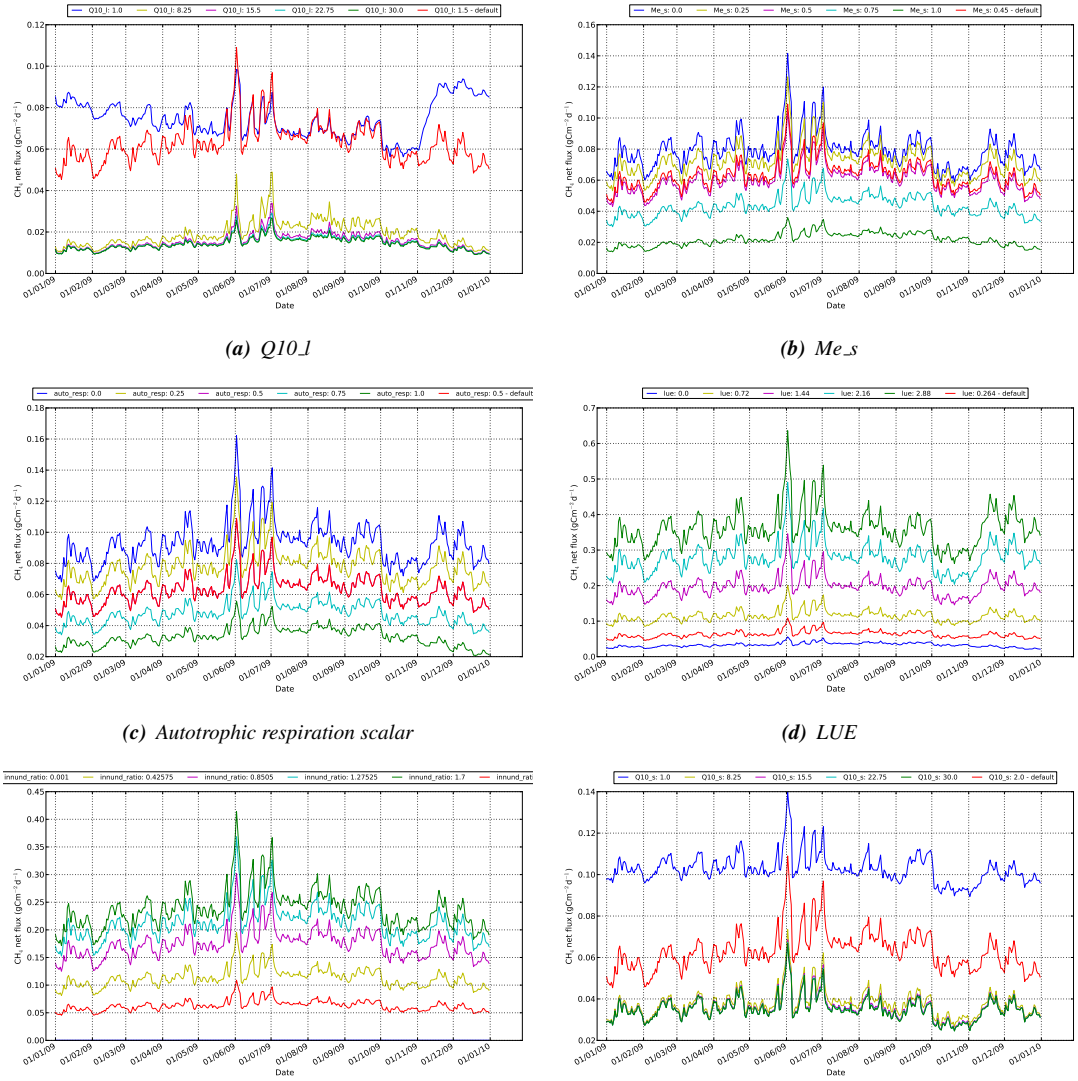

(a) *Q10_l* ***(b)*** *Me_s*

(c) *Autotrophic respiration scalar* ***(d)*** *LUE*

(e) *Inundation ratio* ***(f)*** *Q10_s*

Figure 4.13: OAT sensitivity analyses of the effect of different related parameters on the CH_4 flux.

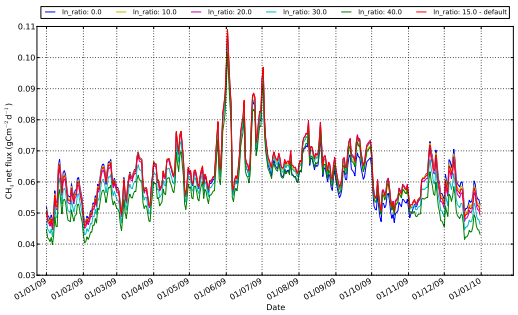

(a) *Lignin-to-Nitrogen ratio*

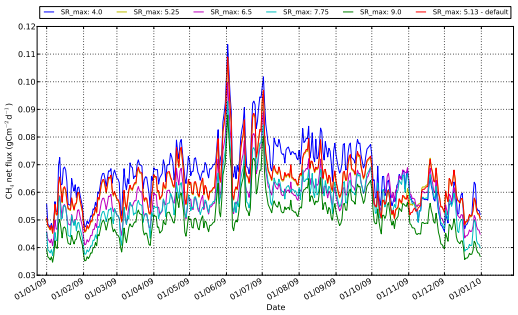

(b) *SR_max*

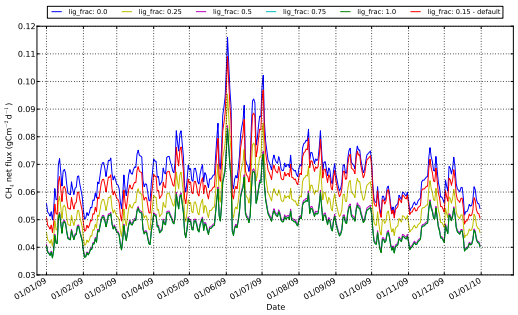

(c) *Lignin fraction*

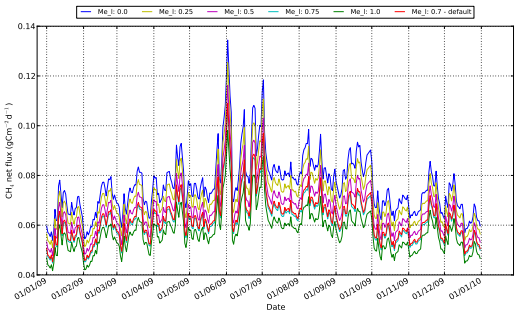

(d) *Me_l*

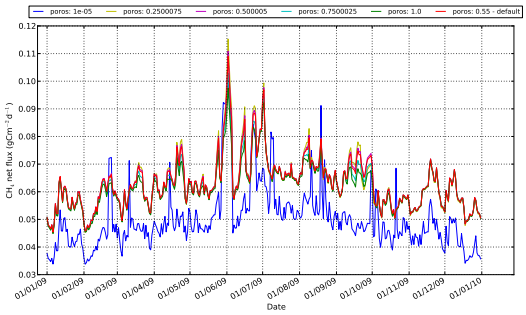

(e) *Porosity*

Figure 4.14: OAT sensitivity analyses of the effect of different related parameters on the CH_4 flux.

remaining model parameters,with some exceptions. The CH_4 flux only appears to be sensitive to changes in the maximum LAI between values of ~3 to 5.0, and noticeably only at times of a decreased flux. An increase in the soil microbial scalar results in a small increase in CH_4 flux, whereas an increase in the Me_a parameter results in a small, linear decrease in CH_4 flux. Like the NEP the CH_4 flux only appears to be sensitive to changes in the wilting point parameter between the values of 0.3 and 0.5. The rdr_a parameter only affects the peak CH_4 flux, as this is when the soil moisture dips below its maximum value. An increase in rdr_a results in a decreased flux, but an increase in rdr_b results in an increased flux (but only above a certain value). The plant mediated transport parameters have almost no bearing on the CH_4 net flux, and the soil suction parameter results in an extremely small increase. Like the NEP the CH_4 is insensitive to the Kb parameter. The soil suction and Kb parameters are involved in soil temperature calculations.

4.6 Discussion and conclusions

This chapter has introduced the model and has outlined the modifications made to the model and the reasoning behind them. The results of a global (Morris) and OAT sensitivity analysis were also presented. The Morris sensitivity analysis crucially enabled a ranking of parameters in terms of their impact on the C fluxes. This has informed which observations should be used to constrain the model, the choice of which parameters should be included in the Bayesian calibration, as outlined in Chapter 3. The OAT sensitivity analysis is useful for understanding the behaviour of the model in response to the parameters constrained by the Bayesian inversion, as presented in the following chapters.

4.6.1 Value of EO data

As discussed in Chapter 2, EO data are particularly useful in being able to drive a model, validate the model outputs and in an assimilation framework aimed at improving a model, over a wide area where other ground-based data may not be available. The advantages of using satellite NDVI data to drive a model such as this have also already been discussed in Chapter 2. Both soil moisture and temperature control the daily variability of the C fluxes. In particular the magnitude of the peak fluxes is controlled by the decrease in soil moisture. Estimates of both variables can be derived from satellite measurements. These data are useful in that they take measurements frequently over a wide area. In addition satellite C flux estimates are now becoming available (see Chapter 2 Section 2.3.2). All these data could be useful in validating and/or calibrating the model in an assimilation framework.

4.6.2 Observations required to constrain the most important model parameters

The results of sensitivity analysis showed that soil moisture data and satellite C flux data would be the most useful for constraining the parameter estimates of the model. This is because the C fluxes are most sensitive to parameters directly related in the C flux calculations, and next to the soil moisture-related parameters, in particular the porosity. Land surface temperature (LST) data could be used in a data assimilation framework, such as the one used in this thesis. to constrain the

soil temperature-related parameters, but the sensitivity analysis showed these were the parameters to which the C fluxes were least sensitive. This is because air temperature is used to force the diffusion of heat in the top layer of the soil in the model. LST could also be used to force the soil temperature submodule at the upper boundary if no good-quality air temperature data were available. The global sensitivity analysis is crucial for determining which are the most important parameters that require calibration. Without the rankings provided by the Morris sensitivity analysis it would be unclear as to which parameters should be included in the inversion.

4.6.3 Parameters and processes constrained using soil moisture and C flux observations

The soil moisture observations will be used to constrain the soil moisture-related parameters. If the inversion results in good parameter constraint this will lead to improved estimates of soil moisture. Soil moisture is used to calculate scalars which modify the amount of C assimilated into the system as well as the cycling of C between the litter and soil C pools. Soil moisture is also involved in determining the ratio of CH_4:CO_2 flux, as this depends on the saturation of the soil.

NEP is most sensitive to parameters associated with the assimilation of C into the system (LUE, autotrophic respiration scalar and to some extent SR_max) and in the decomposition of C in the litter layers (Q10_l). Parameters relating to the decomposition of soil C and transfers of C between soil pools do not impact the NEP enough to require calibration. This is due to the dominance of the NPP on the NEP model outputs. The processes involved in the C assimilation and transfer of decomposition of litter operate on a shorter timescale and are more directly affected by changes in atmospheric forcing than the processes in the soil C module. Therefore they result in a higher variability in C flux. The NEP is also sensitive to the porosity. This is due to the impact soil moisture has on the different C flux calculations, as previously discussed.

The CH_4 flux is most sensitive to parameters relating to the cycling of C in the litter and soil, and to the assimilation of C into the system. It is more sensitive to parameters involved in the decomposition of litter and soil C as the magnitude of the CH_4 flux is directly proportional to the amount of decomposed C. However the process of C assimilation exerts a strong control on the amount of C in the system and therefore the relevant parameters also have an impact on the CH_4 flux. As per NEP the CH_4 flux is also sensitive to porosity, again due to the various processes that depend on the soil moisture.

Chapter 5

OSSE using synthetic CH_4 flux observations

5.1 Introduction

As previously discussed data assimilation is useful in providing a robust, statistical framework for combining the information in both the model and observations in order to obtain optimal estimates of the variables under investigation, together with an estimate of their uncertainty. This technique is routed in Bayesian inference (Chapter 2 Section 2.5.1). In this thesis a Bayesian inversion method is used to calibrate the parameters of the CASA-CH_4 flux model in order to improve model predictions of C fluxes (CH_4 and NEP). This provides an estimate of the parameter distributions, not just the most likely value. The resultant (posterior) distributions are conditioned on the information in the model and the observations, as well as prior information as described by the prior parameter distributions. This is a robust framework for combining all sources of information with estimates of the uncertainty in that information.

Chapter 4 examined which observations would be useful in constraining the model, and which were the most important parameters to constrain. However, as discussed in Chapter 2 Section 3.7, it is difficult, if not impossible, to know the observational characteristics (uncertainty and temporal sampling interval) that would be able to a) accurately determine the most likely parameter value and b) reduce the uncertainty in the parameter distributions. To investigate this an synthetic experiment (OSSE) is required, where the "true" values of the parameter are known, and the inversion is tested with synthetic observations with different characteristics. The OSSE method was outlined in Chapter 3 Section 3.7.

The results of Chapter 4 showed that the most CH_4 flux was most sensitive to parameters which were directly related to the calculations of the C cycle. Thus C flux observations are required to constrain those parameters. In this chapter, the OSSE method is used to investigate the ability of synthetic CH_4 flux observations, with different characteristics, to constrain the parameters to which the CH_4 flux is most sensitive. The aim is to determine a set of requirements against which real observations should be compared before they are used in a calibration exercise for a particular site. More generally, this and the following two chapters provide an example how powerful a tool an OSSE can be in assessing how well a Bayesian inversion scheme might work in practice.

The following questions will be addressed in this chapter:

1. Which CH_4 flux observational characteristics, i.e. which temporal sampling interval and observation uncertainty, result in a robust estimate of the model parameters and C flux?
2. Which model processes are constrained by the observations?
3. Do the CH_4 observations result in improved estimates of NEP?
4. Do real observations, both ground-based and satellite, meet the requirements as set out in the OSSE?

The next section provides a summary of the methods used in this chapter, which were detailed in full in Chapter 3. The results are then presented. Firstly the parameter uncertainty (i.e. 95% confidence interval of the marginal distributions of the parameters) will be examined and following this the model predictive uncertainty (i.e. the 95% confidence interval of the forward model runs). Subsequently the results are discussed according to the questions laid out in the introduction to this chapter, and finally the main conclusions of this chapter are detailed.

Finally, a note on the sign of the CH_4 observations. Positive CH_4 fluxes represent a net CH_4 emission from the soil.

5.2 Experimental set-up

Chapter 3 provided an comprehensive overview of the methods used in this chapter. These are briefly summarised below and the specific details which are pertinent to the experiments in this chapter are outlined.

The Bayesian inversion algorithm used to calibrate the model was described in Chapter 3 Section 3.6. The OSSE method was detailed in Chapter 3 Section 3.7. The synthetic observations used to calibrate the model in the following experiments were derived from the CH_4 flux model output using the default parameters (summarised in Chapter 3 Table 3.2). The added random Gaussian noise is outlined in Chapter 3 Section 3.7 in the 4th column of Table 3.3. The temporal sampling interval of the synthetic observations is decreased by the number of days listed in the first column of the Table 3.3. The observational characteristics used to create CH_4 flux synthetic observations in the following experiments are repeated in Table 5.1 for clarity.

The parameters which are included in the calibration in the following experiments are those to which the CH_4 flux is most sensitive, following the Morris sensitivity analysis in Chapter 4 Section 4.4 - see Figure 4.9 and Table 4.1. The default parameters used to create the synthetic experiments are referred to as the "true" parameter values in the following experiments, as the OSSE is testing whether the observations with added noise and decreased temporal sampling interval can retrieve these values. Uniform prior distributions of the parameters are used in this experiment as detailed in Chapter 3 Section 3.6. The maximum and minimum of the uniform distributions are set to the upper and lower limit of the range of parameter values, which were summarised in Chapter 3 Table 3.2). The parameters included in these experiments, their "true" value and their prior distributions are summarised in Table 5.2. The notation U(a,b) is used to define the distributions, where a is the minimum value of the parameter, and b is the maximum.

Temporal Frequency	CH_4 flux error ($gCm^{-2}d^{-1}$)
1	0.002
5	0.005
10	0.01
15	0.02
30	0.05
60	0.1
180	0.2

Table 5.1: The temporal sampling interval and random Gaussian noise used to create the synthetic CH_4 observations.

Parameter	True Value	Prior distribution
Q10_l	1.5	U(1,30)
Me_s	0.45	U(0,1)
auto. resp.	0.5	U(0,1)
inund. ratio	0.2	U(0.001,1.7)
LUE	0.264	U(0,2.88)
LN ratio	15	U(0,40)
Q10_s	2	U(1,30)
lig. frac.	0.15	U(0,1)
SR_max	5.13	U(4,9)
Me_l	0.7	U(0,1)
poros.	0.55	U(1e-5,1)

Table 5.2: A summary of the parameters constrained using CH_4 flux observations in the Bayesian inversion in this chapter.

The outputs of the OSSE experiments were detailed in Chapter 3 Section 3.7.1. Further details relating to the notation and figure captions were also provided in Chapter 3 Section 3.7.1. In brief, the notation $\{t/\varepsilon\}$ is used to denote the observations with a t temporal sampling interval and ε uncertainty. An explanation of what information is provided in the figures and tables in the results section was also provided in Chapter 3 Section 3.7.1, as it is standardised for each type of figure and table. This will be summarised in the first example of each figure and table in the results, and from then on only the information pertaining the specific figure will be given in the caption.

5.3 Results

5.3.1 Parameter posterior PDF (PPDF)

As the observation error increases and the temporal sampling interval decreases, most parameters do not show a gradual transition from being well-constrained, with the true value accurately retrieved, to being poorly-constrained, and/or the true value not clearly estimated. This can be seen in the histogram plots, and in the tables of posterior parameter mode - truth bias and error reduction in the 95% confidence interval. A subset are chosen to highlight general patterns and behaviour.

The Q10_l parameter is the most well-constrained (highest reduction in 95% confidence interval between the prior and posterior), especially at low observational error and high temporal sampling interval (Figure 5.1). This results in a large reduction in the 95% confidence intervals between the prior and posterior parameter distribution (Table 5.3), a small bias between the mode of the posterior distribution and the true value (Table 5.4). In general the posterior uncertainty decreases, and the bias increases as the observational error increases and the temporal sampling interval decreases. However, the results from some observational characteristics do not conform to this pattern, for example the {5/0.005} observations. The Q10_l value is constrained well here (~91% error reduction) but the true value is not well approximated and therefore the bias is quite high. This is due to parameter coupling and model equifinality, and is discussed in more detail below. Similarly some observations do not result in well-constrained Q10_l posterior, for example for the {15/0.02} observations. In this case the posterior is wider than the prior.

	0.002	**0.005**	**0.01**	**0.02**	**0.05**	**0.1**	**0.2**
1	98.7	99.9	99.5	97.4	75.3	42.6	94.2
5	99.8	91.2	98.5	99.2	92.5	20.7	77.1
10	98.4	99.0	98.6	80.4	29.2	73.9	43.1
15	99.5	88.8	98.8	-1.19	46.5	18.5	33.8
30	99.6	98.5	98.2	97.3	96.6	54.7	7.4
60	99.5	44.1	10.5	97.1	12.5	2.59	41.4
180	53.1	20.7	67.0	96.8	10.4	2.82	90.9

Table 5.3: Reduction in uncertainty (%) between the prior and posterior distributions (95% confidence interval) for the Q10 litter parameter, for each observational characteristic. (Prior 95% C.I.: 27.55). The magnitude of the observation uncertainty is listed in the top headings of the table, and the temporal sampling interval is listed in the headings in the left-hand column.

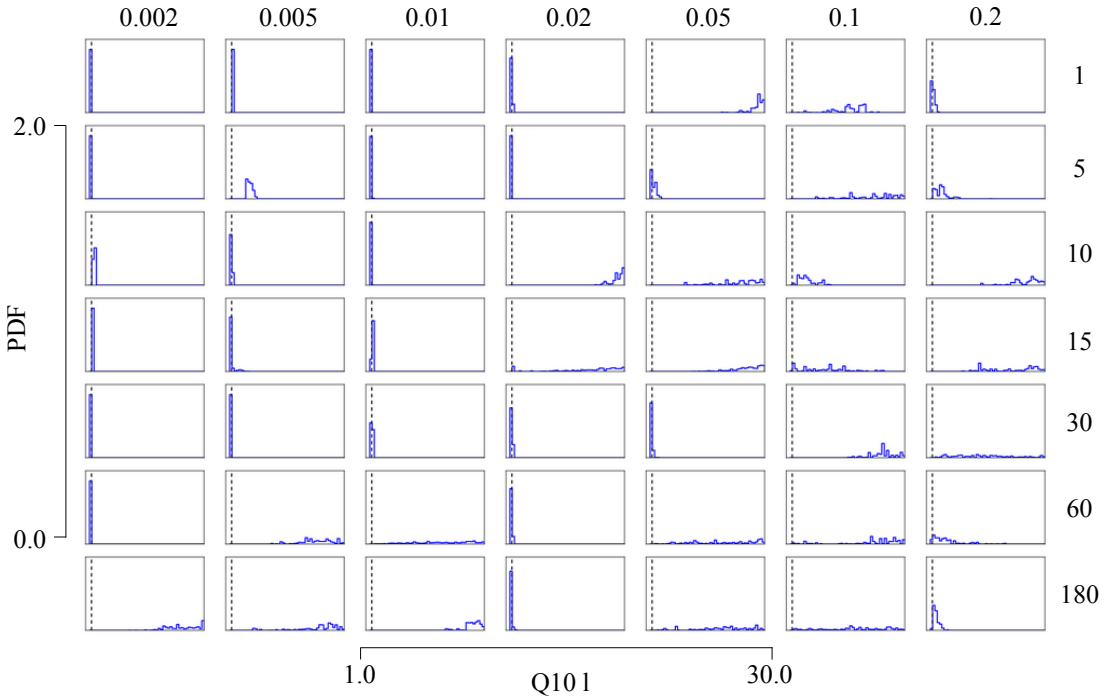

Figure 5.1: Posterior distributions for the Q10 litter parameter, using CH_4 flux observations, for each observational characteristic. The axes are the same for all histograms, and are shown at the bottom and left hand side of the figure. The x-axis is the width of the prior distribution and the blue, the posterior. The vertical black dashed line shows the true value. In all other histogram plots the red lines shows the prior distribution. The histogram plots are arranged with increasing observation uncertainty along the columns and increasing temporal sampling interval down the rows. The magnitude of the observation uncertainty is given in the top row, and the temporal sampling interval is given in the right-hand column.

	0.002	**0.005**	**0.01**	**0.02**	**0.05**	**0.1**	**0.2**
1	-0.158	0.225	-0.038	-0.017	27.2	17.	0.280
5	-0.024	4.11	-0.068	-0.340	-0.053	15.0	2.90
10	0.538	-0.004	-0.242	23.4	19.1	7.79	25.3
15	0.244	-0.100	0.339	0.453	26.9	0.212	12.0
30	-0.220	-0.345	0.148	-0.486	-0.371	23.1	7.26
60	-0.119	22.9	10.5	-0.143	27.5	20.0	5.49
180	28.1	24.5	24.3	-0.221	5.95	15.3	0.561

Table 5.4: The bias between the mode of the Q10 litter posterior parameter distribution and the true parameter value for each observational characteristic.

This general pattern is to be expected as Q10_1 is the parameter the CH_4 flux is most sensitive to (see Chapter 4 Figure 4.9). Figure 5.2, Figure 5.3 and Figure 5.4 show examples of a departure from the general pattern for the autrotophic respiration scalar, porosity and inundation ratio parameters respectively. The reduction in 95% confidence intervals is often high (>80%) for observations with low error and high temporal sampling interval. This reduces with increasing error and decreasing frequency. However the bias between the MAP estimate and the true value of the parameters is also quite high for most parameters, even those constrained using the "best-case" observational characteristics. High biases can exist both for cases where the parameter is well constrained but to the wrong value, and where the parameter is not well constrained but the values are skewed. The former tends to occur for observations with a lower associated error, and the latter for parameters constrained using observations with a higher associated uncertainty.

The uncharacteristic behaviour is not limited to a few specific observational characteristic sets for each parameter. As can be seen in these figures, it is also often the case that the parameter can be poorly constrained but exhibit a significant bias or skewed behaviour. This is demonstrated in the error reduction and mode-truth bias values (e.g. for the autotrophic respiration parameter Tables 5.6 and 5.8).

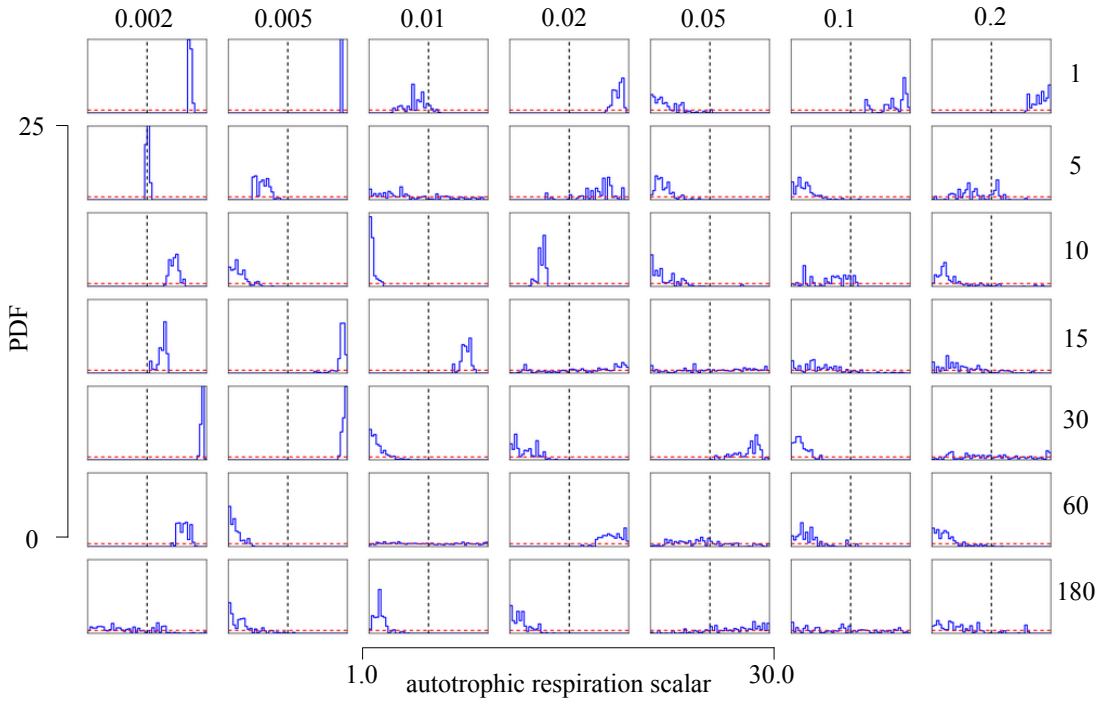

Figure 5.2: Posterior distributions for the autotrophic respiration scalar parameter, using CH_4 flux observations, for each observational characteristic.

The light use efficiency (LUE) parameter generally increases in spread with increasing observational error and decreasing temporal frequency (Figure 5.5). The pattern of bias between the mode of the posterior parameter PDF and the true value is not systematic, with some observational characteristics resulting in a high positive bias or negative bias (Table 5.5).

For parameters to which the CH_4 flux is slightly less sensitive, there is a generally lower parameter constraint, even with observations with low error and high temporal sampling interval.

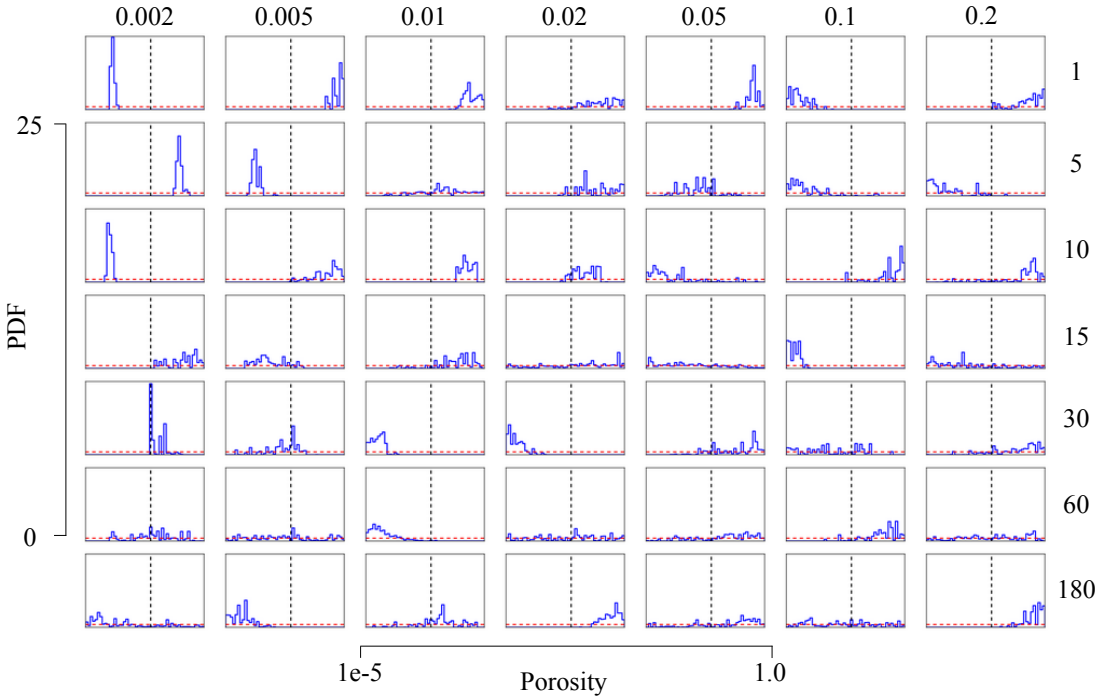

Figure 5.3: Posterior distributions for the porosity parameter, using CH_4 flux observations, for each observational characteristic.

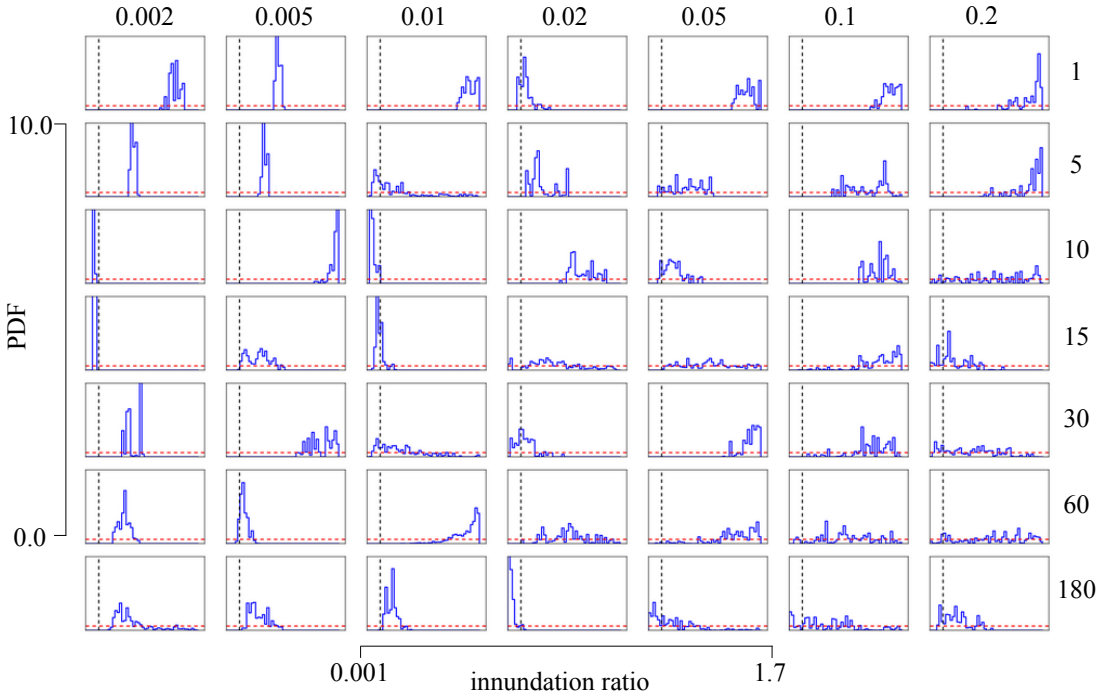

Figure 5.4: Posterior distributions for the innundation ratio parameter, using CH_4 flux observations, for each observational characteristic.

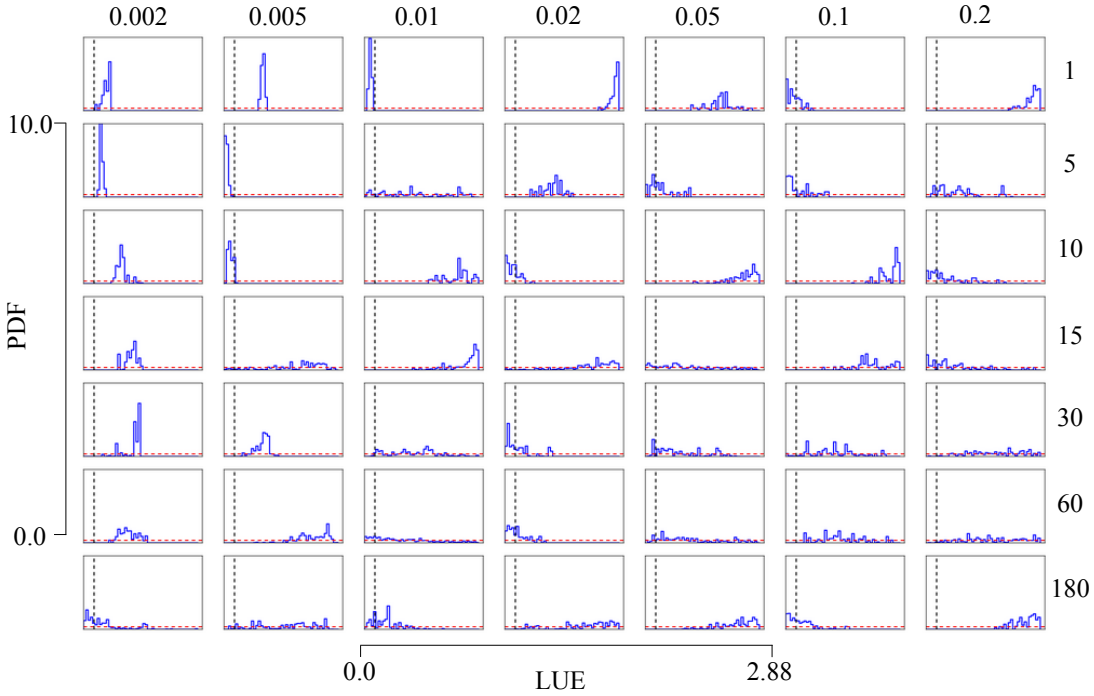

Figure 5.5: Posterior distributions for the light use efficiency parameter, using CH_4 flux observations, for each observational characteristic.

	0.002	**0.005**	**0.01**	**0.02**	**0.05**	**0.1**	**0.2**
1	0.276	0.683	-0.066	2.56	1.75	-0.244	2.611
5	0.154	-0.215	2.12	0.868	-0.223	0.283	1.661
10	0.701	-0.012	2.50	-0.054	2.48	2.45	-0.137
15	1.14	1.75	2.52	2.06	0.444	1.68	-0.256
30	1.16	0.742	1.32	-0.177	1.07	0.299	2.107
60	1.39	2.37	0.000	-0.201	2.00	1.09	1.691
180	-0.160	0.605	-0.124	1.33	1.58	-0.084	2.581

Table 5.5: The bias between the mode of the light use efficiency posterior parameter distribution and the true parameter value for each observational characteristic.

This doesn't change as dramatically with increasing error and decreasing frequency. This is because the observations is not providing any information which can reduce the prior PDF. Therefore the posterior approximates the prior.

	0.002	**0.005**	**0.01**	**0.02**	**0.05**	**0.1**	**0.2**
1	94.9	98.5	62.9	86.0	51.9	62.0	80.2
5	96.3	82.2	4.1	32.1	72.5	64.5	39.6
10	85.0	73.6	89.7	87.4	63.6	45.0	42.4
15	86.5	76.7	82.0	8.09	-1.27	18.5	20.7
30	96.1	94.1	73.9	68.8	56.6	74.7	3.37
60	81.6	81.1	-0.60	69.1	8.89	49.0	55.4
180	23.3	56.5	78.2	73.5	2.00	3.00	16.7

Table 5.6: Reduction in uncertainty (%) between the prior and posterior distributions (95% confidence interval) for the autotrophic respiration scalar parameter, for each observational characteristic. (Prior 95% C.I.: 0.95).

	0.002	**0.005**	**0.01**	**0.02**	**0.05**	**0.1**	**0.2**
1	89.6	86.2	70.2	54.2	91.9	25.1	17.5
5	93.1	82.0	23.3	84.1	73.3	45.5	9.18
10	97.5	31.6	83.0	84.6	42.7	50.4	26.7
15	88.3	51.5	76.7	26.2	7.93	10.0	-0.76
30	87.6	72.1	9.60	60.4	13.0	81.2	43.7
60	91.3	77.2	15.6	11.2	11.5	5.77	48.0
180	34.0	60.9	27.4	9.54	4.17	1.57	19.9

Table 5.7: Reduction in uncertainty (%) between the prior and posterior distributions (95% confidence interval) for the standard microbial C efficiency parameter, for each observational characteristic. (Prior 95% C.I.: 0.95).

	0.002	**0.005**	**0.01**	**0.02**	**0.05**	**0.1**	**0.2**
1	0.369	0.451	-0.045	0.373	-0.427	0.455	0.305
5	0.026	-0.263	-0.233	0.331	-0.377	-0.361	0.059
10	0.230	-0.367	-0.494	-0.257	-0.500	-0.400	-0.394
15	0.162	0.444	0.355	-0.379	-0.134	-0.375	-0.373
30	0.458	0.489	-0.492	-0.266	0.352	-0.429	0.468
60	0.370	-0.455	-0.423	0.254	-0.370	-0.330	-0.370
180	0.091	-0.500	-0.426	-0.383	0.484	-0.067	-0.163

Table 5.8: The bias between the mode of the autotrophic respiration scalar posterior parameter distribution and the true parameter value for each observational characteristic.

5.3.2 Parameter correlation

Whilst some systematic patterns are seen in these results, the fact that the observational characteristics don't conform to the systematic pattern of gradually decreasing constraint of the parameter posterior PDF, and the fact that parameters which are well-constrained often have a high bias in

the MAP estimate, suggests that the parameters might be correlated and the model has a high degree of model equifinality. If this is the case, even if a certain parameter value is wrong, another parameter will diminish the effect on the model output by also having an incorrect value.

To examine this further each of the parameter posterior PDFs has been assigned a colour based on whether the posterior is well-constrained or not and the level of bias between the MAP and the true value of the parameter (Table 5.9 and Figure 5.6). This gives an idea of the more general patterns that exist between the parameters and tests the hypothesis that the parameters are correlated. Figure 5.6 shows that the correlations are generally higher for observations with a lower uncertainty and higher temporal sampling interval. Therefore observations with a small error and a high temporal sampling interval are better able to constrain the model parameters but potentially to the wrong value. Observations every day and 5 days with an error of <=0.005gCm^{-2}d^{-1} have a high number of parameters that are very well constrained but with a high bias (red colour in Figure 5.6). For most observational characteristics many parameters are relatively well-constrained (>50%), with either a high or low bias (blue, cyan, red and yellow colours). Generally as observational error increases and temporal sampling interval decreases fewer parameters are constrained well (green and grey colors) and mostly show a relatively high bias (grey colour code).

Colour code	**Error reduction**	**Bias (% of param. prior range)**
Blue	>90%	<10%
Red	>90%	>10%
Cyan	50% - 90%	<10%
Yellow	50% - 90%	>10%
Green	<50%	<10%
Grey	<50%	>10%

Table 5.9: The codes used to group the parameter posterior PDFs in Figure 5.6 on the basis of their posterior parameter constraint and the level of bias between the MAP and the true value of the parameter.

Figures 5.1 and 5.6 show that the Q10_l parameter is most well-constrained and approximates the truth better than all other parameters. It is also the case that if the Q10_l parameter is not relatively well-constrained then the Q10_s parameter is, at least for lower observational error and higher temporal sampling interval of observations. Examining the correlation coefficients between each pair of parameters for all the observational characteristics does not help to identify patterns in the parameter correlations. As as can be seen in Figure 5.6, it is not always the same pairs of parameters that are correlated. Even the correlation coefficient between the Q10_l and Q10_s parameters, which might be expected to show a more systematic pattern, are wide ranging and of differing sign (Table 5.10). High correlation coefficients are observed between the two parameters for certain observational characteristics though, proving that these parameters can have a great impact on each other if the conditions allow it. This is true for many of the parameter pairs, for example the LUE and inundation ratio (Table 5.11). This also can be the case between two parameters that the model is relatively insensitive to, for example the lignin fraction and lignin-to-nitrogen ratio (Table 5.12) and the SR_max and Me_s parameters (Table 5.13). Even correlation coefficients of 0.4-0.5 are significant.

Rather than looking at all possible pairwise correlations it is more informative to examine

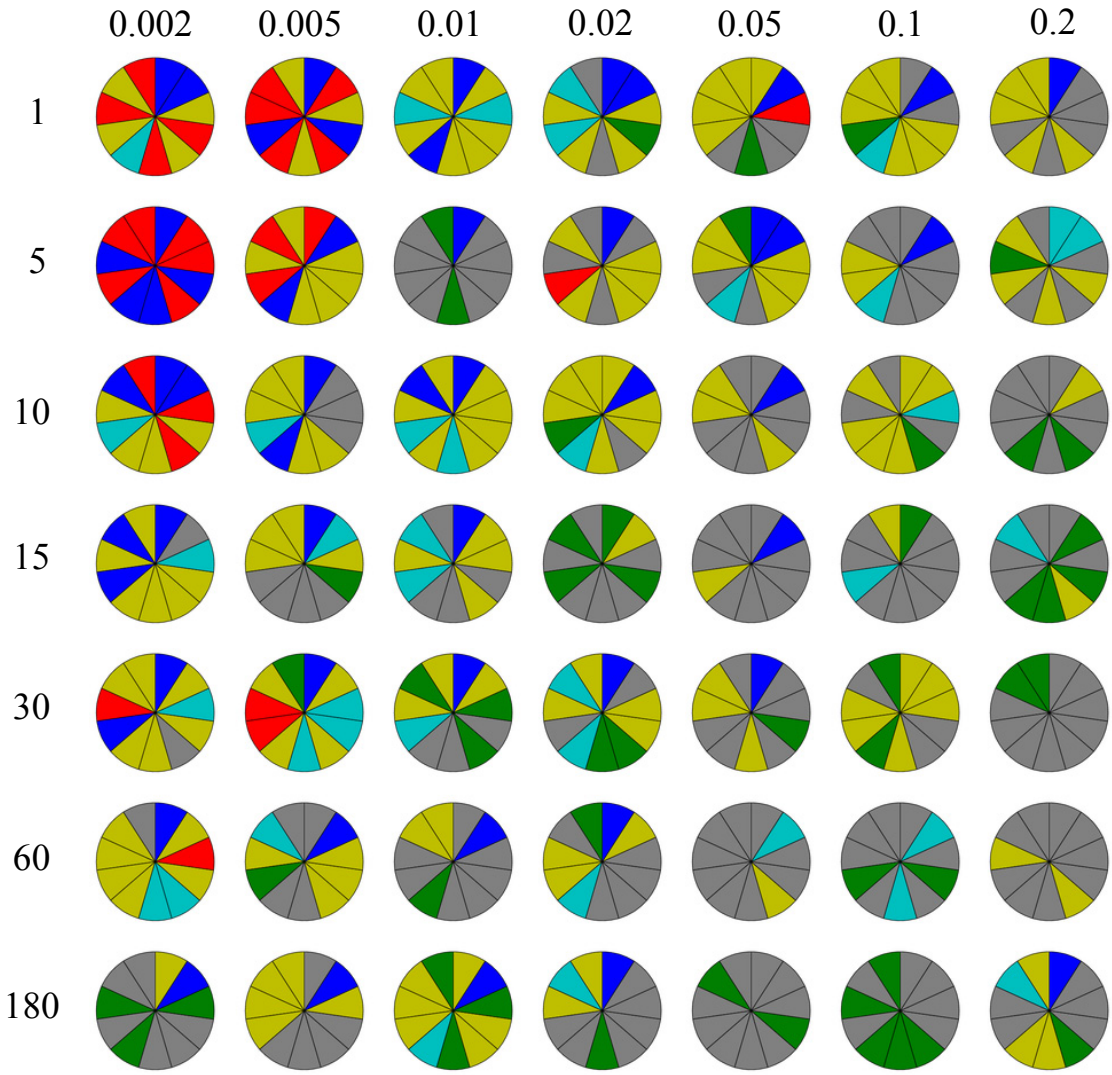

Figure 5.6: Plots to show the level of parameter constraint and bias from the true value in the parameter posterior PDFs. Parameters are in order clockwise from top: Q10_l, Q10_s, Me_s, Me_l, LN_rato, lignin fraction, LUE, SR_max, autotrophic respiration scalar, inundation ratio and porosity. Parameter PDFs are grouped as per Table 5.9

	0.002	**0.005**	**0.01**	**0.02**	**0.05**	**0.1**	**0.2**
1	-0.68	0.41	0.64	-0.16	0.07	0.15	-0.33
5	0.32	0.26	0.61	0.49	-0.14	-0.41	-0.20
10	-0.59	0.11	0.45	0.09	0.00	-0.00	0.07
15	0.92	-0.52	0.33	-0.63	0.05	-0.16	0.48
30	-0.33	0.61	0.05	-0.29	-0.12	-0.16	-0.11
60	-0.01	0.48	0.23	-0.10	-0.35	-0.08	0.13
180	0.39	-0.08	-0.20	0.01	-0.15	0.06	-0.05

Table 5.10: Correlations between the Q10_l and Q10_s parameters using synthetic CH_4 flux observations from 2009 with different observational characteristics and no underestimation of observational error.

	0.002	**0.005**	**0.01**	**0.02**	**0.05**	**0.1**	**0.2**
1	0.34	-0.62	0.28	0.04	-0.42	-0.14	-0.11
5	-0.83	-0.53	-0.45	0.58	-0.85	0.30	0.27
10	-0.30	0.16	0.29	-0.51	-0.16	0.14	-0.17
15	-0.29	0.09	-0.40	-0.23	0.15	-0.21	0.04
30	-0.53	0.05	-0.17	-0.64	-0.23	0.21	-0.26
60	0.13	-0.67	0.13	-0.22	0.06	0.15	-0.17
180	0.02	-0.57	-0.46	-0.69	0.13	0.20	-0.48

Table 5.11: Correlations between the LUE and innundation ratio parameters using synthetic CH_4 flux observations from 2009 with different observational characteristics and no underestimation of observational error.

	0.002	**0.005**	**0.01**	**0.02**	**0.05**	**0.1**	**0.2**
1	0.03	-0.04	0.29	-0.01	0.37	0.08	-0.09
5	-0.14	0.37	-0.06	0.58	0.38	-0.37	-0.15
10	-0.26	0.11	-0.29	0.91	-0.24	0.06	-0.43
15	-0.21	0.06	0.10	0.17	0.29	0.13	-0.08
30	0.94	0.67	0.47	-0.17	-0.73	-0.19	-0.09
60	0.37	-0.26	-0.15	-0.23	0.05	0.28	-0.18
180	-0.02	0.55	-0.34	0.14	-0.00	0.13	-0.22

Table 5.12: Correlations between the lignin-to-nitrogen ratio and lignin fraction parameters using synthetic CH_4 flux observations from 2009 with different observational characteristics and no underestimation of observational error.

	0.002	**0.005**	**0.01**	**0.02**	**0.05**	**0.1**	**0.2**
1	-0.40	-0.07	-0.02	0.02	0.03	-0.16	-0.06
5	-0.16	-0.54	-0.09	-0.58	-0.28	0.21	0.43
10	0.11	-0.12	-0.36	0.51	-0.10	0.50	-0.31
15	-0.52	0.17	-0.35	-0.19	-0.11	0.20	-0.07
30	-0.08	-0.29	0.13	-0.16	0.27	0.01	0.32
60	-0.43	0.01	-0.05	-0.08	0.27	-0.02	0.19
180	-0.02	0.26	-0.69	-0.05	0.13	0.18	0.27

Table 5.13: Correlations between the Me_s and SR max parameters using synthetic CH_4 flux observations from 2009 with different observational characteristics and no underestimation of observational error.

	0.002	0.005	0.01	0.02	0.05	0.1	0.2
1	0.72	0.54	0.40	0.27	-0.23	0.41	0.22
5	-0.36	-0.45	0.05	-0.01	-0.13	0.36	0.00
10	-0.74	0.03	0.51	-0.06	-0.14	-0.18	0.22
15	-0.59	-0.04	0.52	0.03	0.07	-0.05	-0.03
30	-0.32	0.48	0.13	0.23	-0.15	-0.24	0.02
60	0.12	-0.01	0.02	0.10	-0.48	-0.05	0.13
180	-0.03	-0.02	-0.17	0.41	-0.01	0.20	0.27

Table 5.14: Correlations between the lignin fraction and innundation ratio parameters using synthetic CH_4 flux observations from 2009 with different observational characteristics and no underestimation of observational error.

whether those observational characteristics which appear to have a high number of correlated parameters actually do so by looking at the correlation coefficients between all the parameters for that particular set of observational characteristics. Comparing correlation coefficients constrained using the {1,5/0.002} observations (Tables 5.15 and 5.16 respectively), which result in a high number of relatively well-constrained but with a high bias between the MAP and true value, to parameter correlation coefficients constrained using the {30,60/0.2} observations (Tables 5.17 and 5.18 respectively), which result in poorly-constrained parameters, this is indeed the case. The "good" ({1,5/0.002}) observations result in 26 and 19 out of 55 pairs of parameter correlation coefficients that are >0.4, respectively, whereas the "poor" ({30,60/0.2}) observations result in only 2 and 3 out of the 55 pairs of parameter correlation coefficients that are >0.4, respectively. The information provided by the observations is fairly low therefore.

	Q10_l	Q10_s	LUE	POROS	ME_S	ME_L	LN_RATIO	LIG_FRAC	SR_MAX	innund_ratio	AUTO_RESP
Q10_l	1.00	-0.68	-0.29	-0.17	-0.74	0.61	0.29	-0.37	0.16	-0.66	-0.12
Q10_s	-0.68	1.00	0.62	0.28	0.67	-0.37	-0.48	0.12	0.15	0.64	0.04
LUE	-0.29	0.62	1.00	0.24	0.62	0.26	-0.66	-0.34	0.30	0.34	0.19
POROS	-0.17	0.28	0.24	1.00	0.07	-0.15	0.24	-0.33	0.57	-0.08	0.03
ME_S	-0.74	0.67	0.62	0.07	1.00	-0.51	-0.53	0.48	-0.40	0.88	-0.11
ME_L	0.61	-0.37	0.26	-0.15	-0.51	1.00	-0.22	-0.83	0.52	-0.66	0.46
LN_RATIO	0.29	-0.48	-0.66	0.24	-0.53	-0.22	1.00	0.03	0.13	-0.54	-0.60
LIG_FRAC	-0.37	0.12	-0.34	-0.33	0.48	-0.83	0.03	1.00	-0.89	0.72	-0.43
SR_MAX	0.16	0.15	0.30	0.57	-0.40	0.52	0.13	-0.89	1.00	-0.62	0.28
innund_ratio	-0.66	0.64	0.34	-0.08	0.88	-0.66	-0.54	0.72	-0.62	1.00	-0.08
AUTO_RESP	-0.12	0.04	0.19	0.03	-0.11	0.46	-0.60	-0.43	0.28	-0.08	1.00

Table 5.15: Parameter Correlations using synthetic CH_4 observations every day with added random Gaussian noise of 0.002 $gCm^{-2}d^{-1}$.

5.3.3 CH_4 flux forward model mode and model predictive uncertainty

Many of the observational characteristics result in a large reduction in the 95% confidence interval between the prior and posterior forward CH_4 model ensembles, and the true magnitude and trend of the flux is often approximated well by the forward CH_4 flux model mode. Although most parameters are not accurately estimated, an accurate measure of CH_4 flux can still be determined due to model equifinality, i.e. where several combinations of parameters result in the same model output. This was summarised in Chapter 2 Section 2.7, and is discussed in more detail later in

	Q10_l	Q10_s	LUE	POROS	ME_S	ME_L	LN_RATIO	LIG_FRAC	SR_MAX	innund_ratio	AUTO_RESP
Q10_l	1.00	0.32	-0.18	-0.14	0.33	-0.26	0.07	-0.62	0.19	0.43	-0.35
Q10_s	0.32	1.00	-0.18	-0.32	-0.00	-0.22	0.15	-0.37	0.29	0.14	0.04
LUE	-0.18	-0.18	1.00	0.30	0.65	0.65	-0.47	-0.12	0.08	-0.83	-0.13
POROS	-0.14	-0.32	0.30	1.00	0.36	0.41	0.38	-0.48	0.10	0.14	-0.56
ME_S	0.33	-0.00	0.65	0.36	1.00	0.05	0.01	-0.41	-0.16	-0.34	-0.09
ME_L	-0.26	-0.22	0.65	0.41	0.05	1.00	-0.59	-0.25	0.59	-0.41	-0.63
LN_RATIO	0.07	0.15	-0.47	0.38	0.01	-0.59	1.00	-0.14	-0.47	0.51	0.19
LIG_FRAC	-0.62	-0.37	-0.12	-0.48	-0.41	-0.25	-0.14	1.00	-0.50	-0.36	0.76
SR_MAX	0.19	0.29	0.08	0.10	-0.16	0.59	-0.47	-0.50	1.00	0.20	-0.73
innund_ratio	0.43	0.14	-0.83	0.14	-0.34	-0.41	0.51	-0.36	0.20	1.00	-0.36
AUTO_RESP	-0.35	0.04	-0.13	-0.56	-0.09	-0.63	0.19	0.76	-0.73	-0.36	1.00

Table 5.16: Parameter Correlations using synthetic CH_4 observations every 5 days with added random Gaussian noise of 0.002 $gCm^{-2}d^{-1}$.

	Q10_l	Q10_s	LUE	POROS	ME_S	ME_L	LN_RATIO	LIG_FRAC	SR_MAX	innund_ratio	AUTO_RESP
Q10_l	1.00	-0.11	-0.00	0.12	0.04	0.25	0.18	-0.18	-0.09	0.00	-0.24
Q10_s	-0.11	1.00	-0.04	0.18	0.03	-0.18	0.03	0.08	-0.09	0.03	0.23
LUE	-0.00	-0.04	1.00	-0.19	0.01	0.08	-0.06	0.09	0.08	-0.26	0.04
POROS	0.12	0.18	-0.19	1.00	0.39	0.01	0.08	-0.29	0.09	0.02	0.12
ME_S	0.04	0.03	0.01	0.39	1.00	-0.08	-0.10	-0.26	0.32	0.11	0.19
ME_L	0.25	-0.18	0.08	0.01	-0.08	1.00	0.21	-0.00	-0.15	-0.12	-0.41
LN_RATIO	0.18	0.03	-0.06	0.08	-0.10	0.21	1.00	-0.09	0.03	0.36	-0.47
LIG_FRAC	-0.18	0.08	0.09	-0.29	-0.26	-0.00	-0.09	1.00	0.04	0.02	-0.11
SR_MAX	-0.09	-0.09	0.08	0.09	0.32	-0.15	0.03	0.04	1.00	0.05	0.09
innund_ratio	0.00	0.03	-0.26	0.02	0.11	-0.12	0.36	0.02	0.05	1.00	-0.18
AUTO_RESP	-0.24	0.23	0.04	0.12	0.19	-0.41	-0.47	-0.11	0.09	-0.18	1.00

Table 5.17: Parameter Correlations using synthetic CH_4 observations every 30 days with added random Gaussian noise of 0.2 $gCm^{-2}d^{-1}$.

	Q10_l	Q10_s	LUE	POROS	ME_S	ME_L	LN_RATIO	LIG_FRAC	SR_MAX	innund_ratio	AUTO_RESP
Q10_l	1.00	0.13	0.44	0.12	-0.57	-0.11	0.03	-0.13	-0.18	-0.18	-0.11
Q10_s	0.13	1.00	0.15	-0.27	0.04	-0.41	-0.05	0.02	-0.21	0.05	0.01
LUE	0.44	0.15	1.00	-0.28	-0.34	-0.15	0.15	-0.26	-0.02	-0.17	-0.08
POROS	0.12	-0.27	-0.28	1.00	-0.21	0.16	0.06	0.23	-0.22	-0.21	-0.19
ME_S	-0.57	0.04	-0.34	-0.21	1.00	-0.09	-0.13	0.36	0.19	0.39	-0.07
ME_L	-0.11	-0.41	-0.15	0.16	-0.09	1.00	-0.10	-0.17	0.04	-0.20	-0.11
LN_RATIO	0.03	-0.05	0.15	0.06	-0.13	-0.10	1.00	-0.18	-0.00	-0.16	0.09
LIG_FRAC	-0.13	0.02	-0.26	0.23	0.36	-0.17	-0.18	1.00	0.02	0.13	0.19
SR_MAX	-0.18	-0.21	-0.02	-0.22	0.19	0.04	-0.00	0.02	1.00	0.07	0.01
innund_ratio	-0.18	0.05	-0.17	-0.21	0.39	-0.20	-0.16	0.13	0.07	1.00	0.12
AUTO_RESP	-0.11	0.01	-0.08	-0.19	-0.07	-0.11	0.09	0.19	0.01	0.12	1.00

Table 5.18: Parameter Correlations using synthetic CH_4 observations every 60 days with added random Gaussian noise of 0.2 $gCm^{-2}d^{-1}$.

this chapter. In order to understand the model mode and the posterior 95% confidence interval, it is necessary to systematically examine the magnitude and trend of the observation-model error, the parameter PPDF simultaneously and the sensitivity of the CH_4 flux to the parameters. Several different catagories of model behaviour are evident in these results:

1. Good constraint (large reduction in 95% C.I.) of the CH_4 flux and true value approximated well.

2. Good constraint of the CH_4 flux with temporal variability well-approximated but the true value under- or overestimated by the forward model mode.

3. Good constraint of the CH_4 flux but the temporal variability and annual trend are poorly approximated.

4. Poor constraint of the CH_4 flux (wide posterior 95% C.I.) with the true value approximated as in points 1, 2 and 3.

Narrow posterior 95% C.I., accurate forward mode

In general the low uncertainty observations ({1-15/<=0.02}, {30,60/<=0.01} and {180/<=0.002}) result in a well-constrained posterior CH_4 flux, with the forward model mode closely corresponding to the true value (e.g. Figure 5.7). This is unsurprising, given the high number of parameters which appear to be relatively well-constrained. Some of these observational characteristics result in a posterior mode which is indistiguishable from the forward model mode, for example observations with a temporal sampling interval of 5 days and a low error of $0.002 gCm^{-2}d^{-1}$.

Narrow posterior 95% C.I., true flux under- or overestimated

Observational characteristics which result in a general negative bias of the posterior forward mode include the {10,15/0.2}, {30/0.1,0.2} and {180/0.05,0.1} observations (Figure 5.8). Most of these observations result in a positive bias for one or both of the Q10 parameters. From the OAT analysis (Chapter 4 Figures 4.13 and 4.14) this results in a large decrease in the CH_4 flux. For some of these observations the negative bias in the forward mode could also have been achieved with a negative bias in the autotrophic respiration scalar and LUE parameters.

In contrast to the negative bias seen above, the {180/0.2} observations result in a significant positive bias in the forward model mode and a large posterior 95% confidence interval (Figure 5.13). Although several parameters are relatively well-constrained, this is likely due good constraint of the LUE parameter posterior PDF and the fact it is positively biased towards the upper end of its prior range (Figure 5.5). This constraint is potentially strengthened by the negative bias of the autotrophic respiration scalar.

Poor approximation of temporal variability annual trend

The temporal variability of the forward model mode varies from that of the true CH_4 flux in three ways: i) the winter months are generally overestimated and the summer underestimated, ii) the opposite case, with some observational characteristics resulting in an overestimation of the

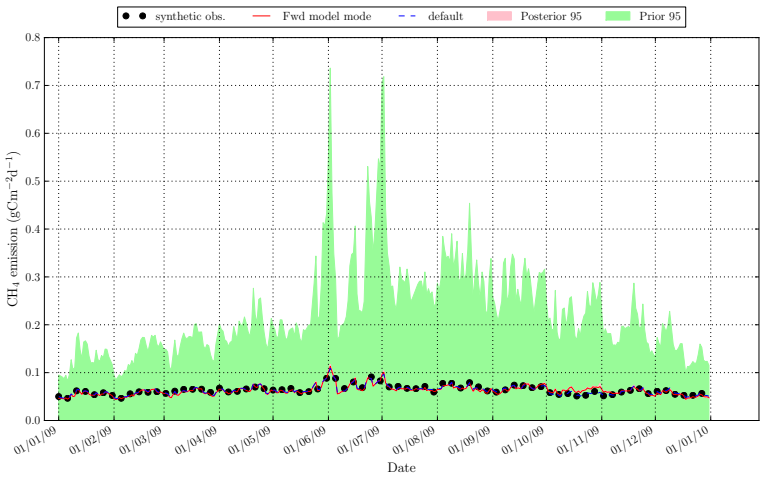

(a) *Synthetic {5/0.002} observations.*

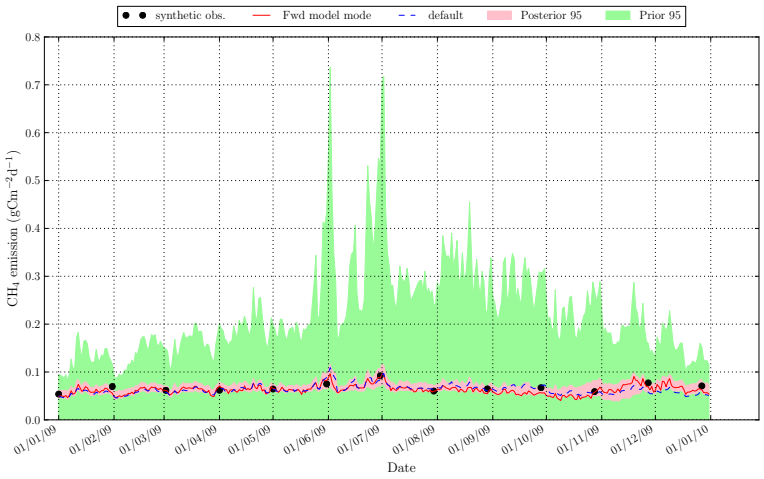

(b) *Synthetic {30/0.01} observations.*

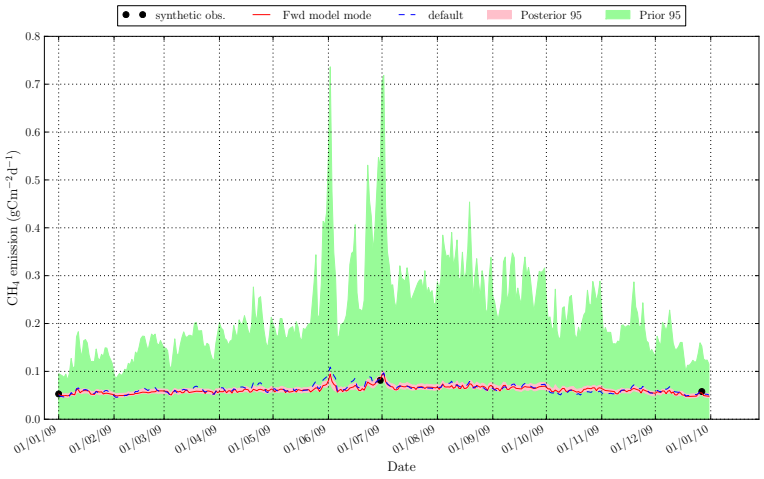

(c) *Synthetic {180/0.002} observations.*

Figure 5.7: The CH_4 net flux from an ensemble of 500 forward model runs using the posterior parameter distributions constrained with synthetic CH_4 flux observations with varying temporal sampling interval and added random Gaussian noise. The green area shows the prior 95% confidence interval of the CH_4 flux using 3000 random samples from the joint prior distribution of the parameters that are being calibrated in this OSSE experiment. The pink area is the posterior 95% confidence interval and the red line is the forward mode. These results are compared to the model run with the true set of parameters, which is denoted by the blue dashed line.

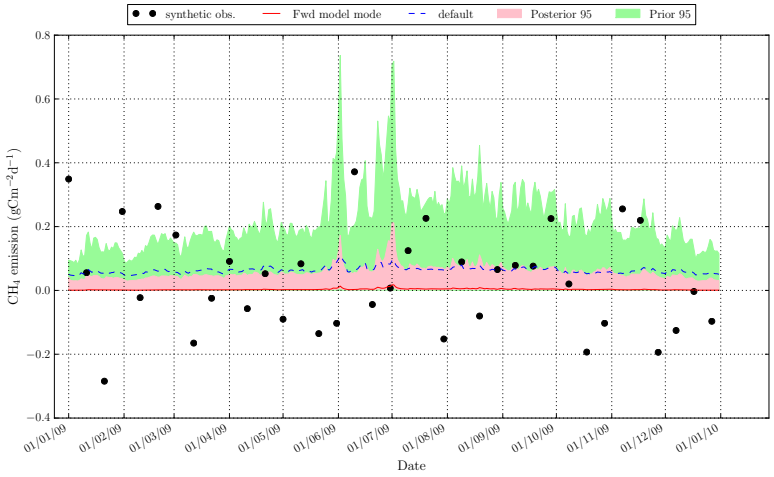

(a) *Synthetic {10/0.2} observations.*

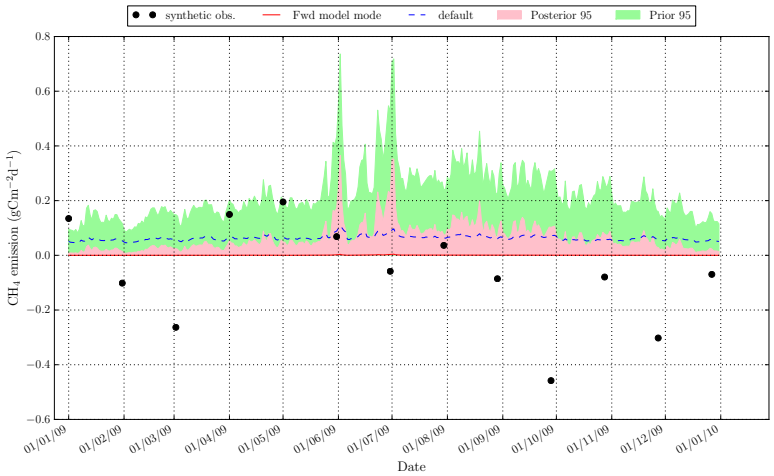

(b) *Synthetic {30/0.2} observations.*

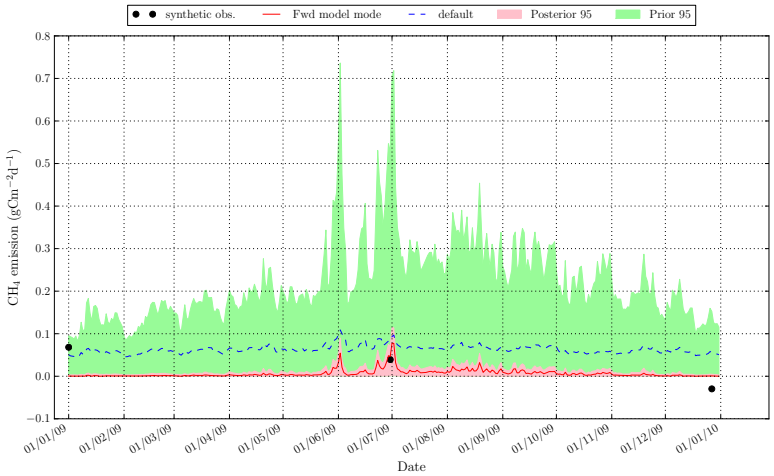

(c) *Synthetic {180/0.1} observations.*

Figure 5.8: The CH_4 net flux from an ensemble of 500 forward model runs using the posterior parameter distributions constrained with synthetic CH_4 flux observations with varying temporal sampling interval and added random Gaussian noise.

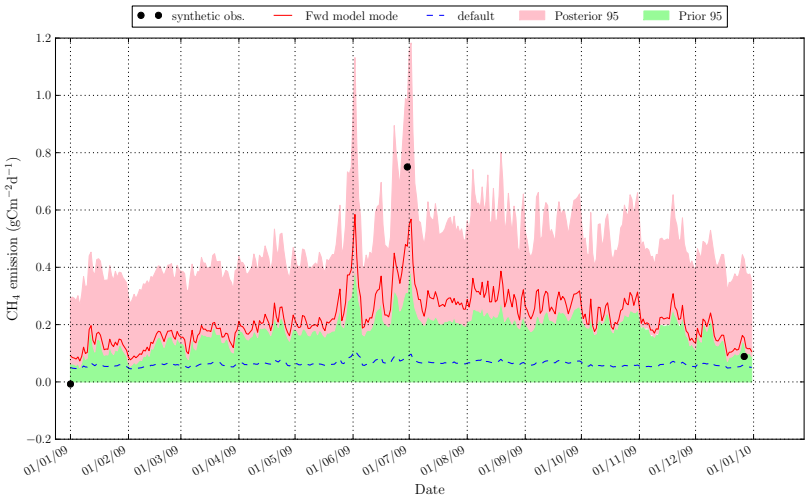

Figure 5.9: The CH_4 net flux from an ensemble of 500 forward model runs using the posterior parameter distributions constrained with synthetic CH_4 flux observations a temporal sampling interval of 180 days with added random Gaussian noise of $0.2 gCm^{-2}d^{-1}$.

peak flux during the summer months, and some in a general overestimation during the summer months, and iii) no clear temporal trend and a loss of daily variability. The first case is seen with the {60,180/0.02}, {30/0.05} and {1/0.2} observations (Figure 5.10). From the OAT sensitivity analyses (Chapter 4 Figures 4.13 and 4.14), it is suggested that this behaviour is the result of a negative bias in the Q10_l parameter as all but the daily observations show a negative bias for the Q10_l parameter, suggesting this could be part of the reason for this departure. The {5/0.1,0.2} and {10,60/0.05,0.1} observations all show a greater amplitude of seasonal cycle than the true CH_4 flux to varying degrees (Figure 5.11).

Examining the OAT sensitivity analyses and the parameter biases, it is likely that an inaccurate temporal variability in the forward CH_4 flux mode is caused by positive biases in the Q10_l, LUE and inundation ratio parameters. A positive Q10_l parameter bias accounts for the underestimate during the winter months. Conversely a positive bias in both the LUE and, for three out of six of these observational characteristics, the inundation ratio, both result in an overestimate of the CH_4 flux, especially during the summer months.

Wide CH_4 flux posterior 95% C.I.

A wider posterior CH_4 flux 95% confidence interval occurs mostly at errors of $>0.1 gCm^{-2}d^{-1}$ (e.g. (Figure 5.12), though not at all temporal frequencies, suggesting that this is not the only cause of a limited reduction in forward model uncertainty.

In contrast to the negative bias seen above, the {180/0.2} observations result in a significant positive bias in the forward model mode and a large posterior 95% confidence interval (Figure 5.13). Although several parameters are relatively well-constrained, this is likely due good constraint of the LUE parameter posterior PDF and the fact it is positively biased towards the upper end of its prior range (Figure 5.5). This constraint is potentially strengthened by the negative bias of the autotrophic respiration scalar.

RMSD between the daily forward mode and the true flux

The root mean squared difference between the forward model daily mode and the true value ranges from 0.0025 to $0.0575 gCm^{-2}d^{-1}$ (Figure 5.14), i.e. between ~4% and 91.3% of the true mean daily flux ($0.06308 gCm^{-2}d^{-1}$). For observations with a temporal sampling interval of >=30 days the RMSD increases more so with increasing observational error, although observations with a temporal sampling interval of 15 days show a slight decrease in RMSD compared to observations every 10 or 30 days. This is possibly due to the periodicities of variation that the 15 day observations are picking out, or just because the random Gaussian error added to the 15 day observations happen to have a slightly lower overall RMSE. However the RMSD increases significantly using observations with a temporal sampling interval of 60 days, except for at the highest associated error of $0.2 gCm^{-2}d^{-1}$.

Annual CH_4 flux

The bias between the annual CH_4 flux MAP estimate at the true value ranges from between -1.0 to $1.0 gCm^{-2}y^{-1}$ for observational characteristics which constrain the flux well, and to ~-

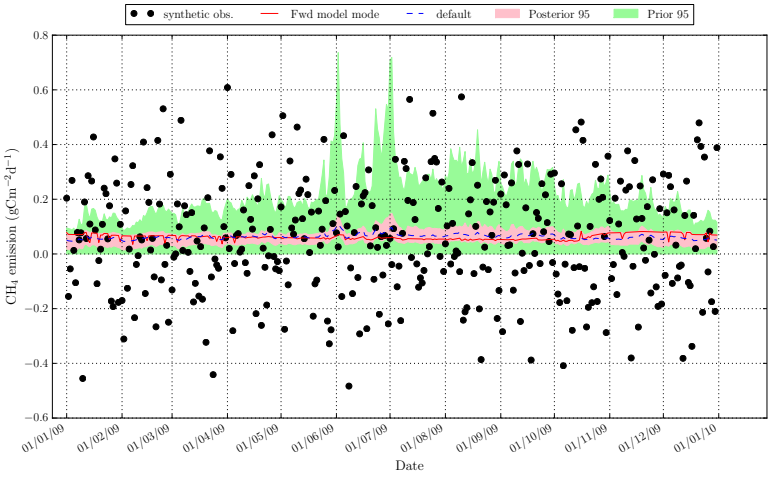

(a) *Synthetic {1/0.2} observations.*

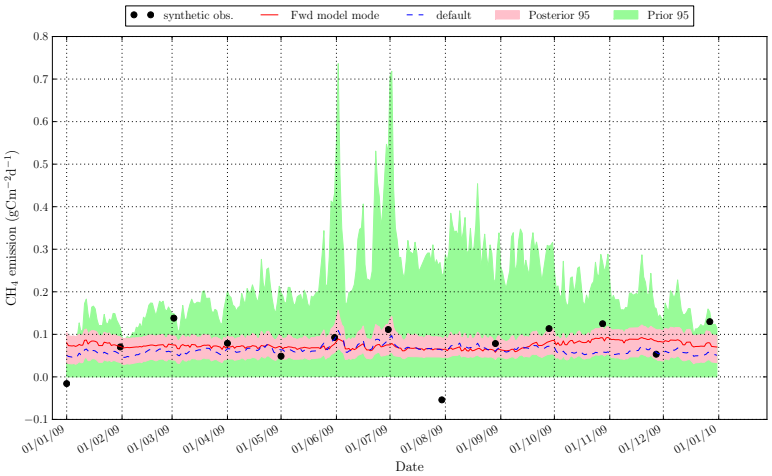

(b) *Synthetic {30/0.05} observations.*

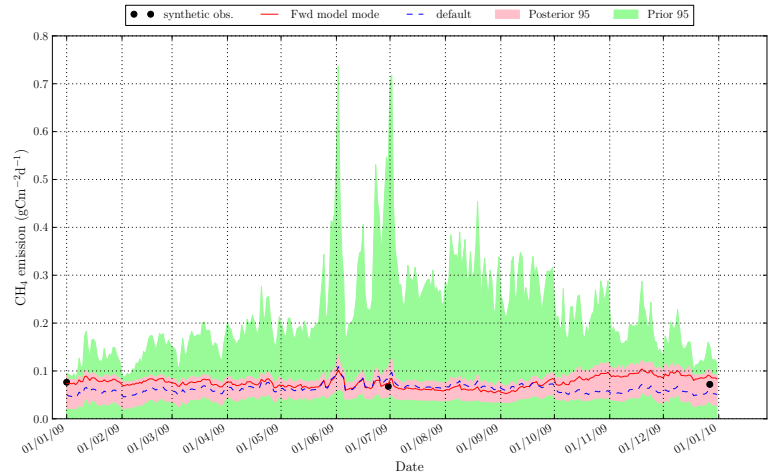

(c) *Synthetic {180/0.02} observations.*

Figure 5.10: The CH_4 net flux from an ensemble of 500 forward model runs using the posterior parameter distributions constrained with synthetic CH_4 flux observations with varying temporal sampling interval and added random Gaussian noise.

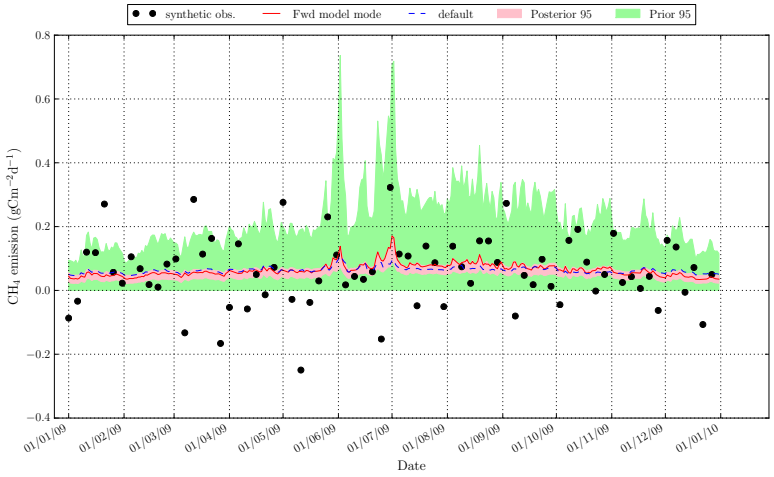

(a) *Synthetic {5/0.1} observations.*

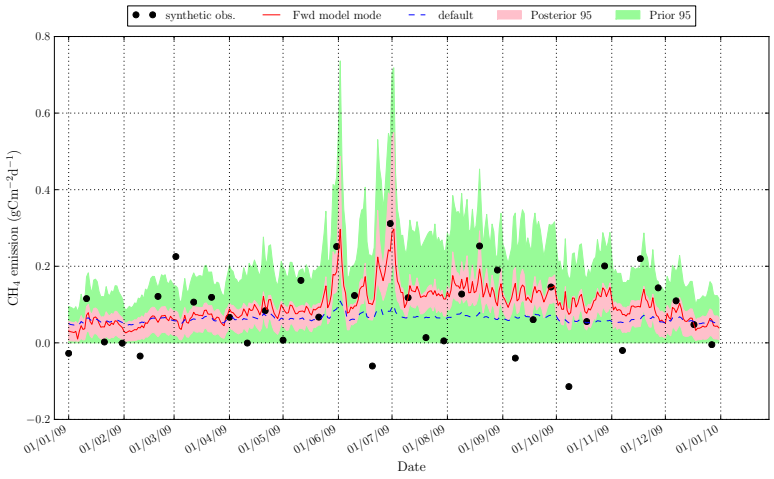

(b) *Synthetic {10/0.1} observations.*

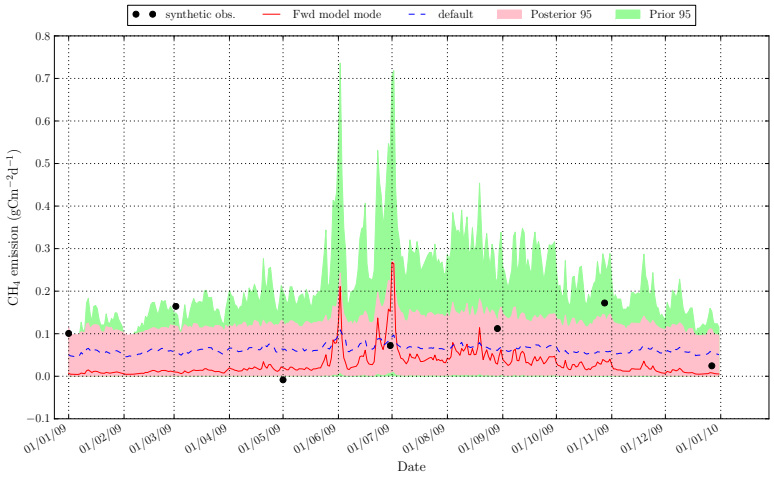

(c) *Synthetic {60/0.1} observations.*

Figure 5.11: The CH_4 net flux from an ensemble of 500 forward model runs using the posterior parameter distributions constrained with synthetic CH_4 flux observations with varying temporal sampling interval and added random Gaussian noise.

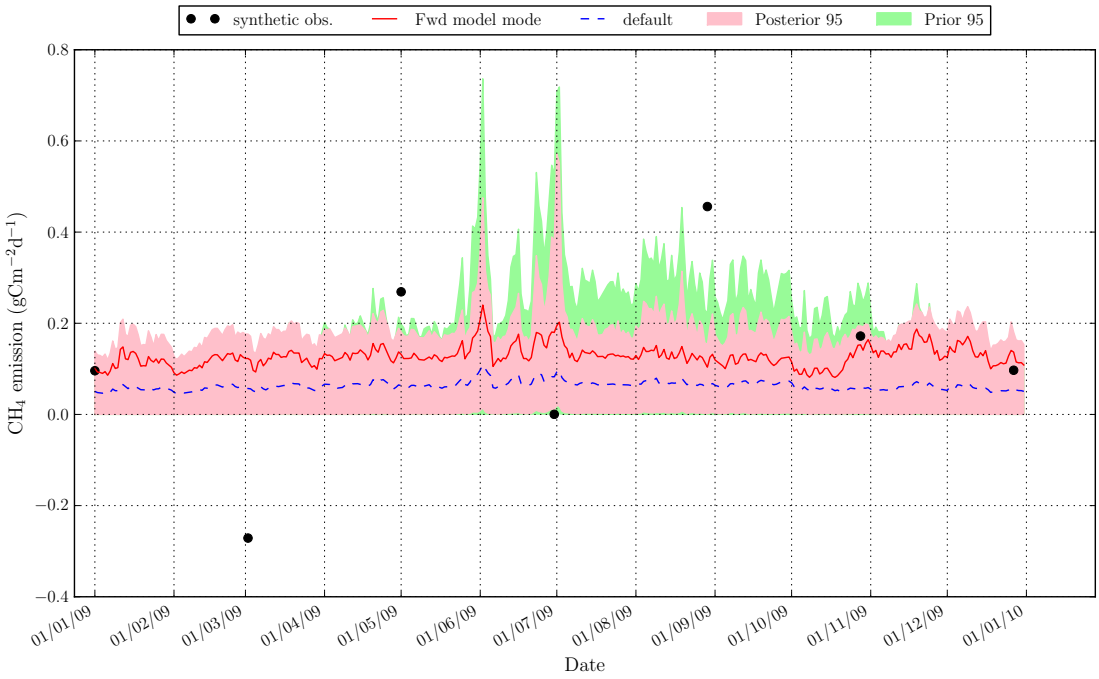

Figure 5.12: The CH_4 net flux from an ensemble of 500 forward model runs using the posterior parameter distributions constrained with synthetic CH_4 flux observations a temporal sampling interval of 60 days with added random Gaussian noise of $0.2 gCm^{-2}d^{-1}$.

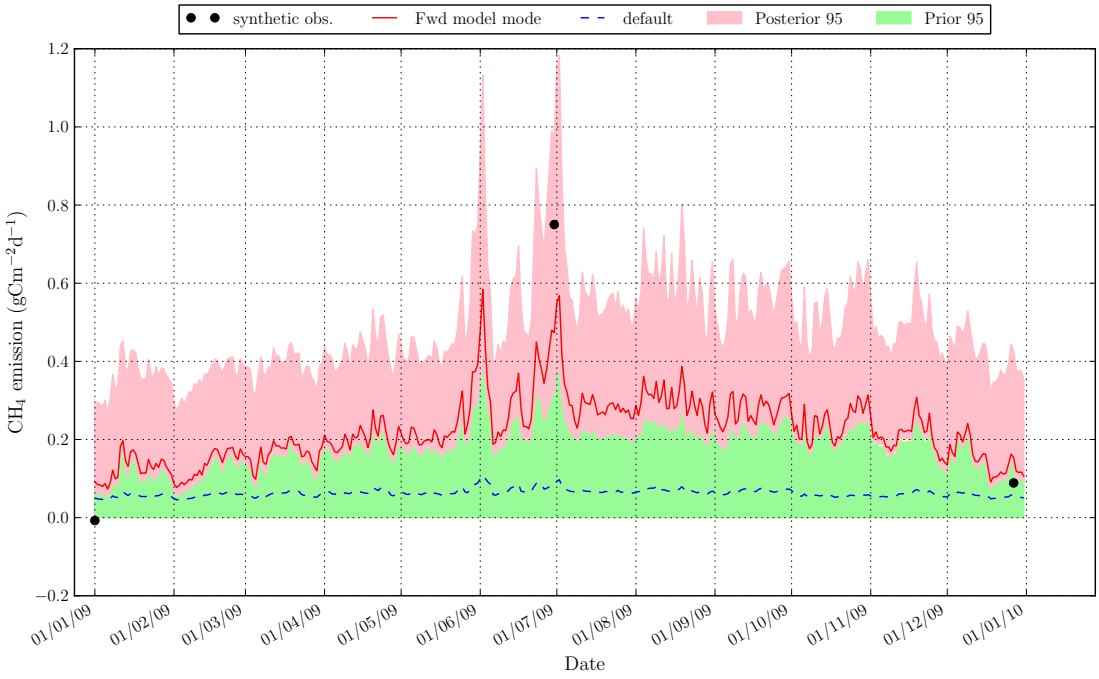

Figure 5.13: The CH_4 net flux from an ensemble of 500 forward model runs using the posterior parameter distributions constrained with synthetic CH_4 flux observations a temporal sampling interval of 180 days with added random Gaussian noise of $0.2 gCm^{-2}d^{-1}$.

$22 gCm^{-2}y^{-1}$ for the worst-case observational characteristics, although the {180/0.2} observations result in a bias of $98.9 gCm^{-2}y^{-1}$ (Figure 5.15). Ignoring the latter outlier, this corresponds to ~ 4 - 95% of the true annual flux of $23.02 gCm^{-2}y^{-1}$.

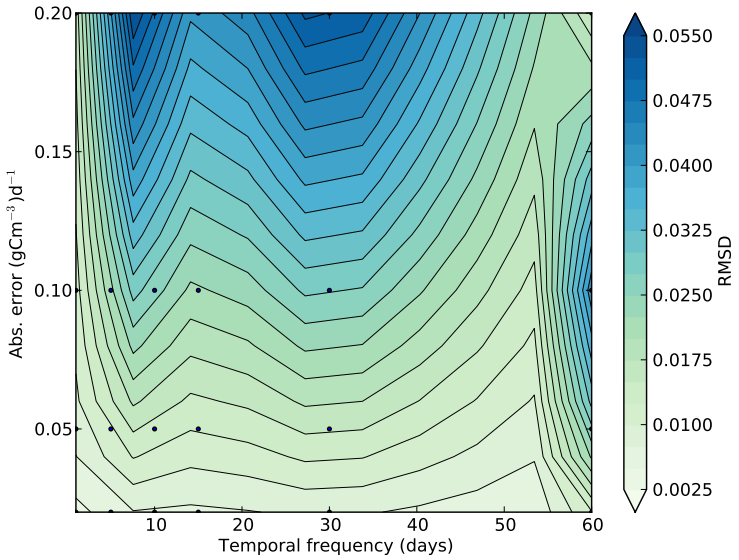

Figure 5.14: Plot to show the root mean squared difference between the MAP of the forward modelled NEP flux and the true daily values using CH_4 flux observations and different observational characteristics.

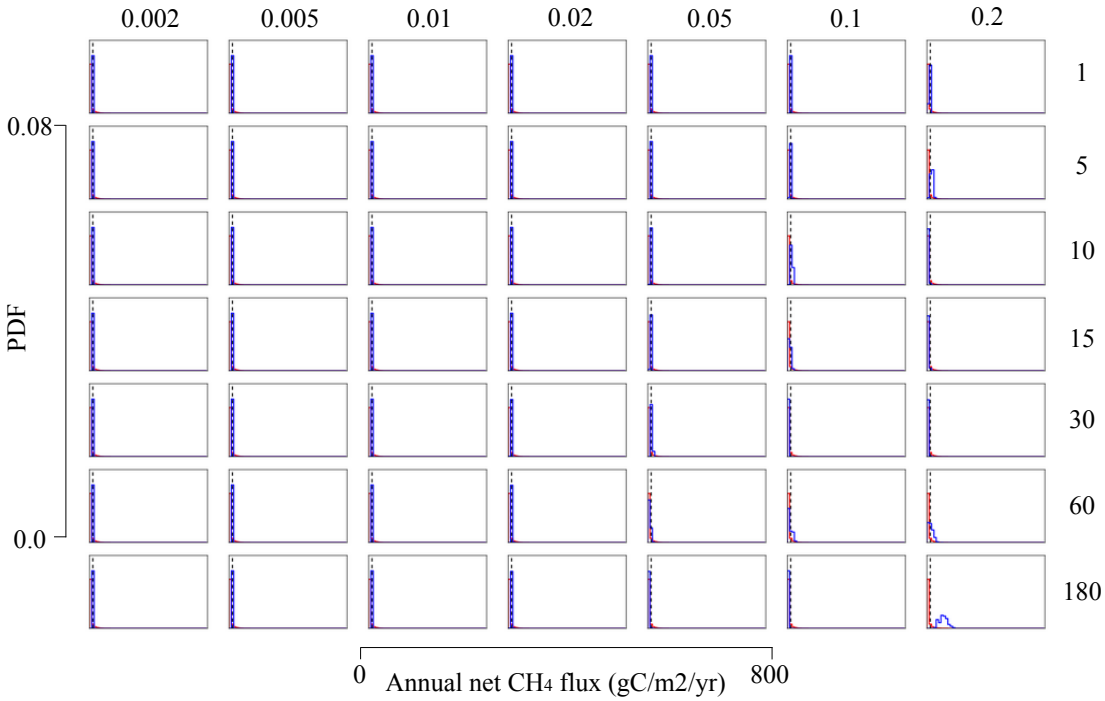

Figure 5.15: Posterior distributions for the annual CH_4 flux, using CH_4 flux observations for each observational characteristic.

5.3.4 NEP forward model mode and model predictive uncertainty

Although all the parameters constrained using the CH_4 flux are involved in the calculation of NEP, it is highly sensitive to only a few of the parameters constrained using the CH_4 flux observations, and mostly to the parameters involved in the NPP calculation (Chapter 4 Table 4.1). It can be seen from the temporal variability that NPP is the dominant control of NEP, especially in the summer months when the variability in flux is highest (Chapter 4 Figure 4.3(b)). An examination of the forward model NEP mode and 95% confidence interval confirms that NEP is mainly controlled by the relative sign and magnitude of the bias in the MAP of the LUE and autotrophic respiration parameters PPDFs and how well-constrained their PPDFs are.

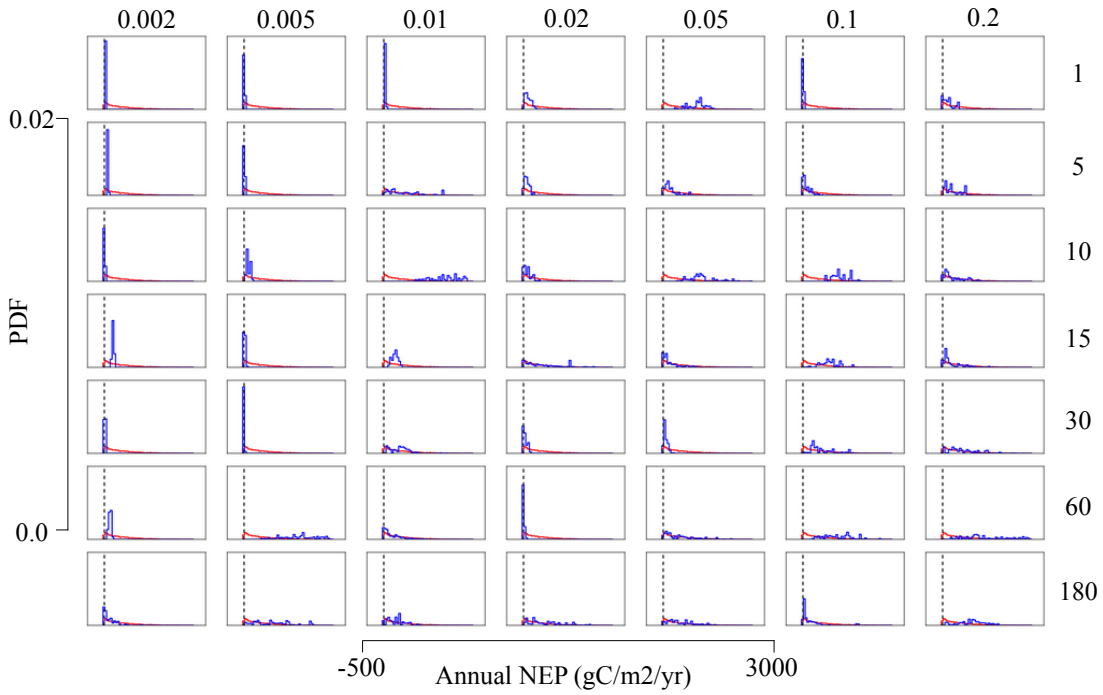

Figure 5.16: Posterior distributions for the annual NEP flux, using CH_4 flux observations for each observational characteristic.

General patterns

The histograms of the annual NEP flux reveal the observational characteristics which result in a constrained NEP posterior flux, and those which do not correspond to the general pattern of decreasing NEP flux constraint (Figure 5.16). The pattern corresponds well with the daily flux timeseries. Generally the {60/0.02}, {<=30/<0.005} and {1/0.01} observations result in a good constraint of the NEP flux and the true value is well approximated, although in most cases the flux is very slightly over- or underestimated (Figures 5.17(a) and 5.17(b) respectively). The bias of the forward modelled mode of the NEP flux is due to under- or overestimation of both the LUE or autotrophic respiration parameters but it is usually the case that one or the other has a slightly greater effect on the NEP flux. For example for the case of the {10/0.005} observations, the biases between the parameter MAP and true value for the autotrophic respiration scalar and LUE parameters were

-0.367 and -0.012 respectively. The relatively large negative bias in the autotrophic respiration scalar results in an increase in NEP flux. On the contrary the relatively small negative bias in the LUE parameter results in a decrease in the NEP flux, but it is not large enough to overcome the positive bias imposed by the autotrophic respiration scalar and as a consequence the modal flux slightly overestimates the true flux. If there is a large positive bias in the LUE parameter and a large negative bias in the autotrophic parameter the forward model mode will greatly overestimate the true value. This can be seen in Figure 5.18.

The above examples resulted in well-constrained posterior NEP fluxes as the LUE parameter constraints were both >90% and the autotrophic respiration scalars were both constrained to >70%. If the posterior parameter PDFs are not well-constrained and slightly biased then the forward model posterior 95% confidence interval will not be as well-constrained.

RMSD between the daily forward mode and the true flux

The RMSD between the forward model daily mode and the true value is shown for all observational characteristics (aside from observations with a temporal sampling interval of 180 days) in Figure 5.19. Values range from 0.0 to 7.2$gCm^{-2}d^{-1}$. The RMSD remains low for observations with a temporal sampling interval of <=30 days and does not increase with increasing observational error. However using observations with a temporal sampling interval of 60 days the RMSD increases significantly, as per the forward modelled CH_4 flux, with a slightly lower RMSD for observations with the highest associated error of 0.2$gCm^{-2}d^{-1}$.

Annual NEP flux

The range in the bias between the NEP annual flux MAP estimate and the true value is large (-62.3$gCm^{-2}y^{-1}$ to ~2141$gCm^{-2}y^{-1}$ - Figure 5.16). For the best-case observational characteristics which result in a well-constrained and accurate forward model mode the bias is generally <100$gCm^{-2}y^{-1}$.

5.4 Discussion

5.4.1 Observational characteristics which result in well-constrained parameters and model

The results show that observations with a low uncertainty are needed to constrain the parameters even if the temporal sampling interval is low, suggesting that it is more important to get a low observation uncertainty that to obtain observations with a high temporal sampling interval. Many of the parameter PPDFs show a significant reduction in the 95% confidence interval with respect to the prior when the {1-15/<=0.02}, {30,60/<=0.01} and {180/<=0.002} CH_4 observations are used to constrain the model. However the with the exception of the Q10_l parameter, the MAP of the parameter PPDFs are biased with respect to the true parameter value. However, the same observations result a well-constrained posterior CH_4 flux, with the forward model mode closely corresponding to the true value. This suggests that many different sets of parameter values exist

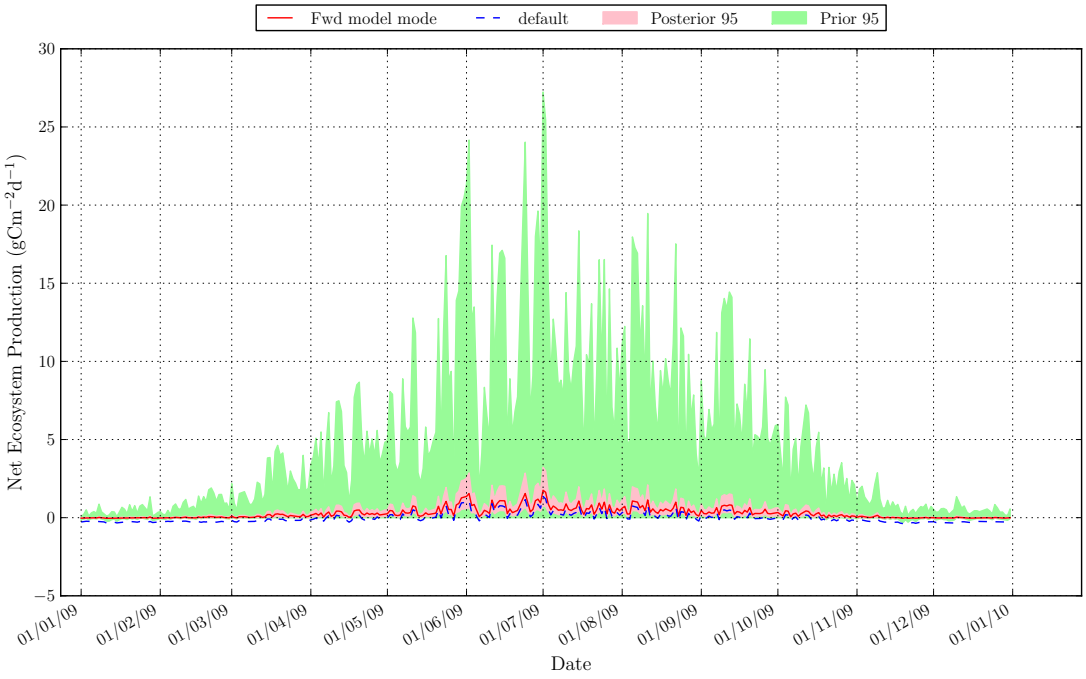

(a) *Synthetic {10/0.005} observations result in a slight overestimate of the NEP flux.*

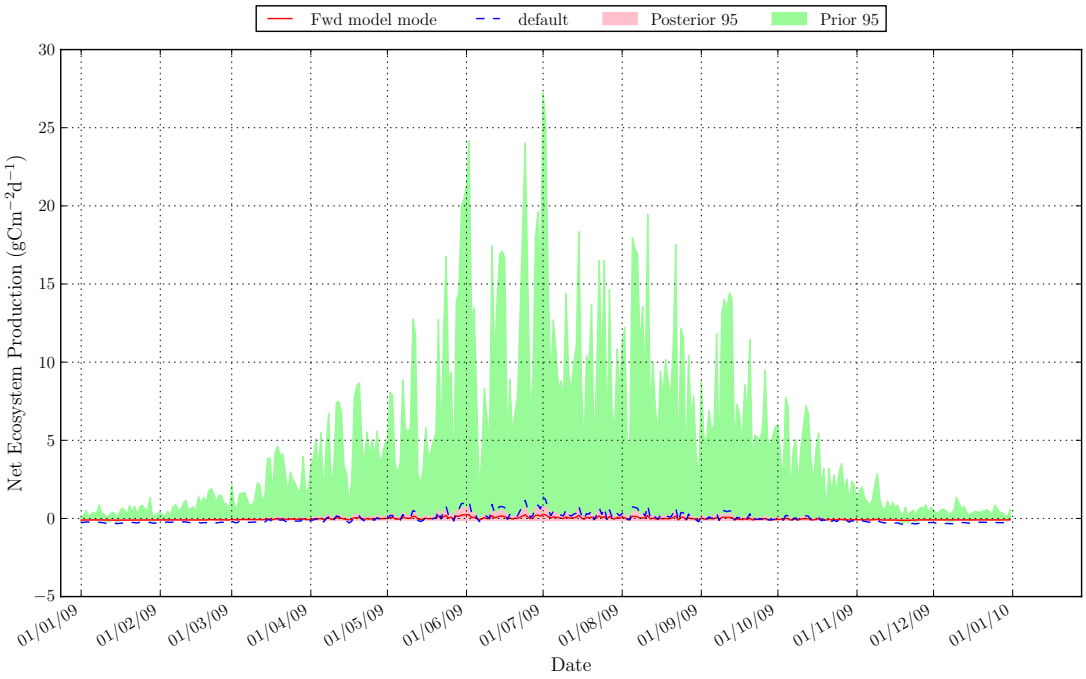

(b) *Synthetic {5/0.005} observations result in a slight underestimate of the NEP flux.*

Figure 5.17: The NEP flux from an ensemble of 500 forward model runs using the posterior parameter distributions constrained with synthetic CH_4 flux observations with varying temporal sampling interval and added random Gaussian noise.

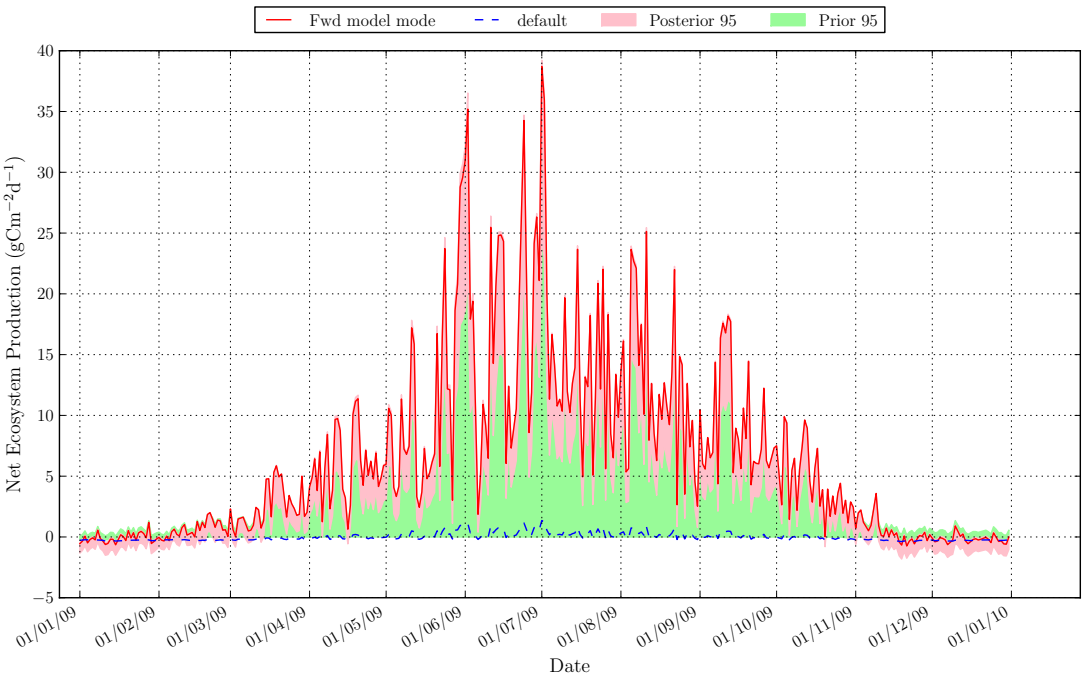

Figure 5.18: The NEP flux from an ensemble of 500 forward model runs using the posterior parameter distributions constrained with synthetic CH_4 flux observations observations every 10 days and an error of 0.01gC^{-2}d^{-1}.

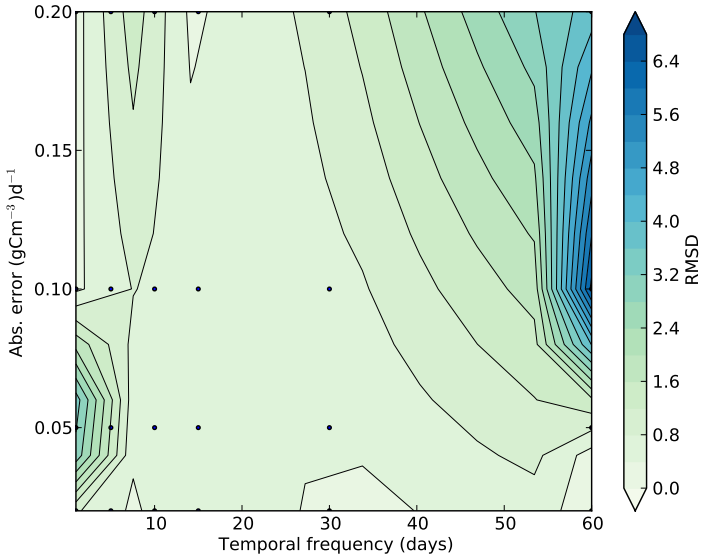

Figure 5.19: Plot to show the root mean squared difference between the MAP of the forward modelled NEP flux and the true daily values using CH_4 flux observations and different observational characteristics.

which produce the same model output - i.e. there is a high degree of model equifinality. The high correlation coefficients between the parameter pairs for these observations confirm this. The correlation magnitude and sign of each parameter pair are not the same for all the observational characteristics however. This is because the correlation structure depends on the bias of the MAP of each parameter and its reduction in uncertainty. This is discussed in more detail below. If the Q10_l parameter is not accurately retrieved the forward mode and posterior uncertainty will be incorrect. This confirms the results of the sensitivity analysis which showed that the CH_4 flux is most sensitive to the Q10_l parameter (Chapter 4 Figure 4.9).

5.4.2 Causes of non-systematic patterns in the parameter bias and correlations

There is no clear pattern in the biases between the MAP estimate and true value for each parameter, nor in the correlations between the parameter pairs. The bias in the well-constrained parameters depends on i) the magnitude, sign and trend of the observation-model difference, and ii) the sensitivity of the CH_4 flux to the parameters. The random noise added to the observations (noise realisations) in each synthetic experiments may happen to produce specific observations which result in biased parameter PPDFs. Extreme values in the observations should therefore be examined carefully before being used in the calibration therefore. Strong biases in a few parameters, specific to each noise realisation of the observations, might govern the resultant correlations between all the parameters.

It might also be the case that only part of the range of two parameters would result in a strong interaction and therefore high correlation between them. If the parameters are constrained, conditional on the observations, in a region of the parameter space to which the model CH_4 flux is sensitive then a high correlation might exist as a consequence. The same pair of parameters might not be correlated if a different set of observations constrained each parameter in a different part of their parameter space. As a result for different observational characteristics the number of correlated parameters varies as well as the specific parameter pairs which are correlated.

5.4.3 Implications of model equifinality

Apart from the Q10_l parameter the other parameters, albeit well-constrained for the best-case observations, just compensate for each other. If the Q10_l parameter is not accurately retrieved the forward mode and posterior uncertainty will be incorrect, given the prior information and observations that have been used in the inversion. These results suggest the model is over-parameterised. The parameters to which the CH_4 flux is sensitive are directly related to calculations of NPP, soil respiration, or CH_4 flux itself. The one parameter which is not involved, porosity, is indirectly used in the calculation of all three C fluxes (Chapter 4 Table 4.1). The model physics is quite complex, and therefore it is perhaps not surprising that all the parameters are highly correlated.

The issue of model equifinality has been discussed by many authors (*Beven*, 2006; *Medlyn et al.*, 2005; *Wang et al.*, 2009; *Williams et al.*, 2009). If a model has a high degree of equifinality it suggests with the information available, in the observations, prior distributions and the model itself, a unique solution to the problem cannot be found. The inversion is therefore "ill-posed". The well-constrained but inaccurate parameter PPDFs may result in an accurate approximation of

the true flux, but this is conditioned on the observations used in the inversion. The model cannot be reliably used to make predictions at other sites or at a different time period for the same site therefore.

The parameters may well be better constrained if there was more information in the observations (i.e. lower uncertainty) or the prior distributions (i.e. a narrower 95% confidence interval). The latter can be achieved by considering the error model used for the distributions. As seen in the results some parameters have regions of the parameters space to which the CH_4 is relatively insensitive. The uniform distribution should therefore be curtailed. If some parameter values are not very likely, which could be discerned from field-based observations, a different prior distribution could be used that would curtail the influence of the unlikely values.

The fact that most of the parameters to which the CH_4 flux is sensitive cannot be accurately constrained suggests that instead of focusing just on improving the prior distribution of the parameters, the model could be simplified. Further investigation would be required as to how to approach simplifying the model. In addition, this analysis has only looked at using the model in one type of climate and ecosystem. If the drivers of the model were different then the parameters to which the model was sensitive might be different and as such very different parameter correlations might occur. It might be necessary in that case to get a better constraint of a different parameter or group of parameters. A site comparison should be one step which is carried out before the model is simplified, as it may be the case that the complexity of the model is necessary for other locations.

As the correlated parameters are well-constrained for the observations which result in an accurate flux, it would be difficult to determine if the MAP of the PPDF was correct if a synthetic experiment had not been carried out. The degree of equfinality in the model can be robustly analysed with the use of a synthetic experiment, giving further proof of how useful a tool an OSSE can be.

5.4.4 Processes constrained by the observations

The only process which is accurately constrained by the observations is the temperature effect on the decomposition of litter (through the Q10_l parameter). Again this confirms the sensitivity analysis. As already discussed in Chapter 4, There is not a large body of literature on the Q10 parameters, which are often used in C flux models. Although the Q10_l parameter is accurately found and well-constrained by the observations, it is suggested that more experimental work needs to be done to better quantify the value of Q10 for different soil processes in different ecosystems. It might be hypothesised that parameters relating to the assimilation of C into the system would have the greatest impact on C fluxes in the model, as they operate at a shorter timescale and have a higher temporal variability due to the direct response to atmospheric forcing. However the CH_4 flux is one step further removed from the assimilation of C into the system than any other C process in the model. It is directly proportional to the magnitude of C decomposition, therefore it is not surprising that the parameters to which the model is most sensitive are those which control the decomposition (Table 4.1).

5.4.5 Impact of unconstrained parameter PPDFs on the forward model ensembles

Above the uncertainty specified above for each temporal sampling interval, the observations do not provide any new information with which to reduce the parameter prior uncertainty, i.e. there is more room for a range of parameter values to match the observations. Therefore the posterior 95% confidence interval of the forward model ensembles is generally not constrained by the observations. In addition the parameters are not highly correlated, which might otherwise act to constrain the 95% confidence interval of the forward model. The mode can approximate the true value of the C flux if the parameter biases result in roughly equal but opposite behaviour in the forward model ensembles. If one parameter is particularly biased then this will have the dominant effect on the model output. This is all down to the specific noise realisations.

It is possible to have a relatively narrow posterior 95% confidence interval if the parameters a not well-constrained, but skewed to a region of their parameter space to which the CH_4 flux is less sensitive. The posterior CH_4 flux 95% confidence interval is quite narrow for the observational characteristics which result in an underestimate of flux, despite the fact that very few, if any, of the parameters are well-constrained. This is likely due to the fact that the Q10 parameter PPDFs are positively skewed. The CH_4 flux is less sensitive to this end of the parameter range (see OAT analyses - Chapter 4 Figures 4.13(a) and 4.13(f)). As previously discussed, improved parameter priors will result in better parameter constraint, and therefore can also help to avoid large biases in any one parameter.

5.4.6 Ability of the CH_4 observations to constrain NEP model estimates

The parameters are constrained with observations of CH_4 flux which has a different relationship to the parameters than the NEP flux. The biases in the parameters are the result of the interaction between the CH_4 flux sensitivity and observation - model error and therefore the same correlation structures which might act to constrain the CH_4 flux are not the same as those that affect the NEP flux.

The NEP flux behaviour is dominated mostly by the relative biases and posterior parameter constraints of the LUE and autotrophic respiration scalar parameters. This confirms the results of the sensitivity analysis, which showed these are the two parameters to which the NEP is most sensitive (Chapter 4 Figure 4.8). As neither of these alter the trend in the NEP flux with changing parameter value the trend of the NEP flux is always well-approximated but the true flux may well be over- or underestimated and the posterior 95% confidence interval can be relatively high. In order to better constrain the two parameters that dominate the NEP flux behaviour it would be better to use observations of NEP flux instead of CH_4 flux, as the range in RMSD values between the NEP forward model mode and true flux is high, as is the bias in the annual NEP flux MAP estimates. However if no NEP flux observations are available, it appears that if observations with an uncertainty of $<=0.005 gCm^{-2}d^{-1}$ with a relatively temporal sampling interval of up to 30 to 60 days are used, the LUE and autotrophic parameters can be correctly found and well-constrained with CH_4 flux observations and therefore an accurate estimate of NEP flux with a reasonably low associated uncertainty can be determined.

5.4.7 Significance of inaccurate model C flux estimates

Both the RMSD values and the bias in the foward modal annual flux are very large for the worst case observational characteristics. This is hardly surprising as the CH_4 flux tends to be low, so small shifts amount to a high proportion of the true value. These error estimates suggest if the flux is not modelled correctly a significant underestimate, amounting to a near-zero flux, could be the result of the parameter calibration.

The highest value RMSD value for the NEP ($7.2 gCm^{-2}d^{-1}$) is considerable given the mean of the daily true NEP flux is -0.0046$gCm^{-2}d^{-1}$ and the maximum is $\sim$1.35$gCm^{-2}d^{-1}$. As the mean is so close to zero most of the range of RMSD values would result in the daily average net NEP flux switching from a sink to a source. It is crucial to be able to get the daily flux well-constrained in order to understand the net C cycle of an ecosystem.

The same is true for the annual NEP. The true annual NEP flux is -1.68$gCm^{-2}y^{-1}$, therefore even the lowest bias of 1.144$gCm^{-2}y^{-1}$ is close to switching the annual net NEP flux from a sink to a source. Most of the biases in the annual NEP MAP estimates would cause a switch from a slight sink in CO_2 to a considerable source, and some biases would result in a significant underestimate of the NEP net flux. Regardless of whether it is a sink or a source, the bias in the annual NEP flux could undoubtably be considerable when trying to constrain the model with CH_4 flux observations, and for many observational characteristics would result in a very inaccurate picture of the annual net NEP flux.

5.4.8 Real ground-based and satellite observations of CH_4 flux

The literature on ground-based measurements of peatland C fluxes suggests that obtaining observations with the required uncertainty should be feasible. However, two problems exist. One, the uncertainty given in many studies scales with the magnitude of the C flux. Therefore the peak fluxes in the summer months may have an uncertainty which is higher than the requirements set out here. This poses a problem for determining the correct temporal trend. The second problem is that a full characterisation of the error in these observations, including both random and systematic errors, has not been achieved yet, and is certainly not routine for many studies. Studies such as *Hollinger and Richardson* (2005) and *Savage et al.* (2008) have used pairwise comparisons to understand the random nature of the errors in C flux measurements, but their investigation does not include systematic errors. On the other hand many studies have looked into understanding the systematic errors that arise from various parts of the measurement and data analysis, but a formalised and universally adopted protocol for dealing with these errors is not available yet. Some studies report a high proportion of the error is related to the sampling uncertainty. *Oren et al.* (2006) suggested however that this could be alleviated if the flux towers were correctly spaced, and the same would be true for chamber measurements, although this would be much harder to achieve in practice.

In general it is unlikely that chamber measurements will be available at regular temporal sampling intervals. Often such measurements are taken in field campaigns which last a few weeks or months and only at certain times of the year. This will not provide the information required. In addition the sampling uncertainty is likely to be very high as the chambers can only measure

very small patches of the surface. Scaling these fluxes temporally and up to the model spatial scale will result in additional uncertainty in the observations. In contrast eddy covariance measurements from flux towers measure the flux over a whole ecosystem and at regular intervals over the whole day and are often in place for long periods of time. These data can be easily be scaled to the daily flux values and are potentially more representative of the spatial scale of a model grid cell than chamber-based measurements. If two or more flux towers are in place, a good assessment of the random errors, including the spatial uncertainty, can be achieved, following the examples of *Hollinger and Richardson* (2005); *Richardson et al.* (2006). However a coherent method for dealing with the systematic errors, for example the underestimation of the flux at night, would also need to be in place. Flux towers are expensive however and they require a lot of effort to get them in place and to keep them running. There are a few hundred flux tower sites around the world, as part of the FLUXNET project, which provide very useful CO_2 flux data but not CH_4 flux, as instrumentation required to accurately measure CH_4 fluxes using the eddy covariance technique has not been developed until recently, and is expensive. However this could feasibly be achieved. Obtaining and setting up a flux tower in a different ecosystem/location that might only be being studied for a short period of time will be difficult, and prohibitively so if a large team is not involved in the project. If a modeller wants to calibrate a particular small-scale model or a particular region which doesn't have a flux tower, they should not rely upon being able to obtain ground-based measurements to do so.

Satellite CH_4 flux observations will alleviate this problem. No CH_4 flux measurements from satellites are operationally available yet but this is likely in the near future with new satellites such as GOSAT which are dedicated to C flux measurements. Methane emission results from several studies have been published (*Bergamaschi et al.*, 2009, 2010; *Frankenberg et al.*, 2011) using SCIAMACHY data. Although only three-monthly average daily a posteriori values are reported in *Bergamaschi et al.* (2009) it seems likely that the requirements for observations with a temporal sampling interval of 1 to 15 days could possibly be met. *Bergamaschi et al.* (2010) presented results of validation exercises based on ground-based flask measurements at certain sites around the globe and found that the satellite data overestimated the ground-based data. The uncertainty estimation was more qualitative than quantitative due to the difficulties in characterising the uncertainties. Clearly some biases exist in the satellite data that have not been accounted for yet. Full error analyses of the CH_4 flux data, including random errors, errors in the retrieval algorithm and atmospheric chemistry-transport models, are not available yet, and theoretical OSSE studies have not been performed for CH_4 flux observations. As retrieval algorithms are improved upon the uncertainty in the observations will be reduced. However, another problem for a small-scale model is that the resolution of the data is currently ~30 x 60km. The satellite measurements are measuring the net emissions, and this scale this includes anthropogenic emissions which are not modelled by most biogeochemical or land surface models. The pixel size alone is likely to produce biased flux estimates if the model operates on a smaller scale, especially for peatland ecosystems which will have a may have higher CH_4 flux than the surrounding area due to the near-saturation of the soil.s On top of that, ancillary information on these emissions would be required to separate out the anthropogenic emissions from the net surface exchange.

A Bayesian inversion approach is used to calculate the fluxes from average atmospheric C concentrations, using an atmospheric chemistry-transport model. This method essentially "updates" prior estimates of the surface C fluxes. Often a land surface model, plus anthropogenic emissions estimates, is used to produce the prior flux map and the concentration measurements improve those prior estimates in much the same way as the Bayesian inversion works in this study. It is possibly circular to use C flux estimates produced using prior C flux estimates from a different land surface model to constrain the model parameters, although if all the uncertainty is accounted for this is essentially just another retrieval algorithm. In practice it would be much better to use the C flux estimates of the model being calibrated as a prior in the Bayesian inversion of the satellite C concentration data. In this way the parameters and C flux estimates could be constrained at the same time. This has not yet been done using a CH_4 flux model. *Spahni et al.* (2011) use CH_4 inversions from SCIAMACHY to evaluated the distribution of CH_4 emissions of the LPJ-WHyMe model but they don't use it to constrain the model flux estimates.

It is unclear at present whether satellite C flux measurements could be used to constrain the parameters of this model. It is possible the uncertainties are small enough but the resolution is too high for small-scale studies. As technology improves the resolution of the data is likely to increase, which would make the data more useful in this instance. Using the C fluxes from the model as priors in the Bayesian inversion would make better use of the C flux data. Separate OSSE experiments would be required in that case, to investigate the error on the satellite C concentration data that would be adequate for this task.

5.5 Conclusions

The main findings of the experiment in this chapter are summarised as follows:

- The {1-15/<=0.02}, {30,60/<=0.01} and {180/<=0.002} observations result in well-constrained PPDFs only for the most important parameters and therefore in a well-constrained posterior CH_4 flux, with the forward model mode closely corresponding to the true value. However the MAP estimates of the parameters only approximate the true value or the Q10_l parameter to which the CH_4 flux is most sensitive.

- Low observation uncertainty is more important for constraining the parameters of the CH_4 flux - sensitive parameters with CH_4 flux observations than the temporal sampling interval.

- Where the observation uncertainty is low enough to allow good parameter constraint, many combinations of parameter values exist which result in the same CH_4 flux model mode. Therefore there is a high degree of model equifinality.

- Observations with a high uncertainty will result in an inaccurate forward model mode and wide posterior 95% confidence interval, though this depends on the number of biased parameters and whether they are skewed towards a region to which the model is sensitive to.

- As the NEP flux has a different relationship to the parameters than the CH_4 flux the resultant parameter values often result in an over- or underestimate of the NEP flux and a wider 95%

confidence interval. Therefore fewer observational characteristics result in an accurate NEP forward flux mode. These are the {<=60/<=0.005} observations.

- Ground-based observations, ideally eddy covariance data, which would meet the observational characteristic requirements maybe available, but the sampling uncertainty is likely to be very high, especially with chamber measurements. Full error characterisation of the data is not often carried out, which presents a problem.

- It is possible that satellite C flux data that meet the observational characteristic requirements are available, although full error analyses of these data have not yet been carried out. The resolution of the data will also present a problem for small-scale studies.

The results of this experiment have demonstrated how useful a tool an OSSE is for a data-model fusion exercise. The OSSE confirms the results of the sensitivity analysis, but without it it would be unclear as to which observations would be able to accurately constrain the most important parameters. The OSSE also allows for a much fuller understanding of the workings of the model, for example the influence of different parameters and the correlations between parameter pairs can be explored. These results show it is helpful to performing a synthetic experiment before trying to calibrate a model. This type of framework has not previously been used in peatland C flux model calibration studies.

Chapter 6

OSSE using synthetic NEP flux observations

6.1 Introduction

The motivation for performing a Bayesian inversion to calibrate the parameters of a model, and for using an OSSE framework to test the ability of the observations to accurately constrain the parameters, has been discussed in Chapters 1, 2, 3 and in the introduction of the previous chapter.

As also discussed in the introduction of the previous chapter, the results of the sensitivity analysis in Chapter 4 showed the CASA-CH_4 model C fluxes are most sensitive to several parameters directly related to the calculation of the C flux. Therefore C flux observations are needed to constrain these parameters. This chapter uses an OSSE framework to test the ability of NEP observations in constraining the model parameters and C flux predictions.
The following questions will be addressed in this chapter:

1. Which NEP flux observational characteristics, i.e. which temporal sampling interval and observation uncertainty, result in a robust estimate of the model parameters and C flux?
2. Which model processes are constrained by the observations?
3. Do the NEP observations result in improved estimates of CH_4 flux?
4. Which C flux observations are most useful in constraining the model, NEP or CH_4 flux?
5. Do real observations, both ground-based and satellite, meet the requirements as set out in the OSSE?

The lay-out of this chapter is very similar to Chapter 5. The next section provides a summary of the methods used in this chapter, which were detailed in full in Chapter 3. The results are then presented. Firstly the parameter uncertainty (i.e. 95% confidence interval of the marginal distributions of the parameters) will be examined and following this the model predictive uncertainty (i.e. the 95% confidence interval of the forward model runs). Subsequently the results are discussed according to the questions laid out in the introduction to this chapter, and finally the main conclusions of this chapter are detailed.

6.2 Experimental set-up

Chapter 3 provided an comprehensive overview of the methods used in this chapter. These are briefly summarised below and the specific details which are pertinent to the experiments in this chapter are outlined.

The Bayesian inversion algorithm used to calibrate the model was described in Chapter 3 Section 3.6. The OSSE method was detailed in Chapter 3 Section 3.7. The synthetic observations used to calibrate the model in the following experiments were derived from the NEP model output using the default parameters (summarised in Chapter 3 Table 3.2). The added random Gaussian noise is outlined in Chapter 3 Section 3.7 in the 5th column of Table 3.3. The temporal sampling interval of the synthetic observations is decreased by the number of days listed in the first column of the Table 3.3. The observational characteristics used to create synthetic NEP observations in the following experiments are repeated in Table 6.1 for clarity.

Temporal Frequency	**NEP flux error ($gCm^{-2}d^{-1}$)**
1	0.05
5	0.1
10	0.2
15	0.5
30	1.0
60	2.0
180	5.0

Table 6.1: The temporal sampling interval and random Gaussian noise used to create the synthetic NEP observations.

The parameters which are included in the calibration in the following experiments are those to which the NEP is most sensitive, following the Morris sensitivity analysis in Chapter 4 Section 4.4 - see Figure 4.8 and Table 4.1. The default parameters used to create the synthetic experiments are referred to as the "true" parameter values in the following experiments, as the OSSE is testing whether the observations with added noise and decreased temporal sampling interval can retrieve these values. Uniform prior distributions of the parameters are used in this experiment as detailed in Chapter 3 Section 3.6. The maximum and minimum of the uniform distributions are set to the upper and lower limit of the range of parameter values, which were summarised in Chapter 3 Table 3.2). The parameters included in these experiments, their "true" value and their prior distributions are summarised in Table 6.2. The notation U(a,b) is used to define the distributions, where a is the minimum value of the parameter, and b is the maximum.

The outputs of the OSSE experiments were detailed in Chapter 3 Section 3.7.1. Further details relating to the notation and figure captions were also provided in Chapter 3 Section 3.7.1. In brief, the notation $\{t/\varepsilon\}$ is used to denote the observations with a t temporal sampling interval and ε uncertainty. An explanation of what information is provided in the figures and tables in the results section was also provided in Chapter 3 Section 3.7.1, as it is standardised for each type of figure and table. This will be summarised in the first example of each figure and table in the results, and

Parameter	True Value	Prior distribution
auto. resp.	0.5	U(0,1)
LUE	0.264	U(0,2.88)
SR_max	5.13	U(4,9)
Q10_l	1.5	U(1,30)
poros.	0.55	U(1e-5,1)

Table 6.2: A summary of the parameters constrained using NEP observations in the Bayesian inversion in this chapter.

from then on only the information pertaining the specific figure will be given in the caption.

Finally, a note on the sign of the NEP flux. Positive NEP represents a net flux of C into the soil (i.e. a C sink) and vice versa.

6.3 Results

6.3.1 Parameter posterior PDF (PPDF)

Q10_l parameter

Although the sensitivity analysis (Chapter 4 Table 4.1) showed that the Q10 litter (Q10_l) parameter was the least important of the parameters to which the NEP was sensitive, the true value of the Q10_l parameter is correctly found and very well-constrained for most of the "good" observational characteristics, i.e. low error and/or high temporal sampling interval (Figure 6.1). The Q10_l parameter shows a systematic pattern of increase in the bias between the MAP estimate and true value (Table 6.3) and a decrease in the reduction of the 95% confidence interval between the prior and posterior parameter PDF (Table 6.4). The width of posterior parameter PDF doesn't gradually increase with increasing error or decreasing temporal sampling interval but rather broadens slightly or reverts back to the prior at certain values of error for different temporal frequencies. The {<=5/<=1.0}, {10,15/<=0.2} and {<=180/<=0.1} observations result in a well-constrained and accurate Q10_l parameter estimate. For all other observational characteristics the posterior remains unchanged from the prior.

	0.05	**0.1**	**0.2**	**0.5**	**1.0**	**2.0**	**5.0**
1	0.013	0.035	0.032	-0.017	0.112	16.2	19.6
5	0.015	-0.151	-0.265	0.076	-0.086	3.78	7.14
10	0.006	-0.073	1.02	17.9	11.0	25.5	2.47
15	-0.114	0.056	-0.158	28.2	2.15	0.053	5.35
30	-0.005	-0.256	-0.113	25.8	20.7	-0.408	8.72
60	-0.109	0.686	0.795	0.366	19.4	3.56	6.30
180	-0.438	-0.311	1.20	4.81	7.97	28.5	26.5

Table 6.3: The bias between the mode of the Q10 litter posterior distribution and the true parameter value for each observational characteristic. The magnitude of the observation uncertainty is listed in the top headings of the table, and the temporal sampling interval is listed in the headings in the left-hand column.

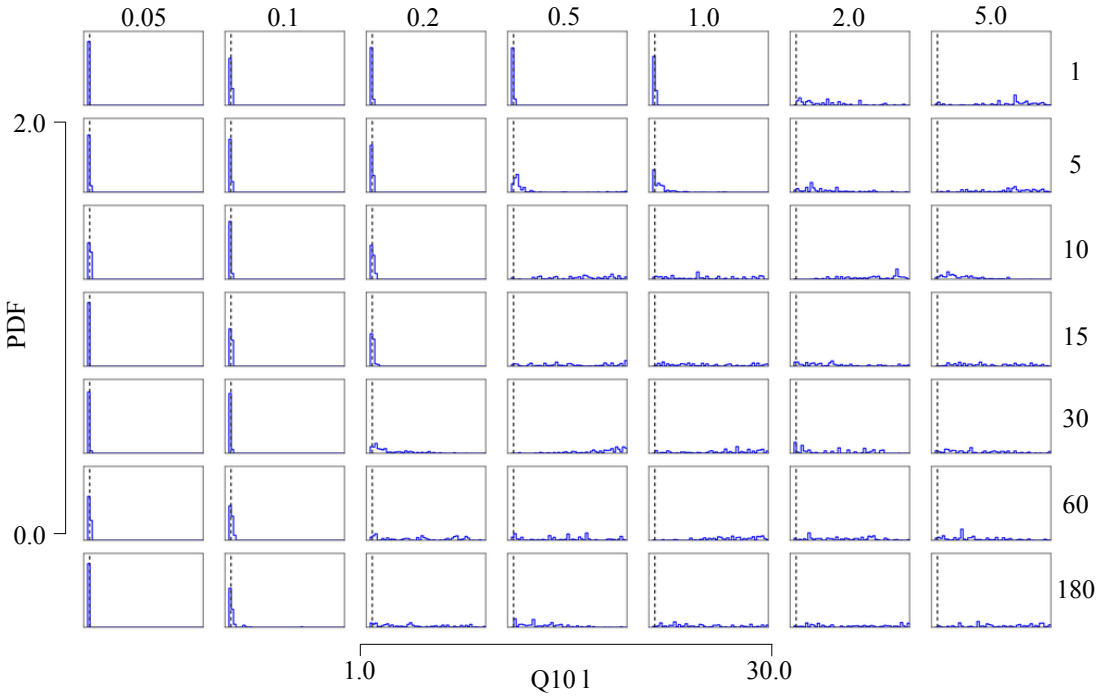

Figure 6.1: Posterior distributions for the Q10 litter parameter, using NEP observations, for each observational characteristic. The axes are the same for all histograms, and are shown at the bottom and left hand side of the figure. The x-axis represents the width of the prior distribution and the blue, the posterior. The vertical black dashed line shows the true value. In all other histogram plots the red line shows the prior distribution. The histogram plots are arranged with increasing observation uncertainty along the columns and increasing temporal sampling interval down the rows. The magnitude of the observation uncertainty is given in the top row, and the temporal sampling interval is given in the right-hand column.

	0.05	0.1	0.2	0.5	1.0	2.0	5.0
1	99.7	99.4	99.1	97.6	96.8	9.67	1.30
5	99.3	98.7	97.6	1.00	56.9	11.6	12.2
10	99.0	98.7	94.8	-3.58	2.49	19.6	35.3
15	99.1	97.1	94.3	-4.15	1.56	0.850	12.9
30	98.7	97.	36.6	22.4	-0.940	18.4	-2.64
60	98.1	95.9	12.0	0.870	17.9	6.80	2.66
180	99.1	85.8	3.51	28.0	-0.730	-3.47	-0.250

Table 6.4: Reduction in uncertainty (%) between the prior and posterior distributions (95% confidence interval) for the Q10 litter parameter, for each observational characteristic. (Prior 95% C.I.: 27.55).

SR_max parameter

The SR_max parameter also shows systematic behaviour of increase in mode - truth bias and decrease in posterior 95% confidence interval with increasing observational error and decreasing temporal sampling interval (Figure 6.2). However even for narrow distributions some bias in the MAP estimate is present. Unlike the Q10_l parameter however this change is more gradual. The {<=30/0.1} observations (or for daily observations an error of <=0.5gCm^{-2}d^{-1}) result in an accurate and well-constrained estimate of the SR_max parameter (Tables 6.5 and 6.6). The {5-15/0.2} observations result in a well-constrained parameter PDF but with a strong negative bias. Most other observational characteristics appear unable tos constrain the parameter well and some result in positively or negatively skewed parameter PDFs, which might be the result of parameter correlation.

	0.05	0.1	0.2	0.5	1.0	2.0	5.0
1	0.006	0.131	0.121	0.308	-1.12	-0.258	-0.584
5	0.097	-0.415	-0.944	-0.939	0.046	2.71	-0.789
10	0.064	-0.360	-1.002	3.69	-0.878	3.28	1.01
15	-0.121	0.061	-0.511	3.21	3.29	1.39	-1.04
30	-0.153	0.628	-0.347	-0.760	0.474	-0.636	3.23
60	-0.974	0.206	0.040	2.82	2.78	1.23	3.73
180	3.53	-0.697	-0.920	0.062	2.67	1.22	3.73

Table 6.5: The bias between the mode of the SR max posterior distribution and the true parameter value for each observational characteristic.

Autotrophic respiration scalar parameter

From the sensitivity analysis he NEP flux is most sensitive to the autotrophic respiration scalar parameter (Chapter 4 Table 4.1) and yet no observtional characteristic result in it being well-constrained and accurately retrieved Figure 6.3). It is often well-constrained but with a positive bias between the MAP estimate and true value (Tables 6.7 and 6.8). This includes all daily observations and all observations with the lowest errors of 0.05 and 0.1gCm^{-2}d^{-1} (except for the

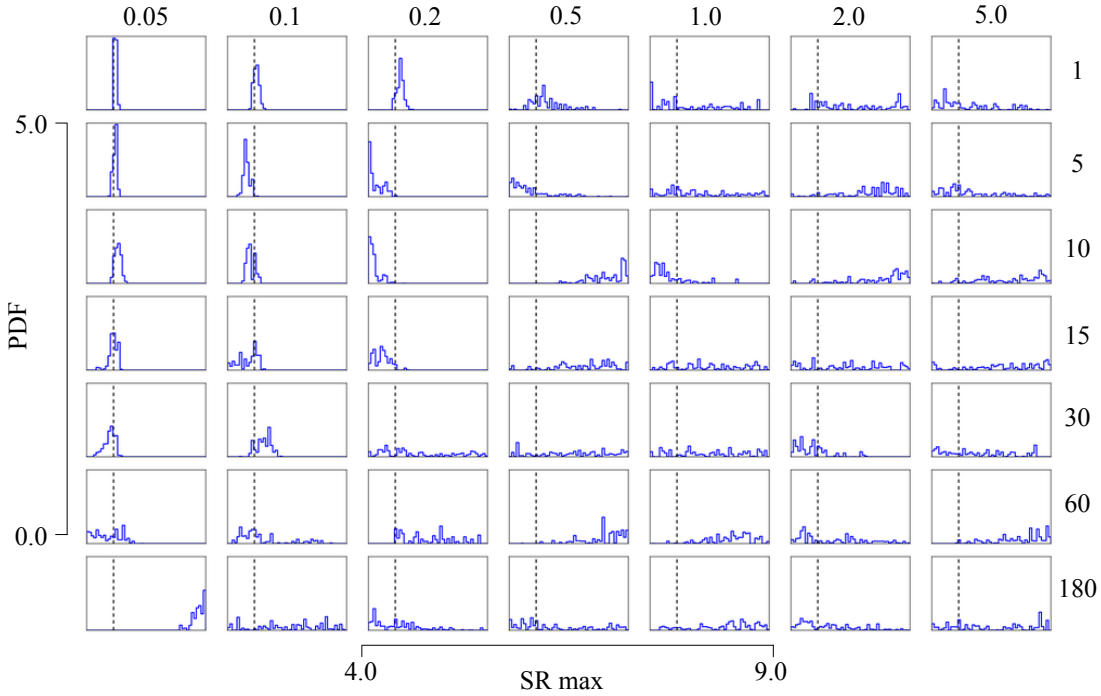

Figure 6.2: Posterior distributions for the SR max parameter, using NEP observations, for each observational characteristic.

	0.05	**0.1**	**0.2**	**0.5**	**1.0**	**2.0**	**5.0**
1	95.8	91.7	87.5	46.2	4.57	17.2	19.8
5	94.3	89.6	79.3	39.4	0.700	8.26	0.290
10	88.7	87.6	83.6	46.0	24.7	14.0	16.0
15	82.5	71.8	77.7	-1.16	7.10	0.500	-1.91
30	82.5	78.3	-0.120	-0.230	-1.01	39.1	9.34
60	62.3	27.7	26.7	34.3	32.7	9.380	20.4
180	78.5	1.88	17.4	-1.07	10.3	15.6	-2.04

Table 6.6: Reduction in uncertainty (%) between the prior and posterior distributions (95% confidence interval) for the SR max parameter, for each observational characteristic. (Prior 95% C.I.: 4.75).

{30/0.1} observations). The {5-15/0.2} observations also result in a well-constrained, positively biased parameter PDF. Most other posterior parameter PDFs are relatively poorly constrained but show either no bias or a strong postive bias, with the exception of observations every 60 days and an error of 0.2gCm^{-2}d^{-1}. The poorly-constrained parameter PDFs show no systematic pattern in how positively skewed they are. This together with the fact posterior PDFs for the "good" observational characteristics produce well-constrained but biased results shows evidence of correlations with other parameters.

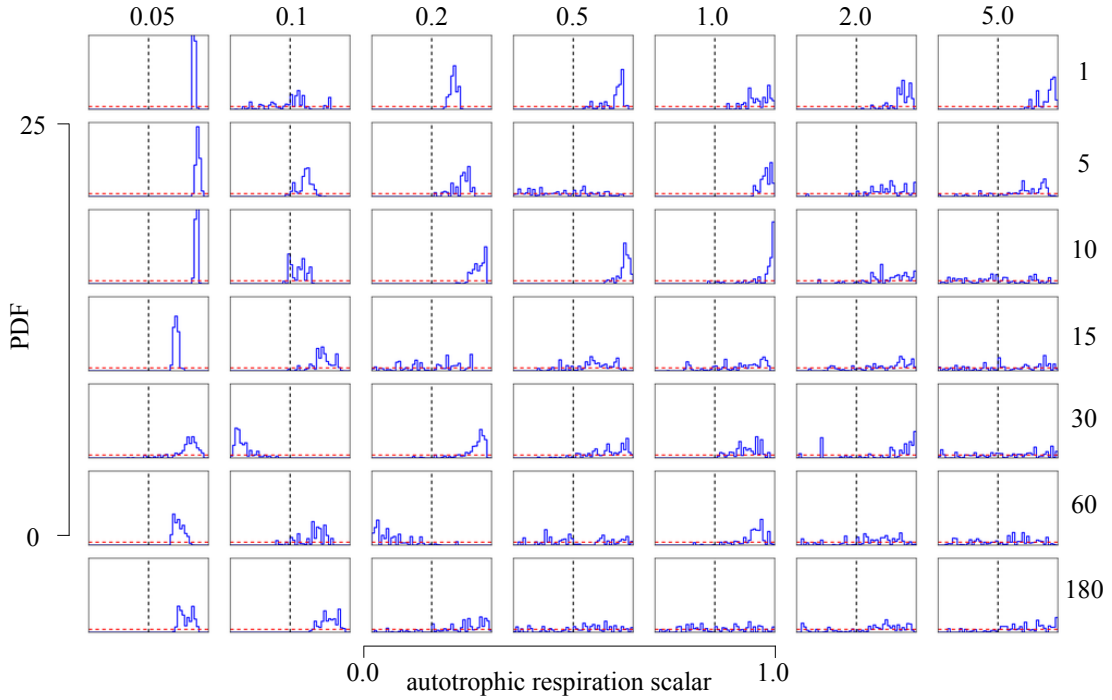

Figure 6.3: Posterior distributions for the autotrophic respiration scalar parameter, using NEP observations, for each observational characteristic.

	0.05	**0.1**	**0.2**	**0.5**	**1.0**	**2.0**	**5.0**
1	0.376	0.007	0.181	0.409	0.484	0.444	0.457
5	0.420	0.150	0.277	-0.272	0.426	0.409	0.200
10	0.397	0.115	0.452	0.438	0.491	0.209	-0.011
15	0.242	0.231	-0.294	0.158	0.085	0.153	0.397
30	0.325	-0.440	0.412	0.294	0.397	-0.290	-0.473
60	0.250	0.237	-0.379	-0.227	0.388	-0.097	0.216
180	0.256	0.361	0.315	0.086	0.296	-0.422	0.481

Table 6.7: The bias between the mode of the autotrophic respiration scalar posterior distribution and the true parameter value for each observational characteristic.

Light Use Efficiency (LUE) parameter

Like the autotrophic respiration scalar parameter the LUE is well-constrained, particularly for temporal frequencies of <=60 days with low observational errors of 0.05 and 0.1gCm^{-2}d^{-1}, but

	0.05	0.1	0.2	0.5	1.0	2.0	5.0
1	96.3	28.2	87.9	64.2	60.2	63.7	76.0
5	93.6	78.5	67.6	10.6	83.1	43.4	18.3
10	95.2	79.5	83.9	79.5	48.9	14.5	10.40
15	92.1	65.1	16.3	39.9	28.3	24.7	1.61
30	51.2	70.6	54.9	45.5	59.1	-1.7	-1.38
60	85.3	51.0	43.9	6.07	52.80	6.00	16.5
180	81.0	74.1	11.8	-0.340	6.71	5.54	16.5

Table 6.8: Reduction in uncertainty (%) between the prior and posterior distributions (95% confidence interval) for the autotrophic respiration scalar parameter, for each observational characteristic. (Prior 95% C.I.: 0.95).

often are postively biased (Figure 6.4 and Table 6.9), though there is no systematic pattern to the bias between the MAP estimate and true parameter value. At higher observational uncertainty the posterior is the approximately the same as the prior (Table 6.10), therefore the observaitons provide no new information to constrain the PPDF. The well-constrained yet biased behaviour of many of the parameter constraints from observations with a low error and high temporal sampling interval suggest that the LUE parameter is correlated with other parameters.

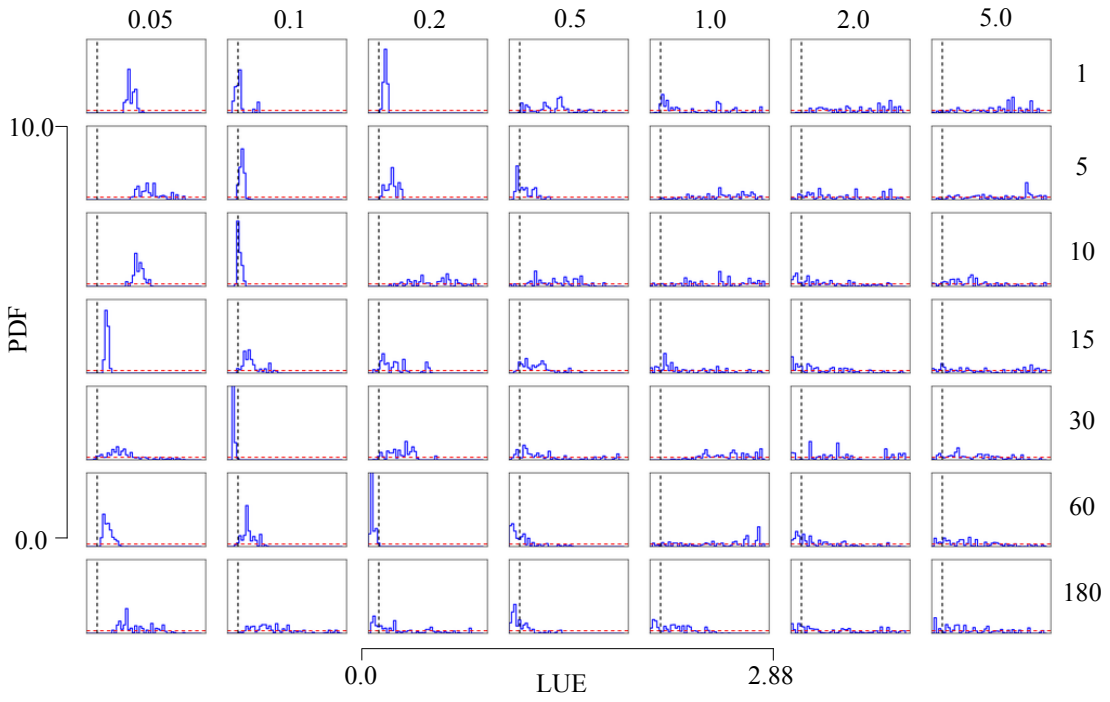

Figure 6.4: Posterior distributions for the light use efficiency parameter, using NEP observations, for each observational characteristic.

Porosity parameter

Most of the porosity parameter PDFs are relatively poorly constrained but often with a positive or negative skew, suggesting they too are sometimes correlated with other parameters (Figure 6.5). Only the {1,5/<=0.1} observations result in well-constrained parameter PDFs.

	0.05	0.1	0.2	0.5	1.0	2.0	5.0
1	0.808	0.050	0.167	1.00	2.53	2.23	2.25
5	1.42	0.124	0.337	-0.040	1.50	2.09	2.11
10	0.983	0.041	1.70	1.56	2.22	-0.177	0.287
15	0.282	0.187	0.068	0.179	0.088	0.211	2.22
30	0.477	-0.114	0.674	0.123	2.50	0.237	0.398
60	0.261	0.566	-0.182	-0.207	2.46	-0.098	0.040
180	0.583	0.656	0.412	-0.147	1.13	-0.076	0.110

Table 6.9: The bias between the mode of the light use efficiency posterior distribution and the true parameter value for each observational.

	0.05	0.1	0.2	0.5	1.0	2.0	5.0
1	87.8	77.7	94.1	35.8	7.72	16.6	10.4
5	53.7	93.3	82.5	69.4	12.7	7.55	9.90
10	78.8	93.7	24.7	18.3	-1.01	10.8	-4.08
15	93.9	66.6	50.0	52.0	2.49	11.3	-3.34
30	31.0	97.7	46.6	4.60	30.8	-4.07	21.6
60	86.0	78.6	91.9	49.8	2.69	11.7	6.90
180	55.1	16.0	9.29	55.0	43.1	-1.55	3.38

Table 6.10: Reduction in uncertainty (%) between the prior and posterior distributions (95% confidence interval) for the light use efficiency parameter, for each observational characteristic. (Prior 95% C.I.: 2.736).

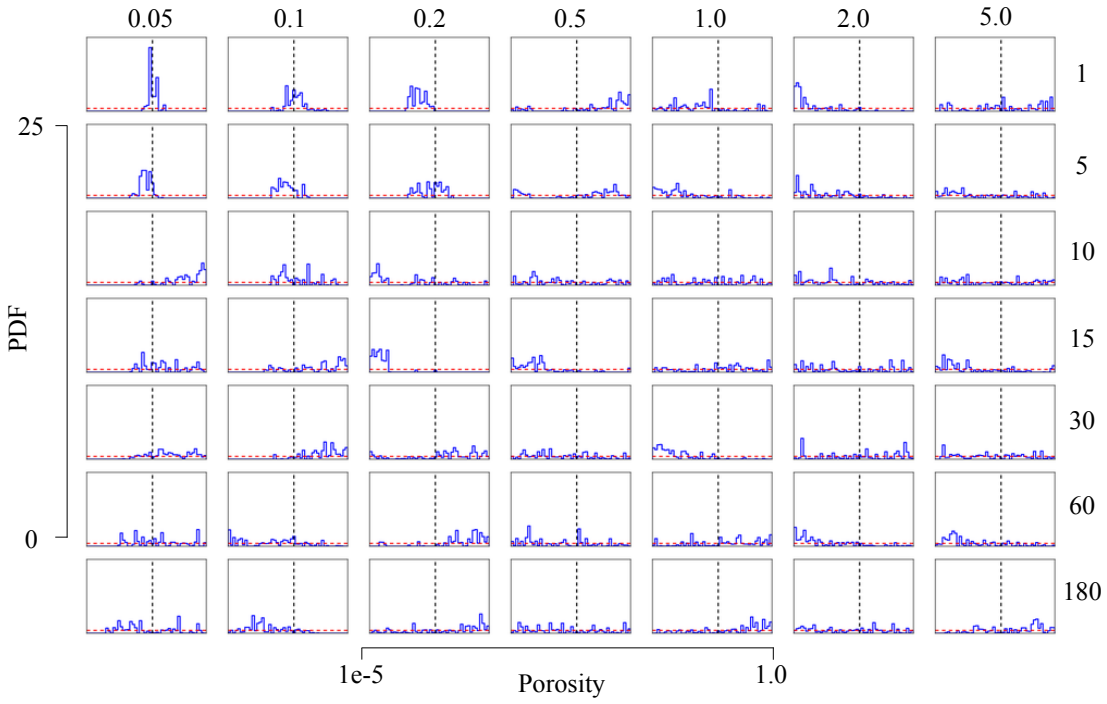

Figure 6.5: Posterior distributions for the porosity parameter, using NEP observations, for each observational characteristic.

6.3.2 Parameter correlation

The correlation coefficients between the LUE and autotrophic respiration scalar parmaters are high for most observation characteristics and are almost always >0.7 for the observational characteristics that result in accurate and well-constrained estimates of the Q10_l parameter (Table 6.11). For all other observational characteristics the correlation coefficient values remain high, and often above 0.4, except for an observation error of 5.0gCm^{-2}d^{-1} for most temporal frequencies. It is likely, as the Morris and OAT sensitivity analysis show that the autotrophic respiration scalar and LUE parameters are the two the NEP flux is the most senstive to, that low observational error in particular allows high correlation coefficient between these two parameters, which in turn forces the good constraint of the Q10_l parameter, as the pattern of the observational characteristic behaviour matches perfectly.

	0.05	**0.1**	**0.2**	**0.5**	**1.0**	**2.0**	**5.0**
1	0.99	0.87	0.93	0.76	0.80	0.66	0.59
5	0.97	0.96	0.92	0.85	0.50	0.51	0.55
10	0.95	0.93	0.74	0.48	0.65	0.43	0.39
15	0.91	0.89	0.90	0.68	0.71	0.54	0.59
30	0.78	0.86	0.71	0.64	0.51	0.64	0.40
60	0.96	0.49	0.67	0.52	0.50	0.35	0.27
180	0.95	0.71	0.71	0.48	0.58	0.51	0.06

Table 6.11: Correlations between the LUE and autotrophic respiration scalar parameters using synthetic NEP flux observations from 2009 with different observational characteristics and no underestimation of observational error.

All other parameter pairs do not show much evidence of parameter correlation. There is a correlation coefficient between the Q10_l and autotrophic respiration scalar parameters for the {60/0.2} observations (0.5) which could be related to that between the Q10_l and SR_max parameters, but this pair of parameters also shows several strong correlation coefficients at other observational characteristics. All but 3 (out of 29) of the parameter pairs (with different observational characteristics and not including the LUE - autotrophic respiration scalar correlation coefficient), with correlation coefficients >=0.4 result in the opposite effect on the NEP flux, according to the OAT sensitivity analysis.

6.3.3 NEP forward model mode and model predictive uncertainty

General patterns

The daily forward model plots show that all of the observational characteristics that show very high correlation coefficients between the LUE and autotrophic respiration scalars, and accurately, well-constrained Q10_l parameter posterior PDFs, result in the daily forward NEP flux mode matching that of the true value, and an extremely narrow posterior 95% confidence interval (Figure 6.6).

As the PPDF of one or both of the of the LUE and autotrophic respiration scalar parameters broadens with increasing observational error, and to a lesser extent, decreasing temporal sampling interval, the correlation becomes weaker. Instead the bias of each parameter, resulting from the a

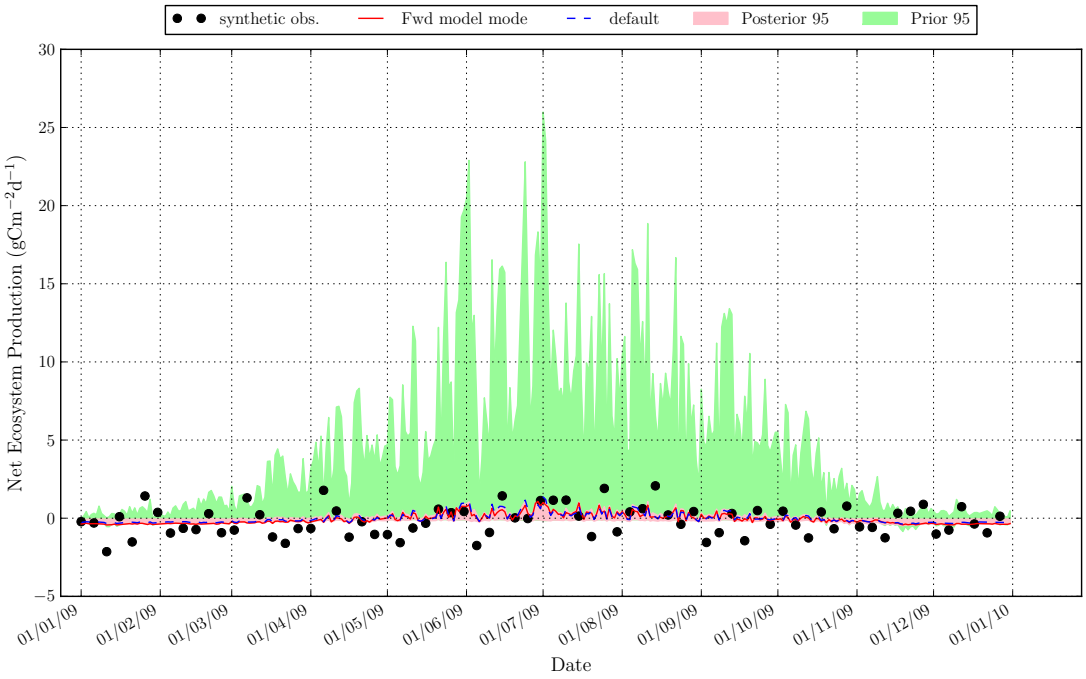

(a) *Synthetic {5/1.0} observations.*

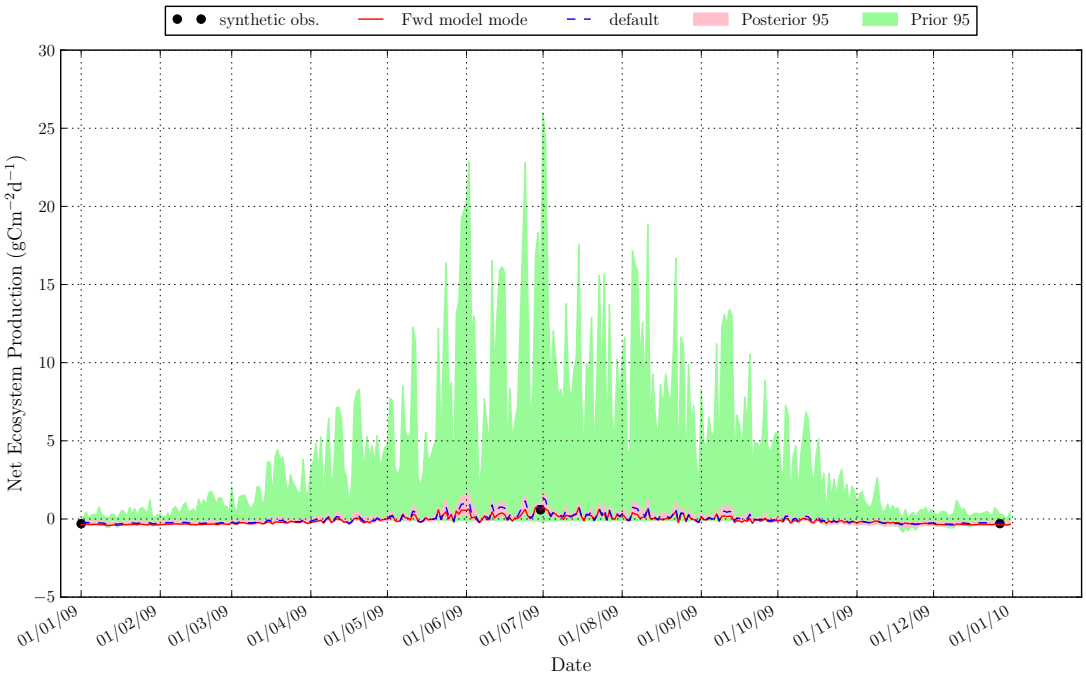

(b) *Synthetic {180/0.1} observations.*

Figure 6.6: The NEP flux from an ensemble of 500 forward model runs using the posterior parameter distributions constrained with synthetic NEP flux observations with varying temporal sampling interval and added random Gaussian noise. The green area shows the prior 95% confidence interval of the CH_4 flux using 3000 random samples from the joint prior distribution of the parameters that are being calibrated in this OSSE experiment. The pink area is the posterior 95% confidence interval and the red line is the forward mode. These results are compared to the model run with the true set of parameters, which is denoted by the blue dashed line. Both plots show a well-constrained and accurate modal NEP flux.

complex interplay between the sensitivity of the flux to the different parameters and the magnitude, bias and trend of the observation-model error, has a more dominant impact on the the mode of the forward flux and the posterior 95% confidence interval. As a result several different groups of forward model behaviour emerge.

1. Well-constrained forward model mode which accurately retrieves the true flux.
2. An overestimate of the true flux throughout the year, but with a wide posterior 95% confidence interval which encompasses the true value.
3. No daily variability, with the modal flux around 0.0gCm^{-2}d^{-1} for the entire year.
4. Underestimation of the true peak flux in the summer months and an overestimation in the winter months (often with the modal flux around 0.0gCm^{-2}d^{-1}).
5. A slight increase in the amplitude of the annual cycle of the mode compared to the true flux (only for the {30/2.0} observations).

The different groups correspond to the same parameter behaviour, unlike the CH_4 flux. The {<=5/<=1.0}, {10,15/<=0.2} and {<=180/<=0.1} observations result in a well-constrained and accurate foward model NEP flux (group one). The forward model behaviour of the second group occurs with high observational errors of 1.0 or 5.0gCm^{-2}d^{-1} which results in poor constraint of all the parameters but a strong positive bias in the LUE parameter, and in most cases a bias in either the autotrophic respiration scalar, SR_max or Q10_1 parameters. These results in an increase in the NEP flux. This is the case for the {5-60/5.0} and {30,60/1.0} observations. An example is shown in Figure 6.7.

The behaviour of the third group occurs mostly when the autotrophic respiration scalar is relatively well-constrained and positively biased, or when the LUE parameter is relatively well-constrained and negatively biased. In both cases all other parameters are poorly constrained. This behaviour from both parameters results in a NEP flux which shows almost no variability throughout the year and remains close to 0.0gCm^{-2}d^{-1}. The correspondance between these parameters' behaviour and the forward model behaviour is unsurprising. The {10,60,180/0.5}, {5,10,180/2.0} and {180/5.0} observations all result in forward modelled NEP fluxes which display this behaviour (e.g. Figure 6.8). The {60/0.5} observations are all close to zero, which will constrain the parameter estimates to produce a forward NEP flux which is also close to zero.

The posterior of the third group tends to be relatively well-constrained, but encompasses the true flux. The only exception to this is for the observations with a temporal sampling interval of 180 days which have the widest posterior 95% confidence interval of all the forward models (e.g. Figure 6.9). This is perhaps due to the very positively biased and poorly constrained Q10_1 parameter (biases of 28.5 and 26.5) due to the high flux in July.

Despite the biases in the autotrophic respiration scalar and LUE, the daily forward model mode is always relatively close to the true value, despite the biases discussed here. The RMSD ranges from 0.0 to 0.57gCm^{-2}d^{-1}.

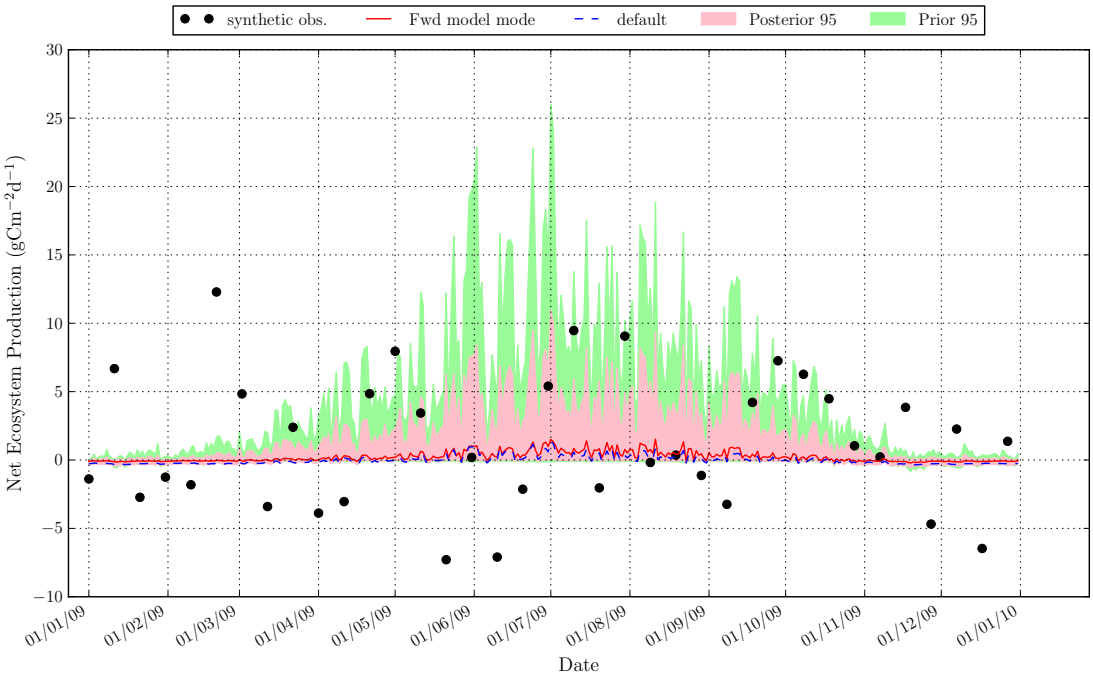

Figure 6.7: The NEP flux from an ensemble of 500 forward model runs using the posterior parameter distributions constrained with synthetic NEP flux observations with a temporal sampling interval of 10 days and added random Gaussian noise of 5.0gCm^{-2}d^{-1}.

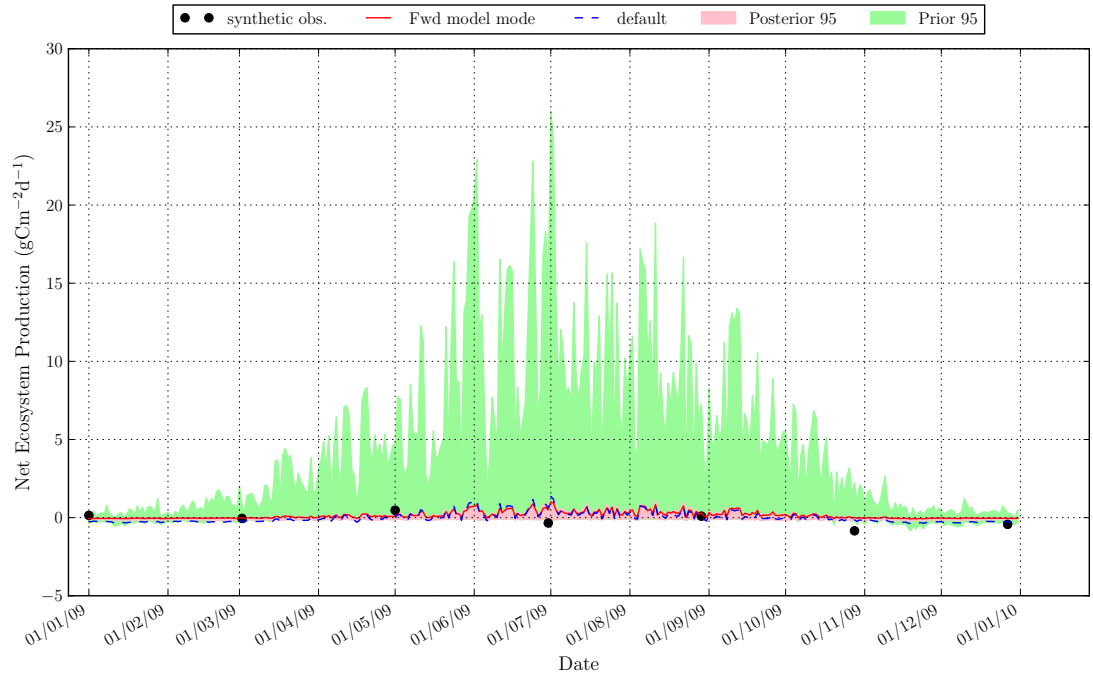

Figure 6.8: The NEP flux from an ensemble of 500 forward model runs using the posterior parameter distributions constrained with synthetic NEP flux observations with a temporal sampling interval of 60 days and added random Gaussian noise of 0.5gCm^{-2}d^{-1}.

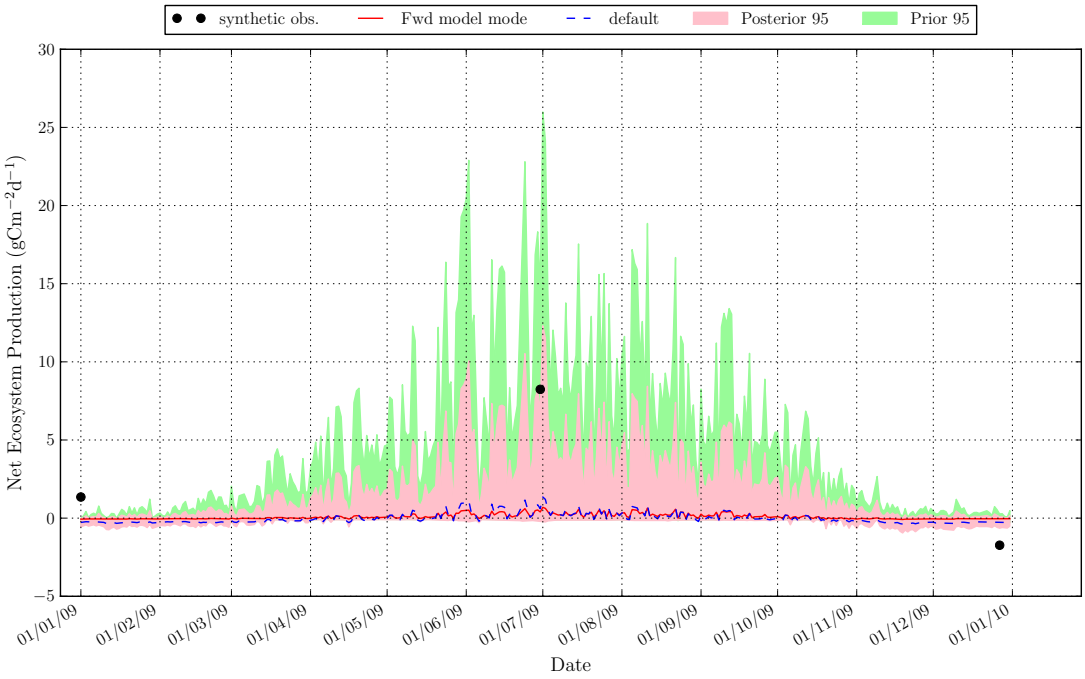

Figure 6.9: The NEP flux from an ensemble of 500 forward model runs using the posterior parameter distributions constrained with synthetic NEP flux observations with a temporal sampling interval of 180 days and added random Gaussian noise of 5.0gCm^{-2}d^{-1}.

Annual NEP

Almost all of the annual NEP flux posterior paramter PDFs are well-constrained (>60%) and the MAP estimate approximates the true value relatively well considering the large prior 95% confidence interval. This shows that whilst some observational characteristics result in a biased daily forward model mode, in general all will result in a relatively accurate annual flux estimate (Figure 6.10). Having said that the pattern of bias between the mode and true value is non-systematic and the range quite high (between -43.63 and +253.22gCm^{-2}y^{-1}), although the observations that constrain the flux well result in very small biases of -1.0 to 1.0gCm^{-2}y^{-1} (Table 6.12).

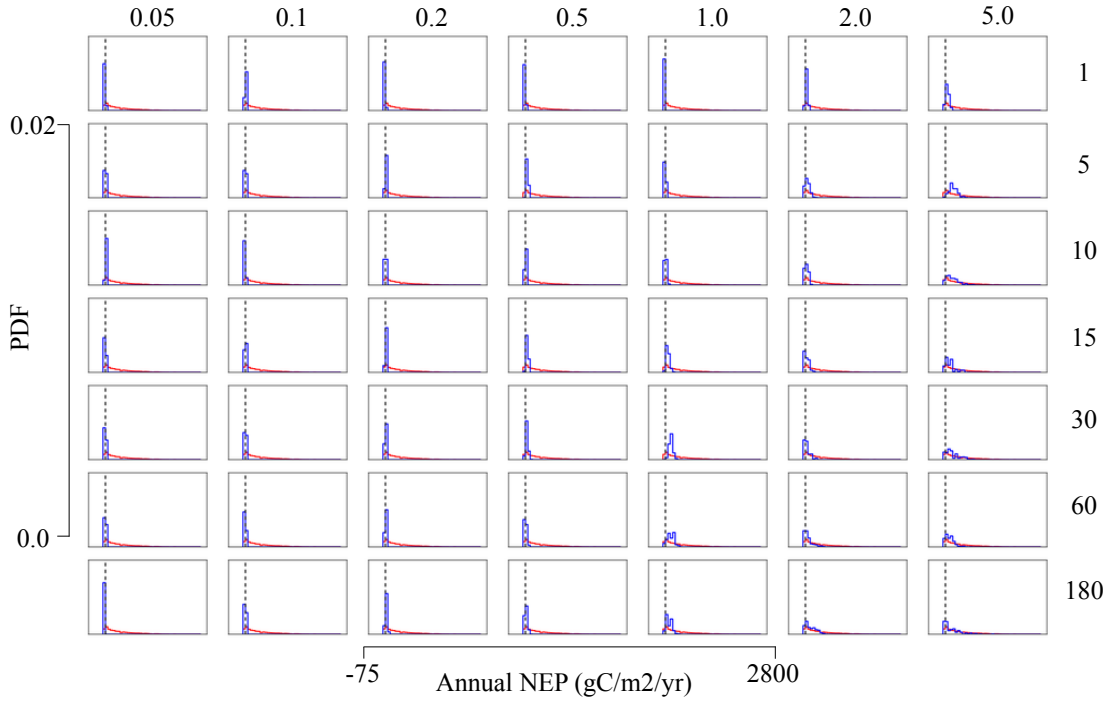

Figure 6.10: Posterior distributions for the annual NEP flux, using NEP observations for each observational characteristic.

	0.05	**0.1**	**0.2**	**0.5**	**1.0**	**2.0**	**5.0**
1	0.671	2.00	-3.19	-6.86	-28.1	42.0	79.8
5	0.100	-0.883	-7.86	83.5	-32.2	-38.0	209
10	1.48	-5.04	1.38	6.18	-5.32	-13.0	214
15	2.02	1.44	1.37	44.4	29.9	0.151	187
30	5.57	-6.40	-13.1	49.1	203	23.8	167
60	-6.71	-0.402	-7.39	-43.6	253	-2.44	168
180	-18.8	-2.15	43.7	-12.6	157	-11.3	-22.1

Table 6.12: The bias between the mode of the annual NEP flux posterior distribution and the true annual flux value for each observational characteristic.

The pattern of constraint shows very systematic behaviour, i.e. it decreases with increasing observational error and decreasing temporal sampling interval, and following the same pattern as the high correlation coefficient in LUE and autotrophic respiration parameters and the well-

constrained Q10_l parameter. As seen in both the daily annual fluxes, none of observational characteristics result in large posterior 95% confidence intervals, which is probably mostly result of the strong, counteractive correlations between the autotrophic respiration scalar and LUE parameters, but also due to the few relatively strong, but counteractive, correlations which do exist between the other parameters that the NEP flux is also sensitive to.

6.3.4 CH_4 flux forward model mode and model predictive uncertainty

General patterns

The patterns of parameter behaviour that result from constraint using NEP fluxes result in a slightly different forward modelled CH_4 flux behaviour, due to the different sensitivity of the CH_4 flux to the parameters. As a result, the CH_4 flux tends to become less well-constrained at a lower observational error than the NEP flux. The forward modelled CH_4 flux mode accurately approximates the true flux and has a narrow 95% confidence interval for the {5,15,30,60/0.05}, {10/0.1} and {1/0.2} observations (e.g. Figure 6.11(a)). At all other observational characteristics the forward modelled CH_4 flux tends to be underestimated, for at least part of the year and often significantly, with the 95% confidence interval only sometimes wide enough to encompass the true value (e.g. Figure 6.11(b)). Only a few observational characteristics result in the CH_4 flux forward model mode overesitmating the true flux (e.g. Figure 6.11(c)). This occurs for the {5/0.1,0.2}, {30/0.2,2.0} and {180/0.05,0.1} observations.

The RMSD values for the CH_4 flux range from 0.0 to 0.052gCm^{-2}d^{-1}, similar to the RMSDs found when using CH_4 flux to constrain the parameters.

Annual net CH_4 flux

The annual flux shows a systematic pattern of decrease in constraint and increase in the bias between the MAP estimate and true value (Figure 6.12 and Tables 6.13 and 6.14). The true flux is accurately found for the {1,5/<=1.0}, {10,15/<=0.2} and {>=30/<=0.1} observations. The reduction in 95% confidence interval can be quite high, even for low temporal frequencies and high observational errors, though this is not the general pattern. The bias between the MAP and true annual flux estimates can be as high as ~-17gCm^{-2}d^{-1} however due to the impact of certain parameters which have the opposite relationship with NEP than the CH_4 flux.

	0.05	**0.1**	**0.2**	**0.5**	**1.0**	**2.0**	**5.0**
1	-0.016	-0.270	0.411	-1.86	-1.31	-17.6	-17.7
5	0.128	1.76	4.01	-10.9	-5.14	-15.2	-17.6
10	-0.823	-0.540	-5.50	-17.6	-17.3	-17.7	-15.1
15	1.05	-0.824	1.14	-17.7	-11.7	1.3	-13.3
30	0.096	1.65	-9.93	-17.5	-17.4	13.0	-16.3
60	-0.408	-1.99	-8.15	-10.0	-17.5	-14.6	-14.5
180	3.08	1.54	-7.24	-16.2	-16.1	-17.60	-17.7

Table 6.13: The bias between the mode of the annual CH_4 flux posterior distribution and the true annual flux value for each observational characteristic.

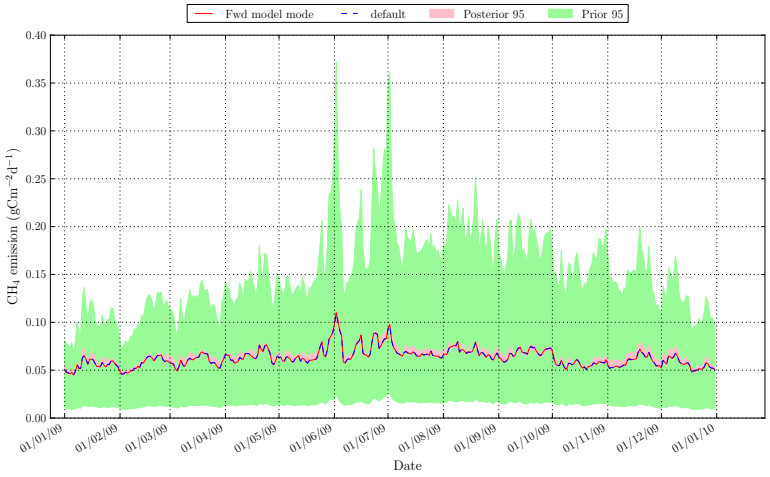

(a) *Synthetic {1/0.05} observations.*

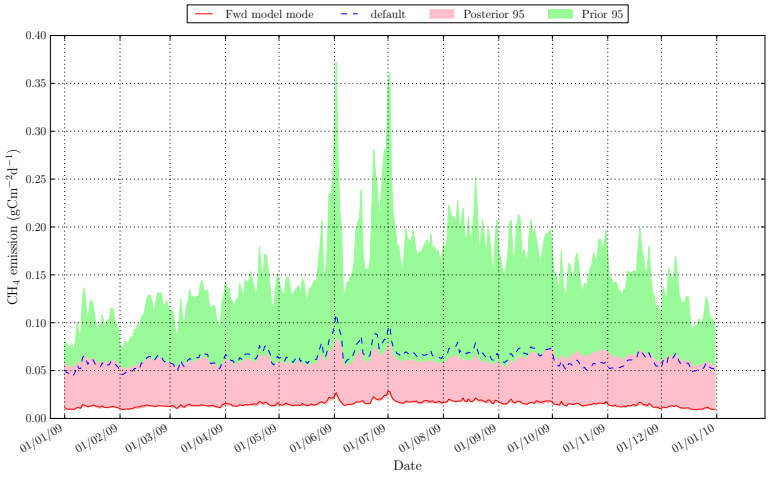

(b) *Synthetic {10/0.5} observations.*

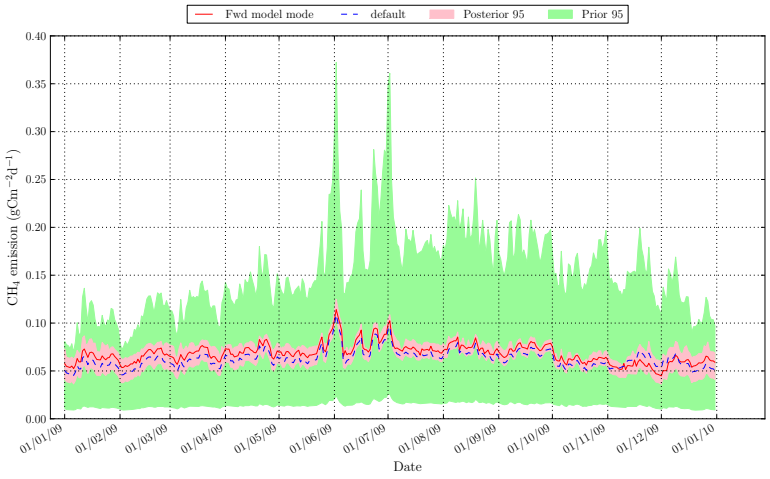

(c) *Synthetic {5/0.2} observations - result in a slight overesimate of CH_4 flux.*

Figure 6.11: The CH_4 flux from an ensemble of 500 forward model runs using the posterior parameter distributions constrained with synthetic NEP flux observations with varying temporal sampling interval and added random Gaussian noise.

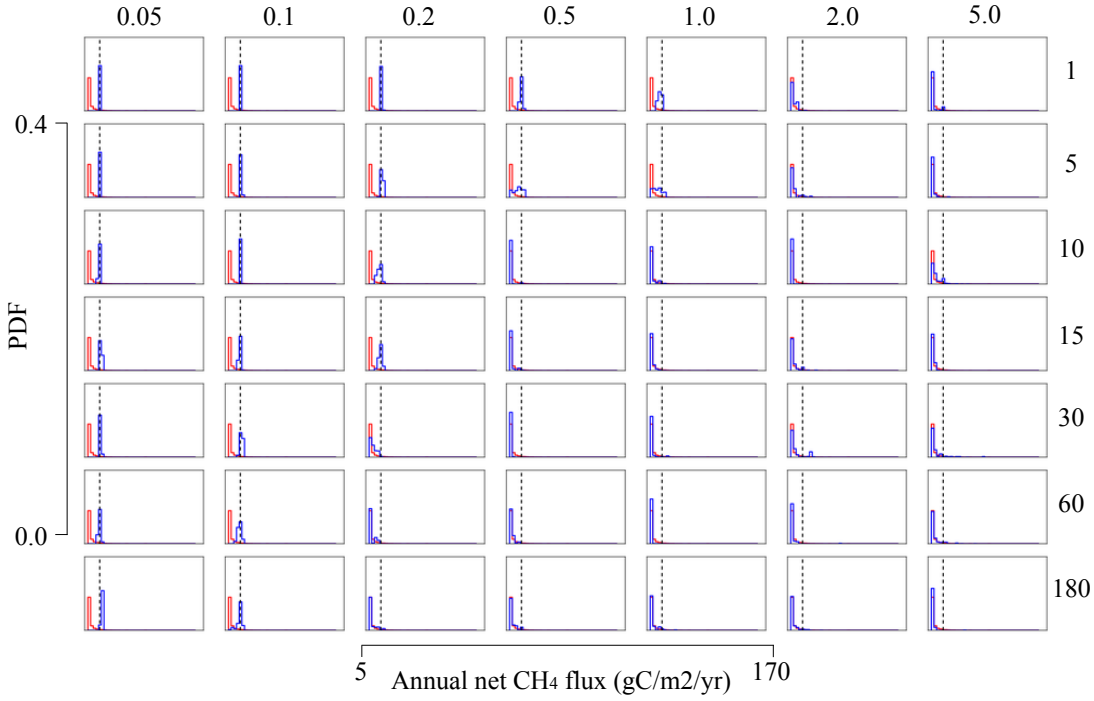

Figure 6.12: Posterior distributions for the annual CH_4 flux, using NEP observations for each observational characteristic.

	0.05	**0.1**	**0.2**	**0.5**	**1.0**	**2.0**	**5.0**
1	97.6	95.4	94.3	86.3	83.3	78.4	65.1
5	96.1	93.2	84.7	53.5	55.1	41.2	83.0
10	93.8	94.3	80.2	66.1	73.3	95.0	44.2
15	94.2	88.6	80.1	69.0	77.0	58.8	85.9
30	93.2	86.2	69.3	97.2	52.3	39.4	19.5
60	88.3	80.9	73.2	72.4	95.6	80.8	24.6
180	90.1	62.4	57.7	63.3	56.6	51.6	85.5

Table 6.14: Reduction in uncertainty (%) between the prior and posterior distributions (95% confidence interval) for the annual CH_4 flux, for each observational characteristic. (Prior 95% C.I.: 50.761287).

6.4 Discussion

6.4.1 Observational characteristics resulting in well-constrained parameters and model

The {<=5/<=1.0}, {10,15/<=0.2} and {<=180/<=0.1} observations result in good constraint but biased LUE and autotrophic respiration scalar parameters and accurate and well-constrained Q10_1 parameter. The correlation coefficients between the LUE and autotrophic respiration scalar parameters are very high (mostly >0.7) for these observations. This is expected from the Morris sensitivity analysis, as their σ value (which represents the effects of higher-order interactions) was very high (Chapter 4 Figure 4.8). This suggests that the correlation between the autotrophic respiration scalar and LUE is causing the good and accurate constraint of the Q10_1. All the other observations (temporal sampling interval of >60 days and a low observation uncertainty (>0.1$gCm^{-2}d^{-1}$) result in a poorly constrained parameter PPDFs as the observations do not contain enough information to improve on the prior estimates. Therefore the posterior PDF approximates that of the prior.

The same observations which allow a high reduction in the parameter PPDFs result in a well-constrained and accurate forward model daily NEP flux. This clearly demonstrates that the high positive correlation between the autotrophic respiration scalar and LUE, which results in counteractive behaviour in the NEP flux, is responsible for the accurate forward models. Several different combinations of the LUE and autotrophic respiration scalar result in a similar model output, as the observations cannot constrain the parameters to their true value. This is more evidence of the high degree of model equifinality, which was also seen with the CH_4 flux observations. The counteractive nature of the parameter correlation is also responsible for the narrow posterior 95% confidence interval. The effect of the high correlation between LUE and the autotrophic respiration scalar on NEP means that the two parameters cannot be separately identified. Their combined retrieval results in a good estimate of the flux in many cases.

6.4.2 Implications of model equifinality

The two parameters to which the NEP flux is most sensitive cannot be accurately retrieved by NEP observations, even with the lowest uncertainty and highest temporal sampling interval. This highlights the issue of model equifinality, where many combinations of parameters result in the same model output. This was also seen, to a higher degree, when the model was constrained with CH_4 flux observations in Chapter 5. The modelling of NEP is aided by model equifinality in this instance, in that the information in the prior and the good quality observations does result in an accurate flux estimate. However model equifinality suggests there is not enough information in the Bayesian inversion to find a unique solution to the parameter estimates. The value of the parameter is just dependent on the noise realisation, i.e. the particular bias and magnitude of the observation uncertainty. Whilst it is arguably fine when just using the model to look at one particular site for one time period, the calibration does not result in parameter estimates which could reliably be used at another site or for a another time period. Therefore the model fails the test of "model generality" - the ability of the model to reproduce flux estimate across a range of different ecosystems. This affects the ability to make predictions with the model and to answer questions about future management and climate scenarios.

How can this problem be dealt with? Assuming the NEP observations are the best-quality (i.e. have the lowest possible uncertainty and highest temporal sampling interval) that is likely to be achieved, there are two possible avenues which might result in more accurate parameter constraints. The first is to obtain observations which might provide unique information with which to constrain the parameters, such as measurements of total respiration or CH_4 flux. These may be able to separate out the processes of CO_2 assimilation and emission. The results of Chapter 5 showed that the CH_4 could more accurately constrain parameters involved in the decomposition of C in the litter than parameters relating to C assimilation, for example.

The other way to more accurately constrain the LUE and autotrophic respiration scalar parameters would be to improve the prior distributions. This could be achieved with field-based measurements. The autotrophic respiration scalar determines the fraction of CO_2 that is released via autotrophic respiration. This can be measured by using dark chamber measurements. The measured CO_2 would be the product of all the respiration terms. If the CO_2 was measured before and after removal of the vegetation, the plant and soil respiration components (autotrophic and heterotrophic respectively) could be determined.

6.4.3 Processes constrained by the observations

The NEP observations mostly constrain parameter which are associated with the assimilation of C into the system (LUE, autotrophic respiration scalar and to some extent SR_max) and in the decomposition of C in the litter layers (Q10_l). This is expected from the sensitivity analysis as already discussed. Parameters relating to the decomposition of soil C and transfers of C between soil pools do not impact the NEP flux enough to be calibrated. This is due to the dominance of the NPP on the NEP model outputs. The processes involved in the C assimilation and transfer of decomposition of litter operate on a shorter timescale and are more directly affected by changes in atmospheric forcing than the processes in the soil C module, and therefore they result in a higher variability in C flux.

6.4.4 Impact of unconstrained parameter PPDFs on the forward model ensembles

When the observation uncertainty is greater than that specified for the observations that resulted in an accurate NEP flux, the parameters are not well-constrained and as a result the forward model mode does not accurately capture the true flux. The flux may be over- or underestimated, or the temporal variability reduced, dependent upon any bias in the observations. This may result in a particular bias of one particular parameter which then controls the model outcome. The posterior 95% confidence interval is also wider if the parameters are skewed towards a part of their range to which the NEP flux is sensitive. The main parameters which result in a bias in the NEP flux are the LUE and autotrophic respiration scalar parameters. This shows that if these two parameters are not well-constrained the model will not be able to replicate the NEP observations.

6.4.5 Significance of an inaccurate model NEP

The annual NEP flux is accurately determined, and well-constrained with respect to the model prior 95% C.I. by almost all the observations, suggesting that the uncertainty in the observations

mainly impacts the daily variability. Whether this is important depends upon what the model is being used for. If annual C budgets are the priority for policy decisions then lower quality observations can be used to determine the annual NEP. If the aim is to understand the drivers of CO_2 sources and sinks over the year then the daily variability is more important and higher quality observations are required. As the annual net NEP flux, and the average daily NEP flux, are close to zero, the bias in the forward model mode would often lead to the model prediction of the net carbon balance changing from a source to a sink. Often the aim of a modelling study is to determine exactly that. In peatland ecosystems in particular this is very important, as they contain a large store of C. Therefore it is imperative that only the "best-case" observations ({<=5/<=1.0}, {10,15/<=0.2} and {<=180/<=0.1}) are used to constrain the NEP flux.

The range in RMSD values for the NEP flux is much lower when NEP flux observations are used instead of CH_4 flux observations. The range in RMSD values between the forward model mode and the true CH_4 flux when using NEP observations is similar to the experiment using CH_4 flux observations. Whilst both C flux observations will cause some bias in the other modelled C flux, it appears this is less of an issue when using NEP flux observations.

6.4.6 Ability of NEP observations in obtaining accurate and well-constrained CH_4 flux predictions

All these results show that it is more important to have NEP observations with a low uncertainty than to have observations with a high temporal sampling interval. This was also the case with CH_4 flux observations. The NEP flux has different sensitivity relationships with the model parameters than the CH_4 flux, and therefore the parameter values that are constrained with NEP flux observations will result in different CH_4 behaviour. The correlations between the parameters will not have the same effect on the CH_4 flux and therefore fewer observational characteristics result in a well-constrained and accurate CH_4 flux. Those that do are the {5,15,30,60/0.05}, {10/0.1} and {1/0.2} observations. Many of the observations result in a positively biased autotrophic respiration scalar which causes the forward CH_4 flux mode to underestimate the true flux. The CH_4 flux has the opposite relationship with the Q10_l to the NEP flux. As the Q10_l is positively biased it will also cause the CH_4 flux to be underestimated.

6.4.7 Comparison of NEP and CH_4 flux observations in constraining the model parameters

These results indicate it would be better to obtain NEP flux observations to constrain the parameters of the model than CH_4 flux observations. In addition, the behaviour of the parameters is much easier to discern using NEP flux observations. Fewer parameters are dominant or have high correlation, suggesting that there is less room for error in obtaining well-constrained parameter estimates and therefore an accurate modelled C flux. The bias in the MAP estimates of the annual C fluxes are similar when using both C flux observations. However, with the "best-case" observations the RMSD values are similar for both C fluxes using both types of observation, so as long as good observations are available the ability to constrain the fluxes should not be too much of a problem.

6.4.8 Real ground-based and satellite-derived NEP observations

The discussion relating to the real C flux observations that might be available and/or might meet the observational characteristic requirements specified by this OSSE experiment is much the same as for the CH_4 flux observations (Chapter 5). However more studies looking at NEP flux are available for chamber, eddy covariance and satellite data. It is more likely that flux towers will be used to collect CO_2 flux data than CH_4, and therefore there might be a greater number of available observations. The same issues arise in terms of availability of instrumentation and error characterisation as discussed in the Chapter 5.

In addition, theoretical OSSE studies which look at the ability of different instruments and retrieval algorithms to constrain the prior emission (e.g. *Hungershoefer et al.* (2010)) have shown that the required uncertainty is achievable with the current and future planned satellite instruments, especially for observations with a temporal sampling interval of <=15 days. *Hungershoefer et al.* (2010) showed if surface networks were also included in the inversion, the posterior uncertainty was reduced, and in that case observations with a lower temporal sampling interval would also meet the requirements. As stated in the previous chapter full error analyses of the CO_2 flux data, including random errors, errors in the retrieval algorithm and atmospheric chemistry-transport models, are not available yet. The observation uncertainties may well be reduced as more data become available for validation and the retrieval algorithms are improved as model structure error become apparent. The same problems relating to spatial resolution of the CH_4 satellite data apply for NEP fluxes. It is also the case that it would be better to use the NEP flux estimates from the model being calibrated as priors in the satellite data inversions. *Nakatsuka and Maksyutov* (2009) did just this with the original CASA model, though they used concentration data from aircraft measurements.

6.5 Conclusions

The main findings of the experiment in this chapter are summarised as follows:

- The autotrophic respiration scalar and LUE have the most influence on the NEP flux. This was expected from the Morris sensitivity analysis.
- The {<=5/<=1.0}, {10,15/<=0.2} and {<=180/<=0.1} observations result in a well-constrained and accurate forward model NEP flux, due to the high correlation between the autotrophic respiration scalar and LUE and the high degree of model equifinality, especially in relation to these two parameters.
- The effect of the high correlation between LUE and the autotrophic respiration scalar on NEP means that the two parameters cannot be separately identified. Their combined retrieval results in a good estimate of the flux in many cases.
- It is imperative to use only the "best-case" observations in this case study in order to accurately determine if a peatland ecosystem is a net source or sink of CO_2. Above a certain uncertainty threshold the observations could result in misleading conclusions. This is important for policy decision-making.

- The {5,15,30,60/0.05}, {10/0.1} and {1/0.2} observations result in a well-constrained and accurately modelled CH_4 flux.
- It is more important to have fewer observations with low uncertainty than to have numerous observations with a high uncertainty.
- NEP flux observations are better suited to producing well-constrained and accurate NEP *and* CH_4 flux than are CH_4 observations, especially if the observational characteristics are not as "good" as they could be.
- Ground-based and satellite data should in theory meet the observational characteristic requirements. However, validation of the satellite data is not yet complete. Standardised uncertainty characterisation procedures are not yet used for either ground-based or satellite observations and therefore good quality uncertainty estimates cannot be provided. In addition satellite data are too coarse a resolution to be used to constrain the parameters of the model at this site.

Once again the OSSE framework has proven to be very useful in improving our understanding of the model and, crucially, for determining which observations would be useful for constraining the parameters of the model. It provides insights into the dominant parameters, thereby extending the model sensitivity analysis, and allows insight into the correlation structures of the model. It also allows a comparison of the ability of different types of observation to constrain the model, which is particularly useful when prioritising obtaining certain datasets or for planning field campaigns.

Chapter 7

OSSE using synthetic soil moisture observations

7.1 Introduction

Again, as in Chapters 5 and 6, the motivation for using an OSSE approach has already been discussed. The results presented in Chapter 4 showed that soil moisture controls the daily variability in the C flux, as well as having a significant impact on the magnitude of the peak flux in the summer when the soil moisture decreases below its maximum value. Furthermore, the sensitivity analysis showed that after parameters directly related to the calculation of C flux, the CH_4 flux and NEP were sensitive to the soil moisture-related parameters, in particular the porosity. Therefore the impact on the C flux predictions from using soil moisture observations to calibrate the model soil moisture-related parameters, is examined in this chapter.

Several OSSE studies are performed to test both volumetric (absolute) and relative (%) soil moisture observations in the inversion. In addition, the impact of a bias in the observations on the results of the inversion is examined for each type of soil moisture observation. This is because operational satellite-derived soil moisture estimates data might be biased due to the coarse resolution of the footprint (see Chapter 2 Section 2.4.2).
The following questions will be addressed in this chapter:

1. Which volumetric and relative soil moisture observational characteristics, i.e. which temporal sampling interval and observation uncertainty, result in a robust estimate of the model soil moisture-related parameters?

2. Do well-constrained soil moisture-parameters result in improved C flux estimates?

3. What is the impact of a bias in the observations?

4. Do real observations, both ground-based and satellite, meet the requirements as set out in the OSSE?

The lay-out of this chapter is as follows. First the results of the OSSE using volumetric soil moisture observations are presented, and then discussed. Following this, the results of an OSSE which was aimed at investigating the impact of reduced prior distributions on the inversion, are

presented and discussed. The motivation for including this extra OSSE study is laid out in the discussion of the first experiment. Following this the results of an OSSE using biased volumetric soil moisture observations are presented. These results are then discussed in terms of the ability of the observations to accurately retrieve the parameters. Finally the results from an two OSSEs using relative soil moisture observations (firstly observations with no bias, and secondly biased observations) are presented, and then discussed. A general discussion of the key findings of all the OSSE studies in this chapter is then provided and conclusions drawn.

7.2 Experimental set-up

Chapter 3 provided an comprehensive overview of the methods used in this chapter. These are briefly summarised below and the specific details which are pertinent to the experiments in this chapter are outlined.

The Bayesian inversion algorithm used to calibrate the model was described in Chapter 3 Section 3.6. The OSSE method was detailed in Chapter 3 Section 3.7. The synthetic observations used to calibrate the model in the following experiments were derived from the volumetric and relative soil moisture model outputs using the default parameters (summarised in Chapter 3 Table 3.2). The added random Gaussian noise is outlined in Chapter 3 Section 3.7 in the 2nd and 3rd columns of Table 3.3 for volumetric and relative soil moisture observations respectively. The temporal sampling interval of the synthetic observations is decreased by the number of days listed in the first column of the Table 3.3. The observational characteristics used to create soil moisture synthetic observations in the experiments in this chapter are repeated in Table 7.1 for clarity.

Temporal Frequency	**Vol. soil moist. error (m^3m^{-3})**	**Relative soil moist. error (%)**
1	0.02	2
5	0.04	5
10	0.06	10
15	0.08	15
30	0.1	20
60	0.15	30
180	0.2	50

Table 7.1: The temporal sampling interval and random Gaussian noise used to create the synthetic soil moisture observations.

The parameters which are included in the calibration in the following experiments are those involved in the calculations of soil moisture. The default parameters used to create the synthetic experiments are referred to as the "true" parameter values in the following experiments, as the OSSE is testing whether the observations with added noise and decreased temporal sampling interval can retrieve these values. Uniform prior distributions of the parameters are used in this experiment as detailed in Chapter 3 Section 3.6. The maximum and minimum of the uniform distributions are set to the upper and lower limit of the range of parameter values, which were summarised in Chapter 3 Table 3.2). The parameters included in these experiments, their "true"

value and their prior distributions are summarised in Table 7.2. The notation U(a,b) is used to define the distributions, where a is the minimum value of the parameter, and b is the maximum.

Parameter	True Value	Prior distribution
poros.	0.55	U(1e-5,1)
rdr_a	7.01e-3	U(1.81e-24,1.24)
rdr_b	-3.48	U(-60.18,-3.41)

Table 7.2: A summary of the parameters constrained using volumetric and relative soil moisture observations in the Bayesian inversion in this chapter.

The outputs of the OSSE experiments were detailed in Chapter 3 Section 3.7.1. Further details relating to the notation and figure captions were also provided in Chapter 3 Section 3.7.1. In brief, the notation $\{t/\varepsilon\}$ is used to denote the observations with a t temporal sampling interval and ε uncertainty. An explanation of what information is provided in the figures and tables in the results section was also provided in Chapter 3 Section 3.7.1, as it is standardised for each type of figure and table. This will be summarised in the first example of each figure and table in the results, and from then on only the information pertaining the specific figure will be given in the caption.

7.3 Synthetic volumetric soil moisture observations

7.3.1 Results

Porosity parameter PPDF

Figure 7.1 shows the porosity PPDF for each set of observational characteristics. The posterior is compared to the prior and the true, known value. With the possible exception of the {180/0.2} volumetric soil moisture observations, the porosity parameter is constrained remarkably well by the observations, compared to the uniform prior, and the true value is well estimated and within the posterior distribution.

The reduction in 95% confidence interval between the prior and posterior PDFs confirms this (Table 7.3). Reductions in relative uncertainty of >90% are found in most cases with generally a decreasing reduction with increasing error and decreasing temporal sampling interval. The posterior PDF is not as well constrained with the {30/0.2}, {60/>=0.15} and {180/>0.08} observations, but the error reduction remains above 50% even for the worst case scenario of {180/0.2} observations.

Table 7.4 shows the bias between the mode or Maximum A Posteriori (MAP) of the porosity posterior parameter distribution and the true value. In general the biases are very small with no pattern to the bias amongst the different observational characteristics. A large bias occurs when the posterior PDFs which are broader. There are a few exceptions where the bias appears to be slightly higher than other PDFs which are less well-constrained, for example, with the {15/0.06}, {30/0.04} and {10,15,60/0.15} observations. The bias has no particular systematic pattern or sign and therefore is not due to the error in the observations, but is just an artifact of the sampling

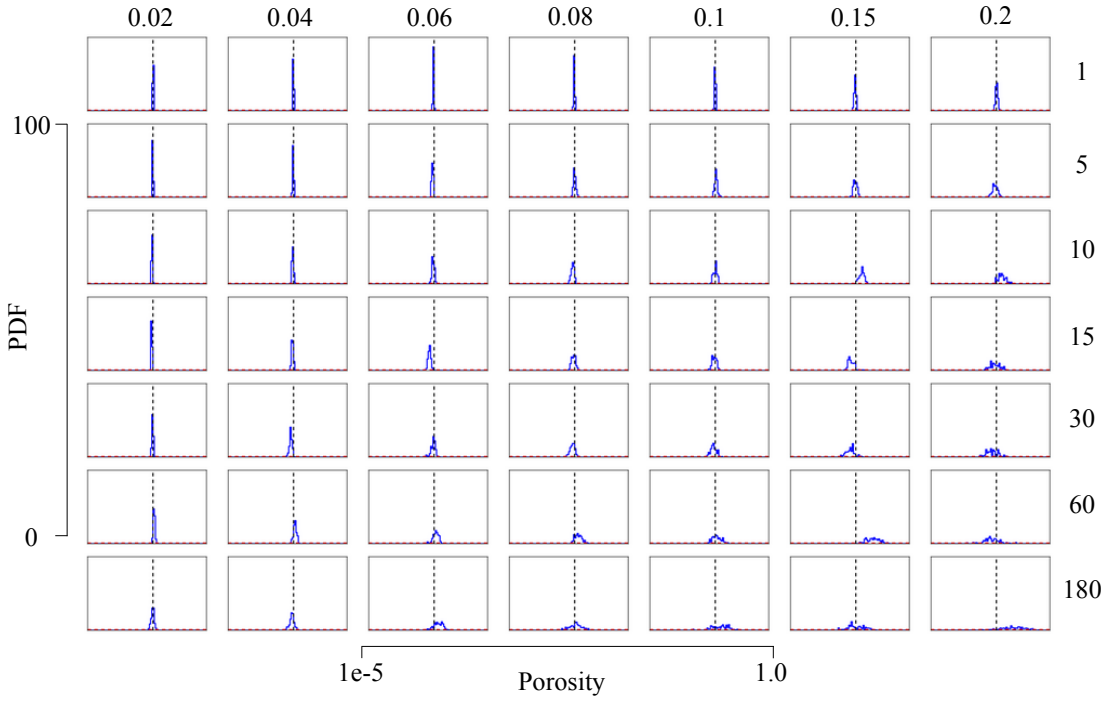

Figure 7.1: Posterior distributions for the porosity parameter using volumetric soil moisture observations for each observational characteristic. The axes are the same for all histograms, and are shown at the bottom and left hand side of the figure. The red line shows the prior distribution and the blue, the posterior. The vertical black dashed line shows the true value. The histogram plots are arranged with increasing observation uncertainty along the columns and increasing temporal sampling interval down the rows. The magnitude of the observation uncertainty is given in the top row, and the temporal sampling interval is given in the right-hand column.

	0.02	**0.04**	**0.06**	**0.08**	**0.1**	**0.15**	**0.2**
1	99.6	99.2	98.7	98.4	98.0	96.8	96.4
5	98.9	98.0	97.2	95.6	94.5	93.1	90.3
10	98.6	97.2	95.7	94.6	94.1	91.1	86.6
15	98.4	96.8	94.8	92.9	92.3	88.8	83.3
30	97.6	95.0	91.3	91.3	89.7	84.1	79.2
60	97.0	94.3	89.4	88.4	86.1	78.1	66.9
180	95.0	91.9	85.7	79.2	67.2	71.1	54.3

Table 7.3: Reduction in uncertainty (%) between the prior and posterior distributions (95% confidence interval) for the porosity parameter, for each observational characteristic. (Prior 95% C.I.: 0.95). The magnitude of the observation uncertainty is listed in the top headings of the table, and the temporal sampling interval is listed in the headings in the left-hand column.

algorithm. This is likely due to the fact that when adding random error to the default model output in the OSSE the added noise realisation, especially for low temporal sampling interval, results in the observations being biased when compared to the default/true model output (e.g. Figure 7.5).

	0.02	**0.04**	**0.06**	**0.08**	**0.1**	**0.15**	**0.2**
1	0.001	-0.000	-0.004	0.001	-0.001	0.007	0.016
5	-0.002	-0.002	-0.013	0.022	0.004	-0.015	-0.022
10	-0.010	-0.017	0.009	-0.001	0.007	0.071	0.028
15	-0.009	-0.014	-0.033	0.005	-0.026	-0.063	-0.042
30	-0.013	-0.030	-0.062	0.009	-0.010	-0.121	-0.040
60	0.005	0.010	0.050	0.067	-0.043	0.075	-0.060
180	0.005	-0.012	0.020	-0.014	0.096	-0.033	0.136

Table 7.4: The bias between the mode of the porosity posterior distribution and the true parameter value for each observational characteristic.

Relative drying rate (rdr) parameter PPDF

The relative drying rate (rdr) parameters a and b are not well constrained in the Bayesian inversion except for the {1/0.02,0.04} and {5/0.02} observations (Figure 7.2 and Figure 7.3). For all the other observational characteristics the posterior is not well constrained and is similar to the prior PDF. The percentage reduction in 95% confidence interval confirms this result (Table 7.5 and Table 7.6). Both rdr parameters are less well constrained with observations every 5 days but the reduction in uncertainty is still >50%.

Therefore a very small bias (-0.006) between the MAP and the true value is only apparent for the {1/<=0.08} observations for the rdr_a parameter (Table 7.7). Interestingly, although resulting in a less well constrained posterior PDF, the {5/0.02} observations result in a smaller bias between the rdr_b true value and the MAP compared to the {1/0.04} observations (Table 7.8. If the parameter is not well constrained a bias between the truth and the mode is not meaningful as many values have a similar frequency with the mode happening to have a slightly higher frequency. Hence a random pattern in the value of the bias for all observations which do not help in constraining the parameters would be expected and that is observed for both rdr parameters.

	0.02	**0.04**	**0.06**	**0.08**	**0.1**	**0.15**	**0.2**
1	98.3	97.9	13.0	4.52	0.55	4.50	-0.05
5	69.1	-1.46	-2.11	9.87	-0.52	1.86	4.01
10	-1.04	6.48	3.93	5.30	14.54	2.98	2.30
15	0.08	-1.52	6.64	3.27	11.9	14.3	2.72
30	1.70	-0.90	13.3	6.03	6.86	4.47	13.9
60	-0.01	11.8	2.46	-0.47	-0.27	1.21	5.87
180	8.56	2.54	1.85	1.22	-1.18	-0.54	-1.44

Table 7.5: Reduction in uncertainty (%) between the prior and posterior distributions (95% confidence interval) for the relative drying rate (a) parameter, for each observational characteristic. (Prior 95% C.I.: 1.178).

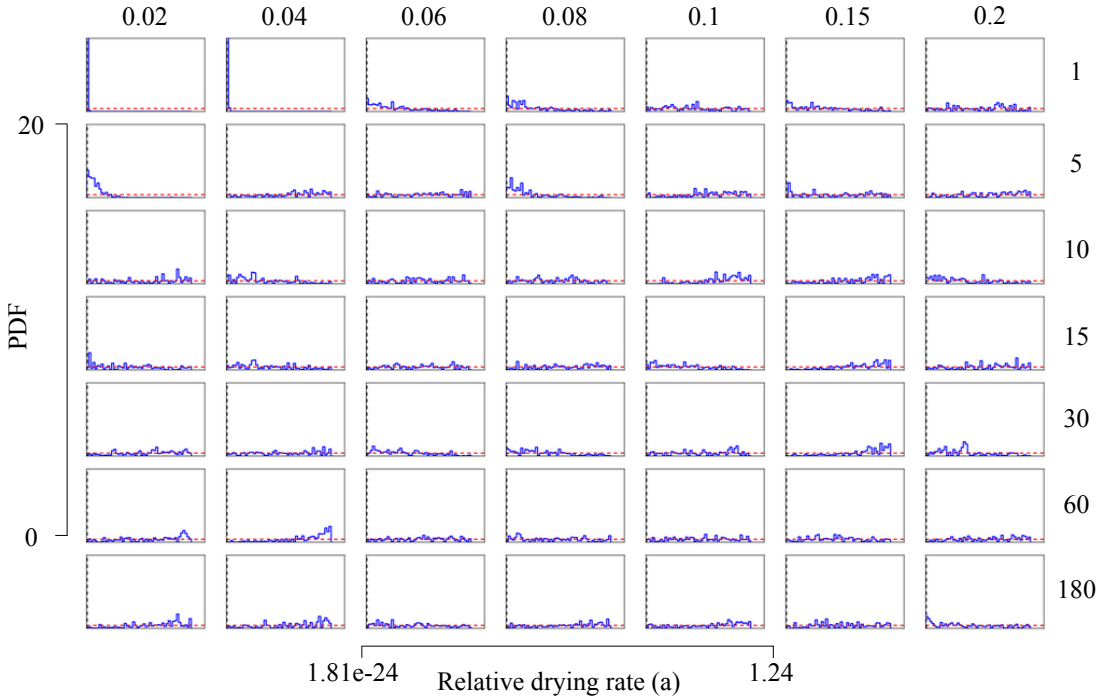

Figure 7.2: Posterior distributions for the relative drying rate (a) parameter using volumetric soil moisture observations for each observational characteristic.

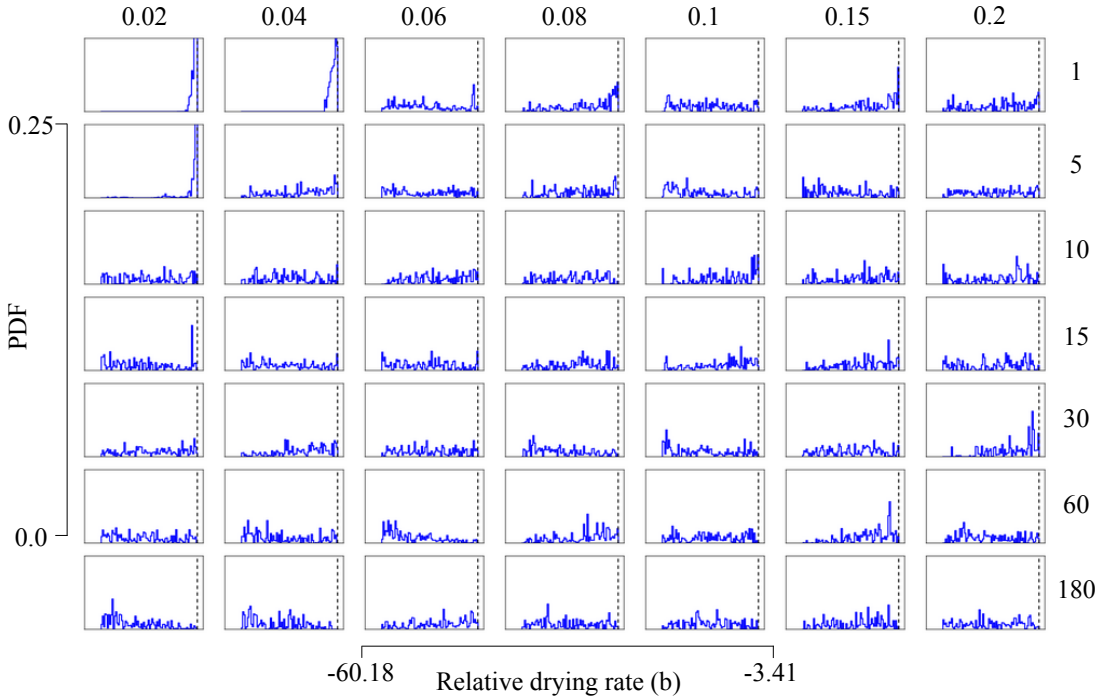

Figure 7.3: Posterior distributions for the relative drying rate (b) parameter using volumetric soil moisture observations for each observational characteristic.

	0.02	0.04	0.06	0.08	0.1	0.15	0.2
1	91.5	86.9	2.79	4.18	1.41	0.44	1.12
5	57.2	5.24	0.25	3.37	-0.90	-2.93	1.66
10	-1.87	-1.70	7.09	8.70	-3.96	1.35	-2.08
15	-0.55	-3.42	-3.89	3.55	1.33	2.05	2.68
30	0.55	0.61	2.08	3.00	0.16	-1.03	10.3
60	0.65	0.25	6.63	4.16	1.91	15.6	3.05
180	4.36	4.71	1.36	1.24	6.03	3.83	1.75

Table 7.6: Reduction in uncertainty (%) between the prior and posterior distributions (95% confidence interval) for the relative drying rate (b) parameter, for each observational characteristic. (Prior 95% C.I.: 53.9315).

	0.02	0.04	0.06	0.08	0.1	0.15	0.2
1	-0.006	-0.007	0.016	-0.005	0.606	0.027	0.255
5	0.091	0.469	1.22	0.045	1.14	0.030	0.556
10	0.898	0.042	0.475	0.130	0.817	1.19	0.107
15	0.020	0.297	0.181	0.120	0.105	0.762	1.07
30	0.797	1.03	0.138	0.364	1.07	1.11	0.475
60	1.13	1.18	0.265	0.150	1.20	0.259	1.23
180	1.08	1.06	0.310	0.864	0.062	0.094	0.056

Table 7.7: The bias between the mode of the relative drying rate (a) posterior distribution and the true parameter value for each observational characteristic.

	0.02	0.04	0.06	0.08	0.1	0.15	0.2
1	-0.357	-4.03	-3.02	-5.03	-53.8	0.044	-14.9
5	0.019	-0.042	-17.3	-1.62	-42.1	-19.2	-47.3
10	-19.2	-47.5	-4.6	-12.0	-3.86	-19.9	-56.0
15	-3.28	-44.3	0.053	-2.30	-14.2	-5.9	-55.1
30	-8.53	-1.97	-29.9	-50.1	-54.2	-29.1	-3.51
60	-55.7	-48.0	-53.0	-12.4	-50.4	-5.8	-8.24
180	-50.0	-51.8	-3.45	-43.2	-36.0	-10.1	-29.6

Table 7.8: The bias between the mode of the relative drying rate (b) posterior distribution and the true parameter value for each observational characteristic.

Parameter correlation

The correlation coefficient between parameters can only be well characterised when the parameters are retrieved successfully. Therefore for this set of observational characteristics it is only possible to determine any correlation coefficients between the porosity and relative drying rate parameters for the {1/0.04} and {5/0.02} observations. The highest correlations are observed between the two relative drying rate parameters with a value of 0.46 for when the parameters are constrained by the {1/0.02} observations and 0.52 using {1/0.04} observations (Table 7.9). No apparent correlation between the two parameters is found when the parameters were constrained with the {5/0.02} observations, despite the fact that both parameters were constrained well with a reduction in uncertainty of >50%. The reduction was lower than for the daily observations however and this might explain the lack of correlation. All other observational characteristics have low correlation coefficients (0.0 to ±~0.21). Overall there is no correlation between the porosity and either of the relative drying rate parameters, even when the parameters are constrained using the "best-case scenario" observational characteristics with the highest temporal sampling interval and lowest error.

	0.02	**0.04**	**0.06**	**0.08**	**0.1**	**0.15**	**0.2**
1	0.46	0.52	-0.15	-0.08	-0.08	-0.10	-0.25
5	-0.09	0.00	-0.13	-0.09	0.04	-0.06	0.22
10	0.00	-0.05	-0.05	0.05	-0.25	0.05	0.33
15	-0.21	-0.13	-0.15	0.08	0.10	-0.04	-0.07
30	-0.03	-0.08	-0.17	0.02	-0.00	0.05	-0.10
60	-0.09	-0.09	0.03	-0.11	-0.15	-0.03	0.22
180	-0.11	-0.04	-0.12	-0.19	0.28	-0.12	0.04

Table 7.9: Correlations between the RDRA and RDRB parameters using synthetic soil vwc observations from 2009 with different observational characteristics and no underestimation of observational error.

Volumetric soil moisture forward mode and model predictive uncertainty

Figure 7.4(a) shows the posterior predictive uncertainty, relative to the prior, for a case where the porosity, rdr_a and rdr_b parameters are all well constrained (for the {1/0.04} observations. As a result the posterior 95% confidence interval is extremely narrow and indistinguishable in this figure. Figure 7.4(b) shows the mode and posterior predictive uncertainty for a case where the porosity is well-constrained but the rdr_a and rdr_b parameter reduction in 95% confidence interval is lower, around 50-60% (for the {5/0.02} observations). The posterior mode is the same as the true value for the maximum soil moisture and approximates the true value reasonably well when the volumetric soil moisture is less than the maximum value. Here the posterior 95% confidence interval is slightly less well-constrained but is still very narrow compared to the prior.

Figure 7.4(c) shows the model and posterior 95% C.I. when the porosity is well-constrained but the rdr parameters' PPDF is not (i.e. the posterior approximates the prior). The PPDF of the rdr parmeters contains a nigher number of values in the parameter range to which the volumetric water content is insensitive, therefore the forward modelled soil moisture is much less variable

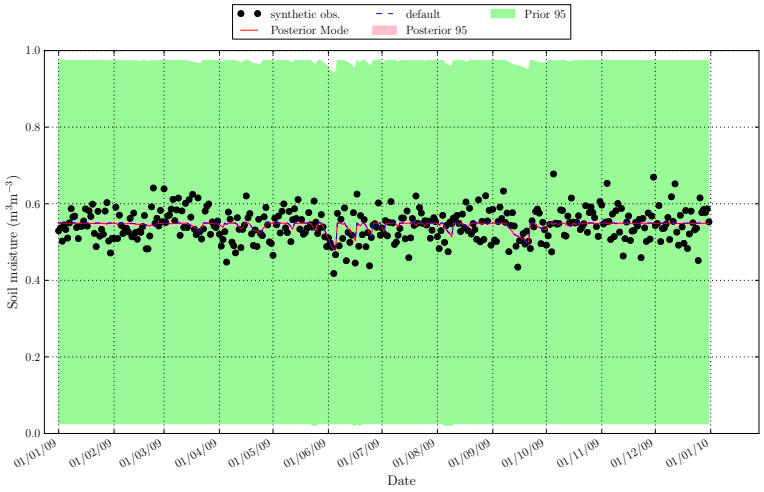

(a) *Synthetic {1/0.04} volumetric soil moisture observations.*

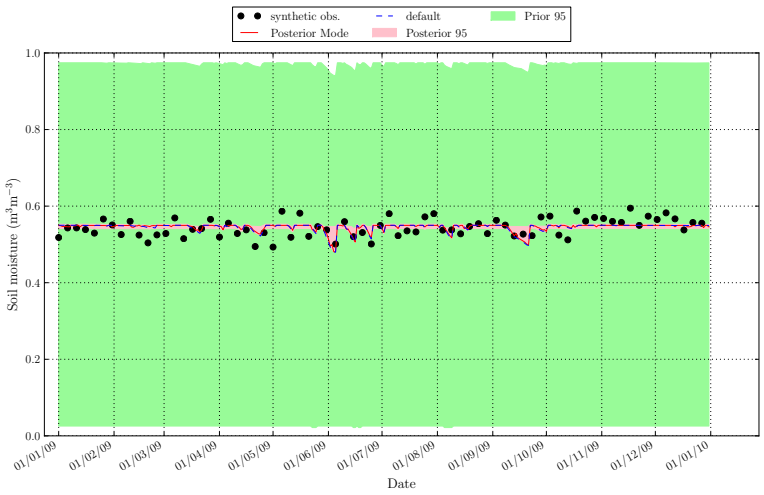

(b) *Synthetic {5/0.02} volumetric soil moisture observations.*

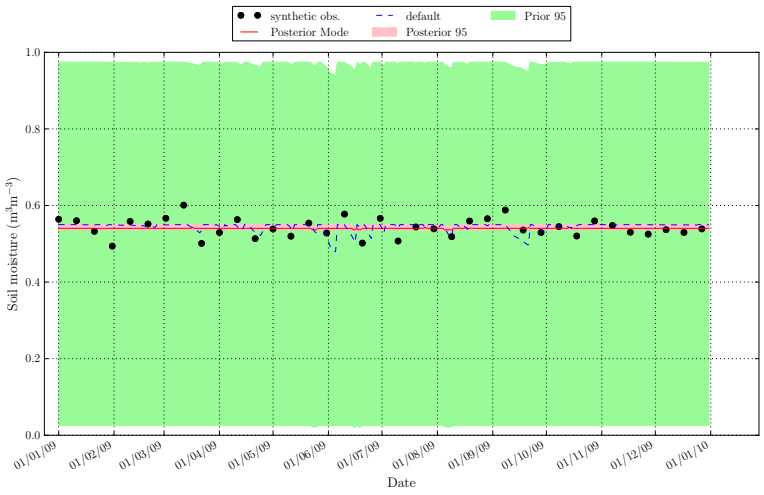

(c) *Synthetic {10/0.02} volumetric soil moisture observations.*

Figure 7.4: The volumetric soil moisture from an ensemble of 500 forward model runs using the posterior parameter distributions from Bayesian inversion using synthetic volumetric soil moisture observations. The green area shows the prior 95% confidence interval of the CH_4 flux using 3000 random samples from the joint prior distribution of the parameters that are being calibrated in this OSSE experiment. The pink area is the posterior 95% confidence interval and the red line is the forward mode. These results are compared to the model run with the true set of parameters, which is denoted by the blue dashed line.

than the truth and the posterior uncertainty is narrow and doesn't encompass the lowest true soil moisture values.

As the porosity parameter is less well-constrained with increasing uncertainty and decreasing temporal sampling interval, the posterior 95% confidence interval of the volumetric soil moisture itself becomes less well-constrained. Where there is a significant positive or negative bias between the truth and the mode of the porosity posterior (e.g. Figure 7.1) the soil moisture is also systematically over- or underestimated, for example with observations every 60 days with an uncertainty of $0.15 m^3 m^{-3}$ which result in a positive bias between the mode and the true porosity value (Figure 7.5).

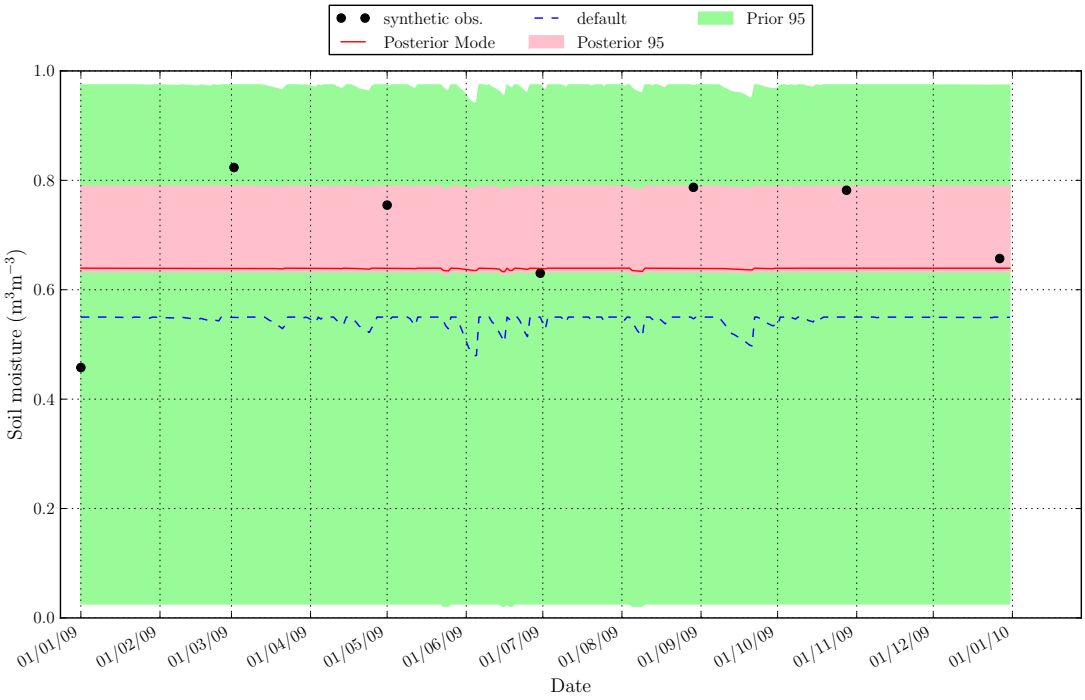

Figure 7.5: The volumetric soil moisture from an ensemble of 500 forward model runs using the posterior parameter distributions constrained with synthetic volumetric soil moisture observations every 60 days with added random Gaussian noise of 0.15 $m^3 m^{-3}$ and no underestimate of observational error. The results are compared to the 'true' model run with the default parameter values and the prior 95% confidence interval.

Figure 7.6 shows the root mean squared difference between the volumetric soil moisture forward model mode and the true value. The RMSD ranges from 0.0 to 0.084, which is up to ~15% of the mean of the true soil moisture. The RMSD increases gradually with both increasing uncertainty and decreasing temporal sampling interval, with a sharper increase in RMSD towards a temporal frequency of 60 days and around an uncertainty of $0.15 m^3 m^{-3}$ (due to the relatively high positive bias in the porosity MAP value).

CH_4 flux forward mode and model predictive uncertainty

This section examines the ability of the volumetric soil moisture observations to improve the CH_4 flux predictions and uncertainty. When comparing the CH_4 net flux forward model runs with the same set of observational characteristics as the volumetric soil moisture, similar patterns emerge. The {1/0.04} observations result in a relatively tightly constrained forward model mode which

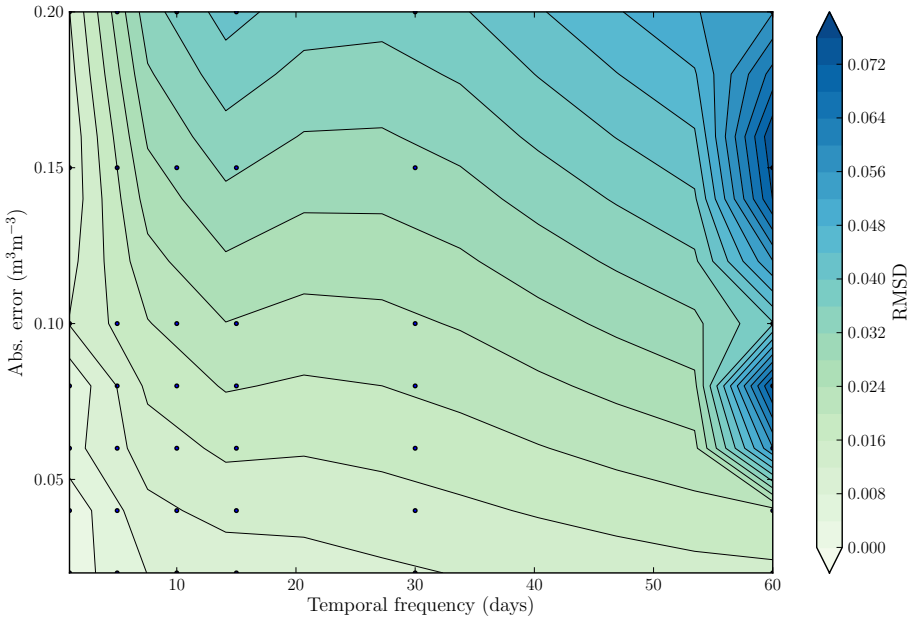

Figure 7.6: Plot to show the root mean squared difference between the MAP of the forward modelled volumetric soil moisture and the true daily values for the different observational characteristics.

corresponds to the true daily variability of CH_4 very well (Figure 7.7(a)). However the true value appears to fall outside of the 95% confidence interval of the prior at certain times of the year, notably when the volumetric soil moisture is lower (corresponding to peaks in CH_4 flux).

Figure 7.7(b) shows the case where the rdr parameters are less well constrained ({5/0.02} observations). The posterior 95% confidence interval is greater and the forward model mode doesn't follow the true flux as well, though the uncertainty in the forward model runs always encompasses the true flux.

Figure 7.17(a) shows forward model runs when the parameters were constrained with the {10/0.02} observations. In this case the rdr parameters were not well constrained by the MH-MCMC run. Although the true CH_4 flux is estimated well at times when the soil moisture is at its maximum value, as the porosity is well-constrained, the peak true flux is often underestimated.

The root mean squared difference between the forward model mode and the true value ranges from 0.00025 to 0.005$gCm^{-3}d^{-1}$, for all observational characteristics (Fig 7.8, which corresponds to 0.4 to 7.8% of the true mean daily CH_4 flux. This is an order of magnitude lower than the RMSD between the daily forward modal CH_4 flux and the true value in the OSSEs using both CH_4 flux and NEP flux observations.

The forward CH_4 ensemble is unable to model the peaks in CH_4 flux correctly, and as the lower values of flux are generally slightly underestimated as well this will have an impact on the annual flux, as seen in Figure 7.9. Only for the{1,5/<=0.02} observations does the true value lie close to the mode of the posterior annual CH_4 flux.

For all other observational characteristics although the posterior is well constrained (Table 7.10), the true annual flux value is underestimated by the posterior mode. The forward model mode - truth bias shows most observational characteristics result in parameter constraints which underestimate the true flux by ~-0.8$gCm^{-2}y^{-1}$ (Table 7.11). This bias is about 3.5% of the true value.

	0.02	**0.04**	**0.06**	**0.08**	**0.1**	**0.15**	**0.2**
1	82.4	80.6	78.3	79.3	73.6	82.4	82.2
5	74.4	82.0	79.1	82.3	75.8	80.1	73.1
10	77.8	80.6	81.8	82.0	82.0	82.0	82.0
15	73.5	72.3	80.6	76.0	82.0	82.1	71.6
30	82.2	80.3	72.0	71.9	81.2	53.4	82.0
60	74.0	73.2	79.6	81.5	81.5	78.9	81.7
180	67.0	72.0	81.3	76.6	81.8	81.2	78.2

Table 7.10: Reduction in uncertainty (%) between the prior and posterior distributions (95% confidence interval) for the annual CH_4 flux, for each observational characteristic. (Prior 95% C.I.: 6.24295).

The high reduction in annual flux uncertainty is mostly due to the constraint of the porosity parameter. These results highlight that it may be possible to reduce the annual model uncertainty but the daily model output can still be wrong (i.e. here the peak flux is underestimated) if the forward ensemble samples parameters to which the CH_4 flux is insensitive. The prior can constrain the parameters so only the regions of the parameter space to which the CH_4 flux is sensitive are sampled in the Bayesian inversion. The choice of prior is crucial. There is a systematic bias for most observational characteristics due to the inability of the observations to constrain the rdr

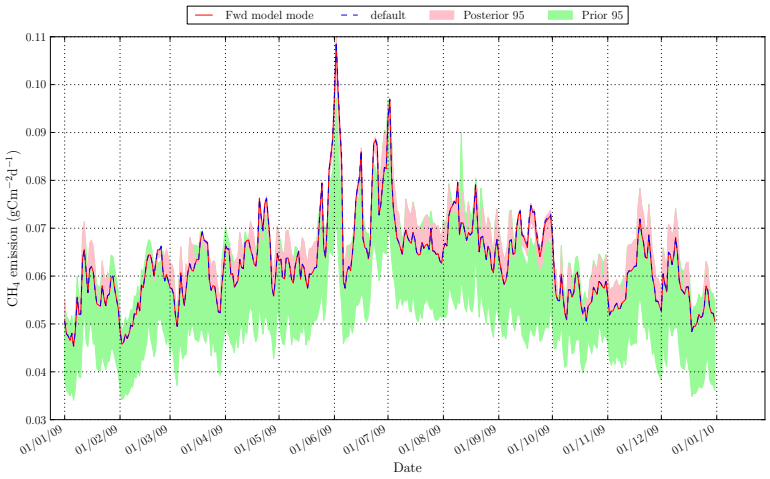

(a) *Synthetic {1/0.04} volumetric soil moisture observations.*

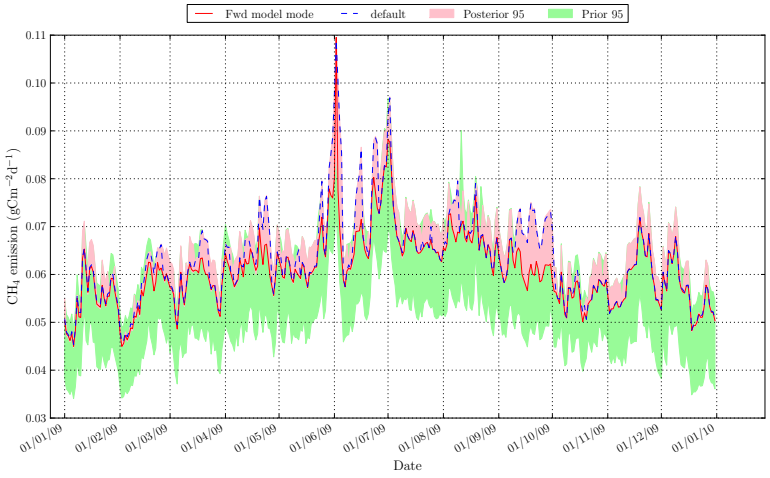

(b) *Synthetic {5/0.02} volumetric soil moisture observations.*

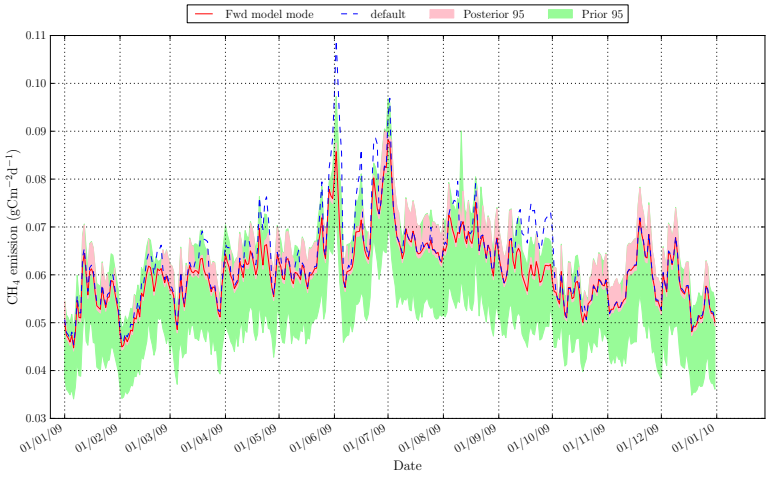

(c) *Synthetic {10/0.02} volumetric soil moisture observations.*

Figure 7.7: The CH_4 net flux from an ensemble of 500 forward model runs using the posterior parameter distributions from Bayesian inversion using synthetic volumetric soil moisture observations.

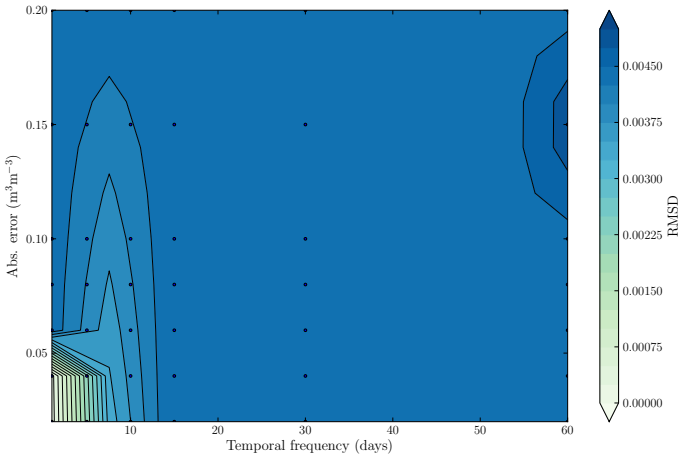

Figure 7.8: Plot to show the root mean squared difference between the MAP of the forward modelled CH_4 flux and the true daily values for the different observational characteristics.

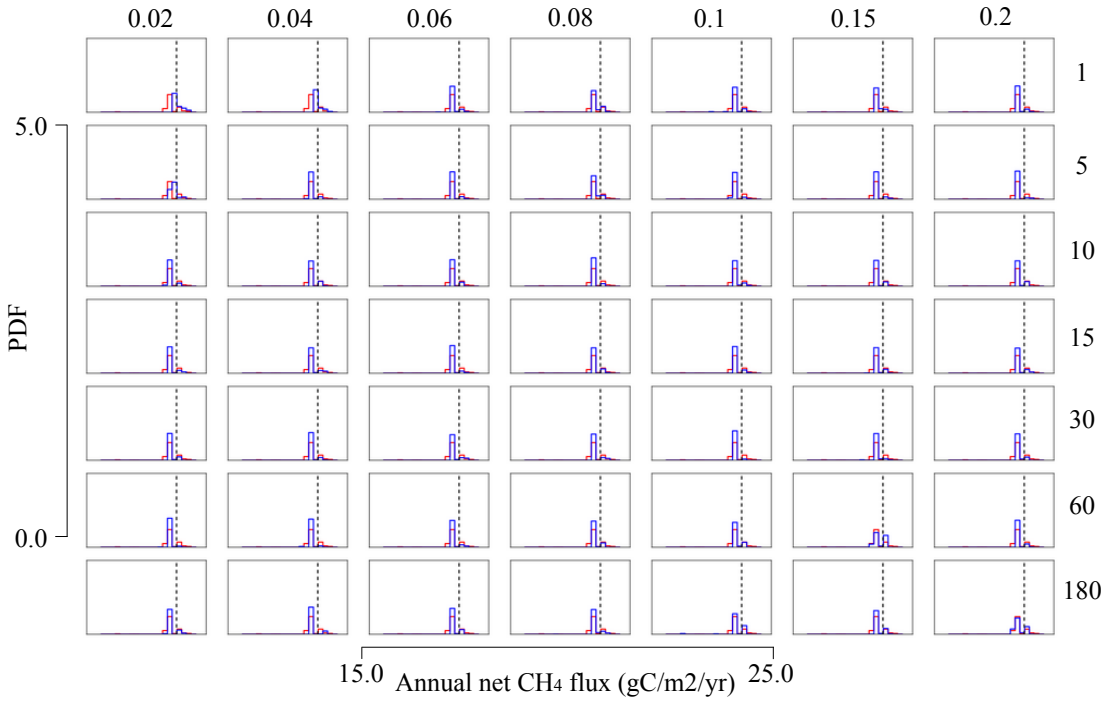

Figure 7.9: Posterior distributions for the annual CH_4 flux using volumetric soil moisture observations for each observational characteristic.

	0.02	0.04	0.06	0.08	0.1	0.15	0.2
1	0.839	-0.003	-0.445	-0.242	-0.834	-0.265	-0.690
5	-0.321	-0.583	-0.798	-0.800	-0.807	-0.807	-0.802
10	-0.816	0.342	-0.752	-0.799	-0.161	-0.831	-0.811
15	-0.515	-0.802	-0.792	0.295	-0.832	-0.794	0.934
30	-0.506	-0.752	-0.797	-0.802	-0.809	-0.814	-0.785
60	-0.808	-0.805	-0.820	-0.865	-0.801	-0.809	-0.812
180	-0.692	0.923	-0.758	-0.794	0.239	-0.818	-0.929

Table 7.11: The bias between the mode of the annual CH_4 flux posterior distribution and the true annual flux value for each observational characteristic.

parameter, even when the porosity parameter, which the CH_4 flux is more sensitive to, is well-constrained.

NEP forward model and model predictive uncertainty

Similar patterns are seen for the NEP flux in terms of which observational characteristics accurately approximate the true value and result in a reduction in 95% confidence interval. The true value is also outside the prior 95% confidence interval for peaks in NEP flux.

The true NEP flux is significantly underestimated (more so than the CH_4 flux) by the forward model mode in the summer months for observations which do not result in a reduction in the prior 95% confidence interval of the rdr parameters (e.g. Figure 7.10).

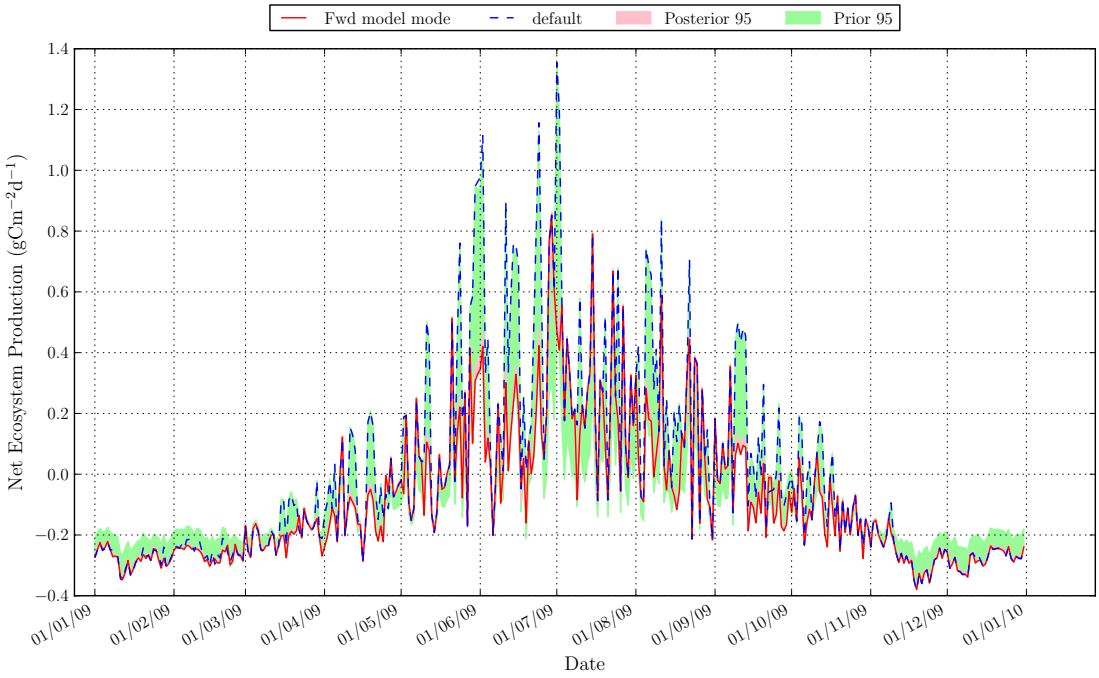

Figure 7.10: The NEP flux from an ensemble of 500 forward model runs using the posterior parameter distributions from a MH-MCMC run, for two sets of synthetic volumetric soil moisture observations with different observational characteristics and no underestimate of observational error. The results are compared to the 'true' model run with the default parameter values and the prior 95% confidence interval.

The signficant underestimation of the true NEP flux in the summer months with due to the poorly constrained rdr parameters is evident in the RMSD between the forward model mode and the true NEP flux as seen in Figure 7.11. The RMSD can be as high as 0.19gCm^{-2}d^{-1} which is quite high given the annual true mean is close to zero (-0.0046gCm^{-2}d^{-1}). This is mainly due to the negative bias of the forward model mode in the summer months. The maximum bias for the NEP flux is lower than for the OSSEs with CH_4 and NEP flux observations, but as discussed in the section on CH_4 flux this is to be expected given only a few parameters are being constrained, with the rest assumed to be known.

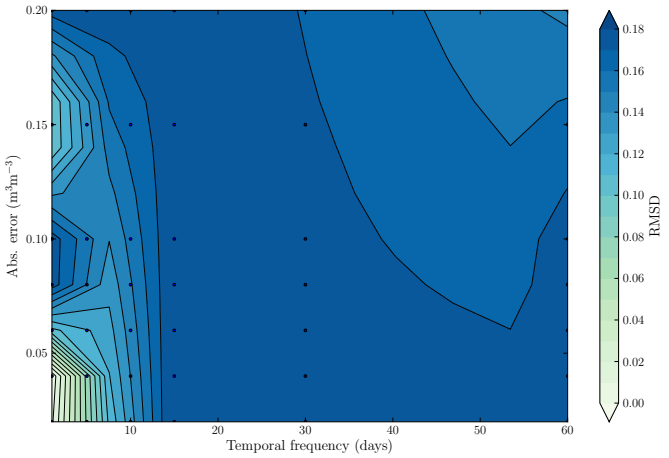

Figure 7.11: Plot to show the root mean squared difference between the MAP of the forward modelled NEP flux and the true daily values for the different observational characteristics.

The significant bias can also be seen in Table 7.12 which shows the bias between the forward model annual NEP flux mode and the true value. This confirms that the rdr parameters are constrolling the bias as the true value is only approximated well (low bias) by the {1/0.0}observations. For all other observational characteristics the true annual flux is not approximated well by the forward model mode and the bias in annual NEP flux is around -28gCm^{-3}yr−1.

	0.02	**0.04**	**0.06**	**0.08**	**0.1**	**0.15**	**0.2**
1	-2.273	0.040	-14.5	-7.00	-27.9	-10.4	-23.9
5	-10.2	-19.1	-27.7	-28.1	-28.0	-28.0	-28.0
10	-28.0	-16.5	-27.9	-28.1	-14.9	-27.9	-28.0
15	-17.3	-28.1	-28.1	-27.0	-27.9	-28.1	-26.4
30	-27.8	-26.6	-28.1	-28.0	-28.0	-28.0	-27.2
60	-28.0	-28.0	-28.0	-27.6	-28.1	-26.1	-28.1
180	-27.8	-26.3	-25.7	-28.1	-26.7	-27.8	-27.3

Table 7.12: The bias between the mode of the annual NEP flux posterior distribution and the true annual flux value for each observational characteristic.

Like the CH_4 flux the annual NEP flux posterior 95% confidence interval is significantly reduced by all observations, despite the negative bias. This reasons for this are discussed for the

CH_4 flux and so are not repeated here. The only exception is for the {5/0.02} observations, which show a very weak reduction in 95% confidence interval of 4.7%. This is because the rdr parameters are partially constrained by these observations, and therefore the true value of flux is better approximated (with a lower bias) but the posterior uncertainty is high.

7.3.2 Discussion

Impact of the joint parameter PPDF on the volumetric soil moisture

As the modelled volumetric soil moisture is very sensitive to the porosity, the posterior predictive uncertainty is heavily reduced by the good constraint of this parameter and the 'true' volumetric soil moisture is accurately determined. Daily narrow 95% C.I. is an example of artificial narrowing of the posterior as a result of the assumption of uncorrelated observations in the likelihood function. In reality daily observations are likely to be correlated and this should be accounted for in the likelihood through an autocorrelation function as in (*Salamon and Feyen*, 2010).

Although the true value is always approximated well by the posterior mode when the volumetric water content is at the maximum value, as it is well-constrained by the porosity, if the rdr parameters are not well constrained the posterior mode fails to fall much below the maximum soil moisture and does not approximate the true value (Figure 7.4(c)). This is because the volumetric soil moisture is only sensitive to a small range around the true value of the rdr parameters and for large part of the rdr parameter range results in only a very slight decrease in volumetric soil moisture (Fig 7.12). The rdr parameters are also important for determining the correct daily variability. The result suggest that below (above) a certain value the rdr_a (rdr_b) parameters completely restrict the daily varaibility in soil moisture and above (below) this value the the volumetric soil moisture is completely insensitive to changes in both parameters. This is confirmed by a "one-at-a-time" sensitivity analsysis of the rdr parameters (Figure 7.12(a) and Figure 7.12(b)). In addition to the restriction of daily variability, if forward model runs sample parameter values from the insensitive regions of the rdr parameters then the posterior predictive uncertainty will be very constrained as the model output won't change with changing parameter value. This suggests the prior should be better constrained if possible with ancilliary information or previous calibration studies. If the rdr parameters were well constrained by the priors, the soil moisture is therefore a function of the porosity.

Impact of the joint parameter PPDF of the CH_4 flux

The true value of CH_4 flux falls outside of the prior because the rdr parameters a and b are at the lower and upper end of their ranges, respectively, and within a small interval where the volumetric soil moisture is highly sensitive to their values. The true value of CH_4 does fall within the maximum value of the prior (Fig 7.13), but not within the 95% confidence interval. However because the majority of the prior parameter space is within the range to which the volumetric soil moisture is insensitive, the prior is biased towards those values of the parameters and the 95% confidence interval of the CH_4 flux is negatively skewed as a result. If the prior was better constrained the truth might lie within this range. It is also the case that the sensitivity of the volumetric soil moisture, and therefore the uncertainty of the posterior CH_4 flux, to the rdr parameters increases when

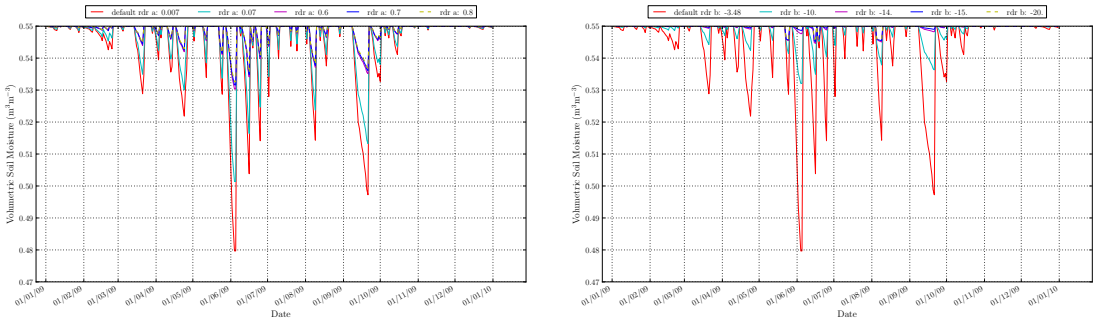

(a) *rdr_a: The original parameter maximum was 1.24 but the graph shows above ~0.7 the model is insensitive to changes in the parameter value.*

(b) *rdr_b: The original parameter minimum was -60.18 but the graph shows below ~-15 the model is insensitive to changes in the parameter value.*

Figure 7.12: "One-at-a-time" sensitivity analyses of the volumetric soil moisture to the rdr parameters

the volumetric soil moisture is lower than the maximum value (i.e. the porosity).

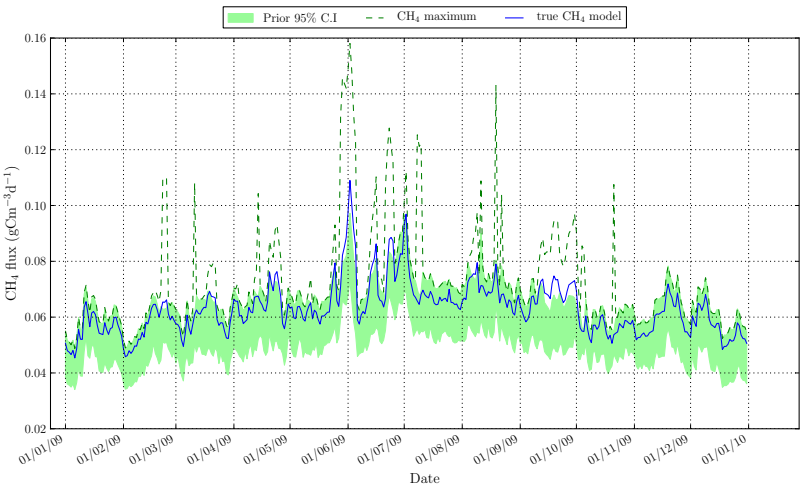

Figure 7.13: Plot to show that although the CH_4 flux peaks are sometimes above the upper limit of the 95% confidence interval they do in fact lie comfortably within the maximum range of CH_4 values.

The true CH_4 flux is often underestimated. This is because the volumetric soil moisture doesn't dip below the maximum value, unlike the true soil moisture, because the rdr parameters are not well-constrained (as previously discussed). As the random parameter values in the forward model runs are taken from the range to which the CH_4 flux is insensitive this also leads to a small posterior 95% confidence interval.

Impact of the joint parameter PPDF of the NEP

The NEP flux is much more variable than the soil CO_2 respiration and the CH_4 flux due to the dominant influence of the NPP flux on the temporal variability. NPP is more variable as it is dependent in part upon atmospheric variables such as solar radiation and temperature. It is also scaled by a moisture-related variable which is heavily dependent upon the estimated evapotranspiration (EET). The EET is a function of the relative drying rate parameters, as well as the overall

volumetric soil moisture. When the rdr_a and b parameters are sampled increasingly towards the upper and lower end of their ranges respectively the EET is very small (thus resulting in the lack of decrease in soil moisture from the maximum value). This has a results in a much decreased NPP flux and therefore the true NEP flux is significantly underestimated (more so than the CH_4 flux) by the forward model mode in the summer months when EET is an important factor in the hydrological balance of the model (e.g. FIgure 7.10).

Significance of the RMSD between the forward mode and true C fluxes

The RMSD between the CH_4 foward mode and the true flux is order or magnitude lower than between when CH_4 observations were used. This is to be expected as the volumetric soil moisture observations are only used to constrain the parameters involved in the soil moisture calculations. These are not the most important in terms of CH_4 flux sensitivity. The other parameters are assumed to be known in this experiment. Nevertheless the possible error in the daily flux is significant just for the case when the rdr parameters are poorly constrained, which were not thought to be that important from the sensitivity analysis. As the CH_4 fluxes are so small it is important to get an accurate estimate of the true flux, especially given its high greenhouse warming potential.

Significance of the bias in the annual net C flux MAP estimates

The annual net CH_4 flux MAP estimate, which is 3.5% of the true value is the result of poor constraint of the rdr parameters which were thought to be unimportant from the results of the sensitivity analysis. However this is due to a very wide prior PDF for the rdr parameters. The high reduction in annual CH_4 flux uncertainty is mostly due to the constraint of the porosity parameter. These results highlight that it may be possible to reduce the annual model uncertainty but the daily model output can still be wrong (i.e. here the peak flux is underestimated) if the forward ensemble samples parameters to which the CH_4 flux is insensitive. The choice of prior is crucial. There is a systematic bias for most observational characteristics due to the inability of the observations to constrain the rdr parameter, even when the porosity parameter, which the CH_4 flux is more sensitive to, is well-constrained.

The bias in the annual NEP MAP estimate for most observations would result in a more significant sink in CO_2 for this ecosystem than the true value. Whilst the biases in the MAP estimates are not as extreme as when CH_4 or NEP flux observations are used, this is still important as in peatlands, which contain large stores of soil C, inaccurate model outputs such as this might affect policy and management decisions, and might result in incorrect assumptions being made about the role of soil C in land-surface feedbacks to climate change. This is another example of how poor constraint of parameters that were thought to be relatively unimportant to the C flux, following the results of the sensitivity analysis, have been shown to be very important in calculating the correct peak fluxes.

7.4 Effect of constraining the rdr parameter priors

7.4.1 Introduction and experimental set-up

As shown in Figure 7.12(a) and Figure 7.12(b), and discussed in the previous section, there is a large region of the rdr parameter prior PDF which the model is insensitive to. It was hypothesised that a more constrained prior PDF for the rdr parameters would result in observations with a higher uncertainty or lower temporal sampling interval being able to constrain the rdr parameters, as the increased information in the prior balances the decreased information in the observations. It was also hypothesised that this would result in a wider forward model 95% C.I. as the parameters would be constrained to a region of their parameter space to which the model is more sensitive. Therefore a higher number of random parameter values in the forward model runs would result in a more variable model output.

To test these hypotheses, the OSSE was therefore repeated with a constrained rdr_a and rdr_b uniform prior PDF. The new prior distributions were therefore U(1.81e-24,0.7) for rdr_a and U(-15.0,-3.41) for rdr_b. Above and below these values for the rdr_a and rdr_b parameters respectively there is almost no change in volumetric soil moisture (and therefore C flux) which changing parameter value (Figure 7.12). Apart from the narrower rdr prior distributions, the OSSE set-up was exactly the same as in Section 7.2.

7.4.2 Results

Analysis of the parameter PPDF

The constrained prior resulted in narrowly constrained rdr posterior parameter PDFs, and accurately determined the true values, for a greater number of observational characteristics. (Figure 7.14 and Figure 7.15). The {1/0.06} and {10/0.02} observations, and to some extent the {5/0.04} and {15/0.02} observations were able to better constrain both rdr parameters compared to the original prior.

This set of observational characteristics (apart from the {5/0.04} observations) had higher correlation coefficients between the rdr parameters (though the value was no higher than those found using the original prior), a higher reduction in prior uncertainty, and a lower mode-truth bias).

As predicted this resulted in slightly higher values for the peaks in CH_4 flux for the lower limit of the prior 95% confidence interval (the 2.5% percentile), but not for the upper limit (Figure 7.16). As the upper limit of the 95% confidence interval didn't increase, the true value still lies outside of the prior range at times of peak CH_4 flux. However for those observational characteristics that result in a narrower rdr parameter constraint with the new rdr prior, the forward model CH_4 flux ensemble mode corresponds to the truth much more closely. For example Fig 7.17 shows the CH_4 flux using parameters constrained with the {10/0.02} observations, for the original rdr parameter prior (Figure 7.17(a)) and the constrained prior (Figure 7.17(b)).

The constrained prior also general results in a wider posterior 95% confidence interval because the parameters are being sampled from values to which the model is sensitive. This is highlighted in Figure 7.18, which shows the forward modelled CH_4 flux using parameters constrained with the {60/0.1} observations, with both the original (Figure 7.17(a)) and constrained (Figure 7.17(b))

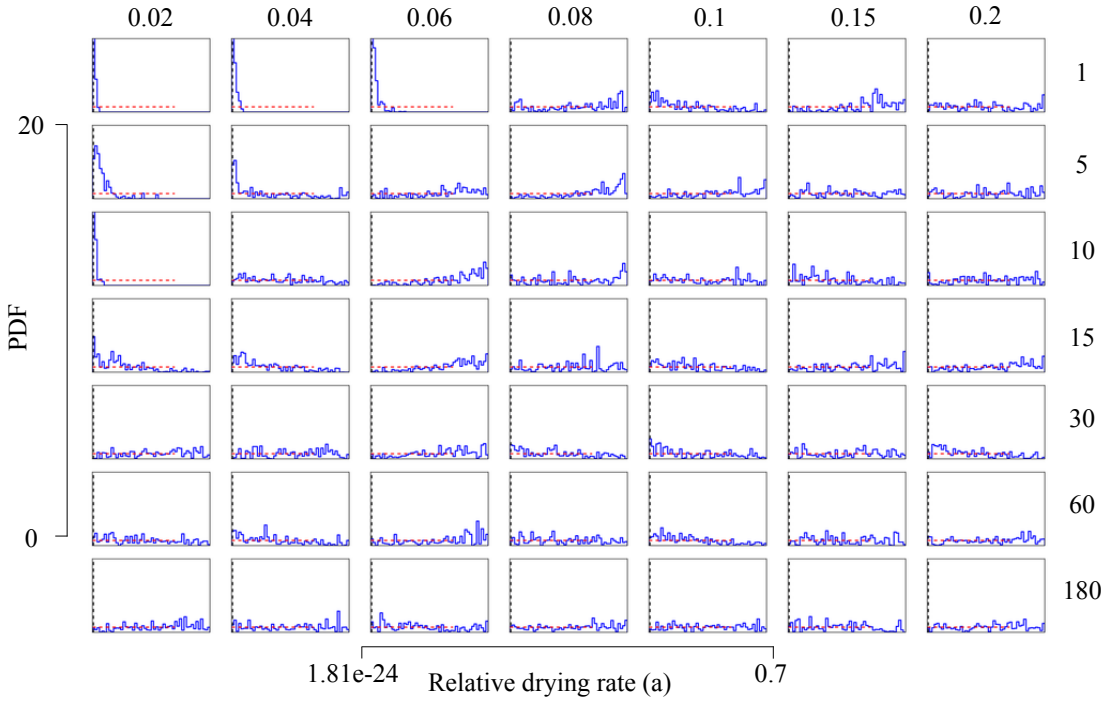

Figure 7.14: Posterior distributions for the relative drying rate (a) parameter using volumetric soil moisture observations for each observational characteristic, with the constrained rdr prior.

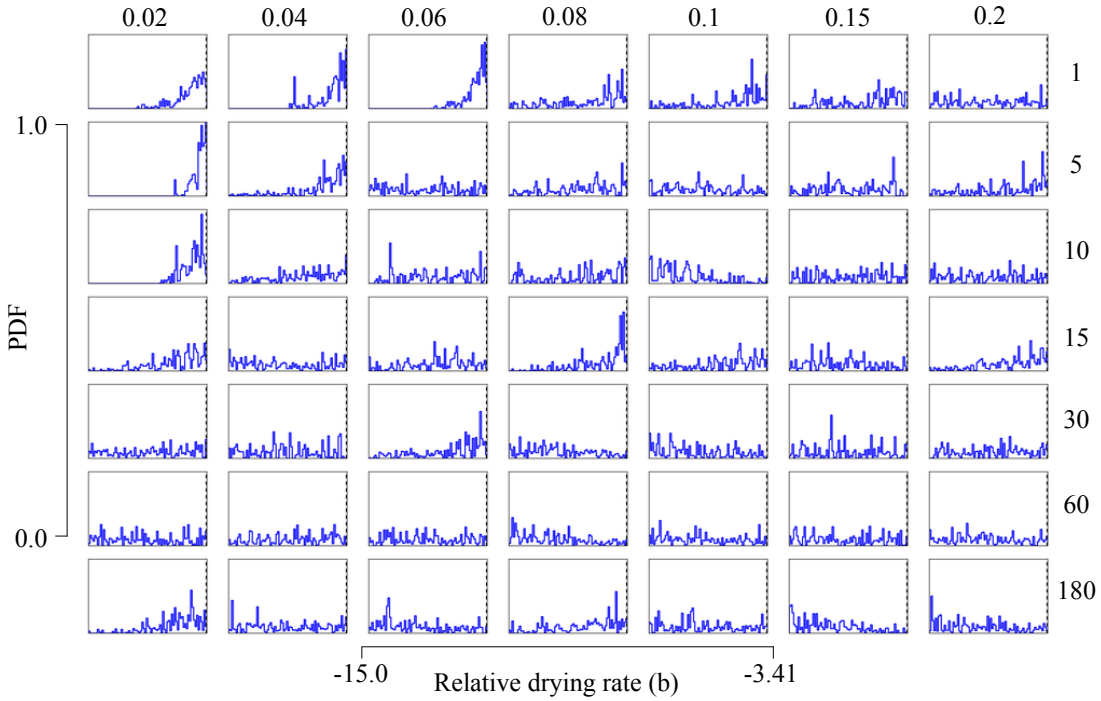

Figure 7.15: Posterior distributions for the relative drying rate (b) parameter using volumetric soil moisture observations for each observational characteristic, with the constrained rdr prior.

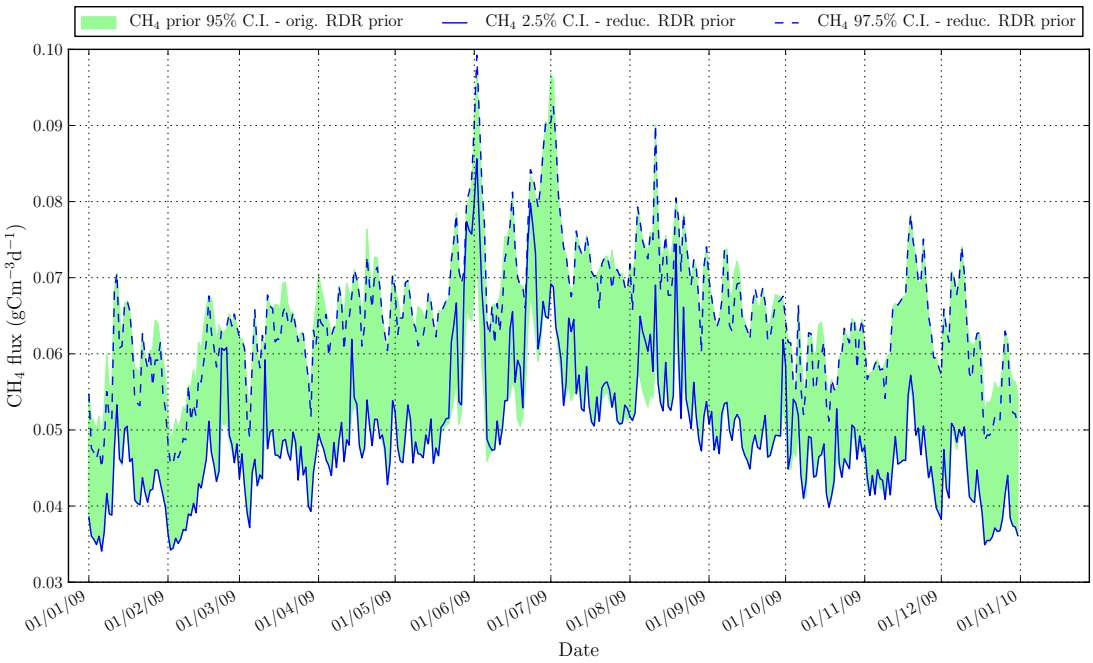

Figure 7.16: A comparison between the CH_4 flux prior 95% confidence intervals using the original and constrained rdr parameter uniform distributions (with all other soil moisture-related parameter prior distributions remaining the same).

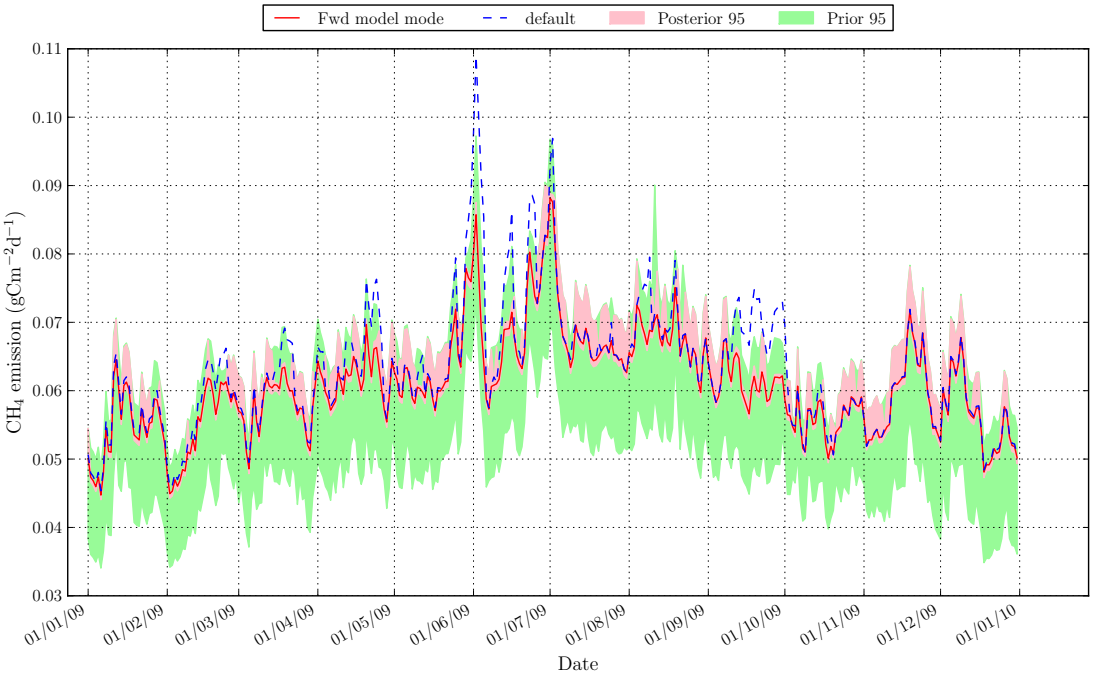

***(a)** Original rdr prior*

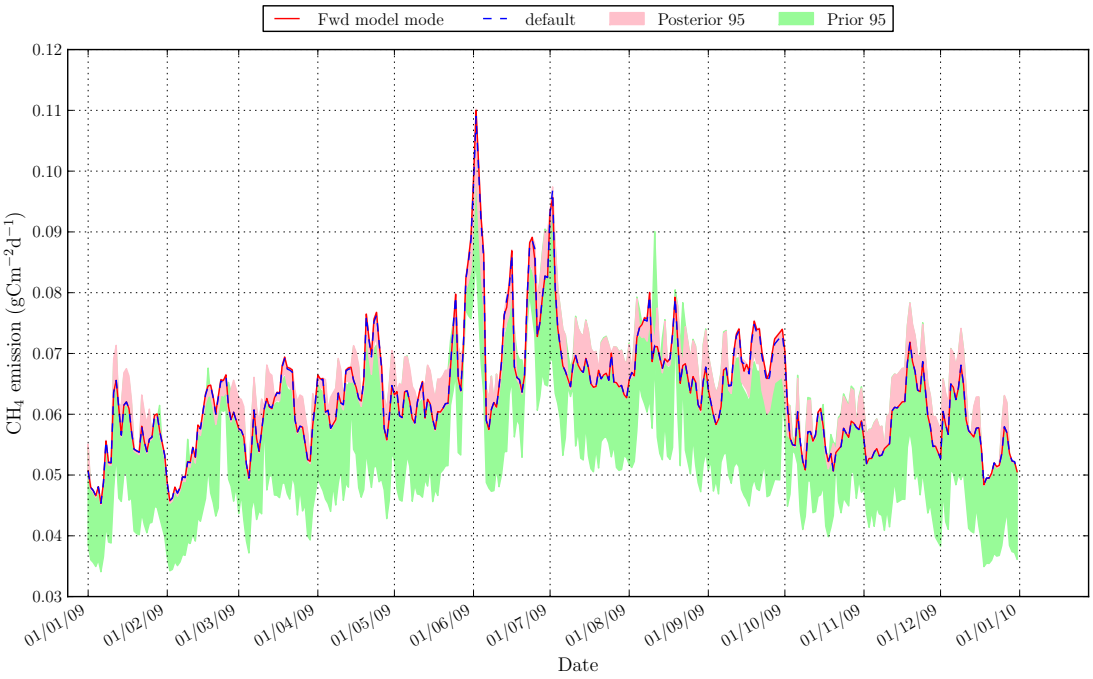

***(b)** Constrained rdr prior.*

Figure 7.17: Comparison of the effect of using the original unconstrained, and the new constrained, rdr priors on CH_4 flux forward models runs, using parameters constrained with observations every 10 days and an associated uncertainty of $0.02 m^3 m^{-3}$.

rdr priors. Neither prior resulted in constrained posterior rdr parameter values, or an accurate approximation to the truth, with this set of observations. However the posterior uncertainty is larger for the constrained rdr priors, as it contains more forward model runs using parameter values that the model *is* sensitive to, and therefore it more accurately represents the uncertainty resulting from inaccurate parameter estimates.

Impact on the forward model mode and predictive uncertainty

For those observational characteristics which result in narrow rdr parameter posterior PDFs using the constrained prior, the forward annual fluxes are also better approximated and the modal value corresponds well to the true value (Figure 7.19). All other observational characteristics which do not constrain the rdr parameter values result in annual fluxes which do not approximate the truth.

There is generally a lower reduction in uncertainty, ~60-80%, compared to ~71-82% with the original rdr prior, (Table 7.13). This is likely due to the more highly constrained rdr priors and/or the increase in posterior uncertainty resulting from a higher number of forward model runs using parameters sampled from the sensitive region of the rdr parameter space. Again there is no systematic pattern to the values, as with the original rdr prior, suggesting a mixture of parameters is responsible for the narrower 95% confidence interval. The relatively high reduction in uncertainty, even for observational characteristics that result in unconstrained posterior rdr parameters for the new rdr prior, suggests that the high reduction in the 95% confidence interval of the porosity parameter is largely responsible.

	0.02	**0.04**	**0.06**	**0.08**	**0.1**	**0.15**	**0.2**
1	73.25	70.26	64.42	72.02	72.67	74.18	74.38
5	67.55	65.24	74.87	73.37	72.72	72.97	67.82
1	70.11	73.66	79.16	73.29	74.57	71.94	74.44
15	66.44	74.71	74.81	72.65	70.40	70.78	71.61
3	74.61	73.73	74.71	74.72	73.57	65.78	74.77
6	63.80	72.99	74.32	74.44	71.73	74.59	71.26
18	79.80	71.15	61.03	70.69	72.63	73.57	71.72

Table 7.13: Reduction in uncertainty (%) between the prior and posterior distributions (95% confidence interval) for the annual CH_4 flux, using the constrained relative drying rate prior, for each observational characteristic. (Prior 95% C.I.: 4.367861).

7.4.3 Effect of constraining the rdr priors - Discussion

This result is a clear demonstration that the choice of prior is crucial, and that a wide and uninformative prior will hamper the ability of the algorithm to constrain parameter values and approximate the true C fluxes and model predictive uncertainty, especially if frequent and very accurate observations are not available. This suggests that any ancillary information or results from previous calibration exercises and a thorough investigation of the prior parameter space, with OAT analyses for example, should be carried out in order to obtain the best estimates of prior parameter ranges.

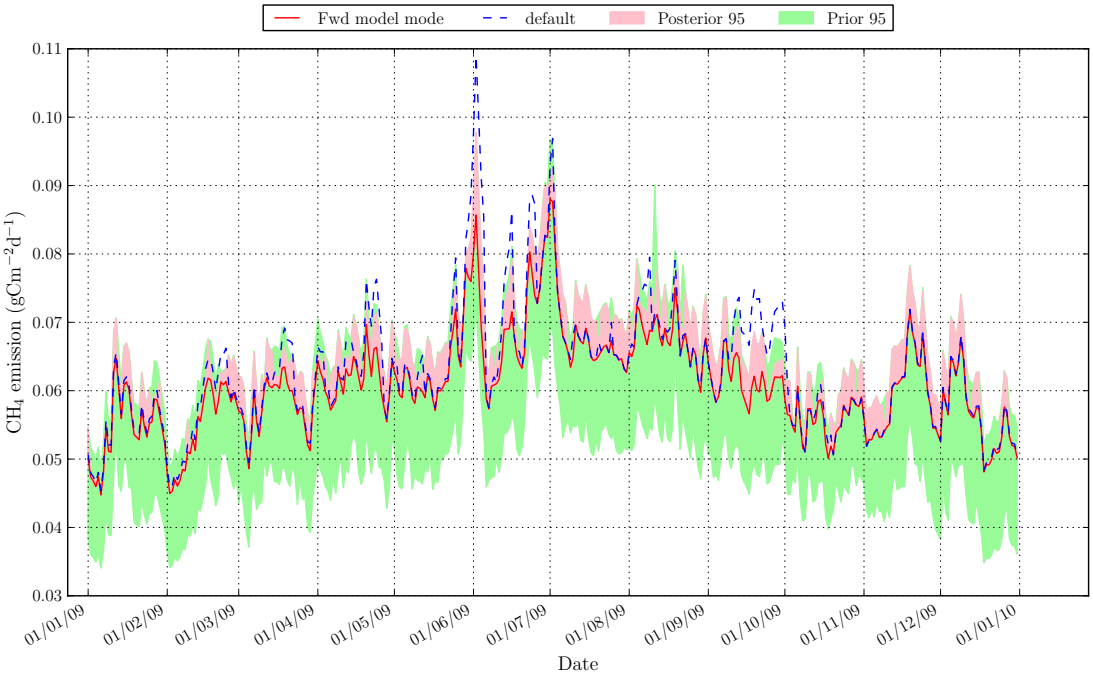

***(a)** Original rdr prior*

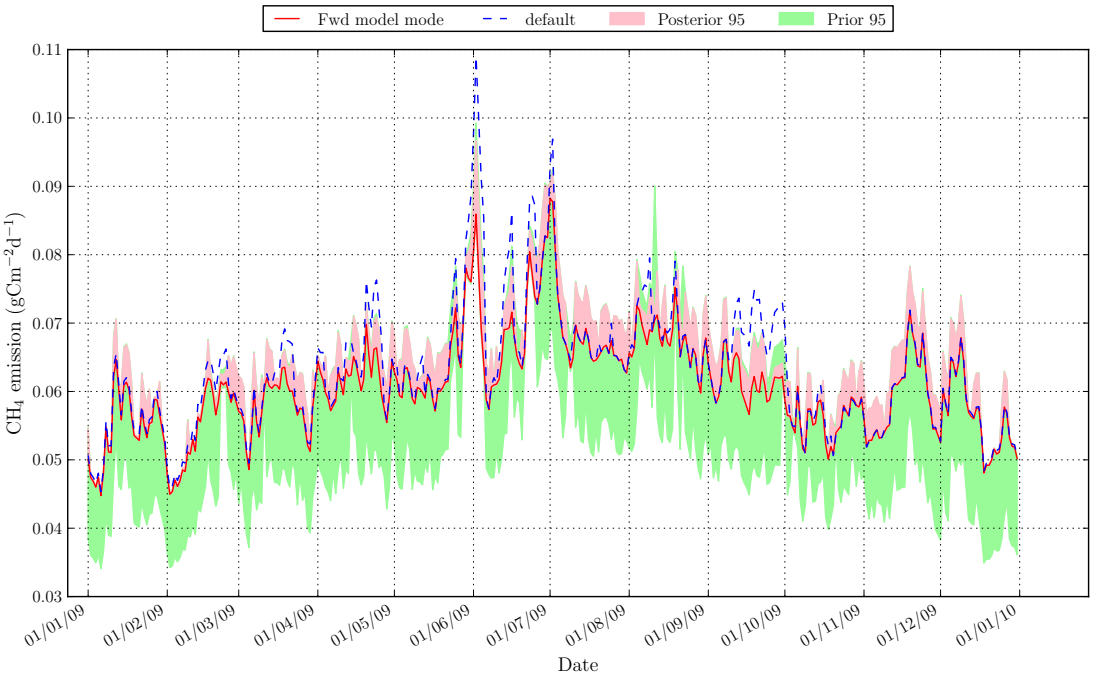

***(b)** Constrained rdr prior.*

Figure 7.18: Comparison of the effect of using the original unconstrained, and the new constrained, rdr priors on CH_4 flux forward models runs, using parameters constrained with observations every 60 days and an associated uncertainty of $0.1 m^3 m^{-3}$.

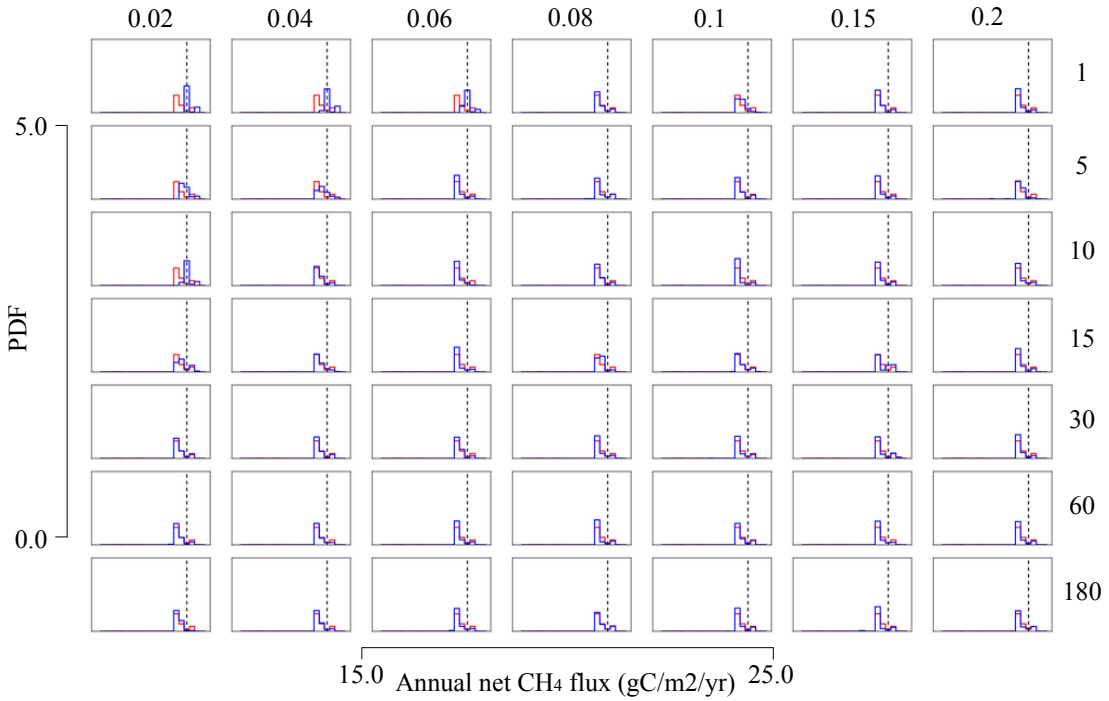

Figure 7.19: Posterior distributions for the annual CH_4 flux using volumetric soil moisture observations for each observational characteristic, with the constrained rdr prior.

7.5 Impact of bias in the volumetric soil moisture observations

As well as random error in the volumetric soil moisture observations, systematic error (bias) can occur as a result of differences in spatial resolution between the model and observations due to poor instrument calibration and inaccuracies in the retrieval algorithms. If the observational bias is not accounted for in the likelihood, the result is likely to be inaccurate parameter estimates. Biased observations will have a similar impact to model error; both would result in an offset between the model and observations, though in reality a mixture of both sources of error will be responsible for the observation-model difference. Bias is much easier to identify and define from comparison with ground-observations however and therefore accounting for the bias is an easier way to reduce the observation - model difference. This will allow for an improved model estimate, or a more detailed investigation of the sources of model structural and/or driver error. The impact of undefined observational bias on the parameter estimates and model predictive uncertainty is examined in this section, before assessing how best to deal with both unknown and known bias in the observations.

7.5.1 Experimental set-up

The OSSE set-up is identical to that described in Section 7.2 but in the following experiments a bias was introduced into the observations. To do this a random Gaussian error with the mean set to increasingly high negative values (instead of being set to zero) was added to the observations. The standard deviation of the random noise (i.e. the observation uncertainty) was set to a value that is typical for real volumetric soil moisture observations ($0.05 m^3 m^{-3}$, *Dorigo et al.* (2010)). The level of bias added to the observations was the same as the uncertainty added to the observations in the previous volumetric soil moisture experiments (i.e. an increasing bias of 0.02, 0.04, 0.06, 0.08, 0.1, 0.15 and $0.2 m^3 m^{-3}$). The temporal sampling interval remained the same.
Two experiments were carried out:

1. The first OSSE assumes the bias is unknown, and repeats the OSSE without taking the bias into account. The impact of the bias on the retrieval of the parameters is investigated.

2. In the second OSSE the bias is assumed to be known and is accounted for in the likelihood of the Bayesian inversion.

The results of both experiments are presented first. The implications of the results are then discussed.

7.5.2 Unknown and undefined bias

Analysis of the Porosity PPDF

This experiment shows that, as hypothesised above, undefined observational bias results in inaccurate and biased estimates of model parameters *if* the bias is larger than the uncertainty in the observations. As the observations were negatively biased, so too was the maximum volumetric soil moisture value, and hence the porosity parameter showed the exact same pattern of posterior MAP - true value bias as did the observations, give or take a little due to random observational

error (Figure 7.20 and Table 7.14). In general the porosity is well-constrained (>=88.5% error reduction), as a relatively small Gaussian random error was added to the observations. The decrease in parameter constraint is the result of the decreasing temporal sampling interval of observations.

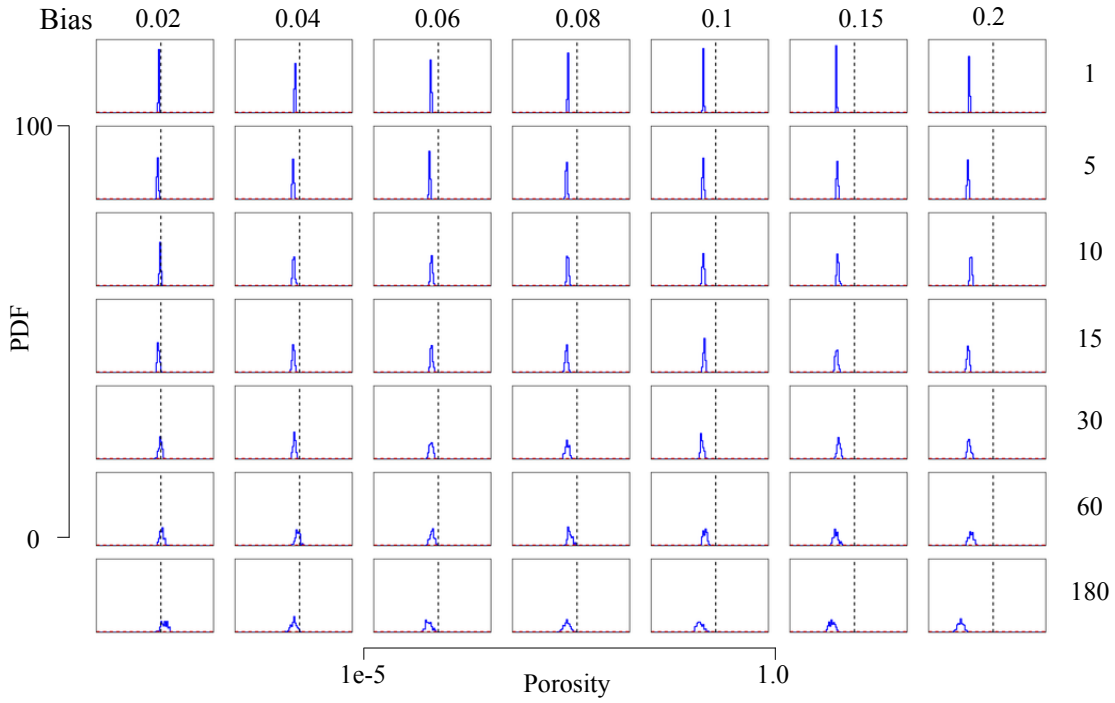

Figure 7.20: Posterior distributions for the porosity parameter using volumetric soil moisture observations, for each observational characteristic, with the constrained rdr prior. The bias, as given in the right-hand column, is not accounted for in the likelihood.

	0.02	**0.04**	**0.06**	**0.08**	**0.1**	**0.15**	**0.2**
1	-0.016	-0.037	-0.061	-0.079	-0.108	-0.156	-0.203
5	-0.018	-0.051	-0.080	-0.093	-0.111	-0.146	-0.224
10	-0.010	-0.028	-0.065	-0.066	-0.103	-0.141	-0.187
15	-0.005	-0.046	-0.059	-0.089	-0.094	-0.164	-0.219
30	0.016	-0.045	-0.033	-0.066	-0.124	-0.128	-0.218
60	-0.001	0.001	-0.043	-0.054	-0.115	-0.160	-0.173
180	0.072	-0.050	-0.110	-0.081	-0.173	-0.194	-0.291

Table 7.14: The bias between the mode of the porosity posterior distribution and the true parameter value for each observational characteristic.

Analysis of the rdr parameters' PPDF

The rdr parameters are both constrained well (>76% and >48% reduction in 95% confidence interval for rdr_a and rdr_b respectively) despite increasing observational bias, for all observations with a daily temporal sampling interval. They are not well-constrained (<27% and <12% error reduction for rdr_a and rdr_b respectively) for temporal frequencies of >5 days. This is contrary to the original observations with increasing random Gaussian error and no systematic negative bias

(see Section 7.3) where the rdr parameters were only well-constrained for the {1/0.04} and {5/0.02} observations.

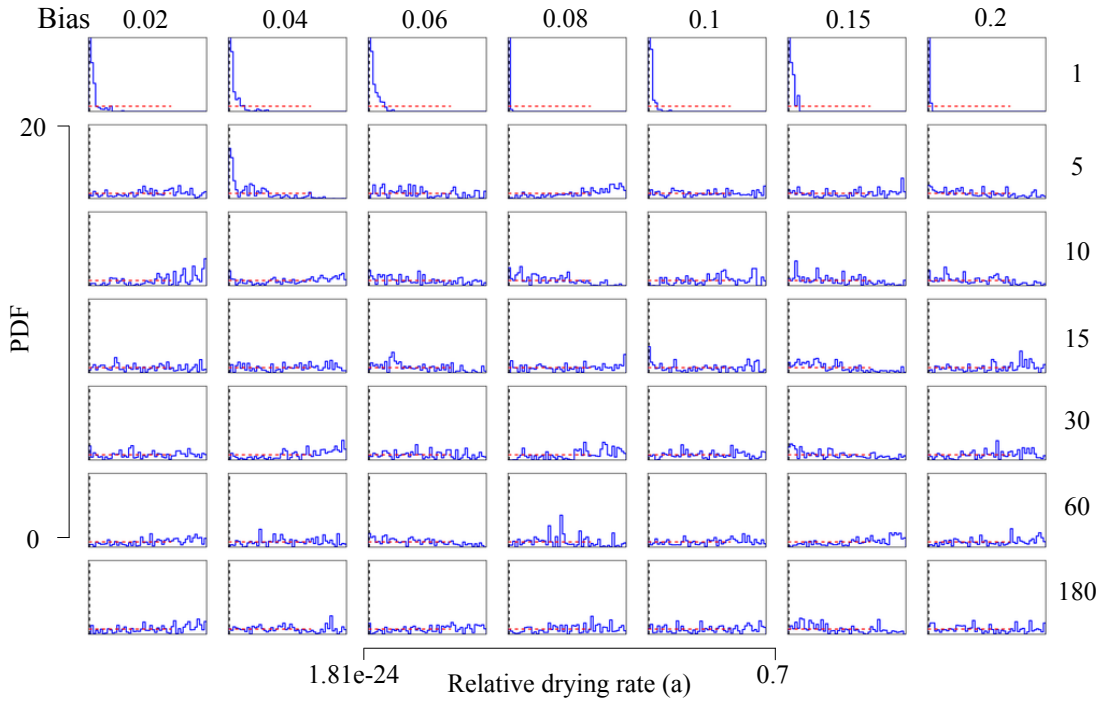

Figure 7.21: Posterior distributions for the relative drying rate (a) parameter using volumetric soil moisture observations, for each observational characteristic, with the constrained rdr prior. The bias, as given in the right-hand column, is not accounted for in the likelihood.

	0.02	**0.04**	**0.06**	**0.08**	**0.1**	**0.15**	**0.2**
1	-0.004	-0.006	0.017	-0.007	-0.006	-0.005	-0.007
5	0.102	0.014	0.022	0.636	0.693	0.677	-0.005
10	0.689	-0.006	0.051	0.007	0.611	0.042	0.209
15	0.664	0.469	0.494	0.683	-0.005	0.005	0.573
30	0.518	0.670	0.472	0.084	0.489	0.068	0.613
60	0.584	0.183	0.004	0.621	0.216	0.691	0.486
180	0.687	0.604	0.673	0.487	0.310	0.017	0.020

Table 7.15: The bias between the mode of the relative drying rate (a) posterior distribution and the true parameter value for each observational characteristic.

Impact on the forward mode and model predictive uncertainty

The forward model mode corresponds well to the biased observations, but therefore cannot capture the "true" value. The calibration works as in the original OSSE with unbiased observations, showing a bias needs to be taken into account in the likelihood. As the OSSE with unbiased volumetric soil moisture observations showed, the forward model modal volumetric soil moisture maximum value is controlled by the porosity parameter, and the decrease in soil moisture is mostly controlled by the rdr parameters. Therefore these results show an increasing negative bias between the modal

daily soil moisture and the true value with increasing bias (Figure 7.22(a)). As seen in the previous volumetric soil moisture OSSEs, where the rdr parameters are well-constrained the soil moisture decreases from the maximum value at times of low precipitation (e.g. Figure 7.22(b)). When the rdr parameters are not well-constrained the soil moisture remains static at the maximum value (e.g. Figure 7.22(c)). The posterior 95% confidence interval increases with decreasing constraint of the porosity value due to decreasing temporal sampling interval. The RMSD between the true volumetric soil moisture and the daily model mode ranges from 0.0 to $0.2 m^3 m^{-3}$, in line with the bias added to the observations.

Although the bias in the volumetric soil moisture observations greatly impacts the porosity MAP estimate, this does not have a considerable effect on the forward modelled CH_4 flux, as it is relatively insensitive to the region of the porosity parameter space that encompasses both the true value and the biased observations.

7.5.3 Accounting for a known observational bias in the likelihood function

If the observational bias is known it can be accounted for in the likelihood function by setting the mean to the value of the bias but with the opposite sign. In this experiment the OSSE with the biased observations (see previous section) was repeated but the mean in the likelihood was set to the value of the bias.

As expected, this results in a well-constrained porosity parameter posterior PDF which has a MAP value very close to the true value (Figure 7.23). The pattern in the constraint of the parameters and forward model mode and predictive uncertainty is therefore dependent upon the observation uncertainty and temporal sampling interval, as discussed in previous experiments. As the error in the observations remains at $0.05 m^3 m^{-3}$, the decrease in porosity constraint is related to the decrease in temporal sampling interval and the rdr parameters are only well-constrained, with a small bias between the MAP and true value, for daily observations.

7.5.4 Impact of bias in the volumetric soil moisture observations - Discussion

In the first experiment the rdr parameters were well-constrained for all daily observations, despite the increase in bias. The true rdr parameters are very close to the limits of their range that results in the maximum possible decrease in soil moisture. Therefore in addition to the low observational error allowing for a good constraint of the parameters, the negative bias acts to constrain these parameters to their true value and towards the limit of their ranges (e.g. the slight negative bias the rdr_a parameter as a result of constraint using daily observations Table 7.15). It is likely that the rdr parameters are only well-constrained for a daily temporal sampling interval because the dips in soil moisture under these specific climatic conditions are very short-lived. Therefore observations with a decreasing temporal sampling interval largely miss them and the observational error is not as low as was required ($<=0.04 m^3 m^{-3}$) by the un-biased observations with a temporal sampling interval of >= 5 days. If the random observational error was larger the observations with a daily temporal sampling interval would also not be able to constrain the rdr parameters. This is a very interesting example of how biased observations can counter-intuitively help to constrain model parameters.

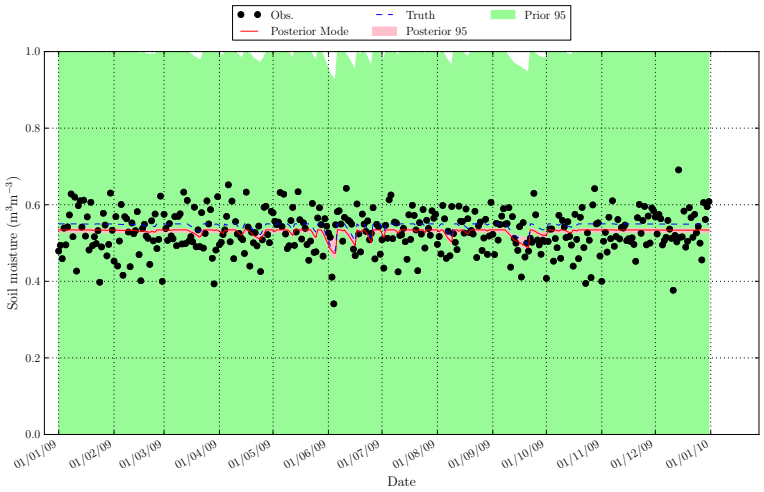

(a) *Synthetic observations with a daily temporal sampling interval and a bias of -0.02m^3m^{-3}.*

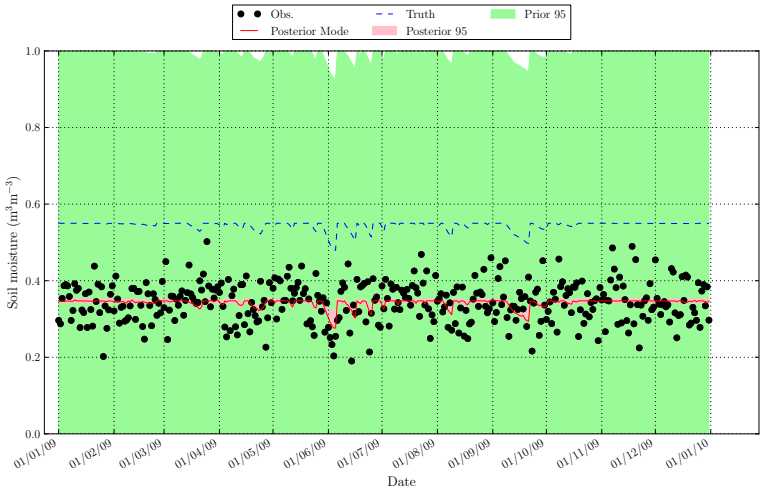

(b) *Synthetic observations with a daily temporal sampling interval and a bias of -0.2m^3m^{-3}.*

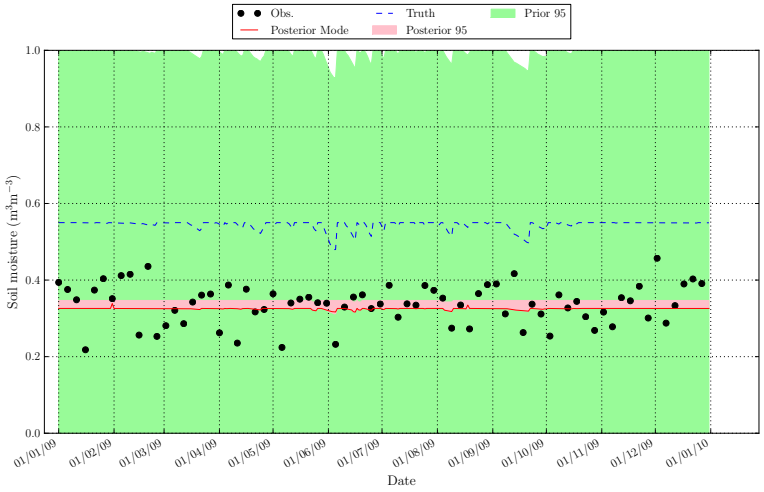

(c) *Synthetic observations with a temporal sampling interval of 5 days and a bias of -0.2m^3m^{-3}.*

Figure 7.22: The volumetric soil moisture from an ensemble of 500 forward model runs using the posterior parameter distributions constrained with *biased* synthetic volumetric soil moisture observations with varying temporal sampling interval and added random Gaussian noise.

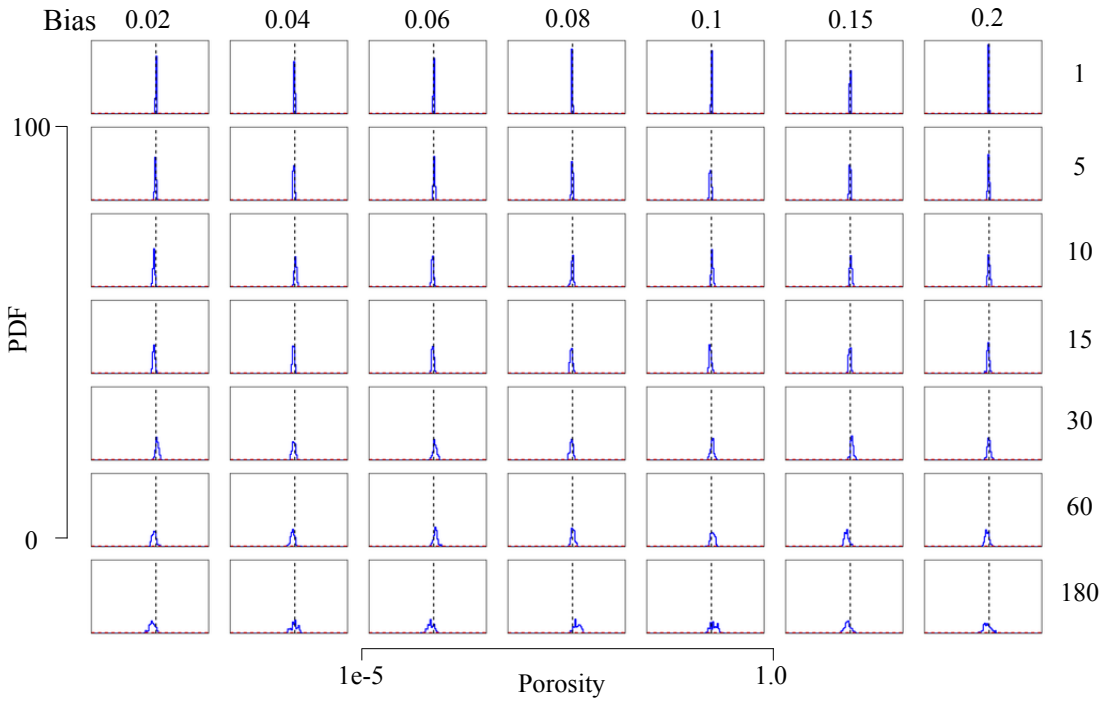

Figure 7.23: Posterior distributions for the porosity parameter using volumetric soil moisture observations for each observational characteristic, with the constrained rdr prior. The bias, as given in the right-hand column, is accounted for in the likelihood.

The peak in NEP and CH_4 flux mode only corresponds to the true peak flux when the rdr parameters are well-constrained, as seen in previous volumetric soil moisture experiments. The same is true for the the annual fluxes - if the rdr parameters are not well-constrained the MAP estimate of the annual flux is biased. The bias in the porosity does not have a significant impact on the CH_4 flux because it is most sensitive to very low values of porosity. However these results show that if the bias in the observations is known it should be accounted for in the likelihood, otherwise the parameter estimates will be incorrect. Whilst this may reproduce the true flux, the values would only be conditioned on the specific observations used, and therefore cannot reliably be used to make model predictions elsewhere.

7.6 Relative (% saturation) soil moisture observations

7.6.1 Introduction

Some soil moisture observations are provided as a percentage of the saturation of the soil. Ground-based instruments sometimes provide a measure of the relative soil moisture, and change detection algorithms, used to retrieve soil moisture from active and passive microwave satellite instruments, also provide a measure of the relative change in soil moisture (e.g. *Wagner et al.* (2003) and see Chapter 2 Section 2.4 for a full description). This is a slightly different measurement to the absolute volumetric soil moisture as the temporal variability will respond slightly differently to different soil textural properties. For example if the porosity is high the relative change in soil moisture will be lower for an equivalent change in absolute soil moisture, than if the porosity is low. This was discussed in Chapter 4 Section 4.5. Relative soil moisture observations therefore might result in slightly different parameter estimates than absolute observations. This is investigated by the OSSE experiments in this section.

Two OSSEs are performed in this section. Firstly an OSSE was performed examine how useful relative soil moisture observations are reducing the prior parameter PDF and therefore constraining the model (Experiment 1). Following this the impact of a strong dry bias in the relative soil moisture on the OSSE results is examined (Experiment 2). As discussed for the volumetric soil moisture observations, there is potential that passive satellite pixels cover an area which does not have the same soil properties as the area under study as the resolution is coarse (~50km). Peatlands characteristically have a near-saturated soil. If the pixel in question also covered a region with a mineral soil the backscatter signal will contain a mixture of the relatively wet peatland soil and the relatively dry mineral soil. For relative soil moisture this would result in lower % soil moisture. However a simple negative bias is not sufficient to characterise the bias for relative soil moisture observations, unlike the volumetric soil moisture, as with a change detection algorithm it is likely that values of 100% will still be reached, despite the fact that one part of the pixel contains soil which can hold less water.

In addition the change detection algorithm (*Wagner et al.*, 2003) assumes that the minimum value of backscatter is related to the minimum (wilting point) soil moisture, but again in such saturated soils this may also never be achieved. A correction is applied to the data for semi-arid and desert soils, where the maximum value might never be reached, and for soils at high-latitudes where the minimum value might never be reached a value for frozen soil is used as it has similar properties to a dry soil (*Wagner et al.*, 2003). For peatland ecosystems at temperate latitudes the soil is never fully frozen and the minimum value is not likely to ever be reached but it appears that no correction is applied for such a scenario. Therefore the apparent range in % soil moisture observations probably does not reflect the true possible range from “wet” to “dry” soil.

These various issues mean that relative soil moisture derived from a change detection algorithm probably has a higher degree of variability, from 100% to low % values of soil moisture, than is the case in reality. Thus in the final relative soil moisture OSSE the impact of an erroneous high amplitude of variability in soil moisture was examined. Values of 100% were still used, which would not be the case if a simple negative bias was put into the observations, but the resultant observations had an overall negative bias and the range of relative soil moisture values

was increased. As the parameters' influence on the model C fluxes has already been discussed at length earlier in this chapter, a limited summary of the impacts on the C fluxes will be given for the results of the experiments in this section, unless the behaviour is markedly different.

7.6.2 Experimental set-up

Designing an OSSE with relative soil moisture observations is difficult because in a relatively wet climate such as the one being studied, the modelled soil moisture values are often at 100%, no matter what the parameter values are. Therefore taking the default model output and adding error to the observations will result in many synthetic soil moisture observations of >100%. Most real observations will not go above 100% if the instrument (or algorithm, in the case of the change detection method) has been correctly calibrated, although it is possible. On the other hand truncating the observations at 100% will result in a 'wet' bias to the observations (i.e. there would be an unrealistically high number of soil moisture values of 100%). However the model soil moisture cannot go above 100%, so the ability of the observations to constrain the model is the same regardless of having observations >100% or equal to 100%.
Two OSSE studies were carried out in this section. The random Gaussian noise that was added to the default model output to create synthetic relative soil moisture observations was detailed in Section 7.2 at the beginning of this chapter.

1. In the first OSSE random Gaussian noise was added to the observations and the resultant synthetic observations were not truncated if the value was >100%.

2. In the second OSSE if the random Gaussian noise resulted in an observation with a value of >100% the noise was subtracted from the default model run, instead of added to it. This simulated observations with an increasing dry bias as a higher magnitude of random noise was added to the observations. Values of 100% were still obtained however. These observations therefore represent the bias that might be present in relative soil moisture observations, as discussed in the introduction. The impact of the bias on the parameter constraints was examined with the aim of investigating whether relative soil moisture observations from satellites would be useful if they showed an unrealistically high variability.

The results of both experiments are presented first, and following this a discussion of the usefulness of relative soil moisture observations is provided.

7.6.3 Relative soil moisture observations with values >100%

Analysis of the parameter PPDF

The most striking result of using relative soil moisture observations is that the porosity parameter is not constrained nearly as well (highest values around 60% reduction in 95% C.I.) for any observational characteristic, and the MAP of the posterior PDF only approximates the true value for the {1/2,5,10} and {5/2} observations (Figure 7.24). A positive skew in the posterior PDF towards the uppermost end of the porosity range, despite the lack of parameter constraint, is visible for many other observations with either a low error of 2% and 5% or a daily temporal sampling interval.

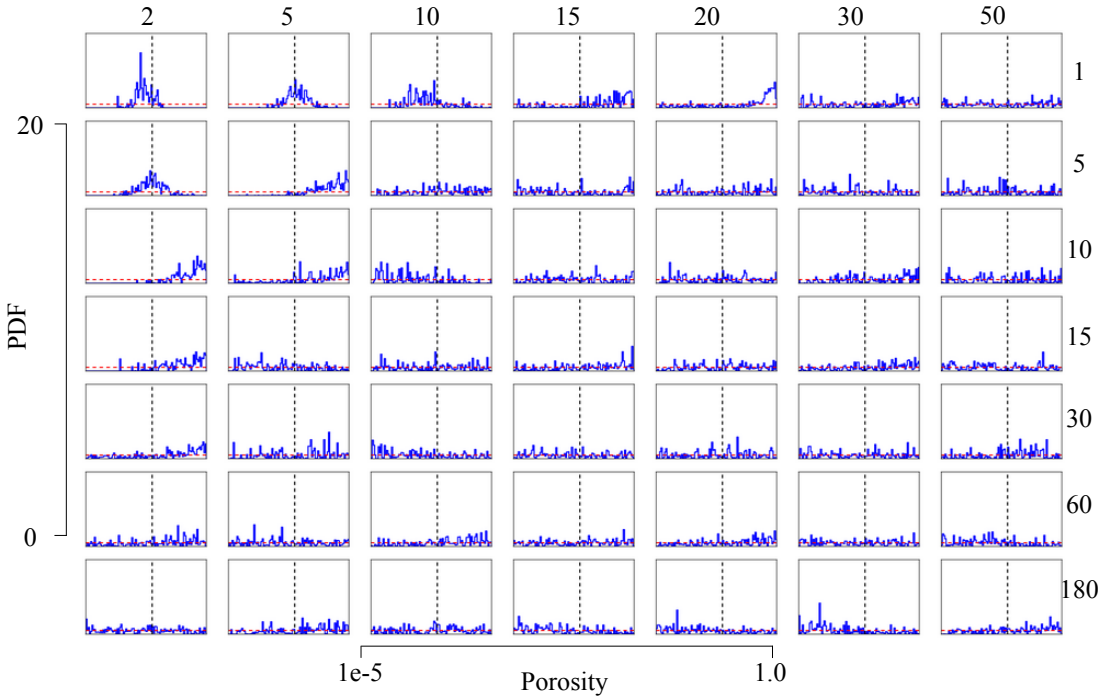

Figure 7.24: Posterior distributions for the porosity parameter using relative soil moisture observations for each observational characteristic.

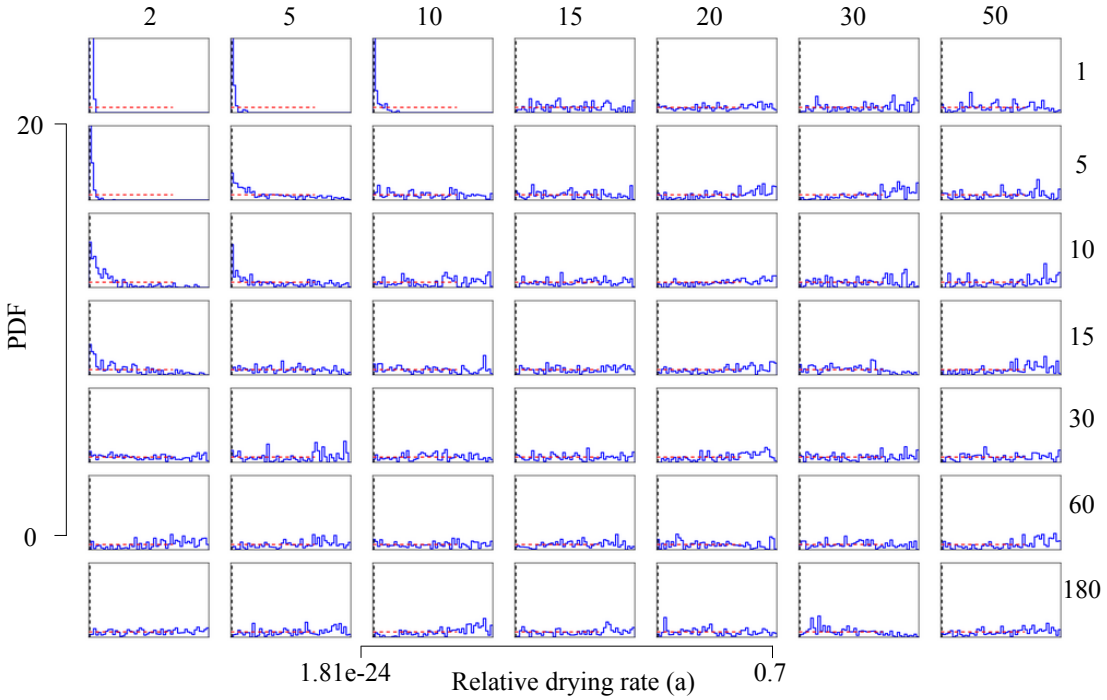

Figure 7.25: Posterior distributions for the relative drying rate (a) parameter using relative soil moisture observations for each observational characteristic.

The rdr parameters exhibit almost the same pattern of behaviour as the porosity parameter (e.g. Figure 7.25 for the rdr_a parameter). Both are well-constrained, with the MAP corresponding closely to the true value for the {1/2,5,10} and {5/2} observations. Both the rdr_a and rdr_b parameters' posterior PDFs show a negative and positive skew respectively towards their true value for the {10,15/2} observations. Observations every 5 and 10 days with an error of 5% also result in a negative skew in the rdr_a parameter, and the {1/15} observations result in a positive skew in the rdr_b parameter PDF.

Impact on the forward mode and predictive uncertainty

As a result of this parameter behaviour, the relative soil moisture mode approximates the true value with a narrow posterior 95% confidence interval where the parameters are relatively well-constrained and the MAP - true value bias is small (e.g. Figure 7.26(a)). As discussed in Section 7.3, the rdr parameters control the amount the volumetric soil moisture decreases from its maximum value. If the rdr parameters are skewed towards their true value a decrease in soil moisture is still evident, although the mode underestimates the decrease in soil moisture.

For the relative soil moisture observations the porosity also affects the decrease in relative soil moisture. A positive bias in the porosity parameter also results in a lesser reduction in soil moisture. Therefore the observational characteristics which result in skewed parameter PDFs result in some dip in the relative soil moisture, but not enough to approximate the true value (e.g. Figure 7.26(b)).

Where the observations result in unconstrained rdr parameters there is often no decrease in the soil moisture, as discussed in Section 7.3. However if the porosity parameter is strongly negatively biased the soil moisture displays odd behaviour where either the mode or at least the posterior 95% confidence interval drops and rises rapidly, producing a "box-like" pattern. This occurs several times in the summer months, but not at other times of the year when a decrease in soil moisture would be expected. This behaviour is consistent with the results of the OAT sensitivity analysis in Chapter 4 Figure 4.11. An example of this can be seen in Figure 7.26(c)). Here the bias between the porosity MAP value and the true value is -0.499. This is behaviour not seen in the volumetric soil moisture OSSE experiments, as the porosity was always very well-constrained by the observations.

Unsurprisingly given the model behaviour is similar, the RMSD between the daily CH_4 and NEP flux mode and true value are similar to the inversion using volumetric soil moisture observations, ranging from 0.00025 to 0.00475$gCm^{-2}d^{-1}$, and 0.0 to 0.18$gCm^{-2}d^{-1}$ (e.g. for the CH_4 flux Figure 7.27). The lowest RMSD values are for daily observations or observations with a very low uncertainty of 2 or 5%. The biases between the CH_4 and NEP annual flux MAP estimates and the true values are again similar to the inversion using volumetric soil moisture experiments.

7.6.4 Relative soil moisture observations with a strong dry bias

Analysis of the parameter PPDF

Observations with the lowest uncertainty (2%) result in relatively well-constrained, accurate parameter values, up to a temporal sampling interval of 15 days (Figure 7.28 for the porosity pa-

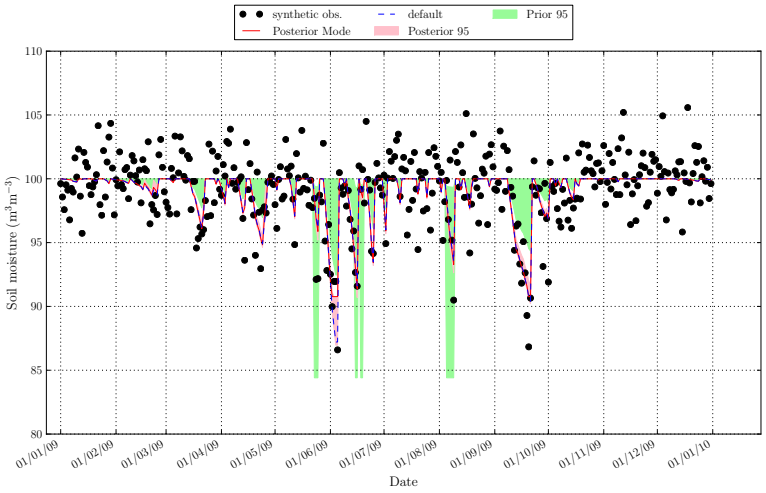

(a) *Synthetic {1/2} observations.*

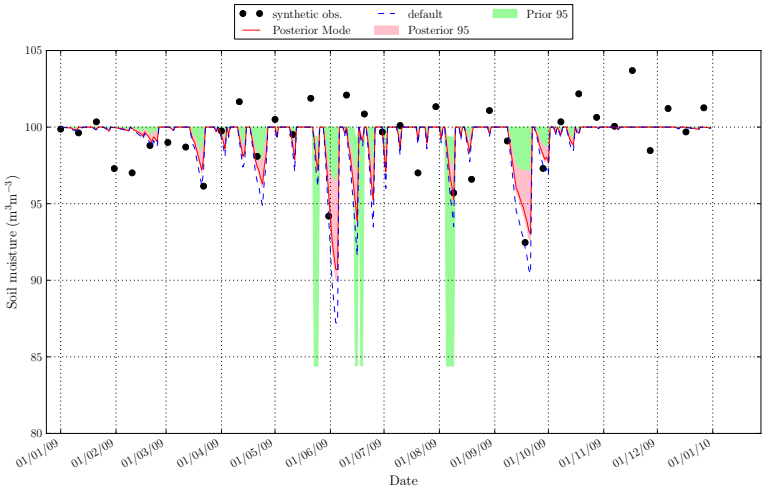

(b) *Synthetic {10/2} observations.*

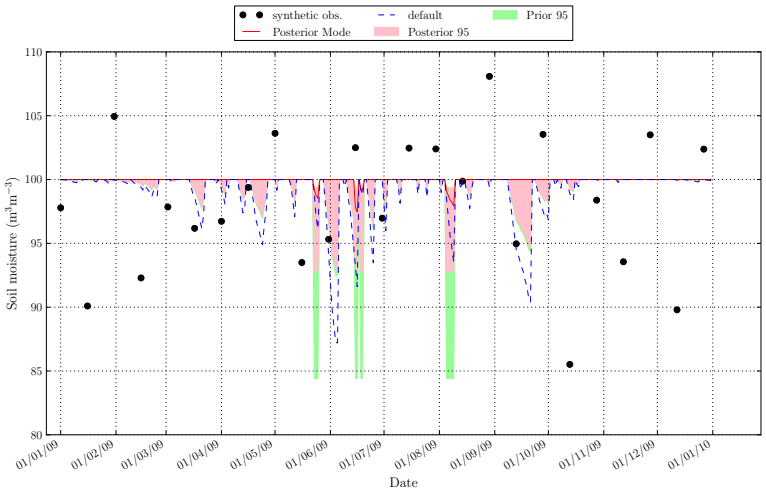

(c) *Synthetic {15/5} observations.*

Figure 7.26: The relative soil moisture from an ensemble of 500 forward model runs using the posterior parameter distributions constrained with synthetic relative soil moisture observations with varying temporal sampling interval and added random Gaussian noise.

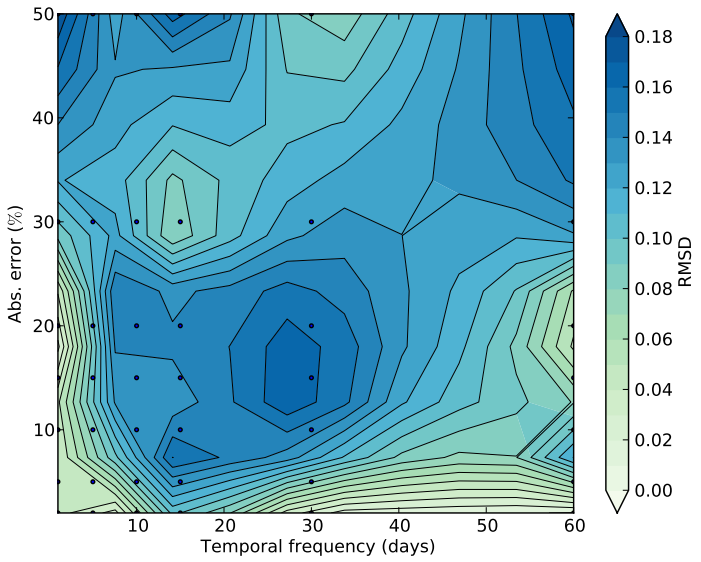

Figure 7.27: Plot to show the root mean squared difference between the MAP of the forward modelled CH_4 flux and the true daily values using relative soil moisture observations and different observational characteristics.

rameter and Figure 7.29 for an example of the rdr parameter behaviour). Observations with a temporal sampling interval of 5 days also show this behaviour at errors of <=5%. Daily observations result in good parameter constraint for errors up to 30%. The rdr parameters are constrained towards their true value and beyond to the limit of their range (biases of up to -0.007 for the rdr_a parameter).

The porosity has a high negative bias (between -0.48 and -0.54) for daily observations and errors between 5 and 30%. This parameter behaviour is due to the high variability in soil moisture, especially at higher observational error. The OAT sensitivity analysis (Chapter 4 Figure 4.11) showed that the lower the value of porosity and rdr_a parameters, and the higher the rdr_b parameter, the greater the variability of relative soil moisture. The negative bias of the observations at high observational error (some values are as low as ~10% for 30% soil moisture), results in the strong biases in the parameter posterior PDFs. However this is only the case for daily observations as less frequent observations do not pick up short timescale decreases in modelled soil moisture.

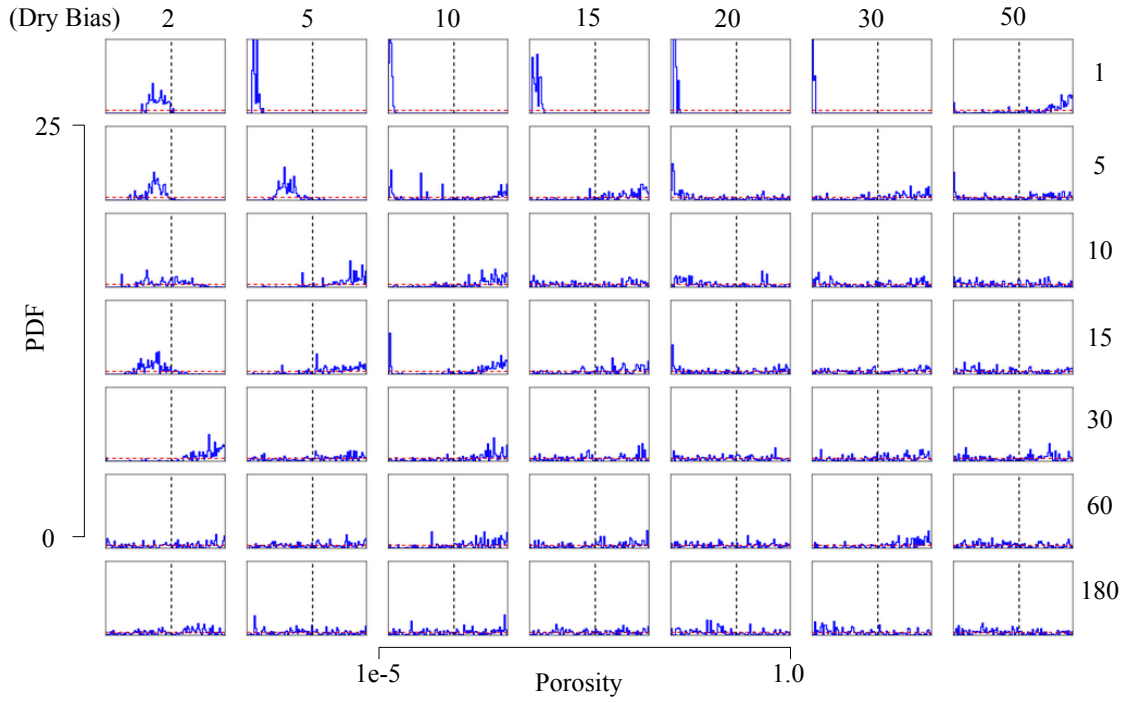

Figure 7.28: Posterior distributions for the porosity parameter using relative soil moisture observations with a dry bias, for each observational characteristic.

Impact on the forward model mode and predictive uncertainty

If the porosity is positively skewed and the rdr parameters are skewed towards their true value there will be some dip in the soil moisture but the C flux peaks might be underestimated. Only the {<=15/2} observations result in accurate approximations of the soil moisture and C fluxes in this experiment as the parameters are tightly constrained to their true value. The remaining observational characteristics result in poorly constrained parameters and therefore generally underestimate decrease in soil moisture and the true peak flux.

However, if the porosity and rdr parameters are strongly skewed towards the end of their

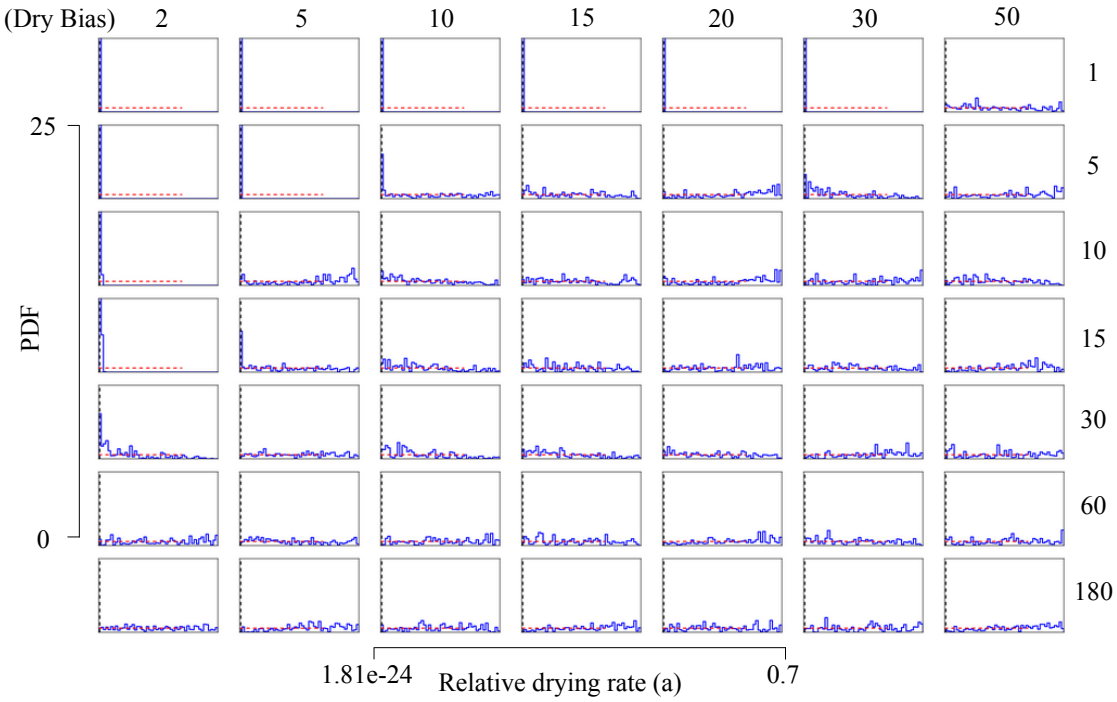

Figure 7.29: Posterior distributions for the relative drying rate (a) parameter using relative soil moisture observations with a dry bias, for each observational characteristic.

ranges which results in the largest dip in soil moisture (negative bias for the rdr_a and porosity, and positive bias for rdr_b), the dip in soil moisture can be very dramatic, and much lower than the true value (Figure 7.30(a)). This can result in an overestimation of the true CH_4 flux and an underestimation of the NEP flux. However this is only significant in the case of the {1/5-30} observations (e.g. Figure 7.30(b) for CH_4 flux observations and FIgure 7.30(c) for the NEP) and the {5/5,10} observations.

7.6.5 Relative (% saturation) soil moisture observations - Discussion

The results showed that similar parameter constraints can be achieved using both volumetric and relative soil moisture observations, with no particular benefit to using either type, if there is no bias in the observations.

The results from these experiments are important as they suggest that relative soil moisture observations that are likely to be obtained in this type of ecosystem from passive microwave satellite change detection methods are likely to have too high a variability to accurately constrain the parameters, unless they have an error of <=2%. If the observations have a daily temporal sampling interval (or in some cases with a temporal sampling interval of <=5 days) it is likely the porosity and rdr parameters will be very biased and therefore will produce a dramatic overestimation of the true CH_4 flux and underestimation of the NEP. For all other observations the parameters will not be well-constrained and the peak flux will be underestimated, though this is the case for unbiased observations as seen in the previous experiment. This requirement is not too different from previous soil moisture (both relative and absolute) OSSE experiments, but the need for a very low observation error is more obvious, even for daily observations.

7.7 Discussion

7.7.1 Observational characteristics which result in a good constraint of soil moisture related parameters

The results of this chapter show that both relative and absolute volumetric soil moisture observations can be used to constrain the soil moisture - related parameters of the CASA-CH_4 model, but only for observations with a high temporal sampling interval and low observational error. For volumetric soil moisture, the {1/<=0.06} and {5,10/<=0.02} observations, and to some extent the {5/0.04} observations, result in good constraint of all of the relevant parameters and therefore accurately modelled C fluxes with narrow posterior 95% confidence intervals. For relative soil moisture only the {1/<=10} and {5/2} observations resulted in accurate and well-constrained parameter and model C flux estimates.

The choice of prior range for the parameters does impact the level of observation uncertainty and the temporal sampling interval of observations which can be used to constrain the parameter estimates and model fluxes. This is the nature of Bayesian inversion; both the observations and the information in the prior distributions are used to improve estimates of the variable being examined. The ability of the algorithm to constrain the model flux estimates will be improved by finding all of the available information on the possible range of parameter values, so as to limit the prior.

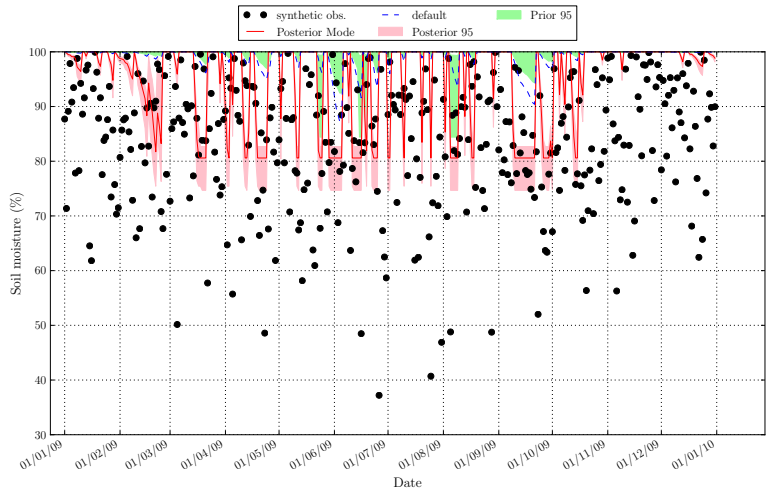

(a) *Relative soil moisture.*

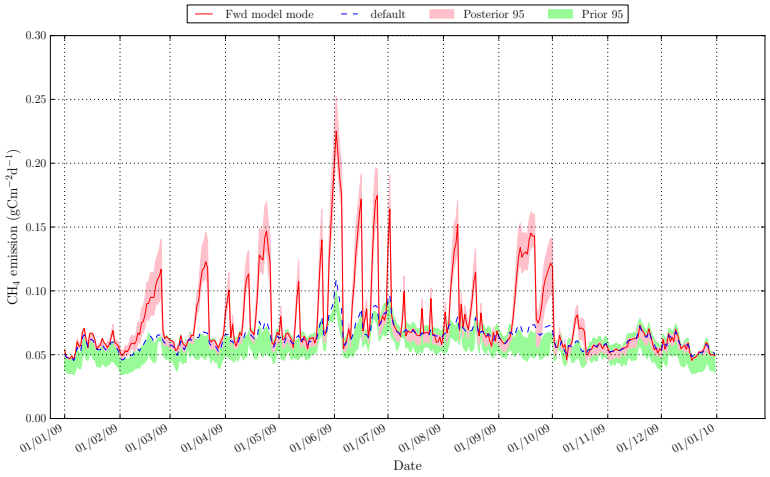

(b) *CH_4 flux.*

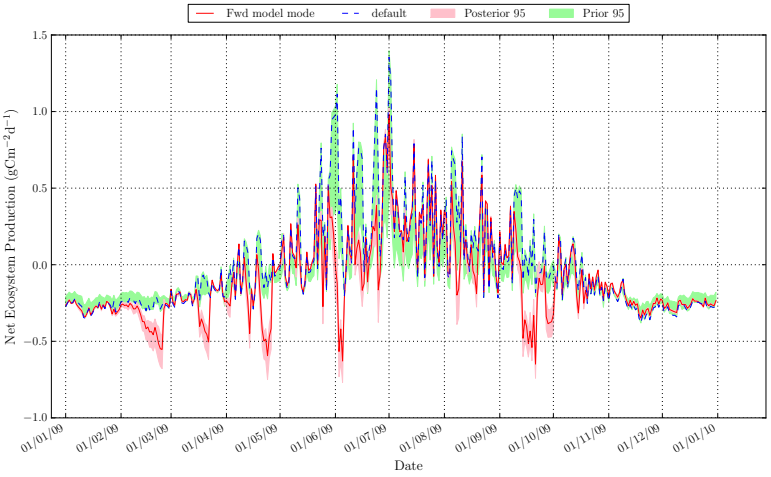

(c) *NEP flux.*

Figure 7.30: The mode and 95% confidence interval for different model state variables from an ensemble of 500 forward model runs using the posterior parameter distributions constrained with synthetic relative soil moisture observations with a daily temporal sampling interval and 20% added random Gaussian noise. The error as been subtracted from the default model output if the value of the resultant observation would be >100%.

This is a necessity if the quality of the observations is poor. This can be achieved through field-based measurements, for example the likely range in porosity values can be measured at the site. Often the parameterisation of soil C models has been designed for mineral soils (*Chimner et al.*, 2002). This is true for the rdr parameterisation in this model. The calculations are based on the soil texture, i.e. % sand and clay etc. Organic soils do not have sand or clay and therefore it is possible parameters that can be used to describe the soil textural properties of organic soils should be used in the model implementation. This would mean the parameters would be more physically based and could be more easily measured (and therefore the prior values constrained) in the field.

7.7.2 Impact of a bias in the volumetric soil moisture observations

A bias in the volumetric soil moisture observations mostly impacted the porosity parameter. However this did not greatly impact the C fluxes as they are relatively insenstive to the porosity parameter in that particular region of the parameter space, even with a negative bias in the observations. The bias did have the unexpected result of allowing a greater constraint of the rdr parameters when the temporal sampling interval was low enough. This surprise result proves that the algorithm's ability to accurately constrain the parameters is not always intuitive. A synthetic experiment can aid our understanding of what is possible with different observational characteristics. If the observations are biased the only way to account for the bias properly is to have an estimate of the bias, from validation with ground-truthed observations for example, and to modify the likelihood accordingly. Although the OSSE studies which examined the impact of bias were applied to soil moisture observations, similar experiments could be done for other observations.

7.7.3 Impact of a bias in the relative soil moisture observations

If there is a strong dry bias in the relative soil moisture observations this can result in poorly constrained and innacurate parameter estimates. Low % soil moisture values are likely to result in extreme biases in the porosity and rdr parameters, pushing them into the regions of their parameter space that greatly impact the C fluxes. A strong negative bias in the porosity and rdr_a and positive bias in the rdr_b parameter will result in a large overestimate of the CH_4 flux and a significant underestimate of the NEP flux. Hence care should be taken with these observations to ensure the variability in the relative soil moisture is not unrealistically high. As this is not a simple bias, as would be the case for the volumetric soil moisture observations, it is not a simple matter to take account of it in the likelihood of the Bayesian inversion. The distribution of the bias in the observations needs to be properly characterised. A new error model in the likelihood is needed to deal with a more complicated bias.

7.7.4 Influence of soil moisture observations on modelled C flux estimates

The RMSD and annual flux biases are smaller for soil moisture observations than for the C flux observations in general (Chapters 5 and 6). This is to be expected, as only a few parameters are being constrained in these experiments. However the values are still significant (the RMSD can be up to 7.8% of the mean daily CH_4 flux and the annual flux bias is 3.5% of the true annual CH_4 flux). The mean of the NEP flux is ~0 and so an RMSD value of $0.19 gCm^{-2}d^{-1}$ is quite

significant. The bias in the annual NEP flux can be up to ~-28gCm^{-2}y^{-1}. Given the true annual flux is -1.68gCm^{-2}y^{-1}, this represents quite a large underestimate. However, as already discussed, for the "best-case" observational charactersitics the errors are very small.

An interesting finding from these experiments is the significance of the rdr parameters on the C fluxes. The constant underestimate of the C fluxes at higher observation error and lower temporal sampling interval is due to the lack of constraint of the rdr parameters. The importance of the rdr parameters was not highlighted in the sensitivity analyses as their impact on the C flux is smaller than for other parameters (the porosity parameter appeared to have a higher importance). This is because the sensitivity analysis takes into account the whole range of parameter values, and only more extreme values of porosity affect the flux, as seen in the relative soil moisture experiments. Also the sensitivity analysis looked at the average daily change in the model C fluxes as a result of a change in the parameters. The rdr parameters only affect the peak fluxes so they will not appear to be as important as other parameters where a change in the value will affect the whole timeseries. However it is crucial to be able to model the peak fluxes, as what appears to be a small change in the peak fluxes will greatly affect the annual net C balance.

7.7.5 Available satellite-derived soil moisture estimates

There are not many satellite datasets that are currently operationally available for the area considered here that could meet the characteristics needed to accurately constrain the soil moisture - related parameters. The passive microwave instruments on board SMOS and AMSR-E (and the associated algorithms), are expected to produce soil moisture estimates with an accuracy of 0.04 and 0.06m^{3}m^{-3} respectively (*Kerr et al.*, 2001; *de Jeu et al.*, 2008). Validation results have shown that this level of error can be acheived but no validation studies in extremely wet sites have yet been carried out. As the study site used here is small, and the surrounding soils will have a lower soil moisture, it is likely that these observations will have a negative bias. Therefore to use them in the calibration framework some ground truth data will be required in order to estimate the bias in the observations. The only other instrument that is currently available and could possibly meet the necessary requirements is the scatterometer, ASCAT, on board the Met-Op satellite. ASCAT soil moisture observations are derived from a change detection algorithm (*Wagner et al.*, 2003) and therefore are relative. Near-daily observations are available but the errors are as high as 10%, so it is not clear that they will be useful. In addition, they are likely to have a strong dry bias, as detailed earlier in the chapter, and therefore will not be useful for constraining parameter estimates of the CASA-CH_4 model. In the near-future operational SAR products may become available or methods to downscale low resolution datasets using other higher resolution EO datasets (optical, thermal and SAR) may become more widespread and an operational product released. It has been tried this for parts of the southern hemisphere (*Wagner et al.*, 2008).

7.8 Conclusions

The main findings of the experiments in this chapter are summarised as follows:

- The {1/<=0.06} and {5,10/<=0.02} volumetric soil moisture observations, and to some ex-

tent the {5/0.04} observations result in good constraint of all of the relevant parameters and therefore accurately modelled C fluxes with narrow posterior 95% confidence intervals.

- The {1/<=10} and {5/2} relative (%) soil moisture observations also result in accurate and well-constrained parameter and model C flux estimates.
- The rdr parameters are important for accurately modelling the peaks in C fluxes, as they control the amount the soil moisture dips below the maximum value at times of decreased precipitation.
- If the observation bias is not accounted for in the likelihood the parameters might be well-constrained but to the wrong value.
- Observations from passive radiometer instruments such as AMSR-E and from active scatterometer measurements are on the threshold of meeting the accuracy and temporal sampling interval requirements specified here. However as the size of the site being investigated is small compared to the size of the pixels it is likely the data contain a bias, therefore its use is dependent on the bias being accounted for, as discussed.
- The choice of priors is of great importance in terms of being able to constrain the model if the observations are of relatively poor-quality.

This chapter has examined the observational characteristics required of volumetric and relative soil moisture observations, as well as issues that might arise when combining EO data with a model in a Bayesian inversion framwork. The OSSE design has proven to be very flexible in this regard, allowing insights into how the calibration process is affected by the observational characteristics and model structure. It has also shown that it can highlight some aspects of the model which were deemed unimportant from other analyses, thereby allowing a greater understanding of the workings of the model and the identification of possible weaknesses.

Chapter 8

OSSE to examine the impact of unknown model error

8.1 Introduction

The previous OSSE studies in Chapters 5, 6 and 7 have assumed there is no error in the model. This is unlikely to be the case in reality. Model structural error should be accounted for in the likelihood function of the Bayesian inversion. If it is not, the parameter posterior distributions will also represent the model error. It is very difficult to identify all sources of model structural error however. This could be due to incorrect processes, or incomplete representation of the dynamics of the system. It is therefore probably that the model structural error will not be fully accounted for in the Bayesian inversion.

The aim of this chapter is to investigate the impact of unknown model structural error on the inversion results. The ability of the observations to constrain the parameters in such a way as to take into account the errors in the model is examined. The impact of such an error on the parameter estimation and constraint, as well as the model predictive uncertainty, is examined by setting up a twin experiment, where the default model was altered to produce new "true" model state variables, which were then used to create "true" synthetic observations. The original (now "inaccurate") model was used in the Bayesian. The details of the experimental set-up are outlined in the following section.
The following questions will be addressed in this chapter:

1. Are the observations able to account for an error in the model used in the Bayesian inversion?

2. How does this change with increasing observation uncertainty?

3. Do the results help to identify the error and whether the parameters can help to account for the model error by a shift in their values away from the true value?

The experimental set-up is detailed in the next section. Following this the results of three OSSE studies, outlined in the experimental set-up, are presented. The discussion at the end of the chapter aims to answer the questions outlined above. The significance of the error in the model,

and possible solutions to the problem of obtaining inaccurate results from the inversion are also discussed. Finally the conclusions of the main findings of the experiments in this chapter are provided.

8.2 Experimental set-up

The experimental set-up is essentially the same as the original OSSE using NEP observations (Chapter 6 Section 6.2). The same parameters are included in the calibration and the same uncertainty and temporal sampling interval are used to create the observations. However in this chapter a "twin" experiment is used to investigate the impact of model error on the inversion. In a "twin" experiment the model used to create the synthetic observations is different from the model used in the inversion. Here this is achieved by modifying the default model NEP flux output in order to create the new "true/accurate" model behaviour, from which synthetic observations were derived. The original (now "inaccurate") model was used in the inversion as the aim is to test the ability of the observations to account for the model error with a shift in the parameter posterior distributions. Two experiments were performed:

1. In the first experiment the amplitude of the annual NEP cycle from the default model outputs was increased. This is the new, accurate model. To achieve this the NEP flux was *decreased* by 30% from in the winter months (January to the end of March, and from October to the end of December). In the spring and autumn (April and September) it was *increased* by 60% and in the summer months (May to the end of August) it was *increased* by 90%. This resulted in a higher NEP flux in the middle of the year and a lower flux in the winter. The original (now "inaccurate") modelled NEP flux is compared to the new (now "true") NEP flux in Figure 8.1. The synthetic observations were created from these the new (true/accurate) model in the same way as the other OSSE studies. This experiment is designed to test the hypothesis that the parameter distributions, conditioned on the observations derived from the true NEP, would account for the error in the model by a shift in the MAP estimate. This hypothesis is derived from the OAT sensitivity analysis which showed that changing parameter values mostly lead to a change in the magnitude of the flux, but not the temporal trend.

2. In the second experiment the amplitude of the annual NEP was changed as per the first experiment. In addition, the phase of the annual cycle was modified by shifting the timeseries forwards by one month (Figure 8.2). This results in a shift in the timing of the period of peak NEP flux. It starts later in the year (beginning of August instead of beginning of July) and decreases later (in mid-November instead of mid-September). The peak flux therefore remains higher later in the year than the original model. This experiment is designed to test the hypothesis, put forward following earlier model experiments, that the parameter distributions, conditioned on the observations derived from the true NEP, can account for a change in magnitude of the flux, but *not* a change in the temporal trend. The reason for this is laid out in the description of first experiment.

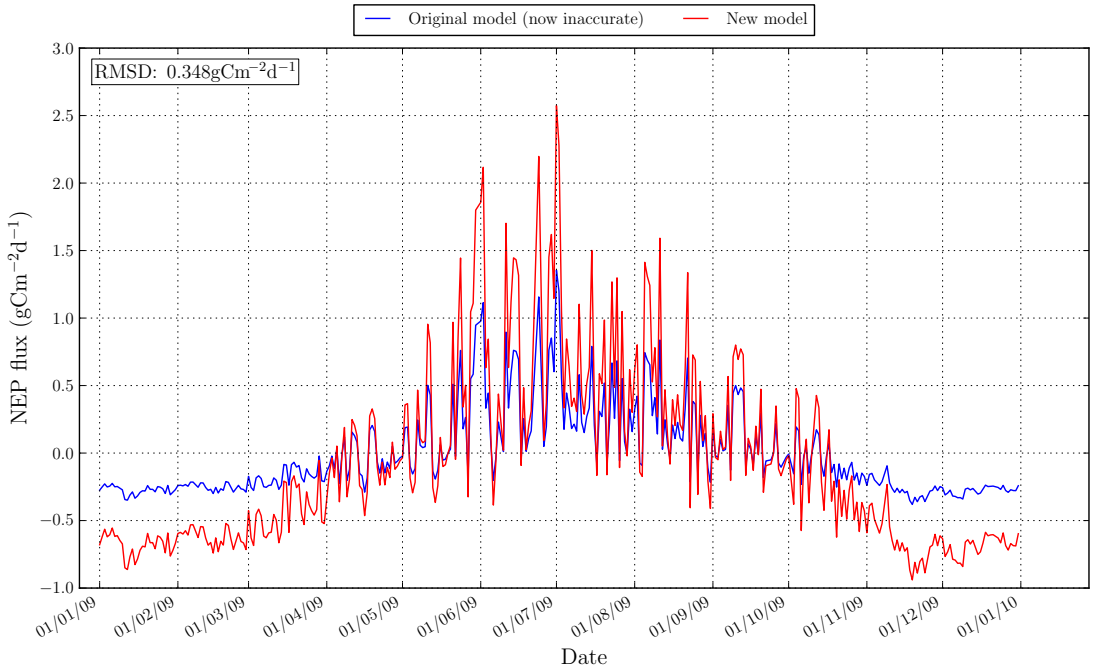

Figure 8.1: Plot to show the difference between the original ("inaccurate") NEP flux and the new ("true") NEP flux created by increasing the amplitude of the annual cycle of NEP flux.

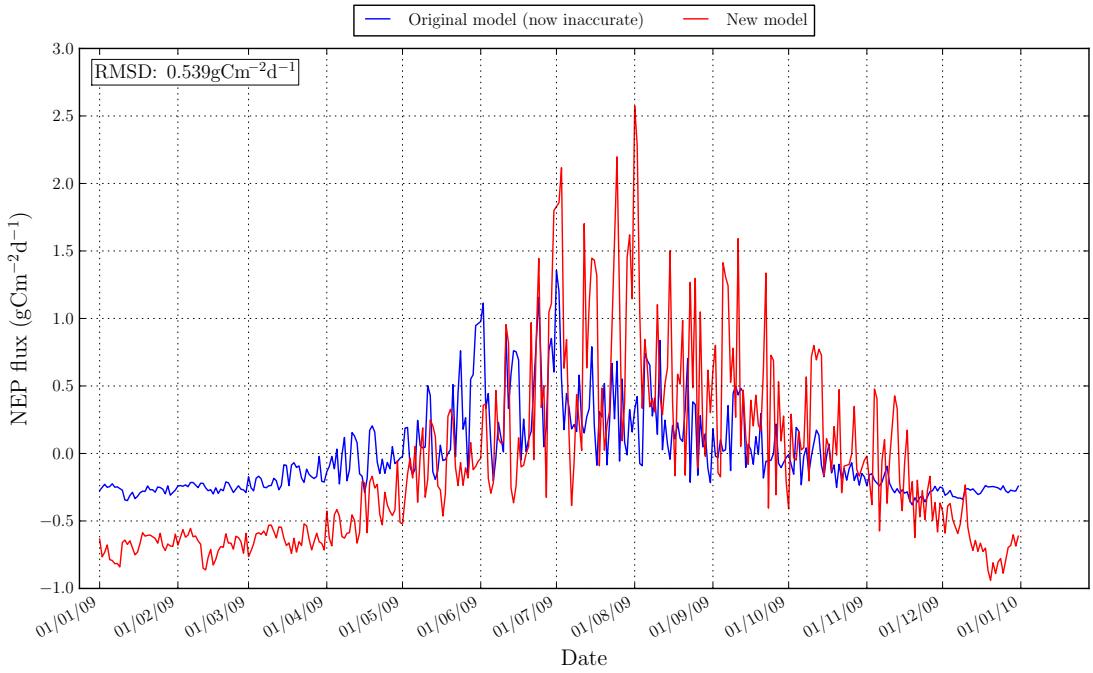

Figure 8.2: Plot to show the difference between the original ("inaccurate") NEP flux and the new ("true") NEP flux created by increasing the amplitude of the annual cycle of NEP flux and shifting the phase of the annual cycle by one month.

An OSSE was carried with the original (inaccurate) model used in the inversion, to investigate whether the observations, created from the accurate ("true") NEP timeseries would result in a shift in the parameter values which would be able to replicate the "true" flux. The results of each experiments are described first. Following this the results of both experiments are discussed. Finally the main conclusions from the experiments in this chapter are outlined.

8.3 Error in the amplitude of the annual cycle of the NEP flux - Results

8.3.1 Parameter PPDF

In the original OSSE experiment with NEP flux observations (Chapter 6), the autotrophic respiration scalar, LUE, porosity and SR_max parameters all displayed correlated behaviour at low observational errors, i.e. the PPDFs were well-constrained with respect to the prior, but the MAP estimate did not correspond to the true value. The forward models however showed good constraint (reduction in the 95% confidence interval) *and* an accurate approximation of the true flux, despite the fact the parameter MAP estimates were significantly biased. This is due to parameter correlation and model equifinality, and was discussed in detail in Chapter 6.

The same parameter behaviour is seen in this experiment, although the Q10_1 parameter is better constrained by the observations at a slightly higher observation error than in the original experiment (Figure 8.3, compared to Figure 6.1). The other parameters show a similar pattern of non-systematic, behaviour, i.e. well-constrained PPDFs with MAP estimates which did not correspond to the default parameter value. (e.g. Figure 8.4 for the autotrophic respiration scalar, compared to the original NEP OSSE study Figure 6.3). The sign of the biases of the MAP estimate of each parameter at low observation error are often different than in the original experiment. In the original OSSE with NEP observations the bias in the parameters was dependent upon the specific noise realisations (i.e. the random Gaussian noise added to the observations) but in this experiments in this chapter, the bias in the parameters may be due to their accounting for the different temporal trend of the new, "accurate" model. The correlation coefficients between the LUE and autotrophic respiration scalar are all very high (0.51 to 0.98) for the observations with an uncertainty of <=1.0$gCm^{-2}d^{-1}$, suggesting that model equifinality has a role to play in the constraint of the MAP of the parameter PPDF.

8.3.2 NEP forward model mode and model predictive uncertainty

As expected there is a number of combinations of the parameters which result in an accurate forward model flux for observations with a low uncertainty (~<=0.2$gCm^{-2}d^{-1}$). The best-case observations are used to investigate whether the parameters can account for the error in the model used in the Bayesian inversion, and therefore whether the true flux could be replicated. Figure 8.5 shows that the forward model mode more closely approximates the true flux (with increased amplitude of the annual cycle) than the original inaccurate model (black line). The NEP flux in the summer months is very accurately depicted by the forward mode, whilst in the winter months the true flux is slightly overestimated by the forward mode. This demonstrates that the parameter

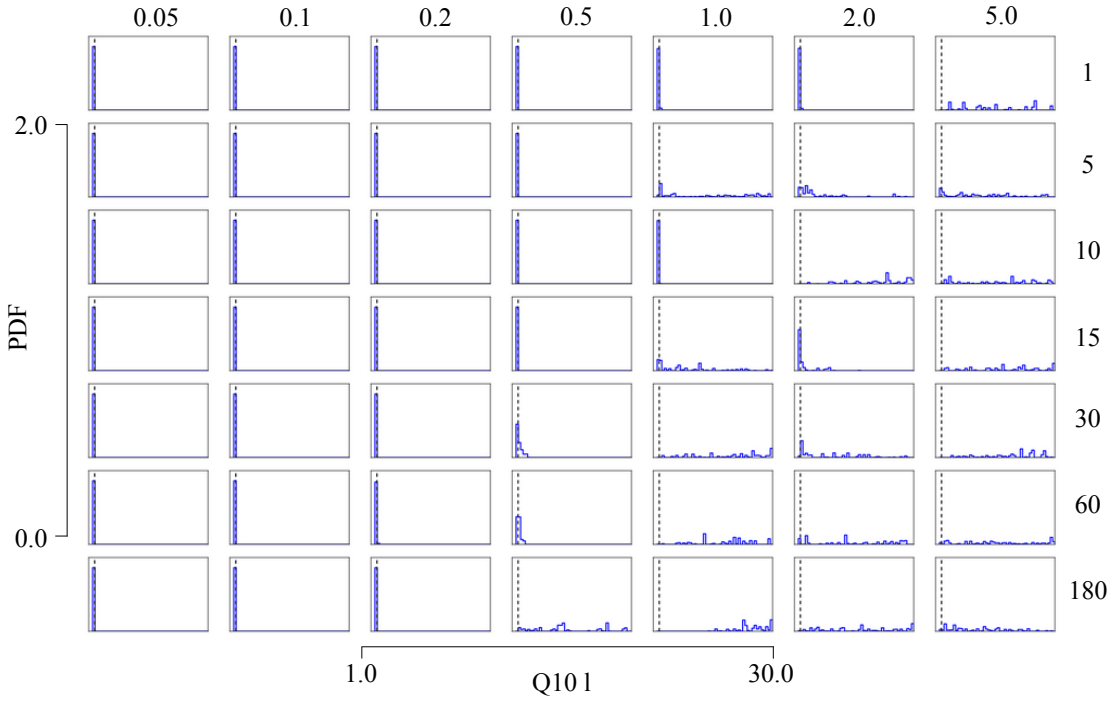

Figure 8.3: Posterior distributions for the Q10 litter parameter, using NEP observations, for each observational characteristic. The axes are the same for all histograms, and are shown at the bottom and left hand side of the figure. The red line shows the prior distribution and the blue, the posterior. The vertical black dashed line shows the true value. The histogram plots are arranged with increasing observation uncertainty along the columns and increasing temporal sampling interval down the rows. The magnitude of the observation uncertainty is given in the top row, and the temporal sampling interval is given in the right-hand column.

PPDF, conditioned on the observations derived from the true flux, have resulted in the mode of the forward NEP ensemble corresponding well to the true NEP. Therefore a shift in the parameters can deal, to some extent, with a error in the magnitude of the flux in the model.

This remains true for most of the observational characteristics which result in constrained parameter PPDFs. As observation error increases and temporal sampling interval decreases the information in the observations is unable to improve on the information contained in the prior, and therefore forward model mode does not approximate the true flux quite as well, resulting in some parts of the year where the forward mode corresponds more closely to the inaccurate model (e.g. Figure 8.6). However for all of these observational characteristics the overall amplitude of the forward mode is close to the that of the true flux.

At higher observational error ($>0.5 gCm^{-2}d^{-1}$) the observation uncertainty is too large to result in an improvement in the prior PDF of the parameters. It is also larger than the model error (see the RMSD value in Figure 8.1), and therefore the lack of information in the observations is more significant in terms of restricting the inversion, than the model error. The forward mode does not correspond to the true flux, or to the original inaccurate model. As found in the OSSE with the original NEP flux observations, forward model behaviour is dominated mostly by the biases in the autotrophic respiration scalar and LUE parameter, which are influenced by the observation - model trend which results from the specific noise realisations.

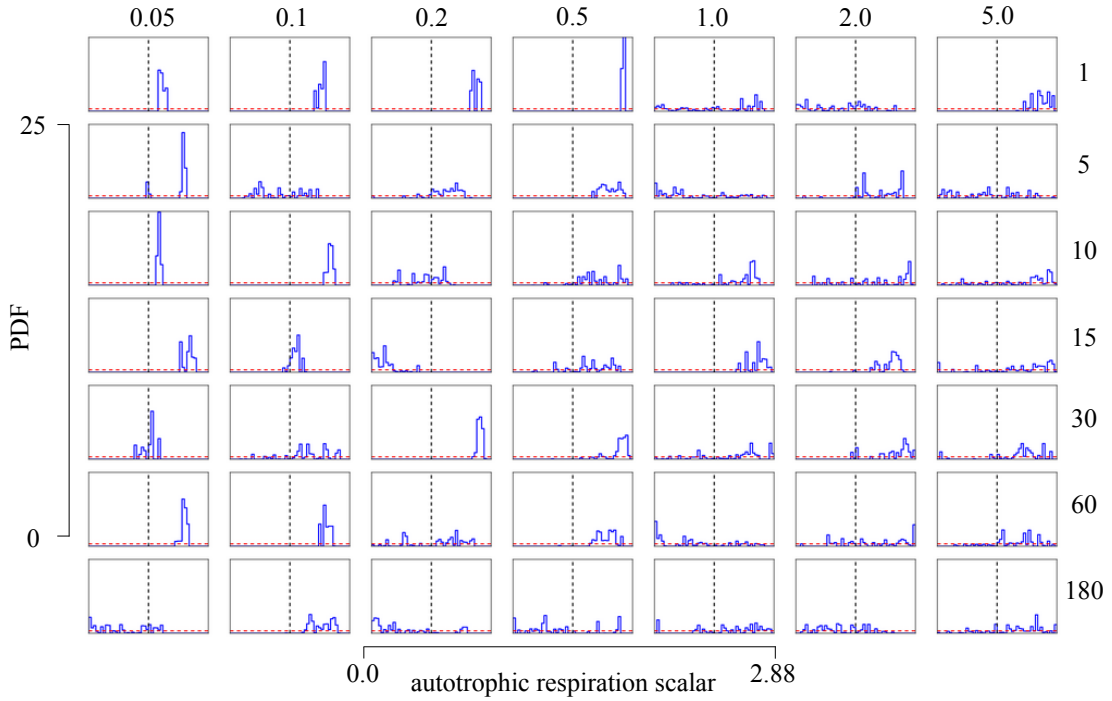

Figure 8.4: Posterior distributions for the autotrophic respiration parameter, using NEP observations, for each observational characteristic.

8.3.3 RMSD between the forward mode and true flux

The RMSD ranges from ~0.3 to ~0.45gCm^{-2}d^{-1} for the low observational characteristics which result in a good approximation of the amplitude of the annual cycle of the true NEP flux (Figure 8.7). This range is comparable to the original OSSE with NEP flux observations for all observational characteristics, not just the observations which constrain the parameters. In this experiment the RMSD increased to 2.8gCm^{-2}d^{-1} for the worst-case observational characteristics (Figure 8.7), which is significantly more than found in the original OSSE.

8.3.4 Annual NEP

The annual NEP flux follows the same pattern of good correspondance to the true value and narrow posterior PDF as the Q10_l parameter, confirming that these observational characteristics do result in the model being able to account for the error in the annual variability by altering the parameter values (Figure 8.8). The bias between the annual NEP flux MAP estimate and the true value is larger for these observational characteristics than in the original NEP OSSE experiment however as the winter flux is overestimated in general. This results in a postive bias of ~30 to 40gCm^{-2}y^{-1}, whereas the bias values in the original OSSE for the low observational error and high temporal sampling interval ranged between ~ -1 to 1gCm^{-2}y^{-1}.

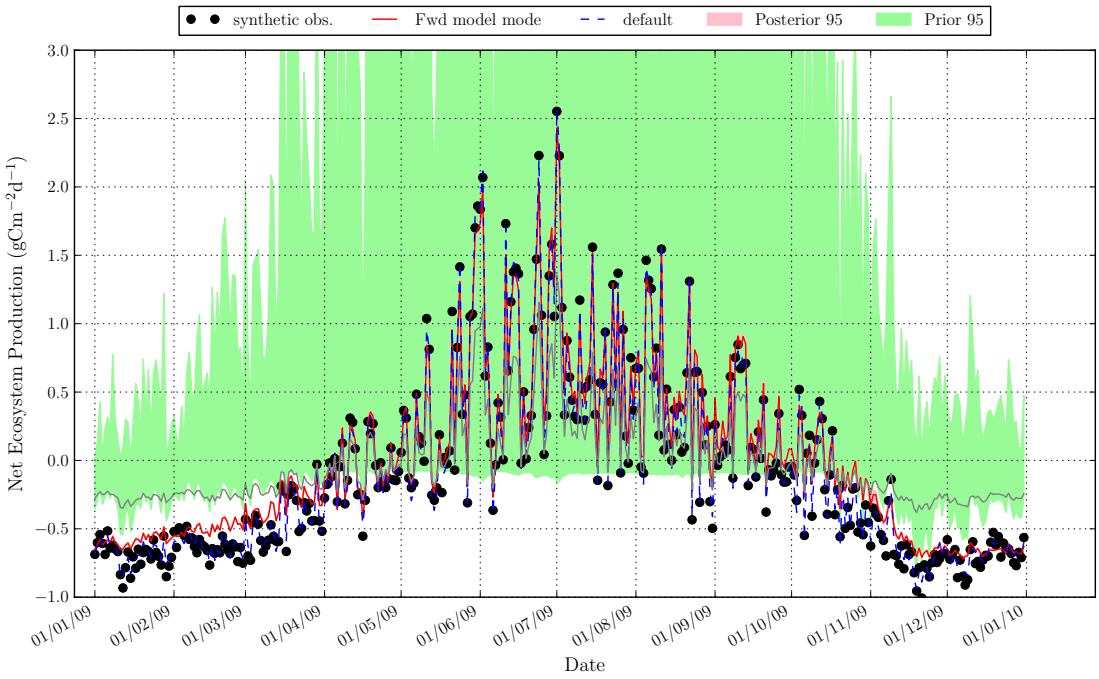

Figure 8.5: A 'zoomed-in' view of the forward modelled NEP flux from 500 model ensembles of the posterior parameter PDFs (red line), using observations with a daily temporal sampling interval and a random Gaussian error of 0.05gCm^{-2}d^{-1}. The mode is compared to the true flux (blue line), the observations used to constrain the parameters in the Bayesian inversion and the "inaccurate" model with the incorrect amplitude of the annual cycle, used in the Bayesian inversion (black line). The green area shows the prior 95% confidence interval of the CH_4 flux using 3000 random samples from the joint prior distribution of the parameters that are being calibrated in this OSSE experiment. The pink area is the posterior 95% confidence interval and the red line is the forward mode. The posteror confidence interval is not clearly visible as it is very narrow.

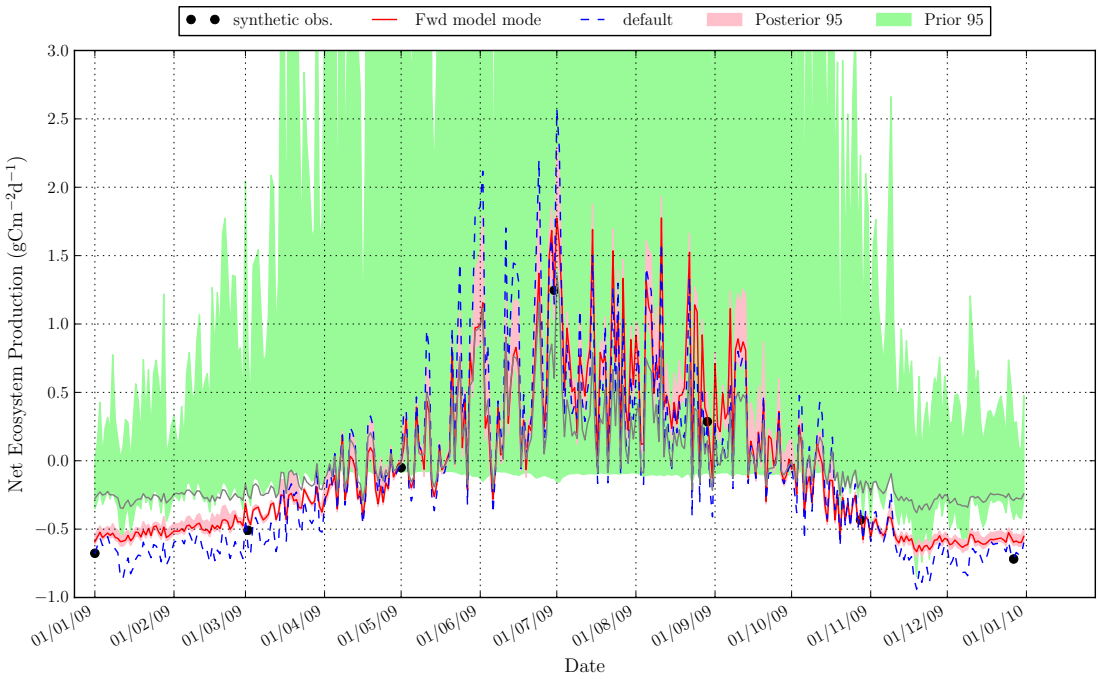

Figure 8.6: A 'zoomed-in' view of the forward modelled NEP flux from 500 model ensembles of the posterior parameter PDFs (red line), using observations with a temporal sampling interval of 60 days and a random Gaussian error of 0.1gCm^{-2}d^{-1}. The mode is compared to the true flux (blue line), the observations used to constrain the parameters in the Bayesian inversion and the "inaccurate" model with the incorrect amplitude of the annual cycle, used in the Bayesian inversion (black line).

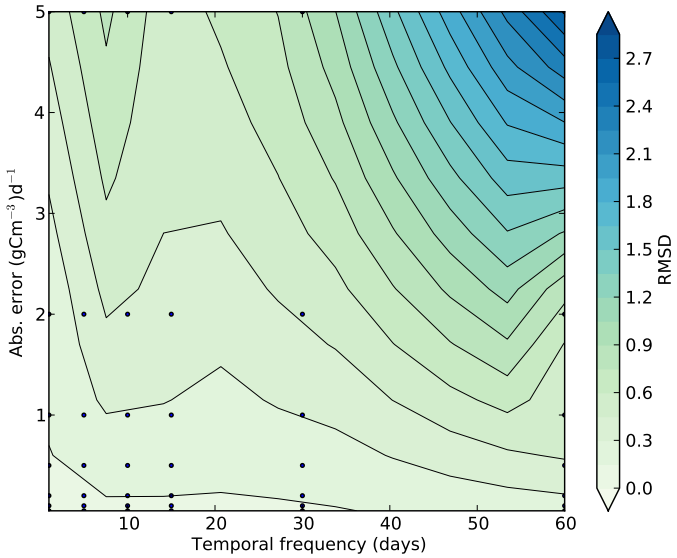

Figure 8.7: The RMSD between the daily forward modelled NEP flux mode and the true flux value for all observational characteristics. The "inaccurate" model used in Bayesian inversion resulted in the incorrect amplitude of the annual cycle but the synthetic observations were produced from the "true" flux.

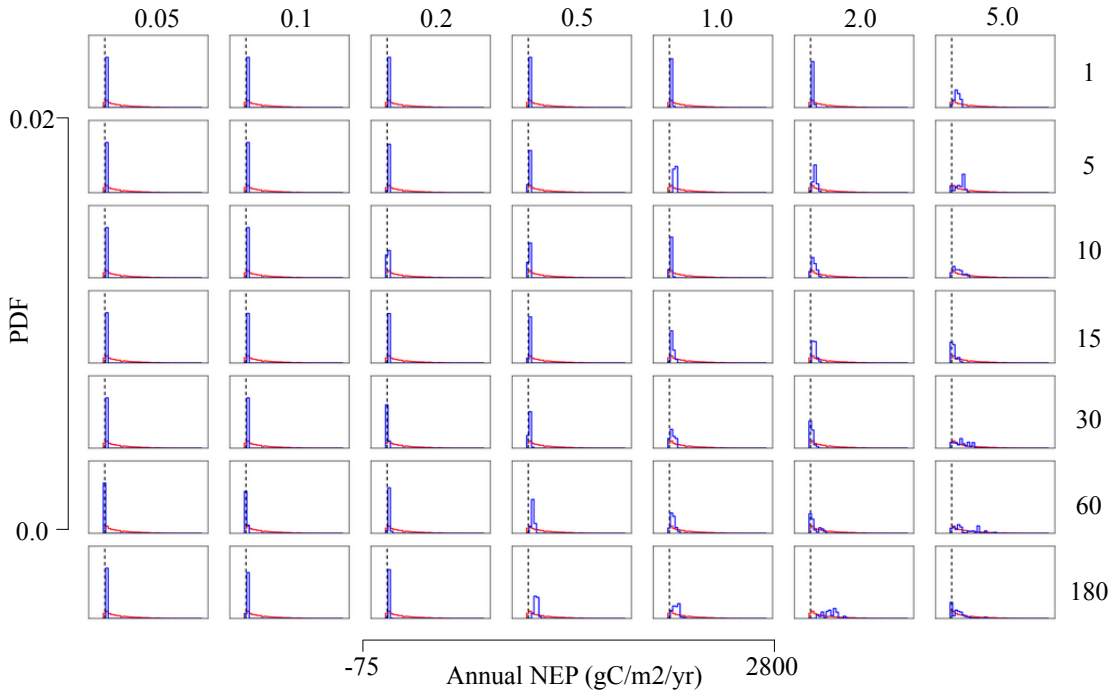

Figure 8.8: Posterior distributions for the annual NEP flux, using NEP observations for each observational characteristic.

8.4 Error in the amplitude and phase of the annual cycle of the NEP flux - Results

8.4.1 Parameter PPDF

The parameters mostly show a very similar pattern of behaviour to all previous OSSE experiments with NEP flux observations, i.e. the Q10_1 parameters are well-constrained for observations with an uncertainty of <=0.2gCm^{-2}d^{-1} (and higher if the temporal sampling interval is smaller). For the same observational characteristics the remaining parameters, specifically the autotrophic respiration scalar and LUE, are well-constrained but not to the default value. This could be due to model equifinality but also due to their accounting for the inaccurate model. However, as in the previous experiment the correlations between the two parameters to which the NEP is most sensitive (LUE and autotrophic respiration scalar) range between 0.46 and 0.98 for observation with an uncertinty of 1.0gCm^{-2}d^{-1}, therefore again model equifinality probably has a role to play in the constraint of the MAP of the parameter PPDF.

8.4.2 NEP forward model mode and model predictive uncertainty

As per the previous experiment, the daily observations, with an error of 0.05gCm^{-2}d^{-1} were examined to investigate whether the parameter PPDFs, conditioned on the observations derived from the true (new, "accurate") flux, could account for the error in the model used in the Bayesian inversion. The results showed that even the "best-case" observations cannot accurately approximate the true flux approximated, and specifically the model cannot replicate the temporal trend (Figure 8.9). Instead it is much closer to the original inaccurate model trend (black line in Figure 8.9). The true peak flux is underestimated by the forward mode and the true flux in the winter months is overestimated by the forward mode. Therefore the annual variability is lower than it should be. The increase in the true flux occurs later in the year and this is not captured by the forward mode. This shows the parameters, conditioned on these observations cannot reproduce the shift in phase caused by the error in the model used in the Bayesian inversion. In the winter months the mode is inbetween the truth and the incorrect model, suggesting that the parameters might be accounting in part for the different magnitude of the flux, but it is clear that the observations have not resulted in a shift in the parameters which would account for a shift in the phase of the annual cycle, and thus in general the magnitude of the flux is wrong.

As in the previous experiment, at a certain level of observation error the parameters are not able to be well-constrained and the observation error is larger than the error between the inaccurate model and true flux, which is ~0.5gCm^{-2}d^{-1}. Thus, especially for lower frequency observations with a larger error, the parameters are not well-constrained and therefore neither is the forward model 95% confidence interval (e.g. Figure 8.10 for the {10/2.0} observations). The wider uncertainty in the forward model captures most of the peaks in the true flux, despite the inability of the model to replicate the truth. However the decrease in NEP in the winter months is outside the prior 95% confidence interval. This is the case for all observational characteristics.

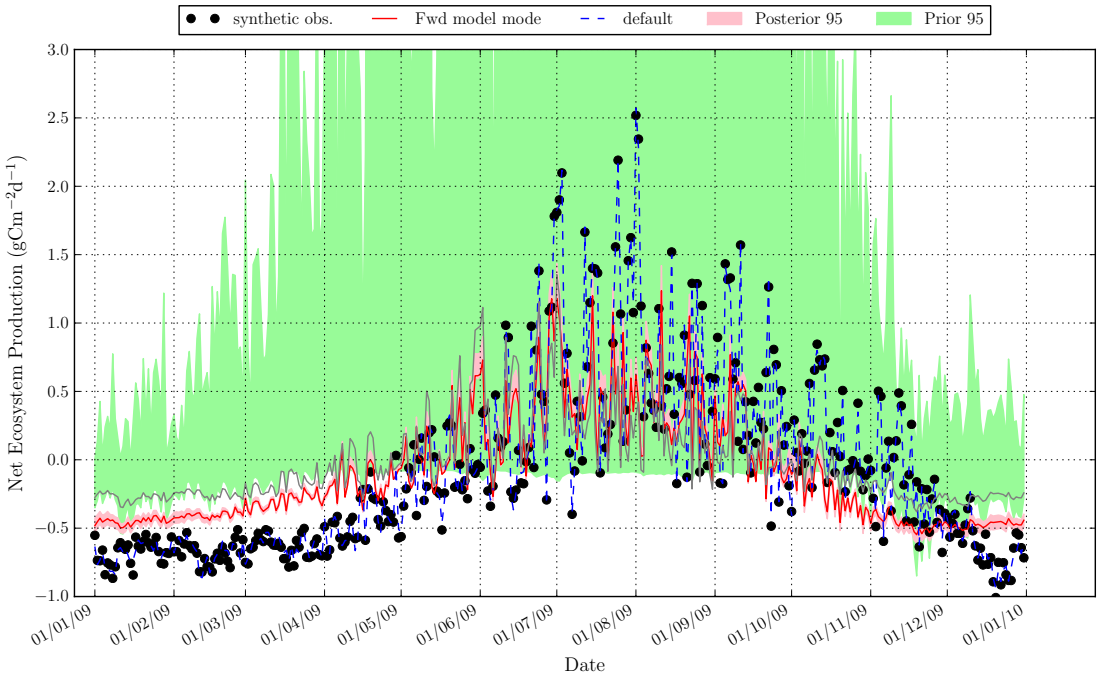

Figure 8.9: A 'zoomed-in' view of the forward modelled NEP flux from 500 model ensembles of the posterior parameter PDFs (red line), using observations with a daily temporal sampling interval and a random Gaussian error of 0.05gCm^{-2}d^{-1}. The mode is compared to the true flux (blue line), the observations used to constrain the parameters in the Bayesian inversion and the "inaccurate" model with the incorrect amplitude and phase of the annual cycle, used in the Bayesian inversion (black line).

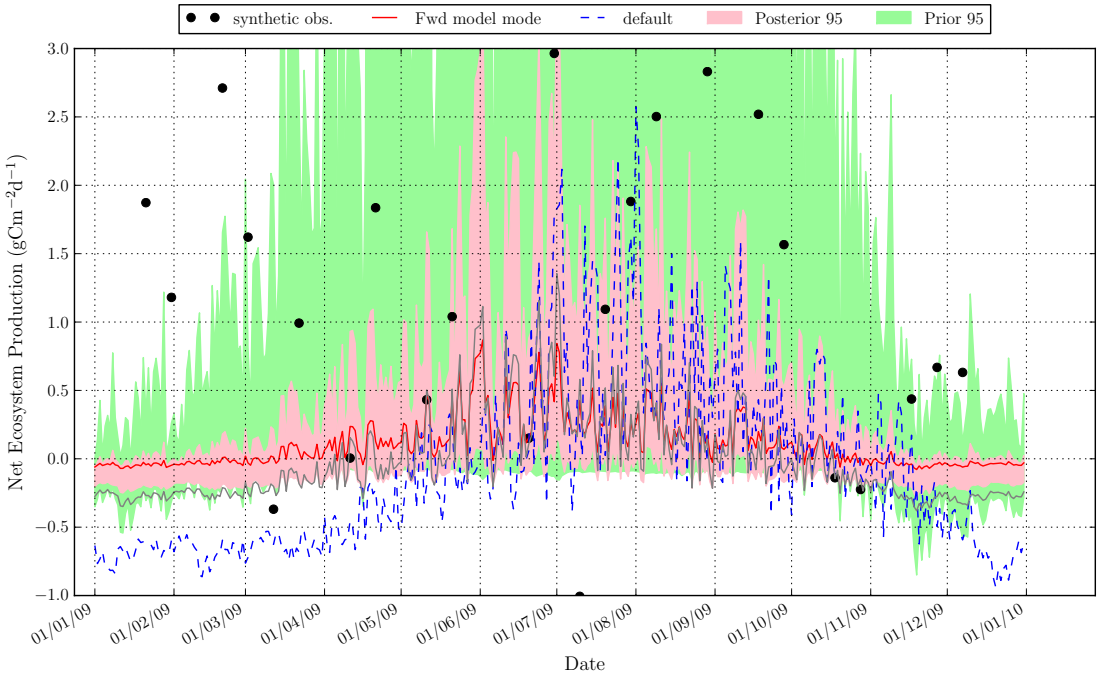

Figure 8.10: A 'zoomed-in' view of the forward modelled NEP flux from 500 model ensembles of the posterior parameter PDFs (red line), using observations with a temporal sampling interval of ten days and a random Gaussian error of 2.0gCm^{-2}d^{-1}. The mode is compared to the true flux (blue line), the observations used to constrain the parameters in the Bayesian inversion and the "inaccurate" model with the incorrect amplitude and phase of the annual cycle, used in the Bayesian inversion (black line).

8.4.3 RMSD between the forward mode and the true flux

The RSMD ranges from 0.4 to 0.8gCm^{-2}d^{-1}, for the "best-case" observational characteristics where the parameters and forward model are well-constrained. The range is ~0.4gCm^{-2}d^{-1} higher than for the previous NEP model error experiment with just an inaccurate representation of the magnitude of the flux.

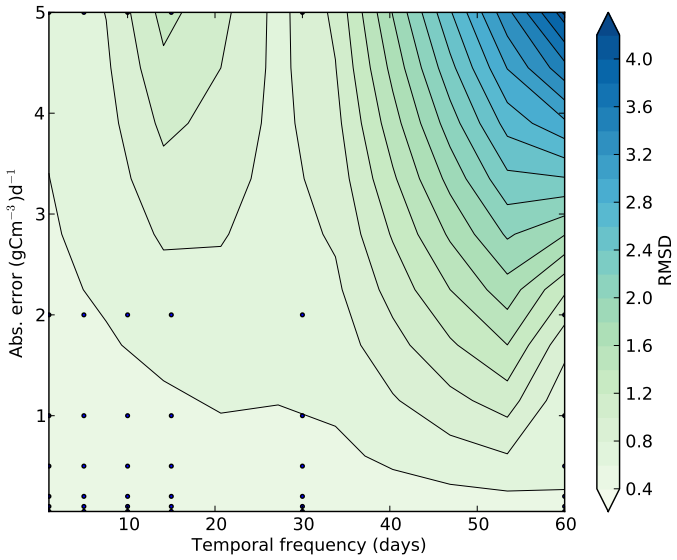

Figure 8.11: The RMSD between the daily forward modelled NEP flux mode and the true flux value for all observational characteristics. The "inaccurate" model used in Bayesian inversion resulted in the incorrect amplitude of the annual cycle but the synthetic observations were produced from the "true" flux.

8.4.4 Annual NEP

Although the daily forward mode clearly does not accurately reproduce the true flux as well, the bias between the annual flux MAP estimate and the true value ranges between ~-15 to 16gCm^{-2}d^{-1} for those observational characteristics which result in good parameter constraint, which is lower than for the same observational characteristics in the previous experiment.

8.5 Discussion

8.5.1 Ability of the observations to account for an error in the model used in the Bayesian inversion

The main finding of the experiments in this chapter is that a shift in the parameter PPDF, conditioned on the prior and observations derived from the true (new, "accurate") flux, may well be able to account for an error in the amplitude of the annual C cycle in the model which consitutes a change in the magnitude of the resultant C fluxes. However the parameters cannot reproduce a change in the temporal trend or shift in the phase of the annual cycle. This can be hypothesised from the sensitivity analysis, which showed that a change in parameter values mostly resulted in a

shift in the magnitude of the fluxes, but not a change in the annual temporal trend. The results of the OSSE add weight to this hypothesis.

A change in the magnitude of the flux as a result of structural error in the model could also be thought of as analgous to a bias in the observations. As seen in Chapter 7 the parameters cannot always account for a bias in the observations; it depends upon the sign and magnitude of the bias and the effect of the parameters on the model state variables. The C fluxes are sensitive to many parameters, and therefore it is possibly more likely that some of the parameters will be able to account for some of the change in magnitude of the flux.

It is interesting that the behaviour of the parameters is much the same. The inversion results in well-constrained parameters (for observations with a low uncertainty) but is unable to reproduce the true flux. It might be expected that a poorly estimated C flux might result from poorly-constrained parameters. There are two possible reasons why this might not be the case. Firstly, the error in the model only affects parts of the year. The amplitude of the annual trend is larger, and the flux remains high later in the year than the original model, but between the middle of April and the end of July, and in August the fluxes are a similar magnitude.

Secondly, differences between the inaccurate model trajectory and the observations derived from the true flux sometimes smaller than the change in flux as a result of the sensitivity of the parameters. The wide prior 95% confidence interval of the NEP is testament to that. The OAT analyses showed for example that the NEP could reach values of $\sim 17 \mathrm{gCm^{-2}d^{-1}}$ with high LUE values (Chapter 4 Figure 4.12(b)). If interactions with other parameters are included the daily model sensitivity could be even higher. For these two reasons it is not surprising that the parameters are reasonbly well-constrained, despite the error in the model used in the inversion. This demonstrates that good-constraint of parameters does not always lead to an accurate prediction of the daily flux, which is key finding of the experiments in this chapter. Well-constrained parameters result in a narrow forward model 95% confidence interval. It is possible that if a model calibration were performed, a high reduction in the prior uncertainty of the parameters and would give false confidence in the calibration results.

8.5.2 Significance of the RMSD between the forward mode and the true flux

The range in RMSD values between the forward mode and true flux is higher for these experiments than for the original OSSE with NEP fluxes, even for the first experiment where the parameters could account for the model error. However even with the error in the model the range of RMSD values is lower than if CH_4 observations were used to constrain the parameters with the accurate model. The highest value ($0.45 \mathrm{gCm^{-2}d^{-1}}$) is larger than the RMSD between the accurate and inaccurate models, suggesting that for observations with a higher uncertainty and lower temporal sampling interval the RMSD is at least partly due to error in the observations.

The RMSD between the daily forward mode of the NEP flux and the true value in the second experiment show the inability of the parameters to depict the true flux, even with the lowest observation uncertainty. The range is $\sim 0.4 \mathrm{gCm^{-2}d^{-1}}$ higher than the first experiment with just an inaccurate representation of the magnitude of the flux. Given the true mean daily NEP flux in both experiments is close to zero but negative, the RMSD values (lowest $\sim 0.3 \mathrm{gCm^{-2}d^{-1}}$) could result in a switch of the NEP flux from a source to a sink, as has been found for most other OSSE

experiments.

8.5.3 Significance of the bias the MAP and true annual NEP

The bias in the annual flux MAP estimate for the observations which do result in well-constrained parameters in the first experiment is large (30 to 40$gCm^{-2}y^{-1}$). As the true annual flux is -26.5$gCm^{-2}y^{-1}$ this again, as with most other OSSE experiments is a significant bias and would result in a switch in the annual NEP from a source to a sink. Therefore although the best-case observations do result in the parameters accounting for an error in the C flux magnitude in the model, the annual flux estimate would lead to incorrect assumptions about the net C balance. However this is still not anywhere near as large as the biases found for those observational characteristics that do not constrain the flux, which can be in the hundreds of $gCm^{-2}y^{-1}$ as for other OSSE experiments with C flux observations.

This bias in the MAP estimates of the annual NEP is lower for the "best-case" observations in the second experiment than for the first, despite the fact the forward mode is unable to accurately replicate the true flux. This is because the peak NEP in the summer months is generally underestimated, but the NEP in the winter months is overestimated. Therefore the resultant annual NEP is similar for the inaccurate model and the true flux. At these values the net annual NEP would not switch from a source to a sink, unlike most other OSSE NEP flux results. The highest bias reaches 1125$gCm^{-2}y^{-1}$, which is significant, but again is still lower than found for the annual NEP MAP estimates when the model is constrained using CH_4 flux observations.

8.5.4 Causes of the discrepancy between the forward mode and the true flux

Of course in reality the inability of the model to replicate the true flux may be due to other factors than model structural error. It may be that the priors are too conservative. If so it would be impossible for the observations to constrain the parameters to values that could reproduce the flux. It may also be that the uncertainty in the observations is too small, thereby restricting the inversion. The final alternative is that parameters not included in the calibration will be able to account for the difference between the observations and the model. The sensitivity analysis does not provide a incontrovertible answer to the question of which parameters will or will not result in an accurate model output through parameter constraint. These factors should be looked into before a model structural error is considered. However, if the ensemble runs using parameters sampled from the prior distribution show that the trend cannot be replicated by the model, due to the constraint of the inputs and model physics (which is the case here) it will be clear that the mismatch between the observations and the model is due to an error in the model.

8.5.5 Identification of an inaccurate forward mode using real observations

Although in the synthetic experiments where the "true" flux is known it is obvious when the forward model does not correspond well to the true flux, the results of the OSSE have shown that in reality a possible model error can be inferred or identified when the forward model, constrained with observations with a low uncertainty, does not match the temporal trend of the observations. However, if the observation error is larger than the model error it will not be clear whether the

difference between the model and the observaitons is due to an error in the model or the error in the observations, and resultant unconstrained parameters.

8.5.6 Solutions to the problem of an inaccurate forward mode

As discussed above, widening the prior distributions of parameters for which there is little information and only narrowing the prior for the most sensitive parameters. This might result in a better replication of the true flux. If the inversion results in parameter MAP estimates which are unrealistic, or are physically impossible, this would reveal the presence of model deficiency. Another possible method of dealing with the discrepancy between the model and the true flux would be to relax the observation uncertainty. This would probably result in less well-constrained parameter PPDFs, but as a result the model uncertainty might be high enough to encompass the true flux.

Several recent studies have investigated including model and/or driver "error parameters" within the Bayesian Total Error Analysis (BATEA) framework (*Thyer et al.*, 2009; *Renard et al.*, 2010; *Salamon and Feyen*, 2010). These sophisticated studies show that it is possible to identify systematic biases in the model and as a result the model predictive error can be better estimated. This would clearly be useful if it is not apparent which processes or combination of processes are causing the model error as the model error parameters can be placed in different places in the model. However the hydrological models used in these studies are relatively simple compared to typical C flux models and the data used to constrain them are more widely available. In order to make this work well a different model error parameter is needed for each timestep, which would result in a large increase in the number of parameters to be calibrated. For a more complex model this is likely to be too difficult to achieve without a faster method of calibration than the Bayesian inversion. In addition the correlations between the parameters might be prohibitively complex to provide a meaningful estimate of the model uncertainty.

8.6 Conclusions

The main findings of the experiment in this chapter are summarised as follows:

- A shift in parameter values as a result of the calibration may be able to account for an error in the magnitude of the C fluxes, but not a change in the temporal trend.
- Good parameter and forward model constraint can give false confidence to the calibration results.
- The inability of the model to replicate the true flux can be identified if the observation uncertainty is low and the 95% confidence interval does not coincide with the observation error. This suggests the parameters being used in the calibration cannot account for the difference between the model and the observations, or that there is another issue that is hampering the ability of the inversion, such as insufficient prior distributions or observation uncertainty, or a model deficiency.

These OSSE experiments are very useful in demonstrating the impact of model error for this model, and the implications for using observations to constrain model parameters under the as-

sumption of a perfect model. It also highlights how the Bayesian inversion can be used to identify model error, proving again that the OSSE is a powerful tool. To my knowledge, an OSSE framework has not been previously been used to test the impact of unaccounted-for model error on the calibration of a C flux model.

Chapter 9

Application of the Bayesian model calibration framework to the Lake Vyrnwy site

9.1 Introduction

The aim of this chapter is to test the ability the Bayesian inversion to constrain the parameters of the CASA-CH_4 model with real data, where available, for the Lake Vyrnwy site. Conclusions drawn from OSSE studies are used to aid the interpretation of the results of the calibration.
The following questions will be addressed in this chapter:

1. Do the available observations for the Lake Vyrnwy site have the required characteristics (uncertainty and temporal sampling interval) as prescribed by the results of the OSSE studies?

2. Are the CH_4 flux, NEP and soil moisture observations able to constrain the parameter posterior distributions, and does this result in forward model ensembles which replicate the observations?

3. How well do the CH_4 flux observations from each of the three locations at the Lake Vyrnwy site compare, in terms of constraining the parameters, and replicating the observations at the other two locations?

4. What is the range in the magnitude of the annual net CH_4 flux and NEP, and the uncertainty estimates of both C fluxes, across the site? Is the site a net source or sink of C?

5. What are the factors controlling the variability of CH_4 flux and NEP across the site?

The experimental set-up of this chapter is outlined in the following section. Following this the OSSE results from previous chapters are used to decide whether the available observations have an adequate sampling interval and a low enough error to be used in the model calibration. Those observations that do meet the requirements are then used to constrain the model using the Bayesian inversion for each location where measurements were taken at the site. The parameter and model

constraint of each location is compared and parameters constrained at one location are used to run the forward ensembles at another, in order to determine how widely applicable the calibration is. Finally the inversion is repeated with the CH_4 flux, NEP and soil moisture observations, in order to obtain the best estimate, with the 95% confidence interval, of the daily variability in the NEP and CH_4 fluxes for the Lake Vyrnwy site. Annual flux maps for 2009 are also produced for the whole site and the possible causes of spatial variability are considered.

The issues arising from using ground-truth and satellite observations to constrain the parameter and model estimates for the Lake Vyrnwy site are discussed at the end of the chapter. The implications of using this framework for other peatland sites is also discussed. The wider context of the C flux estimates obtained for this site are considered. Finally the conclusions drawn from the experiments in this chapter are summarised.

9.2 Experimental set-up

The Bayesian inversion algorithm used to calibrate the model was described in Chapter 3 Section 3.6. The real observations (ground-based NEP and CH_4 fluxes and satellite-derived soil moisture estimates) that were available to calibrate the model at the Lake Vyrnwy site are described in Chapter 3 Section 3.8. The same parameters were constrained by each type of observation as in the OSSE studies and summarised in Chapter 3 Table 3.4 and in the experimental set-up sections of each OSSE chapter, and are repeated here for clarity (Table 9.1). The prior distributions are again the same as used in the OSSE experiments. Please refer to the experimental set-up sections of each OSSE chapter for the minimum and maximum values of the prior distributions for each parameter. The only two exceptions are the prior distributions of the rdr parameters, as the results of Chapter 7 Section 7.4 showed that narrower distributions resulted in better parameter constraints when observations with a higher uncertainty and lower temporal sampling interval were used in the inversion. In the experiments detailed in this chapter a prior distribution of U(1.81e-24,0.7) was used for the rdr_a parameter and U(-15.0,-3.41) for rdr_b parameter.

Soil moisture	**CH_4 flux**	**NEP flux**
porosity	Q10_l	Q10_l
rdr_a	Q10_s	LUE
rdr_b	LUE	SR_max
wilting point	porosity	porosity
	Me_s	auto. resp.
	Me_l	
	LN ratio	
	lignin frac.	
	SR_max	
	inund. ratio	
	auto. resp.	

Table 9.1: The parameters chosen to be included in the Bayesian inversion for each observation type, based on the sensitivity of the model outputs relating to each observation type to the model parameters.

The same outputs are used to describe the results of the inversion as was detailed in Chapter 3 Section 3.7.1.

9.3 Data requirements

In this section each type of observation (CH_4 flux, NEP and soil moisture) is discussed in terms of whether the observation uncertainty and temporal sampling interval are adequate for constraining the parameters of the CASA-CH_4 model. The required characteristics were determined from the results of the OSSE studies in Chapter 5 for CH_4 flux observations, in Chapter 6 for NEP observations, and in Chapter 7 for soil moisture observations.

9.3.1 Ground-based CH_4 observations

The ground-based CH_4 flux observations collected at three locations (Eunant, Hafod and Hirddu - see Figure 9.1) at the Lake Vyrnwy site were presented and discussed in Chapter 3 Section 3.8.1. The OSSE results for the parameter constraint using CH_4 flux observations (Chapter 5), showed that for observations with a temporal sampling interval of 30 days (as is the case with the available observations), the highest error that resulted in a well-constrained and accurate forward model mode was $0.01 gCm^{-2}d^{-1}$. Some of the highest fluxes, particularly for the Hafod location, have SEM estimates which are higher than this threshold. Only observations with a low enough SEM were therefore used in the Bayesian calibration of the CASA-CH_4 model. This resulted in the exclusion of observations in January for the Hirddu location, and January, June and August to November, inclusive, for the Hafod location. All the observations were included for the Eunant location.

There is an issue with the fact the variance of the CH_4 flux measurements scales with the magnitude of the flux. In the absence of data that could provide a thorough error characterisation of these data, as in *Savage et al.* (2008), it is assumed the data are normally distributed, and independent, and therefore it is appropriate to use a Gaussian likelihood in the Bayesian inversion. Even if the random errors in the observations did have a Laplacian distribution, as found in some studies (e.g. *Savage et al.* (2008)), no study has yet provided a full error analysis of both the systematic and random errors, and the potential changes in the error distribution from scaling over a longer temporal time period. *Richardson et al.* (2010) assumed that random errors in eddy covariance data, which studies show have a Laplacian distribution (e.g. *Hollinger and Richardson* (2005)), would be approximately normal when integrated over half a day.

However, another issue that arises from having higher errors associated with a high flux magnitude is the fact that observations representing the peak fluxes in the summer/autumn months cannot be used due to their high associated uncertainty. Either the high flux measurements are used in the Bayesian inversion, which may well result in poorly constrained parameters and modelled CH_4 flux, or they are ignored, which poses a problem in terms of characterising the true peak CH_4 flux and the correct temporal trend, leading to biased model predictions. The second option is chosen for these experiments, as the results of the OSSE show inaccurate parameter and model estimates will result from using observations with errors higher than the $0.01 gCm^{-2}d^{-1}$ threshold. These observations will not add useful information to the Bayesian inversion.

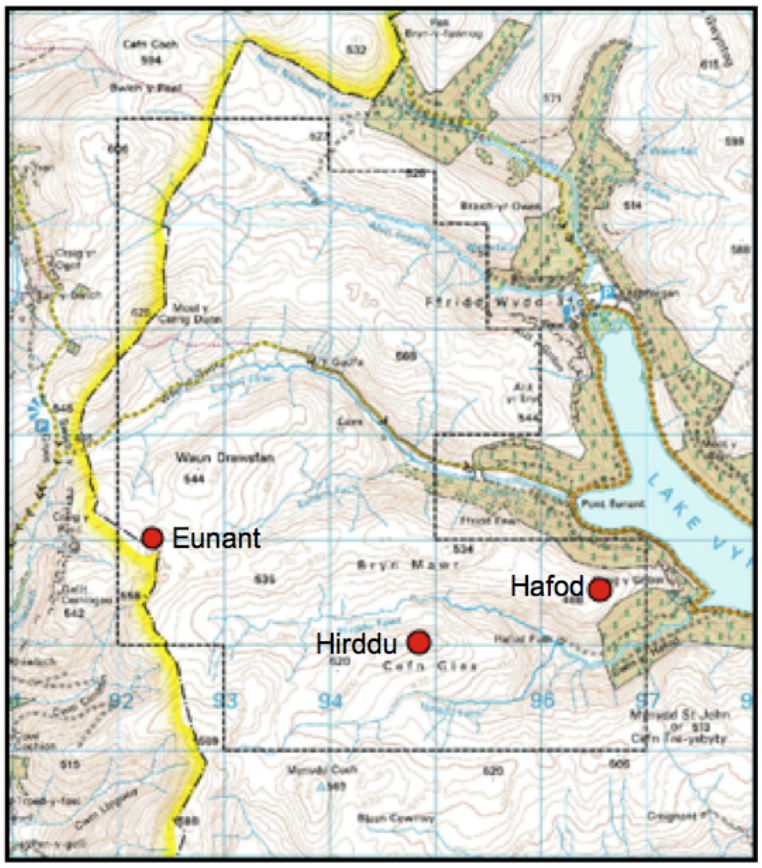

Figure 9.1: Map of the RSPB Lake Vyrnwy Reserve site and the management set-up. Red circles show the locations of the meteorological stations and ground-based CH_4 flux measurements (Section 3.3.6 and Chapter 9).

9.3.2 Ground-based NEP observations

The two available observations of NEP flux the were available from the Lake Vyrnwy site were described in Chapter 3 Section 3.8.2. The OSSE study for the NEP flux observations (Chapter 6), showed that for observations every 60 days the associated error needed to accurately constrain the parameter estimates is <=0.05$gCm^{-2}d^{-1}$. These observations obviously fall sort of that temporal sampling interval and regardless the observation uncertainty (0.0805 and 0.138$gCm^{-2}d^{-1}$) is higher than the required value. This is unfortunate as properly gap-filled flux tower data would provide a more continuous and better estimate of the daily NEP flux as measurements are taken every half hour. In addition, the OSSE results showed it would be better to have NEP flux observations, with the required observation characteristics, than CH_4 flux observations for constraining both fluxes, as the CH_4 flux did not result in good constraint of the NEP forward mode. The inversion was run with these observations regardless to confirm and show their inadequacy.

The footprint of the flux tower which collected the NEP flux measurements is not currently known. In future this can be calculated using footprint modelling approaches, which are reviewed in *Schmid* (2002). It was located closest to the Eunant location, which was approximately WSW. The main wind direction at the site is SW. The NEP observations are used to constrain the model using the meteorological and NDVI inputs from all three locations.

9.3.3 Satellite soil moisture data

AMSR-E data

The AMSR-E volumetric soil moisture data are described in Chapter 3 Section 3.8.3. The OSSE results using volumetric soil moisture observations in the Bayesian inversion (Chapter 7 Section 7.3), showed that for un-biased volumetric soil moisture observations, daily observations with an accuracy of <=0.06m^3m^{-3}, or observations with a temporal sampling interval of 5 days with an accuracy of <=0.04m^3m^{-3}, were required to accurately constrain all of the soil moisture parameters of the CASA-CH_4 model. The temporal sampling interval of the AMSR-E data are typically one to two days, though there are some larger gaps in the dataset. As the specified error is within the limits required for daily observations, it is not clear whether these data will be adequate to constrain the parameter estimates but they are used in the inversions nonetheless.

However as discussed in Chapter 3 Section 3.8.3 the satellite data contain a bias, which needs to be taken into account in the likelihood of the Bayesian inversion if parameters are to be correctly estimated. This was demonstrated in Chapter 7 Section 7.5. The magnitude of the bias was calculated using the available ground-based observations, and amounted to a mean value of -0.356m^3m^{-3} (Chapter 3 Figure 3.14(b)). The ground-based data were only available for the summer months however, so it is unclear as to whether this estimate of the bias in the satellite observations would be accurate for soil moisture observations at other time periods. The annual trend of the AMSR-E data is shown in Chapter 3 Figure 3.14(c). Generally higher values are seen in the winter months, but that is also expected of the ground-based data, as the evapotranspiration decreases in the winter months. Given the relatively good correlation between the satellite and available ground data it is assumed the bias is static throughout the year and can therefore be used to correct for the bias in the satellite observations in the likelihood.

9.4 Results of the CASA-CH_4 model calibration at the Lake Vyrnwy site using each type of observation

The previous section detailed the observations that can be used constrain parameter estimates using the Bayesian inversion. The next three sections focus on the results of the calibration using each different type of observation.

9.4.1 Bayesian inversion using CH_4 chamber measurements

As observations were available for each of the three different weather stations across the Lake Vyrnwy site (Eunant, Hafod and Hirddu), three different MH MCMC runs were set up with each timeseries. The ability of the observations from each site to constrain the parameters were compared as were the parameter PPDFs from each site.

Parameter PPDF

The parameter PPDFs from each site are shown in Figure 9.2, Figure 9.3 and Figure 9.4 respectively. Table 9.2 shows the MAP estimate together with the posterior 95% confidence interval and the reduction in 95% confidence interval for all the parameters for each location.It is interesting how different the parameter PPDFs are for each location based on the information in the observations. If the uncertainty in the observations is very small the parameters are tightly constrained as the observations act as a strong constraint on the possible parameter values. This is seen for the parameter PPDFs using observations from the Hirddu location. The inundation ratio is well-constrained (>90%) at the lower end of its range for all sites as many of the winter CH_4 observations are very close to zero. The only other parameter that are exhibit significant change in their posterior distribution with respect to the prior for the Eunant location is the Me_s parameter. The lignin fraction, lignin-to-nitrogen ratio, Me_l, porosity and Q10_s parameters also show reasonable change in their posterior distribution (>50% reduction in 95% confidence interval) at the Eunant location, with the remainder being poorly constrained. The observations from the Hirddu location result in most parameters being well-constrained, only the porosity and lignin-to-nitrogen ratio are less well-constrained, but both show reductions of >77%. Most of the parameters at the Hafod location are not well-constrained, except for the Me_s and Q10_l parameters. It is interesting how different the parameter PPDFs are for each location based on the information in the observations.

9.4.2 Parameter correlation

The correlation coefficients between the parameters constrained using observations from the Hirddu location show many parameter pairs are very highly correlated (many values of 1.0), owing to the fact that they are all well-constrained (Table 9.3). The most highly correlated parameters are the Q10 parameters, LUE, autotrophic respiration scalar, SR_max, and the microbial efficiency parameters. The observations from the Hafod location result in less well-constrained parameters overall, and therefore the correlation coefficients between the parameters are never >0.5 (Table 9.4).

	Eunant			Hafod			Hirddu		
	MAP	post. 95%C.I.	95%C.I. reduc.	MAP	post. 95%C.I.	95%C.I. reduc.	MAP	post. 95%C.I.	95%C.I. reduc.
Q10_l	16.63	18.09	34.35	2.78	11.89	56.85	13.87	0.02	99.93
Q10_s	28.89	4.74	82.81	25.06	17.58	36.19	27.13	0.09	99.67
lue	0.96	2.73	0.38	0.005	2.83	-3.42	2.4	0.01	99.49
poros	0.97	0.38	59.83	0.09	0.9	5.69	0.005	0.13	85.88
Me_s	0.99	0.06	93.49	0.88	0.48	49.87	0.36	0.05	94.45
Me_l	0.99	0.21	77.61	0.09	0.7	26.25	0.23	0.006	99.32
LN ratio	36.87	12.52	67.06	17.21	36.65	3.54	0.81	8.47	77.7
lignin frac.	0.81	0.44	53.66	0.007	0.95	-0.19	0.89	0.0	99.98
SR max	8.77	2.78	41.58	6.48	4.24	10.65	4.18	0.09	98.07
innund. ratio	0.001	0.0	99.98	0.003	0.08	94.85	0.001	0.0	100.0
auto. resp.	0.36	0.94	1.47	0.12	0.86	10.02	0.73	0.002	99.81

Table 9.2: A summary of the MAP estimate, posterior 95% C.I. and the reduction in uncertainty (%) between the prior and posterior distributions (95% confidence interval) for each parameter and for each site, using CH_4 flux observations.

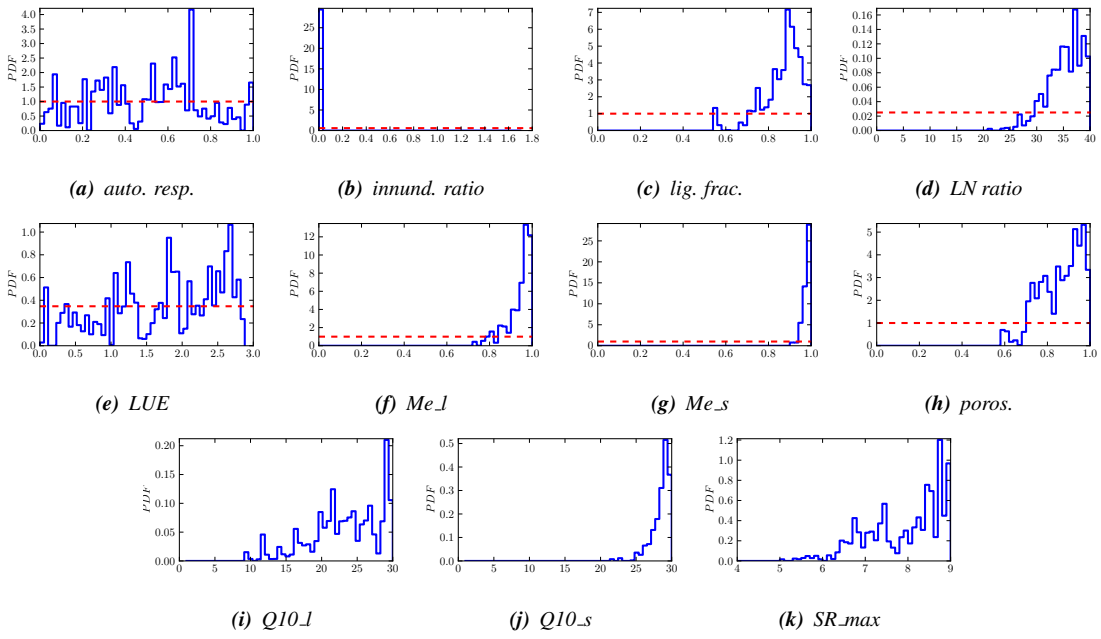

Figure 9.2: The posterior parameter PDFs of the CH_4 flux - sensitive parameters, constrained with CH_4 observations from the Eunant location at the Lake Vyrnwy site.

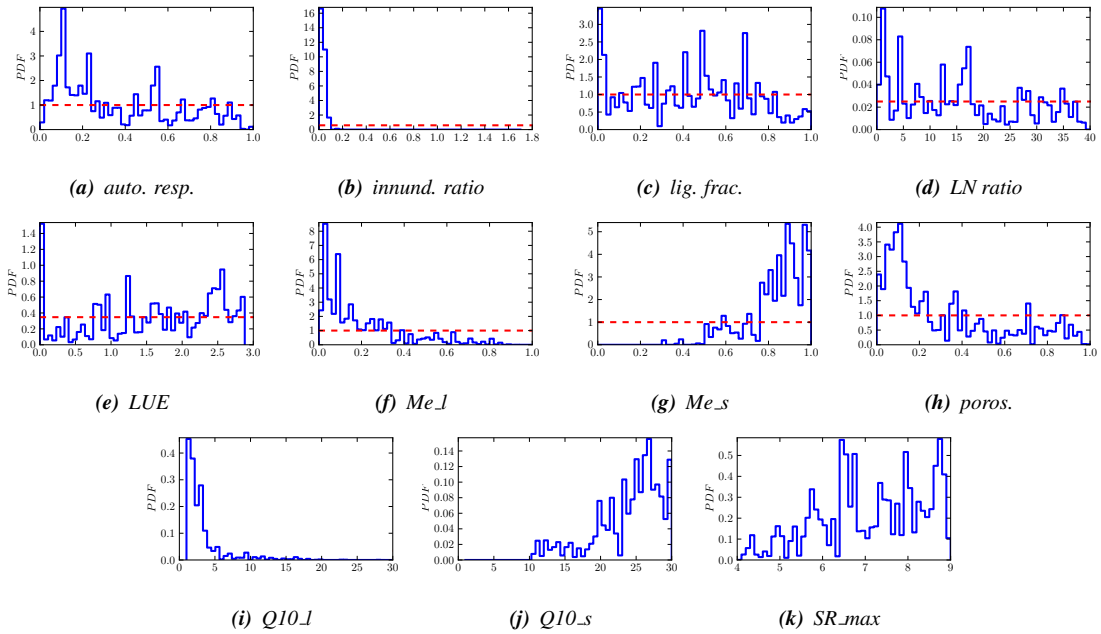

Figure 9.3: The posterior parameter PDFs of the CH_4 flux - sensitive parameters, constrained with CH_4 observations from the Hafod location at the Lake Vyrnwy site.

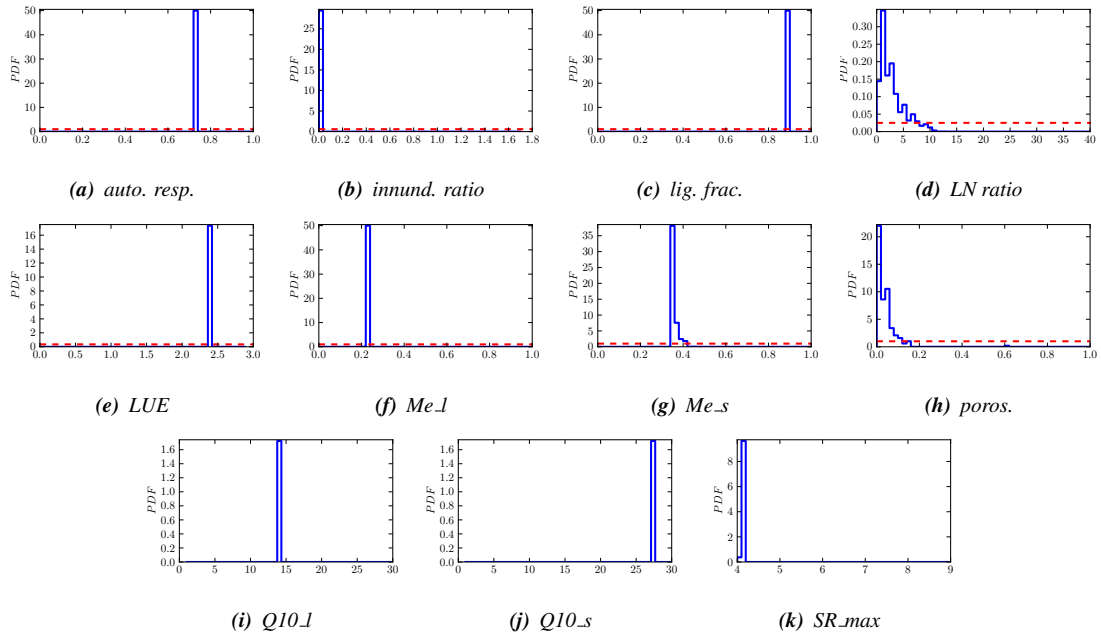

Figure 9.4: The posterior parameter PDFs of the CH_4 flux - sensitive parameters, constrained with CH_4 observations from the Hirddu location at the Lake Vyrnwy site.

	Q10_l	Q10_s	LUE	POROS	ME_S	ME_L	LN_RATIO	LIG_FRAC	SR_MAX	innund_ratio	AUTO_RESP
Q10_l	1.0	1.0	1.0	0.02	1.0	-1.0	0.19	-0.25	-1.0	0.11	1.0
Q10_s	1.0	1.0	1.0	0.01	1.0	-1.0	0.18	-0.20	-1.0	0.11	1.0
LUE	1.0	1.0	1.0	0.02	1.0	-1.0	0.19	-0.28	-1.0	0.11	1.0
POROS	0.02	0.01	0.02	1.0	0.02	-0.02	0.24	-0.10	-0.02	0.04	0.02
ME_S	1.0	1.0	1.0	0.02	1.0	-1.0	0.19	-0.25	-1.0	0.11	1.0
ME_L	-1.0	-1.0	-1.0	-0.02	-1.0	1.0	-0.19	0.25	1.0	-0.12	-1.0
LN_RATIO	0.19	0.18	0.19	0.24	0.19	-0.19	1.0	-0.25	-0.19	0.04	0.19
LIG_FRAC	-0.25	-0.20	-0.28	-0.10	-0.25	0.25	-0.25	1.0	0.25	-0.05	-0.26
SR_MAX	-1.0	-1.0	-1.0	-0.02	-1.0	1.0	-0.19	0.25	1.0	-0.12	-1.0
innund_ratio	0.11	0.11	0.11	0.04	0.11	-0.12	0.04	-0.05	-0.12	1.0	0.12
AUTO_RESP	1.0	1.0	1.0	0.02	1.0	-1.0	0.19	-0.26	-1.0	0.12	1.0

Table 9.3: Parameter Correlations using CH_4 flux observations from Hirddu.

	Q10_l	Q10_s	LUE	POROS	ME_S	ME_L	LN_RATIO	LIG_FRAC	SR_MAX	innund_ratio	AUTO_RESP
Q10_l	1.00	-0.38	-0.06	-0.05	0.15	0.04	0.02	-0.09	-0.12	0.11	-0.00
Q10_s	-0.38	1.00	0.01	0.07	-0.14	-0.02	-0.15	0.21	0.02	0.23	-0.04
LUE	-0.06	0.01	1.00	0.11	0.02	0.23	0.05	0.15	0.10	0.06	0.25
POROS	-0.05	0.07	0.11	1.00	0.17	-0.17	-0.14	0.20	0.05	0.09	0.11
ME_S	0.15	-0.14	0.02	0.17	1.00	-0.14	0.21	0.08	-0.02	0.28	0.05
ME_L	0.04	-0.02	0.23	-0.17	-0.14	1.00	0.15	-0.17	-0.13	0.10	0.16
LN_RATIO	0.02	-0.15	0.05	-0.14	0.21	0.15	1.00	0.14	0.15	-0.06	0.09
LIG_FRAC	-0.09	0.21	0.15	0.20	0.08	-0.17	0.14	1.00	0.18	0.47	0.04
SR_MAX	-0.12	0.02	0.10	0.05	-0.02	-0.13	0.15	0.18	1.00	-0.04	-0.14
innund_ratio	0.11	0.23	0.06	0.09	0.28	0.10	-0.06	0.47	-0.04	1.00	0.28
AUTO_RESP	-0.00	-0.04	0.25	0.11	0.05	0.16	0.09	0.04	-0.14	0.28	1.00

Table 9.4: Parameter Correlations using CH_4 flux observations from Hafod.

CH_4 flux forward mode and model predictive uncertainty

The forward model results, compared to the observation timeseries, provide an insight as to what might be the cause of the poor parameter constraint. Figure 9.5 shows the forward model runs for each location. Observations at the Eunant and Hirddu locations result in a forward model that does not replicate the observation temporal trend. The mode is well-constrained but close to zero, showing limited daily variability.

Observations at the Hafod location were the most incomplete out of all three locations, due to much higher peak fluxes in the months of June and August through to November, inclusive. Figure 9.5(b) shows the observations that were included in the Bayesian inversion in black and those that were excluded in grey. As discussed in Chapter 3 Section 3.8.1, the observations at the Hafod location show an increase in the CH_4 flux at an earlier time in the year compared to the Eunant and the Hirddu locations. The CH_4 flux at the beginning of June is positive, unlike the corresponding observation at the Eunant and Hirddu locations. This corresponds more closely to the peak in the modelled CH_4 flux than the other two locations. Also there is a decrease in the flux at the end of July at the Hafod location which does not correspond with the general increase in CH_4 over the summer. This observation also corresponds more closely to the temporal trend of the model than the other two locations. As a result the forward mode from model runs using parameters constrained with the observations from the Hafod location is generally greater than zero and shows a much higher daily variability than the forward model mode of the other two locations. As the peak observations were excluded from the set of observations that were used in the Bayesian inversion, the remaining observations appear to have a similar temporal trend as the model, but clearly the peak fluxes are significantly underestimated by the forward mode. The

forward model mode is unable to replicate the true temporal trend of the observations, as shown by the grey observations, and the results from the Eunant and Hirddu locations suggest that even if these observations had been included the temporal trend would not be accurately modelled due to the error in the model trend.

If the parameter PPDFs from the Hafod location are used to run an ensemble of 500 forward model runs for the Eunant and Hirddu location, and then compared with the observations, the forward model mode corresponds quite closely to that of the observations (Figure 9.6). This is a very interesting result, given the parameters constrained using the correct observations for each location do not result in a forward mode which closely corresponds to the observations. The temporal trend is still inaccurately modelled, with the peak in the forward model corresponding to times when the observations show a negative CH_4 flux at both locations.

RMSE and correlation coefficient between the forward mode and observations

The correlation and RMSE values between the forward model mode and the observations is shown in Table 9.5. Table 9.6 shows the same for the forward model runs using the parameters constrained using observations at one location with the observations from the other two locations. This correlation is highest at the Hafod site. Overall, considering both the correlation and RMSE, the parameters constrained with the Hafod observations produce a better fit to the other two locations than either Eunant or Hirddu.

	Eunant	**Hafod**	**Hirddu**
Correlation	-0.030	0.650	0.340
RMSE	0.013	0.015	0.017

Table 9.5: The correlation coefficient and root mean squared error between the forward model mode and the CH_4 flux observations from the site used in the MH MCMC algorithm.

	Eunant		**Hafod**		**Hirddu**	
	Hafod	Hirddu	Eunant	Hirddu	Eunant	Hafod
Correlation	0.630	0.320	0.460	0.220	0.030	0.670
RMSE	0.025	0.018	0.013	0.014	0.012	0.024

Table 9.6: The correlation coefficient and root mean squared error between the forward model mode and the CH_4 flux observations from the two sites not used in the MH MCMC algorithm.

These results suggest the parameter PPDFs from the Hafod location are therefore most likely, with the available CH_4 flux observations, to accurately model the CH_4 flux across the site, all the while acknowledging the fact that clearly some areas of the Lake Vyrnwy site have higher CH_4 flux and this will not be accurately modelled with the CASA-CH_4 model.

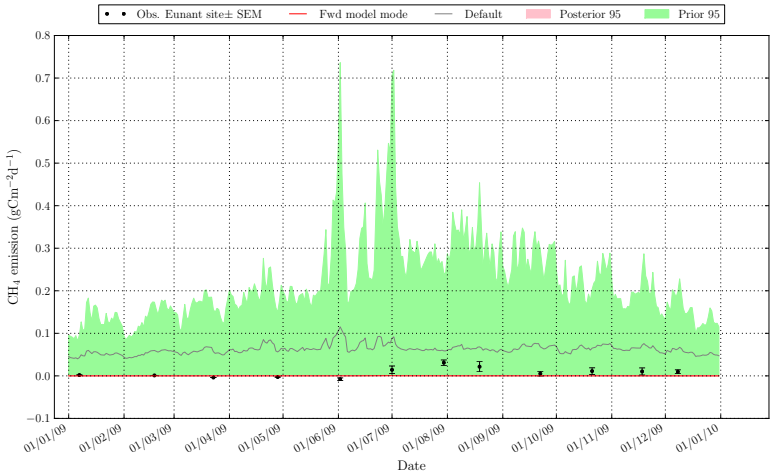

***(a)** Eunant*

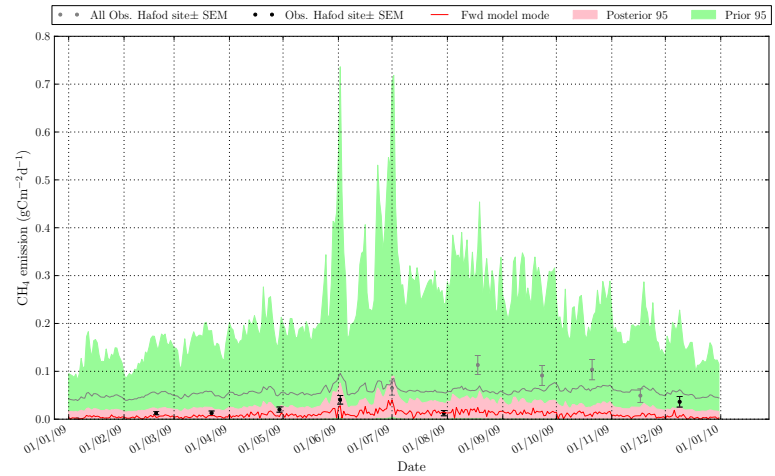

***(b)** Hafod*

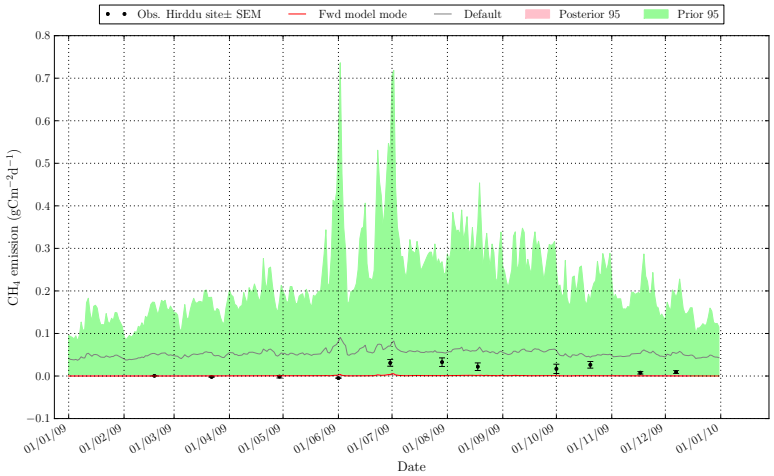

***(c)** Hirddu*

Figure 9.5: Plots showing the forward model mode and 95% confidence intervals of 500 model runs using the posterior parameter PDFs derived from the Bayesian inversion using CH_4 observations from each location at the Lake Vyrnwy site. The forward model runs are compared to the prior 95% confidence interval, the model run with the default parameter values and the ground-based flux observations used in the Bayesian inversion (in black) and those excluded from the observation timeseries (in grey).

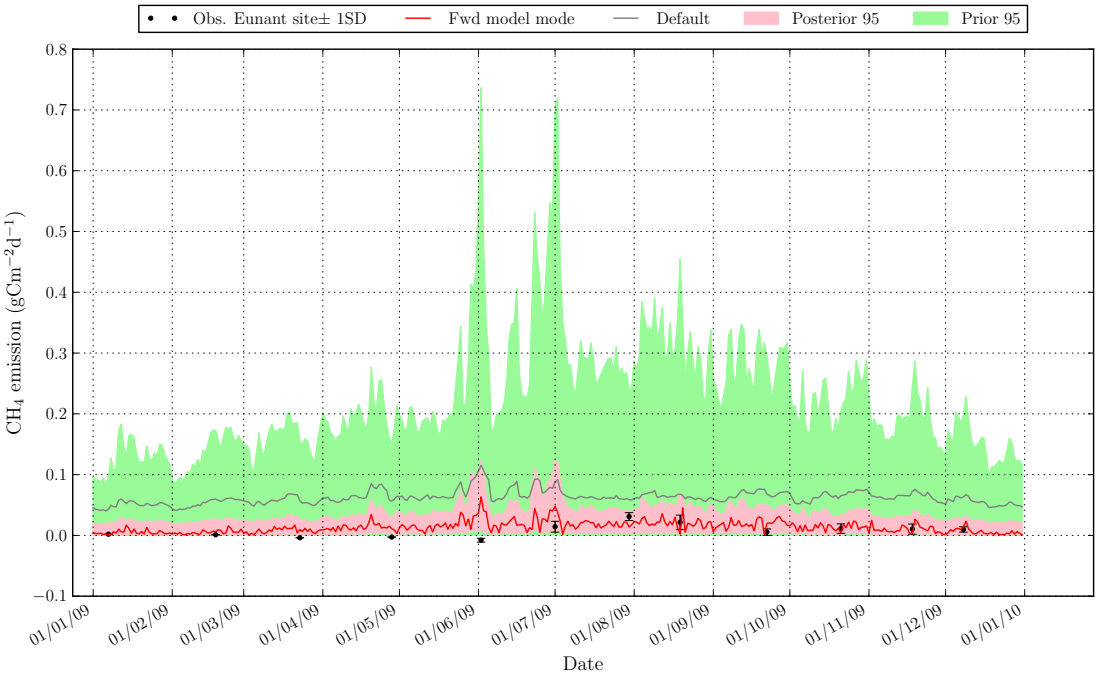

***(a)** Eunant*

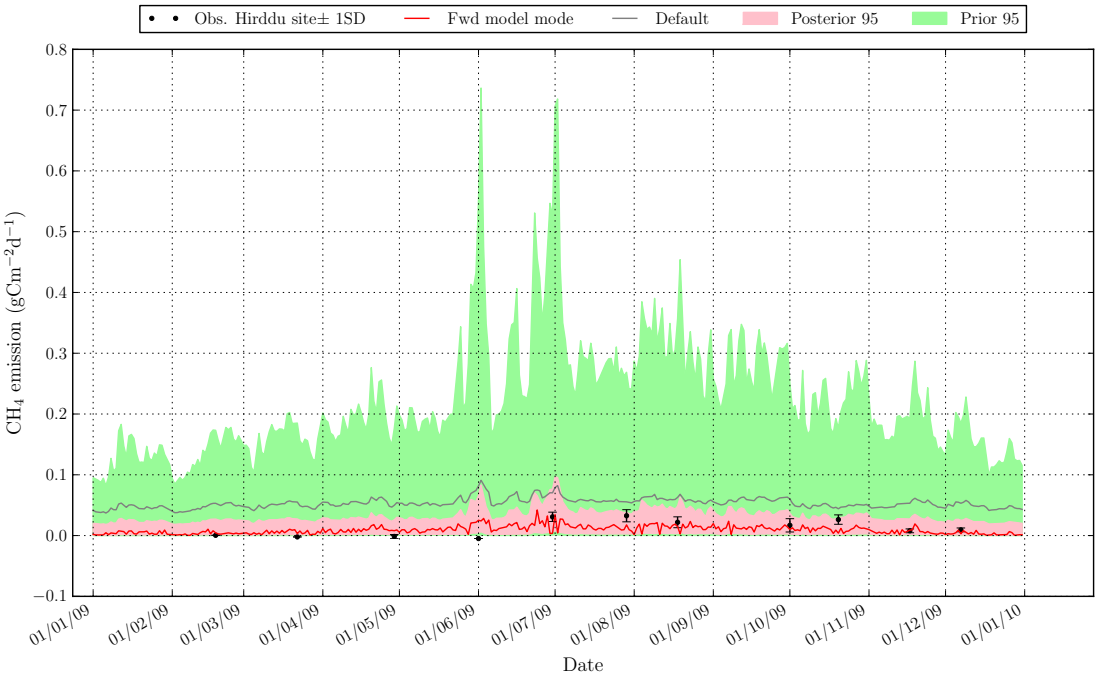

***(b)** Hirddu*

Figure 9.6: Plots showing the mode and 95% confidence interval of the CH_4 net flux from an ensemble of 500 forward model runs for the other two location (Eunant and Hirddu) using the posterior parameter distributions constrained in the Bayesian inversion with CH_4 flux observations from the Hafod location. The forward model is compared to observations from each of the other sites and the model run with the default parameter values and the prior 95% confidence interval.

NEP flux model predictive uncertainty

The forward modelled NEP flux using parameters constrained with the CH_4 flux observations from all three sites showed a very erratic temporal trend with sudden dips in flux in the summer months and wide posterior 95% confidence intervals (e.g. Figure 9.7). None of the sites resulted in a NEP flux which matched the observations, even though there were only two on successive days in August. The posterior distribution is very skewed, therefore the mode lies outside the 95% confidence interval but within the maximum and minimum of the posterior distribution.

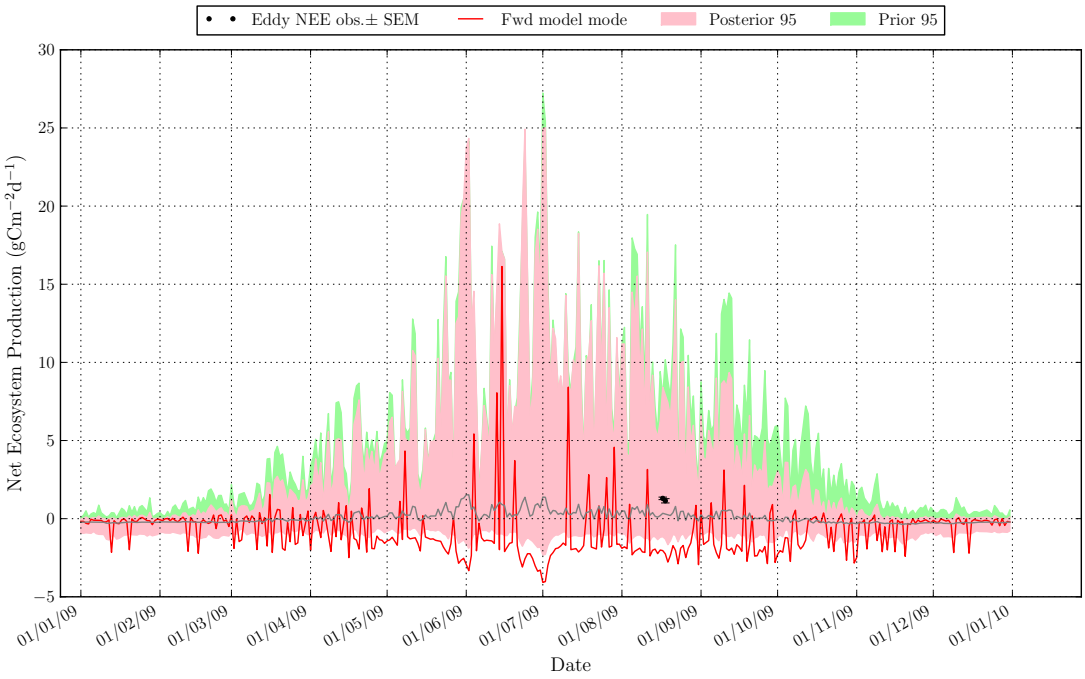

Figure 9.7: Graph showing the mode and 95% confidence interval of the NEP flux from an ensemble of 500 forward model runs for the Hafod location using the posterior parameter distributions constrained in the Bayesian inversion with CH_4 flux observations from the Eunant location. The forward model is compared to observations from each of the other sites and the model run with the default parameter values and the prior 95% confidence interval.

The OSSE experiments showed that CH_4 observations with these characteristics were not useful for constraining NEP flux. The erratic nature of the forward model flux is probably the result of un-constrained parameters, or due to parameters that are constrained to some extent but exhibit biases that result from constraint using CH_4 flux, which has a different sensitivity relationship with each parameter. These CH_4 flux observations cannot be used to constrain the NEP flux for the Lake Vyrnwy site.

Mean daily reduction in uncertainty and annual flux

Tables 9.7 compares the mean daily reduction in 95% confidence interval between the prior and posterior CH_4 and NEP flux for each location. As expected the mean reduction in uncertainty is much lower for the NEP flux, and is deceptively high for the CH_4 flux, given the model trend does not match the observations.

Table 9.8 shows the annual flux metrics (MAP estimate, 95% C.I. and reduction in uncertainty) for all three locations. The NEP posterior 95% confidence intervals are very large, prohibitively so, further proving that the CH_4 flux observations cannot be used to constrain the NEP flux.

	Eunant	**Hafod**	**Hirddu**
NEP	39.610	-32.850	87.120
CH_4	99.940	87.140	99.840

Table 9.7: The average daily reduction in 95%C.I. between the prior and posterior of the forward model ensembles for the NEP and CH_4 flux (using CH_4 flux - sensitive parameters).

	Eunant			**Hafod**			**Hirddu**		
	MAP	post. 95%C.I.	95%C.I. reduc.	MAP	post. 95%C.I.	95%C.I. reduc.	MAP	post. 95%C.I.	95%C.I. reduc.
NPP	31.478	1420.590	21.710	2.281	1772.726	2.300	340.498	1.662	99.910
Soil CO_2	0.151	52.005	56.520	6.396	493.418	-312.550	9.044	155.943	-30.390
CH_4	0.032	0.056	99.930	0.299	10.135	87.210	0.227	0.148	99.810
NEP	-22.238	1419.424	25.000	-688.920	1926.349	-1.790	83.220	156.307	91.740

Table 9.8: A summary of the MAP estimate, posterior 95%C.I. and the reduction in uncertainty (%) between the prior and posterior distributions (95% confidence interval) for each annual C flux and for each site, using CH_4 flux observations.

9.4.3 Bayesian inversion using Eddy Covariance NEP observations

The OSSE results showed that a well-constrained and accurate forward model NEP flux mode was mainly the result of highly correlated, well-constrained but inaccurate LUE and autotrophic respiration scalar parameters. This also resulted in a well-constrained and accurate Q10_1 parameter. None of the parameters are well-constrained by the NEP observations at any location (results not shown), though the autotrophic respiration scalar, LUE and Q10_1 are relatively well-constrained (>50%) for the Eunant location and the autotrophic respiration scalar, porosity and Q10_1 for the Hafod location. The NEP observations were not expected to result in accurate or well-constrained parameters, given their characteristics.

As a result the forward model modes show very erratic temporal variability, despite close correspondence with the two data points, for the Eunant and Hirddu locations, confirming that these observations cannot be used to constrain the model (e.g. Figure 9.8(a)). The results for the Hafod location show less erratic behaviour (Figure 9.8(b)), and therefore could possibly be more reliably used to constrain the NEP flux at the site. As there are only two data points, and the OSSE results showed these observations could not be reliably used, it is unwise to use these data. However combining these observations with CH_4 flux and observations might help to constrain the modelled NEP flux where the CH_4 flux observations alone could not.

9.4.4 Bayesian inversion using both CH_4 and NEP flux observations

As the CH_4 flux observations resulted in an erratic NEP flux forward model mode and given that the NEP flux observations did not have characteristics necessary to constrain the parameters and

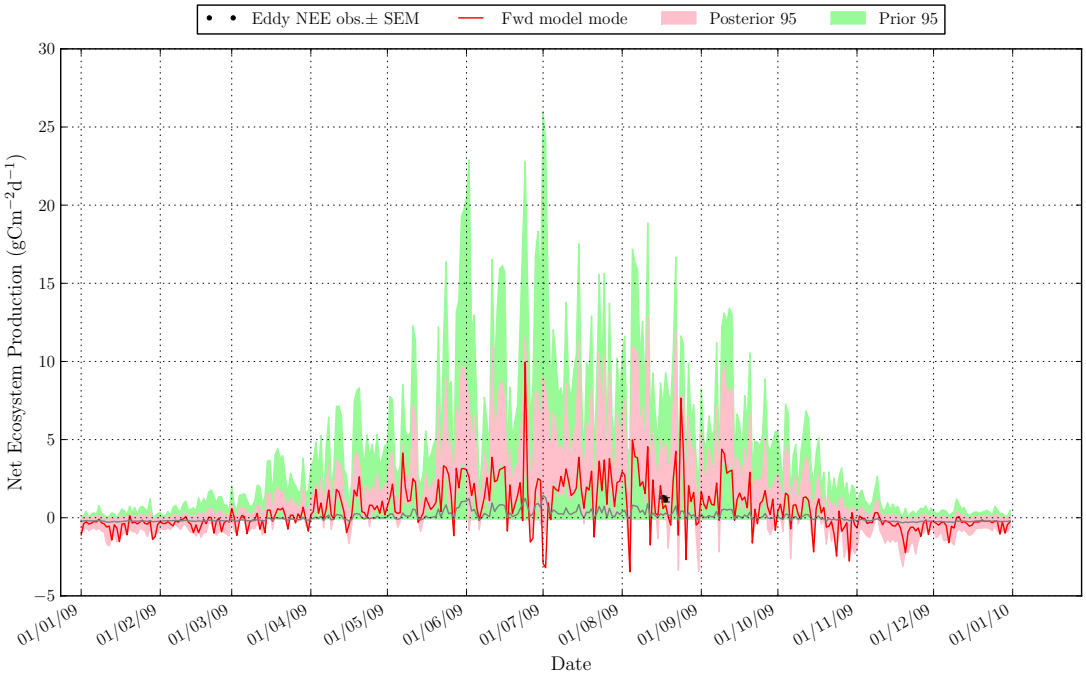

***(a)** Hirddu location*

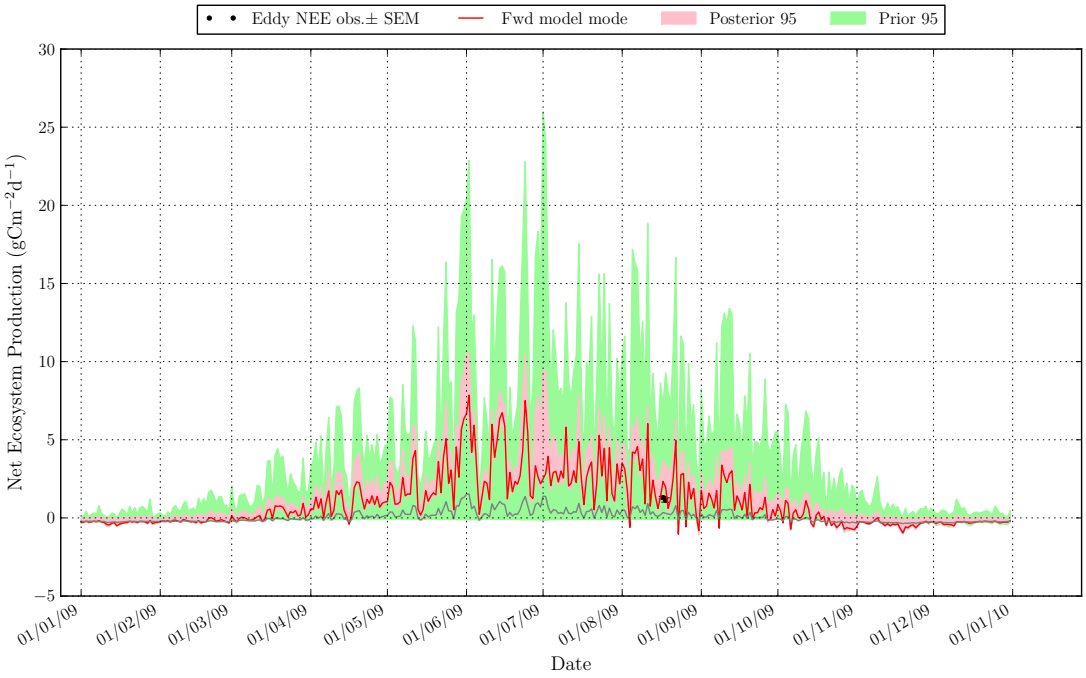

***(b)** Hafod location*

Figure 9.8: Graphs showing the mode and 95% confidence interval of the NEP flux from an ensemble of 500 forward model runs for the Hirddu and Hafod locations using the posterior parameter distributions constrained in the Bayesian inversion with the respective CH_4 flux observations. The forward model is compared to observations from each of the other sites and the model run with the default parameter values and the prior 95% confidence interval.

forward model mode, the inversion was repeated using both CH_4 and NEP flux observations in the Bayesian inversion, assuming the observations are independent.

The results showed a very similar behaviour in the forward CH_4 flux mode but the NEP flux was slightly better defined with the forward mode displaying less erratic behaviour. An example is shown for both fluxes for the Hafod location (Figure 9.9), which as discussed resulted in parameter estimates that best fitted to the observations from all three locations for both the CH_4 and NEP flux. The daily variability in NEP flux still appears quite high, as it did using the NEP flux observations. This is because the NEP flux is dominated by NPP in this model. This has a high daily variability as it is strongly forced by air temperature and solar radiation.

It is clear when comparing Figure 9.9(a) with Figure 9.5(b) that the CH_4 flux behaviour is very similar when using only CH_4 flux observations to constrain the model and when using CH_4 and NEP flux observations. This is because the parameters are very correlated, so new information with a low enough uncertainty results in a shift in the parameter values but the forward model mode remains the same. Comparing Figure 9.9(b)) with Figure 9.7 it is obvious that including the NEP observations in the calibration with the CH_4 flux observations has resulted in a much better defined, less erratic, NEP flux forward model mode.

	Eunant			**Hafod**			**Hirddu**		
	MAP	post. 95%C.I.	95%C.I. reduc.	MAP	post. 95%C.I.	95%C.I. reduc.	MAP	post. 95%C.I.	95%C.I. reduc.
Q10_l	29.662	5.752	79.120	1.517	2.491	90.960	23.863	3.050	88.930
Q10_s	24.790	5.275	80.850	29.621	8.798	68.060	26.535	2.808	89.810
LUE	0.685	0.528	80.700	0.696	1.286	53.020	0.618	0.369	86.520
poros.	0.918	0.258	72.870	0.171	0.219	76.940	0.938	0.053	94.470
Me_s	0.989	0.035	96.270	0.742	0.547	42.460	0.599	0.202	78.770
Me_l	0.960	0.285	69.990	0.950	0.828	12.800	0.721	0.144	84.890
LN ratio	32.136	35.632	6.230	3.166	14.532	61.760	0.101	0.153	99.600
lig. frac.	0.851	0.459	51.670	0.893	0.472	50.330	0.385	0.044	95.410
SR_max	4.276	1.219	74.340	4.039	4.099	13.700	7.825	0.284	94.030
innund. ratio	0.001	0.002	99.900	0.029	0.042	97.420	0.001	0.000	99.990
auto. resp.	0.023	0.406	57.290	0.069	0.615	35.270	0.228	0.166	82.510

Table 9.9: A summary of the MAP estimate, posterior 95% C.I. and the reduction in uncertainty (%) between the prior and posterior distributions (95% confidence interval) for each parameter and for each site, using CH_4 and NEP flux observations.

Combining both C flux observations has resulted in a shift in the MAP estimates of the parameters, particularly the ones to which the NEP is sensitive (LUE, autotrophic respiration scalar, SR_max, Q10_l), as the NEP observations provide a stronger constraint on their PPDFs. This can be seen by comparing the MAP estimates of the parameters in Table 9.9 with Table 9.2. Interestingly the parameters are also better constrained (greater reduction in 95% confidence interval) at all locations, which is to be expected with more information in the observations.

Including NEP observations in the inversion has resulted in higher correlation coefficients between a few parameter pairs, than when the parameters were constrained with CH_4 flux observations from Hafod. The correlation coefficient between the LUE and autotrophic respiration scalar parameter is 0.84, 0.7 for the inundation ratio and Me_s parameters, and -0.65 between the porosity and LUE. The high correlation between the LUE and autotrophic respiration scalar was seen in the original OSSE study using NEP observations (Chapter 6), as the NEP is most sensitive to these two parameters.

Mostly the correlation and RMSEs between the observations are very similar for all locations.

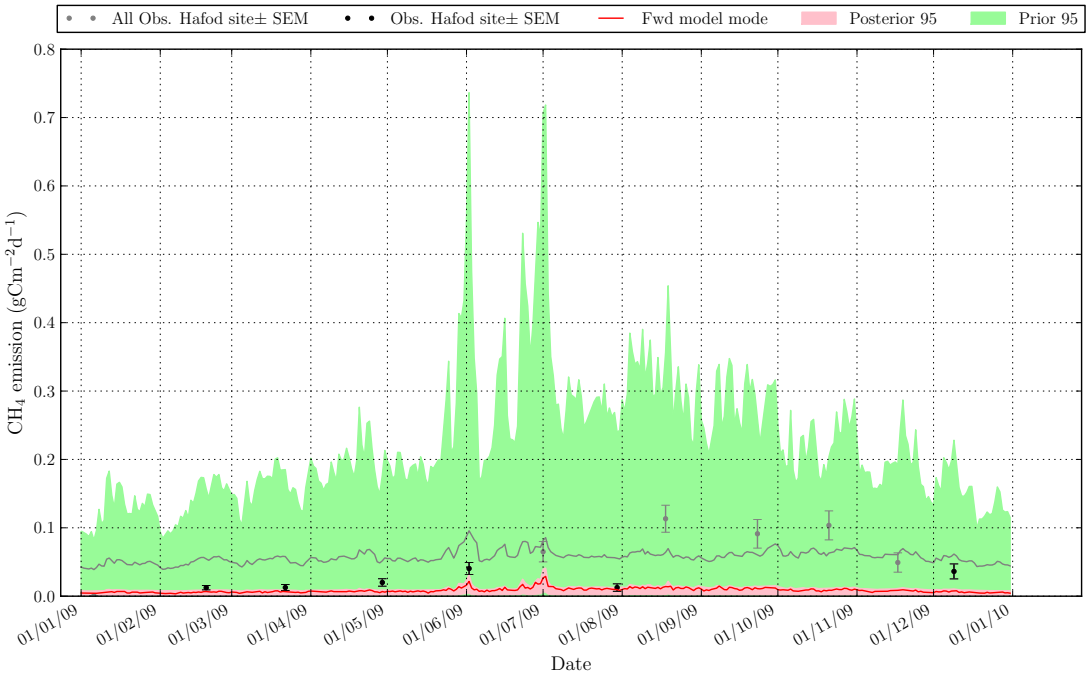

(a)

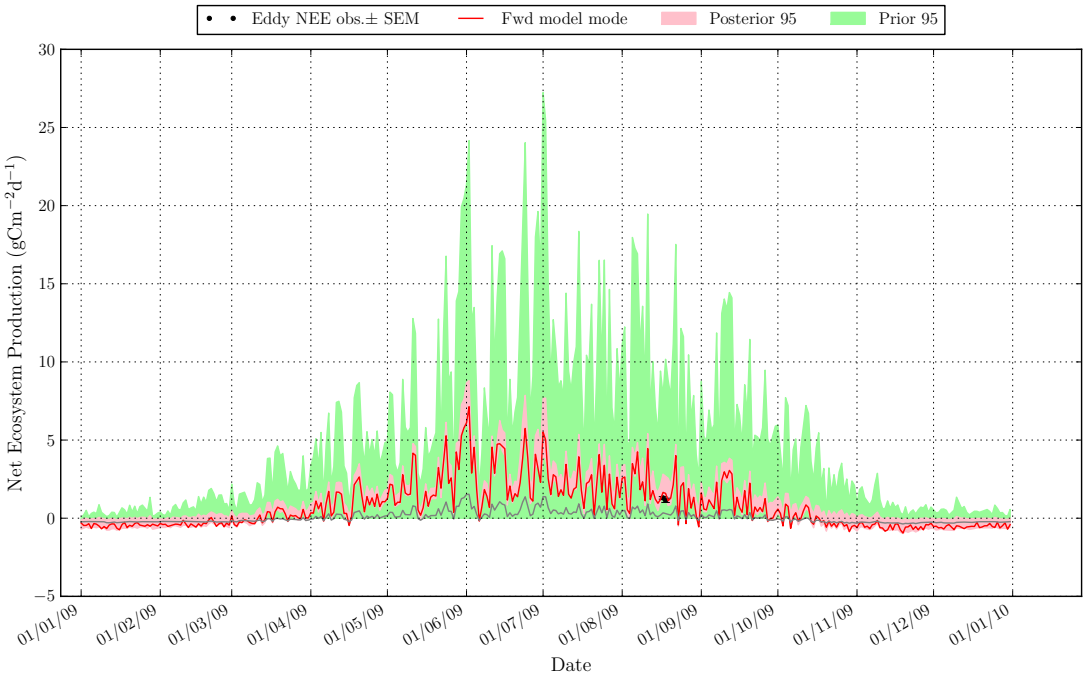

(b)

Figure 9.9: Graphs showing the mode and 95% confidence interval of the CH_4 and NEP flux from an ensemble of 500 forward model runs for the Hafod location using the posterior parameter distributions constrained in the Bayesian inversion with both CH_4 *and* NEP flux observations from Hafod. The forward model is compared to observations from each of the other sites and the model run with the default parameter values and the prior 95% confidence interval.

However the correlation between the Eunant observations and the model ensembles using Eunant driving data and parameters constrained with Hafod observations, is not as not as high and is negative, unlike when only CH_4 observations were used. This is because the lowest, negative observation corresponds to the date where the model peaks at the beginning of July. This is a reminder of the fact that whilst the Hafod observations result in a forward model which corresponds reasonably well with the observations, the trend of the forward mode does not accurately replicate that of the observations. The RMSE errors are still lowest using the Hafod observations when compared to the other locations however.

The outcome of this experiment is positive. The results suggests including the NEP observations provides added information on the LUE, autotrophic respiration scalar and SR_max parameters.

9.4.5 Bayesian inversion using AMSR-E volumetric soil moisture observations

The following sections detail the results of the model calibrated with the AMSR-E volumetric soil moisture observations where the bias was corrected for in the likelihood.

Parameter PPDF

The posterior parameter PDFs for each site and for each parameter are shown in Figure 9.10 and the MAP estimates, 95% confidence interval and the reduction in 95% confidence interval for each site and parameter are summarised in Table 9.10. The porosity was well-constrained and with a MAP value of ~0.9 for all locations. The rdr parameters were not that well-constrained in general, with a range of -1.360 to 48.09% reduction in 95% confidence interval (the highest corresponds to the rdr_a parameter at the Hafod location). Many of the PDFs are skewed toward the lower and upper end of the rdr_a and rdr_b parameter ranges respectively however. MAP estimates for the rdr_a parameter are close to the lower end of the range for the Eunant and Hafod locations and the rdr_b parameter is close to the upper end of the range for the Hirddu location. The OSSE results showed that when the rdr parameters were close to these limits of their ranges the maximum dip in soil moisture following periods of decreased precipitation were modelled correctly, as a large region of the rdr parameter space results in almost no decrease in soil moisture. Dips in soil moisture are expected from both the satellite and ground-truth observations.

	Eunant			**Hafod**			**Hirddu**		
	MAP	**post. 95%C.I.**	**95%C.I. reduc.**	**MAP**	**post. 95%C.I.**	**95%C.I. reduc.**	**MAP**	**post. 95%C.I.**	**95%C.I. reduc.**
rdr_a	0.004	0.65	2.92	0.02	0.35	48.09	0.38	0.53	20.1
rdr_b	-13.59	9.97	9.5	-14.92	11.16	-1.36	-3.52	10.87	1.29
poros	0.93	0.01	98.55	0.92	0.02	98.3	0.92	0.02	98.47

Table 9.10: A summary of the MAP estimate, posterior 95% C.I. and the reduction in uncertainty (%) between the prior and posterior distributions (95% confidence interval) for each parameter and for each site, using AMSR-E volumetric soil moisture observations.

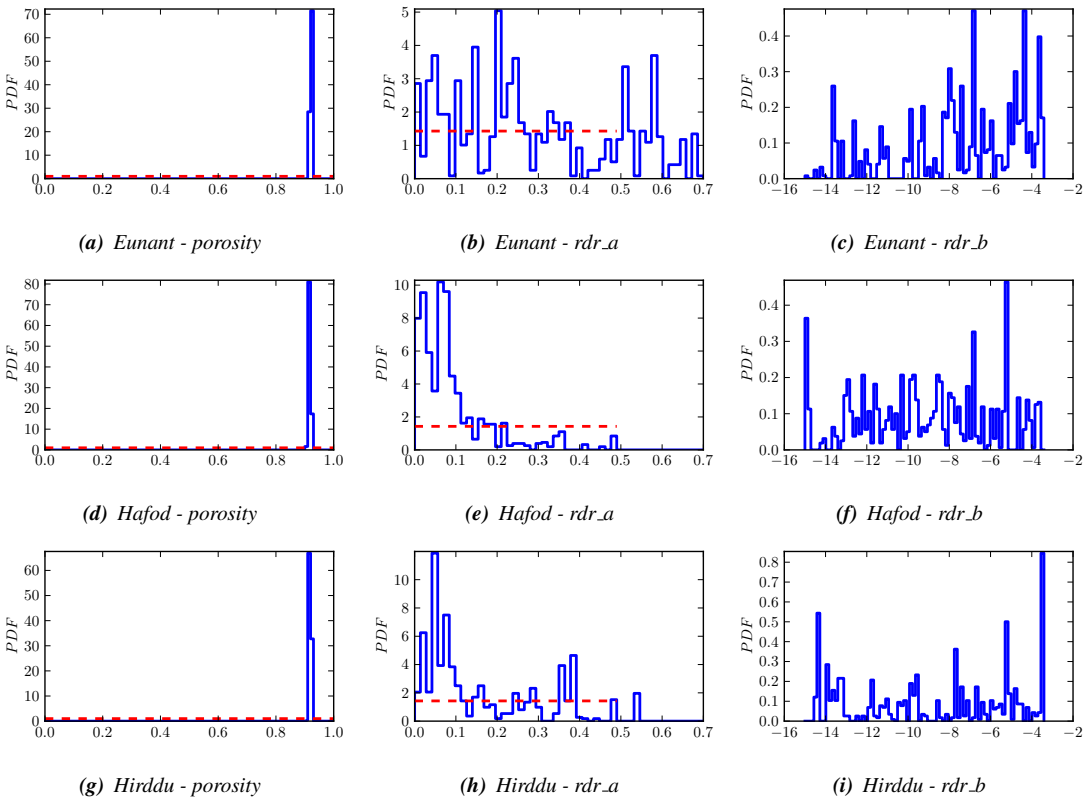

(a) *Eunant - porosity* ***(b)*** *Eunant - rdr_a* ***(c)*** *Eunant - rdr_b*

(d) *Hafod - porosity* ***(e)*** *Hafod - rdr_a* ***(f)*** *Hafod - rdr_b*

(g) *Hirddu - porosity* ***(h)*** *Hirddu - rdr_a* ***(i)*** *Hirddu - rdr_b*

Figure 9.10: Posterior parameter PDFs for each parameter at each location resulting from constraint using AMSR-E volumetric soil moisture observations. The blue line denotes the posterior distribution and the red the prior distribution

Volumetric soil moisture forward mode and model predictive uncertainty

The forward models are only shown for the volumetric soil moisture, as the remaining parameters are still set to the default values in this experiment and therefore the C flux forward models are likely to be incorrect. The forward mode of the volumetric soil moisture is well-constrained for all sites and the constraint of the rdr parameters do result in dips in soil moisture (Figure 9.11). The Eunant location shows the greatest decrease in soil moisture at times of low precipitation, whilst the Hirddu location shows the least. All of the sites correspond very closely to the available ground-truth observations, which is a very promising result. This is only possible because the bias in the AMSR-E observations has been accounted for in the likelihood. This is only possible if ground-truth observations are available. However the satellite data provide the temporal sampling interval required to accurately constrain the parameter estimates. The largest dip in soil moisture at the beginning of July is especially well modelled. The last group of ground-truth observations show a greater variability than is produced by the model, suggesting the processes in the model potentially do not operate on a fast enough timescale, or that the vertical resolution of the model does not match that of the observations.

The correlation between the model and the ground-truth observations is high for all sites, (0.88 and 0.89) and the RMSE between the ground-truth observations and the model ranges from 0.041 to 0.054m^3m^{-3}.

9.5 Daily and annual NEP and CH_4 flux predictions for the Lake Vyrnwy site in 2009

The previous section showed that the AMSR-E volumetric soil moisture observations constrain the porosity and rdr parameters well-enough to produce a model trend which corresponds well to the ground-truth observations. Using both the available CH_4 and NEP flux observations resulted in good constraint of both fluxes, compared to using each type of C flux observation by itself. In order to obtain the best-possible estimate of the daily variability and annual net C flux for the whole site, all three sets of observations (ground-based C flux and satellite-derived soil moisture) were used in the inversion. This included the rdr parameters, which as the results of Chapter 7 showed, are useful in obtaining accurate dips in soil moisture and therefore peak C fluxes. CH_4 flux observations from the Hafod location were used as they resulted in the most accurate replication of the observations for all three locations.

9.5.1 Forward mode and model predictive uncertainty

Figure 9.12 shows the forward mode and predictive uncertainty of the CH_4 flux and NEP respectively. The CH_4 flux at the end of July is slightly higher than when CH_4 flux observations were used, and therefore the mode corresponds more closely to the observation at that time of year. The NEP flux is very similar to when CH_4 flux and NEP observations were used to constrain the parameters, though again the peak NEP is higher at the end of July. The mean reduction in the daily 95% confidence interval is 88.7% for the CH_4 flux and 77.4% for the NEP. The forward model plots for the volumetric soil moisture are not shown as they are very similar to the plots in

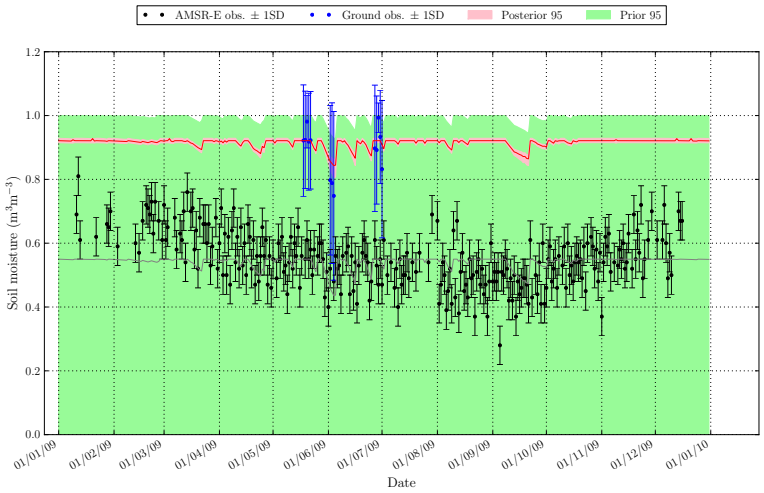

(a) *Eunant*

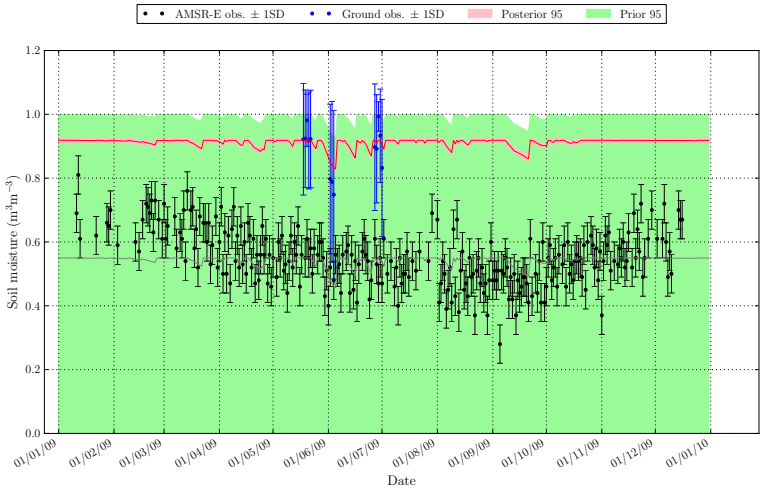

(b) *Hafod*

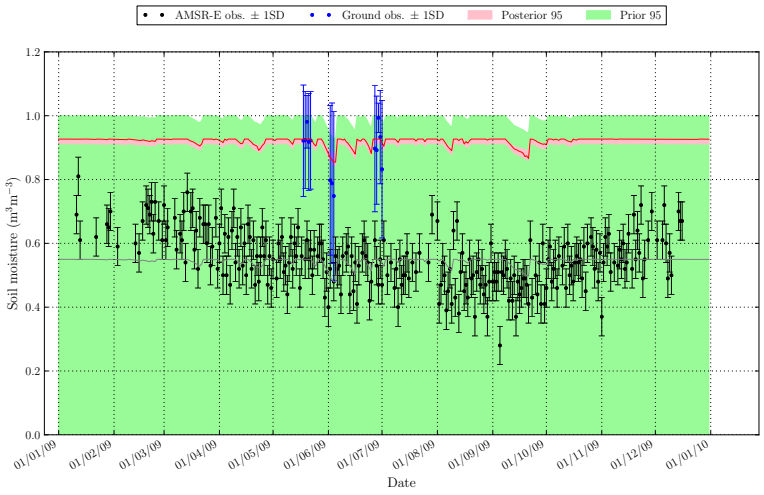

(c) *Hirddu*

Figure 9.11: Plots showing the mode and 95% confidence interval of the volumetric water content from an ensemble of 500 forward model runs using the posterior parameter distributions constrained with AMSR-E soil moisture observations. The bias (-0.356m^3m^{-3}) was corrected for in the likelihood.

Section 9.4.5.

The correlation between the mode of the CH_4 flux and the observations for the Hafod location is 0.69, and the RMSE is $0.015 gCm^{-2}d^{-1}$. The high RMSE is due to the high peak fluxes at the Hafod location. The correlation between the mode of the volumetric soil moisture and the ground-truth observations is 0.89, and the RMSE is $0.049 m^3m^{-3}$, which is lower than the uncertainty in the satellite observations.

9.5.2 Spatial variability of annual net CH_4 flux and NEP

Figure 9.15 shows the annual net CH_4 flux across the Lake Vyrnwy site, the posterior 95% confidence interval and the upper and lower limits of the 95% confidence interval. The equivalent NEP flux plots are shown in Figure 9.16. As the model is run across the whole site using the same set of parameters, the differences are due to changes in the both the climate drivers and the vegetation inputs (satellite-derived NDVI timeseries and the fractional vegetation cover). In order to easily compare the different drivers across the site the spatial variability of the drivers is shown in Figures 9.13 and 9.14. Figure 9.13(a) shows the colour codes of the weather station data used to drive each model grid cell, calculated using nearest neighbour interpolation. This is a simple method but was used so as to preserve the original values. A summary of the annual mean and standard deviation of the air temperature and irradiance together with the total annual precipitation for each weather station is given in Table 9.11. Figure 9.13(b) shows the spatial variability in the annual mean NDVI as derived from the MODIS data. Finally Figure 9.14 shows the fractional cover for each of the major vegetation types that were classified using the aerial images (as described in Chapter 3).

Met. driver	**Eunant**	**Hafod**	**Hirddu**
Air temp. (^{o}C) mean	8.1	7.8	7.1
stdev	4.8	5.3	4.8
Total precip. (mm)	2398	1915	2151
Irradiance (Wm^{-2}) mean	113	133	122
stdev	85	76	78

Table 9.11: The annual mean and standard deviation of the air temperature and irradiance and the annual total precipitation for each of the weather stations.

The spatial variability of the annual net CH_4 flux is mostly controlled by the meteorological data (Figure 9.15). The highest values are seen for the grid cells that are driven using meteorological data from the Eunant weather station. As Figure 9.5(a) shows the peaks in the daily CH_4 flux are higher for the Eunant location, corresponding to larger drops in the soil moisture (Figure 9.11(a)). Each weather station records precipitation on exactly the same dates throughout the year, albeit with differing magnitude. The Eunant site has the highest rainfall. The larger dips in soil moisture are not the result of lower rainfall or a greater number of days with no rain at the Eunant site therefore. The air temperature is slightly higher on many days at the Eunant site, which results in increased C decomposition and therefore slightly higher CO_2 and CH_4 fluxes. The higher temperatures will result in higher evapotranspiration rates, and on days with no precipitation this

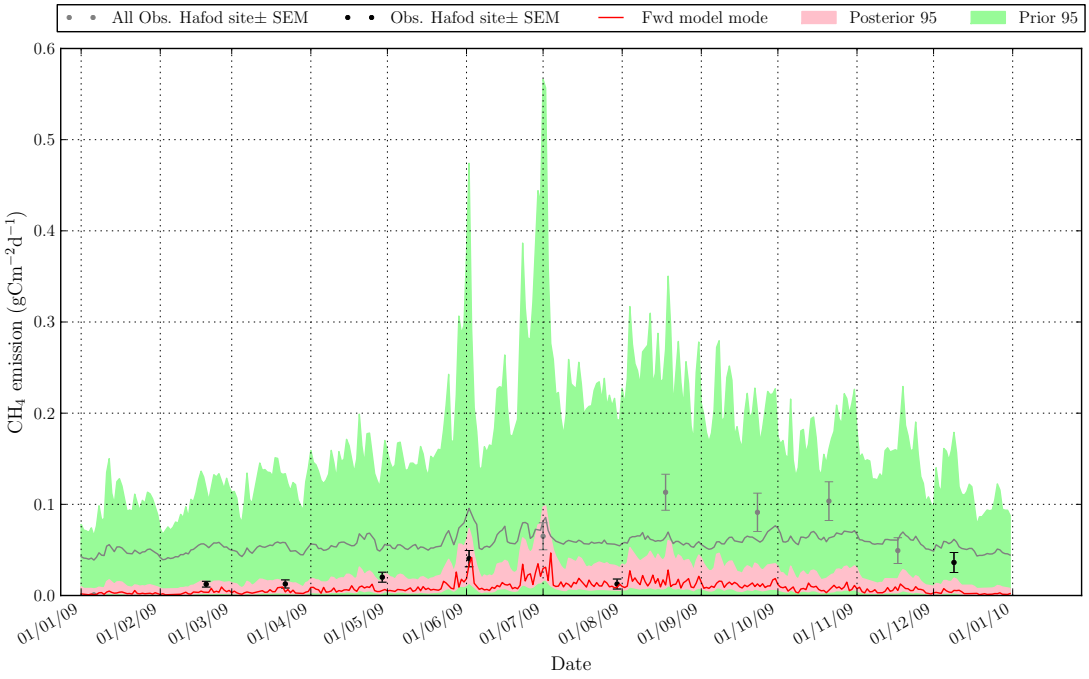

(a) *CH_4 flux*

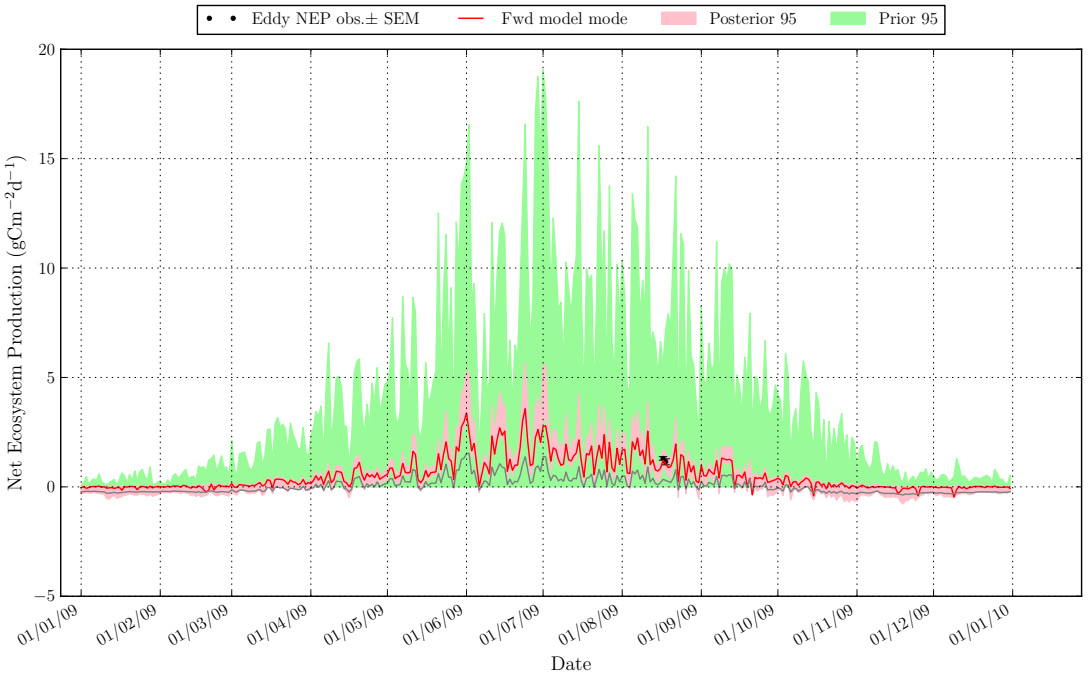

(b) *NEP*

Figure 9.12: Plots showing the mode and 95% confidence interval of the CH_4 flux and NEP from an ensemble of 500 forward model runs each location using the posterior parameter distributions constrained in the Bayesian inversion with C flux and soil moisture observations with the bias corrected for in the likelihood. CH_4 flux observations from the Hafod site were used in the inversion.

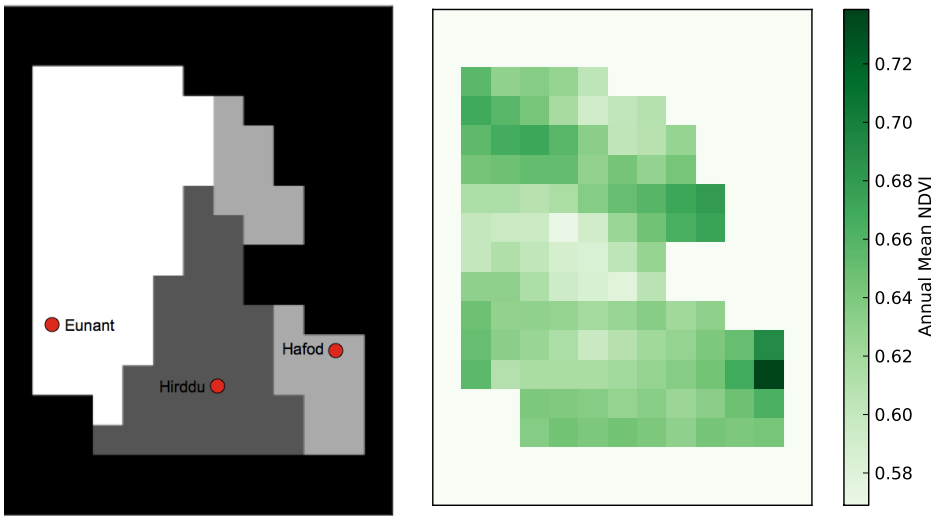

(a) The grid cells driven with data from each weather station.

(b) Annual Mean NDVI

Figure 9.13: Spatial variability of the meteorological and NDVI model drivers for the Lake Vyrnwy site. Coloured areas representing the grid cells driven with the meteorological data from each weather station are shown in the left-hand plot - (white = "Eunant", light grey = "Hafod", dark grey = "Hirddu", black = masked grid cells).(Grid cell = 500 x 500m).

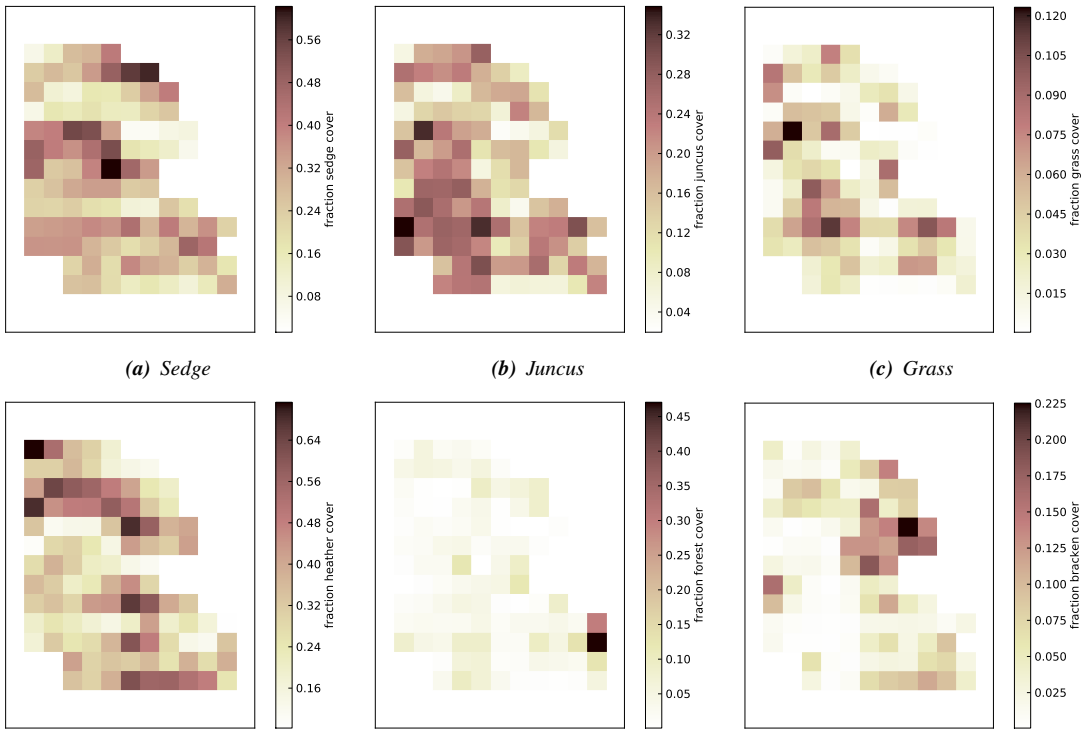

(a) Sedge

(b) Juncus

(c) Grass

(d) Heather

(e) Forest

(f) Bracken

Figure 9.14: Spatial variability of the fractional cover of each vegetation type for the Lake Vyrnwy site (Grid cell = 500 x 500m).

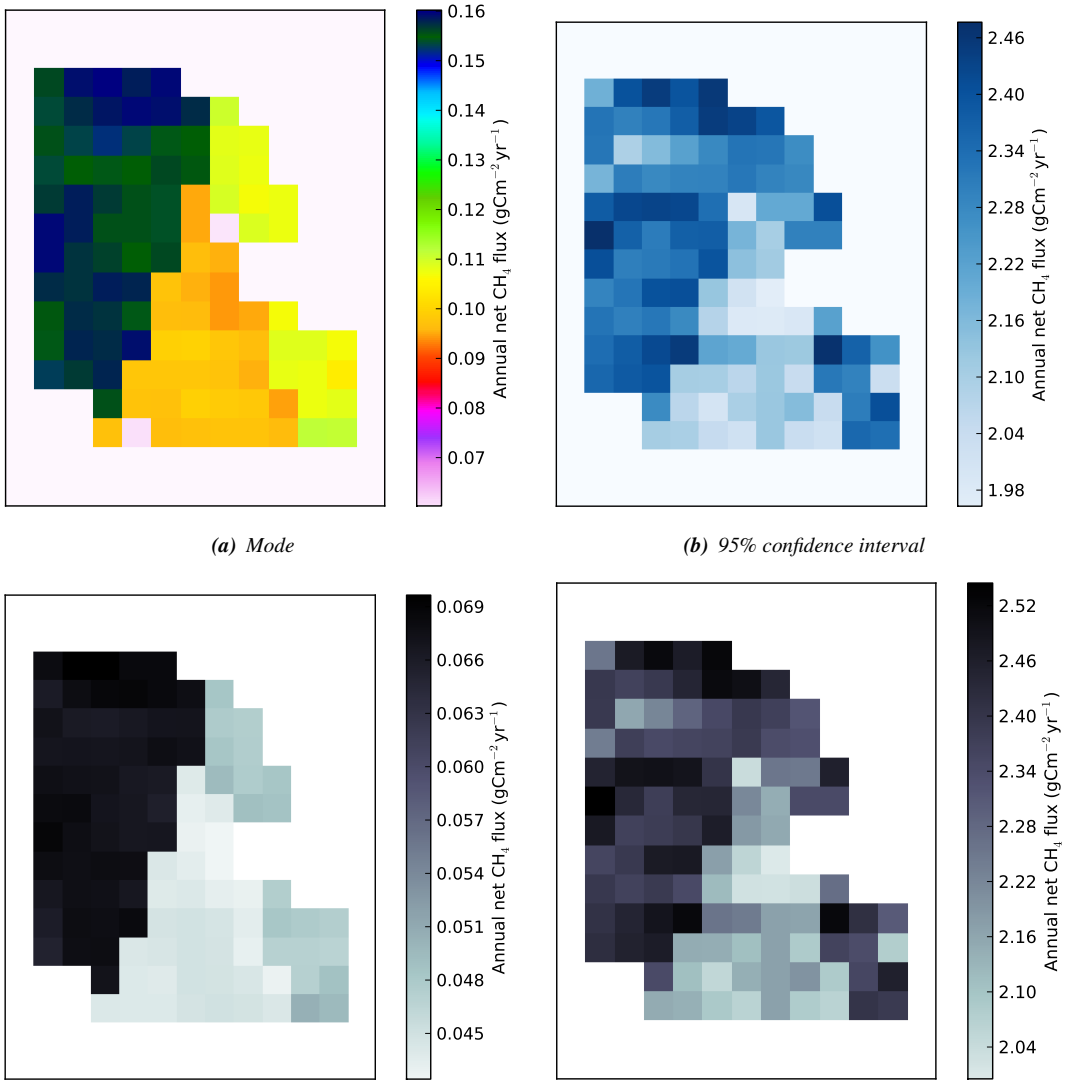

(a) *Mode*

(b) *95% confidence interval*

(c) *Lower limit of the 95% C.I.*

(d) *Upper limit of the 95% C.I.*

Figure 9.15: The mode, 95% confidence interval and the lower and upper 95% confidence limits of the annual net CH_4 flux forward model runs for the Lake Vyrnwy site (Grid cell = 500 x 500m).

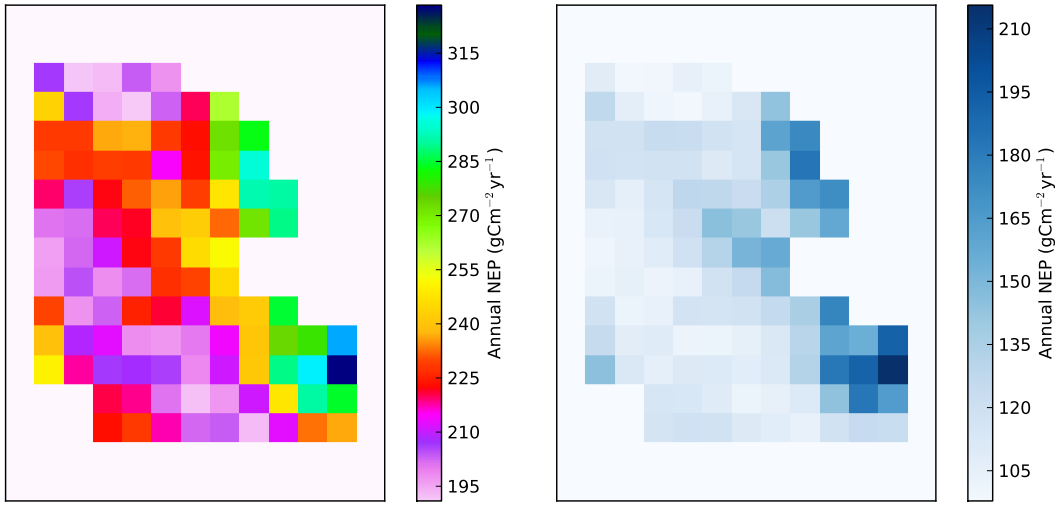

(a) *mode* ***(b)*** *95% confidence interval*

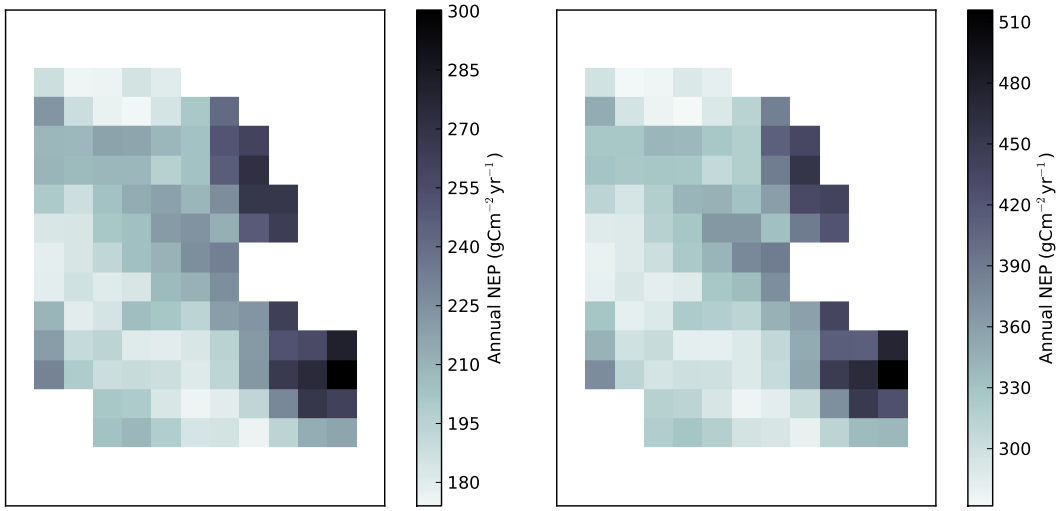

(c) *Lower limit of the 95% C.I.* ***(d)*** *Upper limit of the 95% C.I.*

Figure 9.16: The mode, 95% confidence interval and the lower and upper 95% confidence limits of the annual net NEP flux forward model runs for the Lake Vyrnwy site (Grid cell = 500 x 500m).

will result in a bigger drop in the soil moisture.

The range in the mode of the annual net CH_4 flux is 0.06 - 0.16$gCm^{-2}yr^{-1}$, showing that this site is net source of CH_4. This is not a very high magnitude however. The uncertainty in the annual net CH_4 flux is 1.98 - 2.46$gCm^{-2}yr^{-1}$, which is significant given the magnitude of the mode. As Figure 9.15 shows the mode is closer to the lower limit of the 95% confidence interval showing that the uncertainty in the annual fluxes would result in higher flux estimates.

The range in NEP modal values is ~195 - 315$gCm^{-2}yr^{-1}$, which represents a very large sink of CO_2.The uncertainty in the annual net NEP is ~50-60% of the modal value. The NEP mode and 95% confidence interval is highest for the grid cells driven with the meteorological data from the Hafod weather station (Figure 9.16). This isn't surprising as this is the site with the highest levels of irradiance on average and higher peak temperatures, which results is high NPP values. The NEP is not visibly different between the grid cells drive with the Hirddu and Eunant meteorological data. There is a patch to the south west of the site which has lower NEP values. This corresponds in part to a low mean NDVI, which is possibly due to the relatively high fractional cover of juncus in this area.

9.6 Discussion

9.6.1 Availability of observations with the required characteristics

The results of this chapter have emphasised the difficulty in obtaining observations which have the necessary characteristics for constraining the model parameters and forward model C fluxes. In addition the error in most of the observations has not been fully characterised, and therefore assumptions on the nature of the error, and the magnitude, had to be made. This is not ideal when performing a model calibration as the OSSE results clearly showed the need for a certain level of uncertainty and temporal sampling interval, depending on the observation type, with the uncertainty being the most important for C flux observations. Estimating the uncertainty is difficult however. As discussed in earlier chapters efforts are now being made to standardise error characterisation method (e.g. (*Hollinger and Richardson*, 2005)), which is a positive step forward.

There is a general lack of ground-based CH_4 flux observations. Although the eddy covariance technique can be used to measure CH_4 flux, it is rarely used to do so as the instrumentation required to accurately measure CH_4 fluxes using the eddy covariance technique has not been developed until recently. The monthly CH_4 flux observations taken over a year at this site represent quite a rare example of a long timeseries of data that can be used to better understand the annual CH_4 flux cycle, regardless of any model-data fusion exercise.

Satellite soil moisture observations were easy to obtain. However the resolution is very coarse compared to the scale of the study site and therefore the observations were biased. This could be corrected for in the volumetric soil moisture observations using the ground-based data, but a full validation of the whole year was not possible. This presents a problem when trying to use satellite observations to calibrate a model with a smaller grid-cell resolution. Relative soil moisture observations were obtained for this site from the ASCAT instrument. The observations showed an unrealistically high variability in relative soil moisture (i.e. values of 0 to 100%), probably again due to the coarse resolution of the data. This could not be validated or corrected for as no ground-

based relative soil moisture observations were available. The results of Chapter 7 Section 7.6 showed that if the relative soil moisture observations had a considerable bias this could lead to very low porosity values in the inversion, which resulted in a large overestimate in the CH_4 flux and underestimate of the NEP. These data were not used to constrain the soil moisture parameters of the model therefore.

Satellite C flux observations would alleviate many of the problems faced when trying to obtain observations to constrain the model, if they were a high enough resolution, as they would provide more continuous coverage over a wide area. These data are not currently available however, and are unlikely to be in the near future due to technological and monetary constraints, and the long time it takes for development and launch of a satellite. In addition the nature of the uncertainty associated with satellite C flux data are not fully understood at present, making it difficult to use them in a calibration framework even if they did have a higher resolution. As stated in Chapters 5 and 6 it would be more useful to use the model to provide the prior flux maps which could be updated with satellite C flux concentration data through a Bayesian inversion. This could constrain the parameters as well as the state variables.

As discussed, the two main problems found when trying to obtain satellite observations were the lack of availability, and the coarse resolution. Ideally the scale of the observations and the model would be similar. For a small scale study such as this the optimum resolution would be on the order of 100s metres to a 1-2 kilometres in order to match the scale of dominant the C flux processes, though more information on this is needed. The temporal resolution should also match the model. Data aquired continuously could be used to scale up to a daily measurement would be useful, or alternatively the model could be run at a finer temporal resolution. Flux towers offer the best hope of providing C flux estimates at this spatial and temporal scale for small-scale studies. If global modelling studies are carried out, satellites would be more useful for matching the spatial scale typically used (0.5 - 1 degrees). Hopefully, as discussed in more detail in Chapter 2 Sections 2.4.2 and 2.3.2, the satellite-derived estimates of both soil moisture and C flux will become operationally available in the near future. Efforts are being made to disaggregate coarse resolution soil moisture datasets (e.g. (*Wagner et al.*, 2008)) but this may not be possible for C flux estimates for some time. If models are run on a global scale the grid cell size is much larger and better matches the resolution of the satellite datasets, but for model calibration studies for specific ecosystems that do not cover a wide area, the issue of satellite data resolution will remain a problem.

9.6.2 Ability of the observations to constrain the parameter distributions and to replicate the observation magnitude and trend

The AMSR-E volumetric soil moisture observations resulted in a significant reduction in the prior distributions of the soil moisture related parameters and thus a well-constrained forward mode which corresponded closely to the available ground-truth observations. As a result the peak C fluxes are better approximated, as shown in the OSSE results in Chapter 7 Section 7.3. This highlights the one of the advantages of EO data. Satellite-derived soil moisture estimates are provided on a near-daily basis over a relatively long time period. In contrast the ground-truth observations are only available for eleven dates in the summer months of 2009, due to the length

of time it takes to measure soil moisture over even a small site like this. These data would not meet the observation requirements as set out in the OSSE study (Chapter 7 Section 7.3).

The OSSE results for level of CH_4 observation uncertainty and temporal sampling interval suggested a few more parameters would be highly constrained, if not accurately, due to model equifinality. This suggests that either the removal of some of the observations has potentially resulted in the inability of the observations to accurately constrain the parameters, or that other sources of unknown error, for example model structural or input error, are affecting the results.

Despite the fact that none of the CH_4 flux observations are ideal, the parameters using observations at the Hafod location were reasonably well-constrained and resulted in a forward mode which reproduced the dynamics of all locations well. The observations from the other two locations resulted in a very low CH_4 flux with limited temporal variability. However, even using the observations at the Hafod location, it appears that the model is unable to reproduce the annual dynamics (temporal trend). Some of the observations corresponding to the increase in flux during the summer and autumn months do not result in an increase in the flux at this time, even for the Eunant location where no observations were excluded from the year-long monthly timeseries due to high uncertainty. The summer/autumn peak is not modelled correctly. It can clearly be seen that the observations peak at a later time, and for longer, than the default model run. The observations which correspond to peaks in the modelled flux are actually negative for the Eunant and Hirddu locations.

The relatively high correlation and RMSE between the forward mode and the observations show that whilst the parameters constrained using the Hafod CH_4 observations do result in a better approximation of the forward model mode to the observations, the temporal trend is incorrect and the peak fluxes later in the year and not well captured, resulting in RMSE values that are higher than the magnitude of the flux.

9.6.3 Possible reasons for the inaccurate forward model trend

One possible reason for the inaccurate model trend is that the uncertainty in the observations in the winter/spring is very low, therefore the inversion will fit to those observations well and will in effect give a lower weight to the observations with a higher uncertainty. If the uncertainty in the low magnitude flux observations was increased to the that of the highest uncertainty, there would be more freedom in the inversion for the parameters to fit to the higher flux observations, even if this produced broader parameter PPDFs. This can be seen when comparing the Hirddu and Hafod observations. The observations for the Hirddu site all had lower uncertainty estimates which resulted in a stronger constraint on the parameters in the inversion. For this reason all the parameters are highly correlated but the forward mode is close to zero and shows limited daily variability. The observations taken at the Hafod location had a higher uncertainty. This resulted in a lower constraint of the parameters but the forward mode was better able to replicate the CH_4 flux dynamics, even though the model posterior 95% confidence interval was wider.

This highlights another issue of using observations with uncertainties that scale with the magnitude of the flux. Greater weight will be given to the lower uncertainty observations but this will bias the parameter estimates toward low flux magnitudes. In such cases it might be pertinent to increase the observation uncertainty to that of the maximum uncertainty, so the low flux observations

do not bias the calibration.

Another possible reason for the inaccurate forward model trend is that the prior parameter distributions are too narrow. Some parameters appear to be tightly constrained to the limit of their prior distribution, such as the inundation ratio parameter. If the prior distributions were wider the parameters may be able to better replicate the trend of the observations. If this resulted in "effective" parameters, i.e. parameters that had no biogeochemical basis, this might point to an error in the model representation of the processes. If the parameter can be constrained by the observations then arguably there is no need to modify the model. However effective parameters might result in incorrect model predictions at other sites.

It may also be that some parameters are time-varying, and should be calibrated using a smaller time window of observations than one year. This could be the case for the inundation ratio parameter for example. Again, this suggests that a time-varying processes connected to the parameter in question is not correctly represented in the model. As so few observations are available, it would be better to modify the model than to attempt a calibration over a shorter time window with fewer observations.

As discussed in Chapter 8, in general the magnitude of the C fluxes changes with different parameter values in the CASA-CH_4 model but not the temporal trend. The daily variability and annual trend is controlled by the inputs and the model physics. The parameters mostly scale the magnitude of the model outputs. This suggests no shift in the parameter distributions would result in the model being able to replicate the trend of the observations. A model structural error might therefore be the reason for the inaccurate forward model trend.

The OSSE experiments which looked at an error in the temporal trend of the model showed this could not be accounted for using the Bayesian inversion, even with the best possible observations. Therefore none of these observations would result in an accurately modelled CH_4 flux for this site, using this model, as it has a structural error which cannot be accounted for with a shift in the parameters. This is an unfortunate but interesting result and highlights the usefulness of the OSSE framework in understanding the limitations of possible observations and/or the model before the calibration is carried out. If a synthetic experiment has not been performed it is not known whether the difference between the forward mode and the observations is just the result of inaccurate parameter estimates. The OSSE therefore makes interpreting the results of the calibration of the model with real data much easier.

Further investigation is needed before the presence of a model structural error can be confirmed. Regardless, given the information in the observations, prior and model, the model has not been able to replicate the trend in the observations. The forward model mode is well-constrained by these observations, highlighting the important issue that the posterior 95% confidence interval may well be deceptive and lead to inaccurate assumptions about the quality of the calibration and the confidence placed in the model predictions.

9.6.4 Possible sources of model error in the CH_4 flux dynamics

The possible "late-autumn shoulder" of high CH_4 flux into the autumn months, as seen in the observations but not in the model, was discussed in *Mastepanov et al.* (2008). It is assumed that the CH_4 annual cycle closely corresponds to that of CO_2 in the CASA-CH_4 model, and as

discussed in Chapter 2 Section 2.2.2 most models follow a similar formulation. If this assumption is incorrect then the CH_4 dynamics in most peatland models will produce inaccurate CH_4 flux temporal trends.

The cause of the different temporal trend is unclear. It might be the result of a lag in the methanotrophic productivity following a decrease in soil moisture in the summer months. A lag of two to three months in the response time of CH_4 flux to changing water table has been observed in an experiment looking at small-scale manipulations in controlled environment chambers (S. Toet, pers. comm.). Modelling microbial populations is probably too complex for a biosphere model such as this, but if a lag time in response to decreasing soil moisture were proven a simple relationship which expressed this could easily be added to the model. More ground-based and satellite data are required to confirm the existence of a "late-autumn shoulder" of high CH_4 fluxes. If this is proven to be the case in many different locations, more experimental work needs to be done to confirm that a lag in the microbial activity would be substantial enough to cause a very different CH_4 flux annual temporal trend when compared to CO_2 flux dynamics. In order to properly model the dynamics, the cause of the delayed response in the methanogens or methanotrophs needs to be anaylsed experimentally. The above experiment looked at water table, but temperature, soil characteristics and vegetation type may also be factors.

The CASA-CH_4 model formulation of the varying transport mechanisms of CH_4 is also fairly simple and based on a relatively small number of empirical studies. There is no mechanism for storage of CH_4 in the soil, and indeed no formulation for CH_4 uptake by the soil, as is clearly seen in the observations. It is possible that the addition of a number of more detailed processes relating to CH_4 production and consumption in the model would be able to correctly model the observed CH_4 temporal trend.

If the inaccurate trend of the model is due to an incomplete knowledge controls on CH_4 emission, satellite CH_4 flux observations maybe of use in identifying gaps in our understanding and could provide information on the possible sources of error in the models. Anomalies in the CH_4 emissions provided by satellite data (e.g. *Frankenberg et al.* (2011) might provide further evidence of as yet unidentified processes which important in controlling the pattern in CH_4 emissions.

9.6.5 C flux dynamics at the Lake Vyrnwy site

The model predictions in these experiments suggest that the Lake Vyrnwy site is a net C sink, even though it is a source of CH_4. Even when considering that the global warming potential of CH_4 is roughly 23 times that of CO_2, this is still positive in terms of the net radiative forcing of the C fluxes from this site.

Although estimates of the daily C flux variability and annual net C flux have been provided for the Lake Vyrnwy site, it is likely that the peak CH_4 flux is not accurately modelled for some areas of the site, resulting in an underestimate of CH_4 flux. Whilst the forward NEP flux approximates the two observations that are available this is not adequate enough to confidently say the true NEP flux is accurately modelled, both in magnitude and trend.

From other studies which have investigated the net C balance of UK or temperature peatlands, this is a significant overestimate (estimates of a net sink of $23 gCm^{-2}yr^{-1}$ *Roulet* (2000), $\sim 71 gCm^{-2}yr^{-1}$ *Lafleur et al.* (2003), $15 \pm 12 gCm^{-2}yr^{-1}$ *Worrall et al.* (2003)). *Yu et al.* (2011)

reported that peatland site averages are around 20 - 30gCm^{-2}yr^{-1}. The OSSE studies showed that a wide range of annual net NEP values could result from constraint using the CH_4 observations alone, especially if the uncertainty and temporal sampling interval were not as good as they could be. Here a couple of NEP observations were included in the calibration which resulted in a less erratic temporal trend, but without more NEP data it is impossible to know if this estimate is an overestimate or not. The uncertainty in the annual NEP estimates was very high, further proving that there are not enough observations here to properly constrain the NEP. It is likely from the OSSE experiment results, that a higher number of NEP observations, even with this level of uncertainty, would be result in a better constraint of the model parameters and forward modelled NEP and CH_4 flux.

The width of the 95% confidence interval clearly scales with the magnitude of the C fluxes. This is partly due to the fact the sensitivity of the fluxes to the parameters increases at higher values, so there is a higher range in the peak flux with changing parameter value, as seen in Chapter 4, Section 4.5. This is related to the model physics. For example a drop soil moisture this results in a non-linear increase in the C decomposition and therefore C flux, due to the way the soil moisture is used to scale the decomposition rates in the soil. Therefore it might be better to obtain more observations in the summer months to better constrain the peak fluxes, as this is the largest source of uncertainty.

One of main controls on peak fluxes is the magnitude of decrease in soil moisture following periods of no rainfall or increased evapotranspiration. The rdr parameters mainly control the dip in soil moisture. The decrease in soil moisture that results from the rdr parameter constraint is never very large. More ground-truth observations are required to see if this is realistic or not for this site. If the model is inaccurate in this respect, and the soil moisture does decrease further, this would result in lower NEP values and higher CH_4 flux, potentially resulting in the site becoming a net C source. The rdr parameters are constrained to the values which result in the largest dip in soil moisture possible. Only a porosity value close to zero would result in significant drops in soil moisture and this would not be realistic for a peat soil. Hence if the true variability in soil moisture is greater than the model can predict, the parameters of the model would not be able to account for this model error. More observations are needed before this can be properly assessed however.

9.6.6 Controls on the spatial variability of annual net C flux

The results suggest the spatial variability in the annual net CH_4 flux across the site is mainly controlled by the meteorological data, and in particular the air temperature, while smaller-scale variations are controlled by changes in vegetation phenology and fractional cover. The annual NEP is dominated by both the meteorological drivers and the NDVI. The difference between the two fluxes is not surprising as the NEP is dominated by NPP. The calculation based on NDVI and meteorological inputs. The CH_4 flux is more dominated by soil moisture and temperature effects on decomposition, and is further removed from the drivers which determine the amount of C assimilated into the system. This suggests it is more important to have good quality meteorological data than vegetation-related drivers, though more in depth analysis is needed to interpret this result with confidence. However it is not clear whether the simple representation of the phenology of the different vegetation is adequately captured using a satellite-derived vegetation index. This might

not affect the annual net flux but might impact the daily variability of C flux.

9.6.7 Implications of using this framework for other peatland studies

The OSSE results from the previous chapter not only guided the decision as to which data would be adequate for constraining the parameters of the model, but they allowed a much easier and clearer interpretation of the results of the calibration. In particular they were useful in helping to identify model structural error, and gave confidence to the conclusion that it was this and not poor constraint of the parameters which was responsible for the difference between the model and the observations. This further proves that such a framework is highly useful if not absolutely necessary when performing a model-data fusion exercise such as this.

Model studies of peatland C fluxes, and in particular the CH_4 dynamics, are in their relative infancy. The results of this experiment suggested that there is a possible model deficiency which results in an inaccurate model CH_4 flux temporal trend. Without more observations it is unclear whether this is also true of the NEP. The cause of the discrepancy between the forward mode and the observations needs to be investigated further. If the cause is an error in the model representation of CH_4 dynamics this has a much wider application for modelling of CH_4 fluxes, as discussed earlier in this section.

A Bayesian inversion takes into account all the information and associated uncertainty estimates, and therefore provides a robust framework with which to better estimate C flux estimates, and crucially, the uncertainty in those estimates. The results of this chapter have demonstrated an application of such an approach for estimating peatland C fluxes. To my knowledge a Bayesian inversion framework has not previously been used to estimate the uncertainties associated with peatland CH_4 flux dynamics, therefore this work provides a significant advance over previous studies of this type of ecosystem.

9.7 Conclusions

The main findings in this chapter can be summarised as follows:

- Obtaining observations with the required level of uncertainty in particular is very difficult. This significantly hampers the ability to constrain the parameters of the model and to make reliable predictions of the C flux.
- Calibrating the model with the available CH_4 flux observations has shown that there is a possible structural error with the CASA-CH_4 model which results in an inaccurate temporal trend. This is likely to result in an underestimate of the true CH_4 flux for some areas of the Lake Vyrnwy site and therefore little confidence is placed in the model predictions.
- Calibrating the model with poor-quality observations can result in a deceptively low uncertainty for the C fluxes, which would result in mis-placed confidence in the model predictions.
- Model predictions of NEP are likely to be an overestimate. However the NEP results suggest that this site is a sink of CO_2, which is to be expected of peatland ecosystems.

- Model predictions of the CH_4 flux suggest the site is a source of CH_4. The magnitude of the NEP suggests however that overall the site is a net C sink.
- The spatial variability in annual net C fluxes at the Lake Vyrnwy site appears to be mostly controlled by changes in the meteorological drivers.
- The OSSE results from previous chapters helped significantly, to both identify those observations which would be adequate to constrain the model parameters and predictive uncertainty, and in the interpretation of the calibration results.

Chapter 10

Conclusions

The aim of this thesis was to investigate the ability of a combined observation - modelling approach to improve estimates of CO_2 and CH_4 fluxes from peatlands. The processes that control the balance of CO_2 and CH_4 emission from peatlands are generally well-understood, but the uncertainty in peatland C fluxes remains high, therefore there is a need to better quantify these estimates. Given model inaccuracies and uncertainty in observations, the method of statistically combining the two sources of information (so-called data assimilation) results in optimal estimates. This study has developed and implemented a data assimilation framework that can be used to examine the ability of ground-based and EO data to calibrate, test and improve model estimates of peatland C fluxes. This provides a significant advance over previous studies for this type of ecosystem.

A Bayesian inversion approach was used to constrain the parameters of a simple C flux model that contains a representation of CH_4 flux dynamics (the CASA-CH_4 model). Observation Systems Simulation Experiments (OSSEs) were carried out to determine the type of observations, and the uncertainty and temporal sampling interval, that would be best suited to improving C flux estimates using this model. An application of the Bayesian inversion approach was then used to constrain the model at a UK upland peat site, using ground-based C flux observations and satellite-derived soil moisture estimates.

Chapter 4 presented an initial summary of the workings of the model and the results of a sensitivity analysis of the parameters, in order to decide which were the most important state variables and related parameters that required calibrating. The C flux was most sensitive to parameters directly involved in the calculation of C fluxes, and to the soil moisture-related parameters. Therefore ground-based C flux and satellite-derived soil moisture observations were required to constrain most of the variability in the model resulting from unknown parameters.

Chapters 5 to 7 used an OSSE framework to determine the type of observations and the associated characteristics (uncertainty and temporal sampling interval) which were best in terms of constraining the parameters of the CASA-CH_4 model. These experiments mostly focused on the case where the model was assumed to be correct and the difference between the observations and the model was due to random uncertainty in the observations alone.

The OSSEs performed with CH_4 flux (Chapter 5), NEP (Chapter 6) and soil moisture observations (Chapter 7) identified the level of uncertainty and temporal sampling interval for each type of observation which would result in well-constrained parameters and a forward mode which ac-

curately approximated the true value. For the CH_4 flux and NEP observations, if the observation uncertainty was low enough to allow good parameter constraint, many combinations of parameter values existed which resulted in an accurate forward model mode. The parameters were therefore often constrained to the wrong value, suggesting there was a high degree of parameter correlation and model equifinality. To better constrain the parameters to their accurate values further information is needed; either different types of observation, or an improved knowledge of the prior range of the parameter values.

Model equifinality aided the modelling of NEP and CH_4 flux in this study as an accurate approximation of the true flux could be found with well-constrained parameters, even if they were not constrained to their true value. However these parameter estimates were conditioned on the specific uncertainty in the observations. They could not be used with confidence to make predictions of C flux for different locations or time periods, or to answer questions regarding changing management or climate change scenarios.

The different C fluxes had a different sensitivity to each of the parameters. It was shown that this restricted the ability of each type of C flux observation to accurately constrain the other C flux model estimates. If parameters constrained using one type of C flux were biased due to parameter correlation, they did not always result in an equally good approximation of the other C fluxes in the model. This was seen for the CH_4 flux experiments, where some of the observations that resulted in an accurate and well-constrained CH_4 flux mode did not result in accurate and well-constrained model NEP. The NEP observations were generally better at accurately approximating the CH_4 flux observations than vice versa, though if the best-case observations were available, observations each C flux could replicate the true flux of the other.

For the C flux observations, uncertainty was more important in constraining the parameters than the temporal sampling interval. This was because a change in parameter value affected the whole timeseries. The bias was key to whether that magnitude of flux was correct. For the volumetric soil moisture observations both the uncertainty and the temporal sampling interval were important. This was because it is mainly the relative drying rate (rdr) parameters which can or cannot be well constrained by the observations. The porosity was well estimated by the volumetric soil moisture as it represents the maximum value the soil moisture can have. The rdr parameters on the other hand control the decrease in soil moisture at times of a lack of precipitation. Therefore the temporal sampling interval was important, as if it was too large the observations missed the time periods where the soil moisture decreases with limited precipitation. There were therefore generally fewer soil moisture observational characteristics that resulted in a good constraint of the soil moisture- related parameters.

The synthetic observation framework allowed an investigation of the potential problems that may arise when implementing a data assimilation experiment. Chapter 7 examined the impact of bias in the observations, and the possible ways of dealing with it in the Bayesian inversion. The issue of having an unknown bias was examined for the volumetric soil moisture observations as this was likely to be an issue when using coarse resolution satellite data. The results showed (unknown) bias in the observations can result in inaccurate but well-constrained parameter estimates, which could cause a bias in the modelled fluxes depending on the sensitivity of the model to the parameter in question. Therefore systematic biases in the observations need to be properly ac-

counted for in the likelihood of the Bayesian inversion. This indeed was the case using AMSR-E volumetric soil moisture observations for the Lake Vyrnwy site. The bias was approximated using ground-based data, and used to account for the bias in the likelihood. This resulted in forward model volumetric soil moisture mode that corresponded well to the ground-truth observations.

The final OSSE study in Chapter 8 investigated the impact of unknown errors, in both the amplitude and phase of the model, on the ability of the observations to constrain the model parameters. Results suggested that a shift in the parameters away from the correct value could account for an error in the magnitude of the fluxes, but not a change in the temporal trend. Again, as was shown in the other OSSE experiments, good parameter and forward model constraint could result in false confidence being placed in the model predictions. This is a key finding. Without the OSSE framework it would be impossible to know if this was the case. If the observation uncertainty is low and does not coincide with the posterior forward model uncertainty, the parameters that were included in the calibration cannot account for the error in the model. If the uncertainty estimates on the model and observations do not overlap this identifies the possible presence of the error in the model or inappropriate prior distributions. Several possible methods of accounting for the model uncertainty and/or investigating which part(s) of the model are inaccurate were proposed.

In the final experimental chapter the observation - modelling framework was applied to an upland UK peat site using ground-based C flux observations and satellite-derived soil moisture estimates. The temporal sampling interval of satellite observations is one of the major advantages of using these data, coupled with the continuity over a period of years. Operational satellite soil moisture observations were available for the AMSR-E instrument but the coarse resolution, when compared to the area of the site, resulted in biased observations when compared to ground-based observations. The bias was accounted for in the likelihood of the Bayesian inversion. Validation studies and preliminary attempts at the random error characterisation of soil moisture observations suggested the uncertainty of the AMSR-E observations was adequate for calibration of the soil moisture-related parameters of this model.

Constraining the CASA-CH_4 model with observations of C flux for the Lake Vyrnwy site suggested that there was an error in the temporal trend of the CH_4 flux in the model. The peak fluxes occurred later in the year than the peaks in the modelled CH_4 flux. There were not enough observations to confirm if this was also the case for the CO_2 fluxes. The cause of this error may be related to a lag in the microbial response to changing soil moisture and temperature conditions in the summer months. If there is an error in the temporal trend of the model, satellite C flux observations can help identify whether this error was localised or representative of a significant gap in our understanding of the the controls on CH_4 emissions. In addition further field-based experimental work needs to be carried out to confirm the existence of a "late-autumn shoulder" of high CH_4 fluxes, and the possible causes of this. If it is found that the annual trend of CH_4 is different to CO_2 this is a significant finding in terms of CH_4 flux modelling, as many models include a similar representation of CH_4 dynamics which is heavily coupled to that of soil CO_2 dynamics.

Using parameters constrained with CH_4 flux, NEP, and volumetric soil moisture observations, the annual net CH_4 flux at the site was found to range from 0.135 - 0.188$gCm^{-2}yr^{-1}$ with a posterior 95% confidence interval of around 85-90%. These results are an underestimate the ground-

based CH_4 flux for some areas of the site however, which showed significantly higher magnitude of flux in the summer and autumn months. The annual NEP values suggested the site was a significant sink of CO_2 (450-600g$Cm^{-2}yr^{-1}$). This outweighed any increase in the net GWP of the site from net CH_4 emission.

A key finding of this work was that a low model predictive uncertainty can be deceptive in terms of knowing how good the the model calibration is. Without doing a synthetic experiment it is unknown how well the calibration will work and what the impact of any possible issues relating to poor quality observations, inadequate prior or model error will be. The OSSE framework allows a much clearer interpretation of the results of a model calibration, aside from the fact it provides the necessary information on which observations are likely to result in good parameter and model constraint. It is a valuable tool for better understanding a model and the subtle technicalities of the data assimilation approach. It is arguably imperative that such a study should be carried out before any "real" observations are used. The discrepancy between the model and observation temporal and spatial scale was highlighted in the discussion of the OSSE chapters. It is suggested to the modelling community that the temporal and spatial resolution of the observations must match that of the model in order that biases in the parameter values are not introduced in the calibration. For a small-scale study such as this, data are required on the order of 100s metres to 1 to 2 km. Satellite C flux data do not meet that requirement currently, therefore it would be better to use flux towers to measure C fluxes, and to have at least three in order to properly characterise the error in the observations. Flux towers also provide the necessary half-hourly temporal sampling interval, which can be used to scale to daily measurements. Satellite C flux data would be more suited to the calibration of global models as the resolution is similar to the 0.5 to 1 degree grids used. However, higher temporal sampling intervals than the current revisit periods would be required for future satellite missions.

In terms of soil moisture data, satellite observations are useful in that they offer near daily measurements. The spatial scale of passive microwave data is too large for a study on small-scale, but as discussed many efforts are currently underway to provide operational disaggregation algorithms which would provide soil moisture estimates at the correct spatial scale. This should be a focus for research, as should providing operational soil moisture products from high resolution SAR sensors.

Finally it is clear from this work that modellers and field-based biologists need to work together more in order to improve the observations required to calibrate the models, and to discuss possible sources of model error. In this way experiments that need to be undertaken in order to understand the processes better can be carried out. There is a lack of ground-based CH_4 data. The dataset used in this study is extremely rare. As such it is difficult to say whether the discrepancy between the observations and the model is due to inaccurate process representation on a wider scale. Further collaboration with the team that collected this data will allow for an improvement in our understanding of CH_4 dynamics and therefore more accurate model estimates over wider regions.

10.1 Contribution to scientific understanding

1. This thesis has presented the development and implementation of a framework that can be used to robustly incorporate observations of different types into a process based model of peatland C fluxes. This is the first such study of this type of ecosystem.

2. This work also presented a global sensitivity analysis of a C flux model, which was used to understand what the main drivers of the model are and which observations should be used to calibrate the model.

3. The use of an OSSE approach to identify the observations which will and will not result in an accurate constraint of the model parameters and state variables was demonstrated. Experiments proved the OSSE is a useful and necessary tool for interpreting the results of a model calibration. In particular it was shown that the OSSE can highlight issues that arise in the presence of observational bias and model error.

4. An application of the Bayesian inversion to a test site using the available observations confirmed the usefulness of this approach in obtaining CO_2 and CH_4 flux estimates from a complex peatland system.

5. This work provides a case study for one particular ecosystem but this framework could be used in any model-data fusion context.

6. This thesis also presents the first comprehensive use (as far as I know) of satellite soil moisture in a data assimilation context with C flux models. Mostly soil moisture data assimilation has been conducted with hydrological models, or to improve the hydrology and energy balance of land surface models. To my knowledge only one study (*Verstraeten et al.*, 2011) has had the specific purpose of improving C flux estimates, and that study simply replaced the modelled soil moisture estimates with the satellite data.

10.2 Future work

The work presented in this thesis can be expanded on in several ways. The study should be extended to test the increase in information which would be provided if the prior distributions of some parameters could be better constrained. This may lead to model equifinality having a lower impact on the ability of the observations to accurately constrain the parameters.

The issue of what might be causing the inability of the model to reproduce the observations at the Lake Vyrnwy site should be investigated further. A first step would be to test the model at different locations, to determine whether this is a localised effect. If not there are several ways to deal with the problem. The prior distributions on the parameters could be widened to determine whether parameter values outside the current priors would result in a better retrieval of the observations. This might result in 'effective' parameters, i.e. parameters which enable to model to match the observations but which have no physical meaning. Alternatively the time window of observations which is used to constrain the parameters could be shortened. This might result in a better constraint of the parameters, but the MAP estimates may vary with each calibration

period. Knowledge as to whether this is realistic or not might identify a potential problem in the model physics. For example, the results of four different model calibrations for 2009, performed with observations which span a period of three months, might result in different estimates of the inundation ratio. This would suggest the process which partitions the decomposed C into CO_2 and CH_4 is responding to a time-varying factor which is not accounted for in the model physics. The aim is not to add unnecessary complexity to the model however, but to find the simplest process representation in the model which would result in more accurate CH_4 flux dynamics at many different sites.

Secondly, only the ability of the observations to constrain the parameters of the model has been investigated. In order to make a full assessment of the possible sources of the differences between the model and the observations, uncertainties in the inputs could be examined as parameters in the model, as could the initial conditions. For example the magnitude of the various litter and soil C pools could be estimated in the same framework as in *Yeluripati et al.* (2009).

The OSSE studies which examined the impact of a possible unknown error in the model could be expanded to include 'model error parameters' (hyper-parameters), which in theory would account for the error in the model. The parameters could be linked to any of the model state variables, allowing the possible identification of the source of the model error. This method of simultaneously quantifying the parameters, initial conditions and the error in both the inputs and the model is referred to as Bayesian Total Error Analysis and was briefly discussed at the end of Chapter 8. Studies by *Thyer et al.* (2009), *Renard et al.* (2010) and *Salamon and Feyen* (2010) have shown this can work well, though they were using simpler catchment hydrological models with fewer parameters and state variables.

If the model structural error is to be properly diagnosed and resolved, closer collaboration with biologists who make field-based measurements is needed. Specific issues can be addressed with manipulation experiments, and the models adapted if necessary. This approach would work well with the issue of an inaccurately modelled temporal trend in the CASA-CH_4 CH_4 flux. If this is to be corrected, a dialogue with the experts in the biological and environmental processes that control CH_4 flux needs to take place. As well as field-based measurements, satellite C flux data, which will be increasingly available over the coming years, can be used to identify where there are deficiencies in our the current understanding of the processes. These data will be enormously useful for testing and validating the C flux component of land surface models on a global scale.

Thirdly, future work should include the testing of different temporal and spatial model scales and the impact of the mismatch between the observations and the model. This issue was also discussed by *Raupach et al.* (2005) and *Rayner* (2010). It may be useful to have a model with an hourly timestep (rather than daily) for example, so the model output and observations will correspond to the same time of the day. It is clear from the results in this study that the resolution of the model grid cell should match that of the observations. If the observation is made over a much smaller area than the model grid cell then there could be just as high a spatial uncertainty as for the satellite observations with a resolution that is greater than the model grid cell. Which spatial scale is most useful for obtaining the best C flux estimates? Should the model be run at a very fine scale so as to compare to ground-based data, or at a coarser scale to match the satellite data? Arguably the latter is the most sensible option as satellite data have a high temporal

sampling interval, which may not be possible for ground-based observations. Some studies argue the same result could be achieved with an extensive ground monitoring network for a similar amount of money than it would take to put a satellite in orbit (*Hungershoefer et al.*, 2010). Even if it makes sense practically for the model grid size to be larger, few studies have examined the difference in the C flux estimates over a certain region that are obtained from averaging several higher resolution model grid cells, or from having one grid cell that covers the whole area. As the processing speed and memory size of computers continues to be improved, models could in theory be run at higher resolutions, if it was deemed necessary to do so. This is an interesting and pertinent area of research.

Finally, and on a more technical note, the subtle workings of the Bayesian inversion, given the nature of the observations and their error structures, should be examined further, especially as the error in the observations become better characterised. For example, studies have shown the random error in ground-based C flux observations have a Lagrangian distribution and scale with the magnitude of the flux (*Hollinger and Richardson*, 2005; *Richardson et al.*, 2006). Error models other than the Gaussian distribution (as used in the likelihood of the Bayesian inversion) should be tested if it is thought the uncertainty in the observations warrants this change. Temporal and spatial autocorrelation has also not been examined in this study. It is likely the autocorrelation in daily observations will result in an underestimate of the true uncertainty in the model. This can be accounted for by adapting the likelihood in the Bayesian inversion. All these issues were explored in studies by *Yang et al.* (2007b), *Thyer et al.* (2009), *Renard et al.* (2010) and *Salamon and Feyen* (2010) using the BATEA framework. They focus on improving hydrological models, but it would be very useful to apply this comprehensive approach to C flux and land surface models.

In conclusion, this thesis has provided an example of a rigorous test of a combined observation-modelling approach. This was mainly achieved through the implementation of an OSSE framework. In this case the aim was to constrain the parameters of a the C dynamics of a simple land surface model model in order to improve C flux estimates from peatlands, but this framework could be applied to any data assimilation study. The work in this thesis has shown a synthetic study is valuable in providing a clearer interpretation of the results when using the available ground-based and satellite observations. The task of improving land surface flux estimates, both of C fluxes and water and energy balance, is becoming increasingly important for climate change studies. Data assimilation is being used as a tool in tackling this problem but the usefulness of the available data is largely untested in a synthetic framework. Arguably this is crucial for a more complete understanding of the models, and the information that the observations can provide in improving the model estimates and the quantification of the model uncertainty.

Bibliography

Albergel, C., C. Rudiger, D. Carrer, J.-C. Calvet, N. Fritz, V. Naeimi, Z. Bartalis, and S. Hasenauer (2009), An evaluation of ASCAT surface soil moisture products with in-situ observations in Southwestern France, *Hydrological Earth System Sciences*, *13*, 115–124.

Asner, G., J. Scurlock, et al. (2003), Global synthesis of leaf area index observations: implications for ecological and remote sensing studies, *Global Ecology and Biogeography*, *12*(3), 191–205.

Baker, D., H. Bosch, S. Doney, D. O'Brien, and D. Schimel (2010), Carbon source/sink information provided by column co2 measurements from the orbiting carbon observatory, *Atmospheric Chemistry & Physics*, *10*, 4145–4165.

Baldocchi, D. (2003), Assessing the eddy covariance technique for evaluating carbon dioxide exchange rates of ecosystems: past, present and future, *Global Change Biology*, *9*, 1–14.

Baldocchi, D., B. Hincks, and T. Meyers (1988), Measuring biosphere-atmosphere exchanges of biologically related gases with micrometeorological methods, *Ecology*, *69*, 1331–1340.

Barbu, A., J. Calvet, J. Mahfouf, C. Albergel, and S. Lafont (2011), Assimilation of soil wetness index and leaf area index into the isba-a-gs land surface model: grassland case study, *Biogeosciences Discuss*, *8*, 1831–1877.

Barkley, M., U. Friess, and P. Monks (2006a), Measuring atmospheric CO_2 from space using Full Spectral Initiation (FSI) WFM-DOAS, *Atmospheric Chemistry and Physics Discussions*, *6*, 2765–2807.

Barkley, M., P. Monks, U. Friess, R. Mittermeier, H. Fast, S. Korner, and M. Heimann (2006b), Comparisons between SCIAMACHY atmospheric CO_2 retrieved using (FSI) WFM-DOAS to ground-based FTIR data and the TM3 chemistry transport model, *Atmospheric Chemistry and Physics Discussions*, *6*, 5387–5425.

Bartlett, K., and R. Harriss (1993), Review and assessment of methane emissions from wetlands, *Chemosphere*, *26*, 261–320.

Bellisario, L., J. Bubier, and T. Moore (1999), Controls on ch4 emissions from a northern peatland, *Global Biogeochemical Cycles*, *13*, 81–91.

Bergamaschi, P., et al. (2009), Inverse modeling of global and regional CH_4 emissiongs using SCIAMACHY satellite retrievals, *Journal of Geophysical Research*, *114*, doi:10.1029/2009JD012,287.

Bergamaschi, P., et al. (2010), Inverse modeling of european ch4 emissions 2001-2006, *Journal of geophysical research. Series D, atmospheres*, *115*(22), D22,309.

Beven, K. (2006), A manifesto for the equifinality thesis, *Journal of Hydrology*, *320*(1-2), 18–36.

Bonan, G. (1989), A computer model of the solar radiation, soil moisture and soil thermal regimes in boreal forests, *Ecological Modelling*, *45*, 275–306.

Bonan, G., P. Lawrence, K. Oleson, S. Levis, M. Jung, M. Reichstein, D. Lawrence, and S. Swenson (2011), Improving canopy processes in the community land model version 4 (clm4) using global flux fields empirically inferred from fluxnet data, *J. Geophys. Res*, *116*.

Bosen, J. (1960), A formula for approximation of the saturation vapor pressure over water, *Monthly Weather Review*, *88*, 275–276.

Braak, C. (2006), A markov chain monte carlo version of the genetic algorithm differential evolution: easy bayesian computing for real parameter spaces, *Statistics and Computing*, *16*(3), 239–249.

Bragg, O., and J. Tallis (2001), The sensitivity of peat-covered upland landscapes, *Catena*, pp. 345–360.

Braswell, B., W. Sacks, E. Linder, and D. Schimel (2005), Estimating diurnal to annual ecosystem parameters by synthesis of a carbon flux model with eddy covariance net ecosystem exchange observations, *Global Change Biology*, *11*(2), 335–355.

Breon, F.-M., and P. Ciais (2010), Spaceborne remote sensing of greenhouse gas concentrations, *Comptes Rendus Geoscience*, *342*, 412–424.

Brocca, L., F. Melone, T. Moramarco, W. Wagner, and S. Hasenauer (2010), ASCAT soil wetness index validation through in situ and modeled soil moisture data in central Italy, *Remote Sensing of Environment*, *114*, 2745–2755.

Bubier, J., and T. Moore (1994), An ecological perspective on methane emissions from northern wetlands, *TREE*, *9*, 460–464.

Buchwitz, M., V. Rozanov, and J. Burrows (2000), A near-infrared optimized DOAS method for the fast global retrieval of atmospheric CH_4, CO, CO_2, H_2O and N_2O total column amounts from SCIAMACHY Envisat-1 nadir radiances, *Journal of Geophysical Research*, *105*, 15,231–15,245.

Buchwitz, M., et al. (2005), Atmospheric methane and carbon dioxide from SCIAMACHY satellite data: inital comparison with chemistry and transport models, *Atmospheric Chemistry and Physics*, *5*, 941–962.

Burrows, E., J. Bubier, A. Mosedale, G. Cobb, and P. Crill (2005), Net Ecosystem Exchange of carbon dioxide in a temperate poor fen: a comparison of automated and manual chamber techniques, *Biogeochemistry*, *76*, 21–45.

Calvet, J., N. Fritz, F. Froissard, D. Suquia, A. Petitpa, and B. Piguet (2007), In situ soil moisture observations for the cal/val of smos: The smosmania network, in *Geoscience and Remote Sensing Symposium, 2007. IGARSS 2007. IEEE International*, pp. 1196–1199, IEEE.

Campolongo, F., J. Cariboni, and A. Saltelli (2007), An effective screening design for sensitivity analysis of large models, *Environmental Modelling & Software*, *22*(10), 1509–1518.

Cao, M., S. Marshall, and K. Gregson (1996), Global carbon exchange and methane emissions from natural wetlands: application of a process-based model, *Journal of Geophysical Research*, *101*, 14,399–14,414.

Ceballos, A., K. Scipal, W. Wagner, and J. Martinez-Fernandez (2005), Validation of ERW scatterometer-derived soil moisture data in the central part of the Duero Basin, Spain, *Hydrological Processes*, *19*, 1549–1566.

Champagne, C., A. Berg, J. Belanger, H. McNairn, and R. De Jeu (2010), Evaluation of soil moisture derived from passive microwave remote sensing over agricultural sites in canada using ground-based soil moisture monitoring networks, *International Journal of Remote Sensing*, *31*(14), 3669–3690.

Chanton, J., and J. Dacey (1991), *Trace Gas Emissions by Plants*, chap. Effects of vegetation on methane flux, reservoirs, and carbon isotropic composition, pp. 65–92, Academic, San Diego, California.

Chanton, J., J. Bauer, P. Gaser, D. Siegel, C. Kelley, S. Tyler, E. Romanowicz, and A. Lazrus (1995), Radiocarbon evidence for the substrates supporting methane formation within northern minnesota peatlands, *Geochim Cosmochim Acta*, *59*, 3663–3668.

Chapin, F., P. Matson, and H. Mooney (2002), *Principles of Terrestrial Ecosystem Ecology*, Springer.

Charman, D. (2002), *Peatlands and Environmental Change*, John Wiley and Sons, Ltd, England.

Chen, F., W. Crow, P. Starks, and D. Moriasi (2011), Improving hydrologic predictions of a catchment model via assimilation of surface soil moisture, *Advances in Water Resources*.

CHEN, H., and H. TIAN (2005), Does a general temperature-dependent q10 model of soil respiration exist at biome and global scale?, *Journal of Integrative Plant Biology*, *47*(11), 1288–1302.

Chen, M., S. Liu, L. Tieszen, and D. Hollinger (2008), An improved state-parameter analysis of ecosystem models using data assimilation, *ecological modelling*, *219*(3-4), 317–326.

Chevallier, F., F. Bréon, and P. Rayner (2007), Contribution of the orbiting carbon observatory to the estimation of co2 sources and sinks: Theoretical study in a variational data assimilation framework, *Journal of geophysical research*, *112*(D9), D09,307.

Chevallier, F., S. Maksyutov, P. Bousquet, F. Bréon, R. Saito, Y. Yoshida, and T. Yokota (2009), On the accuracy of the co2 surface fluxes to be estimated from the gosat observations, *Geophysical Research Letters*, *36*(19), L19,807.

Chimner, R., D. Cooper, and W. Parton (2002), Modelling Carbon Accumulation in Rocky Mountain Fens, *Wetlands*, pp. 100–110.

Combal, B., F. Baret, M. Weiss, A. Trubuil, D. Mace, A. Pragnere, R. Myneni, Y. Knyazikhin, and L. Wang (2002), Retrieval of canopy biophysical variables from bidirectional reflectance:: Using prior information to solve the ill-posed inverse problem, *Remote sensing of environment*, *84*(1), 1–15.

Confalonieri, R., G. Bellocchi, S. Bregaglio, M. Donatelli, and M. Acutis (2010), Comparison of sensitivity analysis techniques: A case study with the rice model warm, *Ecological Modelling*, *221*(16), 1897–1906.

Cosby, B., G. Hornberger, R. Clapp, and T. Ginn (1984), A Statistical Exploration of the Relationships of Soil moisture Characteristics to the Physical Properties of Soils, *Water Resources Research*, pp. 682–690.

Cox, P. (2001), Description of the triffid dynamic global vegetation model, *Hadley Centre Technical Note*, *24*.

Cramer, W., D. Kicklighter, A. Bondeau, B. Moore, G. Churkina, B. Nemry, A. Ruimy, A. Schloss, and participants of the Potsdam NPP model intercomparion (1999), Comparing global models of terrestrial net primary productivity (NPP): overview and key results, *Global Change Biology*, *5*, 1–15.

Crow, W., and E.F.Wood (2003), The assimilation of remotely sensed soil brightness temperature imagery into a land surface model using ensemble kalman filtering: a case study based on estar measurements during sgp97, *Advances in Water Resources*, pp. 137–149.

Crow, W., R. Bindlish, and T. Jackson (2005), The added value of spaceborne passive microwave soil moisture retrievals for forecasting rainfall-runoff partitioning, *Geophys. Res. Lett*, *32*.

Das, N., D. Entekhabi, and E. Njoku (2011), An algorithm for merging smap radiometer and radar data for high-resolution soil-moisture retrieval, *Geoscience and Remote Sensing, IEEE Transactions on*, *49*(5), 1504–1512.

Davidson, E., K. Savage, L. Verchot, and R. Navarro (2002), Minimizing artifacts and biases in chamber-based measurements of soil respiration, *Agricultural and Forest Meteorology*, *113*, 21–37.

de Jeu, R., W. Wagner, T. Holmes, A. Dolman, N. van de Giesen, and J. Friesen (2008), Global soil moisture patterns observed by space borne microwave radiometers and scatterometers, *Surveys in Geophysics*, *29*, 399–420.

De Kauwe, M., M. Disney, T. Quaife, P. Lewis, and M. Williams (2010), An assessment of the modis collection 5 leaf area index product for a region of mixed coniferous forest, *Remote Sensing of Environment*.

de Rosnay, P., et al. (2006), Smosrex: A long term field campaign experiment for soil moisture and land surface processes remote sensing, *Remote sensing of environment*, *102*(3-4), 377–389.

Demarty, J., F. Chevallier, A. Friend, N. Viovy, S. Piao, and P. Ciais (2007), Assimilation of global modis leaf area index retrievals within a terrestrial biosphere model, *Geophysical Research Letters*, *34*(15), L15,402.

Denman, K., et al. (2007), Couplings between changes in the climate system and biogeochemistry, *Climate change 2007: The Physical Science Basis. Contribution of the Working Group 1 to the Fourth Assessment Report of the Intergovernmental Panel on Climate Change*, pp. 499–587.

Dinsmore, K., U. Skiba, M. Billett, R. Rees, and J. Drewe (2009), Spatial and temporal variability in CH_4 and N_2O fluxes from a Scottish ombrotrophic peatland: implications for modelling and up-scaling, *Soil Biology and Biogeochemistry*, *41*, 1315–1323.

Dobson, M., F. Ulaby, M. Hallikainen, and M. El-Rayes (1985), Microwave dielectric behavior of wet soil-part ii: Dielectric mixing models, *Geoscience and Remote Sensing, IEEE Transactions on*, *GE-23*(1), 35–46.

Doran, J., L. Mielke, and J. Power (1990), Microbial activity as regulated by soil water filled pore space, *Transactions of the 14th International Congress of Soil Science*, pp. 94–99.

Dorigo, W., K. Scipal, R. Parinussa, Y. Liu, W. Wagner, R. de Jeu, and V. Naeimi (2010), Error characterisation of global active and passive microwave soil moisture datasets, *Hydrological Earth System Sciences*, *14*, 2605–2616.

Dorigo, W., et al. (2011), The international soil moisture network: a data hosting facility for global in situ soil moisture measurements, *Hydrol. Earth Syst. Sci*, *15*, 1675–1698.

Draper, C., J. Walker, P. Steinle, R. de Jeu, and T. Holmes (2009), An evaluation of AMSR-E derived soil moisture over Australia, *Remote Sensing of Environment*, *113*, 703–710.

Drusch, M., E. Wood, H. Gao, and A. Thiele (2004), Soil moisture retrieval during the Southern Great Plains Hydrology Experiment 1999: a comparison between remote sensing data and operational products, *Water Resources Research*, *40*, doi:10.1029/2003WR002,441.

Engman, E., and N. Chauhan (1995), Status of microwave soil moisture measurements with remote sensing, *Remote Sensing of Environment*, *51*(1), 189–198.

Evensen, G. (2003), The ensemble kalman filter: Theoretical formulation and practical implementation, *Ocean dynamics*, *53*(4), 343–367.

Feng, L., P. Palmer, H. B
”osch, and S. Dance (2009), Estimating surface co2 fluxes from space-borne co2 dry air mole fraction observations using an ensemble kalman filter, *Atmos. Chem. Phys*, *9*, 2619–2633.

Forbich, I., L. Kutzbach, A. Hormann, and M. Wilmking (2010), A comparison of linear and exponential regression for estimating diffusive CH_4 fluxes by closed-chambers in peatlands, *Soil Biology and Biogeochemistry*, *42*, 507–515.

Fox, A., et al. (2009), The reflex project: Comparing different algorithms and implementations for the inversion of a terrestrial ecosystem model against eddy covariance data, *Agricultural and Forest Meteorology*, *149*(10), 1597–1615.

Frankenberg, C., U. Platt, and T. Wagner (2005), Iterative maximum a posteriori (imap)-doas for retrieval of strongly absorbing trace gases: Model studies for ch4 and co2 retrieval from near infrared spectra of sciamachy onboard envisat, *Atmos. Chem. Phys*, *5*, 9–22.

Frankenberg, C., J. Meirink, P. Bergamaschi, A. Goede, M. Heimann, S. K
"orner, U. Platt, M. Van Weele, and T. Wagner (2006), Satellite chartography of atmospheric methane from SCIAMACHY on board ENVISAT: Analysis of the years 2003 and 2004, *Journal of geophysical research*, *111*(D7), D07,303.

Frankenberg, C., I. Aben, P. Bergamaschi, E. Dlugokencky, R. van Hees, S. Houweling, P. van der Meer, R. Snel, and P. Tol (2011), Global column-averaged methane mixing ratios from 2003 to 2009 as derived from SCIAMACHY: trend and variability, *Journal of Geophysical Research*, *116*, doi:10.1029/2010JD014,849.

Franks, S., K. Beven, P. Quinn, and I. Wright (1997), On the sensitivity of soil-vegetation-atmosphere transfer (svat) schemes: equifinality and the problem of robust calibration, *Agricultural and Forest Meteorology*, *86*(1-2), 63–75.

Frolking, S., N. Roulet, T. Moore, P. RIchard, M. Lavoie, and S. Muller (2001), Modeling northern peatland decomposition and peat accumulation, *Ecosystems*, *4*, 479–498.

Frolking, S., N. Roulet, T. Moore, P. Lafleur, J. Bubier, and P. Crill (2002), Modeling seasonal to annual carbon balance of Mer Bleue Bog, Ontario, Canada, *Global Biogeochemical Cycles*, *16*, doi:10.1029/2001GB001,457.

Fung, A., Z. Li, and K. Chen (1992), Backscattering from a randomly rough dielectric surface, *Geoscience and Remote Sensing, IEEE Transactions on*, *30*(2), 356–369.

Funk, D., E. Pullman, K. Peterson, P. Crill, and W. Billings (1994), Influence of water table on carbon dioxide, carbon monoxide and methane fluxes from taiga bog microcosms, *Global Biogeochemical Cycles*, *8*, 271–278.

Gao, H., E. Wood, T. Jackson, M. Drusch, and R. Bindlish (2006), Using TRMM/TMI to retrieve surface soil moisture over the Southern United States from 1998 to 2002, *Journal of Hydrometeorology*, *7*, 23–38.

Gelman, A., and D. Rubin (1992), Inference from iterative simulation using multiple sequences, *Statistical science*, pp. 457–472.

Gelman, A., J. Carlin, H. Stern, and D. Rubin (2004), *Bayesian Data Analysis 2nd Ed.*, Chapman and Hall/CRC.

Ghent, D., J. Kaduk, J. Remedios, and H. Balzter (2011), Data assimilation into land surface models: the implications for climate feedbacks, *International Journal of Remote Sensing*, *32*(3), 617–632.

Gifford, R. (2003), Plant respiration in productivity models: conceptualisation, representation and issues for global terrestrial carbon-cycle research, *Functional Plant Biology*, *30*(2), 171–186.

Gorham, E. (1991), Northern peatlands: Role in the carbon cycle and probable responses to climatic warming, *Ecological Applications*, *1*, 182–195.

Gruhier, C., et al. (2010), Soil moisture active and passive microwave products: intercomparison and evaluation over a Sahelian site, *Hydrological Earth System Sciences*, *14*, 141–156.

Hashimoto, S., T. Morishita, T. Sakata, S. Ishizuka, S. Kaneko, and M. Takahashi (2011), Simple models for soil co2, ch4, and n2o fluxes calibrated using a bayesian approach and multi-site data, *Ecological Modelling*.

Heinemeyer, A., S. Croft, M. Garnett, E. Gloor, J. Holden, M. Lomas, and P. Ineson (2010), The MILLENNIA peat cohort model: predicting past, present and future soil carbon budgets and fluxes under changing climates in peatlands, *Climate Research*, *45*, 207–226.

Hendriks, D., J. Van Huissteden, and A. Dolman (2010), Multi-technique assessment of spatial and temporal variability of methane fluxes in a peat meadow, *Agricultural and Forest Meteorology*, *150*(6), 757–774.

Hoeben, R., and P. Troch (2000), Assimilation of active microwave observation data for soil moisture profile estimation, *Water Resources Research*, pp. 2805–2819.

Holden, J. (2005), Peatland hydrology and carbon release: why small-scale process matters, *Philosophical Transactions of the Royal Society*, pp. 2891–2913.

Holden, J., P. Chapman, and J. Labadz (2004), Artificail drainage of peatlands: hydrological and hydrochemical process and wetland restoration, *Progress in Physical Geography*, pp. 95–123.

Hollinger, D., and A. Richardson (2005), Uncertainty in eddy covariance measurements and its application to physiological models, *Tree Physiology*, *25*, 873–885.

Houweling, S., et al. (2010), The importance of transport model uncertainties for the estimation of co2 sources and sinks using satellite measurements, *Atmospheric chemistry and physics*, *10*, 9981–9992.

Hungershoefer, K., F.-M. Breon, P. Peylin, F. Chevallier, P. Rayner, A. Klonecki, S. Houweling, and J. Marshall (2010), Evaluation of various observing systems for the global monitoring of CO_2 surface fluxes, *Atmospheric Chemistry and Physics*, *10*, 10,503–10,520.

Jackson, T. (1993), Iii. measuring surface soil moisture using passive microwave remote sensing, *Hydrological processes*, *7*(2), 139–152.

Jackson, T., and T. Schmugge (1991), Vegetation effects on the microwave emission of soils, *Remote Sensing of Environment*, *36*(3), 203–212.

Jackson, T., M. Cosh, R. Bindlish, P. Starks, D. Bosch, M. Seyfried, C. Goodrich, M. Moran, and J. Du (2010), Validation of Advanced Microwave Scanning Radiometer soil moisture products, *IEEE Transactions on Geoscience and Remote Sensing*, *48*, 4256–4272.

Jensen, J. (2000), *Remote Sensing of the Environment: An Earth Resource Perspective (2nd Edition)*, Prentice-Hall.

Jensen, M. (1973), *Consumptive Use of Water and Irrigation Water Requirements*, American Society of Civil Engineering.

Jensen, M., and H. Haise (1963), Estimating evapotranspiration from solar radiation, *Journal of the Irrigation and Drainage Division*, *89*, 15–41.

Joabsson, A., T. R. Christensen, and B. Wallen (1999), Vascular plant controls on methane emissions from northern peatforming wetlands, *TREE*, *14*, 385–388.

Kerr, Y., and E. Njoku (1990), A semiempirical model for interpreting microwave emission from semiarid land surfaces as seen from space, *Geoscience and Remote Sensing, IEEE Transactions on*, *28*(3), 384–393.

Kerr, Y., P. Waldteufel, J. Wigneron, J. Martinuzzi, J. Font, and M. Berger (2001), Soil moisture retrieval from space: The soil moisture and ocean salinity (smos) mission, *Geoscience and Remote Sensing, IEEE Transactions on*, *39*(8), 1729–1735.

Kettunen, A. (2003), Connecting methane fluxes to vegetation cover and water table fluctuations at microsite level: a modeling study, *Global Biogeochemical Cycles*, *17*, doi:10.1029/2002GB001,958.

Killham, K. (1994), *Soil Ecology*, Cambridge University Press.

Knorr, W. (2000), Annual and internannual co 2 exchanges of the terrestrial biosphere: Process-based simulations and uncertainties, *Global Ecology and Biogeography*, pp. 225–252.

Knorr, W., and J. Kattge (2005), Inversion of terrestrial ecosystem model parameter values against eddy covariance measurements by monte carlo sampling, *Global Change Biology*, *11*(8), 1333–1351.

Knorr, W., T. Kaminski, M. Scholze, N. Gobron, B. Pinty, R. Giering, and P. Mathieu (2010), Carbon cycle data assimilation with a generic phenology model, *J. Geophys. Res*, *115*.

Koike, T., Y. Nakamura, I. Kaihotsu, G. Davva, N. Matsuura, K. Tamagawa, and H. Fujii (2004), Development of an Advanced Microwave Scanning Radiometer (AMSR-E) algorithm of soil moisture and vegetation water content, *Annual Journal of Hydraulic Engineering, Japan Society of Civil Engineering*, *48*, 217–222.

Krinner, G., N. Viovy, N. de Noblet-Ducoudré, J. Ogée, J. Polcher, P. Friedlingstein, P. Ciais, S. Sitch, and I. Prentice (2005), A dynamic global vegetation model for studies of the coupled atmosphere-biosphere system, *Global Biogeochemical Cycles*, *19*(1), 1–33.

Kutzbach, L., J. Schneider, T. Sachs, M. Giebels, H. Nykanen, N. Shurpali, P. Martikainen, J. Alm, and M. Wilmking (2007), CO_2 flux determination by closed-chamber methods can be seriously biased by inappropriate application of linear regression, *Biogeosciences*, *4*, 1005–1025.

Lafleur, P., N. Roulet, J. Bubier, S. Frolking, and T. Moore (2003), Interannual variability in the peatland-atmosphere carbon dioxide exchange at an ombrotrophic bog, *Global Biogeochemical Cycles*, *17*(2), 5–1.

Lai, D. (2009), Methane dynamics in northern peatlands: A review, *Pedosphere*, *19*, 409–421.

Lawrence, D., and A. Slater (2008), Incorporating organic soil into a global climate model, *Climate Dynamics*, *30*(2), 145–160.

Le Hegarat-Mascle, S., M. Zribi, F. Alem, A. Weisse, and C. Loumagne (2002), Soil moisture estimation from ERS/SAR data: toward and operational methodology, *IEEE Transactions on Geoscience and Remote Sensing*, *40*, 2647–2658.

Le Mer, J., and P. Roger (2001), Production, oxidation, emission and consumption of methane by soils: A review, *European Journal of Soil Biology*, *37*, 25–50.

Le Quéré, C. (2010), Trends in the land and ocean carbon uptake, *Current Opinion in Environmental Sustainability*, *2*(4), 219–224.

Letts, M., N. Roulet, N. Comer, M. Skarupa, and D. Verseghy (2000), Parametrization of peatland hydraulic properties for the canadian land surface scheme, *Atmosphere-Ocean*, *38*(1), 141–160.

Li, L., P. Gaiser, B.-C. Gao, R. Bevilacqua, T. Jackson, C. Rudiger, J.-C. Calvet, and R. Bindlish (2010), WindSat global soil moisture retrieval and validation, *IEEE Transactions on Geoscience and Remote Sensing*, *48*, 2224–2241.

Limpens, J., F. Berendse, J. Canadell, C. Freeman, J. Holden, N. Roulet, H. Rydin, and G. Schaepman-Strub (2008), Peatlands and the carbon cycle: from local processes to global implications - a synthesis, *Biogeosciences*, *5*, 1475–1491.

MacDonald, J., D. Fowler, K. Hargreaves, U. Skiba, I. Leith, and M. Murray (1998), Methane emissions rates from a northern wetland; response to temperature, water table and transport, *Atmospheric Environment*, *32*, 3219–3227.

Mastepanov, M., C. Sigsgaard, E. Dlugokencky, S. Houweling, L. Str
"om, M. Tamstorf, and T. Christensen (2008), Large tundra methane burst during onset of freezing, *Nature*, *456*(7222), 628–630.

Mather, P. (2004), *Computer Processing of Remotely-Sensed Images An Introduction (3rd Edition)*, Wiley.

Mattia, F., G. Satalino, A. Balenzano, and M. Rinaldi (), Use of multi-temporal PalSAR ScanSAR data for soil moisture retrieval, in *3rd ALOS Joint PI Symposium, Kona, Hawai'i, USA*.

Maybeck, P. (1979), *Stochastic models, estimation and control*, vol. 141, Academic press.

McCabe, M., H. Gao, and E. Wood (2005), Evaluation of AMSR-E-derived soil moisture retrievals using ground-based and psr airborne data during SMEX02, *Journal of Hydrometeorology*, *6*, 864–877.

McCallum, I., W. Wagner, C. Schmullius, A. Shvidenko, M. Obersteiner, S. Fritz, and S. Nilsson (2010), Satellite-based terrestrial production efficiency modeling, *Carbon balance and management*, *4*, doi:10.1186/1750–0680–4–8.

McNamara, N., T. Plant, S. Oakley, S. Ward, C. Wood, and N. Ostle (2008), Gully hotspot contribution to landscape methane (CH_4) and carbon dioxide (CO_2) fluxes in a northern peatland, *Science of the total environment*, *404*, 354–360.

Medlyn, B., A. Robinson, R. Clement, and R. McMurtrie (2005), On the validation of models of forest co2 exchange using eddy covariance data: some perils and pitfalls, *Tree Physiology*, *25*(7), 839.

Meirink, J., H. Eskes, and A. Goede (2006), Sensitivity analysis of methane emissions derived from SCIAMACHY observations through inverse modelling, *Atmos. Chem. Phys*, *6*, 1275–1292.

Meirink, J., et al. (2008), Four-dimensional variational data assimilation for inverse modeling of atmospheric methane emissions: analysis of SCIAMACHY observations, *Journal of Geophysical Research*, *113*, doi:10.1029/2007JD009,740.

Meng, C., Z. Li, X. Zhan, J. Shi, and C. Liu (2009), Land surface temperature data assimilation and its impact on evapotranspiration estimates from the common land model, *Water Resources Research*, *45*(2), W02,421.

Merlin, O., A. Al Bitar, J. Walker, and Y. Kerr (2009), A sequential model for disaggregating near-surface soil moisture observations using multi-resolution thermal sensors, *Remote Sensing of Environment*, *113*(10), 2275–2284.

Merlin, O., A. Al Bitar, J. Walker, and Y. Kerr (2010), An improved algorithm for disaggregating microwave-derived soil moisture based on red, near-infrared and thermal-infrared data, *Remote Sensing of Environment*, *114*(10), 2305–2316.

Mladenova, I., V. Lakshmi, J. Walker, R. Panciera, W. Wagner, and M. Doubkova (2010), Validation of the ASAR Global Monitoring Mode soil moisture product using the NAFE'05 data set, *IEEE Transactions on Geoscience and Remote Sensing*, *48*, 2498–2508.

Moore, T., and R. Knowles (1989), The influence of water table levels on methane and carbon dioxide emissions from peatland soils, *Canadian Journal of Soil Science*, *69*, 33–38.

Moore, T., N. Roulet, and R. Knowles (1990), Spatial and temporal variations of methane flux from subarctic/northern boreal fens, *Global Biogeochemical Cycles*, *4*, 29–46.

Moore, T., A. De Young, J. Bubier, E. Humphreys, P. Lafleur, and N. Roulet (2011), A multi-year record of methane flux at the Mer Bleue Bog, southern Canada, *Ecosystems*, pp. doi:10.1007/s10,021–011–9435–9.

Moradkhani, H. (2008), Hydrologic remote sensing and land surface data assimilation, *Sensors*, *8*(5), 2986–3004.

Moran, M., C. Peters-Lidard, J. Watts, and S. McElroy (2004), Estimating soil moisture at the watershed scale with satellite-based radar and land surface models, *Canadian Journal of Remote Sensing*, *30*(5), 805–826.

Morris, M. (1991), Factorial sampling plans for preliminary computational experiments, *Technometrics*, pp. 161–174.

Morrissey, L., and G. Livingston (1992), Methane emissions from alaskan Arctic tundra, *Journal of Geophysical Research*, *97*, 16,661–16,670.

Myklebust, M., L. Hipps, and R. Ryel (2008), Comparison of eddy covariance, chamber, and gradient methods of measuring soil CO_2 efflux in an annual semi-arid grass, *Bromus tectorum*, *Agricultural and Forest Meteorology*, *148*, 1894–1907.

Naeimi, V., Z. Bartalis, and W. Wagner (2009a), ASCAT soil moisture: an assessment of the data quality and consistence with the ERS Scatterometer heritage, *Journal of Hydrometerology*, *10*, 555–563.

Naeimi, V., K. Scipal, Z. Bartalis, S. Hasenauer, and W. Wagner (2009b), An improved soil moisture retrieval algorithm for ers and metop scatterometer observations, *Geoscience and Remote Sensing, IEEE Transactions on*, *47*(7), 1999–2013.

Nakatsuka, Y., and S. Maksyutov (2009), Optimization of the seasonal cycles of simulated co2 flux by fitting simulated atmospheric co2 to observed vertical profiles, *Biogeosciences*, *6*(12).

Ni-Meister, W., J. Walker, and P. Houser (2005), Soil moisture intialization for climate prediction: characterization of model and observation errors, *Journal of Geophysical Research*, *110*, doi:10.1029/2004JD005,745.

Njoku, E., and S. Chan (2006), Vegetation and surface roughness effects on amsr-e land observations, *Remote sensing of environment*, *100*(2), 190–199.

Njoku, E., T. Jackson, V. Lakshmi, T. Chan, and S. Nghiem (2003), Soil moisture retrieval from amsr-e, *Geoscience and Remote Sensing, IEEE Transactions on*, *41*(2), 215–229.

Norman, J., C. Kucharik, S. Gower, D. Baldocchi, P. Crill, M. Rayment, K. Savage, and R. Striegl (1997), A comparison of six methods for measuring soil-surface carbon dioxide fluxes, *Journal of Geophysical Research*, *102*, 28,771–28,777.

Oren, R., C.-I. Hsieh, P. Stoy, J. Albertson, H. McCarthy, P. Harrell, and G. Katul (2006), Estimating uncertainty in annual net ecosystem carbon exchange: spatial variation in turbulent fluxes and sampling errors in eddy-covariance measurements, *Global Change Biology*, *12*, 883–896.

Owe, M., R. de Jeu, and J. Walker (2001), A Methodology for Surface Soil Moisture and Vegetation Optical Depth Retrieval using the Microwave Polarization Difference Index, *IEEE Transactions on Geoscience and Remote Sensing*, *39*, 1643–1654.

Owe, M., R. de Jeu, and T. Holmes (2008), Multisensor historical climatology of satellite-derived global land surface moisture, *Journal of Geophysical Research*, *113*(F1), F01,002.

Pan, M., E. Wood, D. McLaughlin, D. Entekhabi, and L. Luo (2010), A multiscale ensemble filtering system for hydrologic data assimilation. part i: Implementation and synthetic experiment, *Journal of Hydrolmeteorology*, *10*, 794–806.

Papale, D., et al. (2006), Towards a standardized processing of Net Ecosystem Exchange measured with eddy covariance technique: algorithms and uncertainty estimation, *Biogeosciences*, *3*, 571–583.

Paris Anguela, T., M. Zribi, S. Hasenauer, and C. Loumagne (2008), Analysis of surface and root-zone soil moisture dynamics with ERS scatterometer and the hydrometeorological model SAFRAN-IBSA-MODCOU at Grand Morin watershed (France), *Hydrological Earth System Sciences*, *12*, 1415–1424.

Parry, M., O. Canziani, J. Palutikof, van der Linden P.J., and C. e. Hanson (2007), *Climate Change 2007: impacts, adaptation and vulnerability: contribution of Working Group II to the fourth assessment report of the Intergovernmental Panel on Climate Change*, Cambridge University Press.

Parton, W., D. Schimel, C. Cole, and D. Ojima (1987), Analysis of factors controlling soil organic matter levels in great plains grasslands, *Soil Science Society of Americal Journal*, *51*, 1173–1179.

Parton, W., et al. (1993), Observations and modeling of biomass and soil organic matter dynamics for the grassland biome worldwide, *Global Biogeochemcial Cycles*, *7*, 785–809.

Pathe, C., W. Wagner, D. Sabel, M. Doubkova, and J. Basara (2009), Using ENVISAT SAR Global Mode data for surface soil moisture retrieval over Oklahoma, USA, *IEEE Transactions on Geoscience and Remote Sensing*, *47*, 468–480.

Pathmathevan, M., T. Koike, and X. Li (2003), A new satellite-based data assimilation algorithm to determine spatial and temporal variations of soil moisture and temperature profiles, *Journal of the Meteorological Society of Japan*, *81*(5), 1111–1135.

Petrescu, A., J. van Huissteden, M. Jackowicz-Korczynski, A. Yurova, T. Christensen, P. Crill, K. Backstrand, and T. Maximov (2008), Modelling CH_4 emissions from arctic wetlands: effects of hydological parameterization, *Biogeosciences*, *5*, 111–121.

Pitman, A. (2003), The evolution of, and revolution in, land surface schemes designed for climate models, *International Journal of Climatology*, *23*, 479–510.

Potter, C. (1997), An ecosystem simulation model for methane production and emission from wetlands, *Global Biogeochemical Cycles*, *11*, 495–506.

Potter, C., and S. Klooster (1997), Global model estimates of carbon and nitrogen storage in litter and soil pools: response to changes in vegetation quality and biomass allocation, *Tellus B*, *49*(1), 1–17.

Potter, C., J. Randerson, C. Field, P. Matson, P. Vitousek, H. Mooney, and S. Klooster (1993), Terrestrial ecosystem production: A process model based on global satellite and surface data, *Global Biogeochemical Cycles*, *7*, 811–841.

Potter, C., J. Bubier, P. Crill, and P. Lafleur (2001), Ecosystem modeling of methane and carbon dioxide fluxes for boreal forest sites, *Canadian Journal of Forest Research*, *31*(2), 208–223.

Priestly, C., and R. Taylor (1972), On the assessment of surface heat flux and evaporation using large-scale parameters, *Monthly Weather Review*, *100*, 81–92.

Qin, J., S. Liang, K. Yang, I. Kaihotsu, R. Liu, and T. Koike (2009), Simultaneous estimation of both soil moisture and model parameters using particle filtering method through the assimilation of microwave signal, *Journal of Geophysical Research*, *114*(D15), D15,103.

Quaife, T., P. Lewis, M. De Kauwe, M. Williams, B. Law, M. Disney, and P. Bowyer (2008), Assimilating canopy reflectance data into an ecosystem model with an ensemble kalman filter, *Remote Sensing of Environment*, *112*(4), 1347–1364.

Quesney, A., S. Le Hegarat-Mascle, O. Taconet, D. Vidal-Madjar, J.-P. Wigneron, C. Loumagne, and M. Normand (2000), Estimation of watershed soil moisture index from ERS/SAR data, *Remote Sensing of Environment*, *72*, 290–303.

Raich, J., and C. Potter (1995), Global patterns of carbon dioxide emissions from soils, *Global Biogeochemical Cycles*, *9*(1), 23–36.

Raich, J., E. Rastetter, J. Melillo, D. Kicklighter, P. Steudler, B. Peterson, A. Grace, B. Moore Iii, and C. Vorosmarty (1991), Potential net primary productivity in south america: application of a global model, *Ecological Applications*, *1*(4), 399–429.

Raich, J., W. Parton, A. Russell, R. Sanford, and P. Vitousek (2000), Analysis of factors regulating ecosystemdevelopment on mauna loa using the century model, *Biogeochemistry*, *51*(2), 161–191.

Raupach, M., P. Rayner, D. Barrett, R. DeFries, M. Heimann, D. Ojima, S. Quegan, and C. Schmullius (2005), Model–data synthesis in terrestrial carbon observation: methods, data requirements and data uncertainty specifications, *Global Change Biology*, *11*(3), 378–397.

Rayner, P. (2010), The current state of carbon-cycle data assimilation, *Current Opinion in Environmental Sustainability*, *2*(4), 289–296.

Rayner, P., M. Scholze, W. Knorr, T. Kaminski, R. Giering, and H. Widmann (2005), Two decades of terrestrial carbon fluxes from a carbon cycle data assimilation system (ccdas), *Global Biogeochemical Cycles*, *19*(2), GB2026.

Reichle, R., R. Koster, J. Dong, and A. Berg (2004), Global soil moisture from satellite observations, land surface models, and ground data: inplications for data assimilation, *Journal of Hydrometeorology*, *5*, 430–442.

Reichle, R., R. Koster, P. Liu, S. Mahanama, E. Njoku, and M. Owe (2007), Comparison and assimilation of global soil moisture retrievals from the advanced microwave scanning radiometer for the earth observing system (amsr-e) and the scanning multichannel microwave radiometer (smmr), *Journal of geophysical research*, *112*(D9), D09,108.

Renard, B., D. Kavetski, G. Kuczera, M. Thyer, and S. Franks (2010), Understanding predictive uncertainty in hydrologic modeling: The challenge of identifying input and structural errors, *Water Resources Research*, *46*(5), W05,521.

Ricciuto, D., A. King, D. Dragoni, and W. Post (2011), Parameter and prediction uncertainty in an optimized terrestrial carbon cycle model: Effects of constraining variables and data record length, *Journal of Geophysical Research*, *116*(G1), G01,033.

Richardson, A., et al. (2006), A multi-site analysis of random error in tower-based measurements of carbon and energy fluxes, *Agricultural and Forest Meteorology*, *136*, 1–18.

Richardson, A., et al. (2010), Estimating parameters of a forest ecosystem c model with measurements of stocks and fluxes as joint constraints, *Oecologia*, *164*(1), 25–40.

Richardson, M., A.D. Mahecha, et al. (2008), Statistical properties of random CO_2 flux measurement uncertainty inferred from model residuals, *Agricultural and Forest Meteorology*, *148*, 38–50.

Robock, A., K. Vinnikov, G. Srinivasan, J. Entin, S. Hollinger, N. Speranskaya, S. Liu, and A. Namkhai (2000), The global soil moisture data bank, *BULLETIN-AMERICAN METEOROLOGICAL SOCIETY*, *81*(6), 1281–1300.

Roulet, N. (2000), Peatlands, carbon storage, greenhouse gases, and the kyoto protocol: Prospects and significance for canada, *Wetlands*, *20*(4), 605–615.

Rudiger, C., J.-C. Calvet, C. Gruhier, T. Holmes, A. de Jeu, and W. Wagner (2009), An Intercomparison of ERS-Scat and AMSR-E Soil Moisture Observations with Model Simulations over France, *Journal of Hydrometerology*, *10*, 431–447.

Salamon, P., and L. Feyen (2010), Disentangling uncertainties in distributed hydrological modeling using multiplicative error models and sequential data assimilation, *Water Resources Research*, *46*(12), W12,501.

Saltelli, A., M. Ratto, S. Tarantola, F. Campolongo, et al. (2006), Sensitivity analysis practices: Strategies for model-based inference, *Reliability Engineering & System Safety*, *91*(10-11), 1109–1125.

Santaren, D., P. Peylin, N. Viovy, and P. Ciais (2007), Optimizing a process-based ecosystem model with eddy-covariance flux measurements: A pine forest in southern france, *Global biogeochemical cycles*, *21*(2).

Savage, K., E. Davidson, and A. Richardson (2008), A conceptual and practical approach to data quality and analysis procedures for high-frequency soil respiration measurements, *Functional Ecology*, *22*, 1000–1007.

Saxton, K., W. Rawls, J. Romberger, and R. Papendick (1986), Estimating generalized soil-water characteristics from texture, *Soil Science Society of Americal Journal*, *50*, 1031–1036.

Schaaf, C., et al. (2002), First operational brdf, albedo nadir reflectance products from modis, *Remote Sensing of Environment*, *83*(1-2), 135–148.

Schimel, J. (1995), Plant transport and methane production as controls on methane flux from arctic wet meadow tundra, *Biogeochemistry*, *28*, 183–200.

Schmid, H. (2002), Footprint modeling for vegetation atmosphere exchange studies: a review and perspective, *Agricultural and Forest Meteorology*, *113*(1-4), 159–183.

Scholze, M., T. Kaminski, P. Rayner, W. Knorr, and R. Giering (2007), Propagating uncertainty through prognostic carbon cycle data assimilation system simulations, *J. Geophys. Res*, *112*.

Schrier-Uijl, A., E. Veenendaal, P. Leffelaar, J. van Huissteden, and F. Berendse (2008), Spatial and temporal variation of methane emissions in drained eutrophic peat agro-ecosystems: drainage ditches as emission hotspots, *Biogeosciences Discussions*, *5*, 1237–1261.

Schutz, J., P. Schroeder, and H. Rennenberg (1991), *Trace Gas Emissions by Plants*, chap. Role of plants in regulating the methane flux to the atmosphere, pp. 29–64, Academic, San Diego, California.

Scipal, K., T. Holmes, R. de Jeu, V. Naeimi, and W. Wagner (2008), A possible solution for the problem of estimating the error structure of global soil moisture data sets, *Geophysical Research Letters*, *35*, doi:10.1029/2008GL035,599.

Sebacher, D., R. Harriss, and K. Bartlett (1985), Methane Emissions to the Atmosphere Through Aquatic Plants, *Journal of Environmental Quality*, *14*, 40–46.

Segers, R. (1998), Methane production and methane consumption: a review of processes underlying wetland methane fluxes., *Biogeochemistry*, *41*, 23–51.

Segers, R., and P. Leffelaar (2001), Modeling methane fluxes in wetlands with gas-transporting plants 3. Plot scale, *Journal of Geophysical Research*, *106*, 3541–3558.

Sellers, P., S. Los, C. Tucker, C. Justice, D. Dazlich, G. Collatz, and D. Randall (1996), A revised land surface parameterization (sib-2) for atmospheric general circulation models. part 2, the generation of flobal fields of terrestrial biophysical parameters from satellite data, *Journal of Climate*, *9*, 706–737.

Sellers, P., et al. (1997), Modelling the exchanges of energy, water and carbon between continents and the atmosphere, *Science*, *275*, 502–509.

Shannon, R., J. White, J. Lawson, and B. Gilmour (1996), Methane Efflux from Emergent Vegetation in Peatlands, *Journal of Ecology*, *84*, 239–246.

Shoshany, M., T. Svoray, and P. Foody (2000), The relationship between ERS-2 SAR backscatter and soil moisture: generalization from a humid to semi-arid transect., *International Journal of Remote Sensing*, *21*, 2337–2343.

Shurpali, N., S. Verma, R. Clement, and D. Billesback (1993), Seasonal distribution of methane flux in a minnesota peatland measured by eddy correlation, *Journal of Geophysical Research*, *98*, 20,649–20,655.

Sitch, S., et al. (2003), Evaluation of ecosystem dynamics, plant geography and terrestrial carbon cycling in the lpj dynamic global vegetation model, *Global Change Biology*, *9*(2), 161–185.

Sivia, J., D.S. with Skilling (2006), *Data Analysis: A Bayesian Tutorial 2nd Ed.*, Oxford Science Publications.

Sonobe, R., H. Tani, X. Wang, and M. Fukuda (2008), Estimation of soil moisture for bare soil fields using ALOS/PALSAR HH polarization data, *Agricultural Information Research*, *17*, 171–177.

Spahni, R., et al. (2011), Constraining global methane emissions and uptake by ecosystems, *Biogeosciences*, *8*, 1643–1665.

St-Hilaire, F., J. Wu, N. Roulet, S. Frolking, P. Lafleur, E. Humphreys, and V. Arora (2010), McGill wetland model: evaluation of a peatland carbon simulator developed for global assessments, *Biogeosciences*, *7*, 3517–3530.

Stroud, K., and D. Booth (2003), *Advanced Engineering Mathematics*, Palgrave MacMillan.

Sundh, I., C. Mikkela, M. Nilsson, and B. Svensson (1995), Potential aerobic methane oxidation in a sphagnum-dominated peatland - controlling factors and relation to methane emissions, *Soil Biology and Biochemistry*, *27*, 829–837.

Tallis, J. (1997), The southern pennine experience: an overview of blanket mire degradation, *Blanket mire degradation: Causes, consequences and challenges*, pp. 7–15.

Tarnocai, C., J. Canadell, E. Schuur, P. Kuhry, G. Mazhitova, and S. Zimov (2009), Solving soil temperature profile from discretized diffusion equation, *Soil organic carbon pools in the northern circumpolar permafrost region*, p. GB2023.

ter Braak, C., and J. Vrugt (2008), Differential evolution markov chain with snooker updater and fewer chains, *Statistics and Computing*, *18*(4), 435–446.

Thyer, M., B. Renard, D. Kavetski, G. Kuczera, S. Franks, and S. Srikanthan (2009), Critical evaluation of parameter consistency and predictive uncertainty in hydrological modeling: A case study using bayesian total error analysis, *Water Resources Research*, *45*, 22.

Trudinger, C., et al. (2007), Optic project: An intercomparison of optimization techniques for parameter estimation in terrestrial biogeochemical models, *J. Geophys. Res*, *112*, G02,027.

Ulaby, F., R. Moore, and A. Fung (1982), *Microwave Remote Sensing Active and Passive Volume II*, Addison-Wesley Publishing Company.

Valentine, D., E. Holland, and D. Schimel (1994), Ecosystem and physiological controls over methane production in northern wetlands., *Journal of Geophysical Research D1*, *99*, 1563–1571.

van Huissteden, J., R. van den Bos, and I. Marticorena-Alvarez (2006), Modelling the effect of water-table management on CO_2 and CH_4 fluxes from peat soils, *Netherlands Journal of Geosciences*, *85*, 3–18.

Van Oijen, M., J. Rougier, and R. Smith (2005), Bayesian calibration of process-based forest models: bridging the gap between models and data, *Tree Physiology*, *25*, 915–927.

Verbeeck, H., P. Peylin, C. Bacour, D. Bonal, K. Steppe, and P. Ciais (2011), Seasonal patterns of co2 fluxes in amazon forests: fusion of eddy covariance data and the orchidee model, *Journal of Geophysical Research*, *116*(G2), G02,018.

Verhoest, N., H. Lievens, P. Matgen, M. Montanari, H. Vernieuwe, G. deLannoy, B. de Baets, and L. Hoffmann (2008), Soil moisture retrieval from ALOS PALSAR in the Alzette (Luxembourg) and Zwalm (Belgium) catchments, in *International Workshop on Microwave Remote Sensing for Land Hydrology Research and Applications, Oxnard, CA, USA*.

Verstraeten, W., F. Veroustraete, W. Wagner, T. Roey, W. Heyns, S. Verbeiren, and J. Feyen (2011), Remotely sensed soil moisture integration in an ecosystem carbon flux model. the spatial implication, *Greenhouse Gas Inventories*, pp. 117–136.

Vuichard, N., P. Ciais, L. Belelli-Marchesini, and R. Valentini (2010), New parameterization of a global vegetation model for steppe ecosystem from southern siberian in situ measurements, *Rangeland Ecology & Management*, *63*(1), 51–61.

Wagner, W., G. Lemoine, M. Borgeaud, and H. Rott (1999a), A study of vegetation cover effects on ERS Scatterometer data, *IEEE Transactions on Geoscience and Remote Sensing*, *37*, 938–948.

Wagner, W., J. Noll, M. Borgeaud, and H. Rott (1999b), Monitoring soil moisture over the Canadaian prairies with the ERS Scatterometer, *IEEE Transactions on Geoscience and Remote Sensing*, *37*, 206–216.

Wagner, W., K. Scipal, C. Pathe, D. Gerten, W. Lucht, and B. Rudolf (2003), Evaluation of the agreement between the first global remotely sensed soil moisture data with model and precipitation data, *Journal of Geophysical Research*, *108*, doi:10.1029/2003JD003,663.

Wagner, W., G. Bloschl, P. Pampaloni, J.-C. Calvet, B. Bizzarri, J.-P. Wigneron, and Y. Kerr (2007a), Operational readiness of microwave remote sensing of soil moisture for hydrologic applications, *Nordic Hydrology*, *38*, 1–20.

Wagner, W., V. Naeimi, K. Scipal, R. De Jeu, and J. Martínez-Fernández (2007b), Soil moisture from operational meteorological satellites, *Hydrogeology Journal*, *15*(1), 121–131.

Wagner, W., et al. (2008), Temporal stability of soil moisture and radar backscatter observed by the advanced synthetic aperture radar (asar), *Sensors*, *8*(2), 1174–1197.

Walker, J., and P. Houser (2005), *Advances in Water Science Methodologies*, chap. Hydrologic data assimilation, AA Balkema, The Netherlands.

Walker, J., G. Willgoose, and J. Kalma (2001), One-dimensional soil moisture profile retrieval by assimilation of near-surface measurements: A simplified soil moisture model and field application, *Journal of Hydrometeorology*, *2*(4), 356–373.

Walker, J., G. Willgoose, and J. Kalma (2002), Three-dimensional soil moisture profile retrieval by assimilation of near-surface measurements: Simplified kalman filter covariance forecasting and field application, *Water resources research*, *38*(12), 1301.

Walter, B., and M. Heimann (2000), A process-based, climate-sensitive model to derive methane emissions from natural wetlands: application to five wetland sites, sensitivity to model parameters, and climate, *Global Biogeochemical Cycles*, *14*, 745–765.

Wang, J., and B. Choudhury (1981), Remote sensing of soil moisture content, over bare field at 1.4 ghz frequency, *Journal of Geophysical Research*, *86*(C6), 5277–5282.

Wang, J., and T. Schmugge (1980), An empirical model for the complex dielectric permittivity of soils as a function of water content, *Geoscience and Remote Sensing, IEEE Transactions on*, *GE-18*(4), 288–295.

Wang, S., X. Li, X. Han, and R. Jin (2011), Estimation of surface soil moisture and roughness from multi-angular ASAR imagery in the Watershed Allied Telemetry Experimental Research (WATER), *Hydrological Earth System Sciences*, *15*, 1415–1426.

Wang, Y., C. Trudinger, and I. Enting (2009), A review of applications of model-data fusion to studies of terrestrial carbon fluxes at different scales, *Agricultural and Forest Meteorology*, *149*(11), 1829–1842.

Wania, R. (2007), *Modelling northern peatland land surface processes, vegetation dynamics and methane emissions*, University of Bristol PhD Thesis.

Wania, R., I. Ross, and I. Prentice (2009a), Integrating peatlands and permafrost into a dynamic global vegetation model: I. evaluation and sensitivity of physical land surface processes, *Global Biogeochemical Cycles*, *23*, GB3014.

Wania, R., I. Ross, and I. Prentice (2009b), Integrating peatlands and permafrost into a dynamic global vegetation model: Ii. evaluation and sensitivity of vegetation and carbon cycle processes, *Global Biogeochemical Cycles*, *23*, GB3014.

Whiting, G., and J. Chanton (1992), Plant-dependent ch_4 emission in a subarctic Canadian fen, *Global Biogeochemical Cycles*, *6*, 225–231.

Wigneron, J., A. Olioso, J. Calvet, and P. Bertuzzi (1999), Estimating root zone soil moisture from surface soil moisture data and soil-vegetation-atmosphere transfer modeling, *Water Resources Research*, *35*(12), 3735–3745.

Wigneron, J., J. Calvet, T. Pellarin, A. Van de Griend, M. Berger, and P. Ferrazzoli (2003), Retrieving near-surface soil moisture from microwave radiometric observations: current status and future plans, *Remote Sensing of Environment*, *85*(4), 489–506.

Wikle, C., and L. Berliner (2007), A bayesian tutorial for data assimilation, *Physica D: Nonlinear Phenomena*, *230*(1-2), 1–16.

Williams, M., P. Schwarz, B. Law, J. Irvine, and M. Kurpius (2005), An improved analysis of forest carbon dynamics using data assimilation, *Global Change Biology*, *11*(1), 89–105.

Williams, M., et al. (2009), Improving land surface models with fluxnet data., *Biogeosciences*, *6*, 1341–1359.

Woodward, F., T. Smith, and W. Emanuel (1995), A global land primary productivity and phytogeography model, *Global biogeochemical cycles*, *9*(4), 471–490.

Worrall, F., M. Reed, J. Warburton, and T. Burt (2003), Carbon budget for a british upland peat catchment, *The Science of the Total Environment*, *312*(1-3), 133–146.

Xi, X. (2008), Solving soil temperature profile from discretized diffusion equation, *EAS8803 special topics on numerical modeling and computer programming in geosciences*.

Xu, T., L. White, D. Hui, and Y. Luo (2006), Probabilistic inversion of a terrestrial ecosystem model: Analysis of uncertainty in parameter estimation and model prediction, *Global Biogeochemical Cycles*, *20*(2), GB2007.

Yang, J. (2010), Convergence and uncertainty analyses in monte-carlo based sensitivity analysis, *Environmental Modelling & Software*.

Yang, J., P. Reichert, and K. Abbaspour (2007a), Bayesian uncertainty analysis in distributed hydrologic modeling: A case study in the thur river basin (switzerland), *Water resources research*, *43*(10), W10,401.

Yang, J., P. Reichert, K. Abbaspour, and H. Yang (2007b), Hydrological modelling of the chaohe basin in china: Statistical model formulation and bayesian inference, *Journal of Hydrology*, *340*(3-4), 167–182.

Yang, K., T. Watanabe, T. Koike, and X. Li (2007c), Auto-calibration system developed to assimilate AMSR-E data into a land surface model for estimating soil moisture and the surface energy budget, *Journal of the Meteorological Society of Japan*, *85*, 229–242.

Yeluripati, J., M. van Oijen, M. Wattenbach, A. Neftel, A. Ammann, W. Parton, and P. Smith (2009), Bayesian calibration as a tool for initialising the carbon pools of dynamic soil models, *Soil Biology and Biochemistry*, *41*(12), 2579–2583.

Yin, X., and P. Arp (1993), Predicting forest soil temperatures from monthly air temperature and precipitation records, *Canadian Journal of Forest Research*, *23*, 2521–2536.

Yu, Z., D. Bkilman, S. FrouciNC, G. MacDonalu, N. Roullt, and P. Camill (2011), Peatlands and their role in the global carbon cycle, *Eos*, *92*(12).

Zhu, L., J. Chen, Q. Qin, J. Li, and L. Wang (2009), Optimization of ecosystem model parameters using spatio-temporal soil moisture information, *Ecological modelling*, *220*(18), 2121–2136.

Zhuang, Q., J. Melillo, D. Kicklighter, R. Prinn, A. McGuire, P. Steudler, B. Felzer, and S. Hu (2004), Methane fluxes between terrestrial ecosystems and the atmosphere at northern high latitudes during the past century: a retrospective analysis with a process-based biogeochemistry model, *Global Biogeochemical Cycles*, *18*, doi:10.1029/2004GB002,239.

Zribi, M., C. Andre, and B. Decharme (2009), A method for soil moisture estimation in Western Africa based on ERS Scatterometer, *IEEE Transactions on Geoscience and Remote Sensing*, *46*, 438–448.